

Friends of the Pleistocene
Pacific Cell 2006



Signatures of Quaternary crustal deformation and landscape evolution
in the Mendocino deformation zone, NW California

CONTRIBUTORS

This year's FOP fieldtrip represents the collaboration of numerous people and their resources we can't possibly list everyone that has helped make this trip happen, but we thank you all. The folks responsible for putting the guidebook together are (for the weekend) known as "the MONGOs" (the Multidisciplinary Order of Neotectonic Geologic Observers). The MONGOs are:

Mark Hemphill-Haley: markhh@humboldt.edu
Tom Leroy: toml@pacificwatershed.com
Bob McPherson: rm4@humboldt.edu
Jay Patton: jrp2@humboldt.edu
Jay Stallman: jay@stillwatersci.com
Diane Sutherland: to_digs@pacbell.net
Todd Williams: williams@unavco.org

Throughout the preparation for this trip, the MONGOs have been guided by the infamous advice from the famous Raymond "Bud" Burke. We would like to thank him for his invaluable comments.

MONGO Disclaimer:

We would like to take responsibility for the contents of this guidebook. If contributions are not correctly formatted or displayed, please blame us. We are, however, not responsible for the content of individual contributions.

We would like to thank the following, without whom this guidebook and field trip would not have possible...

Guidebook Contributors:

Ken Aalto: kra1@humboldt.edu	Tagg Nordstrom: tnordstrom@scopac.com
Hans AbrahamsonWard: HAbramsonward@geomatrix.com	Danny O'Shea: danny-oshea@redwoods.edu
Frank Bickner: bicknerf@lacoassociates.us	John Oswald: ozzy@hughes.net ; joswald@scopac.com
Gary Carver: cgeol@alaska.com	Bill Page: WDP7@pge.com
Gilbert Craven: gcraven@scopac.com	Chad Pritchard: chad-pritchard@sccd.org
Lori Dengler: lad1@humboldt.edu	Ian Pryor
Rocco Fiori: rfiori@parks.ca.gov	Michelle Roberts: mroberts@shn-engr.com
Jeff Freymueller: jeff@giseis.alaska.edu	Dane Robinson: DTRobinson@missiongeo.com
Kevin Furlong: kevin@geodyn.psu.edu	Joshua Roering: jroering@uoregon.edu
Carrie Garrison-Laney: cegl@u.washington.edu	Susan Schwartz: sschwartz@es.ucsc.edu
Harvey Kelsey: hmk1@humboldt.edu	Gary Simpson: gsimpson@shn-engr.com
Caroline Lavenda: levendac@lacoassociates.us	Bonnie Smith: for_bonnie@yahoo.com
David Lindberg: lindbergd@lacoassociates.us	Steve Thompson: thompson@lettis.com
Rick Koehler: koehler@seismo.unr.edu	Mark Verhey: markverhey@hotmail.com
Ben Mackey: bmackey@uoregon.edu	Giovanni Vadurro: vadurrog@lacoassociates.us
Orville Magoon:	Patrick Vaughn: pvaughan@parks.ca.gov
Sunshine Mansfield: ssm5@humboldt.edu	Rob Witter: rob.witter@dogami.state.or.us
Gerald Marshall: Gerald.Marshall@conservation.ca.gov	

HFOG Volunteers: Humboldt State University Geology Students

Sarah Balster
Gwen Erickson
Jeri Lyn Riordan
Martha Mitchell Woodward
Beau Whitney

ACKNOWLEDGEMENTS

The 2006 FOP committee would like to thank these organizations and groups for their support and cooperation for this year's field trip:

Humboldt Redwoods State and National Parks

Pacific Lumber Company (PALCO)

County of Humboldt – Parks Dept.

County of Humboldt – Aviation

College of the Redwoods

Pacific Gas & Electric Company (PG&E)

Residents of Elk River Valley

Humboldt Bay National Wildlife Refuge – Lanphere and Hookton Units

City of Arcata

Yurok Nation

Wiyot Nation

TABLE OF CONTENTS

Contributors.....	ii
Acknowledgements	iii
Table of Contents.....	iv
Welcome	vi
Itinerary	vii
Trip Map.....	ix
Geologic and Seismic Setting.....	xi
Stratigraphic Section	xv
 Day One	 1
Itinerary and Map	2
Road Log	5
Papers	16
 <u>Stop 1-1 Fox Camp Road</u>	
Paper 1-1-A Bob McPherson, Ian Prior.....	16
Paper 1-1-B Todd Williams, Harvey Kelsey, Jeffrey Freymueller	28
Paper 1-1-C Rich Koehler	42
 <u>Stop 1-2 Horse Camp Campground</u>	
Paper 1-2-A Bonnie Smith, Diane Sutherland.....	60
 <u>Stop 1-3 Van Duzen River at Root Creek</u>	
Paper 1-3-A John Oswald, Gilbert Craven, Tagg Nordstrom, Tom Leroy	73
 Day Two	 88
Itinerary and Map	89
Road Log	91
Papers	102
 <u>Stop 2-1 Rohnerville</u>	
Paper 2-1-A Todd Williams and Bob McPherson.....	102
Paper 2-1-B Mark Verhey.....	111
 <u>Stop 2-2 College of the Redwoods</u>	
Paper 2-2-A Giovanni Vadurro	114
Paper 2-2-B Giovanni Vadurro, Frank Bickner, Dave Lindberg, Gary Manhart, Chris Watt.....	121
Paper 2-2-C Robert Witter, Jason Patton.....	137
Paper 2-2-D Mark Hemphill-Haley, Robert Witter, HFOG	157

TABLE OF CONTENTS (cont.)

Stop 2-3 King Salmon

Paper 2-3-A Lori Dengler	171
Paper 2-3-B Jason Patton, Robert Witter	181
Paper 2-3-C Jason Patton, Lori Dengler	194
Paper 2-3-D Steve Thompson, Bill Page, Robert Witter	199

Day Three	224
Itinerary and Map	225
Road Log	227
Papers	236

Stop 3-1 Lower North Fork Elk River

Paper 3-1-A Jay Stallman, Harvey Kelsey	236
Paper 3-1-B Ben Mackey, Joshua Roering	250

Stop 3-2 Mad River Beach

Paper 3-2-A Danny O'Shea	254
Paper 3-2-B Chad Pritchard	265
Paper 3-2-C Tom Leroy	269

Day Four	281
Itinerary and Map	282
Road Log	285
Papers	293

Stop 4-1 Lower North Fork Elk River

Paper 4-1-A Gary Simpson, Michelle Roberts	293
--	-----

Stop 4-2 Lagoon Creek

Paper 4-2-A Carolyn Garrison-Laney, Hans AbrahamsonWard, Gary Carver ...	309
Paper 4-2-B Caroline Levenda	324

Stop 4-3 Tsunami Park, Crescent City

Paper 4-3-A Lori Dengler, Orville Magoon	326
Paper 4-3-B Ken Aalto, Carolyn Garrison-Laney, Dane Robinson	334

Appendix	339
Appendix 1 Introduction Setting References	339
Appendix 2 Frank Bickner	342
Appendix 3 Kevin Furlong, Susan Schwartz	345
Appendix 4 Sunshine Mansfield	346
Appendix 5 John Wakabayashi	347

WELCOME

Welcome to the 2006 Friends of the Pleistocene (FOP) gathering in north coastal California. For those who traveled north, you've transitioned from strike-slip to contractional terrane. For those who traveled south, you're in a more complex contractional terrane influenced by the northern terminus of a dextral transform boundary (Oregonians, don't forget to pump your own gas and pay sales tax). For those arriving from the east, the ocean is west, and if anyone traveled east to get here, we salute your dedication! The "Friends" is an informal group (no officers, administrators, or fees) of scientists, educators, students, and fans of Quaternary geology who meet once a year at field locations across the United States. Topics vary according to location and participation, but there's always interesting geology and reunion of long-time friends. The first meeting of the "Friends" occurred in 1934 when Richard Foster Flint (later of Yale University) and Walter Goldthwait (Dartmouth) met in New Hampshire to discuss glacial stratigraphy in the field. They spent the next three days "thinking out loud and arguing." We hope that spirit will infuse this gathering.

When FOP was last held in Humboldt County 14 years ago in June of 1992, it occurred on the heels of a BIG surprise. On April 25 and 26, about a month before the trip, three earthquakes of M 7.1, 6.6, and 6.7 occurred near Cape Mendocino. Typically during the year before the meeting, trip leaders plan the itinerary, compile and summarize research, and tackle numerous logistics in preparation. Even with advanced planning, the last month is organized chaos. Catalyzed by the recent earthquakes and a soaring list of participants, the leaders dramatically adapted the itinerary and executed a memorable gathering. Since that 1992 meeting, a 115 meter-high redwood tree in Redwood National Park was crowned "tallest living thing," gas rose from \$1.20 to \$3.50 a gallon, the Gorda plate moved about 42–70 cm closer to North America, Cape Mendocino has moved about 42 cm to the north, and it's just over 306 years since the last M ~9 Cascadia subduction zone event.

This year's trip features a broad range of topics related to Quaternary crustal deformation and landscape evolution in the Mendocino deformation zone (MDZ). The trip organizers have assembled over 30 contributors who will present a mountain of research at only 11 field trip stops, so at some stops we may talk about more geology than we'll see. Although these presentations build on some of the work presented during the 1992 FOP trip led by Gary Carver, Bud Burke, Dorothy Merritts, and a host of others; we will focus on recent studies conducted over the last decade. In the spirit of good science and FOP tradition, we encourage animated discussion.

Home base for the trip is Pamplin Grove, a Humboldt County campground reserved entirely for FOP. The trip begins in the southern MDZ near the southern edge of the Gorda Plate and will move progressively northward through the Cascadia fold and thrust belt to Crescent City. The first few pages of the guidebook provide an overall itinerary and map of the field trip area, as well as introductions to the geologic and stratigraphic setting. The main body of the guidebook includes four daily sections, each containing an (1) introduction, (2) itinerary and map of stops, (3) road log, and (4) original papers that support the stops for the day.

The trip traverses many private properties, rural communities, and a few larger towns. A group of our size must be extra conscientious in order to maintain our partnerships with private landowners and other decision makers who support ongoing and future geologic research in the area. Please follow the instructions in the introduction to each day, and be aware that we are guests of private landowners at many stops. We look forward to a fun-filled weekend of geologic nirvana.

Let's get started!

TRIP ITINERARY

2006 Pacific Cell Friends of the Pleistocene Signatures of Quaternary crustal deformation and landscape evolution in the Mendocino deformation zone (MDZ)			
Day 1 (Thursday) Southern MDZ to Eel River Valley			
Field Trip Stop	Authors	Title	Reading Material
Stop 1-1: Fox Camp Road: Overview of tectonics in the southern Mendocino deformation zone (MDZ) - seismic, geodetic, stratigraphic, and geomorphic signatures.	Mark Hemphill-Haley	Welcome and overview of trip	Intro section
	Ken Aalto	Neogene stratigraphic evolution of northwestern California	Intro section
	Bob McPherson and Ian Pryor	Seismicity and stress near the Mendocino triple junction: Part 1	paper 1-1-A
	Todd Williams, Harvey Kelsey, and Jeffrey Freymueller	GPS-derived fault slip rates along the northernmost segments of the Maacama and Bartlett Springs fault zones, northwestern California.	paper 1-1-B
	Kevin Furlong and Susan Schwartz	Influence of the Mendocino triple junction on the tectonics of Coastal California	abstract, appdx 1
	Rich Koehler	Terrace formation and drainage adjustment in response to migrating uplift, 80 km east of the Mendocino triple junction, northern California	paper 1-1-C
	Rocco Fiori and Patrick Vaughan	Topographic patterns and geomorphic processes above the southern edge of the subducting Gorda plate: Part 1	abstract
Stop 1-2: Cuneo Creek at Horse Camp: Fluvial terraces, large landslides, and driving forces.	Rocco Fiori and Patrick Vaughan	Topographic patterns and geomorphic processes above the southern edge of the subducting Gorda plate: Part 2	abs stop 1-1
	Bonnie Smith and Diane Sutherland	Historic terrace deposition and incision at Cuneo Horse Camp	paper 1-2-A
Stop 1-3: Van Duzen River at Root Creek: Southern Little Salmon fault zone.	John Ozwald, Gilbert Craven, Tagg Nordstrom, and Tom Leroy	Evidence for deformation of a Pleistocene strath terrace and coseismic deep-seated failure, implications for tectonic deformation at the boundary between the Northern San Andreas fault system and the southern Cascadia subduction zone	paper 1-3-A
Day 2 (Friday) South Humboldt Bay Area			
Field Trip Stop	Authors	Title	Reading Material
Stop 2-1: Rohnerville: Overview of tectonics in the northern MDZ - seismic, geodetic, stratigraphic, and geomorphic signatures.	Mark Hemphill-Haley	Regional setting, northern MDZ	Intro section
	Bob McPherson and Ian Pryor	Seismicity and stress near the Mendocino triple junction: Part 2	paper 1-1-A
	Todd Williams and Bob McPherson	Gorda plate deformation contributes to shortening between the Klamath block and the on-land portion of the accretionary prism to the southern Cascadia subduction zone.	paper 2-1-A
	Harvey Kelsey	Humboldt Bay and lower Eel River neotectonics: major questions and significant uncertainties	abstract
	Mark Verhey	Subsurface seismic reflection in the Van Duzen/Eel River Valley	paper 2-1-B
Stop 2-2: College of the Redwoods: Paleoseismology and seismic hazards in the Little Salmon fault zone.	Giovanni Vadurro	Amount and rate of deformation across the Little Salmon fault and Table Bluff anticline within the onland portion of the southern Cascadia subduction zone fold and thrust belt, NW California	paper 2-2-A
	Giovanni Vadurro, Frank Bickner, Dave Lindberg, Gary Manhart, and Chris Watt	Fault surface rupture and fold hazard evaluation of the Little Salmon fault at the College of the Redwoods Eureka campus, southern Cascadia subduction zone fold and thrust belt, NW California	paper 2-2-B
	Robert Witter and Jason Patton	Upper-plate earthquakes on the western Little Salmon fault and contemporaneous subsidence of southern Humboldt Bay over the past 3,600 years	paper 2-2-C
	Mark Hemphill-Haley, Robert Witter, and Humboldt Friends of Geology	Latest Pleistocene to Holocene Paleoseismology of the Southern Little Salmon Fault, Strong's Creek, Fortuna, California	paper 2-2-D
Stop 2-3: King Salmon: Overview of earthquakes, tsunamis, and Holocene tectonostratigraphy around Humboldt Bay.	Lori Dengler	The 1906 earthquake in Humboldt and Del Norte counties, California	paper 2-3-A
	Jason Patton and Robert Witter	Late Holocene coseismic subsidence and coincident tsunamis, southern Cascadia subduction zone, Hookton Slough, Wigi (Humboldt Bay), California	paper 2-3-B
	Jason Patton and Lori Dengler	Relative Tsunami Hazard Mapping for Humboldt and Del Norte Counties, California	paper 2-3-C
	Steve Thompson, Bill Page, and Rob Witter	Long-term relative sea level change and implications to the nuclear waste storage facility at Buhne Hill, Humboldt County, California	paper 2-3-D

Introductory Section

TRIP ITINERARY (cont.)

Day 3 (Saturday) North Humboldt Bay Area			
Field Trip Stop	Authors	Title	Reading Material
Stop 3-1: Lower North Fork Elk River: Fluvial terraces, large landslides, and driving forces.	Jay Stallman and Harvey Kelsey	Transient geomorphic response to late Pleistocene baselevel change and climate forcing in the southern Cascadia thrust-and-fold belt	paper 3-1-A
	Ben Mackey and Joshua Roering	Identifying deep-seated landslides through the use of high resolution airborne laser mapping – implications for landscape evolution	paper 3-1-B
	Gerald Marshall	Elk River geology, landsliding and related features	abstract
Stop 3-2: Mad River Beach: Holocene dune stratigraphy, coseismic tidal marsh stratigraphy, and offshore sediment dynamics.	Danny O'Shea	Marine stratigraphy of the Eel continental shelf: coastal response to sea level rise since the latest glacial maximum	paper 3-2-A
	Chad Prichard	Coseismic subsidence of Arcata Bay	paper 3-2-B
	Tom Leroy	Coastal Sand Dune Stratigraphy and Geomorphology of the North Spit of Humboldt Bay	paper 3-2-C
Day 4 (Sunday) North Humboldt Bay Area to Crescent City			
Field Trip Stop	Authors	Title	Reading Material
Stop 4-1: School Road McKinleyville: Mad River fault zone	Gary Simpson and Michelle Roberts	Morphology and structure of the Mad River fault from trench exposures at School Road, McKinleyville, CA	paper 4-1-A
Stop 4-2: Lagoon Creek: paleotsunami deposits	Carolyn Garrison-Laney, Hans Abramson, and Gary Carver	A 3,000 year record of tsunami deposition from the southern end of the Cascadia subduction zone	paper 4-2-A
	Caroline Lavenda	Depositional environments and characteristics of the late Miocene Wimer formation, Mill Creek drainage, Crescent City, Del Norte County, California	paper 4-2-B
Stop 4-3: Tsunami Park, Crescent City: 1964 tsunami	Lori Dengler and Orville Magoon	Reassessing Crescent City, California's tsunami risk	paper 4-3-A
	Bob McPherson and Hans Abrahamson	1964 tsunami deposits in the Crescent City area	
	Ken Aalto, Carolyn Garrison-Laney, and Dane Robinson	Evidence for paleotsunami at Crescent City, northern California	paper 4-3-B

THIS PAGE INTENTIONALLY LEFT BLANK
FOR
TABLOID FIELD TRIP STOP MAP

THIS PAGE INTENTIONALLY LEFT BLANK
FOR
TABLOID FIELD TRIP STOP MAP

GEOLOGIC AND SEISMIC SETTING

Mark Hemphill-Haley, Todd Williams, and Jay Stallman

The Pacific, North America, and Gorda plates intersect at the Mendocino triple junction region (Figure 1). The Mendocino fault separates the Gorda and Pacific plates. North of the triple junction, the Cascadia subduction zone separates the Juan de Fuca/Gorda and North America plates. Relative motion between the North America and Pacific plates south of the triple junction region is concentrated along an approximate 100 km wide zone that is the San Andreas transform (Figure 1). The southern Cascadia subduction zone and Mendocino triple junction are overlapping geologic regimes where deformation at the fault-fault-trench triple junction has been migrating north since the inception of the San Andreas fault system in the Oligocene (Atwater, 1970). As the Mendocino triple junction migrates northward, the San Andreas transform elongates and the Cascadia subduction zone shortens.

The southernmost 150 km of the approximate 1,200 km long Cascadia subduction zone is offshore of northern California (Figure 1). Analysis of seismicity and isostatic residual gravity fields in northern California suggests the Gorda plate is subducting eastward beneath North America. The interface between the two plates is a megathrust that dips to the east-southeast at 5° to 14° (Jachens and Griscom, 1983; Oppenheimer et al., 1993; Smith et al., 1993; Pryor and McPherson, 2006).

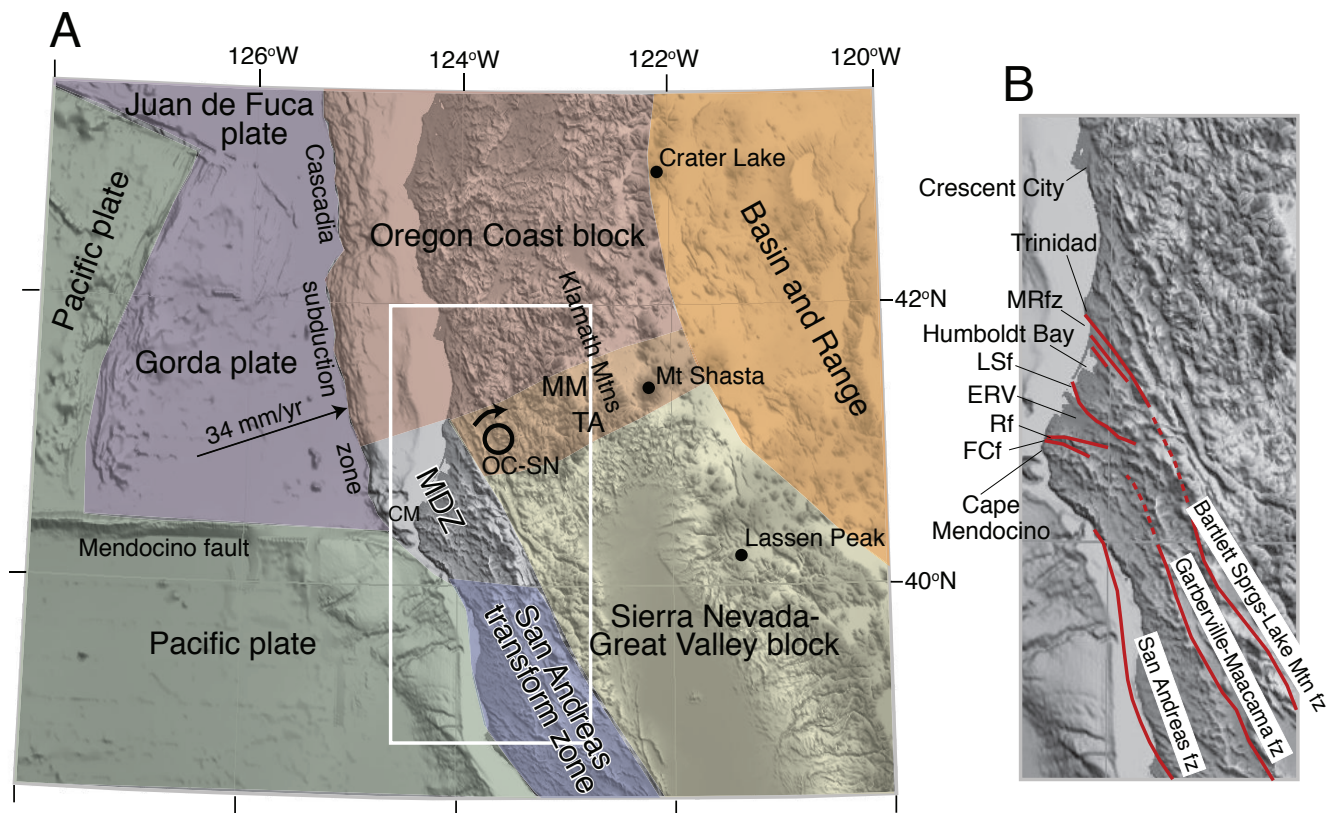


Figure 1. A. Plate and block model for region surrounding the Mendocino deformation zone (MDZ). Boundaries of blocks and plates taken after Wells et al. (1998) and Wang et al. (2003). OC-SN, pole of rotation between Oregon Coast block and Sierra Nevada-Great Valley block after Wang et al. (2003). MM, Marble Mountains; TA, Trinity Alps. The region of distinct shading that includes MM, TA and the OC-SN pole is the diffuse boundary zone between the Oregon Coast block and the Sierra Nevada-Great Valley block. The three volcanic centers (Lassen, Shasta, Crater Lake) delineate the approximate location and trend of the Cascade volcanic arc. CM, Cape Mendocino. B. Map of northernmost coastal California showing the major fault zones and localities discussed in the text. Locations of faults from Kelsey and Carver (1988). MRfz, Mad River fault zone; LSf, Little Salmon fault; ERV, Eel River valley; Rf, Russ fault; FCf, False Cape fault.

The southern section of the Cascadia margin is uniquely distinguished by on-land upper plate thrust faults and associated asymmetric growth folds. In northern coastal California, this fold and thrust belt consists of northwest trending, southwest-vergent growth anticlines and synclines, over northeast-dipping thrust faults (Clarke and Carver, 1992). Faults within the upper North American plate (Figure 2) are sources of seismicity and strain (Dengler et al., 1992; Murray et al., 1996) and displace late Neogene sediment near the coast by hundreds of meters (Carver et al., 1987). Thrust faults that offset Holocene strata in the Humboldt Bay region include structures within the Little Salmon and the Mad River fault zones (Clarke and Carver, 1992). These structures trend approximately normal to the Gorda Plate convergence direction and are evidence of late Quaternary contraction of the North American margin (Carver et al., 1987; Clarke, 1992). Some faults offset 50 ka to >200 ka raised marine platforms and have multiple episodes of Holocene deformation (Burke et al., 1986; Carver et al., 1987; Clarke and Carver, 1992). The western splay of the Little Salmon fault, one of the southernmost structures of the fold and thrust belt, may record up to 4 surface deformation events in the past 2,300 years of up to 1 to 4 m per event (Carver et al., 1987; Clarke and Carver, 1992; Witter et al., 2002; Witter and Patton, 2006). Smaller and less frequent Holocene displacements have occurred in the Mad River fault zone to the north (Carver et al., 1987; Clarke and Carver, 1992; Carver and McCalpin, 1996). Paleoseismic studies indicate that upper plate earthquake recurrence intervals range from hundreds of years for the Little Salmon fault to thousands of years for faults within the Mad River fault zone. It is unknown whether the upper plate thrust faults are independent sources of seismicity or if they only move in conjunction with subduction zone megathrust activity (Clarke and Carver, 1992; Witter et al., 2000; Witter et al., 2001).

On January 26, 1700 A.D., a $M_w \sim 9$ subduction zone earthquake affected the approximate 1,200 km Cascadia subduction zone from northern California to southern coastal British Columbia and caused a devastating tsunami at coastal sites in Japan (Satake et al., 1996; Jacoby et al., 1997; Yamaguchi et al., 1997). During this great earthquake, the locked upper plate was displaced coseismically toward the deformation front. This resulted in coseismic uplift offshore nearest the deformation front and coseismic subsidence near the coast (Savage, 1983; Thatcher, 1984; Hyndman and Wang, 1995). Resultant buried tidal marshes and offshore turbidite flows of similar previous earthquakes provide data to assess recurrence and segmentation of great earthquakes on the Cascadia margin. Using sequences of buried organic layers as time markers, the recurrence interval for slip events on the subduction zone is thought to be on the order of 500 years (Atwater et al., 1995; Atwater and Hemphill-Haley, 1997; Kelsey et al., 2002). Goldfinger et al. (2003) infer that subduction zone earthquakes have triggered large Holocene turbidites in offshore canyons along the Cascadia margin. They observe that the southern 1/3 of the Cascadia margin exhibits about 25% more turbidites than the northern 2/3 of the margin. This may be attributable to segmentation of the subduction zone or higher rates of seismicity due to proximity of the nearby San Andreas fault.

As the Mendocino triple junction migrates, the San Andreas transform elongates. Strike-slip faults of the northern San Andreas fault system (Figure 1) strike northwesterly and merge into the fold and thrust belt from the south (Kelsey and Carver, 1988). Recent GPS geodesy results observe Pacific-North America relative motion 100km north of Cape Mendocino, and suggest that the Eaton Roughs-Lake Mtn. fault zones in the eastern portions of San Andreas transform zone (Figure 2) are accommodating up to 8 mm/yr of dextral strain NNW beyond the latitude of Cape Mendocino (Williams et al., 2006).

Additionally, the northward passage of the Mendocino triple junction is associated with a crustal welt that currently may extend up to 50 km north of the southern margin of the Gorda plate (Verdonck and Zandt, 1994; Beaudoin et al., 1996; Furlong and Govers, 1999; Furlong et al., 2003). In the wake of the triple junction the thickened crust undergoes internal thinning resulting in a decrease in topographic elevation (Furlong and Govers, 1999).

As the San Andreas transform elongates, and the Cascadia subduction zone shortens, the Gorda plate is compressed between the larger, older, Pacific and Juan de Fuca plates (Figure 1). Internal deformation of the Gorda plate accounts for the majority of both onshore and offshore historic seismicity in the region immediately north of the Mendocino triple junction (McPherson, 1989; Smith et al., 1993). Approximately eighty percent of well-located micro-seismicity recorded in the region occurs at Gorda plate depths (McPherson, 1989). Much of this seismicity is

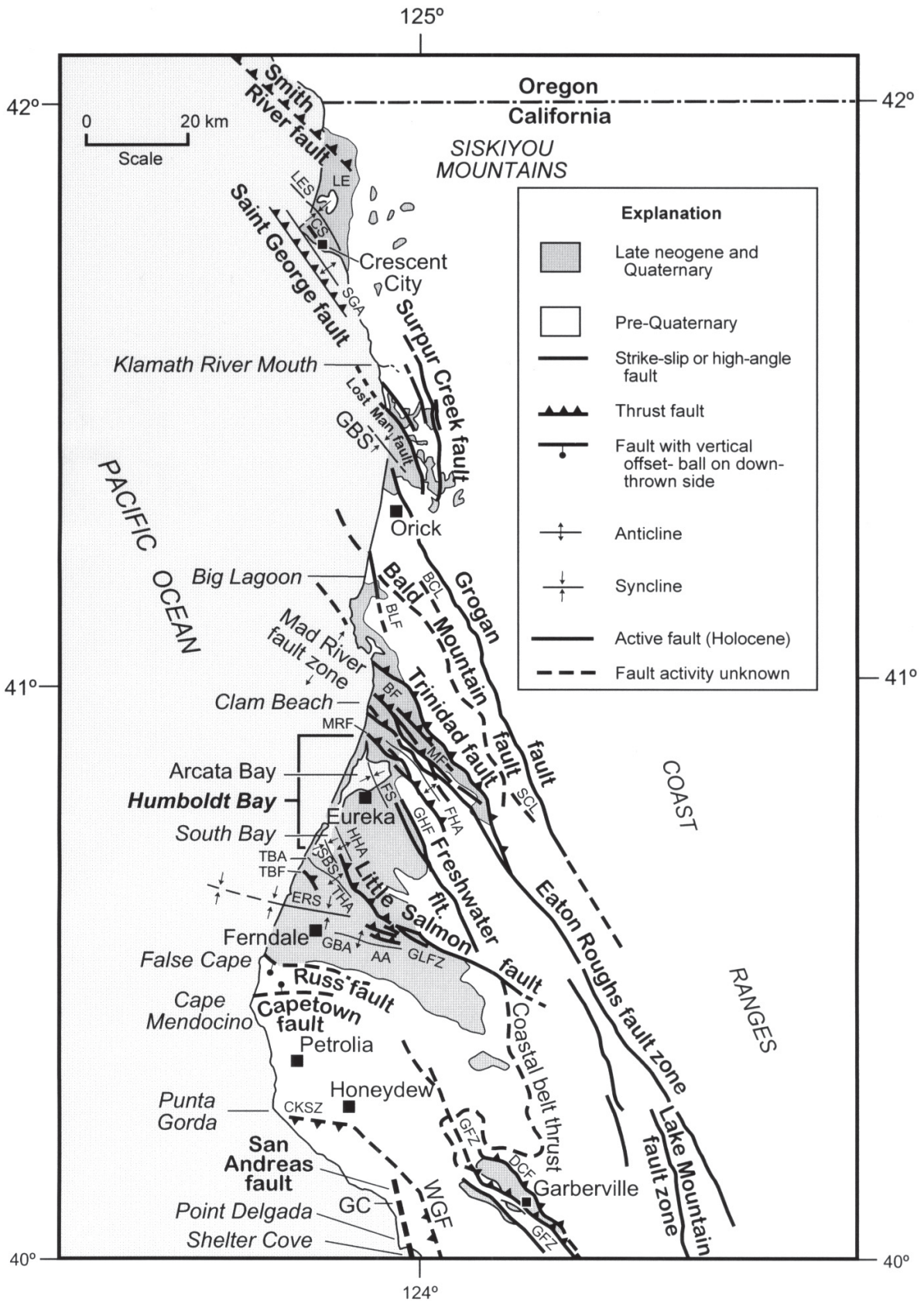


Figure 2. Kelsey, H.M., 2001, Active faulting associated with the southern Cascadia subduction zone in northern California, in Ferriz, H. and Anderson, R. (eds), Engineering Geology Practice in Northern California, Division of Mines and Geology Bulletin 210, Association of Engineering Geologists Special Publication 12, p. 259-274.

due to contraction of the subducting Gorda plate as it is squeezed within the “tectonic die” formed by the older, more rigid Pacific and Juan de Fuca plates (Denlinger, 1992; Smith et al., 1993; Pryor and McPherson, 2006; Williams and McPherson, 2006). This deformation has led some to refer to Gorda as a deformation zone since it does not behave like a plate (McPherson and Dengler, 1992; Williams et al., 2006). Relocated large historic earthquakes ($M \geq 7$) in the study region show that most such earthquakes occur in the offshore Gorda plate or near the Mendocino fault (Bakun, 2000). The notable large historic earthquakes include the 1906 M_w 7.8 San Francisco, 1980 M_s 7.2 Eureka, 1992 M_s 7.1 Petrolia, 1994 M_w 7.0 offshore Mendocino fault, and 2005 M_w 7.2 Gorda plate earthquakes.

In Northern coastal California, “North America” is comprised of a confederation of microplates (Wakabayashi, 2006). This adds complexity to the simplified 3 plate geometry model for the Mendocino triple junction as it migrates northward. During the 2006 FOP, we will discuss this region from many different perspectives. Together we will explore geologic and geophysical phenomena, not from just a mere joining of 3 plates, but from a broad transition zone comprised of the Pacific plate, two fault bounded slivers of the San Andreas transform, a deforming Gorda plate, the Sierra Nevada-Great Valley block, the Klamath block, and the accretionary wedge to the southern Cascadia subduction zone. On this trip we will commonly refer to this transition zone as the Mendocino deformation zone (MDZ; Figure 1), or, the Triangle of Doom if you prefer.

OVERVIEW OF NEOGENE WILDCAT GROUP

Excerpt from:
NEOGENE STRATIGRAPHIC EVOLUTION OF NORTHWESTERN CALIFORNIA

K. R. AALTO

The Wildcat Group (Ogle, 1953) constitutes late Miocene through Pleistocene sediment fill within the Eel River basin (Fig. 1). McCrory (1989) argued that the Eel River basin formed rapidly as a stratigraphic basin near the base of an inner trench slope, in response to subduction of the Gorda plate, and that the initial accumulation of sediments occurred at bathyal depths. Wildcat sediments were previously thought to have been derived from chiefly Coast Range sources to the southeast (Nilsen and Clarke, 1987). Moley (1992) and Aalto et al. (1996) instead suggested that basal sediments of the Wildcat Group accumulated at shallow depths as part of a shelf sediment blanket, that the Eel River basin is chiefly a mid-Pleistocene structural basin formed in response to a combination of Gorda – North American plate convergence and the northward migration of the Mendocino triple junction, and that at least some Wildcat Group sediments were derived from the northeast, possibly from Idaho as discussed below.

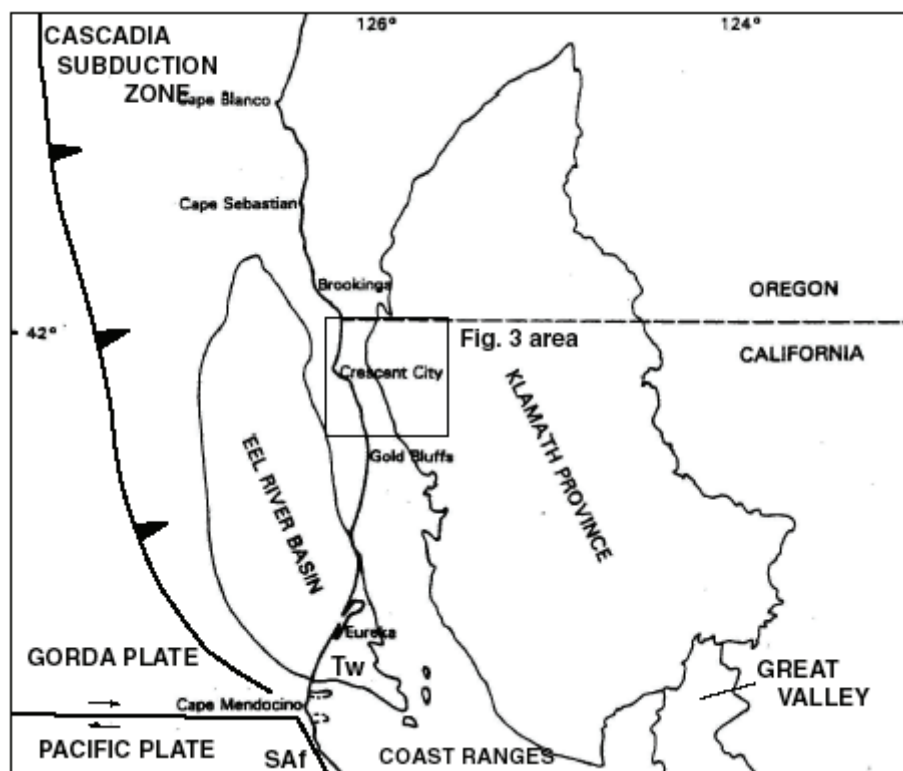


Figure 1. Regional location map showing plate boundaries and general outcrop areas of the Eel River basin, Wildcat Group (Tw), Klamath Mountains and Coast Range provinces, and location of the Mendocino triple junction (at Cape Mendocino). SAF – San Andreas fault.

Overall, the Wildcat Group records an eastward transgression during the late Miocene and Pliocene, with initial deposition of sediments within a near-shore environment, then rapid deepening of the continental shelf to bathyal – abyssal depths, later infilling of the shelf during the Plio-Pleistocene, and westward regression of the shoreline during early to medial Pleistocene (Ogle, 1953; Nilsen and Clarke, 1987; Clarke, 1992; Fig.2). The lowest stratigraphic unit in the Wildcat Group, the Pullen Formation, is believed to be coeval with the Wimer and Saint George Formations.

The marine portion of the Wildcat Group includes 1,900 – 2,600 m of mudstone and subordinate sandstone that range in age from late Miocene to middle Pleistocene, arranged in an overall coarsening-upward

sequence (Ogle, 1953; Haller, 1980; Ingle, 1987; Nilsen and Clarke, 1987). At Scotia, inland along the Eel River, and in logging road cuts some 12 km southeast of Scotia, an angular unconformity separates tightly folded Eocene Yager Complex turbidites and tilted, but relatively undeformed, late Miocene Pullen Formation (Moley, 1992; Aalto et al., 1996). Above the unconformity are sandy shoreface deposits that contain locally derived Yager Complex clasts, indicating that a certain amount of erosional stripping occurred in this region during post-Yager, pre-Wildcat time. East of Eureka, on the northeastern flank of the Eel River basin, facies relations suggest that similar unconformities exist (Knudsen, 1993).

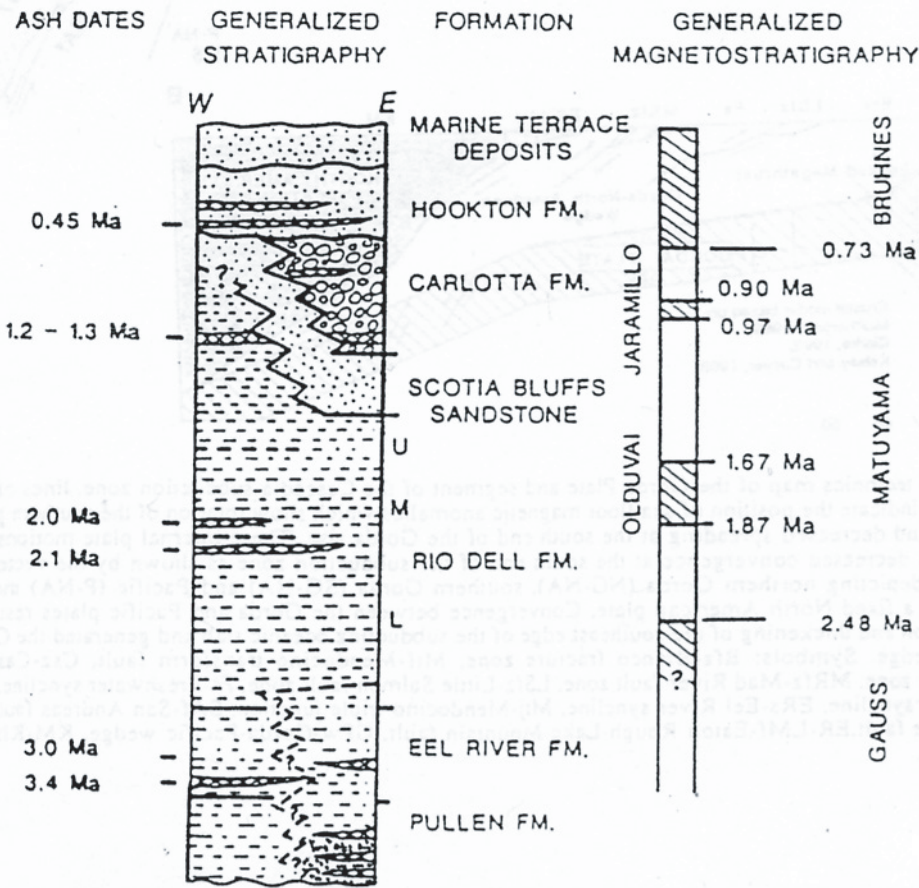


Figure 2. Generalized section of the Miocene to Pleistocene Wildcat Group (Ogle, 1953). Dated volcanic ash deposits, stratigraphy, formations, and magnetostratigraphy are shown.

The nonmarine portion of the Wildcat Group is middle to late Pleistocene and consists of a series of fluvial clastic wedges that thin and intertongue with marine sediments to the west. Thickness ranges from 800 to 1,000 m (Nilsen and Clarke, 1987). Marine – nonmarine cycles are probably glacioeustatic in origin. Patches of similar coeval sediments exist inland of the northeastern flank of the Eel River basin and isolated from basin exposures by basement rock uplifted along active thrust faults.

Moley (1992) determined that Pleistocene fluvial conglomerates of the Wildcat Group were chiefly derived from Franciscan Complex basement of the northern Coast Ranges. However, she noted that late Miocene – early Pleistocene

marine sandstones of the Wildcat Group have an unexpectedly high K-feldspar content, given the relative lack of K-feldspar in local basement rocks. Significant K-feldspar content suggests possible sediment input from sources other than the Klamath Mountains or Coast Ranges since these provide comparatively K-feldspar-poor sands (Underwood and Bachman 1986; Aalto 1989b, 1992). ⁴⁰Ar/³⁹Ar laser probe analyses of some micas from Wildcat Group marine sands (Moley, 1992; Aalto et al., 1995, 1998) suggest an Idaho batholith source, which indeed is compatible with the unusually high K-feldspar contents observed.

It seems apparent that Wildcat-equivalent marine and fluvial sediments covered a significant portion of the northern Coast Ranges, but have been removed by erosional stripping in conjunction with active tectonism.

Day 1 Introduction (Thursday)

Welcome to the first day of the FOP!

We'll begin by gathering at the fire circle in Pamplin Grove at **7:30 AM** to briefly discuss trip stop logistics and carpooling. We'll line up at 8:00 and **roll out of Pamplin Grove at 8:30 AM**.

Day 1 - Logistical Considerations: The first stop has one of the tightest parking limitations of the whole trip. *Please carpool as much as possible for Stop 1-1.* There is parking space at Stop 1-2 on the way out to Stop 1-1 where you can jump in together, but we would prefer that everyone try to fit into as few cars as possible at camp before departing. **Stops 1-2 and 1-3 will involve getting wet feet**, so plan accordingly. Bring river sandals if you have them. The parking at Stop 1-3 is a rough river channel. Most of the parking will be to the right as you turn off Highway 36. Park cars with low clearance single file along the same side. The road is a thoroughfare for logging operations, so don't constrict the road by parking on both sides or more than one car width.

When we return to camp from stop 1-3, the left turn into Pamplin Grove is very tight and can be dangerous. **We strongly recommend that you drive a little further down the road, make a U-turn at the store, and come back to Pamplin Grove so you can make an easy right turn into camp heading east on Highway 36.** It's much safer!

Science of the day: The first day of the trip will focus on some of the geomorphic signatures in the southern Mendocino deformation zone.

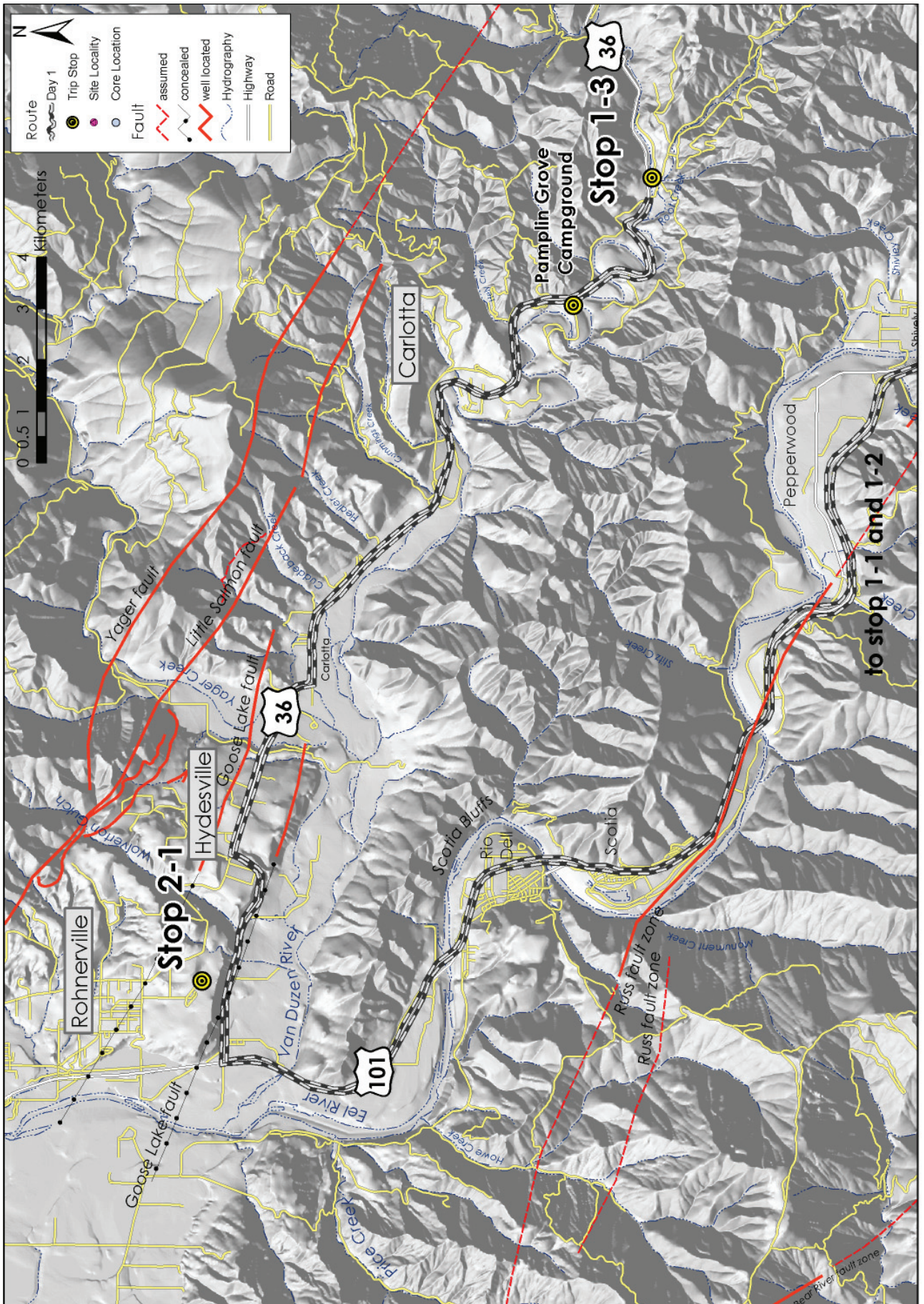
Stop 1-1 is located at Fox Camp road. We will get an overview of the regional tectonics, stratigraphy, seismicity, geodetics, and crustal modeling at the southern boundary of the Mendocino deformation zone. We will then describe the influence of the Mendocino "conveyor" on the tectonics of coastal California, including hillslope processes, terrace formation, and drainage adjustments related to its migration.

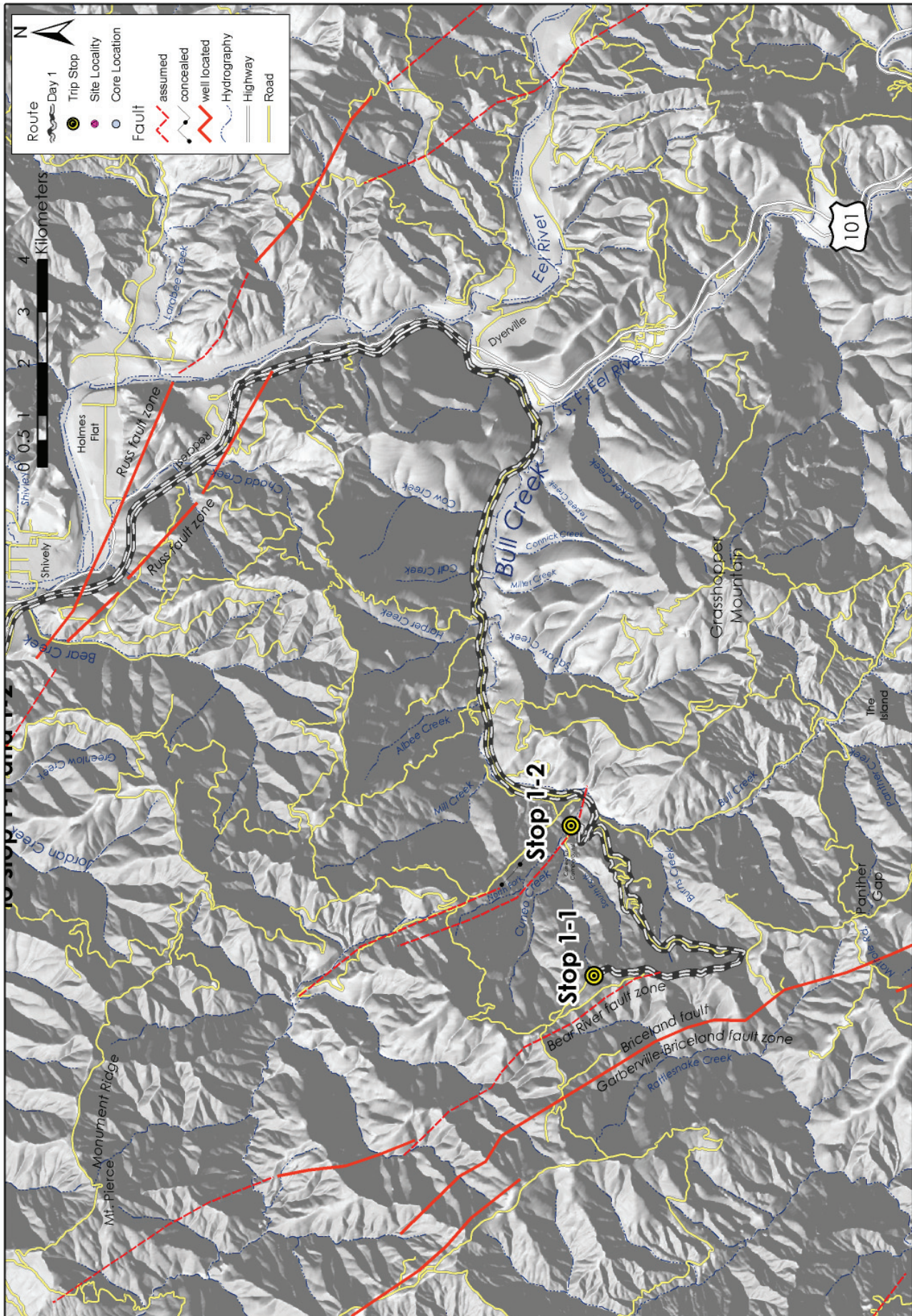
Stop 1-2, located in Cuneo Creek drainage at Horse Camp, will examine fluvial terraces, hillslope processes, and post-1964 channel deposition and incision.

Stop 1-3 will be at the Van Duzen River at Root Creek. At this location we will describe deformation of a Pleistocene strath terrace and possible coseismic deep-seated landslide failure related to the southern Little Salmon fault zone at the transition between the northern San Andreas fault system and the southern Cascadia subduction zone. The exposures at Stop 1-3 (guarded by poison oak) involve hiking a few 100 meters of the river bar and crossing a small (>1ft deep) stream. There's a good swimming hole near the stop for rinsing off that poison oak or just taking a dip.

Day 1 Itinerary

Day 1 (Thursday) Southern MDZ to Eel River Valley			
Field Trip Stop	Authors	Title	Reading Material
Stop 1-1: Fox Camp Road: Overview of tectonics in the southern Mendocino deformation zone (MDZ) - seismic, geodetic, stratigraphic, and geomorphic signatures.	Mark Hemphill-Haley	Welcome and overview of trip	Intro section
	Ken Aalto	Neogene stratigraphic evolution of northwestern California	Intro section
	Bob McPherson and Ian Pryor	Seismicity and stress near the Mendocino triple junction: Part 1	paper 1-1-A
	Todd Williams, Harvey Kelsey, and Jeffrey Freymueller	GPS-derived fault slip rates along the northernmost segments of the Maacama and Bartlett Springs fault zones, northwestern California.	paper 1-1-B
	Kevin Furlong and Susan Schwartz	Influence of the Mendocino triple junction on the tectonics of Coastal California	abstract, appdx 1
	Rich Koehler	Terrace formation and drainage adjustment in response to migrating uplift, 80 km east of the Mendocino triple junction, northern California	paper 1-1-C
	Rocco Fiori and Patrick Vaughan	Topographic patterns and geomorphic processes above the southern edge of the subducting Gorda plate: Part 1	abstract
Stop 1-2: Cuneo Creek at Horse Camp: Fluvial terraces, large landslides, and driving forces.	Rocco Fiori and Patrick Vaughan	Topographic patterns and geomorphic processes above the southern edge of the subducting Gorda plate: Part 2	abs stop 1-1
	Bonnie Smith and Diane Sutherland	Historic terrace deposition and incision at Cuneo Horse Camp	paper 1-2-A
Stop 1-3: Van Duzen River at Root Creek: Southern Little Salmon fault zone.	John Ozwald, Gilbert Craven, Tagg Nordstrom, and Tom Leroy	Evidence for deformation of a Pleistocene strath terrace and coseismic deep-seated failure, implications for tectonic deformation at the boundary between the Northern San Andreas fault system and the southern Cascadia subduction zone	paper 1-3-A





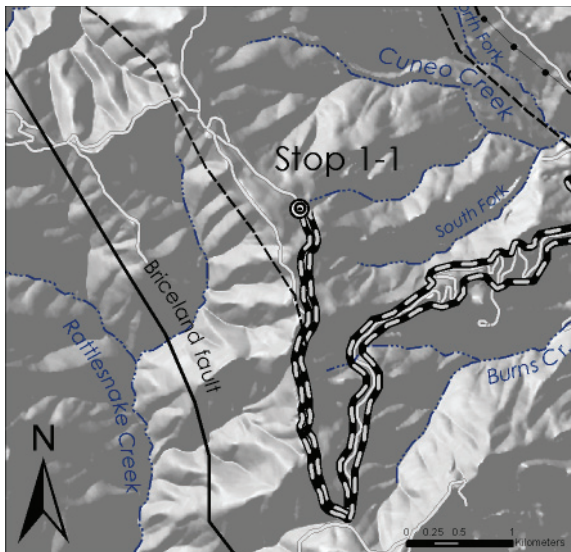
Day 1 Road Log

<u>Mileage</u>	<u>Distance</u>	<u>Description</u>
0.0		Pamplin Grove Gate
0.3	0.3	Turn Left onto Hwy 36. Please drive defensively on these rural roads, the locals drive very fast!
0.8	0.8	Martin & Shirley's Store
2.6	1.8	[from 2.6 to 3.5] Redwoods thrive on alluvial terraces such as this one. An important contributor to the development these terraces and adjacent hillslopes is the intensity of storms we receive in Humboldt County. In northern California, precipitation occurs from October thru March, averaging about 60 inches (1.6 m) per year in Eureka, and twice that in areas of heavy orographic precipitation such as the mountains around Stop 1-1. The thick vegetative cover reflects the mild temperatures and ample precipitation of the north coast, and can make good geologic exposures hard to find. Streams and other failures often provide some of the best exposures for geologists. Rates of terrace formation and incision are topics for discussion at Stop 1-2 this afternoon, and at Stop 3-1 on Saturday.
3.5	0.9	City of Carlotta - Continue west on Highway 36. Please drive slowly through town.
4.4	0.9	[from 4.4 to 5.5] At 3 o'clock, the Grizzly Creek fault cuts the hillslope in the foreground, about half way up the hill. Surface expression of the fault is hard to see - look for the change in in the vegetation. Thick vegetation in Humboldt County obscures the surface expression of many features, and vegetation breaks are often the key to identifying geologic features from the highway.
5.8	1.4	Carlotta Sign
6.1	0.3	Yager Creek Bridge
6.3	0.2	Little Salmon fault cuts hills on skyline (see Figure 1) - 1st description of the Little Salmon fault
6.9	0.6	[6.85 - 7.7]: Driving up steps in the Yager Creek terraces
8.1	1.3	GAS
8.2	0.1	BEAR LEFT and continue East on Hwy 36. DO NOT go right toward Rhonerville Road
9.0	0.9	View of the Van Duzen River valley to the south (9 o'clock). Almost out of view to the west (12 o'clock), a series of hogback ridges typifies the Wildcat Group, Pleistocene-age sedimentary rocks. Resistant units form ridges, and more erodible facies form the valleys that drain into the Salt River. Geologic mapping of Ogle in the 1950's defined many of the Wildcat units along these hogback ridges and in the ocean bluff exposures to the west. We will discuss the stratigraphic section that we see this weekend, including the Wildcat Group, at Stop 1-1 this morning.
10.9	2.8	Highway 36 ends. TURN LEFT ONTO HWY 101. Northbound traffic does not stop, so be careful as you cross the highway!!
11.2	0.3	Mile marker 57.5

<u>Mileage</u>	<u>Distance</u>	<u>Description</u>
11.7	0.5	Van Duzen River bridge - This bridge was replaced after it was washed out in the December 22, 1964 flood. Looking at the hills to the southwest (2 o'clock), Pleistocene river terraces of the ancient Eel River come into view.
12.6	0.9	Modern stream terraces of the Eel River to the west of the highway.
13.6	1.0	Scotia Bluffs come into view at 11 o'clock. This is the location of the type section for the Scotia Bluffs sandstone, one of the members of the Wildcat Group.
14.5	0.9	Eel River Bridge. The northbound lane of the bridge looks newer than the span we're driving across. The northbound lane was stabilized after flooding in the mid-80's, and the southbound lane was constructed after the 1964 floods. Upstream (at 10 o'clock) is a good view of the Scotia Bluffs.
15.2	0.7	Rio Dell - Although the Eel River is alluvial throughout most of its length, this reach flows thru bedrock.
16.6	1.4	Eel River Bridge
16.7	0.1	Scotia Exit
18.4	1.7	road to Scotia
19.8	1.4	Shivley turnoff - continue straight on HWY 101 south
20.2	0.4	Eel River Bridge #3
20.5	0.3	Exit # 676 Stafford Exit. This is the site of a debris flow from the 1997 New Year's storms.
22.5	2.0	Jordan Creek
23.1	0.6	Greenlaw Creek
25.4	2.3	Weott
25.7	0.3	Bear Creek bridge
28.9	3.2	Redcrest sign
29.5	0.6	Exit 667A Avenue of the Giants exit - Continue South on Hwy 101.
32.5	3.0	View of confluence of the south fork and main stem of Eel River (railroad trestle). The town of Dyerville was located on the south bank of this confluence before it was moved upstream after the 1964 flood. We will talk about historical flooding, and associated terrace development and incision at Stop 1-2 today.
32.8	0.3	Bear Right onto Exit 663 "South Fork Honeydew"
33.0	0.2	Stop Sign - Turn Right towards Albee Creek
33.3	0.3	View of alluvial point bars on the South Fork of the Eel River at 9 o'clock. The Eel River is a dynamic river system. High uplift, coupled with relatively incoherent bedrock and intense precipitation events result in some of the highest sediment transport rates of any river in the world.
34.4	1.1	Glimpse of Bull Creek Delta - the size of the delta changes as a general response to the sediment load coming out of the Bull Creek basin. Sedimentation in lower Bull Creek has been an issue for land managers trying to avoid old-growth redwoods from being lost from the park to stream bank erosion for the past several decades.

<u>Mileage</u>	<u>Distance</u>	<u>Description</u>
34.5	0.1	Rockefeller Grove. The Lower Bull Creek Flats were one of the first groves of Old-Growth Redwoods to be put into preservation by Save the Redwoods League. In the summer of 1917, Madison Grant, Henry Osborn, and John Merriam, three noted conservationists, stopped at Bull Creek and witnessed the logging operations moving toward this stand of old-growth. In 1918, they helped establish the Save-the-Redwoods League and in 1921, with the addition of State funds, the League purchased its first grove, now a part of the Humboldt Redwoods State Park. John D. Rockefeller, Jr. brought his family to Bull Creek Flat in 1930. The Rockefeller's \$2 million donation to the League in 1931, helped purchase 9,000 acres in the Bull Creek - Dyerville flats area that remains in preservation along the Avenue of the Giants corridor.
35.9	1.4	Cow Creek
36.6	0.7	Calf Creek
36.8	0.2	Bull Creek. This is the first view of Bull Creek. As we drive upstream along the Mattole Road, note the changes in the channel cross section. Here, in the lower Bull Creek Flats, rip rap along the channel margins precludes the channel banks from eroding. In the storms of 1955 and 1964 (before the rip rap was installed), hundreds of old-growth redwoods were lost to bank erosion.
37.0	0.2	Look Prairie - View of rip-rapped channel to the left. The grassy prairie to the right, called "Look Prairie," is an earthflow in the sheared Franciscan terrane known as 'blue goo'. Note the tilted trees in the eastern edge. The prairie extends nearly to the ridge top because trees can't get established in this material - it is both physically unstable and high in toxic magnesium as a result of the serpentization. Left unmanaged, most of the landscape that's not in earthflow would be forested. However, historically, native peoples burned grasslands to preserve prairies as hunting areas, and for other cultural resources.
37.3	0.3	Harper Creek Bridge
37.5	0.2	Tall Trees turnoff - Continue straight (west) on the Mattole Road
38.1	0.6	Albee Creek Campground - Continue west on Mattole Road
38.3	0.2	Bull Creek Bridge - To the right (upstream), the metal protrusion in the stream is USGS stream gaging site #11476600. The present site was established after the 1964 flood. During the flood, a log deck from a mill site ~1/4 mile upstream of here was incorporated into the flow, and created a dam just around the corner. When the dam of logs and debris broke, the original gage was wiped out. Flood peaks from the '64 flood are therefore estimates.
38.4	0.1	Headlights off - end of big trees. [38.4-38.6] Before the December, 22, 1964 storm, the mill and associated log deck were located here, between the road and the creek.
39.4	1.0	Second Bull Creek Bridge. At 3 o'clock, Mill Creek enters Bull Creek just downstream of here from river left. Upstream, (9 o'clock), instream structures have been placed by Fish and Game & Humboldt Redwoods State Park to enhance fish habitat.

<u>Mileage</u>	<u>Distance</u>	<u>Description</u>
39.7	0.3	[39.7 to 39.8] The Bull Creek town site (“downtown”). Before the 1955 and 1964 floods, the basin was home to hundreds of residents. On both sides of the road, the deposits are 1964 flood terraces (valley wall to valley wall). Flooding in 1955 caused many residents move out of the basin, and the flood of 1964 convinced the rest to leave. The house on the right marks the upstream extent of the main town site.
40.4	0.7	Cuneo Creek Bridge. This is the site of several meters of aggradation as a result of the 1955 and 1964 storms, collectively. The post-1955 concrete bridge is visible in the channel, and served as base level control for Cuneo Creek until ~ the 90’s. You can’t see it from the car, so please don’t stop! We will refer to this bridge site at Stop 1-2.
40.8	0.4	Cemetery. Before the December 22, 1964 flood, this cemetery was located on a terrace closer to Cuneo Creek. Many of the coffins buried here today had to be dug out of flood deposits from the ‘64 flood and relocated to this site.
41.0	0.2	Cuneo Horse Camp - Continue Straight (left up the hill) on Mattole Road - When we come back down the hill, this will be the turnoff for Stop 1-2
41.3	0.3	Glimpse of Upstream Bull Creek Headwaters. You may notice many flat-topped ridges in this landscape. In contrast to the geomorphic origin of features like these in other regions, in the triangle of doom, these flat ridges are not necessarily underlain by more resistant lithologies. The origin of these planar ridge tops will be a topic of discussion at our first stop this morning.
42.2	0.9	Switchback #2
42.4	0.2	Lower Quarry
43.2	0.8	Devil’s Elbow Slide - This is one of the deep-seated landslides that will be a topic of discussion at Stop 1-1, and throughout this weekend. The mechanisms that trigger these features is one of the themes of this trip.
43.5	0.3	mile marker 12.33
43.8	0.3	Cracks in the road - Devil’s Elbow slide has forced the road to be moved several times over the past few years.
44.4	0.6	Water tank Stop 1-1 is at the headwaters of the tributary that feeds this water tank
45.6	1.2	DRIVE SLOWLY as you approach the turnoff to Fox Camp Road
45.7	0.1	Turn Right into the pullout past the gate to turn around so we can keep the roadway clear. This stop is limited to 30 cars at the stop. Everyone needs to carpool !! Cars carrying less than 4 people will be asked to either pick up or become hitch-hikers. Once we exceed the number of cars allowed, we will have trucks available to shuttle people in to Stop 1-1, so be prepared for that eventuality. Shuttles will pick up hitch-hikers near the gate entrance, so be ready with your jacket and backpack, and follow directions of the MONGOs.
47.2	1.5	Park along the edge of the main road, leaving room for other vehicles to pass, and please don’t drive on the grass. Even if it has rained recently, we are very concerned about fire danger, and we need to be extremely diligent about our fire safety. This grassy prairie is burned periodically by Humboldt Redwoods State park to maintain grasses against conifer invasion.



Stop 1-1 Fox Camp Road

Overview of tectonics in the southern Mendocino deformation zone (MDZ) - seismic, geodetic, stratigraphic, and geomorphic signatures.

Assemble at the rocky knob on the ridge near the south side of the prairie for a welcome and introduction to this year's FOP. A host of speakers will introduce the geologic setting for the trip and present field evidence for the crustal conveyor model.

[0900-1100]

STOP 1-1 ABSTRACTS

Seismicity and Stress Near the Mendocino Triple Junction

Ian Pryor and Bob McPherson

We will summarize the salient features from over 30 years of well-located seismicity that surrounds the Mendocino Triple Junction. Some of the questions we will answer at our stops are: What is the geometry of the plates that make up the triple junction? How do the plate boundaries interact and deform? How do the stresses within each plate change as one moves offshore, or north and south of the triple junction? We will present new focal mechanism plots and compare them with past mechanism/centroid moment tensor studies. Also, we will summarize the decades-long debate of the southern edge of the Gorda Plate by showing where it really is. Additionally, we will present new data of the Gorda-North American locked zone evidenced by a bend in the descending Gorda Plate. This information that we will present at stops 1-1 and 2-1 is intended to be the groundwork for later, more specific discussions on recent faulting, geodetics and crustal modeling both north and south of the Mendocino Triple Junction.

GPS-derived fault slip rates along the northernmost segments of the Maacama and Bartlett Springs fault zones, northwestern California.

Todd B. Williams, Harvey M. Kelsey, and Jeffrey T. Freymueller

GPS-derived velocities (1993-2002) in northwestern California show that processes other than subduction are in part accountable for observed upper-plate contraction north of the Mendocino triple junction (MTJ) region. After removing the component of elastic strain accumulation due to the Cascadia subduction zone from the station velocities, two additional processes account for accumulated strain in northern California. The first is the westward convergence of the Sierra Nevada-Great Valley (SNGV) block toward the coast and the second is the north-northwest impingement of the San Andreas fault system from the south on the northern California coastal region in the vicinity of Humboldt Bay. Sierra Nevada-Great Valley block motion is northwest toward the coast, convergent with the more northerly, north-northwest San Andreas transform-fault-parallel motion. In addition to the westward converging Sierra Nevada-Great Valley block, San Andreas transform-parallel shortening also occurs in the Humboldt Bay region. Approximately 22 mm/yr of distributed Pacific-SNGV motion is observed inland of Cape Mendocino across the northern projections of the Maacama and Bartlett Springs fault zones but station velocities decrease rapidly north of Cape Mendocino. The resultant 6-10 mm/yr of San Andreas fault-parallel shortening occurs above the southern edge of the subducted Gorda plate and at the latitude of Humboldt Bay. Part of the San Andreas fault-parallel shortening may be due to the viscous coupling of the southern edge of the Gorda plate to overlying North American plate. We conclude that significant portions of the upper-plate contraction observed north of the MTJ region are not solely a result of subduction of the Gorda plate, but also a consequence of impingement of the western edge of the Sierra Nevada-Great Valley block and growth of the northernmost segments of the San Andreas fault system.

Influence of the Mendocino Triple Junction on the Tectonics of Coastal California

Kevin P. Furlong and Susan Y. Schwartz

The migration of the Mendocino triple junction through central and northern California over the past 25–30 million years has led to a profound change in plate interactions along coastal California. The tectonic consequences of the abrupt change from subduction plate interactions north of the triple junction to the development of the San Andreas transform system south of the triple junction can be seen in the geologic record and geophysical observations. The primary driver of this tectonism is a coupling among the subducting Juan de Fuca (Gorda), North American, and Pacific plates that migrates with the triple junction. This coupling leads to ephemeral thickening of the overlying North American crust, associated uplift and subsequent subsidence, and a distinctive sequence of fault development and volcanism.

Terrace formation and drainage adjustment in response to migrating uplift, 80 km east of the Mendocino Triple Junction, Northern California

Rich D. Koehler

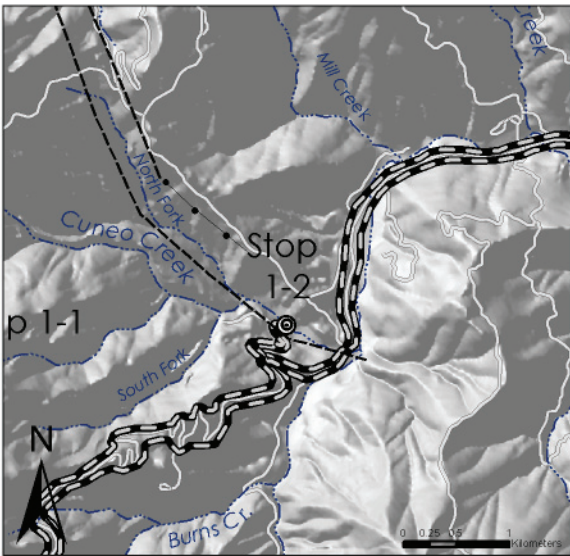
Terrace formation and drainage adjustment in response to migrating uplift is distinguished by a series of fill and strath terraces in the Van Duzen/North Fork Eel Rivers headwaters region, northwestern California. Differences in soil development, amount of incision, and terrace stratigraphy imply a history of non-synchronous terrace formation. The Refuge Valley fill terrace in the drainage divide between the Van Duzen and North Fork Eel Rivers records a transition in geomorphic process from aggradation to incision due to uplift. Well documented uplift to the west in the Cape Mendocino region and the lack of evidence supporting alternative mechanisms of terrace formation (i.e. landslide damming and climate variation) suggests tectonic uplift is the dominant mechanism of drainage adjustment and terrace formation. Tectonic uplift induced channel gradient shallowing in the North Fork Eel channel, promoting the aggradation of the North Fork Eel fill terraces and Hettenshaw Valley. As a consequence of uplift, the Van Duzen River captured the headwaters of the North Fork Eel River, leaving a former North Fork Eel fill terrace at the new drainage divide in late Pleistocene time. Continued uplift, since the time of capture, has steepened the Van Duzen channel, resulting in downcutting and strath terrace formation into the Holocene. The tectonic model driving the uplift is regional bulging associated with the northward migration of the Mendocino Triple Junction.

Topographic Patterns and Geomorphic Processes above the Southern Edge of the Subducting Gorda Plate.

Rocco Fiori and Patrick Vaughan

Uplift rates inferred from a series of marine terrace flights spanning the southern edge of the Gorda Plate correspond to topographic profiles of the prominent northwest trending ridgecrest located approximately 15 - 20 km inland. Profiles taken on and perpendicular to the topographic grain support the hypothesis that northeast transpressional and convergent deformation produced an uplifted relict landform between the Mattole and Eel Rivers. This relict landform has been dissected and altered by the interaction of several mechanisms over the past 500ka to 1Ma and is currently preserved on the broad crested ridges in the study area. Channel elevations of the major streams that cross the 97 km ridgecrest profile are at a similar grade, suggesting steady-state incision across the region. Interestingly, a slight bulge in the profile of these channel elevations lags to the south of the high relief zone shown in the ridgecrest profile. Several mechanisms are implicated: (i) isostatic adjustment, (ii) renewed uplift and deformation associated with near surface faulting, (iii) asthenospheric upwelling, (v) timing of static and dynamic loading relative to incision, and (vi) variations in rock resistance and stream power. In the high relief zone several ridgetop depressions and uphill facing scarps (interchangeably referred to as sackung) have been identified. Many of these features are at the head of mountain-scale bedrock landslides that are consuming the relict landscape. The distribution of ridgetop widths, sackung and other geomorphic features, along with ridgecrest and stream profiles, examined relative to the south to north trend of marine terrace uplift rates, suggest that much of the relict landscape has been evacuated from headwater basins in the south but remains as remnant surfaces in the north where the current locus of high uplift is expressed. Our conceptual model for drainage basin evolution in this region suggests that large scale debris slide amphitheatres are the result of denudation processes that involve: a) uplift and incision, b) foundering of the high relief topography by static and dynamic loading that produces mountain-scale bedrock landslides, c) dissection of the remnant slide mass by debris slides, d) catastrophic valley fill events, and e) cut-in-fill and strath terrace genesis. At Stop 1 we will view and discuss field examples and analysis of topics a through c, and at Stop 2 we will view and discuss field examples and analysis of topics d and e.

<u>Mileage</u>	<u>Distance</u>	<u>Description</u>
42.7		Return to Cars & Return back out Fox Camp Road to the Mattole Road
48.7	1.5	Gate to Fox Camp Road. Turn Left from Fox Camp back onto the Mattole Road. Again pull into turn around for a better view of oncoming traffic & be aware that the locals drive these roads very fast!!
50	17.4	View of Burns Creek to the south (3 o'clock)
50.4	0.4	Devil's Elbow Landslide - At 11 o'clock and level with the current road, note opening in trees. Road used to go thru this opening before a series of storms in the mid-1990's caused the slide to re-activate. Also note arcuate fractures on current road - where can the road be re-routed next?
51.0	0.6	Switchback - to the west is another view about half-way down Devil's Elbow Slide - the South Fork of Cuneo Creek drains the base of this slide. One of the topics at Stop 1-2 is the incision rates of the terraces at Cuneo Creek.
51.4	0.4	Cross under power lines. At 9 o'clock, you may be able to see glimpses of a terrace near eye-height thru small openings in the trees. This terrace is over 80 m thick, and documents a landslide from the paleo-Devil's landslide at ~ 10ka. We will discuss this terrace at our next stop.
51.8	0.4	Quarry Road
52.9	1.1	At 3 o'clock - fire scar up the mountain
53.2	0.3	Turn Left into Horse Camp
54.3	1.1	Pull thru the campground to turn around, but please don't park in the campground. Park along the road on the surface above the campground, again being sure not to drive on the grass and leaving room for cars to pass on the right of the parked cars.



Stop 1-2 Cuneo Creek & Bull Creek Terraces at Horse Camp

Cuneo & Bull Creek fluvial terraces, large landslides, and driving forces in the southern MDZ.

Grab a quick snack and assemble on the terrace downstream of the bathrooms at Horse Camp campground. Diane, Bonnie and Rocco will give a ~45 min presentation, then have time for lunch and to walk around at Cuneo Creek to look at terraces. Poison-oak abounds in this campground. If you don't know what poison-oak looks like, now is the time to ask a MONGO to point it out to you, so you can avoid it.

[1200-1400]

STOP 1-2 ABSTRACT

Historic terrace deposition and incision at Cuneo Horse Camp

Bonnie Smith and Diane Sutherland

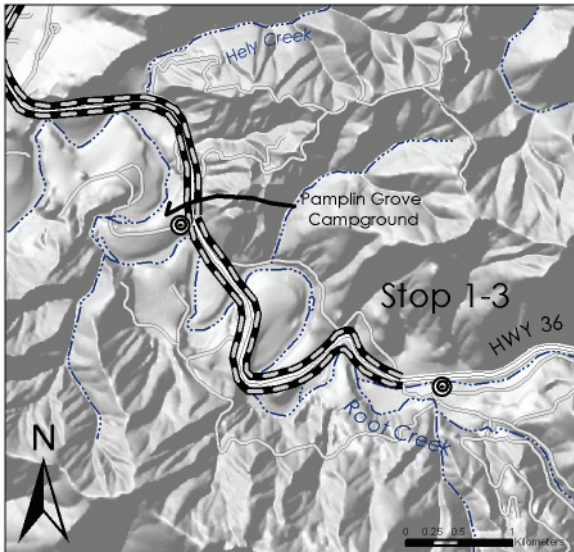
The storms of 1955, 1964, and 1997 produced extensive mass wasting, channel aggradation and widening throughout all major north coast river systems including the Eel, Mad, Van Duzen Rivers, Redwood Creek, and Bull Creek. The community of Bull Creek was damaged in the 1955 storm, and after the 1964 flood, residents abandoned the flooded town and the watershed was incorporated into State Park ownership. Cuneo Creek was identified as a primary source of sediment to Bull Creek, and mitigation efforts to avoid deleterious effects on the old-growth redwoods in the lower Bull Creek flats have been ongoing since the early 1970's.

Stop 1-2 will outline the topographic surveys in Cuneo Creek from 1976 – 2005 that document the erosion into the 1964 maximum aggradation terraces. The combined aggradation from both '55 and '64 storms totals at least 7 meters of fill at the Cuneo Bridge. Surveys in 2000, 2003 and 2005 document exhumed alder trees, bedrock reaches, and stratigraphic layers that indicate the channel may have scoured close to the pre-55 elevation in some places. We estimate that nearly 500,000 m³ of sediment has been eroded from the Horse Camp terraces over the 33-year study period, at least half of it in the first 12 year time step. This stop is intended to give trip participants a sense of scale for the dynamic sediment flux of north coast river systems within the Mendocino Deformation Zone.

<u>Mileage</u>	<u>Distance</u>	<u>Description</u>
54.3		Return to Cars and head back to the Mattole Road
54.5	0.2	Gate to Horse Camp Campground - Turn Left onto the Mattole Road.
55.1	0.6	On the left is the remnants of an orchard, a house used to stand here. To the right, the vegetated surface is a 1964 terrace, and the mouth of Cuneo Creek.
55.2	0.1	Cuneo Bridge - This is the site of ~5 m of fill from the combination of 1955 and 1964 storm events. Please don't stop in the middle of the road to try and see the 1964 bridge.
56.2	1.0	Bull Creek Bridge #2
61.4	5.2	Bull Creek delta at 4 o'clock

<u>Mileage</u>	<u>Distance</u>	<u>Description</u>
62.7	1.3	Proceed straight at the Stop Sign under Highway 101 - Do not go right over the Eel River. On December 22, 1964, you would have been under ~ 2 to 3 meters of water here. There is a high water marker at the entrance to Founder's Grove, a favorite stop for tourists visiting the redwood forest on the south side of the Eel River Bridge. Unfortunately, we don't have time to go there today, but keep it in mind for those traveling thru here on Sunday.
62.8	0.1	Turn Left on to Hwy 101 North.
65.7	2.9	Many redwoods along the Highway 101 corridor have dead tops. One theory about why this occurs is that the water table was intercepted during road construction. Before the highway was built, the trees were able to pump water to higher branches, and the dead tops represent the decrease in water table elevation.
66.4	0.7	Exit # 667 Redcrest
69.5	3.1	Bridge over Bear Creek
74.7	5.2	Stafford Exit
82.4	7.7	The Eel River terraces on the left will be a topic of discussion at stop 2-1 on Friday morning. Mark Verhey will discuss seismic profiles that run parallel to the highway from about mile 82.4 (where the highway swings turns north) to the town of Fortuna (north of the junction of Hwy 36 and 101). We are now paralleling the seismic profiles that show the Grizzly Creek anticline, which are deforming the overlying terraces west of the river.
84.2	1.8	Van Duzen River Bridge - Rhonerville Terrace @ 12 o'clock is Stop 2-1 tomorrow morning
84.7	0.5	Highway 36 turnoff - Turn Right
86.6	1.9	View of Van Duzen River valley on the right. At Stop 2-1 on Friday, we will discuss possible underlying structural features that help explain why the Van Duzen River is hugging the south side of the valley, and the progressive tilting with age of terraces to the north.
87.4	0.8	White Church
87.45	0.05	Intersection with Rhonerville Road. Continue straight and stay on Highway 36 heading east.
87.8	0.3	Van Duzen Fluvial Terraces
88.2	0.4	Little Salmon fault and Yager Creek at 10 o'clock. We will discuss the Little Salmon and associated faults at stop 1-3 and tomorrow.
89.5	1.3	Yager Creek Bridge. Entering the town of Carlotta - please drive slowly.
91.9	2.4	Store (no services)
94.9	3.0	Martin & Shirley's Store - Some supplies; <i>no gas</i>
95.6	0.7	Entrance to Pamplin Grove, campsite for the trip. Continue straight on Hwy 36 to stop 1-3. Note that when we come back to the campsite after stop 1-3, please don't turn left directly into the campground - eastbound traffic cannot see you, and this is not a safe place to turn. After stop 1-3, we ask you to please proceed west a few miles to the marked, safe turn around spot, so you can enter the campground from the eastbound lane.
97.4	1.8	Van Duzen Bridge

<u>Mileage</u>	<u>Distance</u>	<u>Description</u>
97.7	0.3	Van Duzen Bridge - notice the inner gorge slide. 2006 was a relatively big water year in the Van Duzen watershed and caused numerous streamside failures.
98.8	1.1	More streamside landsliding related to recent flooding
99.0	0.2	Base of the escarpment coming in from the north (10 o'clock) points toward the mouth of Root Creek, which enters the Van Duzen River from the south. Stop 1-3 is at an exposure along the Van Duzen River where this escarpment crosses the highway
99.2	0.2	This bedrock strath on the south side of the Van Duzen (3 o'clock) is a continuation of the feature we will see at Stop 1-3.
99.7	0.5	Turn Right - onto dirt (rock road); proceed down onto floodplain. Watch out for oncoming traffic (LOG TRUCKS!!) and boulders in the road.
99.8	0.1	Park along the left side of the gravel road. WATCH FOR LOG TRUCKS coming up the road from the Van Duzen River. Park off the road, allowing enough room for logging trucks to pass. Please be careful as you walk upstream to assemble - logging trucks drive fast!!



Stop 1-3 Van Duzen River at Root Creek

Structural and stratigraphic evidence for faulting and landsliding at the southern end of the Little Salmon fault zone.

Ozzy, Leroy, Gilbert, and Tagg will present evidence for faulting and associated stream terrace warping at Root Creek

[1500-1700]

STOP 1-3 ABSTRACT

Evidence for deformation of a Pleistocene strath terrace and coseismic deep-seated failure, implications for tectonic deformation at the boundary between the Northern San Andreas fault system and the southern Cascadia subduction zone

Oswald, J.A., Craven, G.F., Nordstrom, T.S., and Leroy, T.

The Chalk Mountain landslide complex is an approximately 640 acre, dormant, deep-seated, translational/rotational rock slide complex. The main scarp of the rock slide is located at the ridgetop and is defined by a 130-foot wide ridge-parallel sackung. Uplift along the inferred southern extent of the Little Salmon fault and/or movement on the landslide complex have reduced the width of the Van Duzen River valley along the inner gorge reach. Downstream from the inner gorge, the Van Duzen River occupies a broad valley and shows a series of entrenched meander loops, indicating uplift or incision of a former alluvial valley.

Downstream of the gorge near the mouth of Root Creek the bank of Van Duzen River exposes a series of faults within the undifferentiated Wildcat formation that deform the strath surface of the lower of two terraces. Structural analysis of fault striae and offsets of fractures and concretion nodules demonstrate right-oblique transpression accommodated on northwest striking, north and south dipping faults. The north-south directed contractional strain indicated by this analysis is consistent with the regional strain indicated by the Little Salmon fault and other thrust faults mapped in the vicinity. This fault may be related to the south-eastern Little Salmon fault zone. Detailed LiDAR topography also suggests westward tilting of the adjacent two terrace surfaces and vertical deformation of the upper terrace with the same sense as high angle faults that offset the strath surface.

Evidence for faulting extends southeast along Root Creek between the south-east mapped extent of the Little Salmon fault zone and a profound structural discordance along Carson Creek in Larabee Valley. The fault zone truncates a zone of east-west-trending folding and thrusting along the ridge between the Van Duzen and Eel Rivers, and strikes south along Carson Creek in to Larabee Valley. The combined right oblique shear and thrusting appear to represent increased contractional strain to the west related to the Eel River Syncline and may provide a model for the south-eastern terminus of the Little Salmon fault.

Three distinct depots are exposed in the lower strath terrace on the left bank of the Van Duzen River. The stratigraphy is consistent with fault rupture across an active stream channel and followed closely by deposition of landslide debris. We propose that strong ground motion, potentially from rupture of the fault crossing the strath, caused slip on the Chalk Mountain landslide complex and production of a large amount of landslide debris to east of the fault trace.

<u>Mileage</u>	<u>Distance</u>	<u>Description</u>
99.8		Return to Vehicles, Turn Around and Return to Highway 36
99.9	0.1	Turn Left (West) onto Hwy 36 - Return to Thursday Nite Campsite.
102.4	2.5	Swimmers Delight Campground. Continue Straight on Hwy 36. If we fill all the camp sites at Pamplin Grove, this is one of the optional overflow camping areas.
103.7	0.4	Pamplin Grove campground. DO NOT TURN LEFT INTO PAMPLIN GROVE. Proceed East on Highway 36
104.5	0.8	Turn Left into the pullout at Martin & Shirley's store. Turn around and head west on Highway 36.
105.3	0.8	Turn Right into Pamplin Grove campground

Day 1 Papers

Seismicity and Stress Near the Mendocino Triple Junction

Ian Pryor and Bob McPherson

Geology Department, Humboldt State University, Arcata CA, 95521

ABSTRACT

We will summarize the salient features from over 30 years of well-located seismicity that surrounds the Mendocino Triple Junction. Some of the questions we will answer at our stops are: What is the geometry of the plates that make up the triple junction? How do the plate boundaries interact and deform? How do the stresses within each plate change as one moves offshore, or north and south of the triple junction? We will present new focal mechanism plots and compare them with past mechanism/centroid moment tensor studies. Also, we will summarize the decades-long debate of the southern edge of the Gorda Plate by showing where it really is. Additionally, we will present new data of the Gorda-North American locked zone evidenced by a bend in the descending Gorda Plate. This information that we will present at stops 1-1 and 2-1 is intended to be the groundwork for later, more specific discussions on recent faulting, geodetics and crustal modeling both north and south of the Mendocino Triple Junction.

TECTONIC FRAMEWORK OF THE MENDOCINO TRIPLE JUNCTION

The geometry of the Mendocino Triple Junction (MTJ) is summarized in the cartoon in Figure 1 and the digital image in Figure 2. It can be seen in the cartoon that south of the MTJ, the Pacific Plate is moving in a northwesterly direction at 51mm/yr, forming a translational boundary with the North American Plate (1-10). Traditionally, the boundary between the North American and the Pacific Plates was thought to be a sharp line defined by the surface expression of the San Andreas Fault (1, 5). Now we can see that as the Pacific Plate moves northwesterly, the translational shearing between the two plates forms a broad area of faulting and seismicity sub-parallel to the San Andreas Fault and within the weaker North American Plate (Figures 1, 3 and 4). The MTJ travels with the Pacific Plate as it pushes the Gorda Plate northwesterly, and in its wake leaves the northwardly growing San Andreas Fault system (1, 5, 8, 10-14). Near the MTJ the northeast corner of the Pacific Plate acts like a bulldozer blade along the Mendocino Fault as it shoves the Gorda Plate northward, breaking up the offshore portion of the Gorda Plate (7, 8, 15-18). This transpressional, right-lateral boundary between the Gorda and the Pacific Plates can be seen in Figure 2 as an east-west trending ridge.

The Gorda Plate, youngest, smallest and weakest of the three plates, forms offshore along the Gorda Ridge (Figures 1 and 2), and it moves eastward away from the ridge, eventually plunging beneath the North American Plate at a shallow angle of between 5-11 degrees (7, 8, 16-22). Below in this paper, we will show that the Gorda Plate is wedged between thicker, bigger, and stronger adjacent plates to the north and south, and it is being crushed in the process as it is squeezed through this "tectonic die"(17, 23). Actually, the southern Gorda Plate is considered a deformation zone (see discussion below) and is currently not behaving as a coherent tectonic plate (24-35).

Since the Pacific Plate is older, colder and thicker than its adjoining plates, it is not deforming at all and is mostly devoid of earthquakes (or deformation). Of the three plates that form the triple junction, the Pacific Plate is the only one functioning like a true tectonic plate, with earthquakes occurring along its edges and not within it (7, 8, 17).

MAP VIEW OF SEISMICITY

Two map views of seismicity from 1979 to 2006 are presented in Figures 3 and 4. We would like to point out several significant features in these figures.

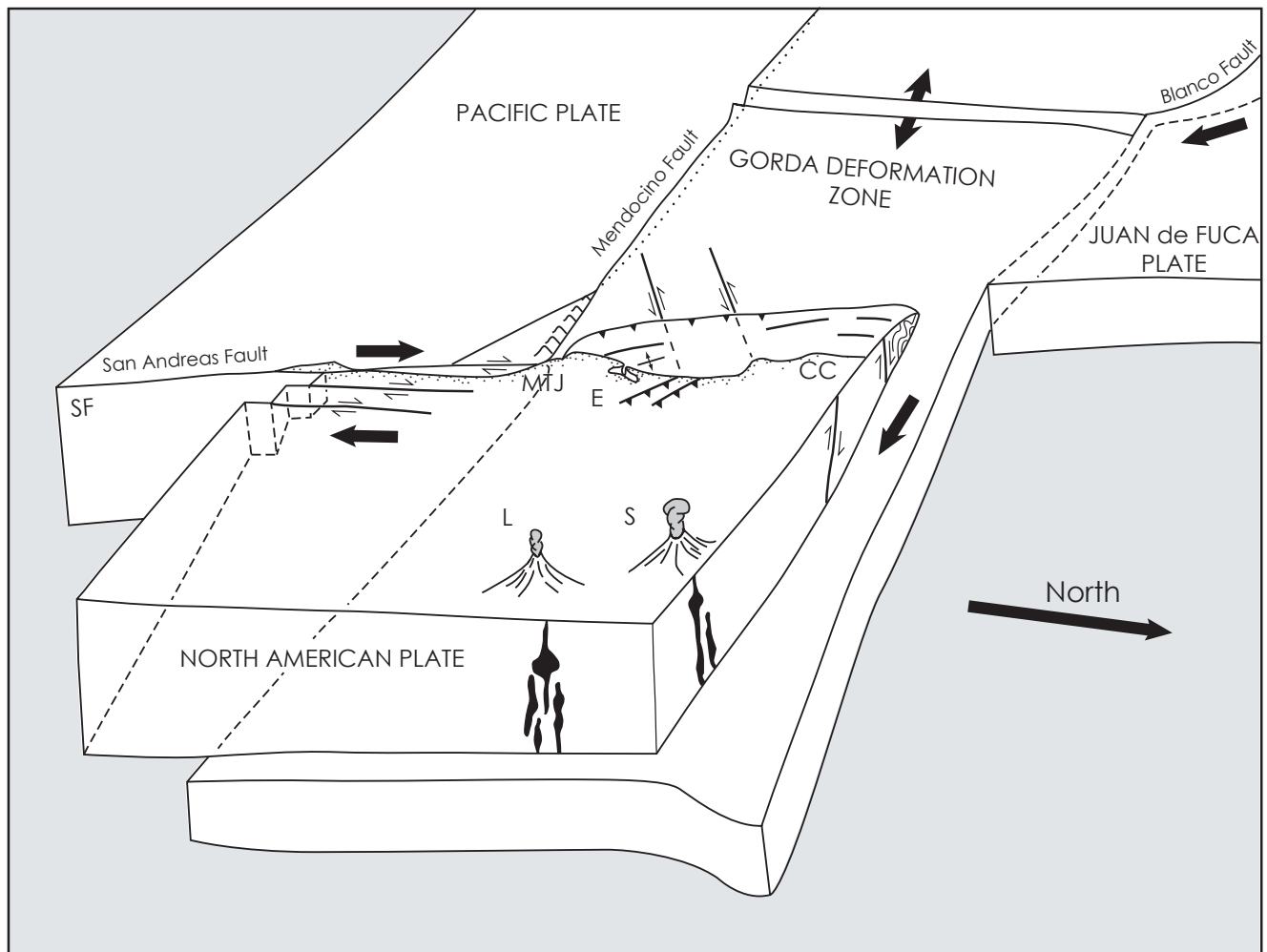


Figure 1. This drawing shows the setting of the three plates that make up the Mendocino Triple Junction. To the south the Pacific and the North American Plates slide past each other along a transtensional boundary that produces a series of right-lateral faults within the North American Plate. The Pacific and Gorda Plates meet along the Mendocino Fault, an active, vertical, right-lateral fault. It is along this boundary that the northwesterly-moving, older, colder, thicker Pacific Plate shoves the younger, warmer, thinner Gorda Plate and concentrates the stresses near this, its northeast corner. The North American and Gorda Plates converge and form the southern Cascadia Subduction Zone. Abbreviations used in this figure are: CC-Crescent City, E-Eureka, SF-San Francisco, L-Mt. Lassen, and S-Mt. Shasta.

First, notice in Figure 3 that there is a “shotgun” pattern of seismicity centered near the MTJ, north of the northeast corner of the Pacific Plate (17, 23). This is where the Pacific Plate’s influence of shoving the MTJ northwesterly is concentrating the stress, the result being the internal brittle failure of the thinner, younger and smaller Gorda Plate (7, 8, 17). Since the Gorda Plate is undergoing such a high level of seismic activity, many researchers refer to the southern part of the Gorda Plate as a deformation zone (22-35). The earthquakes in this region are all intraplate earthquakes and represent 85 per cent of the activity and 90 per cent of the stress released in this region (7, 8, 17, 22).

A second feature seen in both figures is the now undisputed location of the southern edge of the Gorda Plate, shown clearly as a sharp color contrast in seismicity trending ESE from the MTJ (7, 8, 17). This boundary shows up best in Figure 4. Previously, the boundary had a more SE trend based on gravity and magnetic records, but it is now recognized that the seismicity more precisely shows the correct location of the southern edge of the Gorda Plate as it plunges beneath North America (7, 8, 13, 17, 20, 21, 36-42). The southern edge of the Gorda Plate is thought to be bent downwards as indicated by the cooler (deeper) colors of earthquakes running along this edge (21). Also, notice that the Cascade volcanic arc starts north of this southern edge of the Gorda Plate, with Mount Lassen and Mount Shasta located just north of this boundary.

The third significant feature in both figures is the broad, shallow, strike-slip zone of earthquakes formed by the transtensional boundary of the Pacific Plate's northwesterly motion of sliding past the North America Plate (8, 10-14, 43). This can be seen as the broad band of yellow-colored earthquakes with depths typical of strike-slip faults. Notice that all of the earthquakes are North American intraplate events east of the location of the traditional Pacific-North American Plate boundary, the San Andreas Fault. When the earthquakes are filtered for location quality as in Figure 4, they begin to show alignments with the known traces of the Maacama and Bartlett Springs Faults. Also apparent in this figure is the lack of earthquakes on the northern San Andreas Fault, that part of the fault that moved during the 1906 event and which is presently locked.

CROSS SECTIONS

We will discuss briefly the two cross sections shown in Figure 5 which are as follows: An east-west broad section north of the MTJ and a north-south section through the MTJ.

In the east-west section, the intraplate Gorda earthquakes form a 10km thick band that dips gently at first until 123.5W longitude, then more steeply towards the east, eventually getting deep enough so the slab and sediments

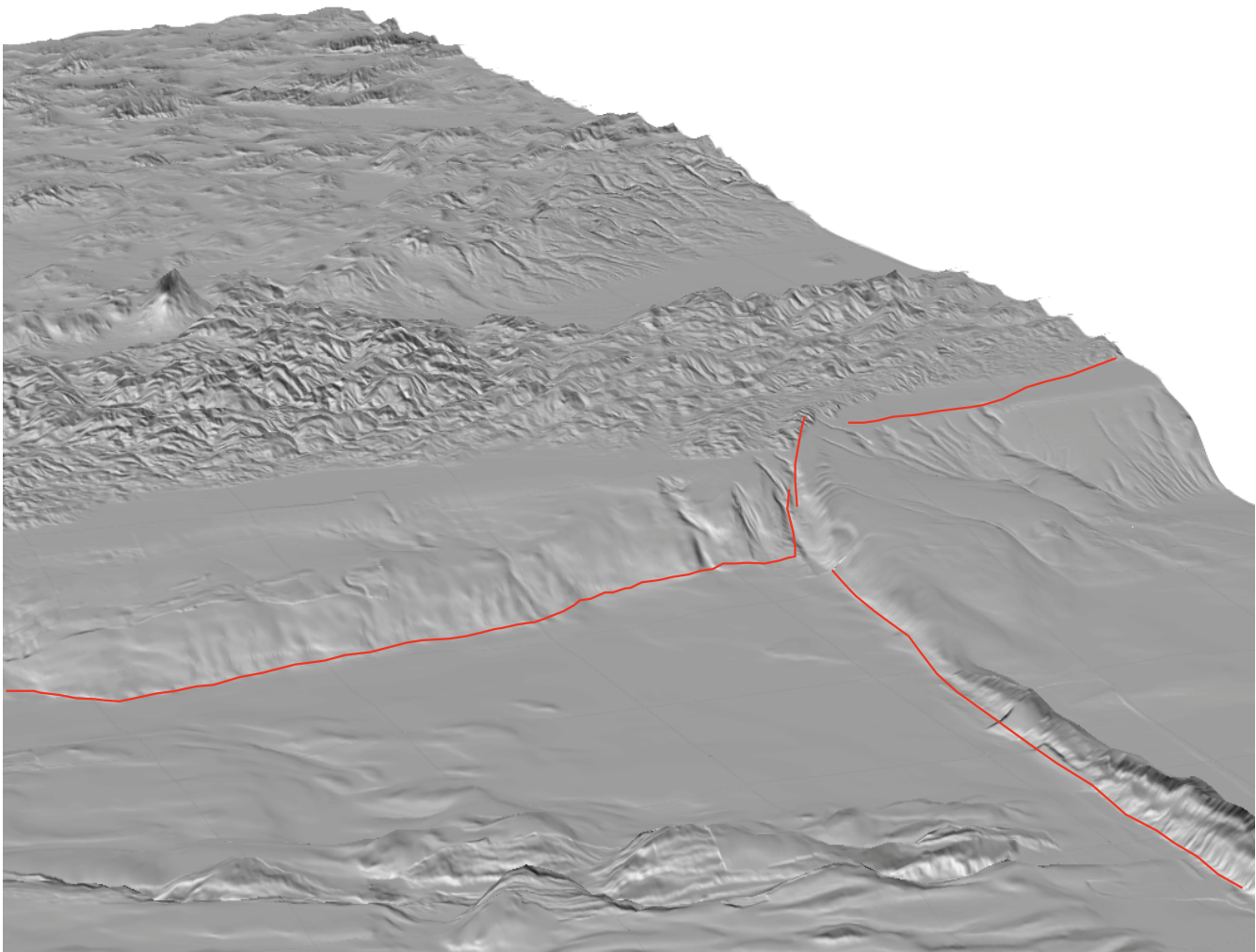


Figure 2. This is an oblique, shaded relief view from offshore looking southeastward towards the Mendocino Triple Junction. The MTJ starts offshore where the North American and Gorda Plates meet. The Mendocino Fault is that section of the east-west trending ridge starting at the triple junction and extending to the Gorda Ridge. The Gorda Ridge can be seen as trending north from the Mendocino Fracture Zone, then veering to the north-east where it meets the Blanco Fracture Zone, the southern edge of the Juan de Fuca Plate.

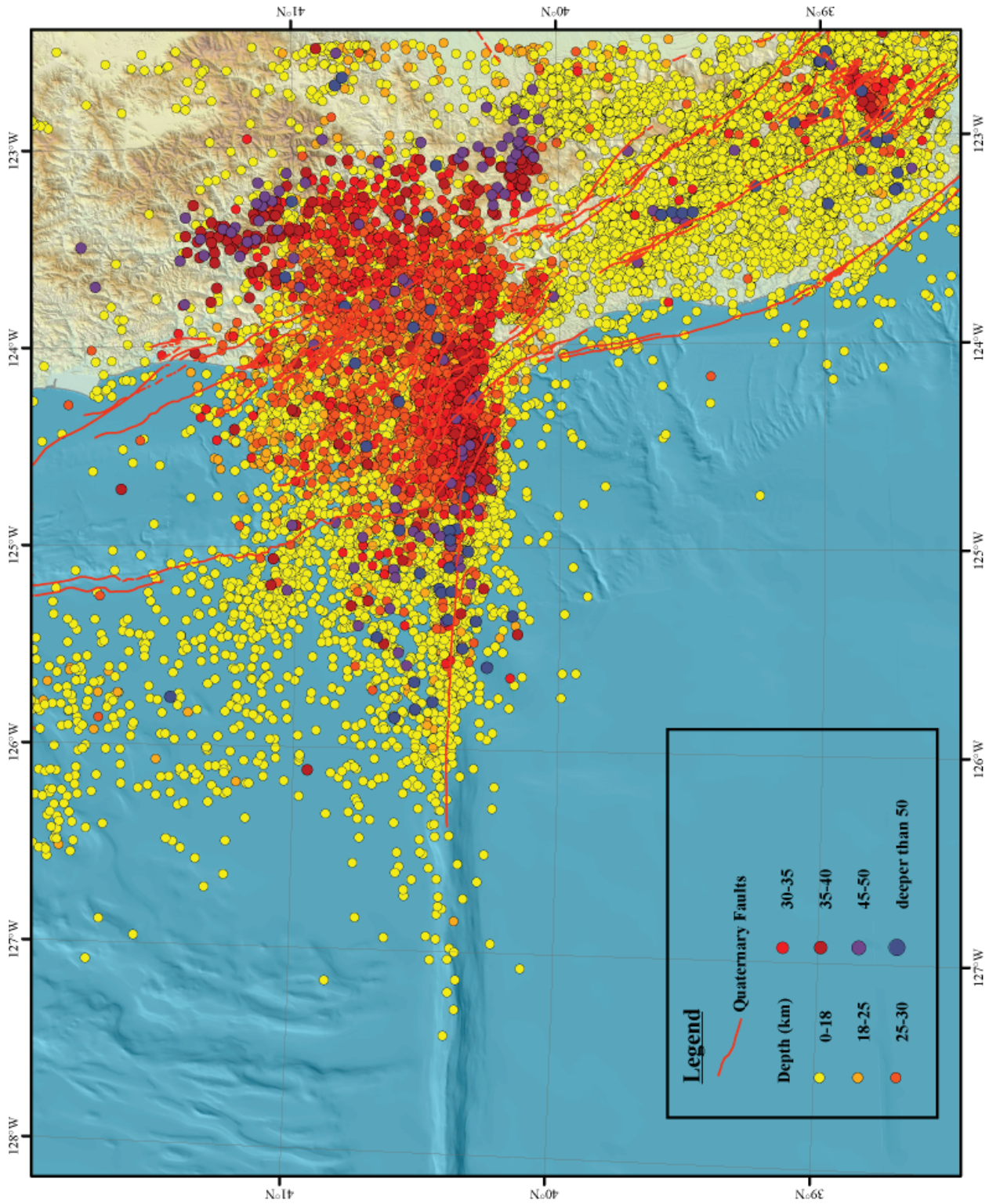


Figure 3. An unfiltered seismicity map shows the regional activity from 1975 to 2006. We did not filter the location quality in this version in order to include most of the offshore Gorda Plate events. The strike-slip boundary is shown by the yellow-colored events coming from the Bay Area, and the depth change in earthquakes represents the beginning of the subduction zone or the south edge of the Gorda Plate.

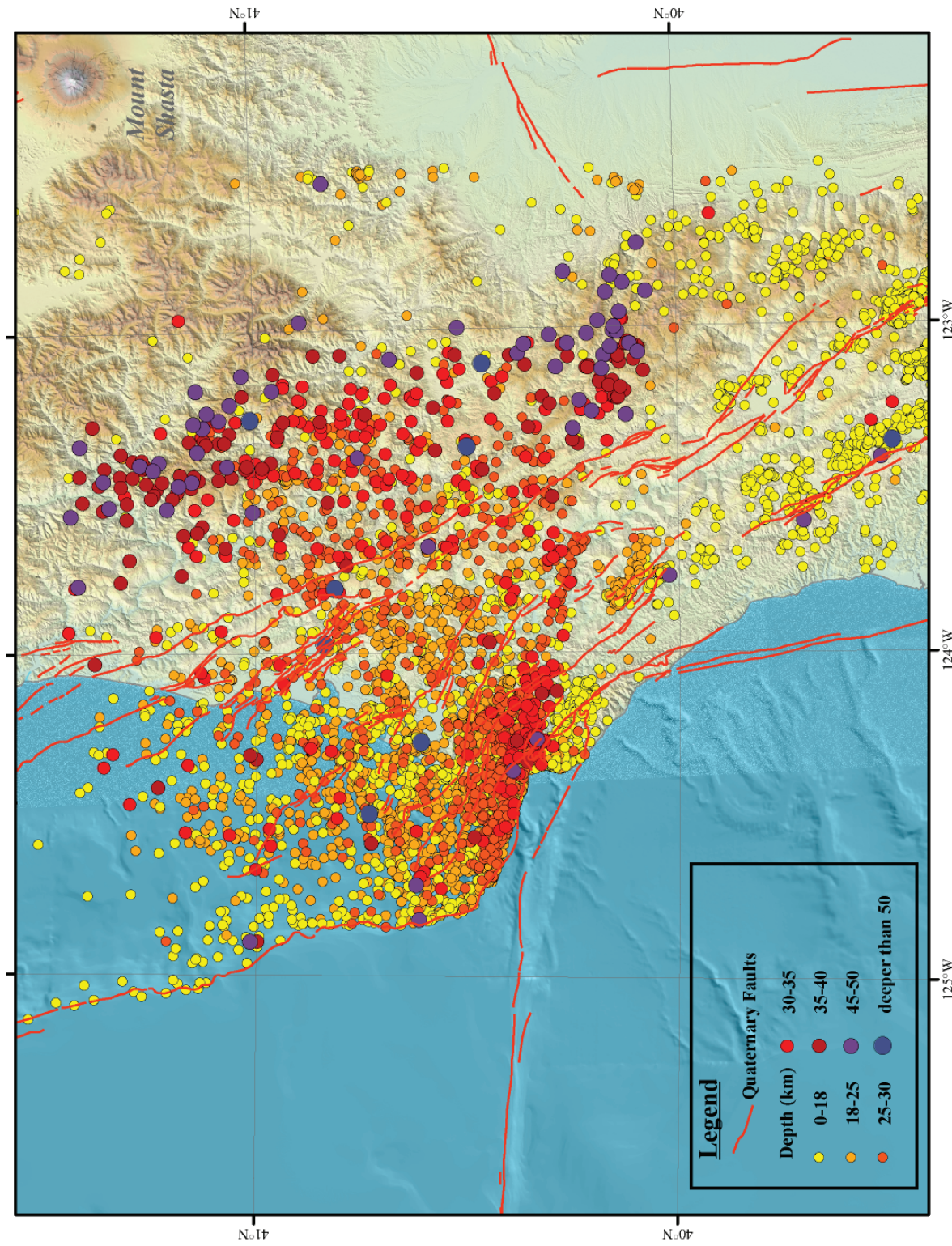


Figure 4. We zoom into the triple junction region with this filtered seismicity map. We show only those earthquakes with location errors of less than 2km, and travel time residual errors of less than .02 seconds. The southern edge of the Gorda Plate is even sharper in this plot, as is the deepening of earthquakes as one moves eastward. Also notice that the epicenters align along the trends of the Maacama and Bartlett Springs Faults, inboard of the locked and seismically quiet San Andreas Fault, shown by the red lines offshore. The Garberville activity is also apparent as an isolated cluster of orange circles, just south of the Gorda Plate in the “slabless window” region.

partially melt and form the southernmost Cascade volcanoes (Figures 1 and 4). This flexure, or change in dip in the Gorda Plate, can also be seen in Figure 4 as a subtle color change from orange to red, blue and purple. The shallow dip to the west of the flexure represents the locked portion of the subduction zone, which is approximately 85-90km wide. East of the flexure point, the increase in dip of the Gorda Plate represents the beginning of the transition that separates the locked zone from the constantly slipping zone deeper to the east (44, 45). Notice also the ratio of earthquakes in the North American Plate versus the Gorda Plate, again with the majority within the Gorda Plate. There is a dense cloud in both plates near the corner of the Pacific Plate at 124.15W longitude, indicative of the plates being locked together in this region of high stress.

The north-south section shows a shift from a subduction zone environment in the north to that of a strike-slip environment in the south. The Gorda Plate can be seen at a depth of 15-25km as one moves from the north, ending abruptly at 40.3N latitude, which demarks the southern edge of the plate (7, 8, 17). Moving farther south one can see the small cluster that represents some activity in the “slabless window” region. This cluster began with a magnitude 3.4 event in 1979, followed by a burst of over 50 smaller events (8). These events are near the bottom of the North American Plate and align along a NW trend. Earlier researchers hypothesized that this cluster may have represented a broken-off piece of the Gorda Plate or may have been related to an asthenospheric upwelling phenomenon (8, 46). It is our view that this swarm relates to heating and asthenospheric upwelling occurring in the wake of the Gorda Plate’s passing (8). Moving farther south, a transition takes place with the occurrence of strike-slip faulting inboard of the San Andreas Fault which is shown by the band of earthquakes less than 20km deep.

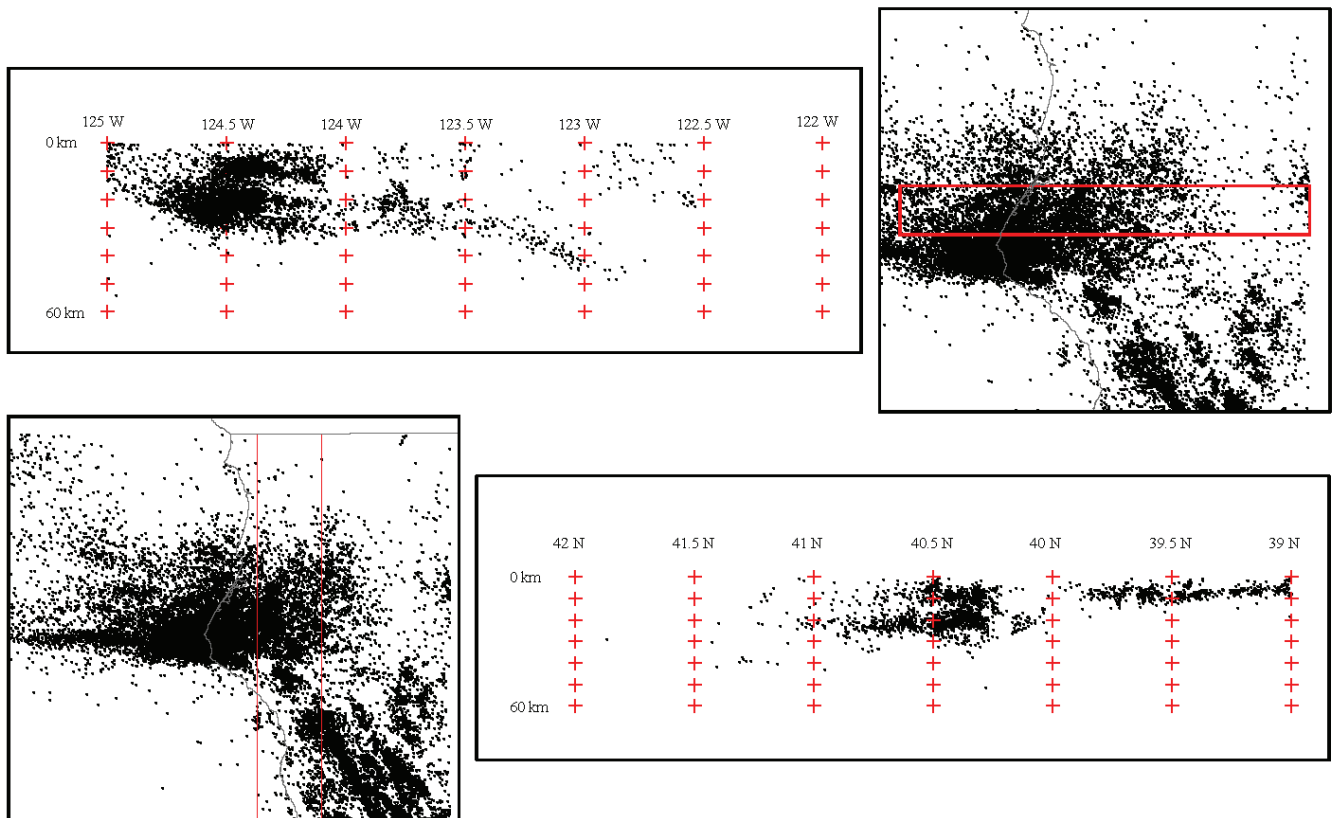
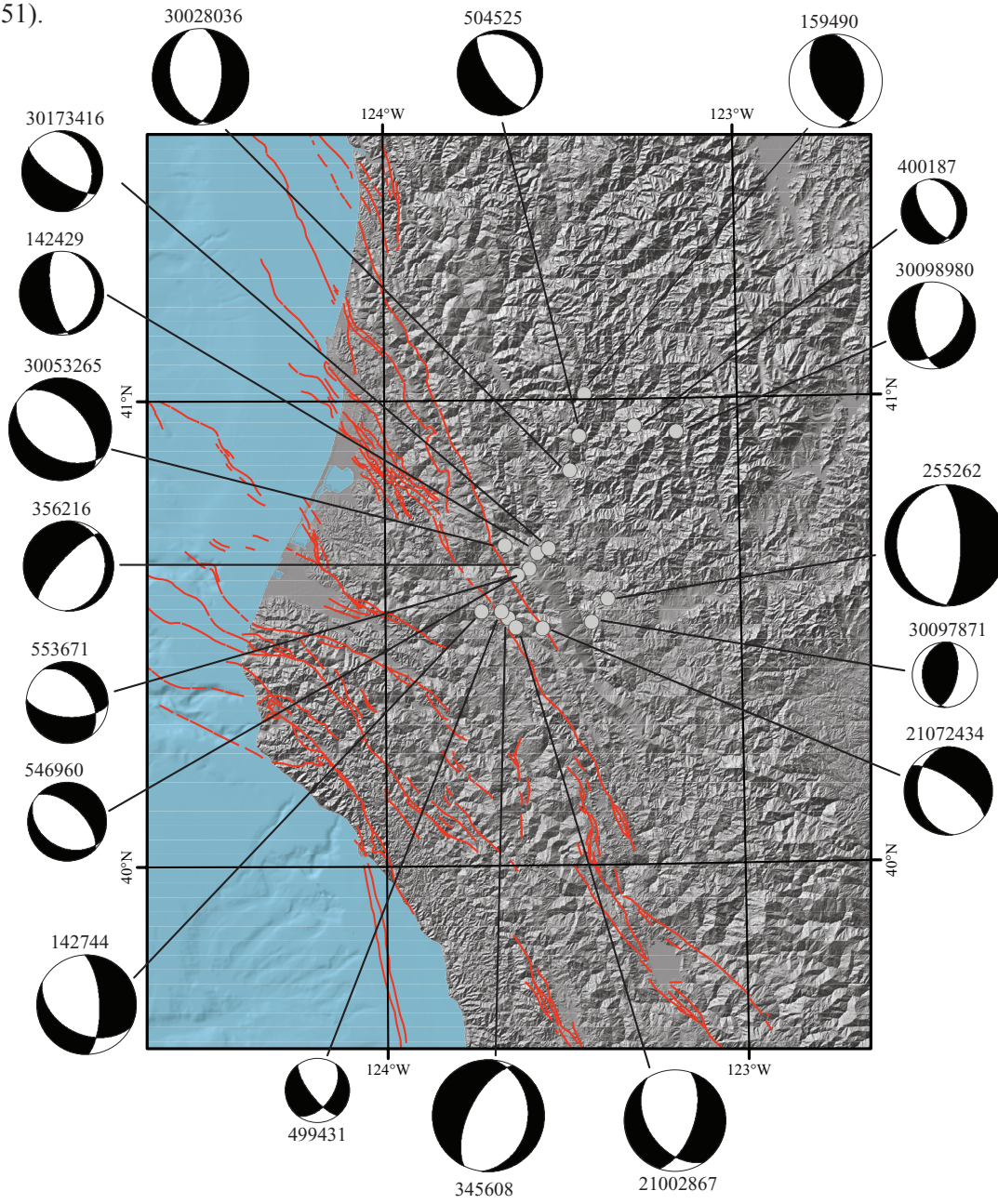


Figure 5. Displayed in this figure is an east-west and a north-south section, with the inset maps showing the rectangles in map view used to generate sections. In the east-west section, the Gorda Plate is a band of earthquakes emerging from the dense cloud of seismicity in the MTJ region, then dipping shallowly to the east until 123.5W longitude, then steepening and disappearing. In the north-south section as one moves from north to south, one can see the sharp southern edge of the Gorda Plate, then the isolated cloud of the Garberville area, then the transition into the shallow, inboard, strike-slip activity along the Maacama and Bartlett Spring Faults.

FOCAL MECHANISMS

In Figures 6 and 7, we present new focal mechanism results and will discuss how they are consistent with past studies (47-51).

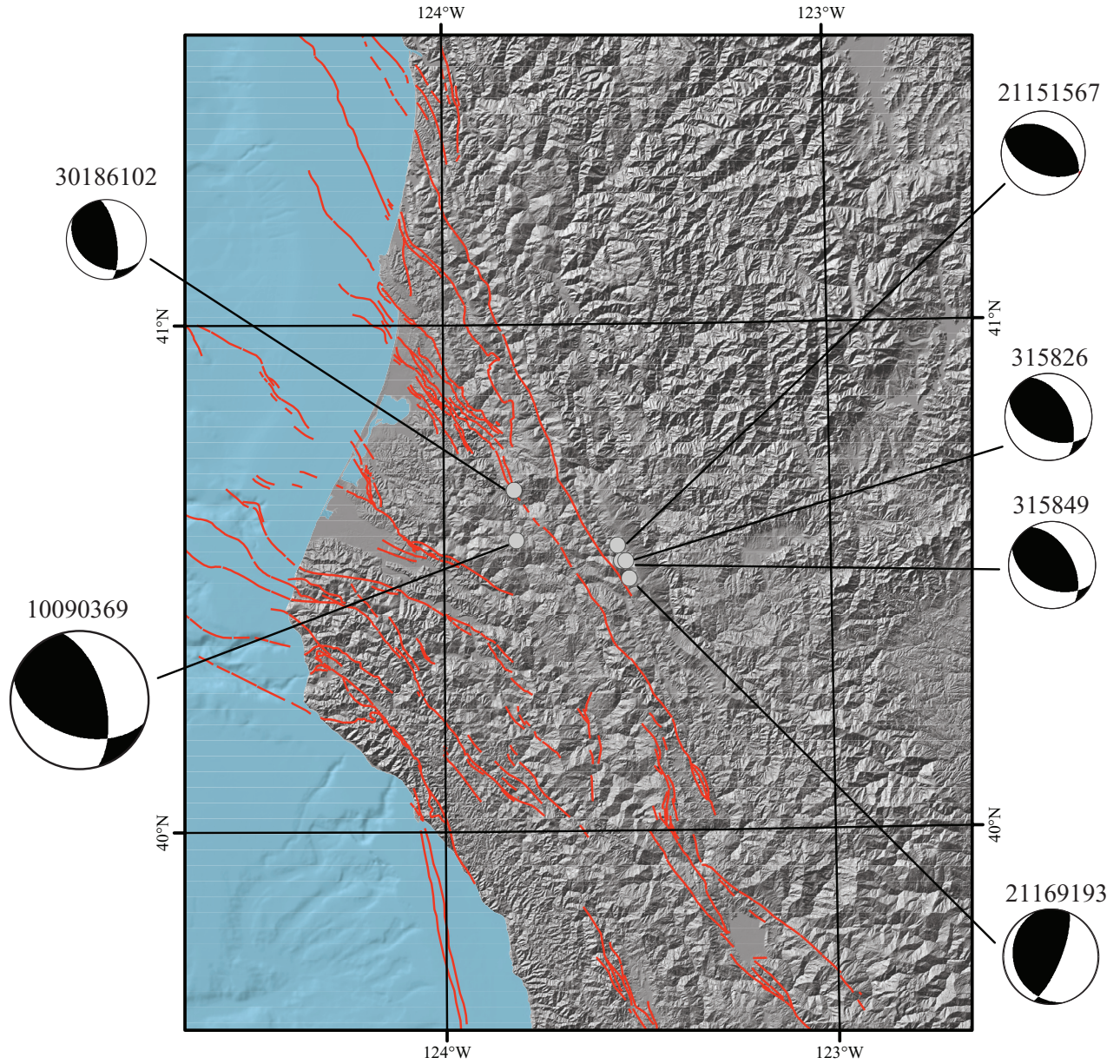


Event ID	Date	Depth (km)	Magnitude	Event ID	Date	Depth (km)	Magnitude
142429	8/17/1989	28.51	2.7	30097871	2/26/1996	25.97	2.1
142744	8/22/1989	27.89	3.2	30098980	3/10/1996	32.83	2.8
159490	6/17/1990	30.66	3	499431	3/25/1997	33.84	2.06
255262	3/9/1992	35.34	4.4	504525	5/10/1997	28.31	2.74
345608	4/15/1993	30.62	3.6	546960	12/29/1997	22.3	2.53
356216	6/18/1993	26.53	2.9	553671	1/26/1998	22.85	2.62
375403	8/19/1993	33.87	2.6	30173416	5/10/1998	30.13	2.6
30028036	9/10/1993	28.41	3.1	21002867	2/22/1999	28.27	3.26
400187	4/10/1994	18.85	2.1	21072434	12/18/1999	22.27	2.84
30053265	7/21/1994	26.82	3.3				

Figure 6. Displayed in this figure is 10 years of well-recorded small events that are within the Gorda Plate under the North American Plate. Most of the mechanisms are consistent with east-west directed tension, which we will show contrast with the offshore Gorda events. All focal mechanisms are upper hemisphere projections in this figure and Figure 7.

Gorda Plate

The Gorda Plate can be divided into two regions: 1) An offshore region that is being crushed between the Pacific and the Juan de Fuca Plates and, 2) That region of the Gorda Plate emplaced under the North American Plate and east of the “tectonic die” formed by the Pacific and the Juan de Fuca Plates to the west.



Event ID	Date	Depth (km)	Magnitude
315826	9/15/1992	11.26	1.9
315849	9/15/1992	9.01	1.9
10090369	12/10/1989	0.22	2.9
21151567	3/7/2001	8.82	1.83
21169193	6/8/2001	11.08	2.07
30186102	7/21/1998	7.49	1.73

Figure 7. Shown in this figure are North American Plate earthquakes that are well recorded. All the events are consistent with NNE-SSW directed, maximum compression. These earthquakes are within the North American Plate, above the activity in the Gorda Plate which was shown in the previous figure.

Offshore, the Gorda Plate has experienced many large events in the past 100 years, and all of these intraplate earthquakes have mechanisms that are consistent with left-lateral motion along northeast-southwest faults (17, 22, 52). Presumably, this is reactivation of emplaced weaknesses within the plate representative of old spreading ridge faults that are now distorted and rotated to a northeast-southwest trend (26-29). The same mechanisms and moment tensors for the larger events all are consistent with north-south compression resulting from the convergence of the Juan de Fuca and Pacific Plates (53).

Once the Gorda Plate moves past the buttressing corner of the Pacific Plate to the south, thereby releasing the confining forces, the mechanisms change from strike-slip solutions to north-south oriented, normal mechanisms which we believe represent down-slab tension and/or the result of bending (8, 15,17).

North American Plate

The North American Plate focal mechanisms change significantly as one crosses the southern edge of the Gorda Plate from north to south as do the depths of seismicity.

North of the southern edge of the Gorda Plate, the focal mechanisms within the overriding North American Plate are reverse mechanisms as seen in Figure 7, consistent with maximum compression trending \approx N20-25E (7, 8, 17). These data agree quite well with the Quaternary faulting and folding as well as geodetic data seen in the North American Plate (54-62).

South of the MTJ the focal mechanisms are strike-slip events consistent with motion along the northwest-trending, right-lateral faults that are inboard of the locked San Andreas Fault (10, 12). We will show moment tensor solutions from 1990 to present that support this statement.

DISCUSSION

The map views of seismicity show clearly that the Gorda and North American Plates are deforming presently as evidenced by the long history of intraplate earthquakes and therefore are not behaving as tectonic plates (63). In the triple junction region, only the Pacific Plate is devoid of earthquakes and behaves like a rigid plate. The North American Plate is shown to be a series of slivers inboard of and parallel to the San Andreas Fault south of the triple junction. That contrasts with the Northern American Plate north of the triple junction where it is being squeezed in a N22E direction in a triangular region enclosing Humboldt Bay (see other talks in this guidebook). Offshore, the southern Gorda Plate is also shown to be presently deforming, consistent with left-lateral earthquake sequences throughout this region. Once the Gorda Plate moves eastward past the corner of the Pacific Plate, the earthquakes within the Gorda Plate change dramatically to normal events, consistent with east-west directed tension.

The southern edge of the Gorda Plate has been a vigorously debated topic for over two decades, but now the debate has quelled as the edge is quite well delineated by Gorda Plate seismicity in map view. There will be several presenters that will use this important boundary location in their modeling, so we hope this data helps their arguments. Also, new information showing the location of the locked-transitional boundary between the North America and Gorda Plates is shown in map view and section, giving modelers of upper plate deformation new data to incorporate in their strain modeling. Large earthquakes offshore have been shown to move onshore GPS benchmarks, as evidenced by the September 1, 1994 event (64). Todd Williams will speak more about this locked zone when he summarizes geodetic signatures of large earthquakes later today.

After stops 1-1 and 2-1, we hope to have convinced you that by using seismic evidence logged for more than 30 years, some of the interactions in the Mendocino Triple Junction have been demystified. We hope that other studies can add to this general information to further our understanding of the kinematics of this complex region, newly named the FOP committee, the Mendocino deformation zone.

ACKNOWLEDGEMENTS

We would like to thank David Oppenheimer for a set of figures that he sent us (RM) years ago that inspired Figures 3 and 4 of this report. The new focal mechanisms and Figures 2-7 within this report will be part of Ian Pryor's senior thesis at HSU. We also would like to thank Todd Williams for assistance on the first versions of the focal mechanism figures. Doug Dreger made time in his very busy schedule helping to produce the moment tensor summary figure (shown at stops). Jay Patton improved several of the figures as he compiled this guidebook. And finally, much thanks to Susan McPherson for her helpful comments, typing and editing that indeed improved this paper.

REFERENCES CITED

- (1) Atwater, T., Implications of plate tectonics for the Cenozoic tectonic evolution of western North America, Geological Society of America, vol. 81, pp. 3513-3536, 1970.
- (2) Atwater, T., J. Stock, Pacific-North America Plate Tectonics of the Neogene southwestern United States: An Update In: International Geology Review, vol. 40, pp. 375-402, 1998.
- (3) Dickinson, W.R., W.S. Snyder, Geometry of subducted slabs related to the San Andreas transform, Journal of Geology, vol. 87, pp. 609-627, 1979.
- (5) Dickinson, W., W. Snyder, Geometry of triple junctions related to the San Andreas transform, Journal of Geophysical Research, vol. 84, pp. 561-572, 1979.
- (6) Dickinson, W., Overview: Tectonic Implications of Cenozoic Volcanism in Coastal California. GSA Bulletin, vol. 109, no. 8, pp. 936-954, 1997.
- (7) McPherson, R. C., Seismicity and stress at the southern end of the Cascadia Subduction Zone, (in field trip guide book): Tulsa, Oklahoma, American Association of Petroleum Geologists-SEPM, pp. 19-28, 1992.
- (8) McPherson, R.C., Seismicity and Focal Mechanisms near Cape Mendocino, northern California: 1974-84, M.S. Thesis, Humboldt State University, pp. 1-74, 21 figures, 2 plates, 1989.
- (9) Godfrey, N., A. Meltzer, S. Klemperer, A. Trehu, B. Leitner, S. H. Clarke, A. Ondrus, Evolution of the Gorda Escarpment, San Andreas fault and Mendocino triple junction from multichannel seismic data collected across the northern Vizcaino Block, offshore northern California, Journal of Geophysical Research, vol. 103, pp. 23813-825, 1998.
- (10) Wallace, R., The San Andreas Fault system, California, USGS Geological Survey Professional Paper 1515, 283 pages, 1990.
- (11) Castillo D., W. Elsworth, Seismotectonics of the San Andreas Fault system between Point Arena and Cape Mendocino in northern California: implication for the development and evolution of a young transform, Journal of Geophysical Review, vol. 98, pp. 6543-6560, 1993.
- (12) Freymueller, J., M. Murrar, P. Segall, D. Castillo, Kinematics of the Pacific-North American plate boundary zone, northern California, Journal of Geophysical Research, vol. 104, pp. 7419-7441, 1999.
- (13) Furlong, K., S. Schwartz, Influence of the Mendocino Triple Junction on the tectonics of coastal California, Annual Review of Earth Planet Science vol. 32, pp. 403-433, 2004.
- (14) Furlong K, R. Govers, Ephemeral crustal thickening at the triple junction: The Mendocino crustal conveyor , Geology, vol. 27, no. 2, pp. 127-30, Feb., 1999.
- (15) Cockerham, R. W., S. W. Smith, R. C. McPherson, S. H. Clarke, Jr., Earthquake Epicenter and Selected Fault Plane Solutions of Northern California Margin, California Continental Margin Map Series, Map No. 7B, California Division of Mines and Geology, 1989.
- (16) Knapp, J., Seismicity, Crustal structure and tectonics near the northern termination of the San Andreas Fault, Ph.D. Thesis, University of Washington, 1982.
- (17) Smith, S.W., J.S. Knapp, R.C. McPherson, Seismicity of the Gorda Plate, Structure of the Continental Margin, and Eastward Jump of the Mendocino Triple Junction, Journal of Geophysical Research, vol. 98, B5, pp. 8153-8171, 1993.
- (18) Smith, S.W., R.C. McPherson, N. Severy, Breakup of the Gorda Plate, Earthquake Notes, vol. 52, p. 42, 1981.
- (19) Cockerham, R., Evidence for a 180km long subducted slab beneath northern California, Bulletin of the Seismological Society of America, vol. 74, pp. 569-576, 1984.
- (20) Jachens, R., A. Griscorn, Three-dimensional geometry of the Gorda plate beneath northern California, Journal of Geophysical Research, vol. 88, pp. 9375-9392, 1983.
- (21) Verdonck, D., G. Zandt, Three-dimensional crustal structure of the Mendocino Triple Junction Region from Local Earthquake Travel Times, Journal of Geophysical Research, vol. 99, B12, pp. 23843-23857, 1994.

- (22) Dengler, L., G. Carver, R. C. McPherson, Sources of north coast seismicity, *California Geology*, vol. 45, pp. 40-53, 1992.
- (23) Denlinger, R., A model for large-scale plastic yield of the Gorda Deformation zone, *Journal of Geophysical Research*, vol. 97, pp. 15415-15423, 1992.
- (24) Riddihough, R., Gorda Plate motions from magnetic anomaly analysis, *Earth and Planetary Science Letters*, vol. 51, pp. 163-170, 1980.
- (25) Riddihough, R., Recent movements of the Juan de Fuca Systems, *Journal of Geophysical Research*, vol. 89, pp. 6980-6994, 1984.
- (26) Silver, Eli, Tectonics of the Mendocino Triple Junction, *Geological Society of America*, vol. 82, pp. 2965-2978, 1971.
- (27) Chaytor, J., C. Goldfinger, R. Dziak, C. Fox, Active deformation of the Gorda Plate: Constraining deformation models with new geophysical data, *Geology*, vol. 34, pp. 353-356, 2004.
- (28) Dziak, R., C. Fox, A. Bobbitt, C. Goldfinger, Bathymetric Map of the Gorda Plate: Structural and Geomorphological Processes inferred from Multibeam Surveys, *Marine Geophysical Researches*, vol. 22, pp. 235-250, 2001.
- (29) Gulick, S., A. Meltzer, T. Henstock, A. Levander, Internal Deformation of the southern end of the Gorda Plate: Fragmentation of a weak plate near the Mendocino Triple junction, *Geology*, vol. 29, pp. 691-694, 2001.
- (30) Stoddard, P., A kinematic model for the evolution of the Gorda plate, *Journal of Geophysical Research*, vol. 92, pp. 11524-11532, 1987.
- (31) Stoddard, P., M. Woods, Master event relocation of Gorda block earthquakes: Implication for deformation, *Geophysical Research Letters*, vol. 17, pp. 961-964, 1990.
- (32) Stoddard, P., A comparison of brittle deformation models for the Gorda plate, *Tectonophysics*, vol. 187, pp. 205-214, 1991.
- (33) Wilson, D., A kinematic model for the Gorda deformation zone as a diffuse southern boundary of the Juan de Fuca plate, *Journal of Geophysical Research*, vol. 91, pp. 10259-10269, 1986.
- (34) Wilson, D., Deformation of the so-called Gorda plate, *Journal of Geophysical Research*, vol. 94, pp. 3065-3075, 1989.
- (35) Wilson, D., Confidence intervals for motion and deformation of the Juan de Fuca Plate, *Journal of Geophysical Research*, vol. 98, pp. 16053-16071, 1993.
- (36) Beaudoin, B.C., M. Magee, H. Benz, Crustal Velocity Structure North of the Mendocino Triple Junction, *Geophysical Research Letters*, vol. 21, pp. 2319-2322, 1994.
- (37) Beaudoin, B.C., N.J. Godfrey, S.L. Klemperer, C. Lendl, A.M. Trehu, T.J. Henstock, A. Levander, J.E. Holl, A.S. Meltzer, J.H. Luetgert, W.D. Mooney, Transition from Slab to Slabless: Results from the 1993 Mendocino Triple Junction Seismic Experiment, *Geology*, vol. 24, no. 3, pp. 195-199, 1996.
- (38) Benz, H. M., G. Zandt, Teleseismic Tomography: Lithospheric Structure of the San Andreas Fault System in North and Central California. In: *Seismic Tomography, Theory and Practice*. Edited by H.M. Iyer and K. Hirahara, Chapman & Hall, pp. 440-465, 1993.
- (39) Benz, H. M., G. Zandt, D.H. Oppenheimer, Lithospheric Structure of Northern California From Teleseismic Images of the Upper Mantle, *Journal of Geophysical Research*, vol. 97, B4, pp. 4791-4807, 1992.
- (40) Helferty, M., J. Booker, B. Weertman, D. Auld, Detection of the southern edge of the Gorda plate by geomagnetic induction, *Abstract, EOS*, vol. 67, no. 44, p.125, 1986.
- (41) Hole, J.A., B.C. Beaudoin, S.L. Klemperer, Vertical Extent of the newborn San Andreas Fault at the Mendocino Triple Junction, *Geology*, vol. 28, no. 12, pp. 1111-1114, 2000.
- (42) Simila, G., Azimuthal variations of teleseismic p-wave residuals for northern California, *Journal of Geophysical Research*, vol. 92, pp. 383-392, 1987.
- (43) Dehlinger, P., B. Bolt, Seismic parameters along the Bartlett Springs Fault zone in the coast ranges of northern California, *Bulletin of the Seismological Society of America*, vol. 75, pp. 1785-1798, 1984.
- (44) Murray, Mark, M. Lisowski, Strain accumulation along the Cascadia subduction zone, *Geophysical Research Letters*, vol. 27, pp. 3631-3634, 2000.
- (45) Flueck, P., R. Hyndman, K. Wang, Three dimensional dislocation model for great earthquakes of the Cascadia subduction zone, *Journal of Geophysical Research*, vol. 102, pp. 20539-20550, 1997.
- (46) Eaton, J., Distribution of aftershocks of the November 8, 1980 Eureka earthquake, *Earthquake Notes*, vol. 52, pp. 44-45, 1981.
- (47) Seeber, L., M. Barazangi, A. Nowroozi, Microearthquake seismicity and tectonics of coastal northern California, *Bulletin of the Seismological Society of America*, vol. 60, pp. 1669-1699, 1970.
- (48) Simila, G., W. Peppin, T. McEvelly, Seismotectonic of the Cape Mendocino, California, area, *Geological Society of America*, vol 86, pp. 1399-1406, 1975.
- (49) McPherson, R. C., Focal Mechanisms and Seismicity at the Southern End of the Cascadia Subduction Zone, *Geological Society of America Abstracts*, vol. 21, p. 116, 1989.

- (50) McPherson, R. C., Seismicity and Focal Mechanisms Near the Southern End of the Cascadia Subduction Zone, *Seismological Research Letters*, vol. 60, No. 1, p. 7, January-March, Vancouver, British Columbia, 1989.
- (51) McPherson, R.C., Focal mechanisms and seismicity at the southern end of the Cascadia subduction zone, *GSA program and Abstracts*, Spokane, p. 66, 1989.
- (52) Bakum W., Seismicity of California's North Coast, vol. 90, no. 4, pp. 797-812, August, 2000.
- (53) We will show a poster of moment tensors from the Berkeley Seismographic Station. The moment tensor catalogue can be viewed by year at www.seismo.berkeley.edu.
- (54) Tanioka, Y., K. Satake, L. Ruff, Seismotectonics of the April 25, 1992, Petrolia earthquake and the Mendocino Triple Junction region, *Tectonics*, vol. 14, pp. 1095-1103, Oct 1995.
- (55) Clarke, S., G. Carver, Late Holocene tectonics and paleoseismicity, southern Cascadia subduction zone, *Science*, vol. 255, pp. 188-92, 1992.
- (56) Clarke, S., Geology of the Eel River basin and adjacent region: Implication for late Cenozoic tectonics of the Cascadia subduction zone and the Mendocino triple junction, *Bulletin of AAPG*, vol. 76, no. 2, pp. 199-224, 1992.
- (57) Gulick, S., A. Meltzer, S. Clarke, Effects of the northward-migrating MTJ on the Eel River forearc basin, California: Stratigraphic development, *GSA Bulletin*, vol. 114, no. 2, pp. 178-191, Feb., 2002.
- (58) Kelsey, H., G. Carver, Late Neogene and Quaternary tectonics associated with the northward growth of the San Andreas transform fault, Northern California, *Journal of Geophysical Research*, vol. 93, pp. 4797-4819, 1988.
- (59) Williams, T., The geodetic signature of modern deformation (1993-2001) within the southern Cascadia margin, northwestern California, Master Thesis, Humboldt State University, 2002.
- (60) Prentice, C., D. Merritts, E. Buetner, P. Bodin, A. Schill, J. Muller, Northern San Andreas fault near Shelter Cove, California, *Geological Society of America*, vol. 111, pp. 512-523, 1999.
- (61) McPherson, R., L. Dengler, The Honeydew Earthquake, August 17, 1991, *California Geology*, vol. 45, No. 2, pp. 31-39, March/April, 1992.
- (62) Merritts, D., The Mendocino triple junction: Active faults, episodic coastal emergence, and rapid uplift, *Journal of Geophysical review*, vol. 101, pp. 6051-6070, 1996.
- (63) Dengler, L, K. Moley, R. McPherson, M. Pasyanos, J. Dewey, M. Murray, The September 1, 1994 Mendocino Fault Earthquake, *California Geology*, pp. 43-53, March -April, 1995.
- (64) Goldfinger, C., H. Nelson, J. Johnson, Holocene Earthquake Records from the Cascadia Subduction Zone and Northern San Andreas Fault Based on Precise Dating of Offshore Turbidites, *Annual Review Earth and Planetary Sciences*, vol. 31, pp. 555-577, 2003.

GPS-derived strain in northwestern California: termination of the San Andreas fault system and convergence of the Sierra Nevada-Great Valley block contribute to southern Cascadia forearc contraction

Todd B. Williams

UNAVCO, Inc., Plate Boundary Observatory, 1440 Regatta Blvd, Richmond, CA 94804 williams@unavco.org,
fax: 510 215 8105

Harvey M. Kelsey

Dept. of Geology, Humboldt State University, Arcata, CA 95521, hmk1@humboldt.edu, fax: 707 826 5241

Jeffrey T. Freymueller

Geophysical Institute, University of Alaska, Fairbanks, AK 99775, jeff@giseis.alaska.edu, fax: 907 474 5618

ABSTRACT

GPS-derived velocities (1993-2002) in northwestern California show that processes other than subduction are in part accountable for observed upper-plate contraction north of the Mendocino triple junction (MTJ) region. After removing the component of elastic strain accumulation due to the Cascadia subduction zone from the station velocities, two additional processes account for accumulated strain in northern California. The first is the westward convergence of the Sierra Nevada-Great Valley (SNGV) block toward the coast and the second is the north-northwest impingement of the San Andreas fault system from the south on the northern California coastal region in the vicinity of Humboldt Bay. Sierra Nevada-Great Valley block motion is northwest toward the coast, convergent with the more northerly, north-northwest San Andreas transform-fault-parallel motion. In addition to the westward converging Sierra Nevada-Great Valley block, San Andreas transform-parallel shortening also occurs in the Humboldt Bay region. Approximately 22 mm/yr of distributed Pacific-SNGV motion is observed inland of Cape Mendocino across the northern projections of the Maacama and Bartlett Springs fault zones but station velocities decrease rapidly north of Cape Mendocino. The resultant 6-10 mm/yr of San Andreas fault-parallel shortening occurs above the southern edge of the subducted Gorda plate and at the latitude of Humboldt Bay. Part of the San Andreas fault-parallel shortening may be due to the viscous coupling of the southern edge of the Gorda plate to overlying North American plate. We conclude that significant portions of the upper-plate contraction observed north of the MTJ region are not solely a result of subduction of the Gorda plate, but also a consequence of impingement of the western edge of the Sierra Nevada-Great Valley block and growth of the northernmost segments of the San Andreas fault system.

Keywords: GPS geodesy, Cascadia subduction zone, Sierra Nevada-Great Valley block, San Andreas fault zone

1. INTRODUCTION

Despite evidence for late Quaternary slip on active upper plate faults at the southern Cascadia margin (Kelsey and Carver, 1988; Clarke and Carver, 1992), only a few studies have attempted to measure present-day deformation rates in this region (Lisowski et al., 1991; Snay and Matsikari, 1991; Murray et al. 1996; Murray and Lisowski, 2000). The purpose of this study is to provide, through repeated periodic Global Positioning System (GPS) surveys, an image of recent deformation (1993-2002) occurring near the Mendocino triple junction (MTJ), the southern Cascadia subduction zone (CSZ), and the northern end of the San Andreas fault (SAF) system, a region encompassed within the Mendocino deformation zone (MDZ; Figure 1). We use contemporary GPS velocities to characterize the nature of interaction of Pacific-North America (P-NA) plate boundary deformation with the southern CSZ, and the pattern of distributed deformation of the northern California P-NA plate boundary. We use dislocation modeling based on contemporary GPS velocities to approximate how shear strain is partitioned among faults at the northern termination of the San Andreas transform system.

GPS velocities are derived from the combination of 1999-2002 observations with initial observations at benchmarks of the California High Precision Geodetic Network (HPGN) established in 1991 by the California Department of Transportation (CalTrans) and the National Geodetic Survey (NGS). Observations utilized in solutions include those of CalTrans (1993, 1994, 1998), NGS (1994, 1998), Freymueller et al. (1999), Poland et al. (1999), and J. Svarc, (U.S. Geological Survey (USGS), Menlo Park, written comm., 2001). GPS-derived

velocity solutions (1993-2002) utilize 66 sites (Table 1) and are presented with respect to a fixed North American plate reference frame (Sella et al., 2002). All sites in Table 1 span at least two years from initial to final measurement and most sites span at least 8 years from initial to final measurement.

Previous USGS geodolite and GPS baseline measurements indicate a transition from ~ 25 mm/yr of right-lateral shear south of Cape Mendocino to ~ 15 mm/yr of northeast directed uniaxial contraction north of Cape Mendocino (Murray et al., 1996; Murray and Lisowski, 2000). The USGS has determined coseismic surface displacements from GPS measurements that span the 1992 M_s 7.1 Petrolia, CA earthquake (Oppenheimer et al., 1993; Murray et al., 1996) as well as the offshore 1994 M_w 7.0 Mendocino fault earthquake (Dengler et al., 1995). The USGS Mendocino GPS network spans the MTJ region and is complementary to this study (<http://quake.wr.usgs.gov/research/deformation/gps/auto/Mendocino/>).

2. DATA ANALYSIS

GPS phase and pseudorange data were processed using the GIPSY/OASIS II software (Zumberge et al., 1997) following procedures of Freymueller et al. (1999; 2000). For pre-1995 data, global solutions were used to estimate satellite orbits, station coordinates, and nuisance parameters including phase ambiguities and tropospheric path delays. Pre-1995 solutions are those of Freymueller et al. (1999), which are reprocessed to add newly available data. Post-1995 solutions use the Jet Propulsion Laboratory non-fiducial orbits (Zumberge et al., 1997), and include a subset of the available continuous stations that span NA.

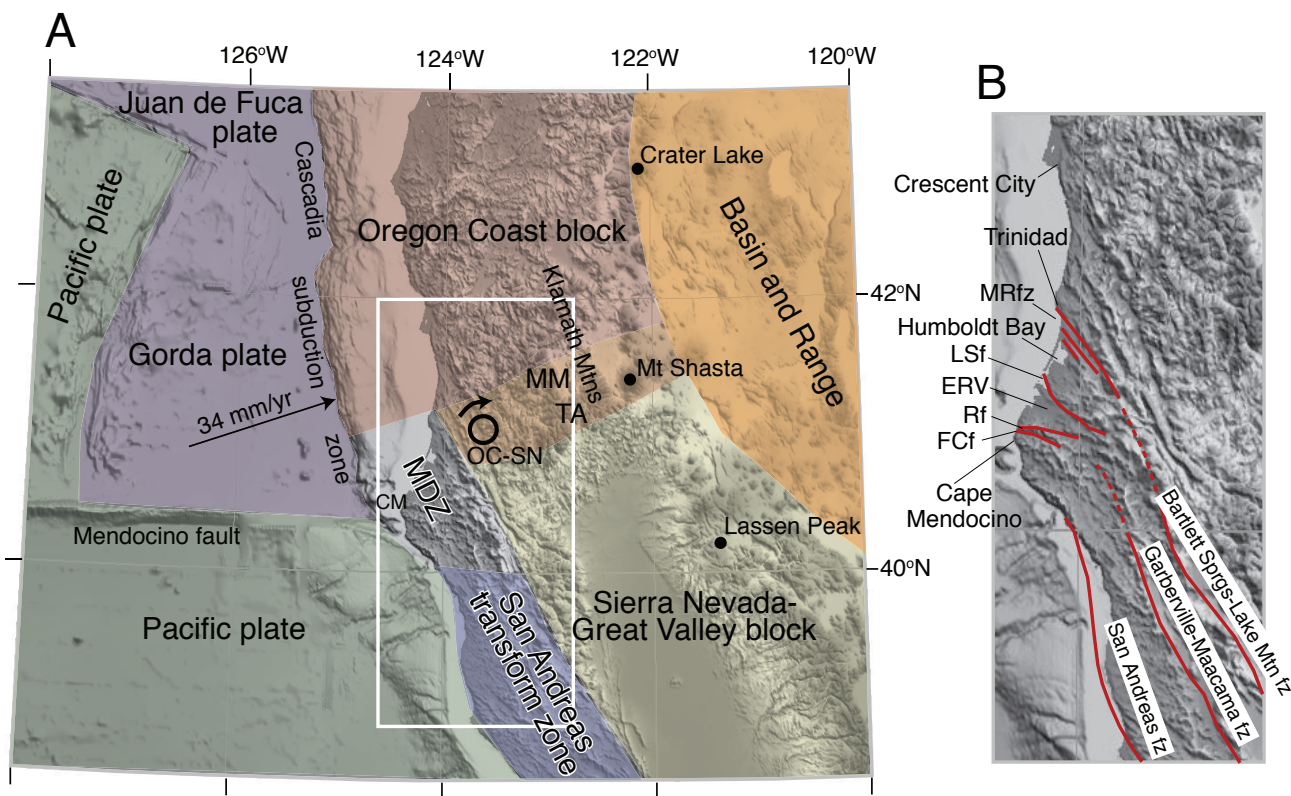


Figure 1. A. Plate and block model for region surrounding the Mendocino deformation zone (MDZ). Boundaries of blocks and plates taken after Wells et al. (1998) and Wang et al. (2003). OC-SN, pole of rotation between Oregon Coast block and Sierra Nevada-Great Valley block after Wang et al. (2003). MM, Marble Mountains; TA, Trinity Alps. The region of distinct shading that includes MM, TA and the OC-SN pole is the diffuse boundary zone between the Oregon Coast block and the Sierra Nevada-Great Valley block. The three volcanic centers (Lassen, Shasta, Crater Lake) delineate the approximate location and trend of the Cascade volcanic arc. CM, Cape Mendocino. B. Map of northernmost coastal California showing the major fault zones and localities discussed in the text. Locations of faults from Kelsey and Carver (1988). MRfz, Mad River fault zone; LSF, Little Salmon fault; ERV, Eel River valley; Rf, Russ fault; FCf, False Cape fault.

Solutions are transformed into the International Terrestrial Reference Frame (ITRF97) (Boucher et al., 1999) evaluated at the epoch of the solution. Each solution contains continuous stations with precise positions and velocities in the ITRF. Each such station is weighted in the estimation of the daily reference frame transformation by the combined uncertainty of its ITRF position and the daily solution. After transformation, three-dimensional root mean square position agreement with ITRF97 is typically ~ 6 mm. The transformed solutions are used to derive velocities of each station in the ITRF97 frame. Observed coseismic displacements of the 1994 Mendocino fault earthquake sequence (Dengler et al., 1995; M.H. Murray, 2000, written communication) were used to interpolate displacement values for HPGN stations without immediate post-earthquake surveys (Williams, 2002). Displacements were then used to correct pre-earthquake surveys used in the velocity solution.

Velocities relative to NA use a global GPS-only defined plate model, REVEL-2000 (Sella et al., 2002), which gives the motion of the plates in ITRF97. Average station velocity uncertainties are ~ 2 mm/yr, including the uncertainty in defining the North American frame.

3. OBSERVATIONS

Northern California GPS station velocities are characteristic of a broadly deforming plate boundary zone (Fig. 2A; Table 1). The northern Sierra Nevada-Great Valley (SNGV) sites are moving 10.8 ± 0.5 mm/yr northwest (QUIN and SUTB; Fig. 2A), consistent with other GPS solutions that span larger portions of the northern SNGV region (10.7 ± 0.4 mm/yr; Prescott et al., 2001). These two northern SNGV sites move northwest ~ 3 mm/yr more slowly than the rigid block motion model prediction of Dixon et al. (2000), however, the majority of the sites used by Dixon et al. (2000) are located in the southern part of the SNGV block. Sites in the eastern Klamath Mountains (7.1 ± 1.1 mm/yr) and the southernmost western Cascade volcanic arc (9.7 ± 1.9 mm/yr) display northwest-directed motion, and sites further north move due north (Fig. 2A and Fig. 3A).

North of Cape Mendocino, inland stations converge upon coastal stations (Fig. 3A). Inland stations as close as ~ 50 km to the coast are moving ~ 10 - 12 mm/yr to the northwest, sub-parallel to northern SNGV block motion. The region separating inland northwest-directed velocities from coastal northeast-directed velocities marks the boundary between subduction dominated interseismic strain at the coast and translational strain of the interior southern Klamath Mountains, where the Klamath Mountains (Fig. 1) are at the northwest end of the P-NA velocity field (Miller et al., 2001; Wells et al., 2001). Inland and north of Cape Mendocino, the Mad River fault zone (MRfz, Figs. 1 and 4) and the Lake Mountain fault zone (BS/LMfz, Figs. 1 and 4) occur at the western edges of the Klamath Mountains and SNGV blocks, respectively.

Stations at and near Cape Mendocino are uniformly moving $\sim N 10^\circ W$ (sub-parallel to the trend of the southern CSZ trench), whereas coastal stations north of Trinidad, CA (TRND) are uniformly moving $\sim N 20$ - $30^\circ E$ (sub-parallel to Gorda-NA convergence)(Fig. 3A). Northeast directed station velocities north of Cape Mendocino (CME1; 31.1 ± 0.5 mm/yr) decrease rapidly northward to 17.2 ± 0.6 mm/yr at Trinidad (TRND) and 12.1 ± 0.6 mm/yr at Crescent City, CA (PTSG)(Fig. 3A).

Station velocities inland of Cape Mendocino increase westward across the northernmost SAF system (0106 to CME1; Fig. 3A). Distributed relative motion of 22.0 ± 1.1 mm/yr occurs inland from Cape Mendocino across an ~ 80 km-wide region (Fig. 3A). This is approximately half the Pacific-SNGV relative plate motion observed in the coast ranges ~ 120 km south of Cape Mendocino (40 - 41 mm/yr; Freymueller et al., 1999).

4. Correction for the Locked Subduction Zone

Strain resulting from the locked CSZ offshore contributes a component of the velocity field for all sites near the coast. This elastic deformation produces contraction in the direction of relative motion between the subducting plate and overriding plate. Sites near the coast move most rapidly in the direction of relative plate motion, with sites far inland being unaffected. Additional complexities result if there are significant along-strike variations in

Table 1. GPS station velocities relative to a fixed North American plate

Station ID	Longitude (°W)	Latitude (°N)	East velocity (cm/yr)	North velocity (cm/yr)	Sigma E (cm/yr)	Sigma N (cm/yr)	Correlation, east–north
0104	123.2010	39.7954	−1.19	0.86	0.07	0.05	−0.2025
0105	123.8352	39.7769	−2.44	2.66	0.07	0.05	−0.2321
0106	123.5235	40.4602	−0.62	0.85	0.08	0.05	−0.2539
0108	123.4935	40.8153	−0.42	0.91	0.09	0.07	−0.2877
0109	124.1174	40.9750	0.36	1.56	0.10	0.07	−0.3057
0110	123.4759	41.4002	−0.29	0.82	0.17	0.12	0.0245
0113	124.1584	41.9325	0.26	1.07	0.30	0.20	−0.3939
0201	123.1930	41.8415	−0.16	0.99	0.22	0.17	0.1056
0202	122.5913	41.9558	−0.26	0.47	0.26	0.20	0.2065
0208	122.2750	41.5321	−0.20	0.62	0.17	0.11	−0.2194
0212	122.4349	40.9571	−0.74	0.56	0.34	0.15	−0.2760
0217	122.9419	40.6521	−0.63	0.74	0.09	0.07	−0.0859
0220	120.3665	40.7992	−0.44	0.45	0.18	0.09	−0.0423
0221	122.9364	40.3696	−0.82	0.62	0.09	0.06	−0.0755
0226	119.9944	40.2450	−0.53	0.53	0.17	0.09	−0.0467
0229	122.5768	40.6476	−1.13	0.48	0.26	0.17	−0.3554
0411	123.0381	38.3240	−2.00	3.17	0.18	0.11	−0.0852
0412	122.4068	38.4411	−1.01	1.53	0.16	0.09	0.0787
0413	123.4008	38.6533	−2.47	3.41	0.12	0.07	−0.0568
0414	122.8121	38.6709	−1.15	2.33	0.14	0.08	−0.0395
1005	120.2667	37.9972	−1.06	0.35	0.28	0.11	−0.0966
1402	123.9852	40.8876	0.23	1.33	0.24	0.13	−0.2162
1436	123.7905	39.6691	−2.08	2.67	0.31	0.12	0.0590
1468	124.1557	40.4481	−0.66	2.47	0.16	0.07	0.0184
8767	124.2176	40.7669	0.60	1.94	0.14	0.09	−0.1297
9750	124.1815	41.7484	0.11	1.01	0.20	0.13	−0.1112
01KD	123.7945	40.0942	−1.59	2.03	0.19	0.08	0.0472
01LD	123.8316	40.2508	−1.26	1.77	0.19	0.08	0.0528
01MC	123.9211	40.3225	−1.09	1.94	0.20	0.08	0.1092
01NC	124.0330	40.4396	−0.53	2.07	0.20	0.09	0.0300
01ND	123.7974	40.4721	−0.28	1.57	0.22	0.16	0.1096
01NE	123.6751	40.4390	−0.80	1.41	0.18	0.06	0.0722
01PA	124.2556	40.5890	0.00	2.18	0.15	0.09	0.0087
01PB	124.2034	40.6393	0.29	1.95	0.28	0.15	−0.3681
01QB	124.1994	40.7447	0.03	1.91	0.26	0.14	−0.3290
01QF	123.3251	40.8145	−0.41	0.57	0.16	0.09	−0.1372
01RB	124.0874	40.9065	0.15	1.59	0.23	0.14	−0.0694
01RD	123.7724	40.8964	−0.50	0.98	0.14	0.07	−0.2192
01RE	123.6225	40.9439	−0.60	0.99	0.12	0.07	−0.1262
ALEN	124.0951	41.1917	0.40	1.17	0.16	0.11	0.1622
ALGO	78.0714	45.9558	−0.04	0.03	0.05	0.03	0.0544
ANDE	122.2906	40.4195	−1.05	0.74	0.21	0.14	−0.0411
BLDK	123.8654	40.8820	−0.34	1.37	0.13	0.08	−0.0053
BRR2	124.2945	40.4977	−0.68	2.58	0.26	0.08	0.0296
CABL	124.5633	42.8361	0.71	1.33	0.04	0.03	−0.0262
CME1	124.3963	40.4418	−0.61	3.05	0.04	0.03	0.0090
GOL2	116.8893	35.4252	−0.72	0.58	0.04	0.03	0.0423
GOLD	116.8893	35.4252	−0.68	0.57	0.04	0.03	0.0405
GREN	122.5259	41.5550	−0.32	0.36	0.17	0.12	−0.0715
HATC	121.4713	40.8177	−0.63	0.46	0.14	0.10	−0.3177
HOPB	123.0747	38.9952	−1.82	2.11	0.04	0.03	0.0237
KNEE	123.9748	40.7266	0.13	1.44	0.12	0.08	−0.5126
MUMB	122.5326	41.1844	−0.47	0.65	0.07	0.05	−0.0119
NEW2	117.5089	39.6856	−0.20	0.06	0.04	0.04	0.0107
NLIB	91.5749	41.7716	−0.03	0.06	0.04	0.03	0.0270
PENT	119.6250	49.3226	0.20	0.03	0.04	0.04	−0.0872

(continued on next page)

plate coupling near the MTJ where the subduction zone ends. The exact contribution of the locked subduction zone to the velocity field depends on the orientation of plate convergence between the downgoing plate and forearc, the width of the locked zone, and the width of the transition zone from fully locked to fully creeping at the base of the locked zone.

Table 1 (continued)

Station ID	Longitude (°W)	Latitude (°N)	East velocity (cm/yr)	North velocity (cm/yr)	Sigma E (cm/yr)	Sigma N (cm/yr)	Correlation, east-north
PILG	121.9819	41.2597	-0.68	0.57	0.17	0.11	0.0185
PTRB	123.0187	37.9962	-2.40	3.56	0.07	0.05	0.0234
PTSG	124.2552	41.7827	0.40	1.14	0.05	0.04	-0.0050
QUIN	120.9444	39.9746	-0.76	0.69	0.04	0.03	0.0064
SAGE	120.0388	39.7909	-0.59	0.27	0.13	0.09	-0.0713
SHIN	120.2250	40.5917	-0.46	0.42	0.04	0.03	0.00321
SHLD	119.0157	41.8684	-0.27	0.21	0.04	0.04	-0.0063
SUTB	121.8206	39.2058	-0.95	0.66	0.04	0.03	0.0205
TRND	124.1509	41.0539	0.52	1.64	0.05	0.04	0.0017
YBHB	122.7107	41.7317	-0.12	0.65	0.04	0.03	-0.0152

To evaluate other tectonic signals independently from subduction, we use a dislocation model modified from Flück et al. (1997) to calculate, and then remove, the component of interseismic strain caused by the locked CSZ. The dislocation model incorporates a fully locked zone 50 km wide and a transition zone from locked to creeping of the same width (Flück et al., 1997). For comparison, an earlier model developed by Verdonck (1995) utilized a locked zone of 75 km and a transition zone of 125 km. The plate convergence rate and direction depends on the assumed motion of the forearc relative to North America (e.g., Wang et al., 2003).

Because the transition between the SNGV block in the south and the Oregon Coast forearc block in the north occurs near the Mendocino deformation zone (Fig. 1), the appropriate convergence rate and direction may vary from south to north across the study area. Miller et al. (2001) derived a Juan de Fuca-North America pole of rotation by combining the DeMets and Dixon (1999) Pacific-North America pole with the alternate Pacific-Juan de Fuca pole of Wilson (1993). Wells and Simpson (2001) determined a new Juan de Fuca-Oregon Coast forearc pole (also reported in Wang et al. (2003)), which included the motion of the Oregon Coast relative to North America. In the southernmost part of the study area, the Juan de Fuca-Sierra Nevada relative motion may be more appropriate to drive the dislocation model, but the Juan de Fuca-Sierra Nevada relative velocity near Cape Mendocino is almost identical to the Juan de Fuca-Oregon Coast velocity (SNGV-Oregon Coast relative velocity is no more than ~10% of the subducting plate velocity at this location).

The Wells and Simpson (2001) pole predicts a relative convergence rate of 34 mm/yr toward 72° in our study area (Fig. 1). This convergence vector results in a maximum model site velocity of 17 mm/yr at Cape Mendocino. Farther north, velocities along the coast are ~10 mm/yr, with the change resulting from the fact that at Cape Mendocino the land protrudes farther west and thus closer to the trench than the northernmost California coastline. Model velocities drop off smoothly but rapidly with distance from the coast, reaching 1-2 mm/yr at the Great Valley or Mt. Shasta area.

The residual velocities (Figs. 2B and 3B), computed by subtracting the modeled interseismic velocities from the observed velocities, represent permanent deformation of the overriding plate and include deformation from upper plate faults, the SAF system and the influence of the SNGV block, as well as errors in the subduction model and measurement error. Residual velocities far inland are the same as the observed GPS velocities (Figs. 3A vs. 3B) because far field stations are unaffected by interseismic strain above the locked subduction zone. Rates of deformation discussed in the following sections are derived from the residual velocity field, which has removed the influence of the southern CSZ.

The main uncertainty in the subduction correction results from possible variations in the width of the locked and transition zones. We use widths estimated from thermal models and extrapolated from elsewhere in Cascadia (Flück et al., 1997; Wang et al., 2003), but along-strike variations in this width are reported both in Cascadia (e.g., McCaffrey, 2002) and elsewhere (e.g., Zweck et al., 2002). The distribution of slip in the transition zone can also have a measurable impact on the model vectors (Wang et al., 2003). In addition, repeated slow slip events (ETS, Episodic Tremor and Slip) have been identified along the southern Cascadia margin (at site YBHB, Fig. 2) (Szeliga et al., 2004). These events show that the width of these zones is not constant in time. Our site velocities

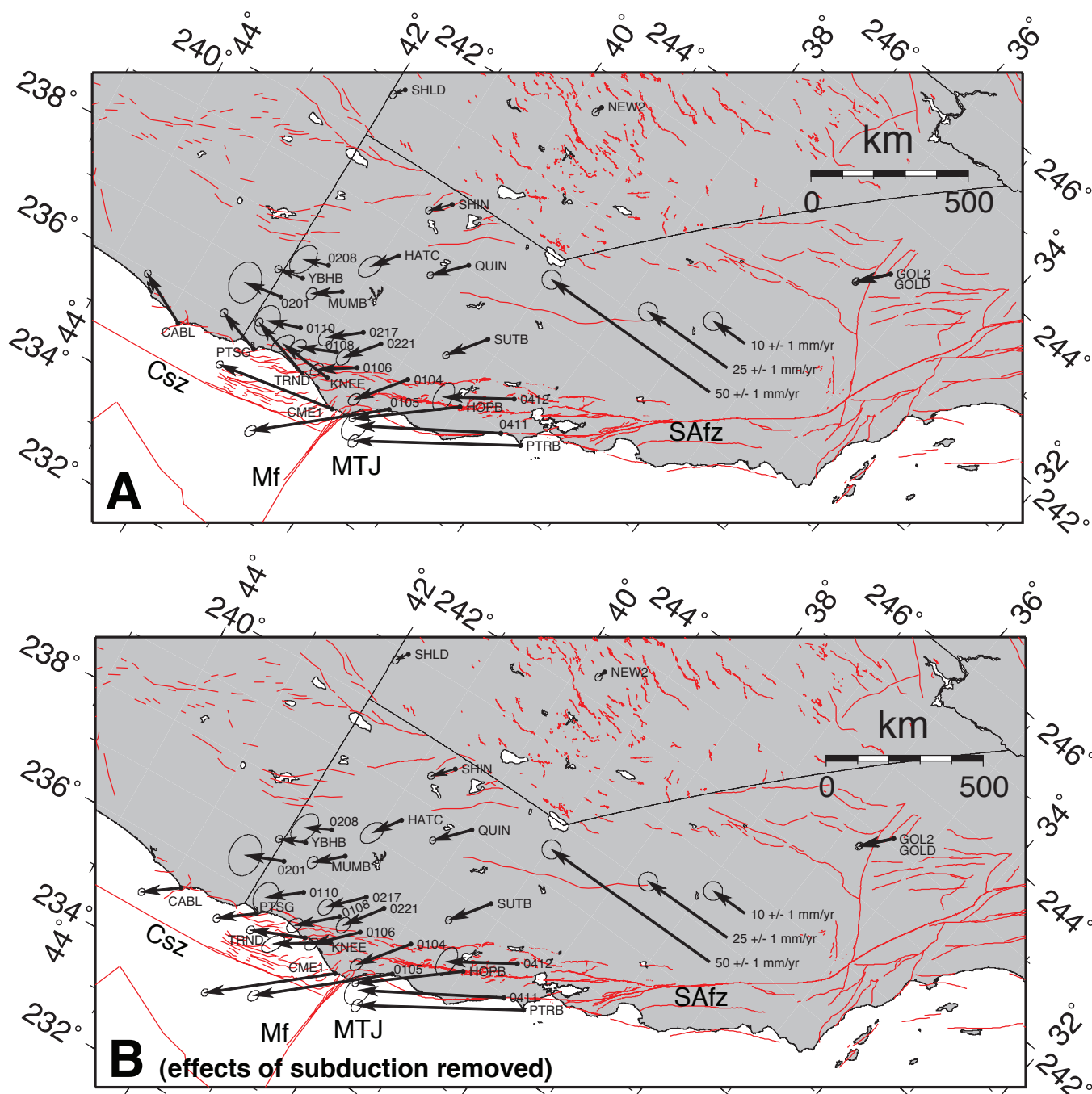


Figure 2. A. Oblique Mercator projection about a pole of rotation determined for observed P-NA relative plate motion (Sella et al., 2002) with base of figure parallel to P-NA relative motion. GPS station velocities (1993-2002) are shown relative to the NA plate (Sella et al., 2002). Uncertainty ellipses at velocity vector tips show 2-sigma (95%) confidence regions. Red lines are mapped faults (Jennings, 1994). Mf, Mendocino fault; MTJ, Mendocino triple junction; SAfz, San Andreas fault zone; Csz, Cascadia subduction zone. B. Residual velocities after subtracting the modeled interseismic strain accumulation on the southern Csz.

are all averaged over a few years to a decade, or several cycles of ETS. The appropriate locked and transition zone width in this case represent the part of the subduction interface that remains fully or partially locked even in the ETS events.

We ran models using a wider or narrower locked zone, in order to evaluate the potential impact on the residual velocities from errors in the assumed subduction model. In general, the model corrections will be smaller if the

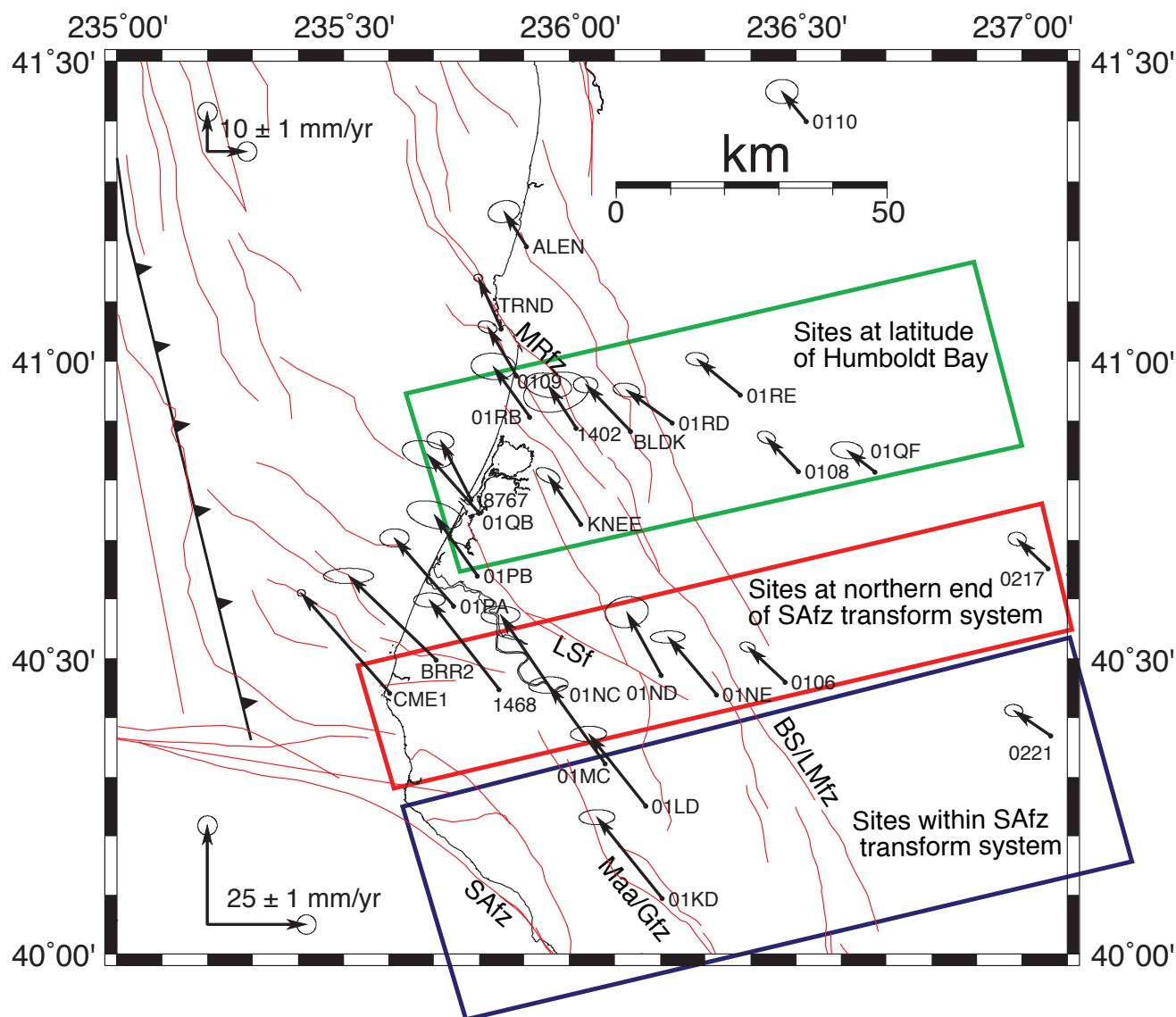


Figure 4. Distributed deformation related to northward migration of the Mendocino triple junction, based on GPS residual velocities (velocities with subduction signal removed). Red lines are mapped faults (Jennings, 1994). Barbed fault represents southern Cascadia subduction zone. The three rectangles (green, red and blue) enclose the green, red and blue GPS stations depicted on the profiles in Figure 5. LSf, Little Salmon fault; MRfz, Mad River fault zone; SAFz, San Andreas fault zone; Maa/Gfz, Maacama/Garberville fault zone; BS/Lmfz, Bartlett Springs/Lake Mountain fault zone.

blocks. This boundary zone may be diffuse (Fig. 1), but relative motions are too small and GPS sites too sparse at this point to resolve whether one or several active faults takes up the difference in forearc block motions between the OC and SNGV blocks.

5.2. Cape Mendocino and the northern San Andreas fault system

In northern California, residual velocities are sub-parallel to the SAF system and related SNGV block motion, reflecting the influence of the P-NA plate boundary on the southern CSZ (Fig. 2B). Slivers of crust between the faults of the northern SAF system move in a right-lateral sense relative to the SNGV block at least as far as Cape Mendocino (0411, HOPB, 0412; Fig. 2B). Continuous station CME1 located above Cape Mendocino is moving 33.8 ± 0.5 mm/yr sub-parallel to P-NA relative motion (Figs. 2B and 4). Although the extension of the San Andreas fault itself is offshore at this latitude, elastic strain from the locked SAF will contribute to this velocity. The distributed right-lateral motion between Cape Mendocino (33.8 ± 0.5 mm/yr) and station 0106 (13.9 ± 1.1

mm/yr) (Fig. 4), is ~ 34% of the total P-SNGV relative motion observed in the coast ranges ~ 120 km south of Cape Mendocino (Freymueller et al., 1999). The westward increases in velocity that span stations 0106 and CME1 (Figs. 3B and 4) are consistent with right-lateral strain on mapped north-northwest-trending faults (Fig. 4), the Bartlett Springs-Lake Mountain fault zone (BS/LMfz) to the east, the Maacama-Garberville fault zone (Maa/Gfz), and the offshore San Andreas fault zone (Fig. 4) (Kelsey and Carver, 1988).

Right-lateral shear strain is seen in the residual velocity field at the latitude of Cape Mendocino (red rectangle, Fig. 4). Because the offshore San Andreas fault terminates to the south of the latitude of Cape Mendocino, right-lateral shear strain must result from onshore faults, or distributed shear. Distinct strike slip faults reaching the surface with Holocene scarps have not been found on either the Maa/Gfz or the BS/Lmfz north of approximately 40°N; therefore the right lateral shear strain on north of 40°N probably involves distributed shear.

Although right lateral shear strain is expected because strike-slip faults of the SAF system must propagate northward as the MTJ propagates northward (Dickinson and Snyder, 1979), residual velocities show reduced right lateral shear strain at the latitude of Humboldt Bay (~40.75°N, green rectangle, Fig 4). Therefore the northern end of the shear strain associated with the SA transform boundary, as reflected in the residual velocities, is north of the latitude of Cape Mendocino and appears to be at the latitude of Humboldt Bay.

We make a more quantitative comparison among sites with SAF-parallel residual velocities at the northern end of the SAF transform system by projecting the SAF-parallel velocities of Fig. 4 onto a profile that strikes 57°, perpendicular to the average SAF system strike at 40°N, and constructing 2D elastic models (Table 2, Fig. 5). We divided the sites into three latitudinal swaths, sites at the latitude of Humboldt Bay (green rectangle, Fig. 4), sites within the northern end of the San Andreas transform at the latitude of Cape Mendocino (red rectangle, Fig. 4), and sites south of the northern end of the San Andreas transform (blue rectangle, Fig. 4). Because our velocities are referenced to NA, we must include the motion of SNGV relative to NA, plus each of the faults of the SAF system. The uncertainty in SNGV-NA motion is a few mm/yr in all existing plate/block motion models (e.g., Sella et al., 2002), so we used the motion of the site QUIN in the Sierra Nevada (9 mm/yr right-lateral normal to the profile) as the motion of SNGV. For fault location, we recognize that the faults generally show an eastward dip (Castillo and Ellsworth, 1993) and there is an uncertainty of a few km in the fault locations at depth, but our model results are only weakly sensitive to the exact locations of the faults as long as every site is on the correct side of the closest fault.

For those sites within the San Andreas transform system (within the red and blue rectangles, Fig. 4), our modeling results in Fig. 5 show no significant along-strike changes in the San Andreas fault-parallel velocities at the latitude of 40 to 40.5°N (red and blue sites both fit with solid blue profile line, Fig. 5) compared to San Andreas-fault parallel velocities at the latitude of 39° to 39.5°N (dashed blue profile line, Fig. 5). The dashed blue profile (Fig. 5) is a velocity model developed by Freymueller et al. (1999) for a transect ~120 km to the south (best-fitting fault slip rates and locking depths tabulated in Table 2) and does an excellent job of fitting most of the data from the northern part of the transform system with the exception that the locking depth of the eastern most fault has been adjusted because the BS/LMfz shows evidence of shallow creep to the south at 39.5°N whereas evidence of creep is lacking on the BS/LMfz in the latitude range 40° to 40.5°N (Fig. 5). The velocities of the westernmost sites are slightly underpredicted, and the fit could be improved by decreasing the slip rate of the SAFz slightly and increasing the slip rate of the Maa/Gfz correspondingly.

Sites in the northern latitudinal swath through Humboldt Bay (green station velocities, Fig. 5), a region that is north of the northern end of the San Andreas transform, show a different pattern of SAF-parallel velocities from those further south. SAF parallel velocities are similar to sites further south in the eastern part of the area (eastern part of green rectangle) but sites in the western part of the area have progressively faster SAF-parallel velocities, although not as fast as sites to the south-southeast along strike. No simple model involving only known active faults explain the data from this profile well. We show a model in which the BS/LMfz continues northward with the same slip rate as in the southern profile (8 mm/yr), but with a locking depth of 12 km (Fig. 5, Table 2).

Although such a fault model explains about half of the data well, it underpredicts the velocities of the other half of the sites (Fig. 5). In addition, a component of right lateral shear is observed extending much farther to the east than in the southern profiles (note the clear difference in velocity between sites 0108 and 01QF (Fig. 4) and the jump in velocity from ~ 0.8 cm/yr to 1.3 cm/yr at about ~ 30 km east of the BS/LMfz (green site velocities, Fig. 5)). This component of right lateral shear occurs in an area where there is no known active Quaternary fault.

Table 2. 2D elastic models for the faults of the San Andreas fault system

Model	San Andreas fault zone, rate (mm/yr)	San Andreas fault zone, locking depth (km)	Maacama/Garberville fault zone, rate (mm/yr)	Maacama/Garberville fault zone, locking depth (km)	Bartlett Springs/Lake Mountain fault zone, rate (mm/yr)	Bartlett Springs/Lake Mountain fault zone, locking depth (km)
Model for San Andreas transform from Freymueller et al. (1999), (dashed blue profile, Fig. 5) ^a	17	15	14	13	8	0
Model for northern end of San Andreas transform (blue profile, Fig. 5) ^b	17	15	14	13	8	5
Sites at latitude of Humboldt Bay (north of MTJ) (green profile, Fig. 5) ^c	0	0	0	0	8	13

^a Model constructed from sites at latitudes 39° to 39.5°N , ~ 100 – 120 km south of Cape Mendocino (Freymueller et al., 1999).

^b Model constructed from sites within blue and red rectangles of Fig. 4.

^c Model constructed from sites within green rectangle of Fig. 4.

We infer that the SAF-parallel residual velocities at the latitude of Humboldt Bay (green rectangle, Fig. 4) are a product of both Gorda-NA plate interaction and Pacific-NA interaction. The right lateral shear strain evident at the latitude of Humboldt Bay reflects right lateral shear propagating north-northwestward on the BS/LMfz (Pacific-NA interaction) as depicted by the model (Fig. 5). However, the origin of the SAF-parallel velocities to the north of the latitude of Cape Mendocino, which is not predicted by a right slip model that stops at the latitude of Cape Mendocino (south edge of the Gorda plate), may be the viscous coupling of the Gorda plate to the North America (NA) plate through the slab window (Furlong and Govers, 1999). Even though we subtracted out the subduction zone component (subduction interface coupling) from these SAF-parallel velocities, we did not subtract out the interplay of Gorda-NA in the slab window region where upper mantle and lower crust is coupled viscously to both the southern edge of the Gorda slab and the overlying NA plate, thereby dragging NA northward (Furlong and Govers, 1999). The viscous drag produces the northward residual velocities of ~ 0.3 to 0.8 cm/yr, accounting for the additional velocity not predicted by the right slip fault model.

5.3. Pacific-North America margin parallel contraction

The transition from predominately translational strike-slip to predominately convergent subduction tectonics occurs over a ~ 80 km distance from the Eel River mouth (near 01PA) to Trinidad, CA (TRND) where station velocities indicate SAF-parallel shortening. The northwest-southeast (SAF-parallel) shortening occurs at the tips of the northern SAF fault system (Figs. 1B and 4) and is a consequence of the rapid decrease in residual station velocities immediately north of Cape Mendocino, a region coincident with the southern edge of the subducted Gorda plate (Smith et al., 1993). Average northwest-southeast shortening among three pairs of sites at the latitude of Cape Mendocino (1468-01PA, 01NC-01PB, and 01NE-KNEE; Fig. 4) is $\sim 8.0 \pm 2.0$ mm/yr. Similarly, there is $\sim 9.0 \pm 5.0$ mm/yr of SAF-parallel shortening between the Trinidad area (stations ALEN and TRND) and stations inland of Cape Mendocino (stations 01IND and 01NE, Fig. 4). This SAF-parallel shortening is essentially orthogonal to the strain direction predicted from the subduction strain model, and is not affected by variation in the width of the locked zone nor variations in the assumed convergence direction of up to ~ 30 degrees. The SAF-parallel shortening cannot be explained as a result of elastic deformation from the locked offshore SAF, because the SAF does not extend this far north.

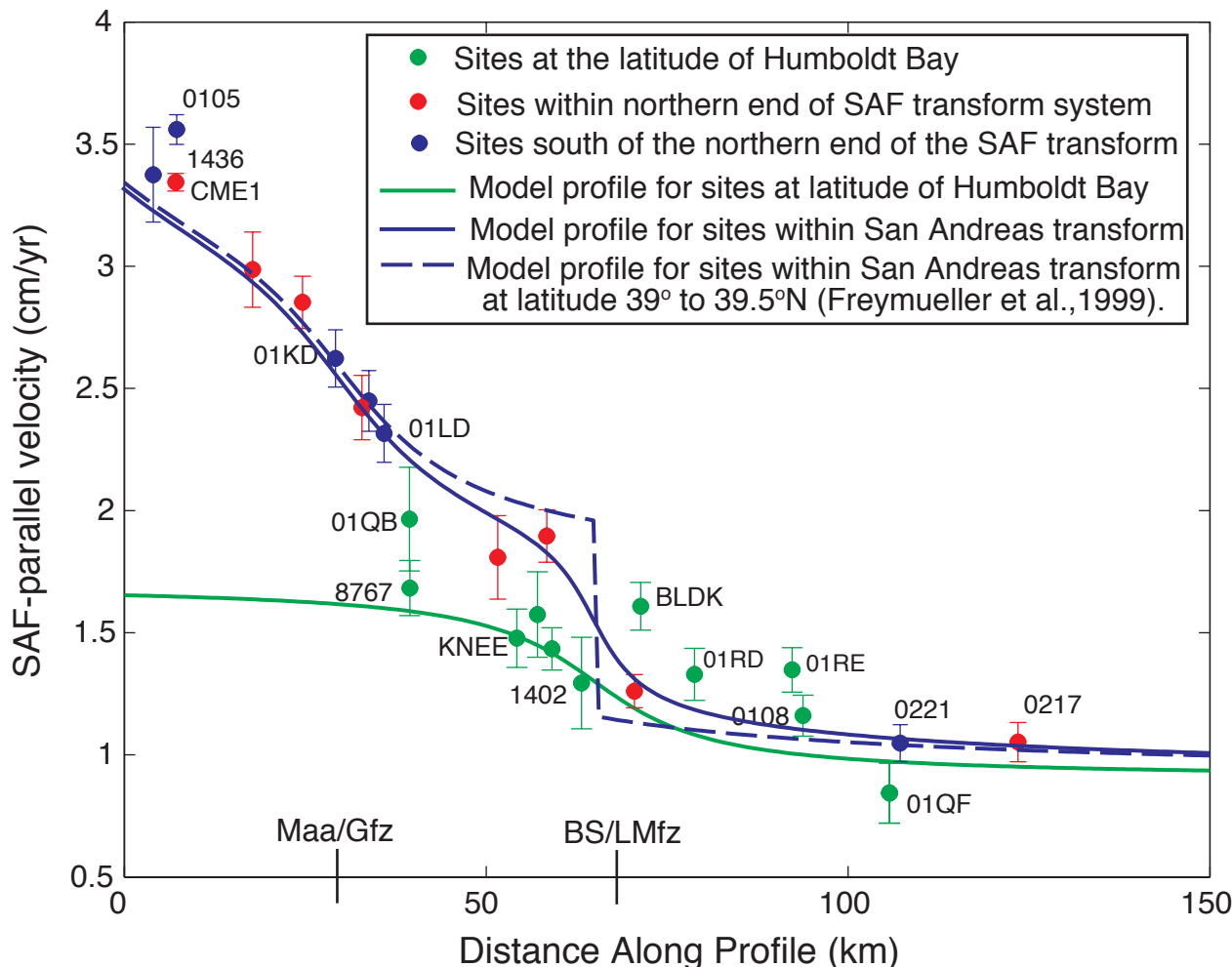


Figure 5. Three velocity profiles from three fault dislocation models perpendicular to trend of San Andreas fault plate boundary (see Table 2 for model parameters). Distributed strike-slip motion occurs across the two eastern strands of the San Andreas fault system, with velocity increases near surface traces of the Maacama/Garberville fault zone (Maa/Gfz) and the Bartlett Springs/Lake Mountain fault zone (BS/LMfz). The (arbitrary) origin of the profiles is near Punta Gorda, the Maa/Gfz is at 30 km distance, and the BS/LMfz is at 65 distance km. The model curves are based on trial and error fits to their respective data. The green model curve is fit to the green stations (those within the green rectangle, Fig. 4), and the blue model curve is fit to the blue and red stations (those within the blue and red rectangles, Fig. 4). The dashed blue model curve (from Freymueller et al., 1999), which is identical to the blue curve except that the BS/LMfz is creeping at the surface, is the velocity profile across the San Andreas fault system ~ 120 km further south at latitude range 39° to 39.5°N.

SAF-parallel shortening north of the latitude of the MTJ may result from two processes, crustal slivers within the eastern SAF system impinging northward on the SNGV and OC forearc blocks as the SAF system propagates northward and viscous coupling of the NA plate (SNGV block) to the underlying south edge of the Gorda slab. In the first instance, rapid velocities west of the Maa/Gfz from the south impinge on slower velocities along strike to the north in the Humboldt Bay region (Figs. 4 and 5), producing SAF parallel shortening west and north of the north-northwest extension of the Maa/Gfz. In the second instance, shortening is the product of bulk strain associated with the Mendocino crustal conveyor, whereby lower crust and upper mantle viscous coupling within the slab window at the south edge of the subducted Gorda plate drives north-south shortening in the North American plate above the southern edge of the subducted plate (Furlong and Govers, 1999; Furlong et al., 2003).

SAF-parallel shortening in the MTJ region is accommodated as permanent strain on several sets of mapped structures in the general latitude of the Eel River valley and Humboldt Bay area north of Cape Mendocino. Faults accommodating SAF-parallel contraction include the high angle reverse faults immediately north of Cape Mendocino (Russ fault and False Cape fault; Rf and FCf, Fig. 1) and the active upper plate thrust faults of Mad River fault zone and Little Salmon fault (MRfz and LSf, Fig. 1) (Ogle, 1953; McLaughlin et al., 2000), where contraction would be accommodated by oblique reverse motion. Folds accommodating SAF-parallel contraction include the long wavelength (~10 km), east-west trending folds apparent both in the margins of the Eel River valley (ERV, Fig. 1) (Ogle, 1953) and in the marine terraced upland near station TRND (Trinidad, Fig. 1) (McCroory, 2000).

5.4. Convergence of Sierra Nevada-Great Valley block with the coast

Stations in the northern SNGV block greater than 100 km inland of the SAF display velocities oriented slightly westward of the P-NA relative motion direction (Fig. 3B; long axis of Fig. 3B is parallel to P-NA relative motion direction). Convergence of SNGV block motion with the MTJ region results in a zone of contraction that begins ~ 130 km east of the coast near station 0217 near Weaverville, CA (Figs. 2 and 4) and persists westward towards the Humboldt Bay region. The western edge of this contraction is within the MRfz to the north of Humboldt Bay and further south the edge is just west of the BS/LMfz (note converging GPS-derived velocities across these fault zones, 01RD to 1402 across the MRfz and 0106 to 01NE across the BS/LMfz, Fig. 4). Similarly, near the San Francisco Bay area >300 km south, the SNGV block is converging at ~ 2-4 mm/yr with the eastern SAF system (Prescott et al., 2001). The contraction between the interior of the SNGV and the coast appears to require contraction on structures both at the western edge of the Great Valley (east of station 0217, Fig. 2) and on fault zones near the coast such as the Mad River fault zone. Although the residual velocity field shows zones of concentrated contraction corresponding to the upper crustal fault zones, errors in the subduction strain model might result in more broadly distributed contraction. Better resolution of the details will require both more precise velocities and greater site density, and also further constraints on the subduction strain model.

6. CONCLUSIONS

Although characterized as a triple junction region on the basis of simple plate boundary geometry, we show on the basis of GPS station velocities that the north coastal California area is more accurately depicted as a quadruple junction of four blocks, the Mendocino deformation zone (MDZ, Fig. 1); the four blocks are the Pacific plate, the Gorda plate, the Sierra Nevada-Great Valley block and the Oregon Coast block (Fig. 1). The San Andreas transform zone is a broad boundary between the Pacific plate and the western edge of the Sierra Nevada Great Valley block, with the northern end of the transform zone overlying the southern edge of the subducted Gorda plate that is viscously coupled to the overlying western margin of the Sierra Nevada-Great Valley block. The northern end to the Sierra Nevada-Great Valley block bounds the Oregon Coast block; the diffuse boundary between the two blocks occurs inland from Humboldt Bay at the approximate latitude of elevated topography of the Trinity Alps and the Marble Mountains (TA and MM, Fig. 1). The southernmost Gorda plate subducts beneath the upper plate at the latitude of Humboldt Bay. The Humboldt Bay region (the upper plate) is a zone of crustal deformation that is both at the northern end of the San Andreas fault transform system and at the western end of the westward converging Sierra Nevada Great Valley block.

Using GPS station velocities, we depict the pattern of strain among these four crustal blocks in northern California. After removing the component of elastic strain accumulation caused by the Cascadia subduction zone, we infer that observed strain accumulation in the region is a consequence of the northern termination of the San Andreas transform system and the westward convergence of the Sierra Nevada-Great Valley block. Right lateral shear strain propagates northward of the latitude of Cape Mendocino along the two eastern strands of the San Andreas transform system, the Bartlett Springs/Lake Mountain fault zone and the Garberville/Maacama fault zone (Fig. 1B). Further north at the latitude of Humboldt Bay, San Andreas fault parallel velocities are less and therefore shortening parallel to the trend the San Andreas fault occurs in the Humboldt Bay region.

The San Andreas fault parallel shortening is expressed as contractional strain on several major structures in the Humboldt Bay area. San Andreas fault parallel shortening is accommodated by the east-west trending folds in the Eel River valley and near Trinidad, by slip on the east-west trending Russ and related faults east of Cape Mendocino and by oblique slip on the northwest trending Little Salmon fault and the Mad River fault zone (Fig. 1B).

The Sierra Nevada Great Valley block converges toward the coast; based on station velocities, a component of this convergence probably is accommodated at or near the western edge of the northern Sacramento Valley while the westernmost component of convergence may be accommodated by east-west shortening across the Mad River fault zone within 20 km of the coast. Although the active upper plate reverse faults in the Humboldt Bay region (Little Salmon fault and Mad River fault zone, Fig. 1B) are perpendicular in trend to the Gorda-North America convergence direction, strain on these faults probably has a polygenetic origin, with a converging forearc block on the east, an impinging transform system and viscously coupled slab window to the south and strain associated with a convergent plate boundary to the west.

ACKNOWLEDGEMENTS

Supported by USGS NEHRP grants 01HQGR0152 (Kelsey) and 01HQGR0151 (Freymueller). Discussions with R. Burgmann, R. M. Burke, G. A. Carver, R. C. McPherson, and M. M. Miller improved this manuscript, as did reviews by P. Segall and K. Wang. Initial GPS measurements are from CalTrans, National Geodetic Survey, Stanford University, and the USGS (M. Murray, M. Poland, and J. Svarc). Field support in 1999 provided by CalTrans District 1, Central Washington University (CWU), Lane Community College, and the University of Oregon. G. Erickson, A. Lutz, J. Wellik, and A. Woolace assisted with reoccupation of GPS stations (2001-2002). GPS equipment provided by CWU, University Alaska at Fairbanks and the University NAVSTAR Consortium (UNAVCO, Boulder, CO). Figures created with GMT (Wessel and Smith, 1995) and USGS SRTM30 gridded DEM data product (http://topex.ucsd.edu/WWW_html/srtm30_html). Online GPS archives employed include: Bay Area Regional Deformation network (<http://quake.geo.berkeley.edu/bard/bard.html>), International GPS Service (http://igs.cb.jpl.nasa.gov/components/prods_cb.html), NGS (<http://www.ngs.noaa.gov>), Pacific Northwest Geodetic Array (<http://www.geodesy.cwu.edu>), and Scripps Orbit and Permanent Array Center (<http://sopac.ucsd.edu>). Sites SHIN and NEW2 (New Pass) are part of the Caltech/Harvard BARGEN network.

REFERENCES CITED

- Boucher, C., Altamini, Z., Sillard, P., 1999. The 1997 International Terrestrial Reference Frame (ITRF97). in IERS Technical Note 27, Observatoire de Paris, Paris, France.
- Carver, G. A., McCalpin, J. P., 1996. Paleoseismology of compressional tectonic environments. In: McCalpin, J. P. (Ed.), Paleoseismology. New York, p. 183-270.
- Castillo, D.A., W.L. Ellsworth, 1993. Seismotectonics of the San Andreas Fault System between Point Arena and Cape Mendocino in Northern California: Implication for the Development and Evolution of a young transform. *Journal of Geophysical Research* 98, 6543-6560.
- DeMets, C., Dixon, T.H., 1999. Kinematic models for Pacific-North America motion from 3 Ma to present, I: Evidence for steady state motion and biases in the NUVEL-1A model. *Geophysical Research Letters* 26, 1921-1924.
- Dengler, L., Moley, K., McPherson, R., Pasyanos, M., Dewey, J. W., Murray, M. H., 1995. The September 1, 1994 Mendocino fault earthquake. *California Geology* 48, 43-53.
- Dickinson, W. R., Snyder, W. S., 1979. Geometry of triple junctions related to San Andreas transform. *Journal of Geophysical Research* 84, 561-572.
- Dixon, T. H., Miller, M. M., Farina, F., Wang, H., Johnson, D. J., 2000. Present-day motion of the Sierra Nevada block and some tectonic implications for the Basin and Range province, North America Cordillera. *Tectonics* 19, 1-24.
- Flück, P., Hyndman, R. D., Wang, K., 1997. Three-dimensional dislocation model for great earthquakes of the Cascadia subduction zone. *Journal of Geophysical Research*, 102, 20,539-20,550.
- Freymueller, J. T., Murray, M. H., Segall, P., Castillo, D., 1999. Kinematics of the Pacific-North America plate boundary zone, northern California. *Journal of Geophysical Research* 104, 7419-7441.
- Freymueller, J. T., Cohen, S. C., Fletcher, H. J., 2000. Spatial variations in present-day deformation, Kenai Peninsula, and their implications. *Journal of Geophysical Research*, 105, 8079-8101.

- Furlong, K.P., Govers, R., 1999. Ephemeral crustal thickening at a triple junction: the Mendocino crustal conveyor. *Geology*, 27, 127-130.
- Furlong, K.P., Lock, J., Guzowski, C., Whitlock, J., Benz, H., 2003. The Mendocino crustal conveyor: making and breaking the California crust. *International Geology Review* 45, 767-779.
- Jennings, C., 1994. Fault activity map of California and adjacent areas. Department of Conservation, California Division of Mines and Geology, Sacramento, CA.
- Kelsey, H. M., Carver, G. A., 1988. Late Neogene and Quaternary tectonics associated with the northward growth of the San Andreas transform fault, northern California. *Journal of Geophysical Research* 93, 4797- 4819.
- Lisowski, M., J.C. Savage, W.H. Prescott, 1991. The velocity field along the San Andreas fault in northern California. *Seismological Research Letters* (abs) 62, 11.
- McCaffrey, R., M. D. Long, C. Goldfinger, P. Zwick, J. Nabelek, C. K. Johnson, and C. Smith, Rotation and plate locking along the southern Cascadia subduction zone, *Geophys. Res. Lett.*, 27, 2117-2120, 2000.
- McCaffrey, R., 2002. Crustal block rotations and plate coupling. in *Plate Boundary Zones*, AGU Geodynamics Ser. 30, S. Stein and J. Freymueller, eds., 101-122,
- McCrorry, P. A., 2000. Upper plate contraction north of the migrating Mendocino triple junction, northern California: implications for strain partitioning. *Tectonics* 19, 1144-1160.
- McLaughlin, R.J., Ellen, S.D., Blake, M.C., Jayko, A.S., Irwin W. P., Aalto, K.R., Carver G.A. and Clarke, S.H., 2000, Geology of the Cape Mendocino, Eureka, Garberville and southwestern part of the Hayfork 30 x 60 minute quadrangles and adjacent offshore area, northern California, Miscellaneous Field Studies MF-2336.
- Miller, M. M, Johnson, D.J., Rubin, C.M., Dragert H., Wang, K., Qamar, A., Goldfinger, C., 2001. GPS-determination of along-strike variation in Cascadia margin kinematics: Implications for relative plate motion, subduction zone coupling, and permanent deformation. *Tectonics* 20, 161-176.
- Murray, M. H., Marshall, G. A., Lisowski, M., Stein, R. S., 1996. The 1992 M=7 Cape Mendocino, California, earthquake: Coseismic deformation at the south end of the Cascadia megathrust. *Journal of Geophysical Research* 101, 17,707-17, 725.
- Murray, M. H., Lisowski, M., 2000. Strain accumulation along the Cascadia subduction zone. *Geophysical Research Letters* 27, 3631-3634.
- Ogle, B. A., 1953. Geology of the Eel River Valley area, Humboldt County, California. California Division of Mines Bulletin 164, 128 p.
- Poland, M. P., Burgmann, R., Fink, J. H., Dzurisin, D., 1999. Deformation field at Medicine Lake Volcano, Northern California; new results from GPS measurements. *EOS, Transactions, American Geophysical Union* 80, 960.
- Prescott, W. H., Savage, J. C., Svarc, J. L., Manaker, D., 2001. Deformation across the Pacific-North America plate boundary near San Francisco, California. *Journal of Geophysical Research* 106, 6673-6682.
- Oppenheimer, D., and 19 others, 1993. The Cape Mendocino, California, earthquakes of April, 1992: Subduction at the triple junction. *Science* 261, 433-438.
- Sella, G. F., Dixon, T. H., Mao, A., Stein, S., 2002. REVEL: A model for Recent plate velocities from space geodesy. *Journal of Geophysical Research* 107, 10.1029/2000JB000033.
- Smith, S. W., Knapp, J. S., McPherson, R. C., 1993. Seismicity of the Gorda plate, structure of the continental margin, and an eastward jump of the Mendocino triple junction. *Journal of Geophysical Research* 98, 8153-8171.
- Snay, R. A., Matsikari, T., 1991. Horizontal deformation in the Cascadia subduction zone from serendipitous data. *Tectonophysics* 94, 59-67.
- Szeliga, W., Melbourne, T.I, Miller, M.M., Santillan, V.M., 2004. Southern Cascadia episodic slow earthquakes, *Geophysical Research Letters*, 31, L16602, doi:10.1029/2004GL020824.
- Wang, K., Wells, R., Mazzotti, S., Hyndman, R.D., Sagiya, T., 2003. A revised dislocation model of interseismic deformation of the Cascadia subduction zone. *Journal of Geophysical Research* 108(B1) 2026, doi:10.1029/2001JB001227.
- Wells, R. E., C. S. Weaver, R. J. Blakely, 1998. Forearc migration in Cascadia and its neotectonic significance. *Geology* 26, 759-762.
- Wells, R. E., Simpson, R. W., 2001. Northward migration of the Cascadia forearc in the northwestern U.S. and implications for subduction deformation. *Earth Planets Space* 53, 275-283.
- Wessel, P., Smith, W. H. F., 1995. New version of the Generic Mapping Tools released, *EOS, Transactions, American Geophysical Union*. 76, 329.
- Williams, T. B., 2002. The geodetic signature of modern deformation (1993-2002) within the Southern Cascadia Subduction Zone, northwestern California, M.S. thesis, Humboldt State University, Arcata, 102 p.
- Wilson, D.S, 1993. Confidence intervals for motion and deformation of the Juan de Fuca plate. *Journal of Geophysical Research* 98, 16053-16071.
- Zumberge, J. F., Heflin, M. B., Jefferson, D. C., Watkins, M. M., Webb, F. H., 1997. Precise point positioning for the efficient and robust analysis of GPS data from large networks, *Journal of Geophysical Research* 102, p. 5005-5017.
- Zweck, C., Freymueller, J.T., Cohen, S.C., 2002. Elastic dislocation modeling of the postseismic response to the 1964 Alaska Earthquake. *Journal of Geophysical Research* 107(B4) doi:10.1029/2001JB000409.

Terrace formation and drainage adjustment in response to migrating uplift, 80 km east of the Mendocino Triple Junction, Northern California

Rich D. Koehler

University of Nevada, Reno Center for Neotectonic Studies

ABSTRACT

Terrace formation and drainage adjustment in response to migrating uplift is distinguished by a series of fill and strath terraces in the Van Duzen/North Fork Eel Rivers headwaters region, northwestern California. Differences in soil development, amount of incision, and terrace stratigraphy imply a history of non-synchronous terrace formation. The Refuge Valley fill terrace in the drainage divide between the Van Duzen and North Fork Eel Rivers records a transition in geomorphic process from aggradation to incision due to uplift. Well documented uplift to the west in the Cape Mendocino region and the lack of evidence supporting alternative mechanisms of terrace formation (i.e. landslide damming and climate variation) suggests tectonic uplift is the dominant mechanism of drainage adjustment and terrace formation. Tectonic uplift induced channel gradient shallowing in the North Fork Eel channel, promoting the aggradation of the North Fork Eel fill terraces and Hettenshaw Valley. As a consequence of uplift, the Van Duzen River captured the headwaters of the North Fork Eel River, leaving a former North Fork Eel fill terrace at the new drainage divide in late Pleistocene time. Continued uplift, since the time of capture, has steepened the Van Duzen channel, resulting in downcutting and strath terrace formation into the Holocene. The tectonic model driving the uplift is regional bulging associated with the northward migration of the Mendocino Triple Junction.

INTRODUCTION

Hettenshaw Valley and Refuge Valley are two high-elevation, flat alluvial surfaces that occupy the low drainage divide between the Van Duzen and North Fork Eel Rivers approximately 80 km east of the Mendocino Triple Junction (MTJ), northwestern California (Figures 1 and 2). The existence of these two surfaces at a drainage divide, and the presence of steep gradient headwater streams that are actively eroding into the alluvial surfaces, as well as the occurrence of barbed, fishhook shaped drainage patterns are all geomorphic evidence supporting a history of terrace formation and drainage network adjustment. Terraces in the area that are a product of ongoing drainage adjustment include large, deeply incised, alluvial fill terraces that extend to the south of the drainage divide along the North Fork Eel River, and a series of well preserved fluvial strath and fill terraces that extend to the north along the Van Duzen River and tributaries (Figure 2).

Throughout the late Neogene and Quaternary drainage basins in northwestern California have been adjusting to crustal deformation related to the northward migration of the MTJ. Analysis of flights of marine terraces south of the MTJ showed that the region of most rapid uplift, 4 m/ky, is 25-43 km south of the MTJ, and a lower rate of uplift, 1.2 m/ky, exists at Point Delgada 55 km south of the present MTJ (Merritts and Bull, 1989). In a related study, Merritts and Vincent (1989) evaluated three-dimensional morphological properties of 24 coastal drainage basins and determined that the maximum relief and gradients of first to third order stream channels increase progressively from Bruhel Point northward to Randall Creek and then decrease progressively from Randall Creek to Bear River (Figure 1). These temporal and spacial patterns of varying uplift rates along the coast indicate that the maximum amount of present day uplift is centered around the MTJ with progressively less uplift extending to the south.

The location of this study 80 km east of the MTJ provides a unique opportunity to assess whether or not the patterns of uplift observed along the coast persist inland. Therefore, in this paper, field mapping, geomorphic position, deposit stratigraphy, relative degree of soil development, and amount of incision was used to evaluate the relative ages and origins of the Quaternary alluvial terraces distributed across the Van Duzen/North Fork Eel River drainage divide. A chronology was then established of terrace formation and stream capture events consistent with the inferred relative ages and origins of the terraces, from which patterns of late Quaternary uplift were inferred. Comparison of the uplift pattern observed in the Van Duzen/North Fork Eel Rivers area to previously established uplift patterns on the coast has implications to the width of drainage basin adjustment

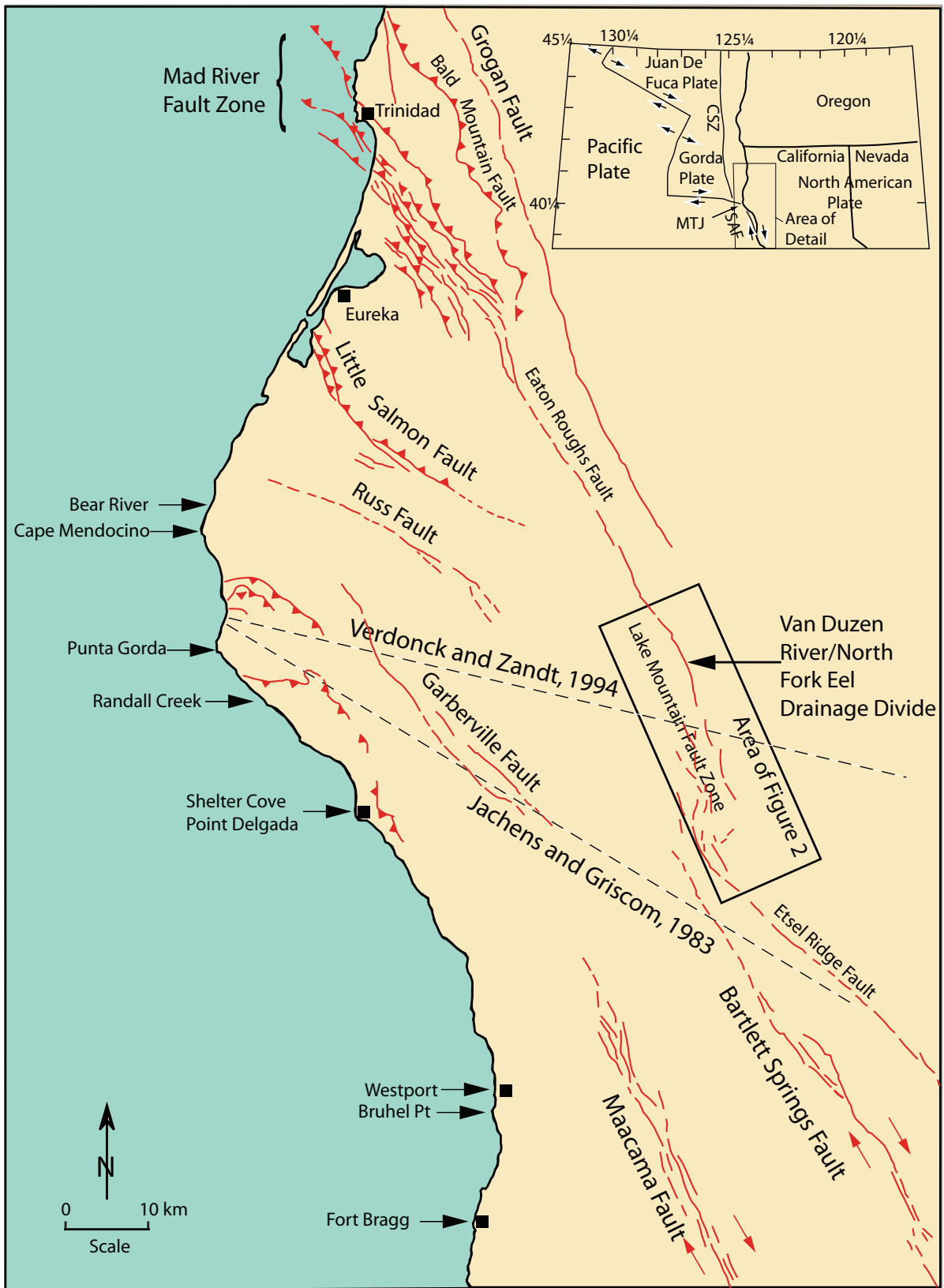


Figure 1. Regional map of Northern California showing major faults and area of detailed field investigation in the vicinity of the Van Duzen/North Fork Eel Rivers drainage divide. Dashed lines represent different interpretations of the southern edge of the subducting Gorda Plate from Jachens and Griscom (1983) and Verdonck and Zandt (1994). Shown on inset are CSZ, Cascadia Subduction Zone; SAF, San Andreas Fault; and MTJ, Mendocino Triple Junction.

related to the tectonic-geomorphic signature generated by the northward migrating MTJ. Additionally, this work provides field based surface geomorphic evidence in support of crustal models (Furlong and Govers, 1999) that show ephemeral crustal thickening in the MTJ region.

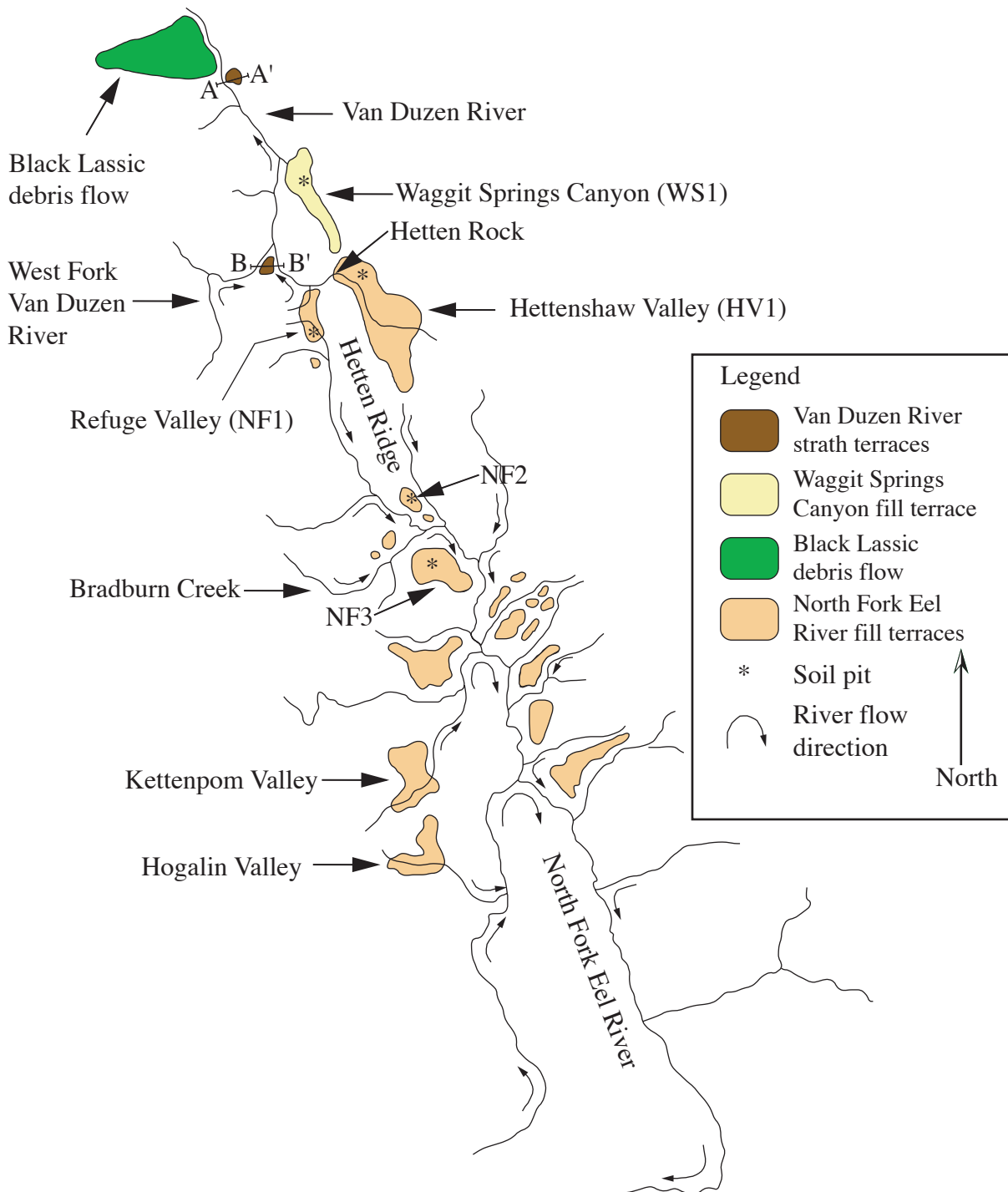


Figure 2. Study area map showing the distribution of strath and fill terraces. Soil pit sampling locations are denoted by asterisk or are shown on cross sections A-A' and B-B' (Figure 3). Fishhook shaped drainage patterns and flow directions for the upper Van Duzen and North Fork Eel Rivers are shown by arrows.

PHYSIOGRAPHIC, GEOLOGIC, AND QUATERNARY TECTONIC SETTING

The drainage divide between the Van Duzen and North Fork Eel Rivers is located within the Northern Coast Ranges Geomorphic Province of California, approximately 80 km southeast of Eureka and 80 km east of the MTJ at Cape Mendocino (Figure 1). From the drainage divide at Refuge Valley and Hettenshaw Valley, the Van Duzen River drains to the northwest and the North Fork Eel River drains to the southeast. The drainage patterns of both rivers are characterized by long, relatively straight, northwest trending valleys with barbed, fishhook-shaped tributary channels. The topography is dominated by northwest trending ridges, steep terrain with thin soil cover, knobby bedrock outcrops, and occasional flat terrace surfaces (Figure 2).

The Van Duzen and North Fork Eel Rivers are cut into marine metasedimentary rocks of the Central Belt Franciscan Formation, a subduction-related accretionary prism of Late Jurassic to Early Cretaceous age (Manning and Ogle, 1950; Ogle, 1953; Irwin, 1960; Bailey et al., 1964; Blake and Jones, 1974, and 1981; McLaughlin et al., 1982; Blake et al., 1985). In the study area, the Franciscan Formation is dominated by interbedded lithic graywacke, mudstone, and conglomerate with lenses of thinly bedded, red radiolarian chert and sparse mafic volcanic blocks (Irwin, 1960). The Franciscan Formation comprises one of the Mesozoic tectonostratigraphic terranes accreted onto the North American Plate during the subduction of the Farallon Plate (Blake et al., 1985). The Late Cretaceous-Paleogene accretion of the Coastal Belt Franciscan terrane to the west (McLaughlin et al., 1982) induced further faulting and folding in the Central Belt Franciscan Formation.

The MTJ was the product of Farallon Ridge collision with the North American Plate approximately 28 Ma (Atwater, 1970). The collision resulted in the formation of two triple junctions and the right lateral San Andreas Fault Zone that grew in length to the north as the triple junction migrated north to its present location near Cape Mendocino. Complex plate interactions associated with the northward migration of the triple junction (Jachens and Griscom, 1983; Furlong, 1993; Dickensen and Snyder, 1979) have resulted in rapid Quaternary uplift rates in the Cape Mendocino region (Kelsey and Carver, 1988; Merritts and Bull, 1989; Merritts and Vincent, 1989; Merritts, 1996; Koehler, 1999).

Tectonism associated with the MTJ region records a transition in tectonic style from transform tectonics in the south to convergent tectonics in the north (Figure 1). In the north, northeastward directed contraction is generated by the subduction of the Gorda Plate beneath the North American Plate along the Cascadia Subduction Zone. Features typical of this region are northwest-trending, north-east dipping thrust faults, and broad folds (Carver et al., 1985, 1986; Witter et al, 2001; 2002). The faults of the Mad River Fault Zone, extending approximately 40 km inland from the coast, offset late Pleistocene marine terraces with scarps of 15-90 m (Kelsey and Carver, 1988), and a Holocene fluvial strath terrace in the lower Mad River by 7 m, (Kelsey and Carver, 1988). A related thrust system, the Little Salmon Fault Zone, has generated 3 large surface displacements, with dip slip of 3.6-4.5 m per event during the last 1700 years (Carver and Burke, 1987; Clarke and Carver, 1989).

South of the MTJ, Quaternary deformation consists of right lateral shear along the San Andreas transform boundary, with localized extension and transpression related to fault geometry. Features typical of this area are northwest trending, high angle strike-slip faults. Also, linear, northwest trending ridges and valleys, aligned sag ponds, ridgetop troughs, and pull apart basins are some of the geomorphic evidence suggesting recent tectonic movement (Herd, 1978). The Maacama Fault Zone has had at least one episode of faulting within the Holocene (Upp, 1982) and the Bartlett Springs Fault Zone has had a minimum of two faulting events in the Holocene (Taylor and Swan, 1986).

East of the MTJ, faults have similar geomorphic expression to, and are aligned subparallel to, faults south of the MTJ, but the fault traces are shorter and less continuous. Tectonic geomorphic landforms including linear valleys, sag ponds, and aligned saddles along both the Eaton Roughs Fault Zone and the Lake Mountain Fault Zone suggest late Quaternary movement on these structures. These observations support a landscape evolution model for the area east of the migrating MTJ in which late Quaternary translational deformation is overprinting topography originally created by contractional deformation.

RESULTS

Reconnaissance Surficial Mapping

The first maps to depict Quaternary terrace deposits in the vicinity of the Van Duzen/North Fork Eel drainage divide (Irwin, 1960; Irwin et al., 1974) grouped Quaternary terraces as Qt, but did not differentiate individual terrace deposits. These studies, however, recognized that Hettenshaw Valley may be correlative with other high-level terrace deposits elsewhere along the Van Duzen and North Fork Eel Rivers. In an effort to differentiate these terrace deposits, geomorphic map units were delineated on color aerial photographs and standard 1:24,000 scale USGS topographic maps (Koehler 1997; 1999). Field mapping of landforms, stream drainages, natural exposures, and road cuts was then performed to confirm geomorphic relations. Initial geomorphic and sedimentologic variables used to differentiate the terraces include geomorphic position, deposit stratigraphy, depth of incision, clast size, clast roundness, and soil development.

Based on geomorphic features observed on aerial photography and in the field, four distinct groups of terraces were identified across the Van Duzen/North Fork Eel drainage divide (Koehler, 1997; 1999). The four terrace groups are: (1) a valley fill terrace deposit within Hettenshaw Valley, (2) fluvial strath terraces on the Van Duzen River, (3) valley fill terraces along the North Fork Eel River drainage, and (4) an alluvial fill terrace at Waggit Springs Canyon. These terraces are shown on Figure 2 and described below.

Hettenshaw Valley (HV1)

Hettenshaw Valley is a north-northwest trending alluvial valley with fill composed of gravel, coarse sand, and fine overbank sand and silt, with sparsely distributed small cobbles. The valley surface consists of a main surface and at least two inset terraces characterized by smooth gently sloping terrace back edges. The elevation of both the valley surface and the underlying bedrock strath decreases to the north. At the southern edge of the deposit, the surface elevation is 976 m with bedrock outcrops at the surface. At the northern edge of the deposit, the surface elevation is 951 m and the depth of alluvium, determined from a local water well, is greater than 23 m. Stream incision depth into the fill is about 1-2 meters. Presently, the headwater stream of the east fork of the North Fork Eel River is actively eroding headward into the southern edge of Hettenshaw Valley (Figure 3). At the northern edge, a low divide separates Hettenshaw Valley from the northwest trending Waggit Springs Canyon, and the valley is drained by Van Duzen River headwater tributaries. The drainage outlet is the west-facing notch between two topographic highs known locally as Hetten Ridge and Hetten Rock (Figure 2).

Van Duzen River strath terraces (VD1-VD6)

The Van Duzen River strath terraces border the Van Duzen River from the confluence of the West Fork Van Duzen River to north of the Black Lassic Debris Flow (BLDF), a late Pleistocene hillslope failure that temporarily dammed the river (Kelsey, 1977; 1978) (Figure 2). These terraces consist of a bedrock strath overlain by 2 to 8 m of cobble size channel deposits overlain by sand and silt overbank deposits (Figure 4). The Van Duzen River terraces usually occur as flights of three prominent terraces (Figure 4), however flights of up to five terraces exist locally. The uppermost terrace surface is at an elevation of 927 m and the lowest terrace surface is at an elevation of 835 m within the zone of modern overbank deposition.

North Fork Eel River fill terraces (NF1-NF3)

The fill terraces in the North Fork Eel River Drainage are composed of fluvial deposits and intercollated debris flow deposits. The fluvial deposits are composed of thin (2 mm to 0.5 m) layers of sand to subrounded cobble size clasts, alternating with thick (1.0-1.5 m) layers of sand and silt (Figure 4). The debris flow deposits are composed of subangular to subrounded boulder to cobble size clasts in a sand matrix (Figure 4). North Fork Eel fill deposits are typically about 30 m thick and step up elevationally in a northerly direction from Bradburn Creek (NF3, 793 m), to Hetten Ridge (NF2, 854 m), to the drainage divide with the Van Duzen River at Refuge Valley (NF1, 951

m) (Figures 2 and 3). Incision through the terraces and into the underlying bedrock is greatest in the south and decreases to the north. Incision below the Bradburn Creek terrace (NF3), Hetten Ridge terrace (NF2), and Refuge Valley terrace (NF1) is 193 m, 166 m, and 75 m, respectively. A much more extensive valley fill deposit prior to incision is suggested by the many flat, concordant ridgetops throughout the North Fork Eel basin.

Waggit Springs Canyon fill terrace (WS1)

The Waggit Springs Canyon fill terrace is underlain by fine grained alluvial sand and silt interfingered with slack water deposits, fine grained debris flow breccia deposits, and thin fluvial cobble layers (Figure 4). The Waggit Springs Canyon fill deposit differs from the North Fork Eel fill deposits by the presence of both slack water deposits and thin, fine-grained debris flow deposits. The Waggit Springs Canyon fill terrace extends continuously northwest from the northern drainage divide at Hettenshaw Valley downstream to the mouth of Waggit Springs

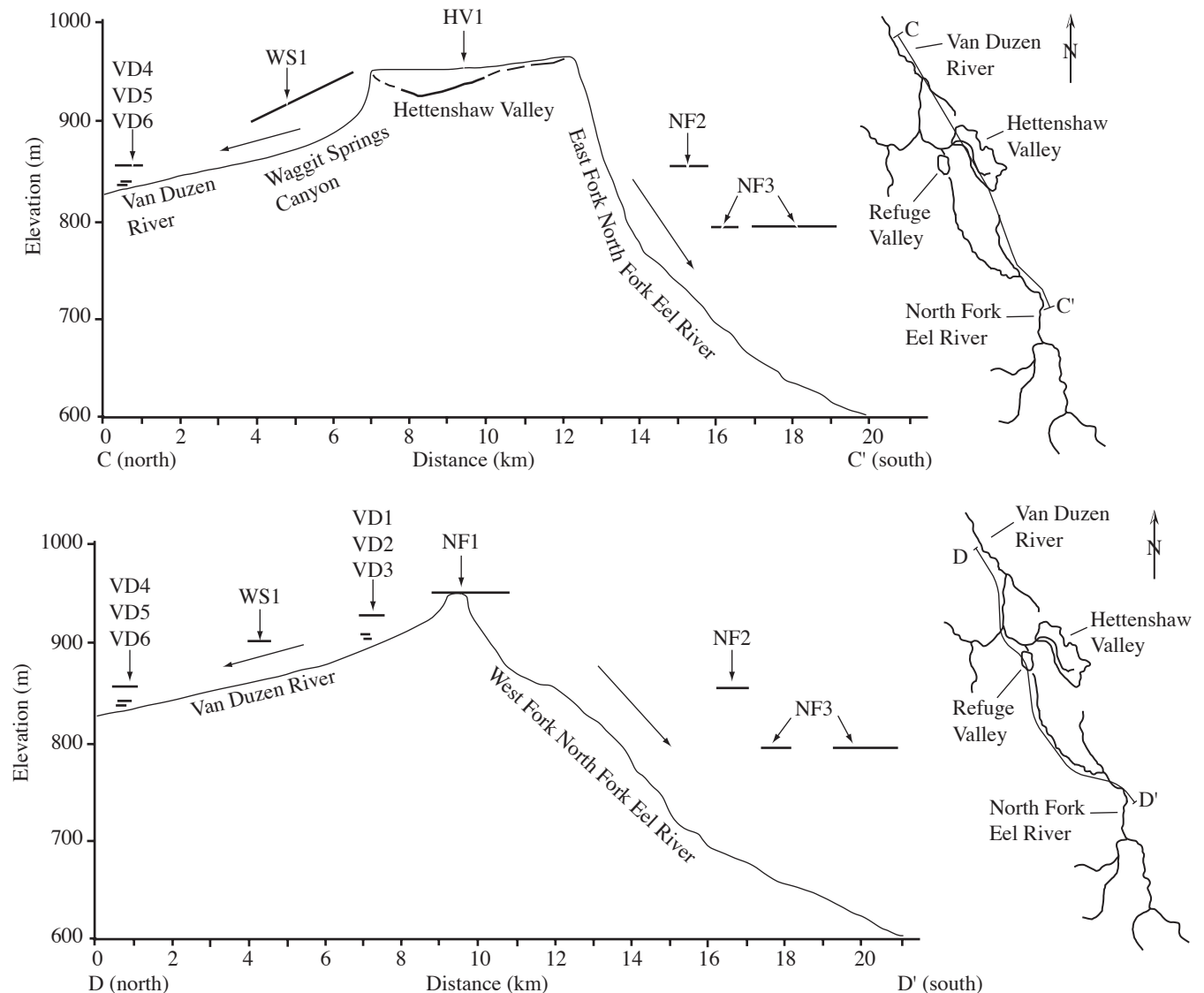


Figure 3. (A) Representative stratigraphy of Van Duzen River strath terraces and cross sections A-A' and B-B'. Asterisks mark locations of soil pits. See Figure 2 for locations of cross sections; (B) Representative stratigraphy of North Fork Eel River fill terraces, and (C) Representative stratigraphy of the Waggit Springs Canyon fill terrace. Each terrace is deposited on Franciscan Formation bedrock. Stratigraphic columns were described at natural stream cut exposures in the field.

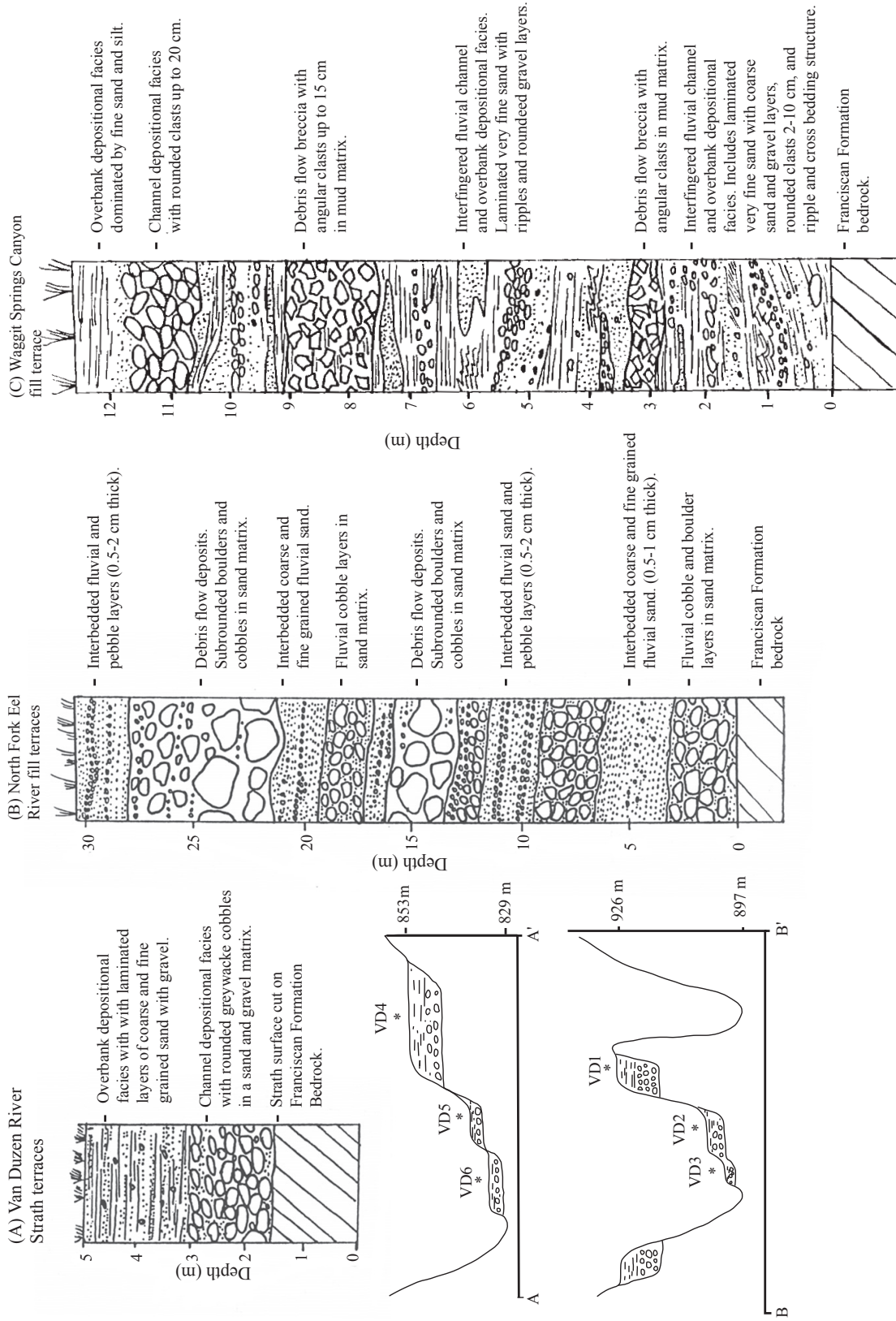


Figure 4. Location maps and topographic profiles C-C' and D-D' showing the distribution of terraces extending to the north and south of the drainage divide between the Van Duzen River and the North Fork Eel River. Profile C-C' crosses the divide at Hettenshaw Valley (HV1) and Profile D-D' crosses the divide at Refuge Valley (NF1). Terraces are indicated by unit designation (eg. NF2). Arrows indicate modern drainage direction. Vertical exaggeration is 10X.

Canyon at the Van Duzen River (Figure 2). The surface of the deposit is flat and the topography of the stream cuts between the top of the surface and the channel is smooth and rounded. Ephemeral creeks have incised up to 18 m into the Waggit Springs Canyon deposit.

Deposit Thicknesses and Amounts of Incision

Deposit thickness and the amount of incision into the deposit varies considerably within the four terrace groups (Table 1; Figure 3). In general, deposit thicknesses for the Van Duzen River strath terraces is thin compared to the deposit thickness for the North Fork Eel River fill terraces, the Waggit Springs Canyon fill terrace, and the Hettenshaw Valley fill deposit. The highest Van Duzen River strath terraces (VD1 and VD4), and the Waggit Springs Canyon terrace (WS1) are incised to a similar depth (18-30 m). The North Fork Eel River fill terraces are incised the greatest amount, ranging from 75 m in the north (NF1) to 193 m in the south (NF3).

Table 1. Deposit thicknesses, depth of incision from terrace surface, and location to drainage divide for each terrace.

Terrace [*]	Deposit thickness (m) ^Ω	Incision from terrace surface ^Σ	Location to drainage divide ^μ
VD1	8	30	N
VD2	6	10	N
VD3	2	5	N
VD4	8	24	N
VD5	4	10	N
VD6	3	5	N
HV1	0-23	2-3	O
WS1	18	18	O and N ^η
NF1	24	75	O
NF2	30	166	S
NF3	30	193	S

* Terraces grouped by similar stratigraphy.

^Ω Estimated in field.

^Σ Estimated using topographic maps, river profiles, and field observation.

^μ N, north of drainage divide; S, south of drainage divide; O, on drainage divide.

^η Suface exists at the drainage divide and extends to the north.

Relative Ages of Terraces based on Topographic Relations and Soil Development

Jenny (1941) noted that if four of the state factors of soil formation (climate, flora and fauna, parent material, and topography) remain constant for a group of soils, soil properties of individual soils can be used to estimate the state factor of time to evaluate relative age differences. For this study, it is assumed that all state factors of soil formation except time are held relatively constant and the parent material resembles Cu horizon materials, loose, non sticky, non plastic sandy loam with a 2.5Y5/3 color. Given this initial assumption, soils with similar property development have similar relative age.

Comparisons of soil properties of the soils developed on the various geomorphic surfaces are used to infer relative surface age. Topographic relations observed in the field are then combined with the soil data to establish a preferred grouping of terrace map units by relative age.

One soil pit was hand excavated on each of the eleven surfaces, including, the Van Duzen River strath terraces (VD1-VD6), the North Fork Eel River fill terraces (NF1-NF3), the Waggit Springs Canyon fill terrace (WS1), and the Hettenshaw Valley deposit (HV1). Soil properties described in the field by methods described in Birkeland (1999) include horizon thickness, nature of boundaries, dry colors, percent gravel, estimated clay content (%), wet and moist consistence, structure, texture, and the abundance of roots and pores. Soil properties determined in the lab by methods outlined in Soil Survey Staff (1992) include percent sand, silt, and clay, and these were used to determine texture. A complete compilation of the soil data can be found in Koehler (1999).

Individual soil properties that qualitatively show the best development through time include maximum clay percent, depth of development, color, texture, and wet consistence and are shown in Table 2 and Figure 5. Based on these data, terraces VD1-VD6 are younger than terraces NF1-NF3, WS1, and HV1, and terraces HV1, WS1

Table 2. Summary of soil properties used in terrace correlation.

Terrace ^β	Elevation (m)	Max clay % and horizon	Depth to C horizon (cm)	Max Color	C horizon gravel % ^φ	Max texture ^ζ	Max wet consistence ^Σ
VD1	927	17 - A	37	2.5Y5/3	>75	SL	ss/ps
VD2	907	17 - A	65	2.5Y3/2	25	SL	ss/ps
VD3	902	15 - Cox	18	2.5Y5/3	50-75	SL	so/po
VD4	854	23 - A1	80	2.5Y4/3	25	SCL	ss/ps
VD5	840	14 - A	49	2.5Y5/3	>75	SL	so/po
VD6	835	25 - Bw	50	2.5Y6/4	75	SCL	so/po
HV1	951	24 - Bt	104	2.5Y5/3	75	L	s/ps+
WS1	951-902	38 - Bt	98	2.5Y6/4	10-25	CL	s/p
NF1	951	33 - Bt	95	10YR5/4	25-50	CL	ss/ps
NF2	854	49 - 2Bw1	>116	7.5YR6/6	N.D.	C	s/p
NF3	793-823	44 - Bt3	>130	7.5YR5/6	N.D.	C	s/p

^β Terraces grouped by similar stratigraphy.

^φ C horizon gravel % estimated by field inspection of soil horizons. N.D., no data.

^ζ Maximum texture determined by laboratory particle size analysis. SL, sandy loam; SCL, sandy clay loam; L, loam; CL, clay loam; and C, clay. Laboratory methods and abbreviations follow Soil Survey Staff (1992).

^Σ Maximum wet consistence determined by field texturing. ss, slightly sticky; ps, slightly plastic; so, nonsticky; po, nonplastic; s, sticky; p, plastic; sp+ plasticity between sp and p. Abbreviations follow Soil Survey Staff (1975).

and NF1 are of similar relative age. Additionally, the North Fork Eel River terraces are relatively younger to the north (NF1) and relatively older to the south (NF2 and NF3)

The six Van Duzen River strath terraces represent two flights of terraces, VD1-VD3 and VD4-VD6 (Figures 3 and 4). Thus, based on topographic position the relative age within the two groups of Van Duzen terraces from oldest to youngest are: VD1, VD2, VD3, and VD4, VD5, VD6. Van Duzen strath terraces are inset into the Waggit Springs Canyon terrace at the mouth of Waggit Springs Canyon, indicating that all the Van Duzen River strath terraces are younger than the Waggit Springs Canyon terrace. The NF2 and NF3 terraces are at a lower elevation than the NF1 terrace, but have been incised to a much greater depth than the NF1 terrace. The NF3 terrace is cut into the NF2 terrace. Therefore, the relative age of the North Fork Eel terraces from oldest to youngest is; NF2, NF3, and NF1. Irwin (1960) recognized that Hettenshaw Valley may be correlative with other high elevation terrace deposits elsewhere along the Van Duzen River. Although direct topographic evidence between terraces HV1, NF1, and WS1 is absent, the close proximity of these surfaces to each other (Figure 2), similar surface elevation, and similar surface morphology (as well as soils) indirectly supports a similar relative age of terraces HV1, NF1, and WS1.

Together, the soils and topographic observations, support the preferred sequence of terrace formation events centered at the Van Duzen/North Fork Eel Rivers drainage divide. This sequence from oldest to youngest is NF2, NF3, combined NF1, WS1, and HV1, VD1 and VD4, VD2 and VD5, and VD3 and VD6 (Table 3).

Terrace Ages Based on Implied Incision Rates and Maximum Clay Percent

Ages inferred for terraces centered across the Van Duzen/North Fork Eel Rivers drainage divide based on implied incision rates and maximum clay percent are shown in Table 4.

For the incision rate age estimates I assume that uplift rates are equal to incision rates (Merritts and Brustolon, 1994; Personius, 1993) and use published uplift rates from the Oregon and California Coast Ranges (Kelsey and Carver, 1988; Merritts and Vincent, 1989; Personius, 1995). The amount of incision into the various terraces

was then used with the various assumed incision rates to calculate terrace ages (Table 4). Terrace age was also estimated by comparing soil maximum clay percent data for soils developed on the terraces to a maximum clay percent vs age relation developed by Merritts et al. (1991) for coastal northern California soils (Table 4). For the maximum clay percent method I assume that soil begins to develop after terrace abandonment and that soil develops at a rate similar to the coast.

Terrace NF3 is the terrace with the most drainage area above it, and thus the most accurate terrace to apply the assumption that uplift rate and incision rate are equal. The calculated soil age for terrace NF3 by the Merritts et al. (1991) approach is 630 ka. This age would imply an incision rate and thus uplift rate of 0.3 m/ky. By

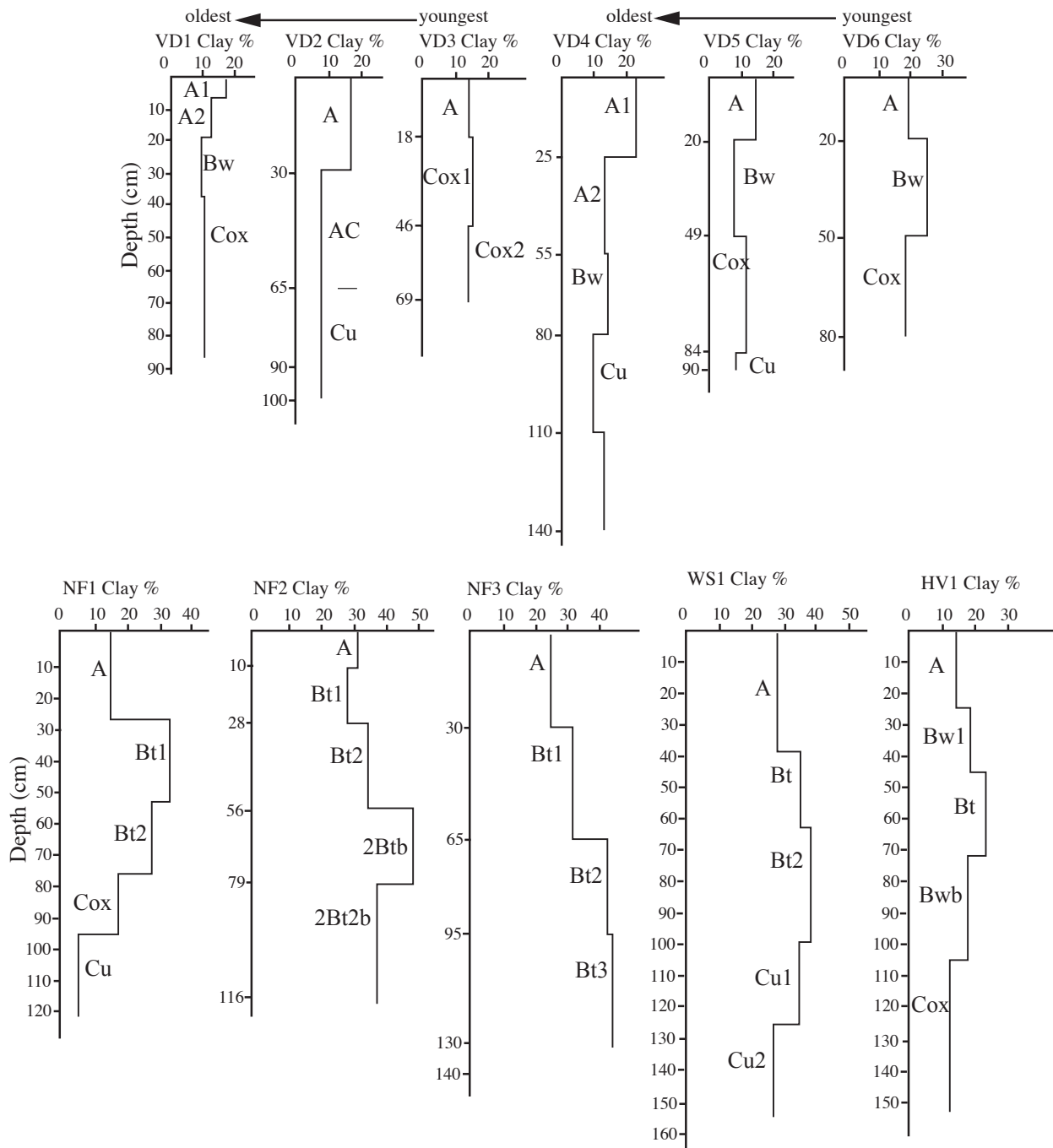


Figure 5. Clay percent vs. depth profiles and horizon designations for soils developed in Van Duzen River strath terraces (VD1-VD6), North Fork Eel River fill terraces (NF1 and NF2), the Refuge Valley fill terrace (NF3), the Waggit Springs Canyon fill terrace (WS1), and the Hettenshaw Valley fill terrace (HV1).

Table 3. Relative age groupings of terrace surfaces based on comparison of individual soil properties, depth of incision for surfaces in similar landscape position, and field topographic relations.

Relative Age	Texture	Clay %	Depth of Development	Color	Depth of incision vs landscape position*	Topographic relations	Preferred Age Relations [#]
younger	VD1-VD6 HV1	VD1-VD6 HV1	VD1-VD6	VD1-VD6 HV1 WS1	VD3, VD6 VD2, VD5 VD1, VD4	VD3, VD6 VD2, VD5 VD1, VD4	VD3, VD6 VD2, VD5 VD1, VD4
↓							
older	NF1, WS1 NF2-3	NF1, WS1 NF3 NF2	HV1, WS1, NF1 NF2 NF3	NF1 NF2-3	NF1 NF2 NF3	HV1, WS1, NF1 NF3 NF2	HV1, WS1, NF1 NF2-3

* Least incision is interpreted to be youngest and most incision is interpreted to be oldest. Relative age of HV1 and WS1 is not assessed by this method because they are located at the drainage divide.

[#] Preferred relative age relation going from youngest to oldest based on rankings in the six columns.

applying an uplift rate of 1 m/ky determined on the California Coast (Kelsey and Carver, 1988), the calculated age of terrace NF3 is 193 ka. Based on published uplift rates from the Central Oregon Coast Range (0.1-0.3 m/ky) located a similar distance east of the subduction zone an uplift rate of 0.3 m/ky is geologically reasonable. Based on soil development and clay percent, an age of 193 ka for terrace NF3 is also geologically reasonable and uplift rates of 0.1 and 4 m/ky result in calculated ages that are too old and too young, respectively. Therefore, the late Quaternary uplift rate in the Van Duzen/North Fork Eel Rivers region is broadly constrained to 0.3-1 m/ky.

Table 4. Inferred ages of each terrace based on; (1) depth of incision and the assumption that uplift rates (U) are equal to incision rates (I) for various published uplift rates in the region; and (2) maximum clay percent. Due to their position in the drainage divide the incision method may underestimate terrace age for HV1, WS1, and NF1.

Terrace ^β	Estimated Age (ka) assuming I=0.1 m/ky and I=U ^ζ	Estimated Age (ka) assuming I=0.3 m/ky and I=U ^ζ	Estimated Age (ka) assuming I=1m/ky and I=U ^η	Estimated Age (ka) assuming I=4m/ky and I=U ^α	Estimated age (ka) based on clay % [#]
VD3	50	16	5	1	10
VD6	50	16	5	1	42
VD2	100	33	10	3	14
VD5	100	33	10	3	9
VD1	300	100	30	8	14
VD4	240	80	24	6	32
HV1	30	10	3	0.75	37
WS1	180	60	18	5	270
NF1	750	250	75	19	133
NF2	1660	553	166	42	1277
NF3	1930	643	193	48	630

^β Terraces grouped by preferred age relations, youngest on top, oldest on bottom.

^ζ Implied incision rate based on published uplift rate from the Central Oregon coast Range, Personius (1995).

^η Implied incision rate based on published uplift rates, Northern California, Kelsey and Carver (1988).

^α Implied incision rate based on published uplift rates near the Mendocino Triple junction, Merritts and Vincent (1989).

[#] Estimated age based on comparison to maximum clay % vs. time relations of Merritts et al., (1991).

Using this range of uplift rates, the Van Duzen/North Fork Eel terraces are mid to late Pleistocene in age and stream capture and river abandonment at the drainage divide (Refuge Valley, NF1) occurred within the last several hundred thousand years but before 75 ka.

Terrace Formation Mechanisms

Differences in soil profile properties and terrace stratigraphy between the strath terraces on the Van Duzen River, the fill terraces on the North Fork Eel River, the Waggit Springs Canyon fill terrace, and the Hettenshaw Valley deposit indicate that the terraces have different relative ages and were formed by different processes. Candidate mechanisms that could cause terrace formation include climatically induced erosion and aggradation, landslide dams, and tectonic uplift. Increased rainfall in northern California during oxygen isotope stages 2, 4, and 6 (Adam and West, 1983) could have increased sediment loads and resulted in region wide aggradation of fill terraces of similar age. However, because the terraces are not synchronous across the Van Duzen/North Fork Eel Rivers drainage divide, terrace formation due to climatically induced sedimentation is unlikely.

Landslide damming is only a viable mechanism of terrace formation for the Waggit Springs Canyon fill terrace. Between the mouth of Waggit Springs Canyon and the BLDF, remnant deposits that match the stratigraphy of terrace WS1 occur along the slopes of the valley wall. These deposits could be remnants of an original continuous fill deposit that extended from the BLDF upstream into Waggit Springs Canyon (Figure 2). If this is the case, then the deposits may represent a deltaic fan system that prograded into a landslide dammed lake. Because Van Duzen River strath terraces are at similar elevations on both sides of the BLDF deposit and lower in elevation than the landslide dam related fill deposits (WS1), they likely post-date the landslide damming event and were formed after the landslide-dam fill deposit was eroded to bedrock in the Van Duzen River channel.

The dominant mechanism for formation and preservation of the terraces distributed across the Van Duzen/North Fork Eel River headwater region is tectonic uplift. Tectonic uplift may induce gradient changes, terrace formation, drainage basin capture, and river flow reversal (Christensen, 1966; Harvey and Wells, 1987; and Prentice, 1989) due to gradient related aggradation and erosion processes (Gregory and Schumm, 1987; Leopold, 1992). The Refuge Valley fill deposit (NF1) in the drainage divide between the Van Duzen and North Fork Eel Rivers is the point of diversion responsible for a stream capture event. Based on the soil relative age data, I infer that the terraces in the Van Duzen/North Fork Eel headwater region are progressively younger to the north. The North Fork Eel River drainage has the oldest terraces (NF1, 2, 3) and a steep channel that is deeply incised into bedrock. The Van Duzen River has younger terraces (VD1-6) and a low gradient channel.

The formation of terraces can be explained by aggradation in response to channel gradient changes generated by uplift in the region. The following sequence of events is proposed to explain the formation of terraces and to account for drainage capture and flow reversal between the north-flowing Van Duzen River and the south-flowing North Fork Eel River (Figures 6 and 7). Initially, a larger North Fork Eel river flowed south, with headwaters in Hettenshaw Valley and the West Fork Van Duzen River (Figures 2 and 6). Uplift in the lower North Fork Eel basin, defeated the gradient of south-flowing channels, promoting aggradation of the North Fork Eel channel, as indicated by the the thick North Fork Eel fill deposits. Then uplift in the vicinity of the Van Duzen/North Fork Eel Rivers drainage divide steepened the gradient of headwater channels of both rivers. Because of prior uplift in the lower North Fork Eel channel the gradient steepening was greater in the Van Duzen channel than in the North Fork Eel channel. This gradient difference promoted the capture of the North Fork Eel headwaters (West Fork Van Duzen River and Hettenshaw Valley) by the modern north-flowing Van Duzen River.

Continued uplift in the vicinity of the drainage divide since the time of capture has resulted in downcutting of both rivers, isolation of the North Fork Eel fill deposits by incision, and the formation of Van Duzen strath terraces (VD1-VD6). Presently, both the East and West Forks of the North Fork Eel River (Figure 3) are headwardly eroding into the Van Duzen River basin, and I infer that the North Fork Eel River may eventually recapture its paleo headwaters, reversing the flow direction again to the south.

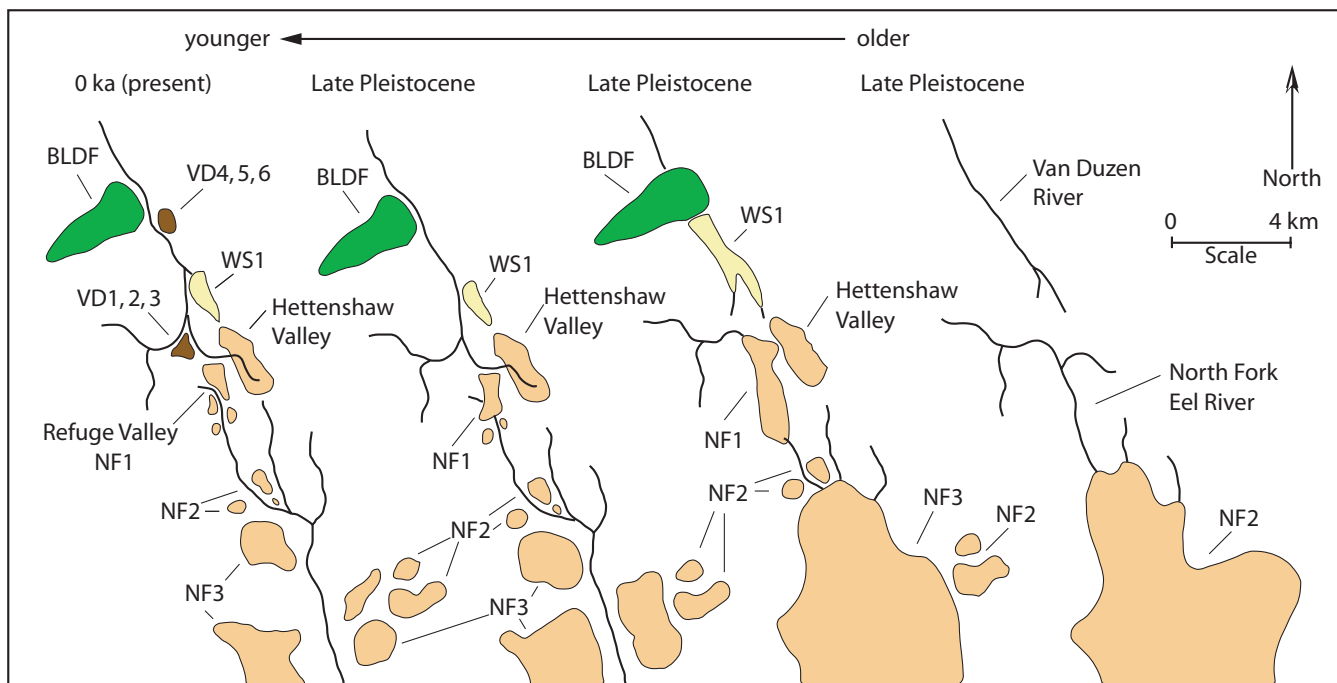


Figure 6. Sequence of terrace formation and stream capture in the Van Duzen/North Fork Eel Rivers headwater region. BLDF, Black Lassic debris flow; NF1, 2, and 3, North Fork Eel fill terraces; WS1, landslide dam related fill deposit of Waggit Springs Canyon; VD1-VD6, Van Duzen River strath terraces.

The above history of past capture and impending recapture is consistent with the soil relative age data and landscape geomorphology. Because the capture model is consistent with the relative ages of the terraces, the apparent stream gradient changes related to tectonic uplift is the dominant terrace forming mechanism.

DISCUSSION

The northward migration of the MTJ has been proposed as the mechanism responsible for temporal changes in uplift rates along coastal northern California (Merritts and Bull, 1989). This migrating bulge of increased uplift rate may be the result of the passage of a slab window (Dickinson and Snyder, 1979; Furlong 1984; 1993) that develops under the North American Plate south of the triple junction as the Gorda Plate is consumed by subduction, producing higher heat flow in the lithosphere. Furlong et al. (1989; 1993) suggested that growth of the slab window is associated with lithospheric thinning, thermal expansion of the crust, and isostatic flexural uplift. Seismic tomography, as well as, reflection and wide-angle refraction imaging studies indicate that thicker crust exists in the region north and south of the trailing edge of the Gorda plate (Verdonck and Zandt, 1994; Beaudoin et al, 1996). Furlong and Govers (1999) attributed the thickened crust to mantle material welded to the trailing edge of the Gorda plate and underlying the North American plate (Figure 7). They defined this process as the Mendocino Crustal Conveyor, in which ephemerally thickened crust moves northward at the speed of MTJ migration and then thins and subsides as the triple junction passes.

The maximum amount of present day uplift along the northern California coast is centered around the MTJ with differentially less uplift extending to the south (Merritts and Bull, 1989; Merritts and Vincent, 1989; Figure 7). A cartoon depiction of this relation and how the uplift effects terrace deposition through time is presented on Figure 8. It is expected and supported by observations that the greatest amount of uplift is coincident with the region of greatest crustal thickening, which occurs directly south of the southern edge of the Gorda Plate (Figure 7). The location of the southern edge of the Gorda Plate varies from different workers, but is thought to be along the southern gradient of an isostatic residual gravity anomaly (Jachens and Griscom, 1983) or, directly beneath the Hettenshaw Valley region, based on seismicity and seismic structure (Castillo and Ellsworth, 1993; McPherson,

1989; 1992; Verdonck and Zandt, 1994; Beaudoin et al., 1996). Therefore, the results of this study suggest that a migrating bulge of uplift similar to the uplift pattern observed along the coast occurred at the same latitude inland in the North Fork Eel basin.

The timing of deformation and location of three previous positions of the MTJ south of its present location is illustrated on Figure 7 (Kelsey and Carver, 1998). Because the field area is directly east of the Garberville sediments, I infer that contractional deformation began uplifting the North Fork Eel basin 2.2-2.5 Ma and that oblique strike-slip deformation along the Lake Mountain Fault began 1.3-1.6 Ma (Figure 7). The timing of

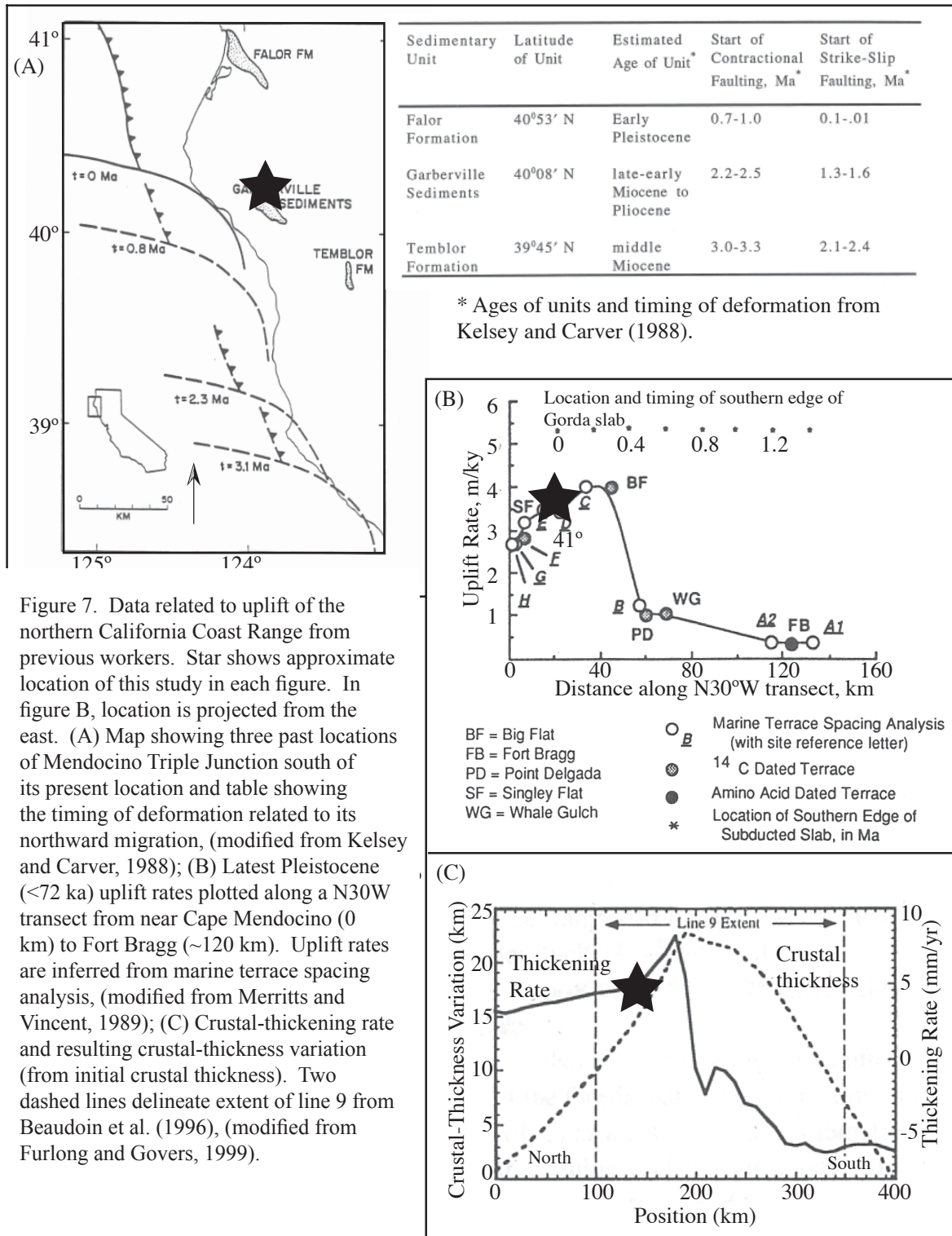


Figure 7. Data related to uplift of the northern California Coast Range from previous workers. Star shows approximate location of this study in each figure. In figure B, location is projected from the east. (A) Map showing three past locations of Mendocino Triple Junction south of its present location and table showing the timing of deformation related to its northward migration, (modified from Kelsey and Carver, 1988); (B) Latest Pleistocene (<72 ka) uplift rates plotted along a N30W transect from near Cape Mendocino (0 km) to Fort Bragg (~120 km). Uplift rates are inferred from marine terrace spacing analysis, (modified from Merritts and Vincent, 1989); (C) Crustal-thickening rate and resulting crustal-thickness variation (from initial crustal thickness). Two dashed lines delineate extent of line 9 from Beaudoin et al. (1996), (modified from Furlong and Govers, 1999).

uplift in the Van Duzen/North Fork Eel Rivers headwater region, generated by the growth of the slab window, is contemporaneous with both contractional and transpressional tectonic regimes. The close proximity of the region to the MTJ allows contractional faulting, strike-slip faulting, and uplift from crustal thickening to be active at the same time. Therefore, I infer that the magnitude of uplift generated at the surface at a particular latitude is related to the magnitude of crustal thickening.

The major geomorphic responses of a river to uplift lag behind the uplift in time. Therefore, a drainage basin currently responding to rapid uplift rates at the latitude of the triple junction may have adjusted to low rates of uplift within the past several hundred thousand years (Merritts and Vincent, 1989). The sequence of channel gradient changes and terrace formation in the Van Duzen/North Fork Eel Rivers headwater region (Figure 6) can be explained as a response to an uplift bulge migrating north with the MTJ.

Within the North Fork Eel basin, uplift rates first increased near the sites of NF2 and NF3 while remaining lower at the divide area upstream, promoting aggradation of fill deposits NF2 and NF3 (Figure 8). At this time, uplift migrated to the north, promoting aggradation of NF1, WS1, and Hettenshaw Valley, as well as, the capture of the headwaters of the North Fork Eel River by the Van Duzen River. Incision in response to uplift migrated to the north as well, resulting in the river cutting into bedrock and isolating the former North Fork Eel channel fills. The fishhook morphology of streams in the North Fork Eel River basin is more developed in the south than in the north (Figure 2), suggesting past stream capture and flow reversal events.

The pattern of gradient shallowing and aggradation of fill deposits followed by incision is the result of the passage of a migrating uplift bulge. This northwardly migrating uplift is responsible for the river adjustment and terrace formation described above, and the impending recapture by the North Fork Eel of its former headwaters will likely occur after the MTJ migrates to the north of its present location.

CONCLUSIONS

A series of fluvial terraces occur within and near the drainage divide of the Van Duzen and North Fork Eel Rivers. Comparison of soil development and stratigraphy for the terraces in proximity to the drainage divide indicates that they formed diachronously and by different processes. The alluvial fill terraces along the North Fork Eel River are older than the drainage divide. The terraces at Refuge and Hettenshaw Valleys, presently at the divide, were deposited just prior to the stream capture that created the present divide. Since that time, the Waggit Springs Canyon fill terrace formed behind the Black Lassic debris flow dam. After the river cut through the Black Lassic debris flow dam, fluvial strath terraces formed along the Van Duzen River.

Presence of alluvial fill deposits in the Van Duzen/North Fork Eel River drainage divide, headward erosion into the divide from the south, progressively younger terraces to the north, and documented uplift associated with the MTJ all support the hypothesis that the terraces formed primarily in response to tectonic uplift. The uplifting landscape caused drainage basin capture and river flow reversal in the late Pleistocene. This work demonstrates that the pattern of uplift documented along the coast persists inland at least to the location of the Van Duzen/North Fork Eel drainage divide and provides field based surface geomorphic evidence in support of the proposed Mendocino Crustal Conveyor of Furlong and Govers (1999).

ACKNOWLEDGEMENTS

This work was made possible by field discussions with Bud Burke, Gary Carver, Tom Leroy, Charlie Narwold, Jennifer Curtis, Joanna Redwine, Giovanni Vaduro, Fred Berman, Vaughn Balzer, Dianne Sutherland, Grant Roden, and Raughley Ann Koehler. Data analysis was improved by thoughtful insight from Harvey Kelsey. This research was sponsored by a \$500 dollar research grant from the Northern California Geological Society, the Pronzini Christmas tree farm, the Salty's Crew, and student research support to Koehler to conduct tsunami studies with Gary Carver for Pacific Gas and Electric Co. Review by Steve Bacon improved the manuscript. Special thanks to HSU.

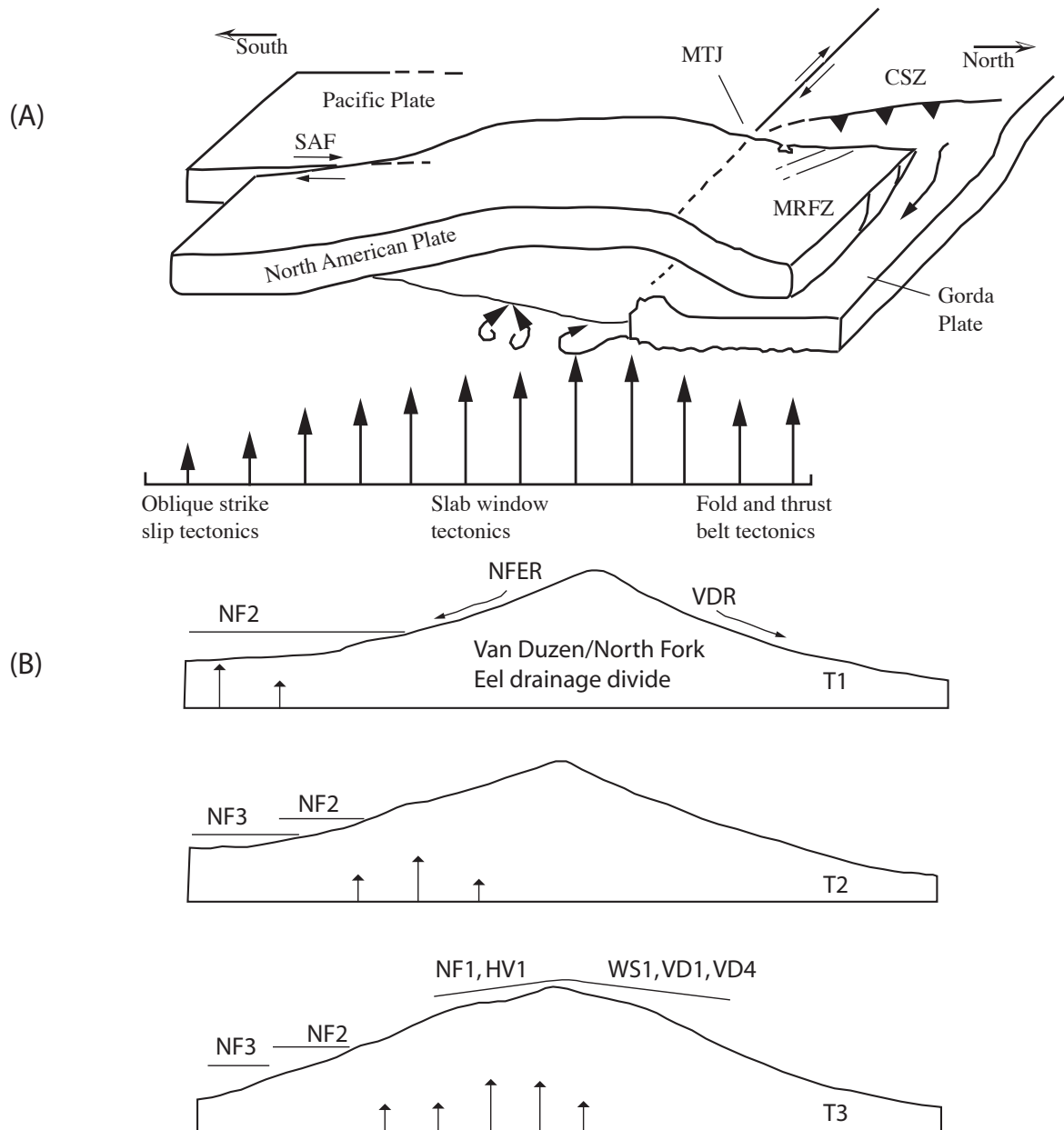


Figure 8. (A) Cartoon shows deformation of the North American Plate in response to the northward migration of the Mendocino Triple Junction. Length of arrows below drawing indicate relative amount of uplift. Circular arrows indicate zone of upwelling magma. SAF, San Andreas Fault; CSZ, Cascadia Subduction Zone; MTJ, Mendocino Triple Junction; MRFZ, Mad River Fault Zone, (modified from McPherson, 1992). (B) Cartoon shows sequence of topographic adjustment and terrace formation in response to uplift migrating through the study area. Length of arrows indicate relative amount of uplift migrating north through time. VDR, Van Duzen River; NFER, North Fork Eel River; T, time; T4, present.

REFERENCES CITED

- Adam, D.P., and West, G.J., 1983, Temperature and precipitation estimates through the last glacial cycle from Clear Lake, California, pollen data: *Science*, v. 219, p. 168-170.
- Atwater, T., 1970, Implications of plate tectonics for the cenozoic tectonic evolution of western North America, *Geological Society of America Bulletin*, 81: 3513-3536.
- Bailey, E.H., Irwin, W.P., and Jones, D. L., 1964, Franciscan and Related rocks and Their Significance in the Geology of Western California, California Division of Mines and Geology, Bulletin 183.

- Beaudoin, B.C., Godfrey, N.J., Klemperer, S.L., Lendl, C., Trehu, A.M., Henstock, T.J., Levander, A., Hole, J.E., Meltzer, A.S., Luetgert, J.H., and Mooney, W.D., 1996, Transition from slab to slabless: Results from the 1993 Mendocino triple junction seismic experiment, *Geology*, v. 24, p. 195-199.
- Birkeland, P., *Soils and Geomorphology*, 432 pp., Oxford University Press, 1999.
- Blake, M.C., Jr., and Jones, D. L., 1974, Origin of Franciscan Melanges in Northern California, *In* Dott, ed., *Modern and ancient Geosynclinal Sedimentation*, Marshall Kay Vol., S.E.P.M. Sp. Pub. 19.
- Blake, M.C., Jr., and Jones, D.L., 1981, The Franciscan Assemblage in northern California: A reinterpretation, in *The Geotectonic Evolution of California*, Rubey vol. 1, ed. W.G. Ernst, Prentice-Hall, Englewood Cliffs, N.J., pp. 306 - 328.
- Blake, M.C., Jr., A.S. Jayko, and R.J. McLaughlin, 1985, Tectonostratigraphic terranes of the northern Coast Ranges, California, in *Tectonostratigraphic Terranes of the Circum-Pacific Region*, Earth Sci. Ser., vol. 1, ed. D.G. Howell, Circum-Pacific Council for Energy and Mineral Resources, Houston, TX., pp. 159-171
- Carver, G.A., R.M. Burke, and H.M. Kelsey, 1985, Quaternary Deformation Studies in the Region of the Mendocino Triple Junction, in Jacobsen, M.L., and Rodrigues, T.R., eds., *Summaries of Technical Reports*, v. 21, National Earthquake Hazards Reduction Program, U.S. Geological Survey Open File Report 86-31, p. 58-62.
- Carver, G.A., R.M. Burke, and H.M. Kelsey, 1986, Deformation of late Pleistocene marine terraces along the California coast north of Cape Mendocino, *Geological Society of America, Abstracts with Programs*, v. 18, p. 93.
- Carver, G.A. and R.M. Burke, 1987, Late Pleistocene and Holocene paleoseismicity of Little Salmon and Mad River thrust systems, N. W. California - implications to the seismic potential of the Cascadia subduction zone, *Geological Society of America, Abstracts with Programs, national meeting*, v.19, n. 7, p. 614.
- Castillo, D.A., and Ellsworth, W.L., 1993, Seismotectonics of the San Andreas fault system between Point Arena and Cape Mendocino in northern California: Implication for the development and evolution of a young transform, *Journal of Geophysical Research*, v. 98, p. 6543-6560.
- Christensen, M.N., 1966, UC Berkeley. Quaternary of the California Coast Ranges, in: *Geology of Northern California*, Bulletin 190, Edgar H. Bailey (editor), California Division of Mines and Geology, Ferry Building, San Francisco.
- Clarke, S.H., and G.A. Carver, 1989, Late Cenozoic structure and seismic potential of the southern Cascadia subduction zone, *Eos Trans. AGU*, 70, 1331-1332.
- Dickinson, W.R. and W.S. Snyder, 1979, Geometry of subducted slabs related to San Andreas transform, *Journal of Geology*, 87, p. 609-627.
- Furlong, K.P., and Govers, R., 1999, Ephemeral crustal thickening at a triple junction: The Mendocino Crustal Conveyor, *Geology*, v. 27, no. 2, p. 127-130.
- Furlong, K.P., 1984, Lithospheric behavior with triple junction migration, an example based on the Mendocino triple junction, *Physics of the Earth and Planetary Interiors*, v. 36, p. 213-223.
- Furlong, K.P., 1993, Thermal-rheologic evolution of the upper mantle and the development of the San Andreas fault system, *Tectonophysics*, 223, p. 149-164.
- Furlong, K.P., Hugo, W.D., and G. Zandt, 1989, Geometry and Evolution of the San Andreas Fault Zone in Northern California, *Journal of Geophysical Research*, vol. 94, p. 3100 - 3110.
- Gregory, D.I., and Schumm, S.A., 1987, River Channels- Environments and Processes; In: *The Effect of Active Tectonics on Alluvial River Morphology*; ed. Keith Richards, chapter 3.
- Harvey, A.M., and S.G. Wells, 1987, Response of Quaternary fluvial systems to differential epeirogenic uplift: Aguas and Feos river systems, southeast Spain, *Geology*, v. 15, p. 689-693.
- Herd, Darrel G., 1978, Intracontinental Plate boundary East of Cape Mendocino, California, *Geology*, v. 6, pp. 721-725.
- Irwin, W.P., 1960, Geologic reconnaissance of the northern Coast Ranges and Klamath , California, with a summary of the mineral resources, *Calif. Div. Mines Bull.* 179, 80 p.
- Jachens, R.C., and A. Griscom, 1983, Three-Dimensional Geometry of the Gorda Plate Beneath Northern California, *Journal of Geophysical Research*, vol. 88, pp. 9375-9392.
- Jenny, H., 1941, *Factors of Soil Formation*, McGraw-Hill, New York.
- Kelsey, H.M. and G.A. Carver, 1988, Late Neogene and quaternary Tectonics Associated With Northward Growth of the San Andreas Transform Fault, Northern California, *Journal of Geophysical Research*, Vol. 93, No. B5, pp. 4797-4819.
- Kelsey, H.M., 1977, Landsliding, channel changes, sediment yield, and land use in the Van Duzen River basin, north coastal California, 1941-1975, [Ph.D. thesis]: Santa Cruz, University of California.
- Kelsey, H.M., 1978, Earthflows in Franciscan Melange, Van Duzen River Basin, California, *Geology*, v. 6, p.361-364.
- Koehler, R.D., 1999, Terrace Formation, Drainage Adjustment, And Tectonic Geomorphology Of The Van Duzen/North Fork Eel Rivers Headwater Region, Northern California [abs.]: *Geological Society of America Abstracts with Programs, Annual Meeting Cordilleran Section*, v. 31, p. 71.
- Koehler, R.D., 1997, Quaternary history of the Van Duzen River headwaters along the northern portion of the Lake Mountain fault zone, northern California [abs.]: *Geological Society of America Abstracts with Programs, Annual Meeting Cordilleran Section*, v. 29, p. 42.

- Koehler, R.D., 1999, Terrace Formation, Drainage Adjustment and Tectonic Geomorphology of the van Duzen/North Fork Eel Rivers Headwater Region, Northern California, [masters thesis]: Humboldt State University.
- Leopold, L.B., 1992, Base level rise: Gradient of deposition, *Israel Journal of Earth Science*, v. 41, p. 57-64.
- Manning, G.A., and B.A. Ogle, 1950, Geology of the Blue Lake Quadrangle, California, *Bull. Calif. Div. Mines Geol.*, 148, 35 pp.
- McLaughlin, R.J., S.A. Kling, R.Z. Poore, K.L. McDougall, and E.C. Beutner, 1982, Post-middle Miocene accretion of Franciscan rocks, northwestern, California, *Geological Society of America Bulletin*, 93, 595-605.
- McPherson, R.C., 1992, Seismicity and Stress at the Southern End of the Cascadia Subduction Zone, *American Association of Petroleum Geologists Guide Book #71, Field Guide to Late Cenezoic Subduction Tectonics and Sedimentation in North Coastal California*, G.A. Carver and K.R. Aalto, editors, pp. 21-30.
- McPherson, R.C., 1989, Seismicity and focal mechanisms near Cape Mendocino, northern California: 1974-1984 [M.S. Thesis]: Arcata, California, Humboldt State University, 75 p.
- Merritts, D.J., and Brustolon, A.E., 1994, The Mendocino Triple Junction: Active faults, paleoseismology, and rapid uplift, U.S. Geological Survey, Open File Report OF 94-0568, In: Prentice, C., Swartz, D., and Yeats, R., *Proceedings of the Workshop on Paleoseismology Sept 18-22, 1994*, published by U.S. Geological Survey.
- Merritts, D.J., 1996, The Mendocino Triple Junction: Active Faults, Episodic Coastal Emergence, and Rapid Uplift, *Journal of Geophysical Research*, v. 101, pp. 6051-6070.
- Merritts, D.J., and W.B. Bull, 1989, Interpreting Quaternary uplift rates at the Mendocino triple junction, northern California, from uplifted marine terraces, *Geology*, v. 17, p. 1020-1024.
- Merritts, D.J., O.A. Chadwick, and D.M. Hendricks, 1991, Rates and processes of soil evolution on uplifted marine terraces, northern California, *Geoderma*, 51, 241-275.
- Merritts, D., and Kirk R. Vincent, 1989, Geomorphic response of coastal streams to low, intermediate, and high rates of uplift, Mendocino triple junction region, northern California, *Geological Society of America Bulletin*, v. 101, p. 1373-1388.
- Ogle, B.A., 1953, Geology of Eel River Valley Area, Humboldt County, California, *Calif. Div. Mines Bull.* 164.
- Personius, S.F., Kelsey, H.M., and Grabau, P.C., 1993, Evidence for Regional Stream Aggradation in the Central Oregon Coast Range during the Pleistocene-Holocene Transition, *Quaternary Research*, 40, 297-308.
- Personius, S.F., 1993, Age and Origin of Fluvial Terraces in the Central Coast Range, Western Oregon, U.S. Geological Survey Bulletin 2038.
- Prentice, C., 1989, Earthquake geology of the northern San Andreas Fault near Point Arena, California, [Ph.D. thesis]: California Institute of Technology.
- Soil Survey Staff, 1992, Soil Survey Laboratory Methods Manual, U.S. Department of Agriculture, Report No. 42, Version 2.0.
- Taylor, C.L., and Swan, F.H., 1986, Geological assessment of the seismic potential of the Bartlett Springs shear zone for Scott Dam, Lake County, California: Final report By Geomatrix Consultants for Pacific Gas and Electric Company, 51 p.
- Upp, R., 1982, Holocene activity on the Maacama Fault Mendocino County, California, [Ph.D. Thesis], Stanford University.
- Verdonck, D., and Zandt, G., 1994, Three-dimensional crustal structure of the Mendocino triple junction region from local earthquake travel times, *Journal of Geophysical Research*, v. 99, p. 23843-23858.
- Witter, R.C., G.A. Carver, J.R. Patton, H.M. Kelsey, C.E. Garrison-Laney, R.D. Koehler, and W.D. Page, 2001, Evidence for progressive folding of late Holocene tidal marsh deposits along the western Little Salmon fault, Humboldt Bay, northern California (abs), *Seismological Research Letters*, 72, 270.
- Witter, R.C., Patton, J.R., Carver, G.A., Kelsey, H.M., Garrison-Laney, C., Koehler, R.D., and Hemphill-Haley, E., 2002, Upper-Plate Earthquakes on the Western Little Salmon Fault and Contemporaneous Subsidence of Southern Humboldt Bay over the Past 3,600 Years, Northwestern California, Final Technical Report to the U.S. Geological Survey, National Earthquake Hazards Reduction Program (award # 01HQGR0125).

Historic terrace deposition and incision at Cuneo Horse Camp

Bonnie Smith and Diane Sutherland

ABSTRACT

The storms of 1955, 1964, and 1997 produced extensive mass wasting, channel aggradation and widening throughout all major north coast river systems including the Eel, Mad, Van Duzen Rivers, Redwood Creek, and Bull Creek. The community of Bull Creek was damaged in the 1955 storm, and after the 1964 flood, residents abandoned the flooded town and the watershed was incorporated into State Park ownership. Cuneo Creek was identified as a primary source of sediment to Bull Creek, and mitigation efforts to avoid deleterious effects on the old-growth redwoods in the lower Bull Creek flats have been ongoing since the early 1970's.

Stop 1-2 will outline the topographic surveys in Cuneo Creek from 1976 – 2005 that document the erosion into the 1964 maximum aggradation terraces. The combined aggradation from both '55 and '64 storms totals at least 7 meters of fill at the Cuneo Bridge. Surveys in 2000, 2003 and 2005 document exhumed alder trees, bedrock reaches, and stratigraphic layers that indicate the channel may have scoured close to the pre-55 elevation in some places. We estimate that nearly 500,000 m³ of sediment has been eroded from the Horse Camp terraces over the 33-year study period, at least half of it in the first 12 year time step. This stop is intended to give trip participants a sense of scale for the dynamic sediment flux of north coast river systems within the Mendocino Deformation Zone.

BACKGROUND

Cuneo Creek is a steep (3%) gravel-bedded stream, draining 10.8 km² of the northern California Coast Range within the Eel River basin. Cuneo Creek is located within the Bull Creek watershed about 25 km east Cape Mendocino, and is the downstream-most major tributary to the south fork of the Eel River. Tributaries of Eel River experience some of the world's highest rates of sediment production as a result of steep topography associated with rapid uplift; erodible, weakly-consolidated sedimentary rocks of the Franciscan and Yager terranes; and heavy, intense precipitation concentrated in the winter months (Brown and Ritter, 1971; Lisle, 1990).

The upper and lower portions of the Bull Creek watershed have had very different land use histories, which contributed to the pattern of historical sediment production, storage, and transport through the watershed. The lower portion of the watershed, from Albee Creek to the confluence with the South Fork Eel River consists of primarily old-growth redwood forest which has been under management as a park since the 1920's (see Map for day 1). In contrast, the upper watershed from approximately Albee Creek to the headwaters, including Cuneo Creek, remained under private ownership until the late 1960's. In the early 1900's, a small town of approximately 300 people was located near the boundary between the upper and lower watershed (LaVen, 1987), and dwellings were scattered throughout the upper basin. Most of the upper watershed was cleared for grazing, livestock, and farming. Accelerated timber harvesting occurred from 1946-1966 as a result of an annual tax on standing timber and an increased demand to fill the post-World War II timber shortage (Short, 1993). In addition, several major wildfires burned much of the upper watershed, including Cuneo Creek, between 1948 and 1964 (Short, 1993).

Aggradation events in Cuneo Creek coincided with three large, regional floods in 1955, 1964 and 1997. These floods produced extensive mass wasting, channel aggradation and widening throughout all major north coast river systems including the Eel, Mad, Van Duzen Rivers and Redwood Creek (Lowdermilk, 1961; Kelsey, 1980; Madej, 1996; LaVen, 1987; Short, 1993; Sloan et al., 2001). In 1955, a large storm delivered intense rainfall, with total estimated precipitation of 93 cm in the Bull Creek watershed (Short, 1993). Mass wasting of the hillslopes in the upper watershed overloaded the channels with sediment and debris, causing severe channel aggradation and widening throughout the Bull Creek watershed, flooding and gravel deposition in the town of Bull Creek, and the loss of approximately 400 old-growth redwood trees within the park. The Devil's Elbow landslide at the headwaters of the South Fork of Cuneo Creek appeared dormant in the 40's, and afterward the '55 storm it was evident as a feature on the landscape. Channel widths in the mainstem Bull Creek that were ~ 60 ft before the storm, were estimated to be ~ 300 ft after this storm (Lehre, 2006).

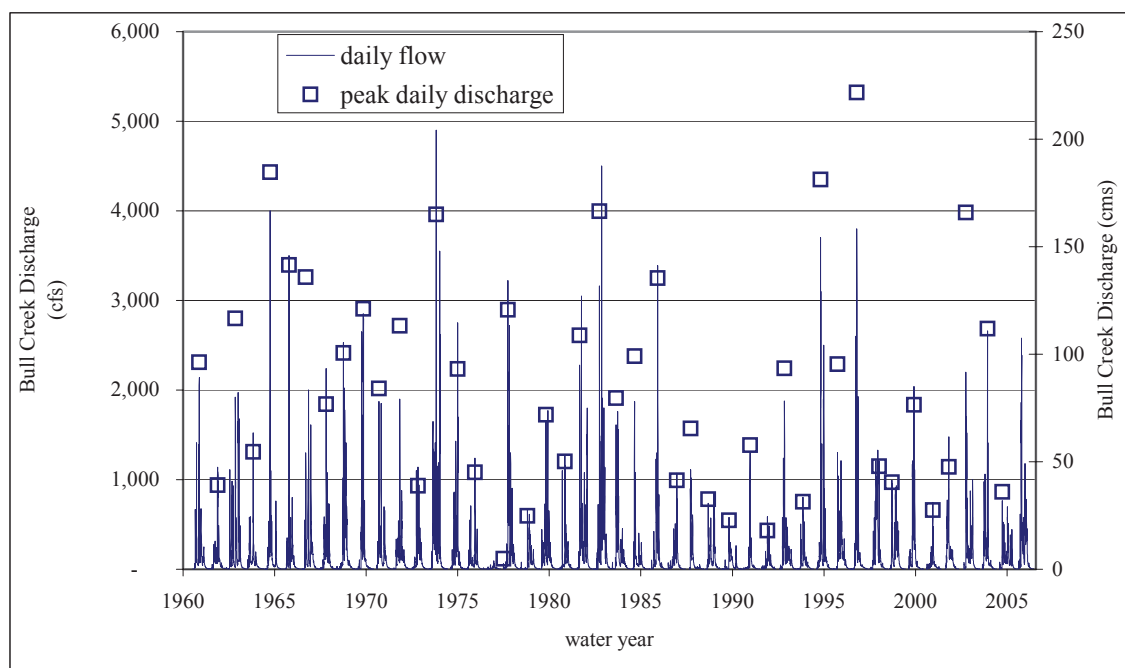


Figure 1. Average daily flow and peak annual discharge for Bull Creek gage (1960 – 2005). Peak annual discharge for storm events in 1964 (estimated to be 185 cms) and 1997 (222 cms) will be discussed at Stop 1-2.

Efforts within the lower Bull Creek watershed to stabilize the channel and route sediment through the lower watershed were all for naught as a second wave of extensive hillslope failures occurred during the December 22, 1964 storm. Large volumes of sediment were again delivered to the channel, and the town site of Bull Creek was again severely damaged and subsequently abandoned. Six hundred more old-growth redwood trees were killed within the park, and the bridge built over Cuneo Creek after the 1955 storm was buried in sediment. Deposits from the 1964 storm buried those from the 1955 storm at every exposure we have seen in the Cuneo Creek study reach and most places in Bull Creek, making deposits from the 1955 and 1964 storms indistinguishable on the surface. After the 1964 flood, the remainder of the upper watershed of Bull Creek was purchased and incorporated into the Humboldt Redwoods State Park. Rehabilitation efforts aimed at reducing sediment loads to streams including building sediment retention structures, road removal, building of in-stream structures, rip-rapping the banks, and a host of other treatments were used throughout the basin starting in the late 1960's and continuing to this day.

The December 22, 1964 peak flow remained the highest on record until the “1997 New Year’s Flood” on December 31, 1996 (Figure 3). Peak flow at the USGS gage was higher in the 1997 storm than in 1964. The 1964 peak had to be estimated because the gauge was demolished in the flood. The 1997 New Year’s flood triggered further mass wasting in the upper Bull Creek watershed. However, the 1997 flood deposits did not leave terrace deposits as extensive or voluminous as those from 1964.

Aggradation in Cuneo Creek

The Cuneo Creek stream channel and floodplain were densely vegetated prior to 1955 and aerial photography provides only coarse estimates of the original channel configuration and width (Figure 2). The 1955 flood stripped nearly all of the vegetation from the channel and floodplain, exposing the channel, allowing for more accurate aerial photographic interpretation of channel planform following the 1955 storm. The only known quantitative reference for aggradation in Cuneo Creek from this storm is Thorp’s (1959) description of 2.4 m of fill in Cuneo Creek, about 200 m upstream of the modern bridge. Short (1993) also speculates that the 1955 bridge was buried by ~ 12 m of sediment, but we believe that the original redwood bridge was more likely carried



Figure 2 is the cross sections at Horse Camp (see .jpg or .tif or .pdf file)

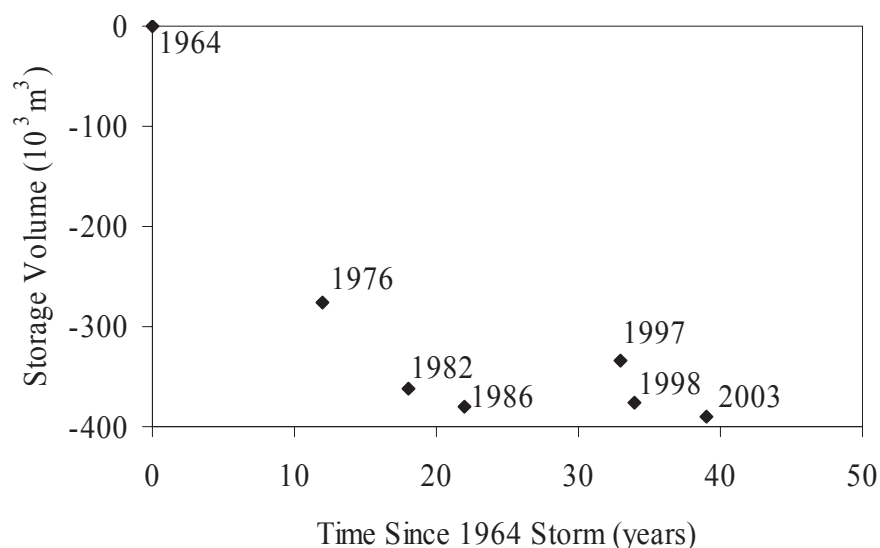


Figure 3. Exponential model fit of measured changes in stored sediment to estimate maximum storage volume in 1964 (time = 0).

attempt to quantify aggradation for the 55-64 time step. We use the 1964 terraces as the maximum fill surface from which to calculate changes in storage from 1964 – 2003.

Cuneo Channel Surveys:

Even before the 1964 storm, Cuneo Creek was identified as one of the largest sources of sediment within the Bull Creek watershed (Lowdermilk, 1961). In 1976, the California State Department of Parks and Recreation established and surveyed 11 channel cross-sections. The cross-sections are on the mainstem of Cuneo Creek, spaced 200 – 400 feet apart from just downstream of the North Fork to the confluence with Bull Creek (Figure 1). In 1982, ten of these cross-sections were reoccupied and permanent endpoints were established with 1-m rebar. The cross-section downstream of the Cuneo Creek bridge was never re-occupied because influence by channel changes in the mainstem Bull Creek made re-surveying impractical. The 10 others were surveyed in 1982, 1983, 1985 and 1986 (Short, 1993), 1998 (Hall, 2000), 2001, 2003 (Smith, 2004) and 2005 (this volume). In addition to cross sections, Smith (2004) identified and surveyed remnant terraces during the 2000-2001 field season. These topographic surveys included terraces, active floodplains and channels from the edge of the 1964 surfaces (valley walls) down to the modern channel.

Quantifying the change in stored material in Cuneo terraces

We used differences in topographic surfaces, including floodplain and channel, to compute changes in storage for time steps six time steps [1964 – 1976, 1976 – 1982, 1982-1986, 1986 – 1997, 1997 – 1998, and 1998 – 2003] by differencing topographic surfaces of the channel, floodplain, and surrounding terraces. Digital elevation models were built from cross-section data, surveys of remnant stream terraces and aerial photographs (Table 1). The maximum aggradation surface in 1964 is estimated by interpolation between remnant stream terraces extant in our 2000 – 2001 topographic surveys. More recent topographic surfaces incorporate channel cross-section data and aerial photographic data. The ten channel cross-sections that were established in 1976 serve as the base for topographic surfaces between 1976 and 2003. A survey of remnant stream terraces in 2000 and 2001 added additional topographic information between cross-sections. Scanned aerial photos were used as a guide to digitize channel location and edges of floodplain and terraces between cross-sections, and the edges were used as break-lines in the interpolation procedure to preserve the abrupt angle of terrace edges channel form. Channel cross-sections surveyed in 1976, periodically from 1982 thru 1986, in 1998, 2000, and 2003 provide further quantitative measures of changes in channel characteristics and sediment storage over the 33-year period from 1964 to 2003.

downstream. Aggradation at the Cuneo Creek bridge as a result of both the '55 and '64 events is therefore estimated at between 7 to 12 meters based on estimates from Short (1993, figure 6).

These three major storms provide a timeframe in which to study the cycles of aggradation and degradation in Cuneo Creek: (1) 1955-1964 – initial channel aggradation, (2) 1964-1997 – net incision into 1964 maximum aggradation surfaces, and (3) 1997-2003 – most recent and detailed measurements of changes in channel storage. Because the 1964 deposits buried 1955 in every exposure we found, we did not

Table 1. Table of data sources used to generate surface for each analysis year.

Year	XS Survey Date Auto-level (AL), Total Station (TS)	Stream terrace Survey date	Aerial Photo Years
1964 (large flood)	None	2000/2001*	None
1976	1976 (Short, 1993)	2000/2001*	1974
1982	1982 (Short, 1993)	2000/2001*	1984
1986	1986 (Short, 1993)	2000/2001*	1984 and 1988
1997 (large flood)	None	2000/2001*	1997
1998	1998* (Hall, 2001)	2000/2001*	None*
2003	2003*	2000/2001*	None**

* Data collected during this study

** No aerial photo interpretation required because of complete total station survey

SEDIMENT TRANSPORT

Sediment-transport function

Intuitively, one can imagine that sediment transport in a channel is a function not only of stream discharge, but also of sediment availability. That is, even given high stream discharge, bed load transport will be low if there is no sediment available. Lisle and Church (2002) reassert Gilbert's (1914) concept of transport capacity: "a change in the rate of sediment supply results in a change in the storage capacity as well as the transport rate which is regulated by channel adjustments. These adjustments determine the quantity transported at a particular sediment stage – the transport capacity of the channel at that stage. Transport capacity is not a fixed quantity but signifies different equilibria between transport and supply rates at different sediment stages." (Lisle and Church, 2002). The channel cross-sections and topographic surveys from Cuneo Creek provide a data set from which we can examine the relation between sediment transport under changing storage conditions, with the ultimate goal of developing a mathematical function that describes the relation between sediment transport and storage volume. Development of a transport-storage (T-S) function requires measurements of stored sediment volume and rate of bed-material transfer from a study reservoir. The sediment reservoir at Cuneo Creek was at maximum storage after the 1964 storms, and there has been net incision into the reservoir until 2003. The latter part of this paper is devoted to developing and examining a sediment-transport function that fits the 1964 – 2003 Cuneo Creek data.

Bed-material output rate is computed by dividing the net volume of sediment removed by the total number of days between measurements. The bed-material output rate is not equal to a sediment transport rate; rather it is a change in channel storage over time. A bed-material output rate equal to zero indicates no net change in channel storage, or an equilibrium condition between sediment input and output. A bed-material output rate greater than or less than zero indicates a disequilibrium condition in which channel storage is changing by way of fill or scour, respectively. In order to account for wet and dry periods, the number of calendar days was replaced by the number of days with a geomorphically significant discharge. The geomorphically significant discharge was assigned to have an exceedance probability of 10% using daily discharge from 1960 – 2002. This discharge was computed for Bull Creek (US Geological Survey gauging station #11476600), and prorated for ungauged Cuneo Creek by using the rating curves developed during the 2002 water year between Bull and Cuneo Creeks. This discharge with an exceedance probability of 10% is 9 cms (317 cfs) in Bull Creek and 2.3 cms (81 cfs) in Cuneo Creek. This flow was arbitrarily chosen, and was capable of moving particles as large as 50 mm during field measurements of bedload and discharge in water year 2001. This grain size is larger than 84% of the bed-material.

Surface grain size characterization

Lisle and Church (2002) proposed that one of the mechanisms for reduction in transport rate is the formation of surface structure and channel armoring. Other mechanisms that explain the decrease in the rate of sediment transport from a sediment reservoir as storage volume decreases include increasing resistance of the channel to entrainment by form resistance (e.g. bars, bedforms, pebble structures in the flow) and the depletion of marginal sources of sediment available to erosion (Lisle and Church, 2002). Armoring is the best understood of these, and easiest to quantify using data available for Cuneo Creek. The degree of channel armor is computed as the ratio of the median particle size of the bed surface (D_{50sur}) to the median size of the subsurface, or bed-material (D_{50sub}).

Historic record of grain size distribution in Cuneo Creek is limited to a single measurement prior to the 1997 aggradation in 1986 (Short, 1993), and to three sets of measurements after the aggradation in 1998 (Hall, 2000), 2001 and 2004. Surface particle size distributions were estimated using the Wolman pebble count procedure (Wolman, 1954) in the active channel. While all measurements utilized the same counting technique, the exact locations of the counts were not duplicated due to lateral channel migration and because the area covered varied between observers. However, the minor differences between the exact locations of these counts are probably not significant enough to affect comparisons between data sets. The pebble counts in 1986 were measured in two adjacent 7.6 by 7.6 meter plots in the active channel 130 meters upstream of the Cuneo Creek bridge (Short, 1993), while Hall (2000) measured in the active channel at xs 38+71, approximately 10 meters upstream of the 1986 counts. Pebble count measurements in 2001 and 2004 covered approximately 70 meters upstream and downstream of xs 38+71, likely covering all areas counted by Short (1993) and Hall (2000). In addition to the data from cross-section 38+71 describe above (1986, 1998, 2001, and 2004), pebble count data are also available for xs 15+00 (1998, 2001, and 2004) and xs 25+46 (2001 and 2004).

RESULTS

Volume of sediment removed the 1964 maximum aggradation datum (0 m^3) decreases generally over time. The 1964-1986 data fit an exponential decay function, which is interrupted by the 1997 aggradation (Figure 3).

Magnitude and Patterns of Sediment Storage (1964 – 1986)

The largest decrease in channel storage occurred in the first time step, the 12 years following aggradation (1964-1976), when fresh terrace deposits provided easily accessible sediment for transport. Topographic changes in Cuneo Creek between 1964 and 1976 showed a significant decrease in bed elevation across most of the valley width following the 1964 event, leaving only isolated pieces of the 1964 surface on the edges of the valley bottom (Figure 4). Depth of incision varied across the surface with the deepest incision occurring in the upstream portion of the reach and decreasing in the downstream direction. Photos showing these channel conditions in 1968 document a braided, or multi-thread channel devoid of much vegetation. Although the photo scale does not allow surface particle size estimation, the channel does not appear armored as fine sediment appears to cover the bed surface.

Cuneo Creek in 1976 was described by Laven (1987) as a “poorly defined, braided stream flowing over massive, nearly level alluvial fill”. Between 1976 and 1982, incision continued, with deep incision ($> 3 \text{ m}$) extending over most of the reach (Figure 4). Channel infilling and deposition on top of previously eroded surfaces represents 13% of sediment storage change, while removal of sediment accounts for 87% of the volume change. Between 1982 and 1986, channel incision ceased and lateral migration became the dominant storage removal process. Channels scoured and filled during this period, but no important changes in channel morphology occurred (Figure 7).

On the whole, stream channel surveys from 1976-1986 show a net reduction in storage volume (Short, 1993). Several large storms, particularly those in 1974 and 1983, had larger average daily flows than the 1964 storm but lower peak discharges (Figure 3), resulting in net sediment removal rather than further aggradation (Short, 1993).

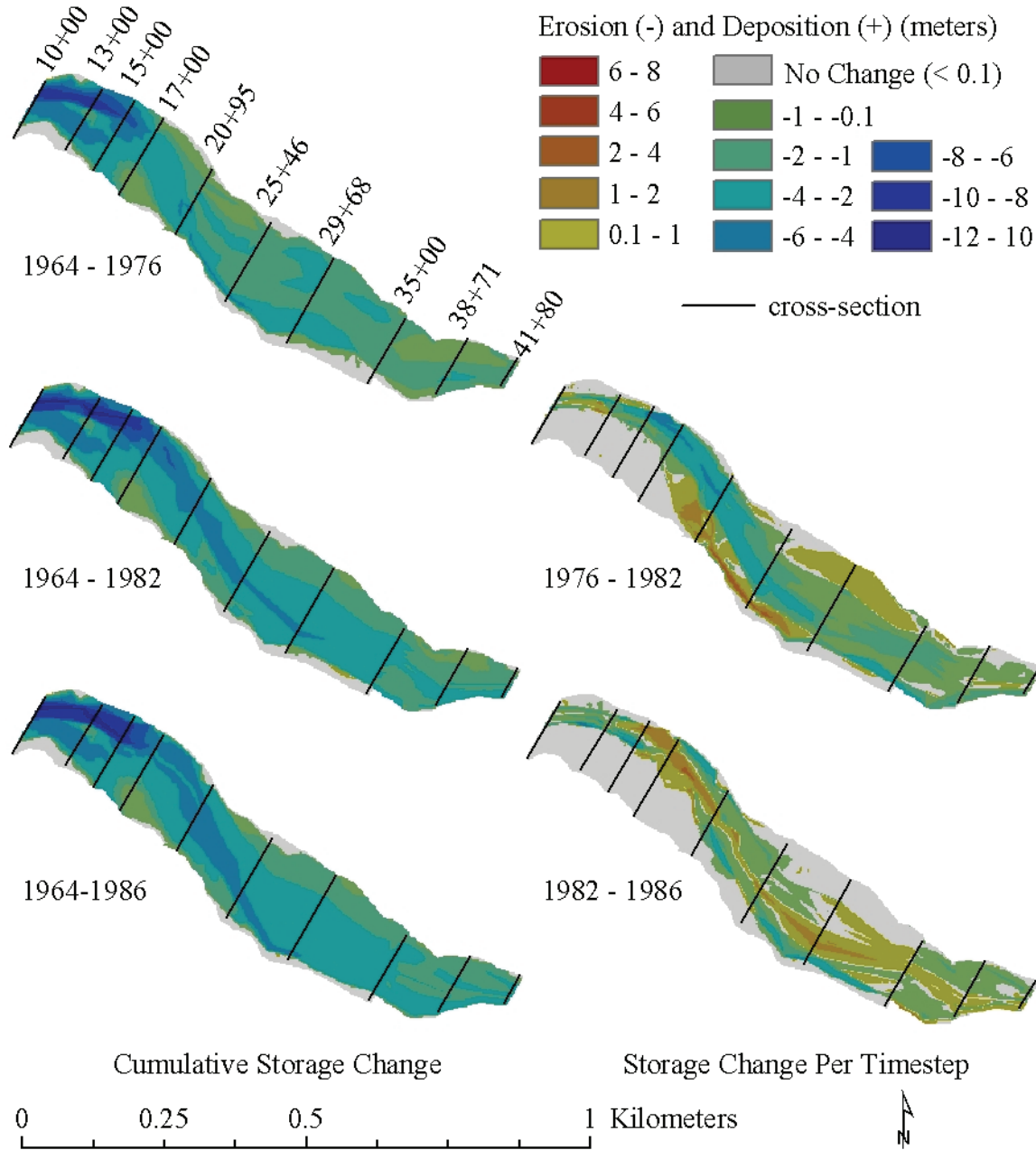


Figure 4. Shaded difference maps showing cumulative changes in storage volume in Cuneo Creek following the 1964 aggradation (1964-1986) and storage volume changes between each time step.

Actual transport through the reach includes both the sediment removed from storage as well as throughput material (sediment that entered and exited the reach within the time period). For this study, throughput was neglected and computed transport rates only include the volume of sediment removed within the study reach during each time period, referred to as bed-material transport rate. Bed-material transport rate is thus computed as the volume of sediment removed by the number of days with flows greater than the geomorphic discharge (2.3 m³/s) during the degradation period (Table 2).

Transport-Storage Function (1964 – 1986)

A transport-storage relation was developed for the degradation period following the 1964 aggradation (1964-1986). Storage volume is reported for the beginning of the time-step and bed-material transport rate is averaged over the time-step.

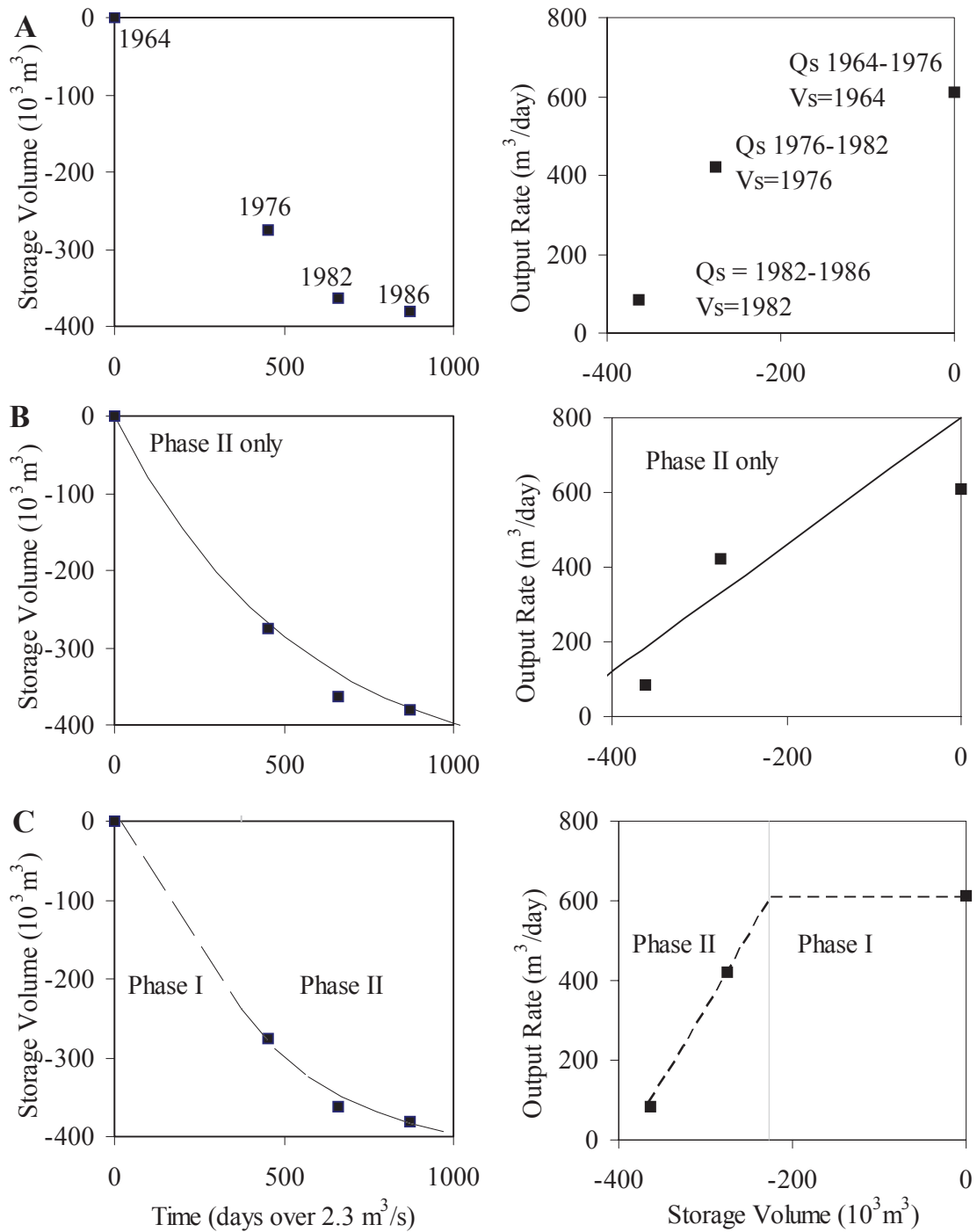


Figure 5. Estimated storage volume and possible transport-storage functions for Cuneo Creek (1964–1986). Changes in storage volume with time (left column) and transport-storage relations (right column) for A. Raw data; B. Relations based on a linear (Phase I) transport-storage relation; and C. Relations based on a non-linear (Phase II) transport-storage relation. Phase I and II nomenclature refer to Lisle and Church (2002).

Magnitude and Patterns of Sediment Storage (1997-2004)

The third cycle of aggradation (1997-2003) has the most complete set of data. Pre-1997 aggradation surveys in 1986 provide a baseline for estimating aggradation volume in 1997, and Hall's (2000) survey documents storage changes in the first year following the 1997 flood. This study extends the Cuneo Creek survey record to include data collection in 2001 and 2003, and surveys of stream terraces provide more detail on the patterns of erosion within the study reach between 1964 and 2003.

Table 2. Sediment storage changes following 1964 aggradation event (1964-1986).

Parameter	1964 – 1976*	1976- 1982	1982- 1986
Cumulative storage volume removed (m ³)	275,939	362,565	380,643
Net volume removed (m ³)	275,939	86,626	18,078
Cut volume (m ³)	275,950	101,406	37,119
Fill volume (m ³)	11	14,780	19,041
Total # days with discharge >2.3 m ³ /s (days)	452	206	214
Net volume removed per day of discharge >2.3 m ³ /s (m ³ /day)	610	421	84

Net sediment removal from Cuneo Creek was interrupted by the 1997 aggradation event. Even though the New Year's 1997 event had a larger peak flow than the 1964 flood, sediment delivery was significantly lower, resulting in aggradation terraces that were contained well within the 1964 flood deposits (Hall, 2000). During the 1997 storm, maximum aggradation (2-3 m) occurred within the channel between xs 10+00 and xs 29+68 (Figure 6). Aggradation was flanked by erosion of the valley wall and earlier flood deposits. Downstream of xs 29+68, aggradation was generally less than a meter. The following year (1998), the Bull Creek stream gage recorded nearly the same volume of water as the previous water year, but as a series of smaller storms. These more

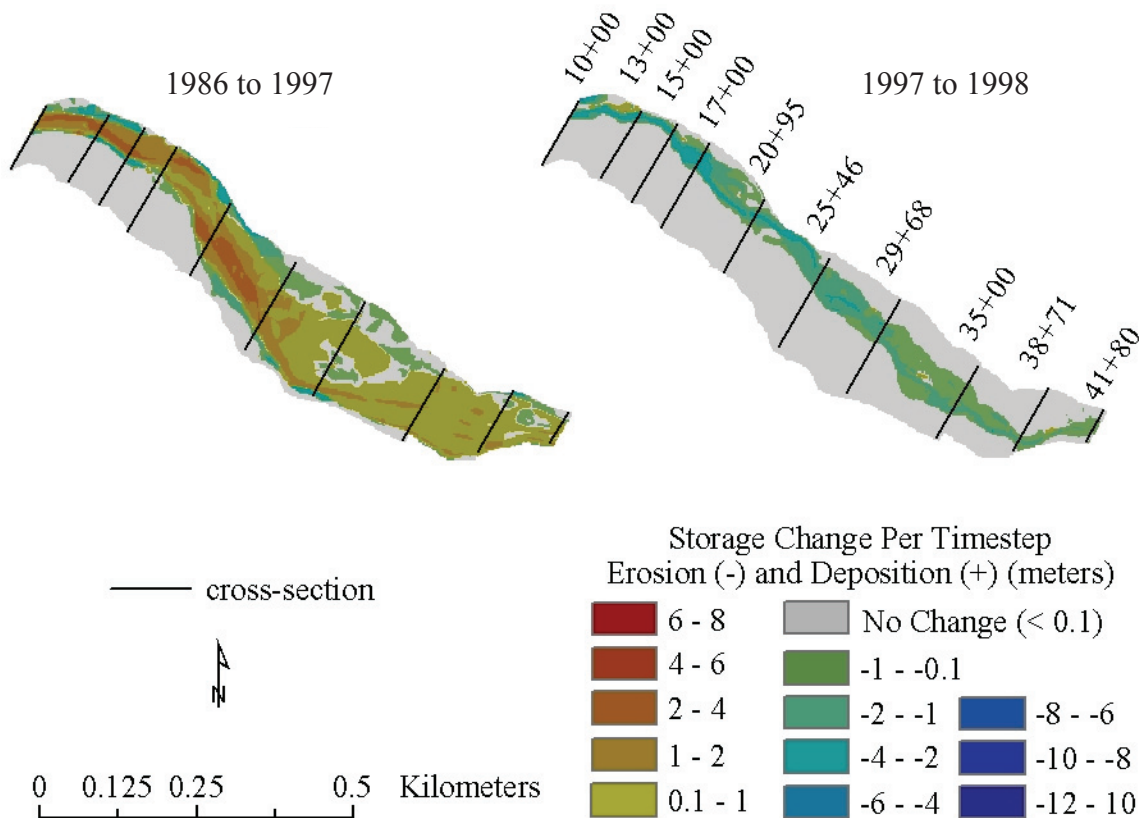


Figure 6. Shaded difference maps indicating changes in storage volume in Cuneo Creek resulting from aggradation (1986 to 1997) and subsequent degradation (1997 to 1998).

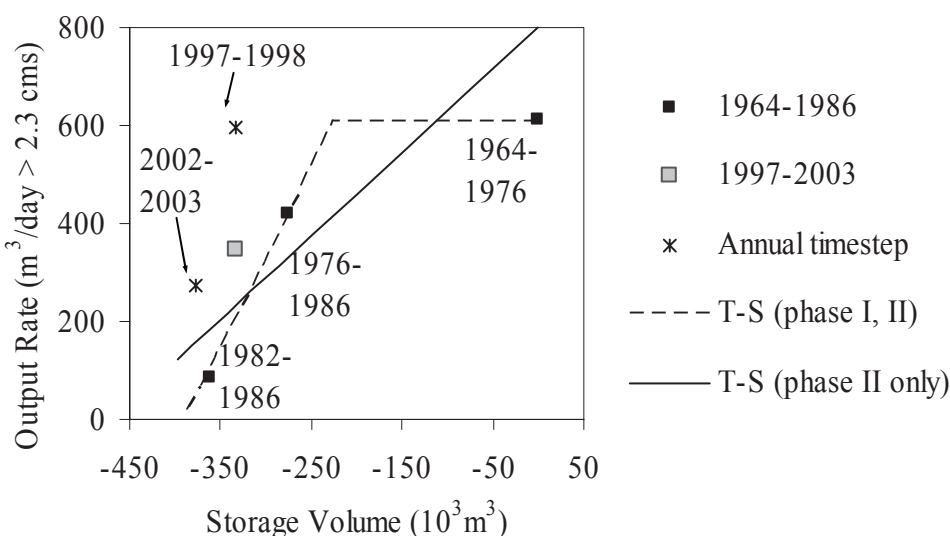


Figure 7. Post-1997 aggradation transport-storage data plotted with transport-storage relations developed for 1965-1986.

frequent but lower peak flows resulted in rapid channel incision throughout the Bull Creek watershed. Within Cuneo Creek, approximately 92% of the net storage gained from the 1997 event was removed in 1998. However, eroded material was not limited to the 1997 flood deposits; rather, the channel avulsed and cut a new channel from just upstream of xs 20+95 to xs 35+00 through older deposits. Furthermore, more sediment was removed during 1998 water year than accumulated from 1986 to 1997 resulting

in a net loss in storage volume between 1986 and 1998 despite the documented channel aggradation in 1997.

Rapid evacuation of material in 1998 shows high transport accompanying high storage volume (Table 3). The average rate of removal is similar to that calculated for the time step following the 1964 event. Subsequent surveys showed no significant change in channel shape from 1999 to 2002.

Table 3. Sediment storage changes following 1997 aggradation event (1997-2003).

Parameter	1997	1997 -1998	2002-2003
Storage volume (m ³)	148,005	105,290	94,898
Net volume change (m ³)	66,606	4,2715	13,190
Cut volume (m ³)	17,018	43,038	16,572
Fill volume (m ³)	83,624	323	29,762
Total # days with discharge >2.3 cms	40	67	48
Net volume removed per day of discharge > 2.3 cms (m ³ /day)	0	596	275

During water year 2003, high water inundated and mobilized the 1997 aggradation surface. Significant channel widening and lateral migration was observed in 8 of the 10 measured cross-sections with more than 15.2 meters of lateral erosion occurring over 67% of the channel length. Average bed elevation of the thalweg through the reach remained nearly constant, decreasing by only 0.024 m (approximately equal to the median grain diameter of the subsurface). Sediment was mobilized over the entire width of the 1997 depositional surface. However, a primary zone of transport appears to have been maintained with the largest bed changes occurring within or adjacent to the main channel through lateral erosion.

Transport-Storage Function (1997-2004)

A transport-storage relation for the period 1997-2003 was developed from survey data in 1998 and 2003. Transport-storage values for each year are given in addition to their combined value to show the average values for the 6-year time step (Figure 6). Transport-storage data for individual years show high transport rates in 1998, similar to those estimated between 1964 and 1976, followed by a significant reduction in 2003. The slope of a transport-storage relation between these two points is similar to slope of the line for the transport-storage relation developed from 1964 to 1986 that includes both Phases of transport. The position of the combined data point (1998-2003) lies between the 1982 and 1986 points, suggesting that current transport conditions are similar to channel conditions in the early to mid 1980's, but with a slightly higher output rate than expected (Figure 7). Higher output rates could be attributed to noise in either of the relations, errors in the data or scaling of time, or a true shift in the transport-storage relation from the 1997 aggradation.

Channel Armoring (1986-2004)

Transport rate is reduced by development of surface structure and channel armor during Phase II transport (Lisle and Church, 2002). Surface particle size distributions were measured in 1986 (Short, 1993) and repeated in 1998 (Hall, 2000), 2001, and 2004. Field measurements of surface grain size distribution of the channel show the surface was coarse relative to the subsurface in 1986, fined to an unarmored state in 1998 (armor ratio < 1), and was coarsened again by 2001 (Table 4). These changes in channel armor are consistent with changes in bed-material transport rates and storage.

Table 4. Surface particle size measurements in the active bed near cross-section 38+71 and 15+00.

Year	Downstream: xs 38+71			Upstream: xs 15+00		
	D50 (mm)	D84 (mm)	Degree of Armoring	D50 (mm)	D84 (mm)	Degree of Armoring
1986 (Short, 1993)	32	128	1.3**	---	---	---
1998 (Hall, 2000)	19	40	0.8	8	106	0.8
2001	38	141	1.6	27	204	2.7
2004	37	108	1.5	39	354	3.9
Bed Material	24	74	---	10*	41*	---

*Sampled 60 meters upstream of xs 15+00 on xs 13+00

**Based on 1997 flood deposits

Measured grain sizes between 1986 and 2001 are equivalent to within the same 0.5 phi size class. Between 2001 and 2004, the upstream measurement location coarsened by one phi size class for both D_{50sur} and D_{84sur} , while the downstream location showed no change in D_{50sur} and a slight fining of D_{84sur} (0.5 phi size class). Although the measured D_{50sur} at both the upstream and downstream locations are nearly equal, the degree of armoring is substantially higher upstream relative to downstream due to the difference in bed-material samples at each location.

CONCLUSIONS

Positive relations between transport capacity and storage are consistent with observed changes in channel condition and patterns of aggradation and degradation. Reductions in bed-material transport rate are consistent with armor development following the 1997 aggradation. Unfortunately, too few data are available to determine if sediment supply was limited by formation of channel armor after the 1964 aggradation event, and if so, for what duration. Arguably, there is evidence that supply did not limit transport for the 1997-1998 water year given the

unarmored condition of the channel in 1998. Low output rates and significant channel coarsening between 1998 and 2001 suggest that supply of mobile material limited transport rates by the onset of the following water year, and continued thru the end of the study period.

The sediment transport relations observed at the Cuneo Horse Camp terraces from maximum aggradation in 1964 thru 2003 suggest that the storage-transport function is not linear. Transport appears to be higher when supply is readily available, and as the storage reservoir is eroded, transport decreases in kind. Field evidence in the form of relic terrace surfaces can only suggest the form of the S-T function due to lack of more detailed yearly data. Terrace erosion rates are consistent with transport-storage theory developed by Lisle and Church (2002), but data are insufficient to rigorously define the form of the transport-storage function, the duration of the Phase I and Phase II transport, and the transport-storage relation for channel aggradation. Using data available from other flume studies and results from the Carnation Creek Experimental Watershed, in Victoria, BC, the form of the S-T relation is better defined. The authors will present these findings at Stop 1-2.

This page is intentionally left blank for notes.

Evidence for deformation of a Pleistocene strath terrace and coseismic deep-seated failure, implications for tectonic deformation at the boundary between the Northern San Andreas fault system and the southern Cascadia subduction zone

Oswald, J.A., Craven, G.F., Nordstrom, T.S., and Leroy, T

ABSTRACT

The Chalk Mountain landslide complex is an approximately 640 acre, dormant, deep-seated, translational/rotational rock slide complex. The main scarp of the rock slide is located at the ridgetop and is defined by a 130-foot wide ridge-parallel sacking. Uplift along the inferred southern extent of the Little Salmon fault and/or movement on the landslide complex have reduced the width of the Van Duzen River valley along the inner gorge reach. Downstream from the inner gorge, the Van Duzen River occupies a broad valley and shows a series of entrenched meander loops, indicating uplift or incision of a former alluvial valley.

Downstream of the gorge near the mouth of Root Creek the bank of Van Duzen River exposes a series of faults within the undifferentiated Wildcat formation that deform the strath surface of the lower of two terraces. Structural analysis of fault striae and offsets of fractures and concretion nodules demonstrate right-oblique transpression accommodated on northwest striking, north and south dipping faults. The north-south directed contractional strain indicated by this analysis is consistent with the regional strain indicated by the Little Salmon fault and other thrust faults mapped in the vicinity. This fault may be related to the south-eastern Little Salmon fault zone. Detailed LiDAR topography also suggests westward tilting of the adjacent two terrace surfaces and vertical deformation of the upper terrace with the same sense as high angle faults that offset the strath surface.

Evidence for faulting extends southeast along Root Creek between the south-east mapped extent of the Little Salmon fault zone and a profound structural discordance along Carson Creek in Larabee Valley. The fault zone truncates a zone of east-west-trending folding and thrusting along the ridge between the Van Duzen and Eel Rivers, and strikes south along Carson Creek in to Larabee Valley. The combined right oblique shear and thrusting appear to represent increased contractional strain to the west related to the Eel River Syncline and may provide a model for the south-eastern terminus of the Little Salmon fault.

Three distinct depots are exposed in the lower strath terrace on the left bank of the Van Duzen River. The stratigraphy is consistent with fault rupture across an active stream channel and followed closely by deposition of landslide debris. We propose that strong ground motion, potentially from rupture of the fault crossing the strath, caused slip on the Chalk Mountain landslide complex and production of a large amount of landslide debris to east of the fault trace.

INTRODUCTION

This paper present the results of regional bedrock and geomorphic mapping between the Van Duzen and Eel Rivers, and an investigation of a riverbank exposure on the Van Duzen River (Fig. 1). The three investigations allow regional bedrock and geomorphic mapping to provide context to interpret the local outcrop. In turn, the local strain conditions derived from the outcrop, have implications for current deformation of the eastern Eel River syncline area.

1:12,000 scale air photos and LiDAR imagery were used to identify lineaments, terraces, and landslides, and as a base map for the more recent regional geologic mapping. Older mapping was done on USGS topographic maps at a scale of 1:24,000. Bedrock map units in the area include Wildcat Group sediments and older of the Franciscan Complex. Structures were mapped and compiled from existing sources of information as shown in Figure 1.

Location and Geography

The geologic and geomorphic mapping was conducted over a broad area between the Van Duzen and Eel Rivers, primarily in the Shively and Root Creek areas of northern California. Root Creek is a tributary to the Van Duzen River. Root Creek extends southeast from the Van Duzen River in a broad, relatively low relief

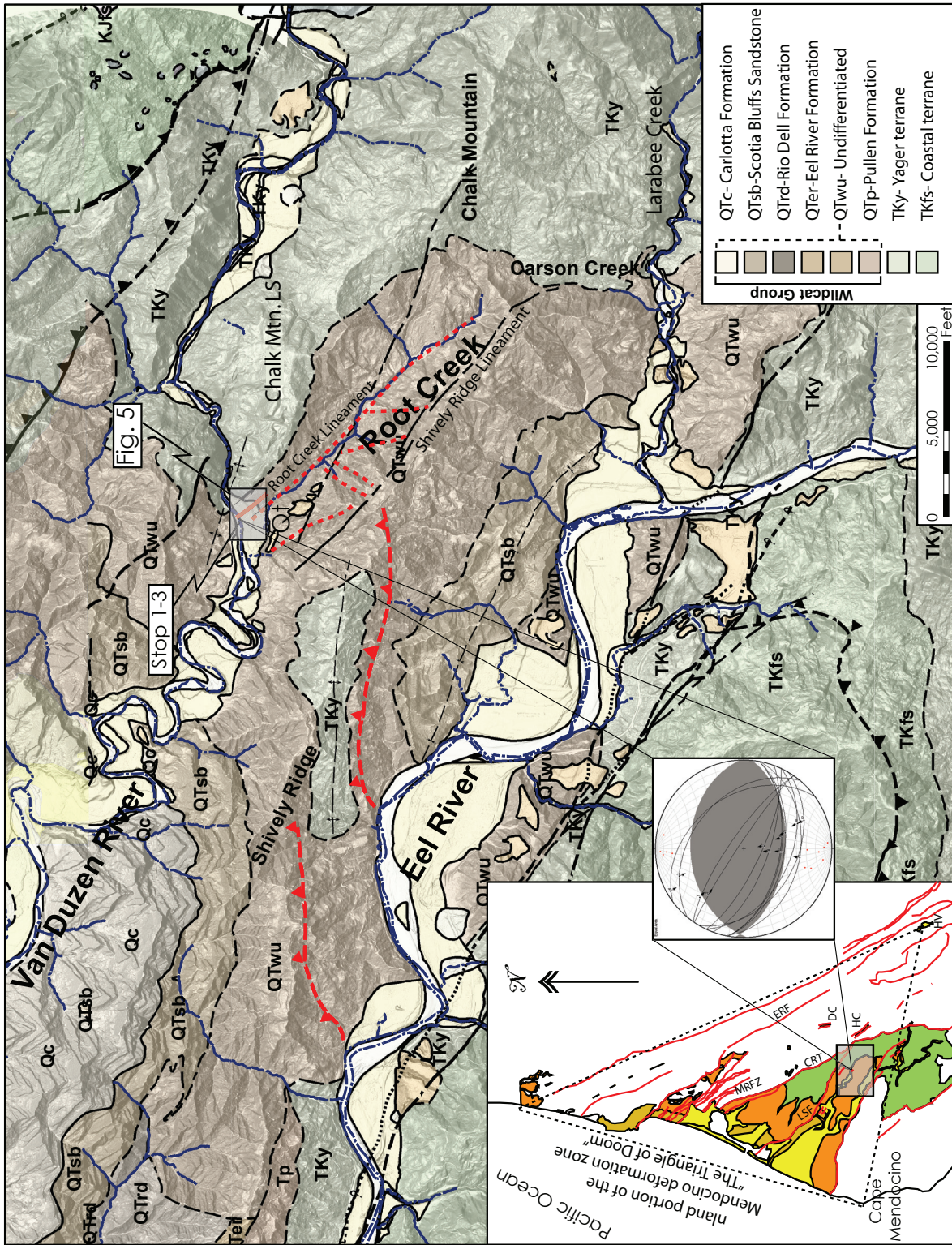


Figure 1. Geologic map of the eastern Eel River syncline draped over a 2m DEM hillshade. Red features indicate newly presented faults and lineaments from this study. (inset) regional tectonic map of the southern Cascadia onshore deformation zone, at the southern termination of the Cascadia subduction zone and the northern termination of the San Andreas Fault system. Geologic units include: Alluvium and dunes (Yellow), marine terraces (brown), Wildcat Group and equivalent (orange), Yager terrane (green), Franciscan Complex and others (white), Major faults in red. The paleo strain solution was determined from fracture data collected at the Root Creek outcrop. Mapping from: McLaughlin et al. 2000, Kelsey and Carver 1988, Ogle 1953, RNP 1981, Carver and Burke 1992, CGS 1999, Kelsey and Allwardt 1987, Allmendinger 2006.

valley. The eastern extent of the Root Creek watershed closely follows the contact between the Yager terrane and Wildcat Group. The valley intersects the Larabee Creek watershed at a broad, topographically low divide in the headwaters of Carson Creek (Fig. 1). Lower Larabee Creek flows essentially east to west and is a tributary to the Eel River. This region is near the boundary of the northern San Andreas fault system and the southern Cascadia subduction zone (Fig. 1)

The deformed strath terrace exposure is located on both PALCO and California State Parks property about 15 miles east of the intersection of highway 36 and highway 101 (See road log). The exposure is on the left bank of the Van Duzen River up-stream of the confluence with Root Creek (Fig. 1). The bedrock strath is continuously exposed, from the private seasonal bridge access, for about 720 feet east, where it is obscured by the active river channel and overlying deposits. The strath exposure also disappears downstream to the west at a series of high angle structures, a small bank slump, and young alluvial deposits. The exposed strath underlies the lower of two abandoned terraces along the left bank of the Van Duzen at this location. The terraces gain elevation to the east and abut a ridge that separates Root Creek from the Van Duzen River.

East of the strath exposure, the Van Duzen River flows through a narrow bedrock canyon deeply incised into the northwestern end of Chalk Mountain. The local relief and steepness of the streamside slopes increase dramatically east of the mouth of the canyon. The bedrock knob ('the monitor') overlooking the southern wall of the canyon mouth forms the lower left lateral margin of the Chalk Mountain landslide (Fig. 1 & 2). Highway 36 twists east through the gorge along the Van Duzen River. The entire far bank of the Van Duzen seen from the highway along the gorge is formed in the toe of the Chalk Mountain landslide (Fig. 1 & 2).

Geologic Setting

Root Creek defines the eastern extent of the contiguous Neogene sediments of the Eel River basin. The local Neogene sediments are the Wildcat Group of Ogle (1953), consisting of marine and non-marine sandstone, siltstone, mudstone and conglomerate. The Wildcat Group is differentiated into deep marine, shallow marine and nearshore/fluvial sedimentary sequences in some areas, but is locally not differentiated.

Shively Ridge between the Eel and Van Duzen Rivers west of the stop is comprised of gently to moderately dipping Scotia Bluffs Sandstone and Carlotta Formation of the Wildcat Group (Fig. 1). The Wildcat Group sediments locally overlie the middle to late Eocene Yager terrane, which represents the final episode of continental shelf and slope deposition associated with the Franciscan Complex (McLaughlin et al., 2000). Regionally the Yager terrane is highly folded, faulted, and sheared but does contain local areas of structurally coherent blocks. The Yager terrane is faulted along its entire base and only depositionally in contact with younger strata. (McLaughlin et al., 2000).

The mapping area is located on the southern limb of the Eel River Syncline, which folds the Neogene strata of the Wildcat Formation (Ogle 1953). The Eel River Syncline is one of the remnants of the Eel River basin, which has been dismembered by tectonic activity with the northward migration of the Mendocino Triple Junction. Uplift of the southern limb of the Eel River Syncline has resulted in a northward regional dip in the Wildcat strata, with dipslope morphology from the coast to just west of this location. The erosion of the dipslope geologic strata forms hogbacks on the steeply dipping strata east of Ferndale and cuesta ridges along the gentle to moderate slopes south of the Van Duzen River. Regionally, the northern limb of the Eel River Syncline is truncated by the Little Salmon and Yager faults (Fig.1 insert). The trip stop is located near the eastern terminus of the Eel River Syncline.

Local Geology and Structure

The Wildcat Group is bound to the east by the Yager terrane (McLaughlin et al., 2000). The contact, which as usual in Humboldt County is not exposed, is in the Van Duzen channel about 500 feet upstream from the eastern extent of the exposed deformed strath terrace near Root Creek.

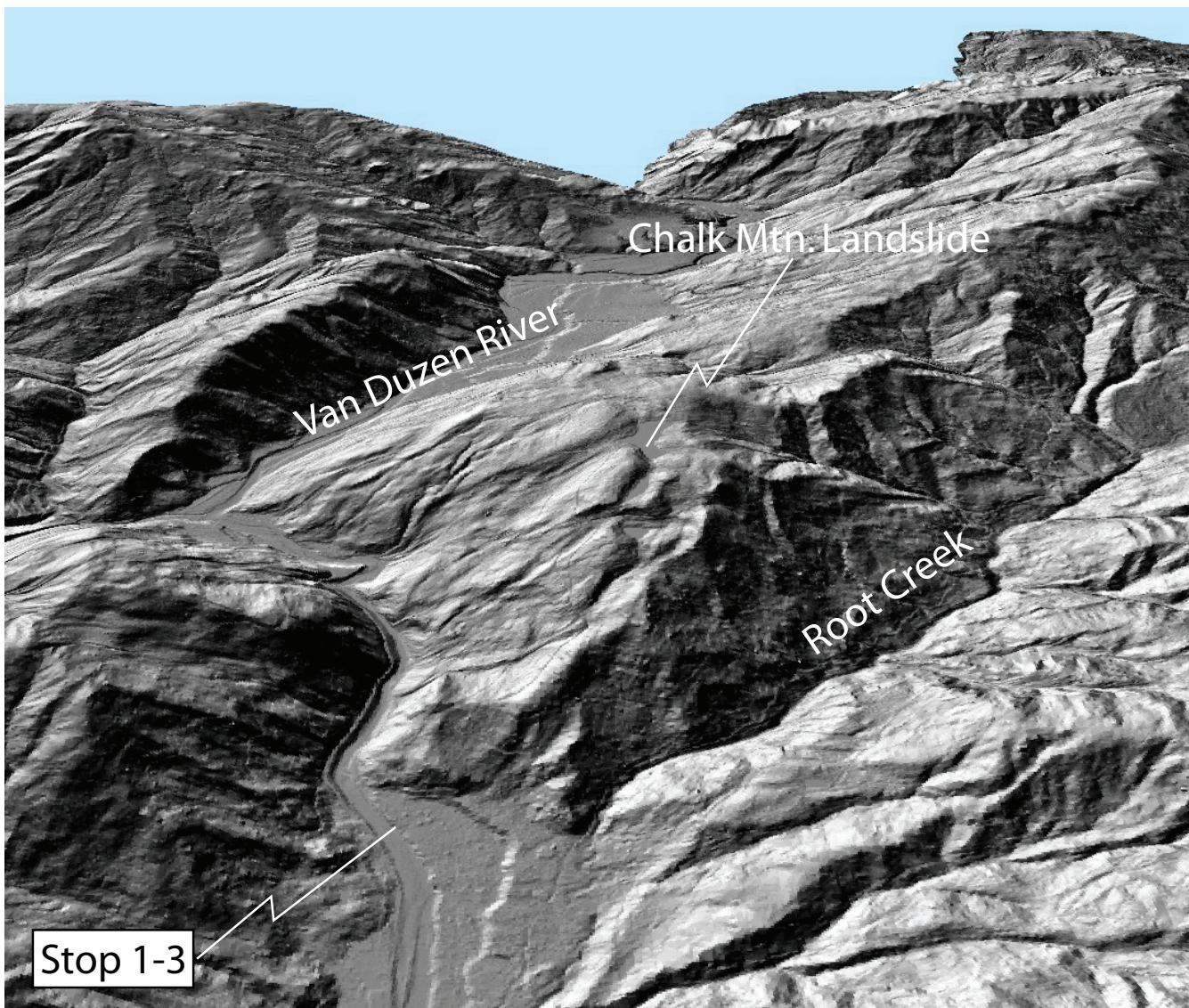


Figure 2. Oblique view looking east up the Van Duzen River valley. The toe of Chalk Mountain landslide (center) forms the narrow gorge east of stop 1-3. A series of sackungen define the main scarp along the ridge between Root Creek and The Van Duzen River. Image generated using 2m LiDAR hillshade product.

The Yager terrane crops out east of the strath exposure as light brown to gray, silty fine sandstone, pebble boulder conglomerate, and dark gray argillite. Within the study area, the Yager terrane strikes predominantly north-west and dips 30-50 degrees to the northeast. The Yager terrane also crops out west of the site at the crest of Shively Ridge and is brought up through the Neogene strata by means of a fault bend fold structure (Fig. 1). The thrust faults shown on Figure 1 are based on our recent geologic mapping along Shively Ridge and existing literature (e.g.: Harmon, 1914) and define an area of conformable Wildcat Group stratigraphy to the west and a mapped zone of undifferentiated Wildcat to the east.

The undifferentiated Wildcat Group within the study area is comprised of light gray to brown, weakly consolidated, inter-bedded siltstone to silty fine sandstone. Measurements of several sandy inter-beds show the strata strike northwest and dip steeply to the south, consistent with other mapping of local structure (CGS, 1999), but in contrast to the northern regional dip. The south-dipping Neogene strata occur directly south and east of the eastern extent of the Little Salmon and Yager faults and southeast along the eastern slope above Root Creek.

The exposed strath outcrop is at the northwestern end of a zone of lineaments originally mapped by Spittler (1983) that extend up the Root Creek valley to the divide between Root Creek and Carson Creek to the southeast.

The most prominent lineament (the Shively Ridge lineament) runs just below the unusually straight, sharp crest of Shively Ridge south of Root Creek (Fig. 1) and consists of a series of enclosed depressions, midslope benches, and notches that consistently occur on spur ridges at their intersection with Shively Ridge. The original mapping of this lineament shows it continuing into the Carson Creek drainage, where it terminates at the contact between Wildcat Group sediments to the west and Yager terrane rocks to the east. The structural discordance between locally east-west-striking Wildcat sediments and Yager rocks indicates that the contact at Carson Creek is not depositional. This lineament becomes less prominent to the west of the stop, where it intersects the projection of fold and thrust structures on Shively Ridge and the orientation of Shively Ridge becomes more westerly. However, sidehill notches, ridgelets, slope inflections, and terrace backedges continue to express the lineament nearly to the bank of the Van Duzen River.

Another prominent lineament occurs along the lower to middle reaches of Root Creek (The Root Creek Lineament), stop 1-3 is along its projection (Fig. 1). It is expressed largely as the straight inner gorge of Root Creek, parallel to the Shively Ridge lineament. It is not as finely expressed as the Shively Ridge lineament, which is to be expected due to the dynamic slope processes along the inner gorge of Root Creek. This lineament becomes obscure toward the upper reaches of Root Creek and branches with the eastern portion of the northern lineament mapped by Spittler (1983) (Fig.1).

Other lineaments occur sub-parallel to, and between the Shively Ridge and Root Creek lineaments, particularly near the lower reaches of Root Creek. These lineaments are expressed as sidehill notches, canyons, and alignments of terrace backedges. The western portion of the northern lineament mapped by Spittler (1983) is considered to be one of these lineaments (Fig. 1).

North-south to northeast trending lineaments near the middle reaches of Root Creek are expressed as small, highly incised watercourses near Shively Ridge, and boundaries between completely brecciated and relatively coherent zones of Wildcat bedrock on the lower slopes. These boundaries are evident in the topography as well. Some of the north-south to northeast trending lineaments branch off the Shively Ridge lineament at spur ridge notches. One block bounded by two of these transverse lineaments has bedding striking N30°E and dipping 46° to the east, off the axis of any structure to the north or south and indicating complete structural dismemberment between the two major northwest-trending lineaments.

The overall lineament pattern and available structural data are suggestive of lateral shear on straight, high angle faults bounding a zone of rotational and shear deformation of internal blocks between Shively Ridge and Root Creek. There is some suggestion of a right step in the shear across the western slope above Root Creek. High angle lateral shear is consistent with the structural data from the exposed strath, described later.

The contact between the Yager and Wildcat east of the strath exposure may be stratigraphic, tectonic, or a combination of both. We interpret exposures of fault breccia and sheared bedrock along the mapped depositional contact east of the Root Creek site to represent the southern extent of a mapped fault that dies at the Chalk Mountain landslide (CGS, 1999; Fig. 1). This fault is directly in line with the southern extent of the Little Salmon fault, and either represents the southern terminus of the existing mapped Little Salmon fault and a right step onto a Root Creek structure or a southward bend and right step of the Little Salmon fault along Root Creek. The southwest dip of the Wildcat sediments east of Root Creek is consistent with folding along the trend of the Little Salmon fault.

Channel Geomorphology of the Van Duzen River

West of the mouth of the canyon, the Van Duzen River valley changes dramatically from a narrow bedrock canyon to meanders entrenched into a broad alluvial valley. The change in expression from deeply incised canyon to entrenched meander occurs at the contact between the more resistant Yager terrane and weaker Wildcat Group, and the deformed strath exposure. The recent entrenchment of the Van Duzen River does not appear related to local conditions, but more regional adjustment of base levels. Several mapped old river terraces on adjacent

slopes of the Van Duzen record a long term downcutting and/or uplift of the basin (Fig. 1). Additionally, the old river terraces are on the southern limb of the Eel River Syncline and may record uplift and northward tilting. The terrace deposits are sometimes difficult to recognize in outcrop because of the high input of colluvial and fine textured source materials locally available in the Wildcat Group, however, where mapped they form laterally extensive low gradient to flat surfaces in a regionally dipping landscape of cuesta and hogback morphology.

Adjacent the modern meandering channel are several mapped old river terraces. A conundrum is presented in explaining a flight of abandoned terraces, located southwest of the deformed strath terrace, that extend up to an elevation of 800 feet, about 600 feet above the current grade of the Van Duzen River (Fig. 1). These terraces are on the footwall block of the down-to-the-west, northeast dipping inferred high angle fault at the deformed strath site. Uplift is required within the footwall block to bring the terraces to such an elevation above present grade. We propose that they are uplifted by a thrust fault that crosses the southern side of the ridge between the Eel River and Van Duzen River, originally mapped by Harmon (1914), that accommodates shortening and folding of the southern limb of the Eel River Syncline. This mechanism provides additional local uplift to get the terraces to their present elevations.

CHALK MOUNTAIN LANDSLIDE

The Chalk Mountain landslide complex is a 640 acre, dormant translational rock slide. The main scarp of the landslide is defined by a 130 foot wide ridge parallel depression that contains undrained depressions up to 30 feet deep (Figures 1 and 2). The ridgetop depression forms a broad arc that curves into the lateral margins of the landslide. The left lateral margin is expressed as a steep planar bedrock ridge. The right lateral margin is less well defined than younger appearing right lateral internal scarps to the west. The right lateral margin of the landslide appears to be advancing westward. The body of the landslide contains several steep bedrock internal scarps with rolling, broadly hummocky, stepped morphology on low gradient benches. The toe of the landslide forms the left bank of the Van Duzen River. The river has undercut the slopes and an inner gorge extends about 6000 feet upstream from the lower extent of the canyon. The inner gorge is characterized by bare raveling slopes, coalescing shallow debris slide scars, and rotational slumps formed by the undercutting of the slopes by the Van Duzen River. The shallow landslide features initiate from the over steepened toe of the Chalk Mountain landslide complex. Below we describe the distribution of the activity status of the landslide, probable triggering mechanism, and structural control on failure mechanism. Later we incorporate our proposal of the triggering mechanism to refine our understanding of the stratigraphy associated with the deformed terrace exposure.

Activity Status

Field reconnaissance shows an increase in the activity level of the landslide downslope as manifest in increasingly sharper and younger appearing landslide morphology downslope. The upper extents of the landslide show no evidence for recent movement in vegetative indicators or in surface morphology. Surface features are subdued and muted by erosion. Old growth stumps show that the trees were undeformed prior to being cut. The morphology of the lower landslide indicates slow, creeping failure of the toe region coupled with the very infrequent movement of the upper mass. The long interval since movement of the upper mass suggests a triggering mechanism that is infrequent yet profound because of the durable nature of its landslide morphology after erosion. The likely candidate would be ground shaking, but earthquakes are a common occurrence on the north coast. The event would have to generate enough shaking to trigger failure of the landslide and would require a source close enough to do so. For an event to trigger movement of the landslide as infrequently as shown by the activity status it would likely be an infrequent, and strong earthquake. Rupture of a local fault would be infrequent and could generate strong ground shaking especially above the hanging wall of a thrust fault.

The shallow landslides across the inner gorge expose large portions of the bedrock within the body of the landslide. Dark bands of sheared argillite and blocks of sandstone are exposed across the steep raveling slopes that lead to the Van Duzen River. The toe provides the source for the abundant large boulder deposits within the Van Duzen River at this location. It is likely in the event of a large movement of the entire landslide that portions

of the Van Duzen would be dammed by landslide debris. This debris would be reworked downstream as debris flows as the landslide dams were breached by the river. This debris flow mechanism is important in interpreting the stratigraphy at the deformed strath exposure.

Structural Control of the Chalk Mountain Landslide

The landslide is located on the projection of a mapped fault that extends to just east of the mouth of the canyon (Fig. 1). This places the landslide on the hangingwall of the fault. While the trace of the fault has not been located south of the Van Duzen River, the south-dipping Wildcat strata east of Root Creek are consistent with an anticlinal fold above a blind thrust (Fig. 3). Such a fold provides a mechanism for extensional features to occur within the hangingwall that could provide deep planes of weakness leading to slope failure. The landslide is also on the dipslope of a relatively coherent block of Yager terrane sandstone and interbedded argillite and conglomerate. The dipslope and fault-related structures provide optimally oriented planes for deep slope failure and are schematically presented on a cross-section of the landslide complex (Fig. 3). The figure shows how the dipslope plane essentially forms the failure plane and the extensional structures related to folding provide optimally oriented planes for the break-away zone at the top of the ridge. The motion of the failure plane is apparently almost pure translation because of the graben-like sackung formed along the ridgeline.

STRATH TERRACE EXPOSURE

The strath exposure is located on State Park Property. Detailed investigation of the exposure would require extensive, permitted, excavation to more confidently interpret the stratigraphic sequences. At this point, we have nothing more to say on the matter. The exposure consists of a strath terrace, cut into steeply dipping Wildcat sediments, capped by a series of alluvial units. Figure 4 shows a photograph mosaic of the exposure. The strath terrace is deformed such that it is exposed for 720° before it descends from view beneath the river level on both ends. Below we describe the site conditions and provide an interpretation of the stratigraphic and structural elements of the exposure. Later we place this interpretation, along with our geologic and geomorphic mapping, into a regional context for deformation along plate margin boundary between the northern San Andreas and Cascadia subduction zone.

Stratigraphy

We have broken the stratigraphy of the site into four units based on age, textural differences, and cross-cutting relationships. The units define the Neogene Wildcat bedrock the strath is eroded into, and the capping deposits exposed at the site. These deposits form the lower of two terrace surfaces preserved between the Van Duzen River to the north and Root Creek to the south (Fig. 2).

Wildcat Group Sediments

The strath bedrock is predominantly composed of massive silty fine sandstone and fine sandy siltstone. There are a few fine sandstone beds and lenses exposed between the low water crossing and the easternmost visible exposure that provide bedding orientations. Consistent with published mapping the average bedding orientation strikes around 130° dips 62° south (CGS, 1999). There are rare mollusks and trace fossils scattered throughout the exposed outcrop, along with a few concretions. Several concretions are offset by small faults within the exposure. The exposure reveals numerous faults, fractures, and shears within the undifferentiated Wildcat sediments.

Unit 1

Unit 1 is discontinuously exposed in the outcrop and it is always in contact with the bedrock strath. It consists of sub-angular to well rounded, clast supported cobble and boulder deposits with lesser amounts of mixed pebbles and sand filling between clasts. The clasts consist of sandstone and conglomerate of the Yager terrane or various lithologies common to the Franciscan Central Belt melange. One 2 foot by 1 foot boulder of wildcat

was identified at the base of unit 1 about 15 feet east of the scarp on the eastern fault trace (Fig. 4). This is an uncommon clast in the deposit because of the weak nature of the wildcat and requires that the clast underwent very little transport in the ball mill composed of harder lithologies. The boulder is underlain by rounded cobbles.

Unit 1 extends continuously east from the eastern fault trace and occurs only in discontinuous pockets to the west. The texture of unit 1 is variable depending on its locality in the exposure, increasing significantly in maximum particle size to the east as the exposure approaches the Wildcat/Yager geologic contact. Much of the exposure in this area is poor due to bank collapse and dense vegetation. The average particle size of the boulders and cobbles in unit 1 appear smaller west of the eastern fault trace.

Unit 2

Unit 2 is found throughout the exposed outcrop capping both the strath and unit 1. It is a mostly matrix supported, heterogeneous mixture of sub-rounded to sub-angular boulders, cobbles, and pebbles in a fine grained matrix. The deposit appears to lack internal fabric or sedimentary structures, and in most places the clasts appear randomly oriented. The clasts consist of lithologies predominantly derived from the Yager terrane. The particle size of unit 2 varies throughout the outcrop although the larger size particles appear to drastically decrease in abundance east of a small side channel cut into the strath (fig. 4 mosaic). Unit 2 is up to 9-12 feet thick and appears to have been laid during a single event.

Unit 3

Unit 3 is only found capping unit 2. It is a medium brown silt that blankets the entire exposure. The contact between unit 2 and 3 varies from relatively sharp to diffuse. The modern forest is rooted in this deposit.

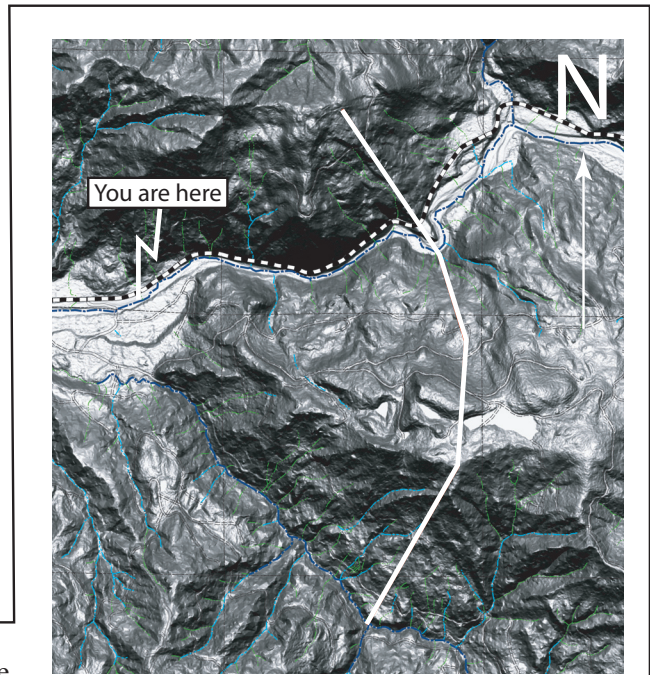
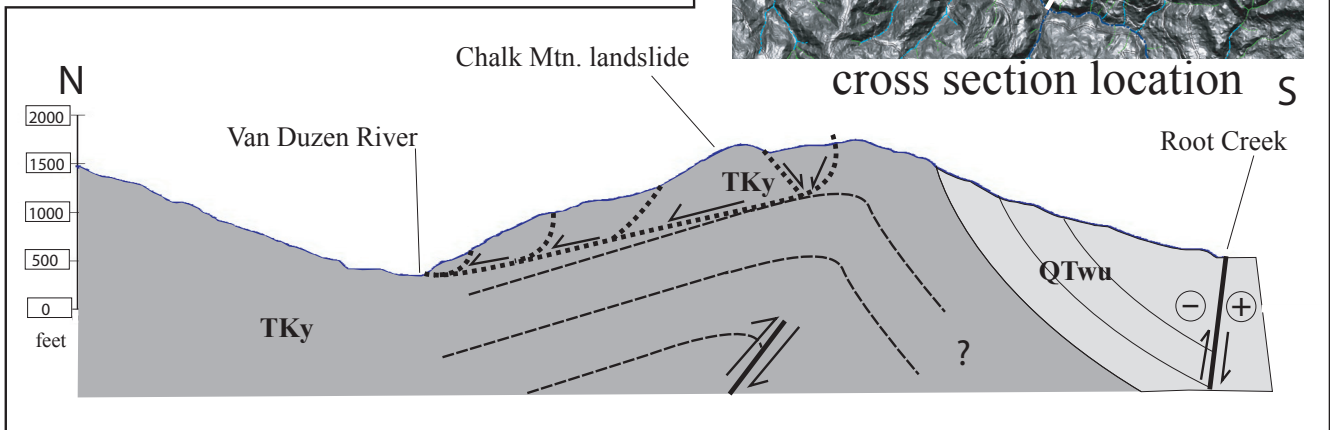


Figure 3. Schematic cross section through the Chalk Mtn. landslide showing the relation between geologic structure and landsliding.



left intentionally blank
for
tabloid oswald figure 4

Figure 4. Photo mosaic of the exposed outcrop near Root Creek in the summer of 2006. (A) The full mosaic from just past the eastern fault trace (east) to the Root Creek summer bridge crossing (west). (B) The same mosaic enlarged with data sites and selected observations labeled. Stereonets show rake of striae for representative sites, paleo-strain solutions are shown for north-dipping and south-dipping faults.

left intentionally blank
for
tabloid oswald figure 4

Discussion of Stratigraphy

Overall we interpret the stratigraphic section exposed at Root Creek as a strath terrace with associated river cobbles and boulders (unit 1) that was stripped and capped by a debris flow (unit 2). The fine grained unit 3 could either be the upper section of unit 2 where a smaller particle size sorted in the debris flow, or alternatively, a subsequent over-bank deposition event.

The thick, clast supported boulder deposit resting against the eastern visible fault trace is an anomalously thick deposit when compared with other exposures of unit 1. We interpret this stratigraphy as representing sediment trapped on the downthrown side of a fault ruptured active stream bottom, because: 1) the presence of the soft Wildcat boulder near the base of the deposit adjacent to the fault scarp that offsets the strath surface, 2) the anomalous thickness of the deposit at this location, and 3) the lack of comparable sized boulders in exposures of unit 1 west of the fault trace.

The Wildcat siltstone boulder is significant; because of its lack of durability, it would require specific circumstances for its preservation in the deposit. It would essentially require origination from a local source, rapid isolation from bedload abrasion by rapid deposition of the overlying boulders, followed by stability of the boulders after deposition. The most likely source for the boulder is the broken tip of the adjacent thrust fault that offset the channel of the Van Duzen River. This would highly suggest the Wildcat boulder was deposited contemporaneously with the fault rupture that offset the strath surface.

The deposition of the anomalously thick, coarse, boulder deposit would be required to be temporally associated with the deposition of the Wildcat boulder and, thus, the fault rupture, in order to preserve it. The rapid deposition and stability of the boulder deposit required to preserve the Wildcat boulder, and the lack of comparably thick or coarse deposits west of the fault trace, suggest that the boulders were deposited in a pulse of sediment that subsequently remained stable because of the inability of stream flow to move them downstream after an initial depositional event. The source for the boulder deposit is inferred to be the channel of the Van Duzen river. The rounding and size range of the deposits are consistent with current deposits in the active channel. The stable boulder deposit appears also to have had a role in preserving the visible offset of the strath surface by preventing subsequent planation across the fault trace by the unit 2 debris flow.

Unit 2 appears to have a close source on the Van Duzen river, as indicated by the sub-angular to sub-rounded nature of the clasts. The most likely source for unit 2 is the Chalk Mountain landslide about .5 miles up river. This slide has a history of large movements as previously discussed, and an actively eroding toe in the boulder strewn Van Duzen River. The distribution of coarse material in unit 2 suggests the faulted and folded strath may have been buried by debris flows initiating from the failed mass of Chalk Mountain landslide. The apparent lack of fluvial reworking of Unit 2 indicates that the exposure was isolated from channel processes after the deposition of Unit 2. This isolation may have resulted from earlier diversion of the channel by the offset along the eastern fault trace and deposition of the large boulder deposit east of it. Alternatively, the isolation could have occurred due to uplift of the entire strath surface.

Structure

Faulting

The Wildcat sediments exposed at Root Creek are pervasively fractured and faulted throughout the outcrop. All the shears, faults and the fractures demonstrate a strong northwest trend and dip steeply southwest and northeast towards a central near vertical zone of faults and shears. Two zones of densely-spaced fracturing and shearing separate mostly undeformed bedrock near the center of the exposure. The easternmost fault shows an estimated 6 feet of apparent vertical offset of the strath surface with an apparent reverse sense of motion. The alluvial units above the strath do not appear faulted (Fig. 4). The density of fractures and micro-faulting gets more concentrated near the eastern trace that offsets the strath. A central vertical to steeply north dipping fault delineates the second

area of dense fracture patterns. The fault does not appear to clearly offset the strath but defines an area of subtle down-warping to the west. The western end of the exposure is cut by numerous high angle north dipping faults. The strath surface rapidly plunges below a bank slump and young terrace gravels to the west. The eastern and central densely fractured zones also coincide with zones of pervasively sheared rock and clay fault gouge.

A limited number of the exposed faults have striations on them suggesting slip direction orientation. We have not documented a fault with obvious offset that has striations on it, but there are numerous striated faults with strikes and dips similar to the ones with documented offset. We recorded 6 striae measurements east of the eastern fault trace and 4 measurements of faults with evident striae within and to the west of the central zone (Fig. 4).

All of the faults with striae data are plotted on an equal area stereonet (Fig. 1). The P-axis predicted for the direction of movement and fault plane orientation is also plotted. Plotting of the fault data demonstrates a change in rake of the fault lineations over a portion of the outcrop that is consistent with the dip of the fault (Fig. 4). Adjacent the eastern fault trace, a series of closely spaced faults shows lineations with a mostly vertical to right-oblique orientation. The central vertical fault trace, and north dipping faults to the west show rakes with a large horizontal component suggesting more right lateral transpression.

One P-axis is consistent for the two differently dipping fault sets, suggesting they were formed together. Solving an average fault solution for the two sets of differently dipping data produces two different mechanism of faulting: thrusting for the eastern set and right-lateral for the central and western sets (Fig. 4). However, if both sets are combined an average solution for the entire data-set indicates north-south directed contraction, with a very small right oblique component (Fig. 1).

Multiple shear zones with similar orientations to the faults were observed along the outcrop (Fig. 4). These shear zones typically consist of a 1"-2.5" Grey-green laminated clay/silt gouge. Offset of the strath surface prior to its emergence would not be preserved due to planation by the river channel unless preserved by a stable armoring deposit as at the eastern fault trace. Much of the motion of the high angle faults with a large lateral component would not be expressed in the strath surface.

Surface Deformation

The strath terrace at the Root Creek outcrop is uplifted such that it is exposed for 720' before it descends from view beneath the river level at both ends. The highest elevation of the strath surface is roughly 17' above the river level, directly above the eastern fault trace, providing a minimum constraint on the total amount of vertical deformation. The total offset of the strath surface is not constrained due to its unconstrained depths east and west of the exposure. Deformation recorded in the strath surface also provides a minimum constraint on vertical offset across faults, since fault offsets beneath the channel would be planated by channel scour.

Further constraints on the vertical component of deformation are provided by the topography of the two terrace surfaces above the strath. The second terrace above the strath shows a down-to-the-west inflection near the eastern slope of the Root Creek valley (Fig. 5), this inflection shows a trend consistent with the Root Creek lineament and projects toward the western end of the strath exposure, which is terminated in a series of down-to-the-west high angle faults. This convergence of observations supports the interpretation of high angle faulting with a down-to-the west component as the origin of the Root Creek lineament.

The fault exposed at the deformed strath terrace location cuts the folded Wildcat sediments, indicating that the folding pre-dates the fault along Root Creek (Fig. 1). If the blind thrust underlying Chalk Mountain and deforming the Wildcat sediments is related to the Little Salmon fault, the fault that deforms the strath is relatively young, cross-cutting the deformation related to the Little Salmon fault along Root Creek. Additionally, the terraces tilt and step towards the southwest, consistent with the westward tilt of the Wildcat along the east side of Root Creek and suggesting deformation associated with the blind thrust underlying Chalk Mountain.

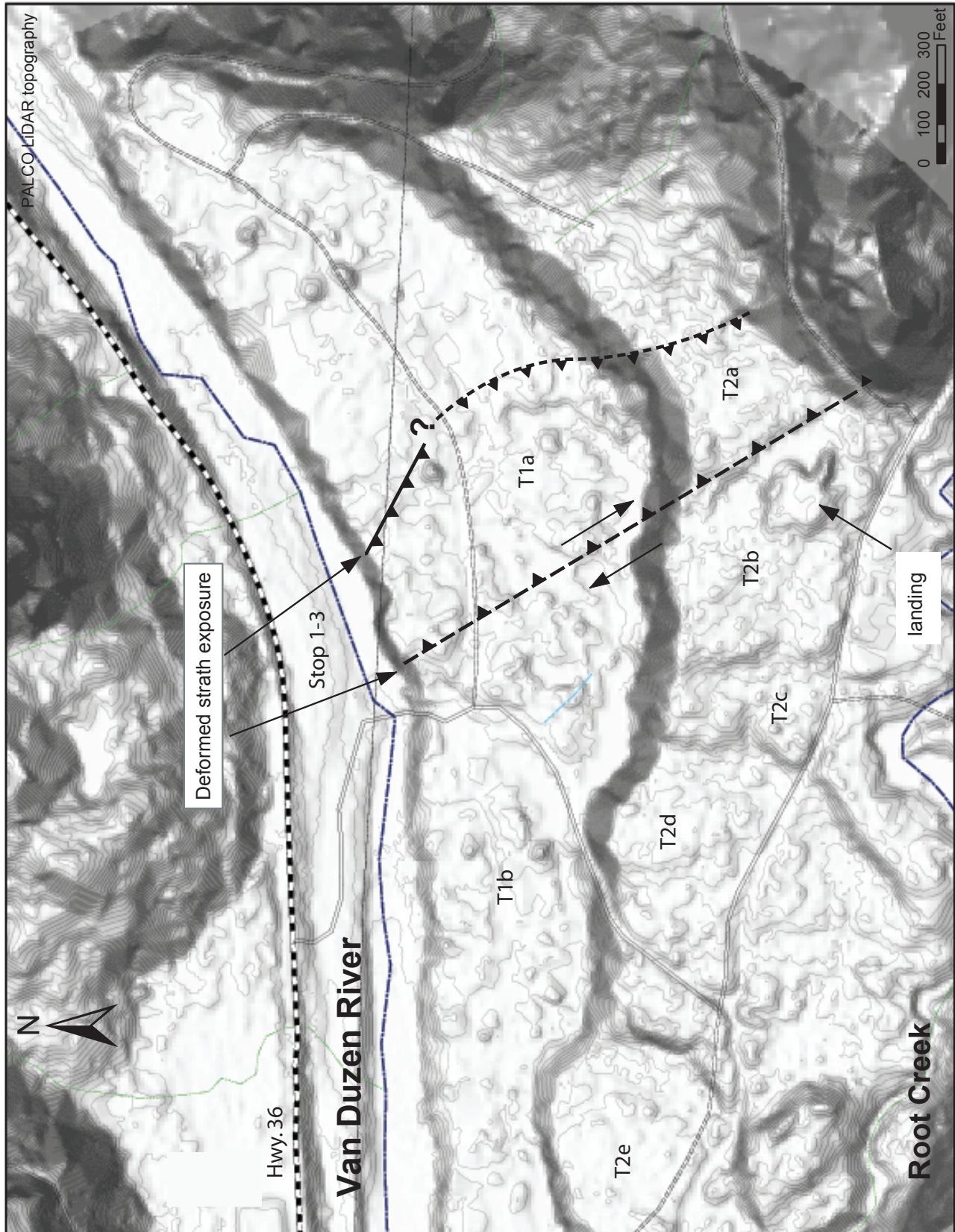


Figure 5. LIDAR generated topography of the stop 1-3 area. The image includes fault traces inferred from exposures in the deformed strath terrace. T1 and T2 correspond to terraces discussed in text. The contour interval is 2', superimposed over a 10ft hillshade product

DISCUSSION

Regional tectonics

The Root Creek area is in a zone of transitioning tectonic regimes where movement along the Pacific/North American plate boundary impinges into the southern Cascadia subduction zone (Williams et. al., 2006; Kelsey and Carver, 1988). Deformation of the North American plate inland from the San Andreas transform margin occurs as a broad zone of roughly north-northwest-trending right-lateral deformation south and east of the Root Creek area. The eastern boundary of the San Andreas related deformation is the Sierra Nevada-Great Valley block (SNGV) east of the Bartlett Springs/Lake Mountain fault zone (Williams et al., 2006). The Maacama fault zone extends roughly along the southern reaches of the Eel River and projects slightly east of the Root Creek area. Williams et. al (2006) present geodetic strain data indicating approximately 22mm/yr of distributed Pacific-SNGV motion observed inland of Cape Mendocino across the northern projection of the Maacama and Bartlett Springs fault zones, with additional strain occurring between the Maacama fault zone and Cape Mendocino. Less northward motion occurs in the Humboldt Bay region (Williams et al., 2006), indicating contractional deformation between the Mendocino Triple Junction and Humboldt Bay. Northward encroachment of deformation related to the San Andreas Transform against the North American plate north of the Mendocino Triple Junction was proposed by Kelsey and Carver (1988) as the driving force behind contractional deformation across the Eel River Syncline. The strain data of Williams et al. (2006) indicate increasing strain accommodated across the western portion of the Eel River Syncline. The eastern limit of the Eel River Syncline is indicated by a change in structural grain of mapped faults to a northwest orientation in the vicinity of Bridgeville, 6 miles east on highway 36 (Fig 1 inset).

Local Faulting

The previously mapped and unmapped structures described in this paper are consistent with contractional deformation at the northern terminus of right-lateral shear. The thrust faults mapped along Shively Ridge project into a zone of high angle faults indicated by the Shively Ridge/Root Creek lineaments. The Root Creek lineaments are continuous with a structural discordancy along Carson Creek in Larabee Valley that is interpreted as a fault. Chaotically deformed Wildcat sediments occur between Larabee Valley and the Dyerville area, but a through going fault in this area has not been mapped. Connecting the Root Creek faults with a San Andreas related structure such as the Maacama fault requires a bit of a punt. However, the kinematic system indicated by transpressional shear along Root Creek combined with the Shively Ridge thrust faults fits the regional model of shear and contraction, with contraction increasing to the west. The shear may or may not be a branch of the shear that would be inferred adjoining the terminus of the Little Salmon fault under the model.

The topography related to lineaments along the Root Creek valley is suggestive of downdropped blocks between the Root Creek lineaments. Such downdropping may result from local relaxation of transpression if the inferred right step in shear is in fact present and results in local extension in a northward direction.

Although the faults measured at Root Creek are oriented northwest-southeast and exhibit a significant amount of lateral shear, the p-axis, and paleo-strain solution suggest faulting driven by a strong north-south contractional strain field. This is consistent with the strain indicated by thrust faults mapped in the area. The exact role of the transpressional faults related to local and regional structures is subject to interpretation, as discussed above.

The relative ages of the Root Creek faults and folding of the Wildcat sediments related to the Little Salmon fault indicate the local onset of shear after development of the Little Salmon fault possibly representing recent northward propagation of San Andreas plate margin shear within the Eel River Syncline.

CONCLUSIONS

The Chalk Mountain landslide is a major bedrock landslide influenced by Yager stratigraphy and tensional structures related to folding on the hanging wall of the Little Salmon fault. It is likely triggered by major seismic events, resulting in catastrophic release of debris into the Van Duzen River.

The exposed outcrop at Root Creek on the Van Duzen river suggests the following stratigraphic events: 1) One faulting event occurred following the planation of the strath surface by the Van Duzen River. 2) Faulting along the eastern fault trace was followed by deposition of a large boulder deposit inferred to originate from the channel of the Van Duzen River, which preserved the offset surface at this location. 3) Debris flow deposition followed emergence of the strath surface or diverted the river away from the strath surface at the outcrop. The fine-grained uppermost unit may be associated with the debris flow deposition. The large event-related deposits may have originated from seismogenic movement of the Chalk Mountain landslide.

The zone of high angle faults that define the western limit of the outcrop, occur along the trend of an inflection of the upper terrace. This inflection indicates the same sense of vertical offset as the faults. These features are aligned with a major lineament occurring near the bottom of the Root Creek valley, supporting the interpretation that the lineaments are related to a system high angle faults extending the length of the Root Creek valley and over the divide to Carson Creek in Larabee Valley.

The paleo-strain solution indicated by fault orientations and surface features indicates transpressional deformation of the strath surface and is consistent with the regional strain indicated by major contractional structures in the area.

REFERENCES CITED

- Allmendinger, R.A., 2006. Faultkin v 4.3.5. url: <http://www.geo.cornell.edu/geology/faaculty/rwa/programs.html>
- Carver G.A., and Burke, R.M., 1992, Late Cenozoic Deformation on the Cascadia subduction zone in the region of the Mendocino triple junction. Pacific Cell, Friends of the Pleistocene guidebook for the field trip to northern coastal California.
- CGS, 1999, California Geological Survey, North Coast Watersheds Mapping, DMG CD-ROM 99-002.
- Harden, D.R., Kelsey, H.M., Morrison, S.D., and Stephens T.A. 1981, Geologic map of the Redwood Creek drainage basin, Humboldt County California. 1:62,500. Redwood National Park water resources investigation, Open file report 81-496
- Harmon Jr., A.K.P., 1914, Eel River Valley, geology and oil possibilities, California State Mining Bureau Bulletin 69, pp 455-459.
- Kelsey, H.M. and Carver, G.A., 1988, Late Neogene and Quaternary tectonics associated with northward growth of the San Andreas Transform fault, northern California, Journal of Geophysical Research, vol. 93, pp 4797-4819.
- Kelsey, H.M., and Allwardt, A.O., 1987, Geology of the Iaqua Buttes 15' quadrangle, Humboldt County, California. California Division of Mines and Geology open file report 87-06.
- Mclaughlin, R.J., Ellen, S.D., Blake, M.C., Jayko, A.S., Irwin, W.P., Aalto, K.R., Carver, G.A., and Clark, S.H.; 2000, Geology of the Cape Mendocino, Eureka, Garberville, and southwestern part of the Hayfork – 30x60 minute Quadrangles and Adjacent Offshore Area, Northern California, U.S. Geological Survey, Miscellaneous Field Study 2336, 1:100,000
- Ogle, B.A., 1953, Geology of the Eel River Valley Area, Humboldt County, California, California Division of Mines Bulletin 164, 128pp.
- Spittler, T.E., 1983, Geology and geomorphic features related to landsliding, Redcrest 7.5 min. quadrangle. CDMG Open file report 83-17.
- Williams, T.B., Kelsey, H.M., and Freymueller, J.T., 2006, GPS-derived strain in northwestern California: Termination of the San Andreas fault system and convergence of the Sierra Nevada-Great Valley block contribute to southern Cascadia forearc contraction, Tectonophysics vol. 413 pp171-184.

Day 2 Introduction (Friday)

Welcome to Day 2!

We will **meet at 7:45 AM** at the fire circle to discuss access at Stop 2-1, and **leave Pamplin Grove at 8:00 A.M.**

Day 2 - Logistical Considerations: Today, like all four days of this year's FOP trip, is a **good day to carpool**. We may (weather depending) drive across a portion of the southern approach to the Rohnerville Airport this morning. After crossing the airport property we will enter a large open field. **Please leave the horses or cattle alone.** When driving on rural roads today between Stops 2-1 and 2-2, please **drive slowly and stay on your side of the road**

Science of the day: Day 2 will focus on the region north of the latitude of Cape Mendocino. During the first half of the day, we will look at regional tectonics and crustal shortening. During the afternoon, we'll have discussions about coseismic burial of tidal marsh stratigraphy, relative long term sea-level change, and effects of the 1906 earthquake in Humboldt County.

We will make 3 stops today:

Stop 2-1 is an overlook stop at Rohnerville Airport, northeast of the confluence of the Eel and Van Duzen rivers. This stop will provide discussions on regional seismicity, GPS geodesy, structure of the Eel River basin, and hopefully a nice view.

Stop 2-2 at College of the Redwoods will examine additional structure of the Eel River basin and paleoseismic studies of the Little Salmon fault from 3 regional study sites.

Stop 2-3 will take place on the south breakwater jetty at King Salmon and will hopefully provide us views of the mouth of Humboldt Bay, the Humboldt Hill anticline above the Little Salmon fault, Table Bluff, marine terraces on the flanks of the Elk River drainage, and the Humboldt Bay power plant.

Day 2 Itinerary

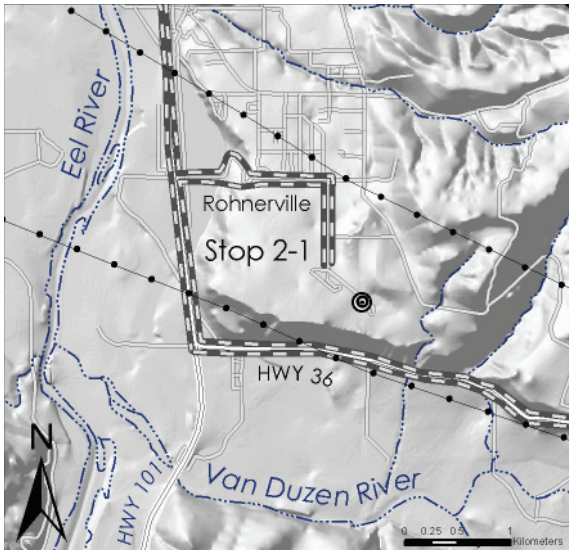
Day 2 (Friday) South Humboldt Bay Area			
Field Trip Stop	Authors	Title	Reading Material
Stop 2-1: Rohnerville: Overview of tectonics in the northern MDZ - seismic, geodetic, stratigraphic, and geomorphic signatures.	Mark Hemphill-Haley	Regional setting, northern MDZ	Intro section
	Bob McPherson and Ian Pryor	Seismicity and stress near the Mendocino triple junction: Part 2	paper 1-1-A
	Todd Williams and Bob McPherson	Gorda plate deformation contributes to shortening between the Klamath block and the on-land portion of the accretionary prism to the southern Cascadia subduction zone.	paper 2-1-A
	Harvey Kelsey	Humboldt Bay and lower Eel River neotectonics: major questions and significant uncertainties	abstract
	Mark Verhey	Subsurface seismic reflection in the Van Duzen/Eel River Valley	paper 2-1-B
Stop 2-2: College of the Redwoods: Paleoseismology and seismic hazards in the Little Salmon fault zone.	Giovanni Vadurro	Amount and rate of deformation across the Little Salmon fault and Table Bluff anticline within the onland portion of the southern Cascadia subduction zone fold and thrust belt, NW California	paper 2-2-A
	Giovanni Vadurro, Frank Bickner, Dave Lindberg, Gary Manhart, and Chris Watt	Fault surface rupture and fold hazard evaluation of the Little Salmon fault at the College of the Redwoods Eureka campus, southern Cascadia subduction zone fold and thrust belt, NW California	paper 2-2-B
	Robert Witter and Jason Patton	Upper-plate earthquakes on the western Little Salmon fault and contemporaneous subsidence of southern Humboldt Bay over the past 3,600 years	paper 2-2-C
	Mark Hemphill-Haley, Robert Witter, and Humboldt Friends of Geology	Latest Pleistocene to Holocene Paleoseismology of the Southern Little Salmon Fault, Strong's Creek, Fortuna, California	paper 2-2-D
Stop 2-3: King Salmon: Overview of earthquakes, tsunamis, and Holocene tectonostratigraphy around Humboldt Bay.	Lori Dengler	The 1906 earthquake in Humboldt and Del Norte counties, California	paper 2-3-A
	Jason Patton and Robert Witter	Late Holocene coseismic subsidence and coincident tsunamis, southern Cascadia subduction zone, Hookton Slough, Wigi (Humboldt Bay), California	paper 2-3-B
	Jason Patton and Lori Dengler	Relative Tsunami Hazard Mapping for Humboldt and Del Norte Counties, California	paper 2-3-C
	Steve Thompson, Bill Page, and Rob Witter	Long-term relative sea level change and implications to the nuclear waste storage facility at Buhne Hill, Humboldt County, California	paper 2-3-D



Day 2 Road Log

<u>Mileage</u>	<u>Distance</u>	<u>Description</u>
0.0		Pamplin Grove Gate - reset daily trip mileage (Day 1 mileage was 105.3)
0.3	0.3	Turn Left onto Hwy 36. Please drive defensively on these rural roads, the locals drive very fast!
0.8	0.8	Martin & Shirley's Store
3.5	2.7	City of Carlotta - Continue west on Highway 36. Please drive slowly through town.
4.4	0.9	[from 4.4 to 5.5] At 3 o'clock, the Goose Lake fault cuts the hillslope in the foreground, about half way up the hill. The Goose Lake, Little Salmon and Yager Creek faults are all associated with the Little Salmon fault zone, which will be a topic of discussion at our first stop this morning. Refer to today's map and the trip map for location of these faults.
5.8	1.4	Carlotta Sign
6.1	0.3	Yager Creek Bridge
6.3	0.2	Little Salmon fault cuts hills on skyline.
6.9	0.6	[6.85 - 7.7]: The fluvial terraces you are ascending were generated from Yager Creek. The back edges of the fluvial terraces trend north-northeast and are faulted by a series of west-northwest trending faults, including the Goose Lake Fault (O'Dea 1992).
8.1	1.3	Gas station - note that there's less than 60 miles of driving today total, and we have a very tight schedule today, so please don't stop for gas unless you really need it.
8.2	0.1	BEAR LEFT and continue East on Hwy 36. DO NOT go right toward Rhonerville Road
9.0	0.9	View of the Van Duzen River valley to the south (9 o'clock).
11.8	2.8	Highway 36 ends. TURN RIGHT ONTO HWY 101. Northbound traffic does not stop, so be careful as you merge into traffic. Stay in the right lane.
12.3	0.5	Hillslope failure at 3 o'clock reveals the Carlotta formation (the uppermost unit of the Wildcat Group) underlying the Rhonerville terrace surface. Note that the underlying bedrock is dipping steeper than the surface of the Rhonerville terrace. Stop 2-1 is on this terrace surface.
12.8	0.5	TURN RIGHT on Drake Road
12.9	0.1	Proceed straight at the 'Burl Country' sign. Drive defensively on this windy, rural road.
13.5	0.6	Please don't stop in the road to see the terrace gravels exposed in the road cut. These gravels and the 2-3' A horizon cap the Rhonerville terrace surface.
13.9	0.4	TURN RIGHT onto Airport Road
14.5	0.6	TURN LEFT towards Rhonerville Air Attack Base
14.6	0.1	Gate to Rhonerville Air Attack Base (Dept. of Forestry, State of Ca.)

- 14.8 0.2 Park on the right side of the road, allowing room for other cars to pass on the left. Walk to the front of the line of parked cars, and proceed straight down the paved road along the fence line thru the trees. Assemble in the field overlooking the bluff for Stop 2-1.**



Stop 2-1: Overview of Rhonerville Terraces & South Humboldt Bay

Mark H-H, Bob, Ian, Todd, and Harvey will overview the geologic setting of today's stops, and Mark V will talk about the structures of the Eel River valley revealed in seismic profiles.

[0900-1100]

STOP 2-1 ABSTRACTS

Gorda Plate Deformation Contributes to Shortening Between the Klamath Block and the On-land Portion of the Accretionary Prism to the S. Cascadia Subduction Zone.

Todd Williams and Robert C. McPherson

Recent GPS studies (Williams et al., 2006) indicate that observed convergence (2-6 mm/yr) between the Sierra Nevada-Great Valley (SNGV) block and the eastern San Andreas Fault Zone (SAFZ), near the latitude of Cape Mendocino, continues into the Southern Cascadia Subduction Zone (SCSZ). Along strike, the northernmost segment of the eastern SAFZ transitions into the convergent boundary between the Klamath Mts. and the backstop to the on-land portion of the accretionary prism to the SCSZ. Earthquakes that accommodate N-S compression in the Gorda plate are commonly SW-NE striking left-lateral strike slip events. These events are documented as having permanently deformed the on-land portion of the accretionary prism ~ 10 mm/event towards the east. The observed displacements confirm that portions of the accretionary prism are coupled to the Gorda plate, and, that these displacements will contribute to convergence with the Klamath Mts at the eastern boundary of the backstop to the accretionary prism of the SCSZ.

Humboldt Bay and Lower Eel River Neotectonics: Major Questions and Significant Uncertainties

Harvey Kelsey

The Humboldt Bay/lower Eel River region provides abundant geologic data with which to address several scientifically significant and societally relevant questions in Quaternary tectonics and Quaternary science.

The following science questions have in common the goal of better understanding the tectonics and geomorphic processes at the western edge of the North American plate within the Mendocino deformation zone and the southern end of the Cascadia subduction zone. Key research techniques include late Quaternary biostratigraphy, lithostratigraphic description, radiocarbon dating, leveling analyses for elevation relative to tidal datum, identification of paleo sea level stratigraphic indicators, and, more recently, satellite based geodesy. All of these approaches have become more sophisticated in the last three decades, requiring ongoing evaluation of older data for accuracy and precision.

The major scientifically significant and societally relevant questions are:

- What is the relation of the Cascadia subduction zone megathrust to the active upper plate faults above the megathrust, in terms of timing of earthquakes and recurrence interval of earthquakes?
- How much deformation on the Cascadia subduction zone is taken up by folding of the upper plate rather than by slip on the megathrust or upper plate faults?
- Can Holocene deformation be documented using folded terraces (fluvial or marine), or folded tidal wetlands? How is folding measured? When is folding of manifestation of contraction?
- To what degree of resolution can radiocarbon age determinations establish a faulting or folding chronology, a tsunami chronology, or a terrace (fluvial or marine) chronology?
- To what degree of accuracy can uplift rates be assigned to coastal late Pleistocene-age landforms? to coastal Holocene-age landforms?

For the questions posed above, it is necessary to ask to what extent should the scientific community use prior research results as a building block for ongoing research? Are past results robust building blocks or smoke screens obscuring progress? If both may be the case, how do we choose what results to use? To pose this question is not to attempt to discredit past research. To the contrary, past work in this region is uniformly creditable and undertaken in good faith with research tools available at the time. However, advances in: 1) radiocarbon research (both criteria for sample selection and how samples are analyzed), 2) other Quaternary dating techniques, 3) geodetic techniques, 4) biostratigraphic data processing using statistics of large data sets, and 5) criteria for identifying paleo sea level in stratigraphic sections means that some creditable work needs to be redone to better standards while other work remains robust and can be used as a building block for ongoing research.

At this introductory field stop, I will briefly explore these concerns using field case studies that will be discussed in the remaining days of the field trip.

Dept of Geology Humboldt State University hmk1@humboldt.edu

Subsurface seismic reflection in the Van Duzen/Eel River Valley

Mark Verhey

The relative development of several soil properties on Eel River terraces, located on the southern limb of the Eel River syncline, records three distinct soil age groups. The highest well-preserved terrace is named the Rohnerville. The relative elevations of similar age terraces/soil age groups records Quaternary growth, and the approximate location of, thrust faults and folds.

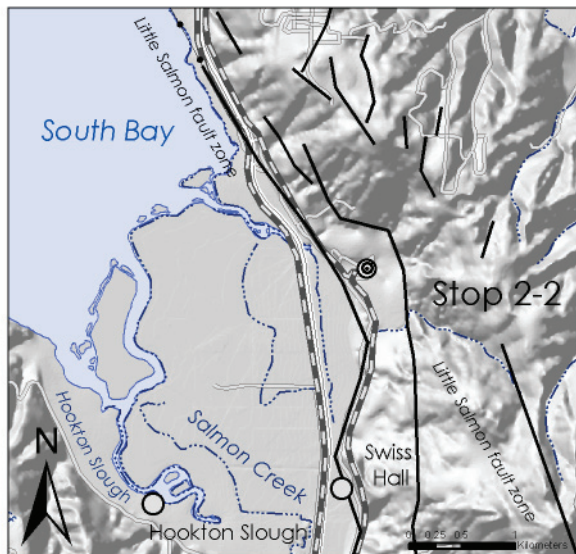
The Grizzly Bluff anticline is an asymmetric fold, with a relatively long and planar northern limb, expressed by the northward tilt of the Rohnerville terrace between Hydesville and Fortuna. A 200-foot down to the south displacement of the Rohnerville terrace across Price Creek expresses the southern limb of the GBA. Additionally, an intermediate terrace, the Weymouth terrace is visibly tilted south, which can be viewed from the highway.

Principal reflection packages across industry seismic reflection lines reveal the GBA is a thin-skinned structure. North dipping thrust faults exposed in Price Creek and Weymouth Bluff Road do not extend to seismogenic depth. Rather, they are rooted in a south dipping detachment surface. The vergence direction is northerly, with some of the slip returning to the surface in a series of backthrusts or antithetic faults. The south dipping detachment surface does not reach the surface. I have provided one of the seismic lines for your review.

<u>Mileage</u>	<u>Distance</u>	<u>Description</u>
14.8		Return to Vehicles. Follow the lead cars to the east end of the parking area to turn around heading west.
15.1	0.3	Turn Right on Airport Road
15.7	0.6	Turn Left onto Drake Hill Road.
16.1	0.4	Road cut in the Rhonerville terrace - watch for oncoming traffic on this 20 mph blind corner.

<u>Mileage</u>	<u>Distance</u>	<u>Description</u>
16.6	0.6	TURN RIGHT and merge onto 101 North
18.3	1.6	View of Strong's Creek basin at 3 o'clock. The Little Salmon fault runs thru Strong's Creek where the confined stream emerges into the valley. Mark Hemphill-Haley will discuss faulting history on the LSF at Stop 2-2 based on a trench near Strong's Creek.
20.3	2.1	EXIT RIGHT onto Palmer Rd. exit (exit 690)
20.7	0.4	TURN RIGHT onto Thompkins Hill Road. DO NOT go straight and re-enter HWY 101! If you miss this turn and re-enter Hwy 101, proceed north on 101 to the Hookton Rd exit and rejoin the trip log at the Swiss Hall entry.
21.1	0.5	Climbing up Tompkins Hill
21.7	0.6	Nice view of the Eel River Valley and Wildcat Ridge at 8:00. South of the Eel River and Wildcat Ridge, the terrane is dominated by the southern Mendocino deformation zone - yesterday's topic of discussion. Today, we are driving thru a landscape dominated by the fold and thrust belt
22.1	0.4	Spectacular glimpse of Eel River Valley behind a barn on the left
22.3	0.2	Graham Way on right, natural gas well access down this road; Go left and follow the main road
22.4	0.1	Wildcat Hills to west-southwest. [21.3 - 21.5] The Loleta ash has been found in road exposures here. The Loleta ash is chemically identical to the Tumelo Tuff, erupted from the Bend, Oregon region (ca. 400 ka ?)
22.8	0.4	[21.7 to 21.8] Watch for oncoming traffic as you enjoy the spectacular view of the Eel River Valley and Table Bluff to the west. We are looking down the axis of the Table Bluff at ~10 o'clock. Giovanni Vadurro will discuss the underlying structures of the Table Bluff anticline at Stop 2-2.
23.0	0.2	View to the east is into an unnamed tributary of Little Salmon Creek. Notice the pressure ridge associated with the Little Salmon fault zone running northwest-southeast at 3 o'clock (between Little Salmon Creek and the unnamed trib). At 11 o'clock is another view down Table Bluff. Be careful not to run over the yappy dog.
23.3	0.3	At 11 o'clock is a nice view of the mouth of Humboldt Bay. The Eel River is to the south at 8:30, and at 10:30, the Holgersen's Dairy (yellow and red barn) comes into view. At 12 o'clock, the western trace of the Little Salmon fault runs along the base of the slope, just to the east of the dairy.
24.0	0.7	Drive slowly as you take this hairpin turn - this turn can be icy in cold weather. After the turn, the grassy hill at 3 o'clock is of the toe of a pressure ridge forming the drainage divide between Little Salmon Creek and the unnamed tributary we are driving along.
24.3	0.3	Field on the right is the location of Carver and Burke's 1988 trenches into the western trace of the Little Salmon fault. See the 1992 FOP guidebook for more information on these trenches.
24.5	0.2	Little Salmon Creek Bridge. Note the interaction between alluvial and fluvial features and young tectonics.
24.9	0.4	cow grazing accentuates scarp expression
25.0	0.1	Salmon Creek Bridge. Entering private property, please drive slowly

<u>Mileage</u>	<u>Distance</u>	<u>Description</u>
25.2	0.2	Road on right leads to Carver and Burke (1988) trenches wherein they mapped the eastern trace of the Little Salmon fault. This was the first trench to document the high magnitude, ~300-year recurrence interval potential of the Little Salmon fault zone.
25.5	0.3	Holocene Bovine terracettes (Hbt) at 2:00 :)
25.7	0.2	Holgersen Dairy residence; Please drive very slowly and respect the private property.
25.8	0.1	Good view of the north limb of the Table Bluff anticline at 11 o'clock.
26.0	0.2	Hookton Road (Beatrice) enters from the left; Go Straight
26.0	0.0	At 12:00 noon is the former location of the town site of Beatrice. Although difficult to see, a horizontal vegetation lineament marks location western trace Little Salmon fault, which Rob Witter will discuss at stop 2-2.
26.5	0.5	In the field on the left, note mole track where cattails define wetland adjacent to fault. This is the site of the Witter et. al trench, which will be discussed at our next stop.
27.2	0.7	At 12 o'clock the roof of College of the Redwoods Administration/Library building comes into view. CR is the meeting place for stop 2-2.
27.9	0.6	TURN RIGHT into CR parking lot: park towards east side of lot. School is in session, so follow parking MONGOS to the designated FOP area.



Stop 2-2: College of the Redwoods paleoseismology: miles and miles of trenches

Giovanni will talk about seismic profiles of Table Bluff; Frank, Dave, Gary and Gio, Mark H-H, and Rob will discuss trenching at CR, Strongs Creek, and near Swiss Hall, respectively.

[1200-1400]

STOP 2-2 ABSTRACTS

Amount and rate of deformation across the Little Salmon fault and Table Bluff anticline within the onland portion of the Southern Cascadia Subduction Zone fold and thrust belt, NW California

Giovanni A. Vadurro, Humboldt State University Geology Department, Arcata, CA

The Little Salmon fault (LSF) and Table Bluff anticline (TBA) with its associated north dipping blind thrust and south dipping back-thrusts accommodate a significant amount of upper plate crustal shortening within the onland portion of the fold and thrust belt (Figure 1). Regionally, these structures deform Yager Terrane basement rocks and younger overlying sediments. The Yager consists of Paleogene marine strata as much as 3000 m thick. Unconformably overlying and in depositional contact with the basement rocks are a sequence of upper Miocene to middle Pleistocene-aged sediments comprising the Wildcat Group (Ogle, 1953). Wildcat Group sediments consist of a marine transgressive-regressive sequence

greater than 3500 m thick (Clarke, 1992). In ascending order this sequence is composed of the Pullen, Eel River, Rio Dell, and Scotia Bluffs Formations. Interfingering with and gradationally overlying this sequence is 800-1000 m of non-marine sandstone and conglomerate of the Carlotta Formation, which is the uppermost unit of the Wildcat Group. The entire sequence is truncated at the top by an unconformity, and is overlain by nearshore marine to coastal plain and fluvial deposits of the Pleistocene Hookton Formation (Ogle, 1953).

Where the LSF underlies the Humboldt Hill anticline (HHA), structure contouring of the fault plane based on petroleum industry exploratory borehole data and boreholes installed by Woodward-Clyde Consultants (WWC, 1980) indicates the fault to strike about N 30-45° W and dip a maximum of 30° NE. Further to the southeast, structure contouring of the fault plane reveals a more westerly strike and similar dip. The depth to the LSF below the fold crest of the HHA ranges from 400-500 m below mean sea level. Northeast of Field's Landing, along the backlimb of the HHA, the fault plane is encountered at an elevation of -900 m. Based on the borehole geophysical and mud logs, the fault is generally observed to emplace mudstone of the lower Wildcat Group sediments over sand and gravel of the Carlotta or Hookton Formations (WWC, 1980).

Total vertical displacements along the LSF generally decrease to the northwest. Borehole data from T.T. Co. Little A-1 within the hanging wall of the LSF and the Holmes-Eureka #3 well at Tompkins Hill within the footwall, indicate the vertical separation of the contact between the Yager and the overlying Wildcat sediments across the LSF to be 1650 m. Further to the northwest, along the HHA, the apparent vertical separation of the Yager/Wildcat contact is 1400 m, based on borehole data from the Blackwood Nichols No. 1 and Brauner wells. In the Fields Landing area, apparent vertical separation of the base of the Hookton Formation, which unconformably overlies the Rio Dell Formation at this location, is estimated to be as much as 560 m (WCC, 1980). Reported age estimates for the base of the Hookton Formation are about 400-500 ky.

Timing for the onset of movement on the LSF and TBA blind thrust is not well constrained. Seismic reflection profiles across the tip of the LSF and through the TBA and Eel River syncline (ERS) reveal onlap sequences along the forelimb of the anticline beginning within the lower Scotia Bluffs Formation (Figures 2 and 3). The thickness of the underlying Rio Dell Formation appears uniform across the width of the fold. The onlap sequences are interpreted to represent growth strata resulting from syntectonic deposition following the onset of folding in response to slip on the underlying blind thrust. The maximum age of the growth strata were determined by following the underlying reflectors in the seismic profiles south to where they are projected to daylight in the coastal bluff at Centerville Beach. Paleomagnetic data obtained from the lower Scotia Bluffs Formation at this location, and continuing up section, indicates normal magnetic polarity (WCC, 1980). This suggests that the onlapping sequences in the lower Scotia Bluffs Formation were deposited following the Brunhes-Matuyama geomagnetic field reversal of 780 ka (Baksi et al, 1992). Therefore, growth of the TBA, a major fault-propagated fold generated by repeated slip on an underlying blind thrust, was initiated post-780 ka. Thus it is assumed that slip on the LSF, and growth of the HHA, also initiated at a similar time.

Long term slip rates for the LSF and TBA blind thrust were calculated from the apparent maximum vertical separation of the Yager/Wildcat contact across the fault zones coupled with the dip of the fault plane, and the timing for the onset of movement. At Tompkins Hill, the vertical separation of 1650 m on the Yager/Wildcat contact yields a net dip-slip displacement of 3300 m and a long term slip rate of 4.2 mm/yr. In the vicinity of the HHA, the net dip-slip displacement on the same contact is 2800 m yielding a slip rate of 3.6 mm/yr.

At Table Bluff the dip of the underlying north dipping blind thrust that is confined to the basement rocks is unknown. A dip of 30°, similar to the dip of the LSF, is therefore assumed. Between the crest of the TBA and axis of the ERS, the maximum vertical separation of the Yager/Wildcat contact, based on its elevation in the Sunset-1 and Texaco Quinn-1 wells, is about 1460 m. The resultant dip displacement is therefore ~2900 m yielding a slip rate of 3.7 mm/yr.

The reported rate of northeast-southwest directed horizontal contraction across the entire fold and thrust belt is reported to be about 20 mm/yr (Clarke and Carver, 1992), which is approximately half of the Gorda-North American plate convergence rate. Of this total, the LSF and TBA with its associated thrusts are accommodating more than 7 mm/yr of upper plate crustal shortening.

Fault Surface Rupture and Fold Hazard Evaluation of the Little Salmon Fault at the College of the Redwoods Eureka Campus, Southern Cascadia Subduction Zone Fold and Thrust Belt, NW California

Vadurro, G. A., Bickner, F. R., Lindberg, D. N., Manhart, G. L., and Watt, C. J.

College of the Redwoods (CR) is located entirely within the Little Salmon fault zone (LSF) and has been extensively investigated for surface fault rupture and fold hazards (Woodward-Clyde Consultants, 1980; LACO, 1999). Between 1989 and 1999, approximately 1,600 lineal meters of exploratory trench were excavated in order to site new facilities and evaluate potential surface fault rupture and fold hazards to existing buildings.

The LSF bounds CR and consists of two northwest striking, northeast dipping, low-angle thrust faults. The west trace of the LSF daylight along the southwesterly edge of campus infrastructure and dips beneath the site at an angle of 25° while the east trace daylight at the base of the Humboldt Hill anticline (HHA), near the northeasterly edge of campus infrastructure. Movement on the LSF during the late Pleistocene and Holocene at CR is accompanied by surface fault rupture, localized uplift, and growth of a broad asymmetric fold within the upper thrust sheet featuring a steeply dipping forelimb, a broad, very gently dipping, back-tilted crest, and shallowly dipping backlimb. This fault-generated fold geometry is evidenced by the present-day topography at CR.

Structural variability along strike of the LSF where it traverses the campus is pronounced. Trench exposures revealed 25-50 m wide zones of deformation displaying primary north dipping thrusts and secondary south dipping back-thrusts, and progressively folded strata. Low and high-angle faults exhibiting reverse and normal offsets, respectively, were observed.

Late Pleistocene slip rates determined for the west trace of the LSF based on the age and amount of uplift of marine terrace surfaces Qtm1 and Qtm2, and the dip of the fault, range from ~5.8 mm/yr to ~7.6 mm/yr. Slip rates obtained from trenching studies conducted south of CR across both the west and east trace of the LSF yield a combined rate of 6-12 mm/yr (Clarke and Carver, 1992). Displaced stratigraphic markers at this site record three slip events totaling 4.6 m to 6.5 m, of which 3.6 m to 4.5 m were measured on the west trace. Greater amounts of slip per event recorded on the west trace compared to that of the east trace suggest the west trace is likely accommodating most of the recent deformation.

Upper-Plate Earthquakes on the Western Little Salmon Fault and Contemporaneous Subsidence of Southern Humboldt Bay Over the Past 3,600 Years

Robert C. Witter and Jason R. Patton

Along the southeastern side of Humboldt Bay the Little Salmon fault zone extends over 100 km in the fold-and-thrust belt of the southern Cascadia subduction zone and includes three northwest-striking imbricate thrust faults that deform intertidal deposits and terraces along the bay margin. The bay deposits contain tidal marsh soils abruptly overlain by intertidal mud interpreted to record sudden regional subsidence caused by plate-boundary earthquakes. Although prior investigations of the western Little Salmon fault documented three earthquakes in the past 2,000 years, the question of whether the Little Salmon fault ruptures independently from the southern Cascadia subduction zone or is coseismically triggered by megathrust events remains unresolved. At the Swiss Hall site we investigated the western trace of the fault where a 1- to 1.5-m-high moletrack scarp projects into southern Humboldt Bay and deforms late Holocene intertidal sediment. Estuarine strata that lap onto the scarp include three buried peaty soils containing tidal marsh diatoms that are progressively folded with increasing depth and form a west-facing monocline. An angular unconformity separates the sequence of soils from a thick (0.7 m) overlying deposit of tidal flat mud. Normal faults in the hanging wall offset the entire sedimentary package in the scarp. We identify three slip events on the western Little Salmon fault during the past 1,700 years. Growth of the scarp occurs through folding and secondary faulting above a shallow, low angle, blind thrust fault. The most recent earthquake disrupted the scarp along subvertical surface fissures that taper downward into normal faults in the hanging wall. The data provide a slip rate estimate of 2.9- to 6.9-mm/yr with 1.3- to 4.1-m of slip per event. Radiocarbon ages that bracket evidence of scarp deformation broadly limit the timing of three earthquakes to between 0 to 460, 540 to 1,230 and 1,530 to 1,710 cal yr BP. The uncertainty spanned by the age ranges precludes a one-for-one correlation between earthquakes on the western Little Salmon fault and regional Cascadia megathrust events. Comparisons between slip-histories for the western Little Salmon fault and regional chronologies of megathrust earthquakes leave open the possibility that some upper-plate events were coseismically triggered by plate-interface seismicity. This inference is strengthened for event 3 where deformed strata in the fault scarp coincide with

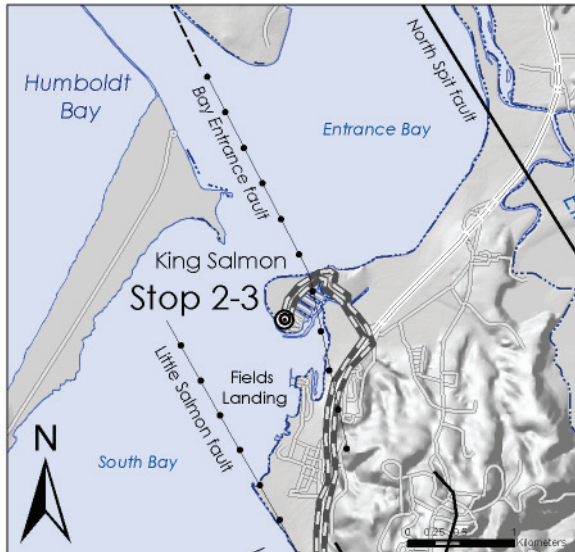
evidence for extensive subsidence of southern Humboldt Bay that extended into the hanging wall of the Little Salmon fault. In contrast, fault slip during event 2 lacks correlation with evidence of coseismic subsidence in the hanging wall and allows the possibility that the Little Salmon fault ruptured independently during the interseismic period between great Cascadia subduction zone earthquakes.

Latest Pleistocene to Holocene Paleoseismology of the Southern Little Salmon Fault, Strong's Creek, Fortuna, California

Mark A. Hemphill-Haley, Robert C. Witter and Humboldt Friends of Geology (F.O.G.)

A trench was excavated along a southern splay of the Little Salmon fault near Fortuna, California. The Little Salmon fault is one of the southernmost reverse faults within the onland fold and thrust belt associated with the Cascadia subduction zone. The trench exposed evidence for at least 3 fold and fault events in terrace gravels and overbank deposits associated with nearby Strong's Creek. A prominent 1 m-wide fault zone dipping between 30 and 60° displaces all but the uppermost unit in the trench which is anthropogenic fill. The majority of deformation appears related to non-brittle folding of the fine-grained deposits. The most recent event consisted of about 2.5 m of vertical uplift and 2.9 m of horizontal shortening in a broad monoclinical fold of a prominent clayey silt deposit accompanied by about 20 cm of reverse offset. This event occurred between about 10,000 to 12,000 years ago. Based on retrodeformation of trench units and radiocarbon-based estimates of deposit ages, we conclude that a total of 5.1 m of fault parallel offset has occurred since about 13,000 to 14,000 years ago providing a slip rate of about 0.4 to 0.5 mm/yr. The three deformation events occurred within a span of less than 4,000 years followed by 10,000 years of quiescence. We conclude that this may represent temporal clustering of events on this particular splay of the fault which is not characteristic of the Little Salmon fault as a whole. Ample evidence for multiple Holocene ruptures on the Little Salmon fault at locations to the north lead us to believe that the splay trenched at Strong's Creek is likely subsidiary to a more active, yet unmapped structure nearby.

<u>Mileage</u>	<u>Distance</u>	<u>Description</u>
27.9		Return to Vehicles and exit out the south entrance to the CR parking lot.
28.2	0.4	TURN RIGHT onto Thompkins Hill Road
28.8	0.6	BEAR RIGHT onto HWY 101 NORTH
29.2	0.4	View of the south spit to the west and Humboldt Bay and Table Bluff to the south. At Stop 2-3 we will talk about the tsunami record in southern Humboldt Bay.
30.9	1.7	PG&E power plant comes into view at 12 o'clock, and Humboldt Hill is to the east. Refer to the map in Vadurro (Stop 2-2A) for the structure underlying Humboldt Hill.
31.2	0.3	TURN RIGHT onto King Salmon Exit
31.4	0.2	TURN LEFT under Hwy 101 and proceed west
31.9	0.5	Road to PG&E power plant on the right. PROCEED STRAIGHT on King Salmon road. Note that the trace of the Little Salmon fault is mapped up to, but not thru this PG&E facility. Safe storage of nuclear waste from this facility is a topic of discussion at our next stop.
32.2	0.3	Follow road as it takes a HARD LEFT
32.3	0.1	Park along the right side of the Buhne Road, and please don't use the parking lot in "Gils by the Bay" There is a short (few hundred meters) hike to an overview near the mouth of Humboldt Bay. Follow the trail at the south end of the parking line to assemble for Stop 2-3. Bring a windbreaker if you have one.



Stop 2-3 King Salmon: earthquakes, tsunami, and other stories

We will meet on the dunes near the mouth of Humboldt Bay where Lori will talk about the 1906 earthquake in Humboldt County, Jay will discuss coseismic subsidence and tsunami hazard in Humboldt Bay, and Steve will tell us about sea-level and land-level changes for the next 100 ka.

[1500-1700]

STOP 2-3 ABSTRACTS

The 1906 Earthquake in Humboldt and Del Norte Counties, California

Dengler, L.

The State Earthquake Investigation Commission (Lawson, 1908) documented the 1906 earthquake in Humboldt County. This study examines that report and additional information including newspapers, diaries and retrospectives and previously unpublished photographs to describe the earthquake and compare its impacts to recent large local earthquakes. Humboldt County of 1906 had thriving timber and agricultural industries, six newspapers in print and populations in the Eel River Valley similar to current levels. Local Historical Societies have compiled a large collection of primary materials. Losses in Humboldt County from the 1906 earthquake are estimated at \$200,000 in 1906 dollars. Damage and eyewitness accounts do not support the Lawson Report isoseismal map for Humboldt County. The Lawson map shows a zone of strongest ground motions around Humboldt Bay. Strongest ground motions (MMI IX) actually occurred in the Eel River Valley and Petrolia areas where all structures reported some damage and a number of injuries occurred. In the Eel River Valley and Ferndale, fewer than 2% of chimneys survived and nearly every structure was damaged. Liquefaction was observed in the Mattole Valley and throughout the Eel River Valley and occurred on a larger scale than any more recent events. Damage in Eureka was much less than in Ferndale and rapidly decayed to the north. Based on the severity of damage and scale of liquefaction, the 1906 earthquake was Humboldt County's strongest historic event with an intensity VII or larger area more than twice the size of the 1992 Cape Mendocino (M_w 7.1) earthquake. The 1906 earthquake triggered at least 22 smaller earthquakes on the North Coast in the 6 weeks following including the largest aftershock ($M \sim 6.7$) of the 1906 sequence.

Late Holocene Coseismic Subsidence and Coincident Tsunamis, Southern Cascadia Subduction Zone, Hookton Slough, Wigi (Humboldt Bay), California

Jason Patton and Robert Witter

In the past 3,650 years (cal. yr. B.P.) evidence of coseismic subsidence was recorded five times in stratigraphy of bay margin deposits in southern Humboldt Bay, California. There are five buried marsh soils along a 1-kilometer long transect adjacent to Hookton Slough, a tidal channel tributary in Humboldt Bay. Using the lateral extent of burial, the abrupt upper contacts to the soils, and the diatom biostratigraphy, soils subsided coseismically and those soil burials were accompanied by abrupt rises in relative sea level. Tsunami-transported sand, observed in the stratigraphy from Hookton Slough, was deposited directly on two soils at the time of subsidence. Buried soils at Hookton Slough are best explained by coseismic subsidence during Cascadia subduction zone earthquakes. Radiocarbon age estimates constrain timing of subsidence and allow me to estimate a recurrence interval of Cascadia subduction zone earthquakes in the Humboldt Bay region. A recurrence interval for these

large earthquakes ranges from 650 to 720 years for the last 2,400 years. Three of the buried soils correlate to similar buried soils found at other sites around Humboldt Bay, and timing of subduction zone earthquakes at Hookton Slough overlaps with timing of earthquakes on the Little Salmon fault.

The largest subsidence estimates based on the paleoelevation method are determined to be a minimum of 0.9 meters. This minimum estimate is increased by utilizing the relief of the upper contact for one buried soil. The relief of the upper contact was over two meters. Since the paleoecology of the soil was freshwater pre-submergence, and the entire soil was coseismically buried by tsunami sands and then by tidal silts to clay-silts, the subsidence estimate is increased from less than one, to greater than two meters.

Relative Tsunami Hazard Mapping For Humboldt and Del Norte Counties, California

Jason R. Patton and Lori A. Dengler

Based on paleoseismic evidence from coastal marshes and on historic teletsunami inundation, coastal Humboldt and Del Norte Counties entertain a considerable tsunami hazard. Tsunami hazard maps are constructed using a raster-based geographical information systems (GIS) approach to depict the relative tsunami hazard of coastal Humboldt and Del Norte County in northern California (<http://www.humboldt.edu/~geodept/earthquakes/rctwg/toc.html>). The raster model is primarily based on topography, so the parameters may be easily adjusted as new hazard-elevation relations are developed through numerical modeling or other methods. In contrast to maps depicting hazard by a single inundation line, the raster model uses a gradational scale. Elevation, normally used for 2.5D surfaces, is substituted with safety units. Hazard is displayed as a safety index, a continuous gradational color scale ranging from red (high hazard) through orange (medium), yellow (low) to white (no hazard). Hazard-elevation relations were developed using existing numerical modeling, paleoseismic studies, historical tsunami flooding, and impacts of recent tsunamis elsewhere. Hazard units are further modified by distance to open water. An advantage to this approach is that tsunami hazard maps can be constructed even when numerical modeling does not exist and can be readily adjusted as new information/modeling results become available. The GIS framework facilitates ready adaptation by planners and emergency managers for use at different map scales. The maps are intended for educational purposes, to improve awareness of tsunami hazards, and to encourage emergency planning efforts of local and regional organizations by illustrating the range of possible tsunami events. The maps have been adopted by the Humboldt County Office of Emergency Services as part of their tsunami hazard mitigation plan.

Long-Term Relative Sea Level Change and Implications to the Nuclear Waste Storage Facility at Buhne Hill, Humboldt County, California

Thompson, S.C., Page, W.D., and Witter, R.C.

A temporary, dry storage facility of nuclear waste (ISFSI) is being constructed at Buhne Hill on Humboldt Bay, the site of the Pacific Gas & Electricity Company (PG&E) Humboldt Bay Power Plant. In response to a request by the California Coastal Commission, PG&E evaluated the site conditions of their proposed facility for stability 'in perpetuity' by forecasting up to 100,000 years in the future potential changes from two geologic hazards: (1) the tectonic uplift of Buhne Hill, and (2) coastal erosion from projected sea level rise and Pacific storm variability that may result from global warming. This paper summarizes the analysis for coastal erosion hazard to Buhne Hill related to projected relative sea level rise over time periods of 100, 1,000, 10,000, and 100,000 years.

Relative sea level change results from both land level change and global sea level change. Land level change at Buhne Hill is dominated by long-term tectonic uplift at a rate of 1.2 ± 0.5 feet per thousand years (0.4 ± 0.1 mm/yr). Short-term land level change is dominated by elastic strain accumulation and release on the Cascadia subduction zone and Little Salmon fault zone, with permissible abrupt uplift or subsidence of up to a few meters during an earthquake on one or both of the sources. Global warming over the next century and beyond will cause a rise in sea level. Current emissions of greenhouse gases, most notably carbon dioxide and methane, have produced higher atmospheric concentrations of those gases than at any time in the past 420,000 years, and projected increases in temperature and sea level are expected to occur at rates that are an order of magnitude or higher than rates typical of the past few thousand years. The context for evaluating sea level change over the very long term is an assumption that the earth's climate remains in the cycle of glacial and interglacial intervals that have persisted for the past 2.5 million years. Changes in earth's orbit around the sun cause predictable variations in the solar

insolation on earth, and these orbital variations closely correlate with glacial and interglacial cycles in the past. Current and projected solar insolation, combined with present day and near-future anthropogenic rise in greenhouse gasses, suggest that the earth may miss the next opportunity to enter the next glacial interval and hence global cooling may not start for another 50,000 years.

Over the next few hundred years sea level is expected to rise between less than one to as much as six feet, based on the 2001 report on climate change by the Intergovernmental Panel on Climate Change. In the thousand to ten thousand year time period sea level may rise and approach the ISFSI elevation of 44 feet (MLLW) with the extreme scenario of it being over topped. The maximum rate of sea level rise is not expected to exceed about 3.3 feet per century (10 mm/yr), the maximum rate of sea level rise recorded during an interglacial interval in the geologic record for the past 400,000 years. In the forecasts that consider climate change over for tens of thousands of years, glacial intervals are expected to resume with a corresponding drop in sea level. In all scenarios the long-term tectonic uplift of the site counters sea level rise.

Rise in sea level is a slow process (0.26 to 3.3 feet/100 years) and will be monitored. As the riprap protection at Buhne Hill is damaged, or possibly impacted, during increased storm activity and other changed conditions, additional riprap or other protection would be placed in front of Red Bluff and around Buhne Hill to insure the protection of the ISFSI. Over the next 100 years, barring a major earthquake on the Cascadia subduction zone, interseismic uplift will likely keep pace with sea level rise. However, a major earthquake on the Cascadia subduction zone would drop King Salmon but may or may not cause abrupt coseismic subsidence of Buhne Hill. In this occurrence, PG&E would evaluate the integrity of the coastal protection works following the event and place additional riprap or other protection in front of Red Bluff to insure the protection of the ISFSI. In the unlikely scenario that the sea level rose above the elevation of the ISFSI in several thousand years, the site would be moved to a safe location.

<u>Mileage</u>	<u>Distance</u>	<u>Description</u>
31.2		Return to cars.
32.6	0.3	Return to camp. Pull to the end of Buhne Road and turn around at Gill's by the Bay
33.0	0.3	35 MPH sign
33.1	0.1	Bear Right onto King Salmon Road
33.9	0.8	TURN RIGHT and get on HWY 101 South
49.1	15.2	TURN LEFT on HWY 36 - Remember, Northbound traffic does not stop!
60.0	10.9	TURN RIGHT and into Pamplin Grove campground

INTENTIONALLY LEFT BLANK FOR WILLIAMS FIGURE 2

Figure 2. Comparison of campaign GPS results (1993-2002) with continuously operating GPS stations (2004-2006) in the Mendocino deformation zone. Continuous stations are operated through the National Science Foundation's EarthScope Project, and data shown are from the USGS Earthquake Hazards Program auto-processing facility in Menlo Park, CA.

INTENTIONALLY LEFT BLANK
FOR
WILLIAMS FIGURE 2

INTENTIONALLY LEFT BLANK
FOR
WILLIAMS FIGURE 2A

Figure 2A. Comparison of campaign GPS results from this study (1993-2002) and the USGS Mendocino network (1993-2005). Slight inconsistencies are present, and are likely due to differences in reference frames (Sella et al, 2002 vs. ITRF 2000).

INTENTIONALLY LEFT BLANK
FOR
WILLIAMS FIGURE 2A

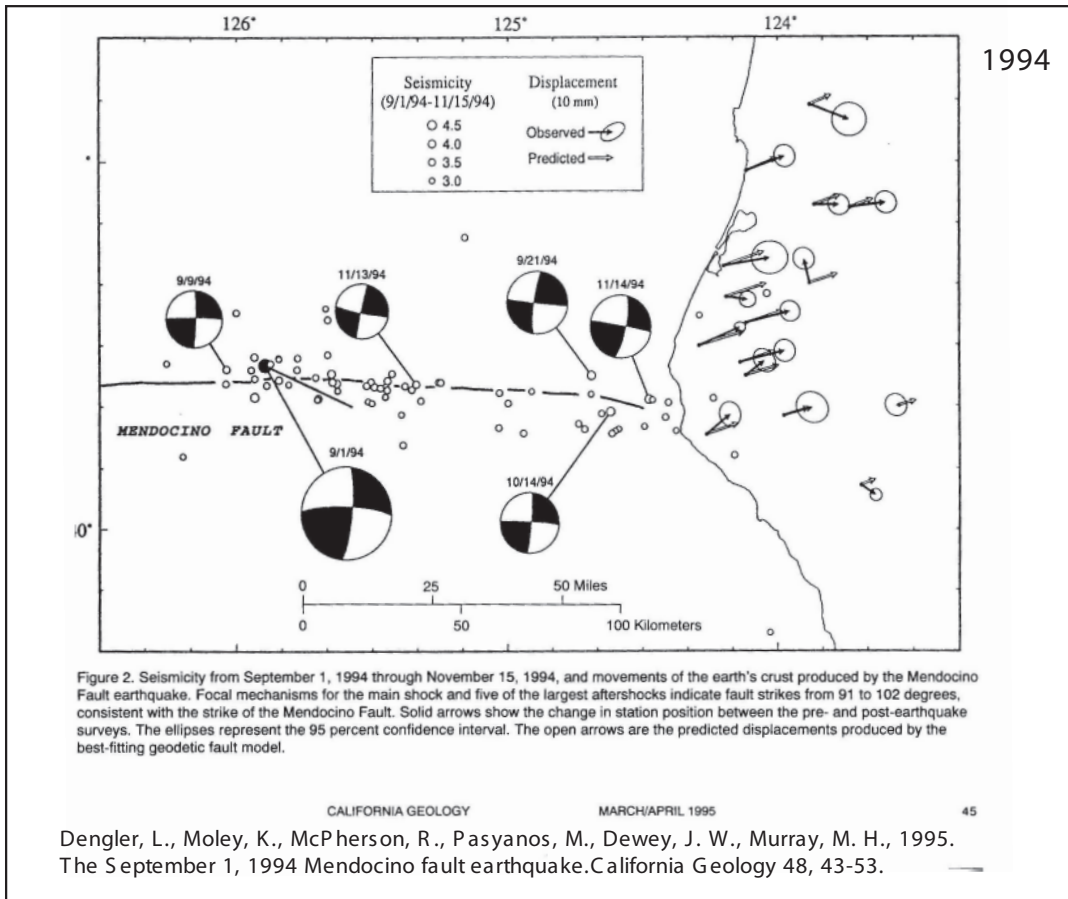
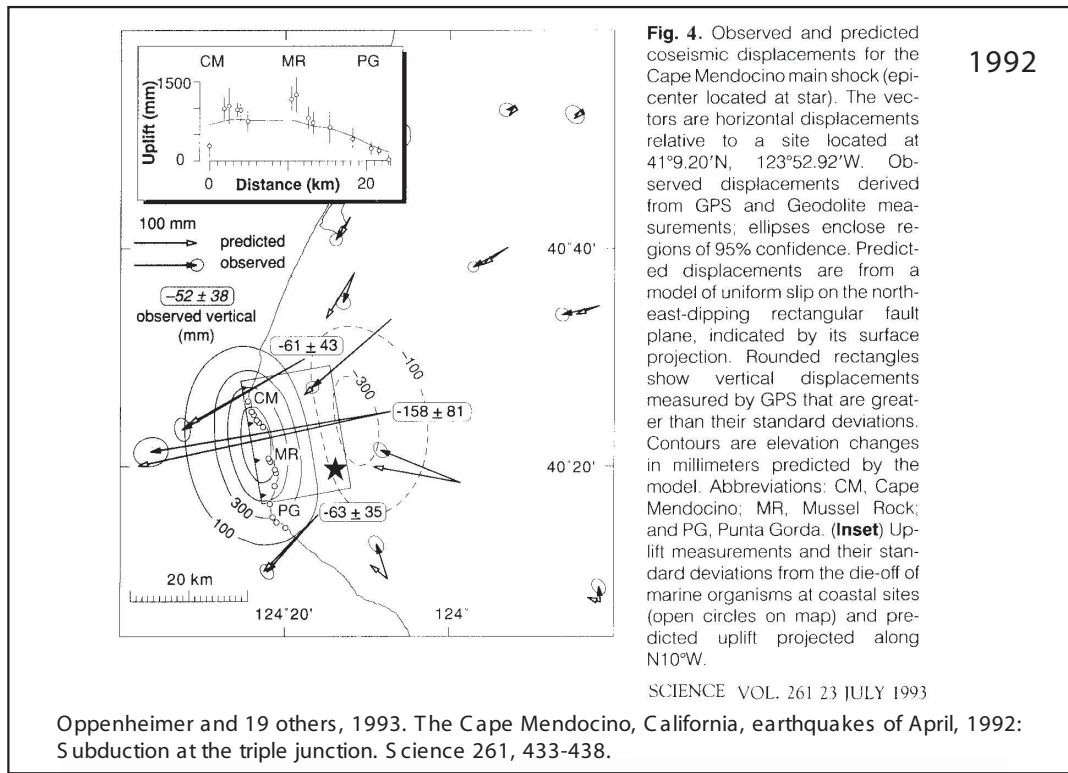


Figure 3. Summary of historic earthquakes in the study area for which repeated GPS surveys are available. The 1992 event involved thrust faulting within the upper plate at the southernmost end of the CSZ (Oppenheimer et al., 1993). Note the eastward push that the on-land portion of the accretionary wedge experienced as a result of the 1994 event (Dengler et al., 1995).

2005

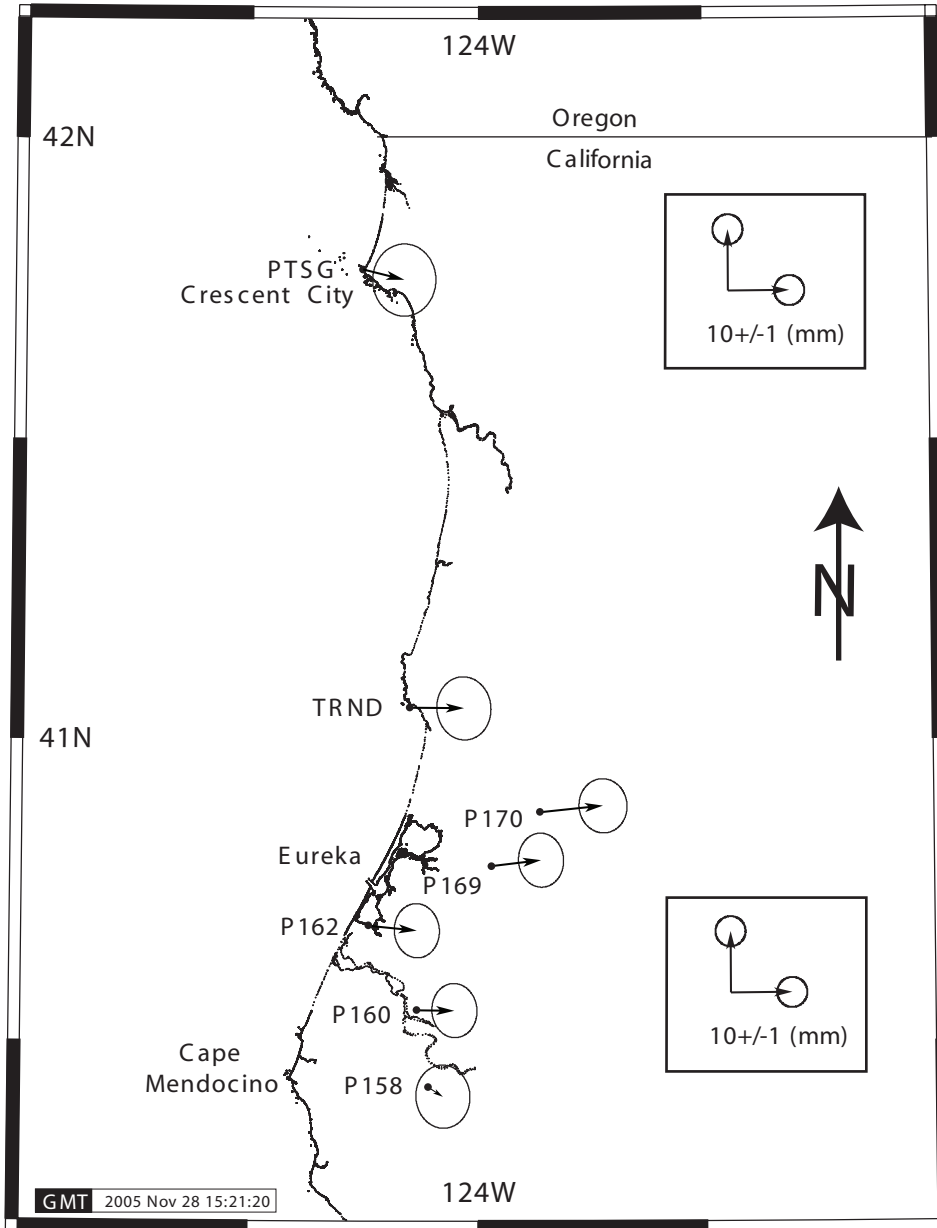
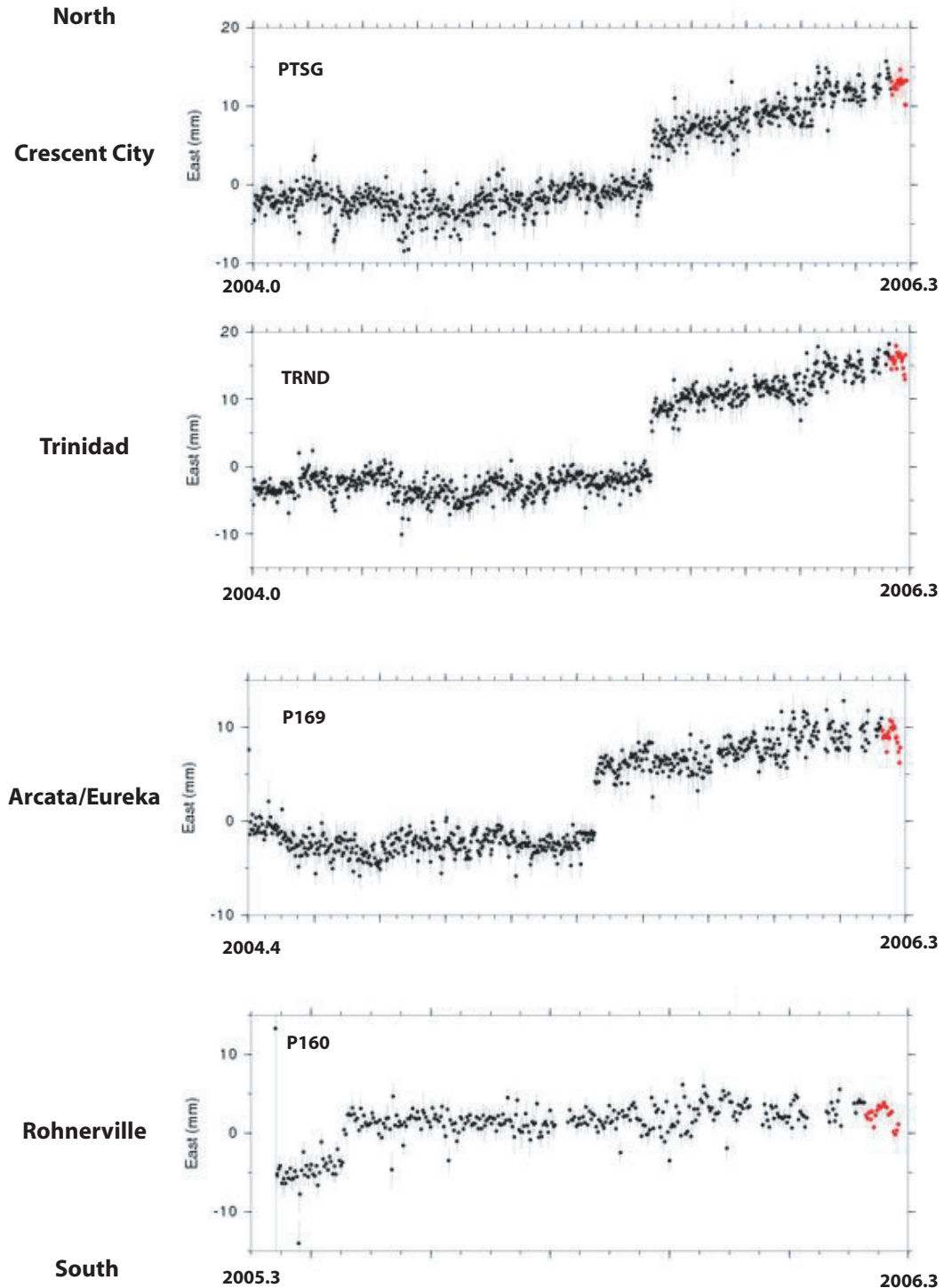


Figure 4. Coseismic displacements from the 15-Jun-2005 M7.2 Gorda plate earthquake located (off the map) 156 km (97 miles) W (280°) from Trinidad, CA and 157 km (98 miles) WSW (251°) from Crescent City, CA. Note the similarity to the deformation pattern of the 1994 event. Continuously operating GPS stations shown here are operated and maintained through the Plate Boundary Observatory component (pbweb.unavco.org) of the National Science Foundation's EarthScope project (www.earthscope.org).

Stations PTSG and TRND were initially built and maintained by (PANGA (www.geodesy.cwu.edu).

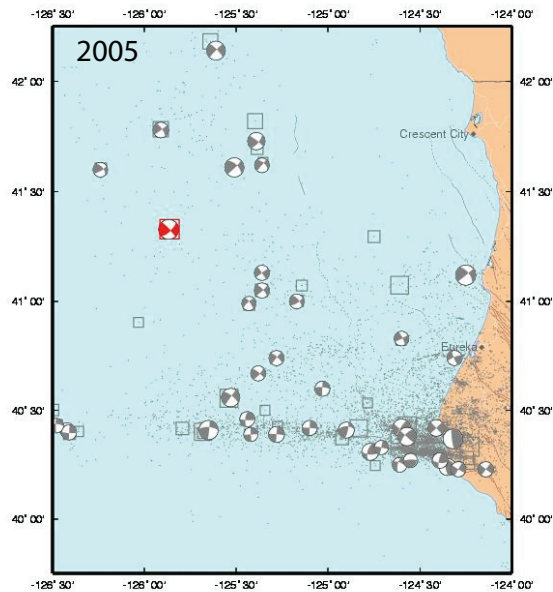
2005 Coseismic Displacements (Eastward)



EarthScope/Plate Boundary Observatory timeseries plots available at:
http://pbweb.unavco.org/stations/?page=station_type&groupid=1#7

Figure 5. Coseismic displacements measured with continuous GPS stations operating in the study area. Timeseries plots show changes in position of longitude (east-west). Abrupt eastward steps of 3 to 8 mm.yr are evident from the 15-Jun-2005 event. Coseismic deformation was detected over the entire coastal region from Cape Mendocino to Crescent City.

Selected Gorda Plate Earthquakes from the Last 25 years



<http://www.cisn.org/special/evt.05.06.15/map.html>

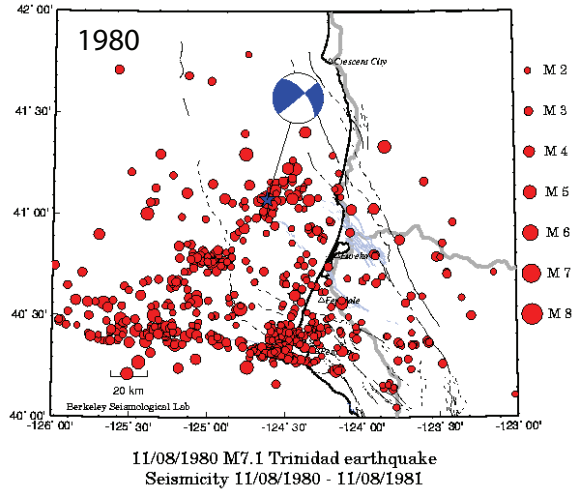
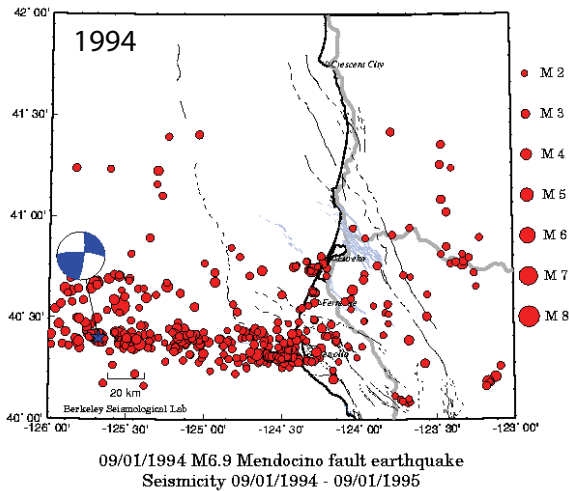
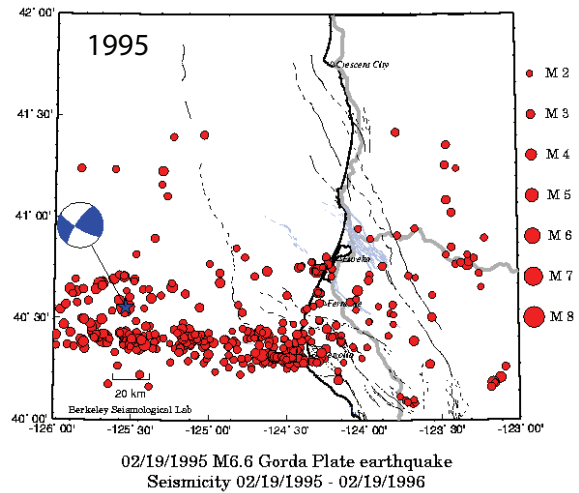


Figure 6. Selected M6 - M7 Gorda plate earthquakes from the last 25 years. Note that the 2005 and 1994 Gorda events produced surface displacements which were detected through repeated GPS surveys (see accompanying figures) . These earthquakes relieve N-S compression within the Gorda plate and exhibit eastward displacements within the on-land portion of the accretionary prism to the S. Cascadia subduction zone (SCSZ). These small displacements likely contribute to convergence between the backstop of the accretionary prism and the Klamath Mts block to the east. There is 2-6 mm/yr of convergence between the Klamath block and upper plate fault slivers of the SCSZ accretionary prism. (Williams et al., 2006).

Images from the CA Integrated Seismic Network (CISN) and the Berkeley Seismological Lab (BSL).

Subsurface seismic reflection in the Van Duzen/Eel River Valley

Mark Verhey

ABSTRACT

The relative development of several soil properties on Eel River terraces, located on the southern limb of the Eel River syncline, records three distinct soil age groups. The highest well-preserved terrace is named the Rohnerville. The relative elevations of similar age terraces/soil age groups records Quaternary growth, and the approximate location of, thrust faults and folds.

The Grizzly Bluff anticline is an asymmetric fold, with a relatively long and planar northern limb, expressed by the northward tilt of the Rohnerville terrace between Hydesville and Fortuna. A 200-foot down to the south displacement of the Rohnerville terrace across Price Creek expresses the southern limb of the GBA. Additionally, an intermediate terrace, the Weymouth terrace is visibly tilted south, which can be viewed from the highway.

Principal reflection packages across industry seismic reflection lines reveal the GBa is a thin-skinned structure. North dipping thrust faults exposed in Price Creek and Weymouth Bluff Road do not extend to seismogenic depth. Rather, they are rooted in a south dipping detachment surface. The vergence direction is northerly, with some of the slip returning to the surface in a series of backthrusts or antithetic faults. The south dipping detachment surface does not reach the surface. I have provided one of the seismic lines for your review.

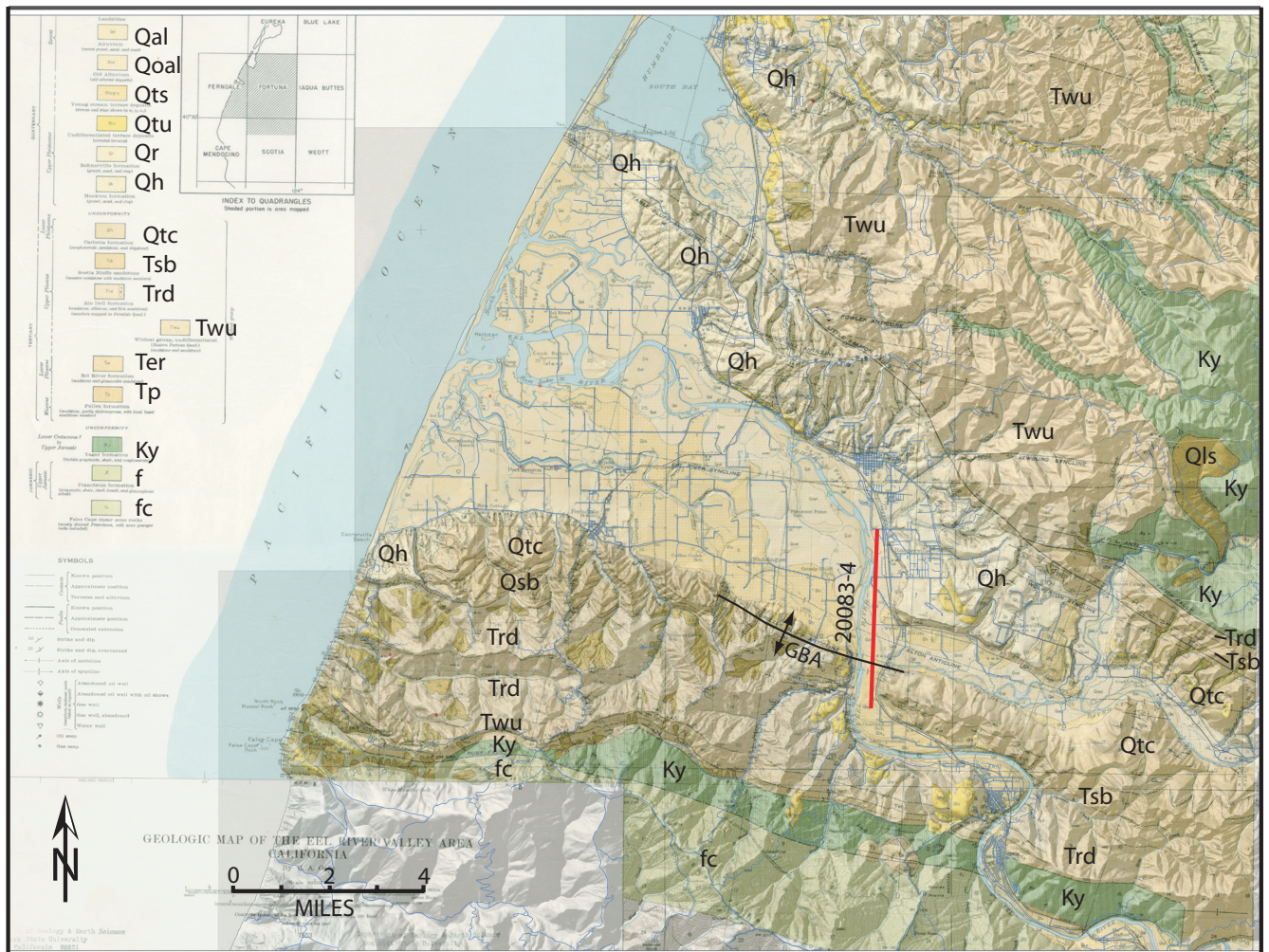


Figure 1. Industry seismic reflection profile 20083-4 shown in red. This profile crosses the Grizzly Bluff Anticline (GBA). Basemap with Neogene stratigraphy (Ogle, 1953) draped over USGS 10 M DEM shaded relief mosaic. Basemap DEM image and geologic map overlay: T. Leroy.

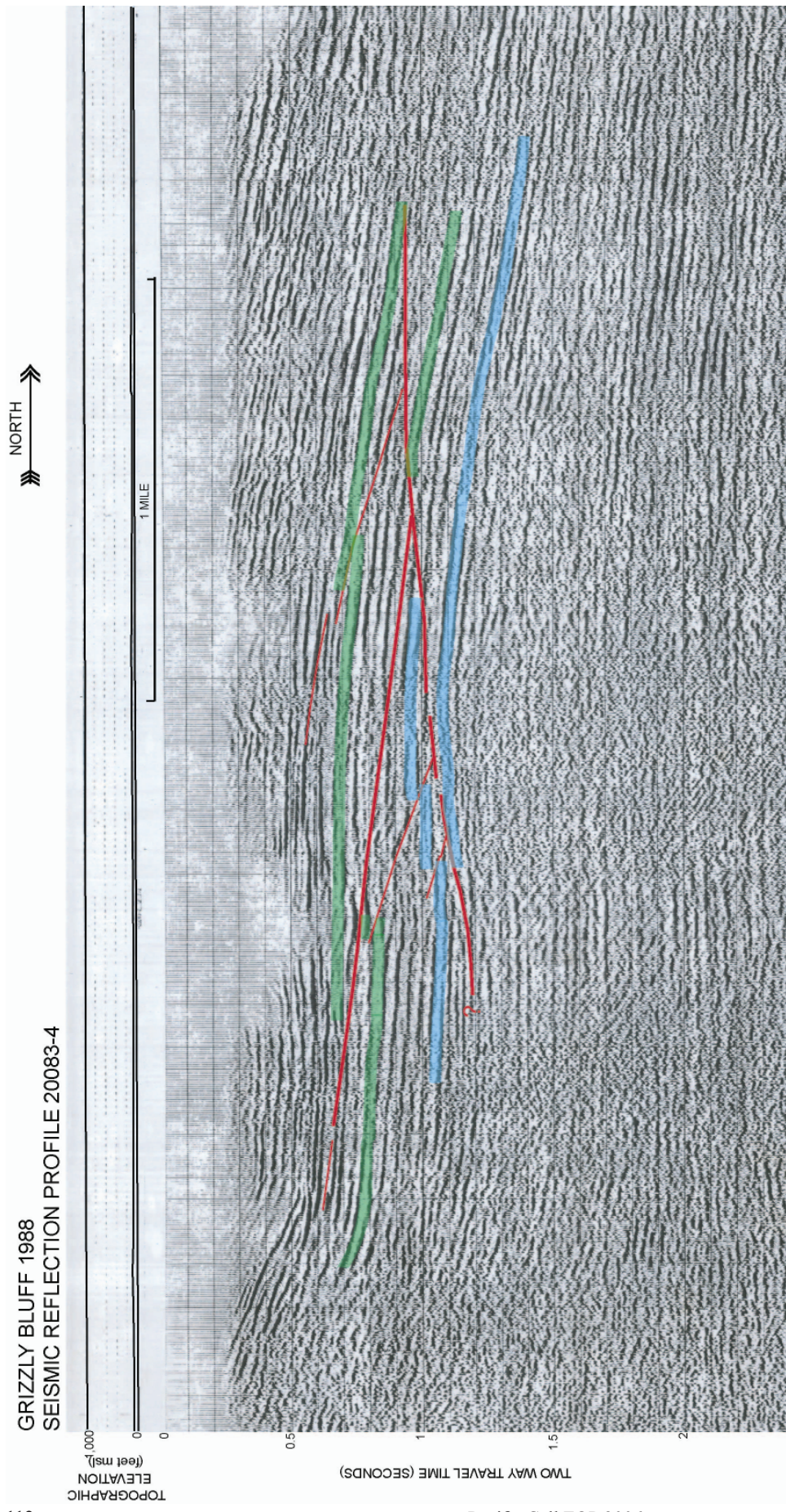


Figure 2. Structural interpretation by Mark Verhey. See Figure 1 for location of seismic line.

Amount and rate of deformation across the Little Salmon fault and Table Bluff anticline within the onland portion of the Southern Cascadia Subduction Zone fold and thrust belt, NW California

Giovanni A. Vadurro, Humboldt State University Geology Department, Arcata, CA

The Little Salmon fault (LSF) and Table Bluff anticline (TBA) with its associated north dipping blind thrust and south dipping back-thrusts accommodate a significant amount of upper plate crustal shortening within the onland portion of the fold and thrust belt (Figure 1). Regionally, these structures deform Yager Terrane basement rocks and younger overlying sediments. The Yager consists of Paleogene marine strata as much as 3000 m thick. Unconformably overlying and in depositional contact with the basement rocks are a sequence of upper Miocene to middle Pleistocene-aged sediments comprising the Wildcat Group (Ogle, 1953). Wildcat Group sediments consist of a marine transgressive-regressive sequence greater than 3500 m thick (Clarke, 1992). In ascending order this sequence is composed of the Pullen, Eel River, Rio Dell, and Scotia Bluffs Formations. Interfingering with and gradationally overlying this sequence is 800-1000 m of non-marine sandstone and conglomerate of the Carlotta Formation, which is the uppermost unit of the Wildcat Group. The entire sequence is truncated at the top by an unconformity, and is overlain by nearshore marine to coastal plain and fluvial deposits of the Pleistocene Hookton Formation (Ogle, 1953).

Where the LSF underlies the Humboldt Hill anticline (HHA), structure contouring of the fault plane based on petroleum industry exploratory borehole data and boreholes installed by Woodward-Clyde Consultants (WWC, 1980) indicates the fault to strike about N 30-45° W and dip a maximum of 30° NE. Further to the southeast, structure contouring of the fault plane reveals a more westerly strike and similar dip. The depth to the LSF below the fold crest of the HHA ranges from 400-500 m below mean sea level. Northeast of Field's Landing, along the backlimb of the HHA, the fault plane is encountered at an elevation of -900 m. Based on the borehole geophysical and mud logs, the fault is generally observed to emplace mudstone of the lower Wildcat Group sediments over sand and gravel of the Carlotta or Hookton Formations (WWC, 1980).

Total vertical displacements along the LSF generally decrease to the northwest. Borehole data from T.T. Co. Little A-1 within the hanging wall of the LSF and the Holmes-Eureka #3 well at Tompkins Hill within the footwall, indicate the vertical separation of the contact between the Yager and the overlying Wildcat sediments across the LSF to be 1650 m. Further to the northwest, along the HHA, the apparent vertical separation of the Yager/Wildcat contact is 1400 m, based on borehole data from the Blackwood Nichols No. 1 and Brauner wells. In the Fields Landing area, apparent vertical separation of the base of the Hookton Formation, which unconformably overlies the Rio Dell Formation at this location, is estimated to be as much as 560 m (WCC, 1980). Reported age estimates for the base of the Hookton Formation are about 400-500 ky.

Timing for the onset of movement on the LSF and TBA blind thrust is not well constrained. Seismic reflection profiles across the tip of the LSF and through the TBA and Eel River syncline (ERS) reveal onlap sequences along the forelimb of the anticline beginning within the lower Scotia Bluffs Formation (Figures 2 and 3). The thickness of the underlying Rio Dell Formation appears uniform across the width of the fold. The onlap sequences are interpreted to represent growth strata resulting from syntectonic deposition following the onset of folding in response to slip on the underlying blind thrust. The maximum age of the growth strata were determined by following the underlying reflectors in the seismic profiles south to where they are projected to daylight in the coastal bluff at Centerville Beach.

Paleomagnetic data obtained from the lower Scotia Bluffs Formation at this location, and continuing up section, indicates normal magnetic polarity (WCC, 1980). This suggests that the onlapping sequences in the lower Scotia Bluffs Formation were deposited following the Brunhes-Matuyama geomagnetic field reversal of 780 ka (Baksi et al, 1992). Therefore, growth of the TBA, a major fault-propagated fold generated by repeated slip on an underlying blind thrust, was initiated post-780 ka. Thus it is assumed that slip on the LSF, and growth of the HHA, also initiated at a similar time.

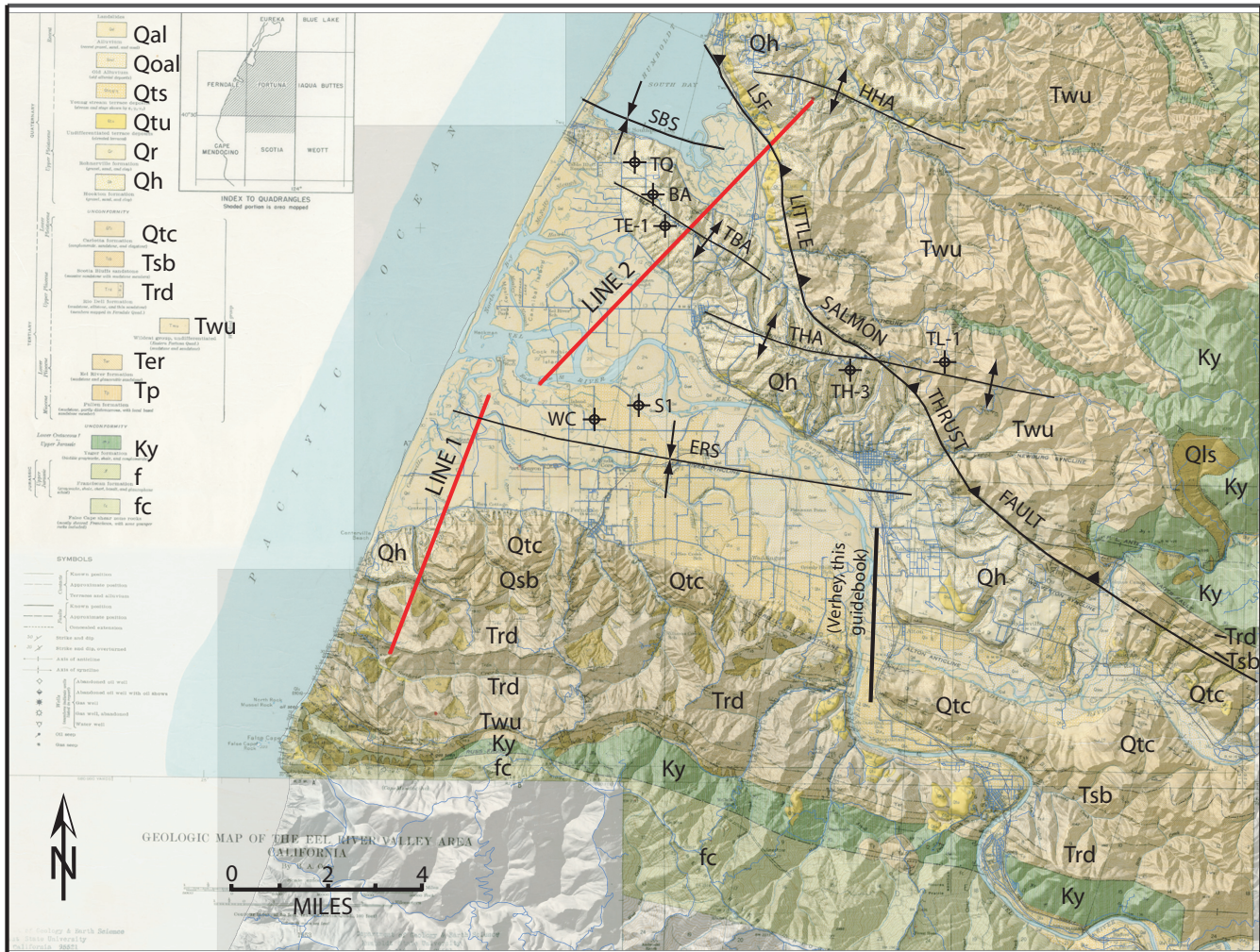


Figure 1. Location map with the “Geology of the Eel Rive Valley Area” by Ogle (1953) draped over USGS 10 M DEM shade relief mosaic. Lines 1 and 2 represent industry seismic reflection profiles across several prominent structures including the Humboldt Hill anticline (HHA), Little Salmon fault (LSF), South Bay syncline (SBS), Table Bluff anticline (TBA), and Eel River syncline (ERS). THA denotes the Tompkins Hill anticline gas field. Industry electric-log data used in interpreting the seismic stratigraphy and fault depths include the following wells: WC = Western Continental I-26, S1 = Sunset 1, TQ = Texaco Quinn, BA = Bishop Anderson, TE-1 = Texaco Eureka-1, TL-1 = Texaco Little A-1, TH3 = Texaco Holmes-Eureka No 3. Note that TL-1 encounters the Yager/Wildcat contact in the hanging wall of the LSF at a depth of -1637 ft (500 m) and intersects the fault plane at a depth of -2037 ft (620 m). The well extends an additional 3000 ft (914 m) into the footwall and does not encounter the Yager/Wildcat contact indicating a minimum vertical separation of this contact of ~3400 ft (1040 m). The Tompkins Hill anticline at this location is actively being under-thrust the LSF. The Yager/Wildcat contact is encountered in TH3, located in the crest of the anticline within the footwall of the LSF, at a depth of -7062 ft (2150 m) suggesting a maximum vertical separation of this contact of ~5400 ft (1650 m). A fault plane dip of <math><30^\circ</math> determined from structure contouring indicates a dip displacement of ~10,300 ft (3.1 km).

Basemap DEM image and geologic map overlay by T. Leroy.

this page left intentionally blank
for
vadurro tabloid fig 2

Figure 2. Time-migrated seismic reflection profiles 1 and 2 across a portion of the Southern Cascadia Subduction Zone fold and thrust belt. The depth to Yager Terrane bedrock within the axis of the Eel River syncline is -9960 ft (3035m) and within the crest of the Table Bluff anticline -5200 ft (1580 m). Seismic reflection data provided by Arco (1991).

this page left intentionally blank
for
vadurro tabloid fig 2

this page left intentionally blank for vadurro tabloid fig 3

Figure 3. Simplified geologic interpretation of seismic reflection lines 1 and 2. Well log projections are shown with depths to contacts in feet below sea level. The plotted depths as shown are determined from two-way travel times. The vertical scale varies with depth and therefore distorts bed thickness and fault dip. Refer to Figure 1 for the name and location of wells. Note the vertical relief on the top of the Yager between the crest of the Table Bluff anticline and axis of the Eel River syncline is upwards of 4800 ft (1460 m). The Table Bluff anticline is interpreted to be a fault-propagated fold generated by a blind thrust that is best explained by the trishear model where “discrete fault zones within the basement diffuse outward and upward in a triangular zone of deformation in the overlying sedimentary section.” The geometry of the folds surface expression suggests that growth of the fold is in part being controlled by a north-verging backthrust as evidenced by the more steeply dipping backlimb compared to the forelimb.

this page left intentionally blank
for
vadurro tabloid fig 3

Long term slip rates for the LSF and TBA blind thrust were calculated from the apparent maximum vertical separation of the Yager/Wildcat contact across the fault zones coupled with the dip of the fault plane, and the timing for the onset of movement. At Tompkins Hill, the vertical separation of 1650 m on the Yager/Wildcat contact yields a net dip-slip displacement of 3300 m and a long term slip rate of 4.2 mm/yr. In the vicinity of the HHA, the net dip-slip displacement on the same contact is 2800 m yielding a slip rate of 3.6 mm/yr.

At Table Bluff the dip of the underlying north dipping blind thrust that is confined to the basement rocks is unknown. A dip of 30°, similar to the dip of the LSF, is therefore assumed. Between the crest of the TBA and axis of the ERS, the maximum vertical separation of the Yager/Wildcat contact, based on its elevation in the Sunset-1 and Texaco Quinn-1 wells, is about 1460 m. The resultant dip displacement is therefore ~2900 m yielding a slip rate of 3.7 mm/yr.

The reported rate of northeast-southwest directed horizontal contraction across the entire fold and thrust belt is reported to be about 20 mm/yr (Clarke and Carver, 1992), which is approximately half of the Gorda-North American plate convergence rate. Of this total, the LSF and TBA with its associated thrusts are accommodating more than 7 mm/yr of upper plate crustal shortening.

This page is intentionally left blank for notes.

Fault Surface Rupture and Fold Hazard Evaluation of the Little Salmon Fault at the College of the Redwoods Eureka Campus, Southern Cascadia Subduction Zone Fold and Thrust Belt, NW California

**Vadurro, G. A., Bickner, F. R., Lindberg, D. N., Manhart, G. L., and Watt, C. J.
LACO ASSOCIATES Consulting Geologists, 21 W. 4th St., Eureka, Ca 95501**

ABSTRACT

College of the Redwoods (CR) is located entirely within the Little Salmon fault zone (LSF) and has been extensively investigated for surface fault rupture and fold hazards (Woodward-Clyde Consultants, 1980; LACO, 1999). Between 1989 and 1999, approximately 1,600 lineal meters of exploratory trench were excavated in order to site new facilities and evaluate potential surface fault rupture and fold hazards to existing buildings.

The LSF bounds CR and consists of two northwest striking, northeast dipping, low-angle thrust faults. The west trace of the LSF daylight along the southwesterly edge of campus infrastructure and dips beneath the site at an angle of 25° while the east trace daylight at the base of the Humboldt Hill anticline (HHA), near the northeasterly edge of campus infrastructure. Movement on the LSF during the late Pleistocene and Holocene at CR is accompanied by surface fault rupture, localized uplift, and growth of a broad asymmetric fold within the upper thrust sheet featuring a steeply dipping forelimb, a broad, very gently dipping, back-tilted crest, and shallowly dipping backlimb. This fault-generated fold geometry is evidenced by the present-day topography at CR.

Structural variability along strike of the LSF where it traverses the campus is pronounced. Trench exposures revealed 25-50 m wide zones of deformation displaying primary north dipping thrusts and secondary south dipping back-thrusts, and progressively folded strata. Low and high-angle faults exhibiting reverse and normal offsets, respectively, were observed.

Late Pleistocene slip rates determined for the west trace of the LSF based on the age and amount of uplift of marine terrace surfaces Q_{tm1} and Q_{tm2}, and the dip of the fault, range from ~5.8 mm/yr to ~7.6 mm/yr. Slip rates obtained from trenching studies conducted south of CR across both the west and east trace of the LSF yield a combined rate of 6-12 mm/yr (Clarke and Carver, 1992). Displaced stratigraphic markers at this site record three slip events totaling 4.6 m to 6.5 m, of which 3.6 m to 4.5 m were measured on the west trace. Greater amounts of slip per event recorded on the west trace compared to that of the east trace suggest the west trace is likely accommodating most of the recent deformation.

SEISMIC SETTING

North of the Mendocino Triple Junction the regional tectonic framework is controlled by the Cascadia Subduction Zone wherein oceanic crust of the Juan de Fuca/Gorda plate is being actively subducted beneath the leading edge of the North American plate. Plate convergence along the Gorda segment of the Cascadia Subduction Zone is occurring at a rate of about 30-40 mm/yr (Heaton & Kanamori, 1984). Upper plate crustal deformation associated with the subduction of the Gorda plate is expressed as a 90 km wide fold and thrust belt that comprises the accretionary complex along the North American plate margin (Carver, 1987).

This accretionary complex is deformed in a prominent system of northwest striking, northeast dipping thrust faults and fault-related folds. The direction of shortening nearly parallels the Gorda and North American plate convergence vector, and accounts for more than half of the overall convergence rate. Convergence is accommodated by growth of the fold and thrust belt (Carver and McCalpin, 1996). Thrust faults form imbricate thrust fans that merge into sole

thrusts that extend into or near the interface between the Gorda and North American plates (Clarke, 1992). Where the fold and thrust belt extends onland between Cape Mendocino and Big Lagoon, cumulative slip of greater than 15 km has been estimated from measured vertical separations of lower Pleistocene sediments across faults (Carver, 1987; Kelsey and Carver, 1988). Coupled with displacements of upper Pleistocene marine terraces, these relations indicate the fold and thrust belt is accommodating at least 20 mm/yr of northeast-southwest horizontal contraction (Clarke and Carver, 1992). The apparent youthfulness of these structures indicates that the subduction zone is strongly coupled and compressive deformation within the North American plate margin is active (Clarke and Carver, 1992).

The Little Salmon fault (LSF) is a major northwest striking, northeast dipping thrust fault located within both the onshore and offshore portions of the Cascadia Subduction Zone fold and thrust belt. Total length of the LSF, including its offshore segment, is 80 km (Petersen et al, 1996). The LSF can be traced from east of Carlotta, northwest to the coast at Humboldt Bay (Ogle, 1953). Offshore, where the LSF was mapped by acoustic-reflection profiling, it is interpreted to terminate along a major structural discordance (Clarke, 1992).

The strike of the onshore portion of the LSF varies from N 60° W near its southeast terminus, to N 35° W in the vicinity of College of the Redwoods (CR). In map view, the surface trace is sinuous and broadly convex to the southwest. Northwest of the Tompkins Hill anticline (THA), the main surface trace splays into two segments comprising the LSF zone. In the vicinity of CR, the west trace of the LSF zone steps over to the north and is projected to daylight along the toe of the low-relief anticline on which CR is situated (Figures 1 and 2). The east trace is postulated to be located at the base of the Humboldt Hill escarpment along the back edge of the campus based on topography and air-photo lineaments.

Where the west trace underlies CR, the fault plane is calculated to dip at about 20-25°. The dip of the fault plane is based on its projected surface trace and the depth to the fault plane of ~55 m encountered in geotechnical borehole GB-1, located near the backlimb fold hinge of the low-relief anticline underlying the campus (Figure 2). A borehole installed by the USGS (2002) at CR near the southwest building corner of the Science Complex near the forelimb fold hinge, encountered the fault at a depth of ~40 m yielding a fault dip of about 25°. At both locations the fault was observed to emplace Pleistocene Hookton Formation over latest Pleistocene (?) bay mud and peat, the implications of which will be discussed later in determining the late Pleistocene slip rates.

Folding generated by movement along the LSF zone consists of northwest trending and northwest plunging asymmetric anticlines with discreet fold hinges. Fold geometries typically display steeply dipping forelimbs with broad, relatively flat-lying crests, and more gently dipping backlimbs. This geometry is observed in both the Humboldt Hill anticline (HHA), generated by the east trace of the LSF, and, at a smaller scale, by the low-relief anticline underlying CR, interpreted to be a growth fold generated by repeated slip on the west trace.

GEOLOGIC SETTING AT COLLEGE OF THE REDWOODS

CR is located entirely within the LSF zone and has been extensively investigated for surface fault rupture and fold hazards (Woodward-Clyde Consultants, 1980; LACO 1989, 1993, 1998, and 1999). In the late 1980's and 1990's, approximately 1,600 lineal meters of exploratory trench was excavated and mapped in order to site new facilities and evaluate potential surface fault rupture and fold hazards to existing buildings (Figures 1 and 2). The LSF zone bounds CR and consists of imbricate, northwest striking, northeast dipping, low-angle thrust faults. The west splay of the LSF zone is projected to daylight along the southwesterly edge of campus infrastructure and underlies the site at a relatively shallow depth, while the east splay of the LSF is interpreted to daylight at the base of the HHA, near the northeasterly edge of campus infrastructure. It is unclear how much slip is actively being distributed between each trace. Trench investigations to the southeast of the CR indicate the west trace to be accommodating the majority of recent displacement (Clarke and Carver, 1992).

At CR, surface fault rupture, localized uplift, and generation of a growth fold within the upper thrust sheet accompany movement on the LSF. The growth fold exhibits a steeply dipping forelimb, a broad, gently dipping

back-tilted crest, and shallow dipping backlimb. The youthfulness of this fault-generated fold geometry is evidenced by the present-day surface topography observed at CR.

Underlying CR is Pleistocene Hookton Formation (Ogle, 1953), late Pleistocene marine terrace deposits, and latest Pleistocene to Holocene landslide and alluvial deposits (Figure 1). The Hookton Formation is composed of sands, silts, clays and gravel, deposited in a near-shore, shallow-water marine to coastal plain and fluvial environment. The Hookton Formation also underlies the hill slopes to the north and east of the campus along the southern limb of the HHA. Late Pleistocene landslide deposits mantle much of the in-place Hookton Formation on the hill slopes behind the campus.

Late Pleistocene marine terrace and latest Pleistocene-Holocene Hookton-derived fluvial-deltaic and alluvial deposits cap much of the Hookton Formation on the developed portions of the campus. The marine terrace and fluvial-deltaic deposits consist of sands, sandy silty clays, and gravelly sand. These materials are generally of medium to high density (100 pcf - 140 pcf). Lateral and vertical textural variation is pronounced due to the complex depositional and tectonic history of the site. The lower parking lot alluvium consists of fluvial-deltaic deposits containing silty to clayey sand interfingering with predominantly fine grained sediments of bay margin origin and of significantly lower density (80 pcf - 86 pcf).

Structural variability along strike of the LSF at CR is pronounced. High and low-angle secondary faults, exhibiting both reverse and normal offsets, were mapped. Trench exposures revealed secondary faulting and folding of the hanging wall distributed over more than 100 meters from the primary fault (Figure 3). Four primary sources of permanent ground deformation were identified including primary fault rupture, secondary fault rupture, fold-limb rotation, and hinge-line fold deformation, similar to that observed during the 1999 Chi-Chi (Taiwan) earthquake (Lettis *et al*, 2003).

Typical secondary fault geometries consist of subparallel reverse faults that dip to the southwest and record up to several meters of cumulative slip. The more steeply dipping secondary back-thrusts are generally located in the forelimb of the growth fold being generated by the primary thrust (see Trench 1-8-C and 9-2-C). The steeply dipping nature of these secondary thrusts may be the result of progressive folding or conversely the high-angle back-thrusts are accommodating additional shortening of the growth fold. The degree of folding also increases significantly toward the primary thrust tip.

Graben structures composed of densely spaced, opposing high-angle normal faults which record upwards of 2 m of cumulative vertical separation were mapped across fold structures in Trench 2-7-C, located due east of the administration building, and 8-1-B located in the far northwest portion of CR. Apparent vertical dip-slip displacements of stratigraphic markers along the normal faults decrease down-dip to zero, at which point the fault traces terminate. The graben structures, and associated extension within the hanging wall, are discontinuous along strike and in cross-section are limited to 30-40 m wide zones in both trenches. Hanging wall extension is interpreted to be the result of the upper thrust sheet migrating over a shallowing thrust ramp in the up-dip direction.

EXPLORATORY TRENCH LOGS

The following selected trench logs are presented in sequential order from northwest to southeast. Presentation of the trench logs in Figure 3 follows in the same order.

Trench 8-1-B and 8-2-C Humboldt Botanical Garden Foundation

Located at the far northwest edge of the campus, the HBGF site is underlain by north dipping, late Pleistocene marine terrace deposits, latest Pleistocene landslide deposits (Q₁s), late Holocene (Qa₄) alluvial deposits and recent fluvial deposits (Qa₅). Landslide deposits consist of reworked Quaternary Hookton Formation derived from the nearby south

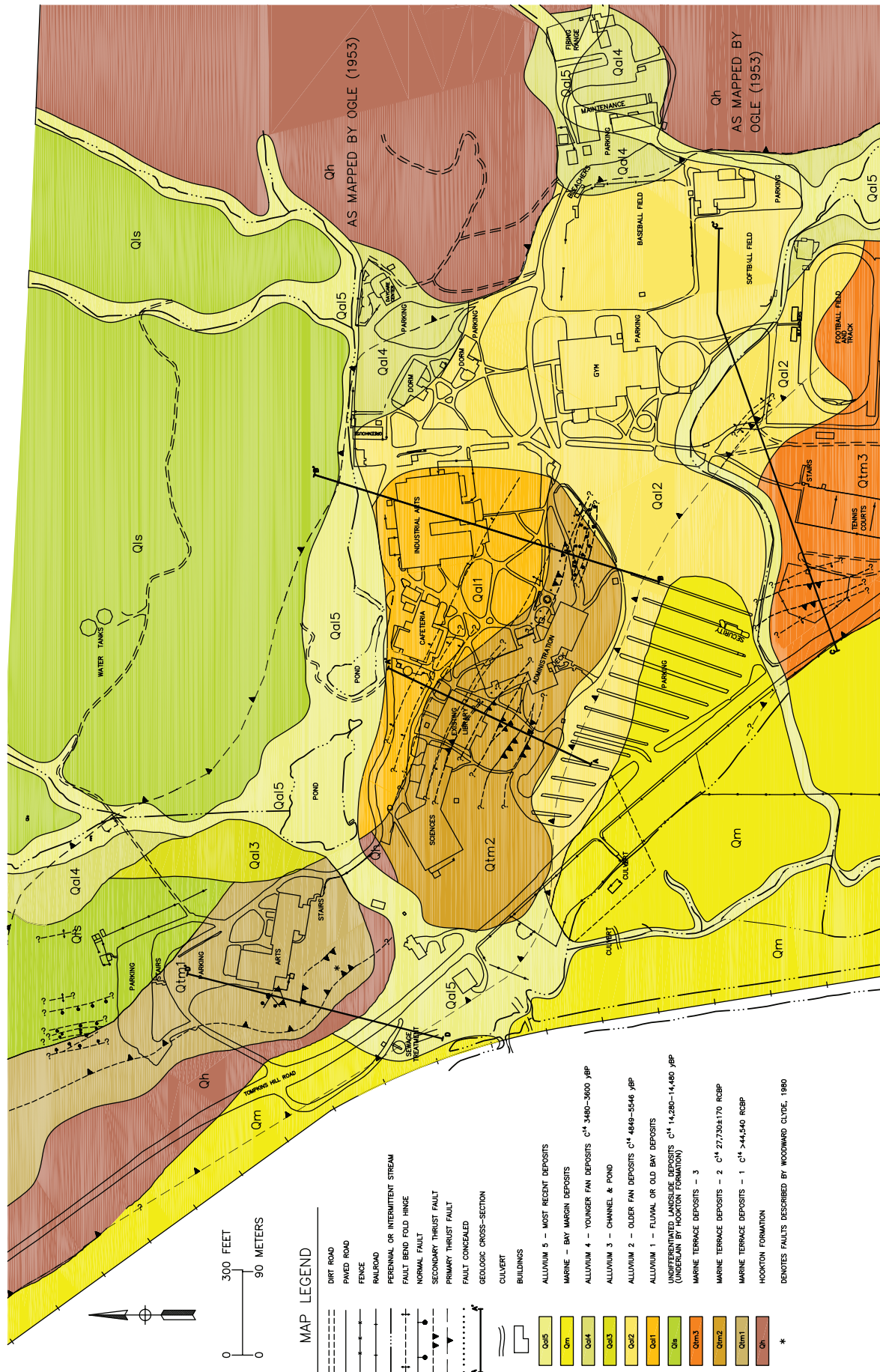


Figure 1. Geologic map.

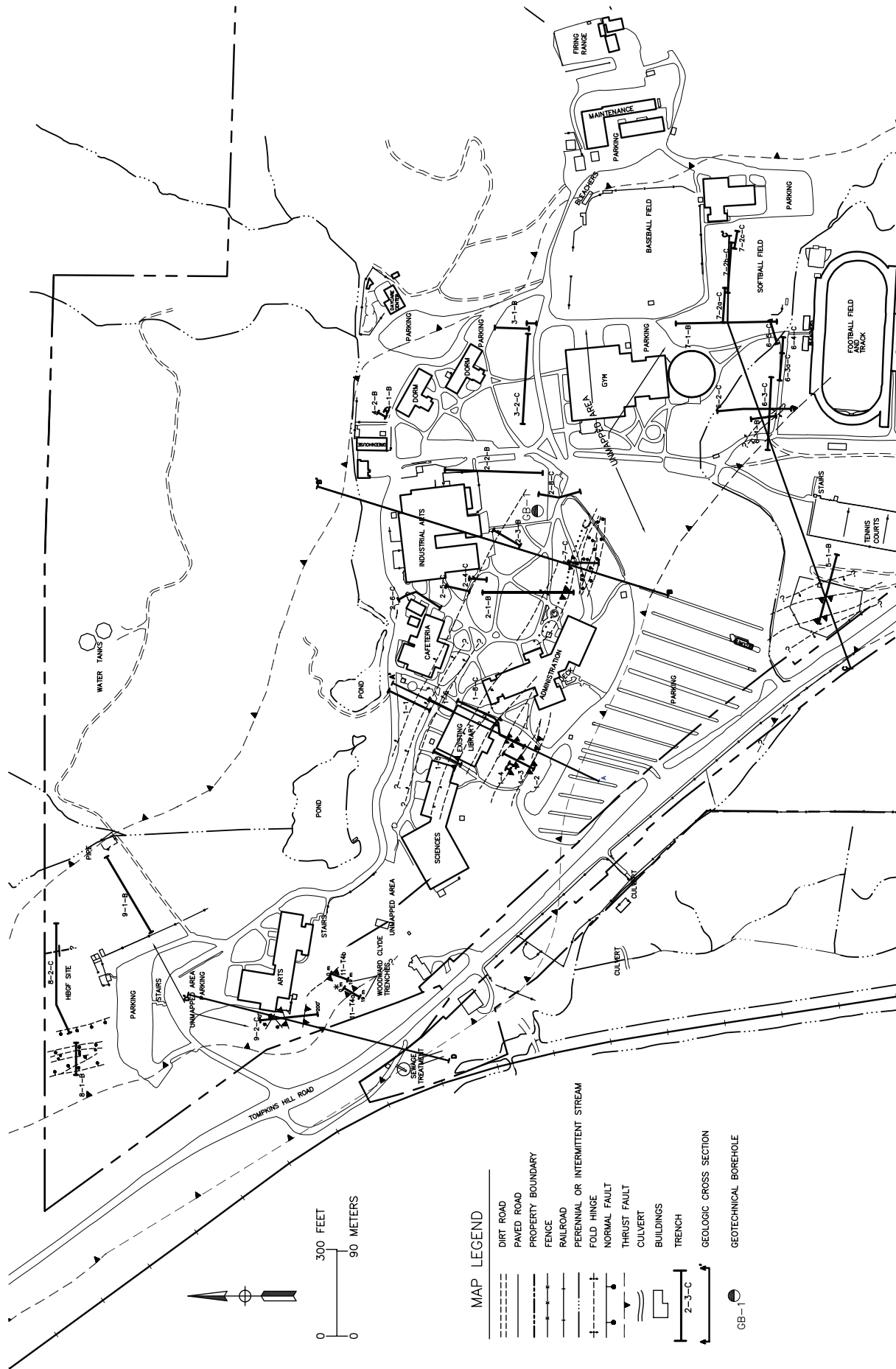


Figure 2. Trench location map.

aspect slope. Five individual landslide deposits were recognized consisting of massively bedded silty clay with sand and clayey silts that contain abundant, matrix-supported, angular clay rip-up clasts, and minor amounts of detrital charcoal. The rip-up clasts were typically enveloped by thin to moderately thick weathering rinds and decreased in abundance and size away from the toe of the slope. Individual landslide deposits generally coarsened upward suggesting they were deposited as a viscous mass. Their lower depositional contacts were observed to be abrupt and wavy. The overlying alluvial deposits, by contrast, contain well sorted sands and rounded pebbles with an abrupt and irregular lower erosional contact.

The late Holocene alluvial deposits and younger fluvial deposits are derived from the drainage swale originating nearly parallel to, and along the toe of the slope of the east trace escarpment. The former through-flowing drainage (it is currently damned creating the existing western pond) is incised through the hangingwall of the LSF at CR and crosses the growth fold at nearly a right angle suggesting it is antecedent to the fold.

Calibrated (2-sigma) radiocarbon dates for detrital charcoal samples collected from an upper landslide deposit in Trench 9-1-B (interpreted to be correlative with similar deposits in Trench 8-2-C) indicate an age of 14,280-14,480 yBP. Calibrated (2-sigma) radiocarbon dates for the overlying alluvial deposits (Qal₄) that occupy the margins of the swale axis at the eastern end of Trench 9-1-B (Figure 2) indicate an age of 3480-3600 yBP.

Deformation observed in the northwest portion of CR is characterized by a broad fold where the crest and backlimb fold hinge contain a 40 m wide zone of high angle normal faults. Surface fault rupture was observed at the west end of the trench 8-2-C. A single high-angle normal fault striking N 12° W and dipping 67° SW records 0.7 m (2.2-2.4 ft) of apparent dip-slip displacement on the lower Qls units and about 0.3 m (1 ft) of displacement on the base of the A-horizon. In Trench 8-1-B, numerous opposing high angle normal faults were mapped that also generally strike north-northwest and dip in excess of 60°. Many of the normal faults, however, terminate upwards and do not appear to displace the base of the A-horizon. Approximately 2 m of cumulative dip-slip displacement is recorded across the zone of normal faulting.

Combined, the two trenches reveal a broad growth fold containing a graben composed of high-angle opposing normal faults within the crest and backlimb hinge line of the fold. The fold records progressive deformation as indicated by the onlapping and subsequent tilting of the overlying sediments along the backlimb. Onlapping and folding of the latest Pleistocene landslide deposits and late Holocene alluvial deposits attest to the youthfulness of the structure. Presence of a broad topographic swale with an axial trend of northwest to southeast along the fold backlimb at the base of the Humboldt Hill escarpment suggests this structure is active.

Approximately 75 feet west of the end of Trench 8-1-B is a subtle break in topography interpreted to be a scarp associated with the primary fault trace deforming the Qtm₁ surface. The scarp is on trend with the projected fault trace mapped by Woodward-Clyde (1980) in trenches located 1000 feet to the south-southeast.

Trench 9-2-C Art's Complex

Stratigraphically, five depositional sequences were observed in Trench 9-2-C. The three middle sequences were delineated by organic-rich material present at the top of each sequence. The oldest sequence (Unit 1) consists of well-stratified sand and silty sand with thin clay stringers. The sands are thinly bedded and grade downward into fine sandy silts. Near the southern end of the trench relatively large (5-10 cm diameter) woody debris were present. This sequence is interpreted as a wash over deposit formed in a backshore environment. Conformably overlying Unit 1 are massive clayey silts with thin silt laminae (Unit 2). A thin, discontinuous layer of organic-rich clay caps this sequence. Unit 3 consists of massive silty clay capped with a 25-30 cm thick, discontinuous layer of organic-rich clay. Unit 4 consists predominantly of clay with interbedded clayey silt. Unit 4 is capped by thin, continuous organic-rich clay. Overlying the entire length of the sequence is a well sorted sand layer, up to 20 cm thick, interpreted to be of storm wave or tsunami origin. Unit 5 consists of clay to clayey silt containing abundant fine roots.

this page left intentionally black
for
vadurro LACO tabloid figure 3

Figure 3. Logs of trench exposures at CR across a portion of the LSF zone. Trenches are spatially oriented from the top to the bottom of the page in the northwest to southeast direction along the trace of the fault. Trench numbers correspond to Figure 2 locations. The fault reaches the ground surface in large part as a growth fold above the fault tip. Progressive deformation is recorded by onlapping of younger sediments, particularly along the backlimb of the fold in 8-2-C. Note that all trench exposures, with the exception of 6-3-C, are limited to the up-thrown hangingwall block.

this page left intentionally black
for
vadurro LACO tabloid figure 3

this page left intentionally black
for
vadurro LACO tabloid figure 4

Figure 4. Simplified geologic cross sections across the width of the LSF zone. Cross sections are spatially oriented from the top to the bottom of the page in the northwest to southwest direction along the trace of the fault. Location of cross sections is shown in Figure 1.

this page left intentionally black
for
vadurro loco tabloid figure 4

Units two through five are predominantly fine-grained and are interpreted to be of eolian origin with intercalated pond deposits deposited in a back dune environment. Radiocarbon dating of charcoal samples collected within the organic-rich horizons yielded conventional C-14 ages of >46,140 years BP in Unit 1; >44,540 years BP in Unit 3; and >45,660 years BP in Unit 4. Combined, this shoreline complex (Q_{tm1}) is thought to represent the marine isotope Stage 3 sea level high stand.

Significant amounts of faulting and folding were encountered in trench 9-2-C. Both reverse and normal faults were observed, dipping both to the north and south. Folding was observed across the entirety of the trench in the form of two distinct anticlines separated by a north dipping thrust. In the north half of the trench, a maximum of 16 degrees of apparent folding was measured along the north dipping backlimb. Less apparent folding was observed in the younger overlying units. Several high-angle, north dipping, discontinuous normal faults with a maximum apparent offset of 0.3 m were observed deforming the backlimb and fold crest. Folding was generated in response to movement along the 35° north-dipping thrust fault, which strikes N 70° E and projects to the ground surface near the midway point of the trench. The amount of dip-slip displacement recorded by this fault, based on repeated section, totals about 10 m. The greater degree of folding recorded in the older units indicates that fold growth was occurring during deposition in response to ongoing slip on the underlying thrust. The lack of a pre-campus construction surface expression associated with this fault, interpreted on the basis of the thin eolian cap lower contact, indicates this fault to likely be inactive.

Further towards the south of the trench, a maximum of 12 degrees of apparent folding was measured along the north-dipping backlimb of the second anticline. In the forelimb, bedding steepens to an apparent dip of 34 degrees. In the crest of the fold a graben generated by two antithetic normal faults displays about 0.3 m of apparent dip-slip displacement. The steeply dipping forelimb is faulted by numerous high-angle south dipping back-thrusts with apparent net dip-slip displacement of 2.1 m.

Folding and high angle reverse faulting observed near the south end of the trench are interpreted to have been generated by movement on an underlying northwest-striking, northeast-dipping primary thrust fault that projects to the ground surface beyond the south end of Trench 9-2-C. This thrust fault is interpreted to be the continuation of the fault mapped by Woodward-Clyde (1980) in a trench exposure located 150 feet to the southeast of this site. The measured orientation of the primary thrust in the Woodward-Clyde trench had a strike of N 30° W and dip of 24°N with apparent net dip-slip displacement of 2 m (6.5 ft) which the authors attributed to possibly a single event. They suggest that the “extreme” folding observed in their trench (similar to that observed in Trench 9-2-C) indicates the apparent 2 m displacement is a relatively small portion of the total deformation across the fault zone.

Trench 1-8-C Former Library

Four depositional sequences were differentiated in Trench 1-8-C. Unit 1, which is mapped in the southern (downslope) half of the trench, only, consists of massively bedded, well-sorted sand with thin discontinuous lenses of clayey silt capped by well rounded, coarse pebbly sands. Unit 2 disconformably overlies Unit 1 and consists of interbedded silty clays and sandy silts that grade vertically and laterally (in the seaward direction) into gravelly sands. The fine-grained sediments consisting primarily of silts and clays are heavily gleyed and are capped by thin organic-rich horizons containing plant roots in growth position. The plant roots are interpreted to have occupied the fringes of a tidal marsh or pond within a back dune hollow. Diatom analysis revealed a few fragments of freshwater species only. The lack of diatoms, however, may be due to acidic soil conditions following subaerial exposure and the establishment of vegetation resulting in oxidation of diatom fragments. Radiocarbon dating of a composite sample taken from the uppermost organic-rich horizon (in the north half of the trench) yielded a conventional C-14 age of 27,730 ± 170 years BP. Units 1 and 2 likely represent a marine transgressive-regressive, sequence with Unit 1 being slightly more deformed as evidenced by the steeper dips exhibited along both limbs of the fold.

Unit 3 consists of stratified gravelly sands, massively bedded, well-sorted sands with very thin discontinuous silt stringers, and interbedded discontinuous lenses of pebbly sand. All clast sizes are well-rounded and generally

range from fine pebbles to coarse cobbles. Unit 3 onlaps the growth fold and is also folded. Unit 3 is interpreted to be of nearshore marine origin deposited during a subsequent marine transgression. Combined, all three units comprise the upper portion of Q_{tm2}.

Unit 4 is limited to the far northeastern end of the trench and consists of clayey silts with minor amounts of pebbles, truncated by poorly sorted pebbly sands. The base of Unit 4 is highly irregular and in abrupt erosional contact with the underlying marine terrace deposits of Unit 3. Unit 4 (Q_{al1}) is interpreted to be of fluvial origin, deposited following uplift and emergence of the nearshore marine deposits comprising the terrace surface.

Folding and faulting were observed throughout trench 1-8-C. Folding is evidenced by the present day topography and was observed in the trench in the form of a relatively tight, asymmetric anticline in the southern half of the trench and a monoclinical warp in the northern half. The anticline exposed in the southern half of the trench is truncated near the downslope terminus of the trench by several densely spaced high-angle back-thrusts with a cumulative displacement of about 2 m. The back-thrusts in turn have refolded a portion of the forelimb in the opposite sense. In general, the dip of both the forelimb and backlimb of the fold decreases up-section through the entire fold width implying syntectonic deposition. Growth of this fold is likely occurring in response to repeated movement along the underlying primary thrust fault that is projected to daylight at the toe of the slope along the edge of the main parking lot.

Folding of the monoclinical warp is constrained in relative age to Unit 2 (Unit 1 is below the bottom of trench at this location) and predates deposition of Unit 3 as indicated by the onlapping nature of Unit 3. Generation of the monoclinical warp is likely due to a northwest striking and northeast dipping thrust fault observed in Trench 1-5-A located on the west side of the library that is on-strike with the monocline. The fore-thrust observed to the northwest is interpreted to be blind at the location of Trench 1-8-C on the east side of the library.

Within the anticline located further downslope, numerous southwest dipping secondary back-thrusts were observed that were generally traceable upward to the contact with the historic fill, where they were truncated by grading. Interestingly, several of the back-thrusts were untraceable downward through the clay-rich horizons comprising the lower portion of Unit 2. Measurable offset, however, was observed in the overlying sands and gravels. It should also be noted that the amount of offset recorded by individual back-thrusts did not increase down-dip suggesting that they are single event faults. Furthermore, a majority of the secondary back-thrusts post-date much of the progressive fold deformation recorded. In total, a minimum of 4 m of apparent cumulative dip-slip displacement was measured along the secondary back-thrusts across the width of the fold.

Trench 2-7-C Administration Building

Two depositional sequences, capped by eolian derived silts, were differentiated at this location. Unit 1 consists of marine terrace deposits (Q_{tm2}) containing well stratified, poorly sorted sands and gravels with thinly bedded silt and fine sand laminae. The gravels are generally rounded to well-rounded consisting primarily of chert and similarly-resistant lithologies derived from reworked Hookton Formation. Cobble and pebble lags were typically observed that graded upward into coarse sand.

Unit 2, which is limited to the north end of the trench, consists of fluvial deposits composed of pebbly fine sand with clay, and sandy silt with scattered pebbles (Q_{al1}). Unit 2 unconformably overlies Unit 1, as indicated by the erosional nature of the contact. Unit 2 truncates a south dipping secondary back-thrust that records about 0.2 m of dip-slip displacement on the underlying terrace sands. Both the marine terrace and fluvial deposits are capped by eolian silt that comprises the A-horizon interpreted to have been deposited during the marine isotope Stage 2 sea level low stand (late Pleistocene to early Holocene).

Deformation observed in the trench is characterized by a monoclinical warp where the forelimb is deformed by numerous opposing high angle normal faults beginning at the fold hinge. Combined, the opposing normal faults form a graben with a cumulative displacement of ~2 m. In general, the normal faults strike nearly east-west to west-

northwest and dip in excess of 60° to the north and south. The normal faults record diminishing amounts of slip in the down-dip direction. Several of the faults terminate in the lower sections of the trench and within the uppermost terrace deposits. The base of the A-horizon is mostly unfaulted with the exception of the area near the north end of the graben. At this location, the base of the A-horizon is clearly faulted with the generation of a fissure infilled with the overlying organic-rich silt. The underlying terrace sands are offset by as much 0.4 m along an east-west striking fault dipping 75° S. The normal faults and graben structure project towards the Administration Building to the west. Where they terminate is unknown. No extensional deformation, however, was observed in trench exposures located to the west of the Administration Building.

Trench 6-3-C Child Development Center

Two depositional sequences were differentiated at this location. Unit 1 consists of marine terrace deposits (Qtm₃) composed of well stratified, poorly sorted gravel with sand, that grades upward into moderately to well stratified, poorly sorted sands with fine pebble lenses. The marine terrace sands and gravels are overlain by and possibly interfinger with fluvial deltaic deposits and distal fan facies of Unit 2 interpreted to be associated with Qal₂. An age of 4849-5546 yBP is assigned for the overlying alluvial deposits based on calibrated (2-sigma) radiocarbon dates derived from detrital charcoal collected from a buried soil in Qal₂ in trench exposures located 250 feet to the northeast.

Evidence of liquefaction, consisting of flame structures and “ball and pillar” structures, was observed at several locations in both this trench and the cross trenches. Deformation observed in the trench is characterized by a broad, gentle fold that is faulted by a primary fore-thrust that strikes N 48° W and dips 32° NE. The fault consists of two closely spaced, subparallel traces that record up to ~4 m (13 ft) of dip-slip displacement on the basal contact of Unit 2 with the underlying terrace sands. The fault becomes untraceable as it approaches the ground surface. However, the base of the A-horizon is vertically separated 1.1 m across the projected surface trace of the fault. Resolving the vertical separation into slip on the fault plane based on a 32° dip yields a displacement of ~1.7 m on the base of the A-horizon. Therefore, the 4 m of cumulative dip-slip displacement recorded by the fault is the product of at least two faulting events that have occurred since deposition of Qal₂, or in approximately the past 5000 years.

SLIP RATES AND RECURRENCE INTERVALS

Published Holocene slip rates for the LSF construed from nearby sites are in general agreement with those presented here. Carver and Burke (1989) reported a slip rate of 5.6 mm/yr for the west trace from initial trenching studies to the southeast of CR near Salmon Creek. Slip rates obtained from subsequent trenching studies at Little Salmon Creek across both the west and east traces of the LSF yield a combined rate of 6-12 mm/yr (Clarke and Carver, 1992). Displaced stratigraphic markers at this site record three slip events totaling 4.6 to 6.5 m each, of which 3.6 to 4.5 m per event was measured on the west trace. Greater amounts of slip per event recorded on the west trace compared to that of the east trace suggest the west trace is probably accommodating most of the recent deformation.

Late Pleistocene slip rates were calculated for the west trace of the LSF zone at CR, with age-control provided by the conventional radiocarbon dates obtained from Trench 9-2-C and 1-8-C, in conjunction with reconstructed sea level curves (Waelbroeck *et al*, 2002), and geologic cross sections (Figure 4). Stratigraphic horizons from which the radiocarbon ages were obtained are interpreted to represent approximate paleo-sea level elevations. The total vertical uplift of Qtm₁ (C¹⁴ >45,000 RCBP) and Qtm₂ (C¹⁴ 27,730 RCBP) is 110 m and 90 m, respectively, yielding average uplift rates of 2.4 mm/yr and 3.2 mm/y. Based on a fault plane dip of 25°, the resultant dip-slip displacements are about 260 m and 210 m, respectively, which yield average slip rates of ~5.8 mm/yr and ~7.6 mm/yr.

A second approach in determining late Pleistocene slip rates at CR is to estimate the age and amount of slip recorded by the under-thrusted bay mud and peat encountered within the footwall in borehole GB-1. The age of Qtm₂ (C¹⁴ 27,730 RCBP) constrains the maximum age for the under-thrusted bay mud and peat since these

deposits (and the creation of the South Bay) post-date the nearshore and beach environment associated with Qtm₂. The slip required to emplace the bay mud/peat to a depth of 55 m is ~140 m. Assuming a maximum age of 27,730 RCBP yields a minimum slip rate of 5 mm/yr.

Simplified geologic cross sections were constructed from overlapping trench logs, geotechnical borehole logs, and geologic mapping (Figure 4) based on methods outlined in Suppe (1983), Mitra and Namson (1989), Mount *et al* (1990), and Medwedeff and Suppe (1997), to assess the amount of slip in relation to the folding observed. Assuming the elevation of Qtm₂ within the footwall of the west trace of the LSF remains at its initial depositional elevation of -75 m, the actual dip-slip displacement of Qtm₂ is therefore on the order of 165 m, based on the projected elevation of the fold forelimb into the fault plane. This is in comparison to the 210 m predicted by using the calculated uplift rate. This suggests that formation of the growth fold at the surface is accommodating a portion of the slip at depth. Therefore, the measurable slip typically observed on primary thrust faults in trench exposures may likely underestimate the actual seismic hazard.

Recurrence intervals of individual slip events on the LSF are constrained by three dated faulting events recorded during the past 1700 years at the Little Salmon Creek trench site and yield a return period of 300 to 560 years (Clarke and Carver, 1992). At CR, use of an estimated 3-5 m of slip per event coupled with an averaged slip rate of 6-7 mm/yr determined from the uplift rate for Qtm₁ and Qtm₂ yields a return period of about 400 to 870 years.

Displacements and deformation along the LSF are believed to be synchronous with movement on the Cascadia Subduction Zone (Clarke and Carver, 1992; Carver, pers. comm. 1997). Paleoseismological evidence from around the Humboldt Bay region records deformation resulting from sudden slip on several major thrust faults, as well as sudden uplift and subsidence of sections of the coast (Carver and Burke, 1987; Carver and Burke, 1989; Vick, 1988; Shivellev *et al*, 1991; Valentine, 1992; Leroy, 1999). The magnitude and distribution of deformation is similar to that observed from historic subduction zone earthquakes worldwide and suggests that subduction-related earthquakes have occurred in this region during the recent past and should be anticipated to recur in the future.

REFERENCES CITED

- Carver, G. A., 1987, Late Cenozoic Tectonics of the Eel River Basin Region, Coastal Northern California; Proceedings of a Symposium on Tectonics, Sedimentation and Evaluation of the Eel River and Associated Coastal Basins of Northern California, San Joaquin Geological Society, Miscellaneous Publications No. 37, pp. 61-71.
- Carver, G. A. and Burke, R. M., 1987, Investigations of Late Pleistocene and Holocene Thrust Faulting in Coastal California North of Cape Mendocino, in Jacobson M. L. and Rodriguez, T. R., National Earthquake Hazards Reduction Program, Summaries of Technical Reports, Vol. XXIII: U. S. Geological Survey Open File Report 87-63, p. 165-168.
- Carver, G. A. and Burke, R. M., 1989, Trenching Investigations of Northwestern California Faults, Humboldt Bay Region, unpublished final report, National Earthquake Hazards Reduction Program; U. S. Geological Survey Grant 14-08-0001-G1082, 53p.
- Carver, G. A. and McCalpin, J. P., 1996, Paleoseismology of Compressional Tectonic Environments, in *Paleoseismology*, ed. J. P. McCalpin, p. 183-270. Academic Press, Inc.
- Clarke, S. H., 1992, Geology of the Eel River Basin and Adjacent Region: Implications for Late Cenozoic Tectonics of the Southern Cascadia Subduction Zone and Mendocino Triple Junction: American Association of Petroleum Geologists Bulletin, V. 76, pp. 199-221.
- Clarke, S. H. and Carver, G. A., 1992, Late Holocene Tectonics and Paleoseismicity, Southern Cascadia Subduction Zone: Science, v. 255, p.188-192.
- Gibbs, J. F., Tinsley, J.C., and Boore, D. M., 2002, Borehole Velocity Measurements at Five Sites That Recorded the Cape Mendocino, California Earthquake of 25 April, 1992: U.S. Geological Survey Open-File Report OF 02-203.
- Heaton, T. H. and Kanamori, H., 1984, Seismic Potential Associated with Subduction in the Northwestern United States: Bulletin of the Seismological Society of America, v. 95, pp. 933-942.
- Kelsey, H. M. and Carver, G. A., 1988, Late Neogene and Quaternary Tectonics Associated with Northward Growth of the San Andreas Transform Fault, Northern California: Journal of Geophysical Research, V. 93, No. B5, pp. 4397-4819.
- LACO ASSOCIATES, 1989, Geologic Investigation, Fault Rupture Hazard Evaluation, Little Salmon Fault Zone, College of the Redwoods Library Addition: Unpublished consulting report for the College of the Redwoods.

- LACO ASSOCIATES, 1993, Geologic/Seismic Hazards-Risk Zoning Phase B Report, Little Salmon Fault Zone, College of the Redwoods Library Addition: Unpublished consulting report for the College of the Redwoods.
- LACO ASSOCIATES, 1998, Geotechnical Report; Liquefaction Evaluation and Seismic Response Spectrum, College of the Redwoods Library Addition: Unpublished consulting report for the College of the Redwoods.
- LACO ASSOCIATES, 1999, Final Report of Seismic Study Phase 3 at College of the Redwoods Eureka Campus: Unpublished consulting report for the College of the Redwoods.
- LACO ASSOCIATES, 1999, Site Evaluation for the Child Development Center, Fault Rupture Hazard Phase C Investigation. Unpublished consulting report for the College of the Redwoods.
- Leroy, T. H., 1999, Holocene Sand Dune Stratigraphy and Paleoseismicity of the North and South Spits of Humboldt Bay, Northern California, M.S. Thesis, Humboldt State University, 44p.
- Lettis, W. R., Kelson, K.I., and Carver, G.A., 2003, Styles of Surface Deformation Associated with Thrust Earthquakes, Examples from the 1999 Chi-Chi (Taiwan) Earthquake: 2003 GSA Seattle Annual Meeting.
- Medwedeff, D. A. and Suppe, J., 1997, Multibend Fault-Bend Folding, *Journal of Structural Geology*, Vol. 19, Nos. 3-4, p. 279-292.
- Mitra, S. and Namson, J., 1989, Equal-Area Balancing, *American Journal of Science*, Vol. 289, p. 563-599.
- Mount, V. S., Suppe, J. and Hook, S. C., 1990, A Forward Modeling Strategy for Balancing Cross Sections, *The American Association of Petroleum Geologists Bulletin*, V. 74, No. 5, p. 521-531.
- Ogle, B. A., 1953, Geology of the Eel River Valley Area, Humboldt County, California: California Division of Mines Bulletin 164, 128p.
- Petersen, M. D., Bryant, W. A., Cramer, C. H., Cao, T., Reichle, M. S., Frankel, A. D., Lienkaemper, J. J. and McCrory, P. A., 1996, Probabilistic Seismic Hazard Assessment for the State of California. DMG OFR 96-08, 59 p.
- Shivelle, C.D., Carver, G.A. and Valentine, D.W., 1991, Foraminiferid Stratigraphy as Evidence for Great Earthquakes on the Cascadia Subduction Zone in Northern California, *Geological Society of America*, Suppe, J., 1983, Geometry and Kinematics of Fault-Bend Folding, *American Journal of Science*, Vol. 283, p. 684-721.
- Valentine, D. W., 1992, Late Holocene Stratigraphy as Evidence For Late Holocene Paleoseismicity of the Southern Cascadia Subduction Zone, Humboldt Bay, California: Humboldt State University, p. 1-99.
- Vick, G. S., 1988, Late Holocene Paleoseismicity and Relative Vertical Crustal Movements, Mad River Slough, Humboldt Bay, California: Humboldt State University.
- Waelbroeck, C., Labeyrie, L., Michel, E., Duplessy, J.C., McManus, J.F., Lambeck, K., Balbon, E., and Labracherie, M., 2002, Sea-level and deep water temperature changes derived from benthic foraminifera isotopic records: *Quaternary Science Reviews*, V. 21, 295-305.
- Woodward-Clyde Consultants, 1980, Evaluation of the potential for resolving the geologic and seismic issues at the Humboldt Bay Power Plant Unit number 3: Unpublished consulting report for Pacific Gas and Electric Company, Summary Report.

Upper-Plate Earthquakes on the Western Little Salmon Fault and Contemporaneous Subsidence of Southern Humboldt Bay Over the Past 3,600 Years

Robert C. Witter¹ and Jason R. Patton

ABSTRACT

Along the southeastern side of Humboldt Bay the Little Salmon fault zone extends over 100 km in the fold-and-thrust belt of the southern Cascadia subduction zone and includes three northwest-striking imbricate thrust faults that deform intertidal deposits and terraces along the bay margin. The bay deposits contain tidal marsh soils abruptly overlain by intertidal mud interpreted to record sudden regional subsidence caused by plate-boundary earthquakes. Although prior investigations of the western Little Salmon fault documented three earthquakes in the past 2,000 years, the question of whether the Little Salmon fault ruptures independently from the southern Cascadia subduction zone or is coseismically triggered by megathrust events remains unresolved. At the Swiss Hall site we investigated the western trace of the fault where a 1- to 1.5-m-high moletrack scarp projects into southern Humboldt Bay and deforms late Holocene intertidal sediment. Estuarine strata that lap onto the scarp include three buried peaty soils containing tidal marsh diatoms that are progressively folded with increasing depth and form a west-facing monocline. An angular unconformity separates the sequence of soils from a thick (0.7 m) overlying deposit of tidal flat mud. Normal faults in the hanging wall offset the entire sedimentary package in the scarp. We identify three slip events on the western Little Salmon fault during the past 1,700 years. Growth of the scarp occurs through folding and secondary faulting above a shallow, low angle, blind thrust fault. The most recent earthquake disrupted the scarp along subvertical surface fissures that taper downward into normal faults in the hanging wall. The data provide a slip rate estimate of 2.9- to 6.9-mm/yr with 1.3- to 4.1-m of slip per event. Radiocarbon ages that bracket evidence of scarp deformation broadly limit the timing of three earthquakes to between 0 to 460, 540 to 1,230 and 1,530 to 1,710 cal yr BP. The uncertainty spanned by the age ranges precludes a one-for-one correlation between earthquakes on the western Little Salmon fault and regional Cascadia megathrust events. Comparisons between slip-histories for the western Little Salmon fault and regional chronologies of megathrust earthquakes leave open the possibility that some upper-plate events were coseismically triggered by plate-interface seismicity. This inference is strengthened for event 3 where deformed strata in the fault scarp coincide with evidence for extensive subsidence of southern Humboldt Bay that extended into the hanging wall of the Little Salmon fault. In contrast, fault slip during event 2 lacks correlation with evidence of coseismic subsidence in the hanging wall and allows the possibility that the Little Salmon fault ruptured independently during the interseismic period between great Cascadia subduction zone earthquakes.

¹Oregon Department of Geology and Mineral Industries Coastal Field Office, 313 SW 2nd St., Suite D, Newport, OR 97365 Phone: (541) 574-7969; Fax: (541) 265-5241 E-mail: rob.witter@dogami.state.or.us

INTRODUCTION

Along the Pacific coast of northern California, evidence for drowned forests, subsided estuaries and uplifted marine terraces attest to repeated episodes of earthquake-induced vertical deformation above the southern Cascadia subduction zone (Carver et al., 1994; Clarke and Carver, 1992; Patton, 2004; Vick, 1988). Geologic and geophysical investigations of the Cascadia subduction zone indicate that the plate interface is currently locked, and has the seismic potential to generate earthquakes of magnitude 8 or greater that release elastic strain as vertical land-level change (Atwater and Hemphill-Haley, 1997; Fluck et al., 1997; Heaton and Kanamori, 1984; Nelson et al., 1995; Satake et al., 1996). However, uncertainty exists regarding the contribution of upper-plate faults and folds to permanent vertical deformation in the overriding plate (Kelsey et al., 1996; McNeil et al., 1998) and whether this strain is a product of independent upper-plate earthquakes that were not triggered by plate-interface seismicity.

Stratigraphic investigations in Humboldt Bay (Figure 1) delineate extensive burial of prehistoric tidal marshes attributed to coseismic subsidence during great megathrust earthquakes (Carver and Carver, 1996; Carver et al., 1996; Vick, 1988; Valentine, 1992), but the component of vertical deformation accommodated by triggered slip of the Little Salmon fault, if any, and other upper-plate faults in the Humboldt Bay region has not been quantified. The 25 April 1992 Cape Mendocino earthquake (M_s 7.1) represents the largest historical reverse-slip earthquake recorded as seismological evidence for subduction on the Gorda-North America plate interface (Oppenheimer et

al., 1993). The main shock resulted in up to 1.4 m of coastal uplift between Cape Mendocino and Punta Gorda (Carver et al., 1994). However, slip on shallow thrust faults in the North America plate triggered by the Cape Mendocino earthquake was not observed (Oppenheimer et al., 1993). If shallow thrust faults, like the Little Salmon fault, rupture independently of earthquakes on the southern Cascadia subduction zone, then these faults represent additional sources of seismic hazards in northwestern California.

This abridged report summarizes the findings of a NEHRP-funded paleoseismic study of the western trace of the Little Salmon fault and the southern part of Humboldt Bay, located about 16 km south of Eureka, California (Witter et al., 2002). Two principal objectives drove the investigation: (1) to assess whether stratigraphic and structural relations in fault-normal trenches and shallow borings could provide evidence to distinguish upper-plate earthquakes from regional megathrust events, and (2) to evaluate whether stratigraphic evidence of buried tidal marsh soils in Hookton Slough reflected subsidence limited to the footwall of the Little Salmon fault or regional subsidence produced by slip on the Cascadia subduction zone. We present evidence for 3 earthquakes that deform tidal-marsh deposits along a 1- to 1.5-m high fault-line fold-generated scarp at the Swiss Hall site. Our results also include stratigraphic evidence for extensive coseismic subsidence in southern Humboldt Bay (South Bay) at Hookton Slough, described by Jay Patton as a component of his Masters thesis from Humboldt State University and summarized in a related section of this guidebook. Finally, through comparison of the earthquake history of the Little Salmon fault with regional chronologies of Cascadia earthquakes and tsunamis, we conclude that at least two of the last three Little Salmon fault earthquakes may have been triggered by slip on the megathrust. Less evidence links upper-plate faulting about 1,000 years ago to a regional plate-interface earthquake recorded in southwestern Washington and Mad River Slough.

APPROACH

Our approach involved paleoseismic trenching across the western trace of the Little Salmon fault at the Swiss Hall site (Figure 2) coupled with investigation of widespread buried tidal marsh soils preserved along the margin of South Bay at Hookton Slough (described by Patton in this guidebook). This design allowed us to evaluate stratigraphic and structural relations between buried tidal marsh soils overlain by sand sheets inferred to record regional plate-interface earthquakes and tsunamis, and deformed estuarine strata that betray evidence for upper-plate earthquakes on the western Little Salmon fault. The location of the Swiss Hall site along the southeastern margin of Humboldt Bay presented an opportunity to examine buried marsh soils that lap onto and are folded within a 1-to-1.5-m-high moletrack scarp (Figure 3) where the western trace of the Little Salmon fault projects across the Salmon Creek delta and into South Bay (Figure 2).

To evaluate whether upper-plate earthquakes may have operated independently of great earthquakes on the Cascadia megathrust we mapped out the lateral continuity of buried tidal marsh soils preserved near Hookton Slough and deformed in the scarp of the western Little Salmon fault at near Swiss Hall. We also compared slip histories for the western fault trace to regional records of great Cascadia earthquakes. Several assumptions guided our interpretations of the relationships between buried marsh soils and slip events recorded in the scarp: First (1), widespread buried marsh soils present in the South Bay that are deformed by the fault scarp probably reflect regional subsidence produced by megathrust events because independent rupture of an upper-plate fault would not produce subsidence in the hanging wall; second (2), 'event horizons' identified in the scarp that are not stratigraphically linked to a buried marsh soil are best explained as an independent upper-plate earthquake not coseismically triggered by megathrust seismicity; and finally (3), radiocarbon age estimates for upper-plate earthquakes that do not correlate with regional earthquake records, given large uncertainties in radiocarbon dating, would be considered evidence for upper-plate events that occurred independently and were not triggered by slip on the megathrust.

RESULTS

The Swiss Hall site hosts upper intertidal bay-margin sediments deformed by late Holocene slip on the western trace of the Little Salmon fault (Figure 2). Bay-margin deposits west of the scarp include buried tidal marsh soils abruptly overlain by intertidal mud interpreted to record coseismic subsidence caused by earthquakes on the

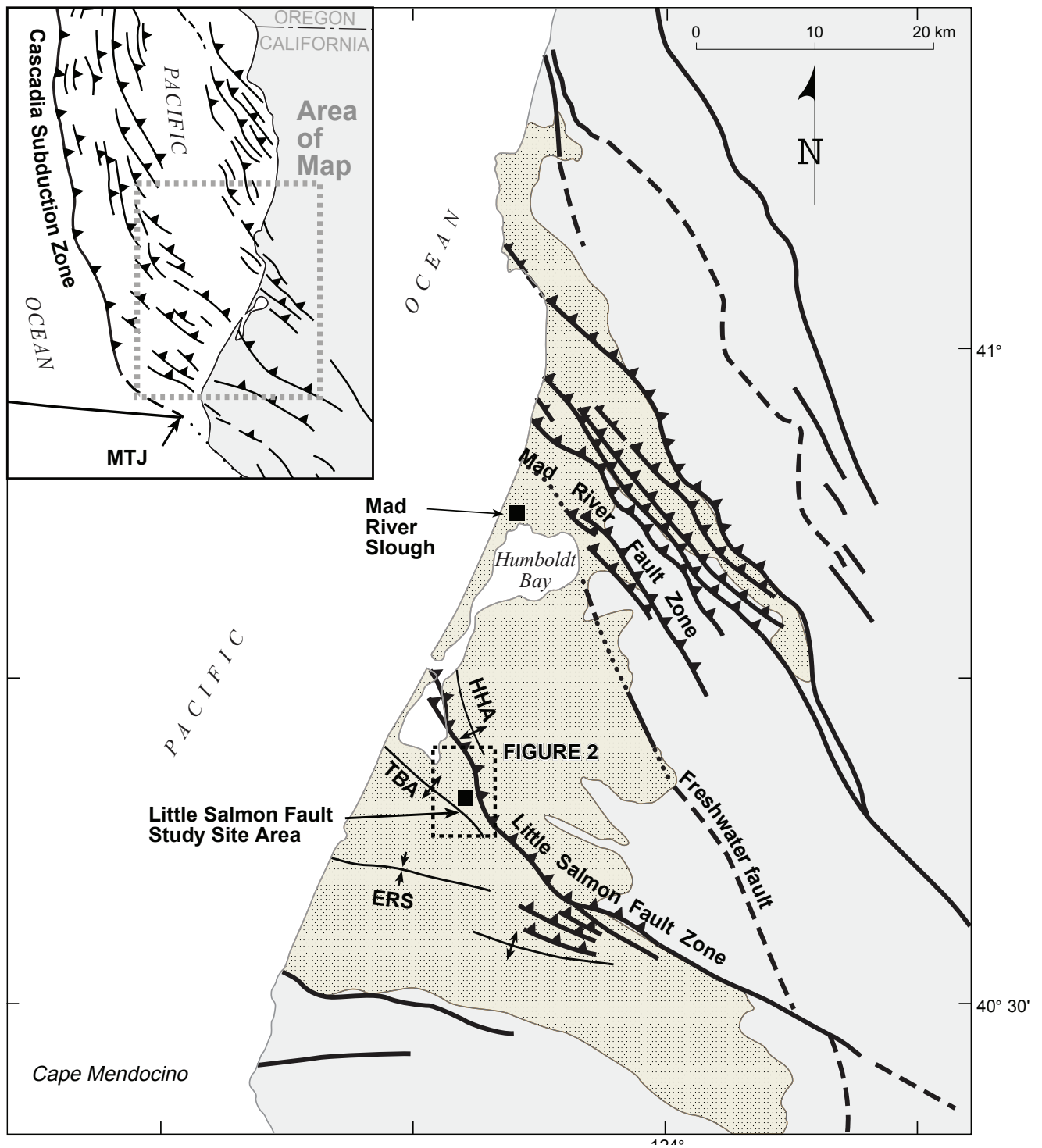


Figure 1. Tectonic map of coastal California north of Cape Mendocino in context of the plate tectonic setting (inset). Crustal contraction in the lower Eel River valley occurs along the Little Salmon Fault zone and along imbricate thrust faults of the Mad River fault zone north of Humboldt Bay. The Little Salmon fault study area is shown in Figure 2. Stippled area delineates late Neogene and Quaternary sediments of the Falor Formation, Wildcat Group and late Pleistocene fluvial and marine terraces (after Kelsey and Carver, 1988). HHA, Humboldt Hill anticline; TBA, Table Bluff anticline; ERS, Eel River syncline; MTJ, Mendocino Triple Junction.

southern Cascadia subduction zone (Clarke and Carver, 1992; Valentine, 1992; Vick, 1988). At the Swiss Hall site a moletrack scarp strikes northwestward across the Salmon Creek delta on the southeastern margin of Humboldt Bay. Presently, the top of the scarp at the Swiss Hall site is about 1-m above mean higher high water (National Ocean Service, 1982).

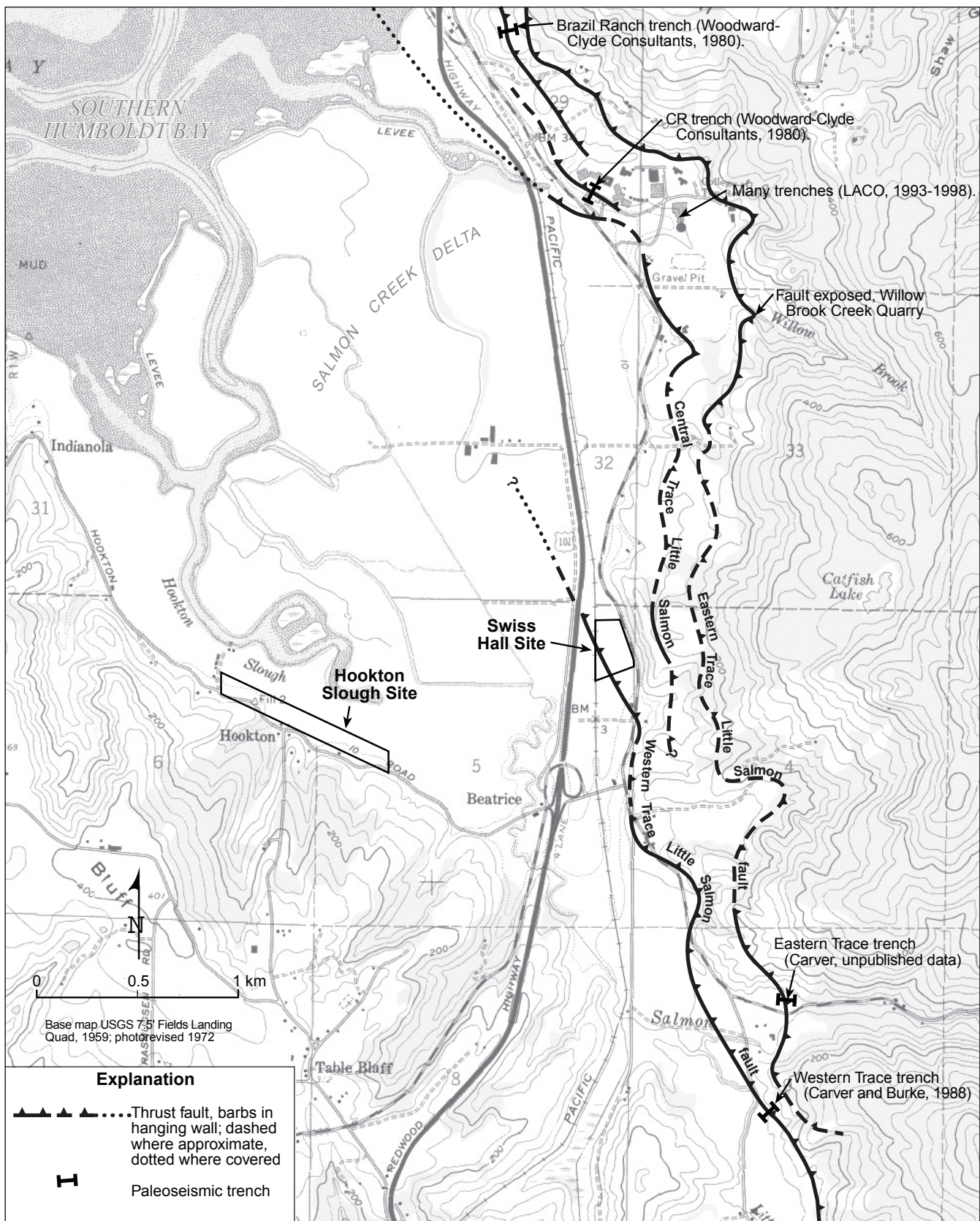


Figure 2. Fault map showing three imbricate east-dipping thrust faults of the Little Salmon fault zone including the eastern trace, the central trace and the western trace. The Swiss Hall and Hookton Slough study sites are indicated on map.

Landforms at the Swiss Hall site, sculpted by fluvial, bay margin and tectonic processes, provide clues to the origin of the western Little Salmon fault scarp. A former channel of Salmon Creek likely cut a 34-m high cliff about 150-m east of the site exposing late Pleistocene fluvial and shallow marine deposits of the Hookton Formation (McLaughlin et al., 2000; Ogle, 1953). West of the cliff, the western trace of the fault deforms late Holocene bay margin deposits creating a left-stepping *en echelon* pressure ridge and secondary scarp in the hanging wall (Figure 4). The primary pressure ridge, also referred to as a moletrack scarp by Carver and McCalpin (1996), rises 1-to-1.5-m above the adjacent pasture directly to the west and spans a width of approximately 50 m. The secondary scarp lies to the east of the primary scarp and measures 0.4-m high by 25-to-50-m wide (Figure 4). The secondary scarp likely relates to a paleo-tidal channel that drained the area to the east of the moletrack scarp. A second uplifted paleo-tidal channel, beheaded by the primary scarp, lies in the northwestern corner of the study area (Figure 3).

Bay Margin Stratigraphy West of the Scarp

The oldest deposits encountered in shallow borings west of the scarp consist of greenish grey, massive silty sand that fines upward to mud (units 9 and 11; Figure 5). These sediments, probably deposited within the subtidal to intertidal zones of the estuary, grade upward into a laterally continuous, black organic-rich mud (unit 6) that laps eastward onto the scarp. In the westernmost cores away from the scarp the upper 2- to 8.5-cm of unit 6 consists of black fibrous peaty soil and contains foraminifera and diatoms that indicate soil development in a high marsh environment (core LS 6; Figure 5).

Two distinct lithologic units abruptly overlie unit 6 and occur at different positions relative to the scarp. In sediment cores to the west, grey mud (unit 5) containing rhizomes and discontinuous peaty laminae abruptly buries unit 6 (Figure 5). However, where it occupies a paleo-tidal channel in the western flank of the scarp, laminated organic-rich mud (unit 4), consisting of interbedded peaty and muddy laminae (ranging from several millimeters to a few centimeters thick), sharply overlies unit 6 (Figure 5). Unit 4 overlies both units 5 and 6 in the paleo-tidal channel and contains laminae that dip away from the scarp at an angle lower than the sharp mud-over-peat contact between units 5 and 6. Unit 4 grades upward into laminated mud (unit 3) that, in turn, grades upward into massive oxidized mud (unit 2). Unit 2 extends eastward, laps onto and buries unit 6 higher up on the western flank of the fault scarp. In addition, the lower contact of unit 2 marks an angular unconformity.

A dark brown granular soil (unit 1), correlative with the surface soil in the crest of the scarp, overlies unit 2. Near the fault scarp the contact between the soil and the underlying mud is sharp. To the west, away from the scarp, this lower soil contact is gradual and the composition of unit 1 shifts to predominantly peat and interbedded mud. The granular soil structure and oxidation of unit 1 reflects sub-aerial exposure and drying of the marsh deposits that mantle the scarp. Historically deposited mud and peat (unit 0) bury unit 1 based on modern radiocarbon ages (Witter et al., 2002).

Stratigraphic Relations in Trench Exposures

The oldest deposits exposed in the trenches include grey mud and sandy mud (units 9 and 11; Figures 5 and 6) that vary from 10- to 80-cm thick, and extend westward as encountered in borings west of the scarp. Above unit 9, peaty tidal marsh soils (units 4, 6, 8 and 10) buried by mud lenses occupy an asymmetrically-folded paleo-tidal channel near the base of the primary scarp. The buried marsh soils converge to the east and west of the paleo-tidal channel forming a single composite buried soil that drapes the entire scarp (Figures 5 and 6). The buried soils exhibit sharp upper contacts and contain diatom assemblages indicative of high marsh environments (Witter et al., 2002).

Lenticular mud deposits bury the marsh soils preserved in the paleo channel and pinch out to the east and west on the margins of the paleo-tidal channel (units 3, 5, and 7; Figure 5). These mud lenses exhibit gradual to sharp lower contacts with the buried soils and contain diatoms from low marsh and mudflat environments (Witter et al., 2002). Peaty laminae in unit 3, 2-to-5-mm thick, dip gently to the southwest subparallel to underlying buried

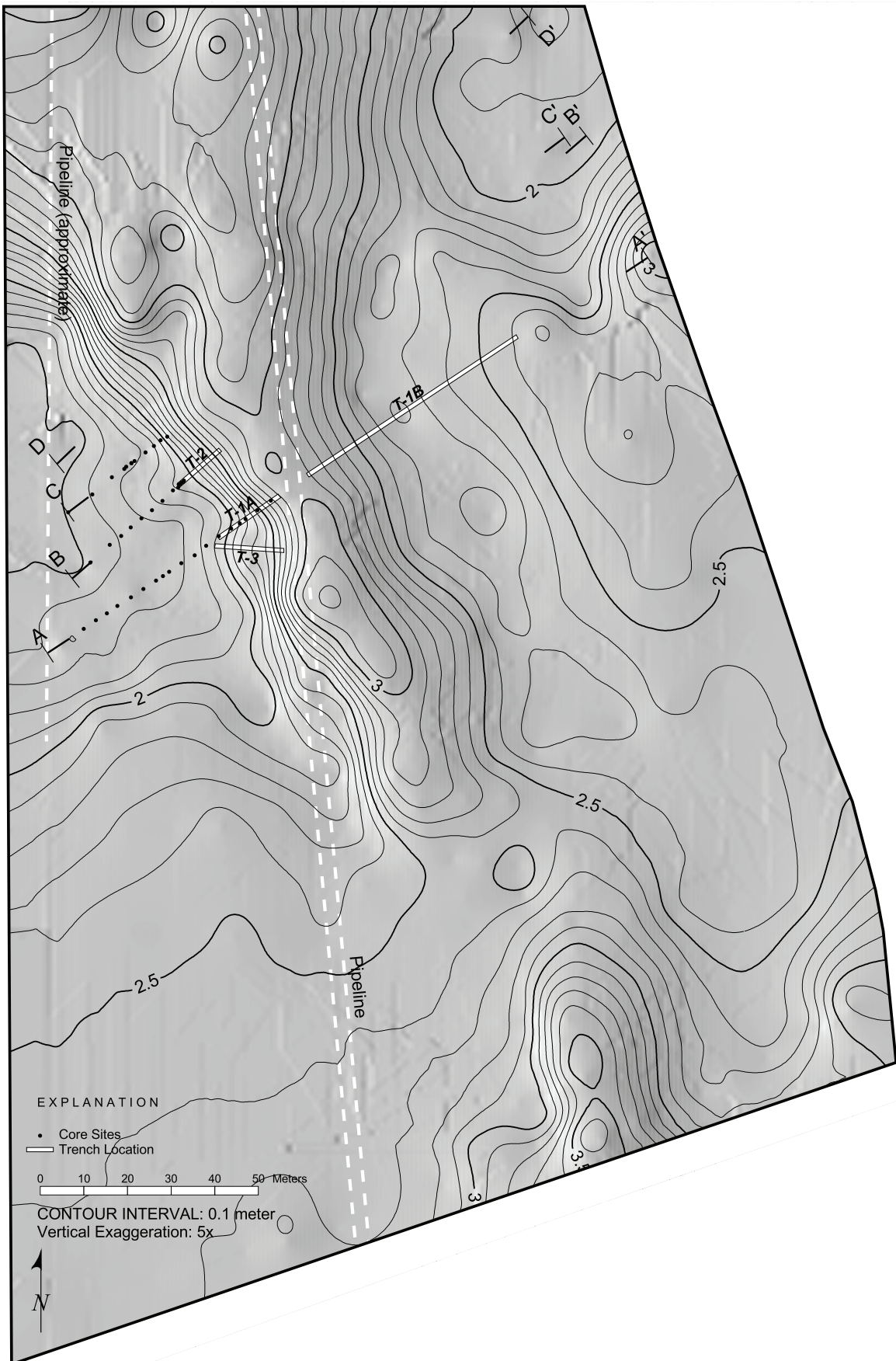


Figure 3. Shaded relief topographic map of moletrack scarp along western Little Salmon fault at the Swiss Hall site. Contour interval 0.1 m, vertical exaggeration of shaded relief 5:1.

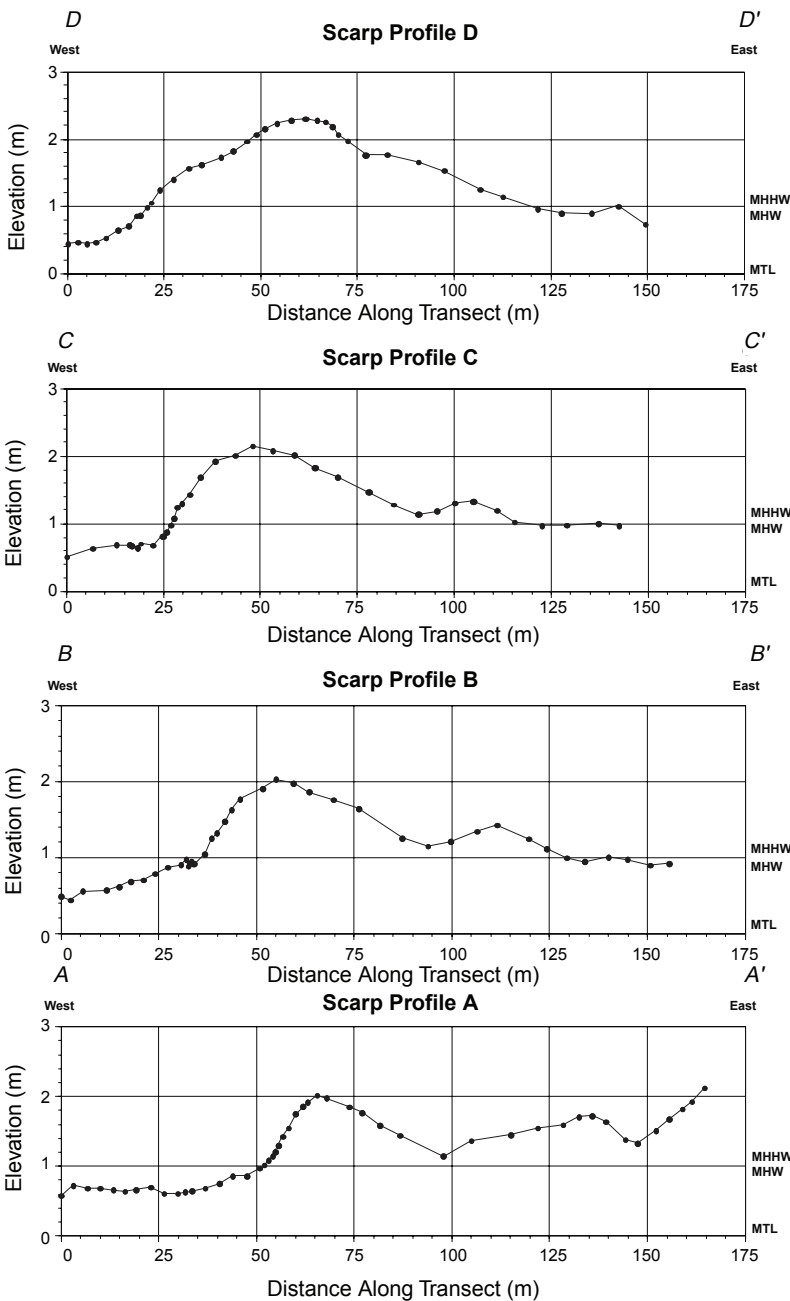


Figure 4. Topographic profiles of moletrack scarp. Profile locations shown on topographic map (left). Tidal datums: MHHW, mean higher high water; MHW, mean high water, MTL, mean tide level. Vertical exaggeration is ~ 18:1.

as a tidal marsh soil catena that reflects transport of sediment from the crest to the base of the scarp over time. Interbedded peat and mud beds (unit 0) that overlie the soil were deposited historically based on a bomb-related radiocarbon spike measured in herbaceous seeds (Witter et al., 2002).

Vertical, soil-filled cracks occur in all the trench exposures on the western side of the scarp (Figures 5, 6 and 7). These downward-tapering fissures converge into normal faults that offset strata in the paleo-tidal channel, occur in opposing trench walls, and trend obliquely to the scarp at an azimuth of $\sim 300^\circ$. We interpret these cracks as earthquake-related features and not as desiccation cracks because they offset bedding, have consistent sense of vertical offset, occur as sub-planar en echelon gashes in the hanging wall, delineate a structural graben, and are associated with groundwater springs. The implication of these cracks on the style of surface deformation is discussed further in the following section.

marsh soils (units 4 and 6; Figure 6). On the basis of their lenticular shapes and from diatom analyses we interpret the mud lenses to represent lower intertidal deposits that filled a paleo-tidal channel at the toe of the fault scarp. The sharp mud-over-peat contacts that exemplify the lower boundaries of some of the mud lenses may indicate erosion by tidal currents in the bottom of a tidal channel. Alternatively, the mud lenses may indicate repeated tectonic subsidence of the scarp.

Above unit 3, a thick (15 to 80 cm), massive bed of mud (unit 2) buries the western flank of the scarp and pinches out to the east before reaching the crest of the scarp (Figures 5 and 6). Unit 2 also occupies a paleo-tidal channel exposed in trench T-1B (Figure 8), east of the primary scarp. Thus, unit 2 laps onto but does not completely cover the primary scarp. A sudden shift in the diatom assemblages across the sharp mud-over-peat contact between unit 2 and unit 6 (Witter et al., 2002) suggests rapid relative sea-level rise nearly submerged the entire scarp.

Overlying unit 2 is a 20- to 70-cm-thick, dark brown soil (unit 1) that contains many fine roots, oxidized root mottles and fine subangular blocky peds. The lower contact of unit 1 is clear to sharp (<1 cm) indicating relatively rapid aggradation of this deposit. Diatom assemblages analyzed from this unit suggest deposition in a high marsh environment (Witter et al., 2002). Also, unit 1 generally thins across the crest of the scarp and thickens toward the base of the scarp and above the paleo-channel in trench T-1B (Figure 5). On the basis of these relationships we interpret unit 1

Near Surface Structural Relations

Structural relations revealed in trench exposures and cores provide information on the style of deformation that formed the moletrack scarp at the Swiss Hall site (Figures 5 and 6). Subtidal estuarine deposits and overlying mud flat and tidal marsh strata parallel the gross topographic profile of the scarp with the exception of a paleo-tidal channel near the base of the scarp that is buried by unit 2. The oldest deposits present in the trench exposures appear to be warped to a greater degree than younger deposits. Thus the stratigraphic data coupled with the topography of the scarp reflect multiple episodes of deformation via folding rather than brittle displacement. The total vertical relief developed across the scarp equals 2.6 to 3.2 m over the last ca. 1,600 years (Table 1) as measured by the deformation of unit 6 in trenches T-1A and T-2 (Figures 5 and 6). Carver and Burke (1988) observed minor reverse displacement and a similar growth-folding style of deformation in excavations across the scarp of the western Little Salmon fault 2.5-km south-southeast of the Swiss hall site. We interpret that growth of the scarp near Swiss Hall occurred through repeated episodes of fault-propagation folding above a shallow, blind, low-angle, northeast-dipping thrust fault. Below, we describe two structural relationships that illustrate the style of deformation that constructed the scarp and a third relationship that suggests broad down warping defeated scarp

TABLE 1. Total Dip Slip, Slip per Event and Late Holocene Slip Rate Estimates for the Western Little Salmon Fault

Vertical offset of ~1.6 ka marsh soil (m) ^a	Dip of fault near surface (degrees) ^b	Cumulative dip slip on fault near surface (m)	Slip per event assuming three earthquakes since ~1.6 ka (m)	Late Holocene slip rate estimates (mm/yr) ^c	Average late Holocene slip rate estimate (mm/yr) ^d
2.6	30	5.2	1.7	2.5-3.4	2.9
2.6	20	7.6	2.5	3.7-4.9	4.2
2.6	15	10.0	3.3	4.9-6.5	5.6
3.2	30	6.4	2.1	3.1-4.1	3.6
3.2	20	9.4	3.1	4.6-6.0	5.2
3.2	15	12.4	4.1	6.0-8.0	6.9

^a On the basis of paleoseismic trenching and sediment coring data across the western Little Salmon fault, a ~1.6 ka buried marsh soil has been folded by three to four slip events.

^b Fault dip estimated from outcrop exposure observed by Carver and Burke (1988).

^c Range of slip rate estimates based on the calibrated radiocarbon age of Unit 6 (1530-1710 yr BP) and assuming the most recent earthquake occurred approximately 250 yr BP.

^d Average slip rate calculated by dividing the cumulative dip slip in millimeters by 1360 yrs. This age represents the average age of Unit 6 minus 250 yrs, the inferred age of Event 1 (Table 1).

growth: (1) progressive folding of strata with age; (2) extensional features including normal faults in the western flank of the moletrack scarp; and (3) evidence of coseismic subsidence of the hanging wall.

Evidence for Growth Folding

Tidal marsh deposits exposed in trenches and cores record contractional deformation in the scarp reflected by progressive folding with age. Using stratigraphic profiles from cores and trenches T1-A and T-2 (Figures 5 and 6), we estimated the magnitude of vertical deformation across the bold buried soil (unit 6), the base of unit 2 and the base of the modern soil profile (unit 1). The maximum estimated vertical deformation across unit 6 is 2.6 to 3.2 m; 1.7 to 1.8 m across the base of unit 2; and about 1 m across the base of unit 1. These values likely overestimate the vertical component of flexure across the scarp because these measurements assume that the strata were originally horizontal prior to deformation. There probably was some existing relief to the scarp prior to each deformation event that was less than the vertical range of the intertidal zone that hosted marsh soils. In Humboldt Bay this vertical range is about one meter (National Ocean Service, 1982). Nevertheless, the increasing amount of warping in progressively older strata demonstrates that three successive deformation events buckled the scarp.

THIS PAGE LEFT INTENTIONALLY BLANK
FOR
WITTER TABLOID FIGURE 5

THIS PAGE LEFT INTENTIONALLY BLANK
FOR
WITTER TABLOID FIGURE 5

THIS PAGE LEFT INTENTIONALLY BLANK
FOR
WITTER TABLOID FIGURE 6

THIS PAGE LEFT INTENTIONALLY BLANK
FOR
WITTER TABLOID FIGURE 6

Evidence for Extension in the Hanging Wall

In three trenches (Figures 5, 6 and 7) thin, wedge-like fissures filled with soil from unit 1 taper downward and join normal faults that offset strata in the paleo-tidal channel and the western limb of the adjacent monocline. Normal faults offsetting unit 6 also occur in the western flanks of the primary scarp (trench T-2; Figure 6) and anticline at the base of the primary scarp (trench T-3; Figure 7). Some normal faults show as much as 8 cm of displacement, although the amount of normal offset across most faults amounted to 2 to 5 cm. The normal faults border a shallow graben centered above the paleo-tidal channel. Faults on the west show down-to-the-east displacement; whereas, faults to the east show down-to-the-west displacement. The trend of the normal faults and related soil-filled cracks were obliquely oriented counter-clockwise from the trend of the moletrack scarp and parallel to the trend of the tidal channel. We interpret these small normal faults as bending-moment faults associated with fault-propagation folding above the fault tip.

The geometry of folding in the primary scarp includes a steeply west-dipping, hanging-wall monocline that dips less steeply near the toe of the scarp. The asymmetric fold displays westward vergence and shows evidence for plastic flow and soft sediment deformation. A paleo-tidal channel at the base of the primary scarp adjoins more gently west-dipping strata at the toe of the scarp. Extension in the hanging wall, evident as a fault-bounded graben occupied by a tidal channel, coincides with the inflection in the monocline at the toe of the scarp. This compound monoclinial fold characterized by an inflection in the dip of the strata near the toe of the scarp probably reflects a subsurface fault bend and propagation of a very shallow (tens of meters deep), blind, thrust fault below the scarp (Carver and McCalpin, 1996).

Evidence for Submergence in the Hanging Wall

Changes in fossil diatom assemblages across mud-over-soil contacts in the scarp attest to multiple occurrences of sudden relative sea-level rise that partially submerged the hanging wall. Fossil diatoms in buried soils (units 4, 6 and 8; Figures 5 and 6) deformed within the fault scarp express affinities for low to high marsh environments. Evidence for sudden submergence of units 6 and 8 includes sharp upper contacts with overlying mud and a shift to fossil diatom assemblages that typically inhabit lower intertidal environments such as tidal sloughs and mud flats (Witter et al., 2002). We assume that uplift of the hanging wall accompanies slip during earthquakes on the western Little Salmon fault. Therefore, evidence for submergence in the hanging wall must be caused by some other mechanism. We propose that the simplest explanation for submergence in the hanging wall of an upper-plate fault is regional subsidence caused by a Cascadia megathrust event.

Trench exposures show that intertidal mud buried a high marsh soil (unit 8) between 1,840 to 2,300 cal yr BP, based on changes in fossil diatoms across the upper soil contact (Figures 5 and 6). The presence of this buried soil in the scarp and its correlation to an extensive buried tidal marsh soil near Hookton Slough 2-km to the west that was submerged 2,040 to 2,310 cal yr BP indicate widespread submergence including the hanging wall of the fault. Ages of delicate detrital macrofossils that estimate the time of submergence at both sites are statistically indistinguishable (Witter et al., 2002).

Extensive submergence of another tidal marsh soil along Hookton Slough between 1,350 to 2,150 cal yr BP correlates with submergence of unit 6 (1,530 to 1,710 cal yr BP) in the hanging wall. Sharp upper contact of the soil with overlying mud revealed in sediment cores and trench exposures is consistent with diatom analyses that indicate a sudden shift from high marsh conditions to low marsh and tidal slough environments.

The gradual contact between unit 4, the youngest buried marsh soil in the hanging wall, and overlying laminated mud of unit 3 suggests a gradual shift from high to low marsh environment based on the difference in fossil diatoms present in each unit (Witter et al., 2002). Slow submergence of unit 4 about 1,310 to 1,690 cal yr BP probably was limited to the area near the Swiss Hall site because it lacks a correlative buried soil at Hookton Slough.

Trend of trench — 095°

Trench T-3

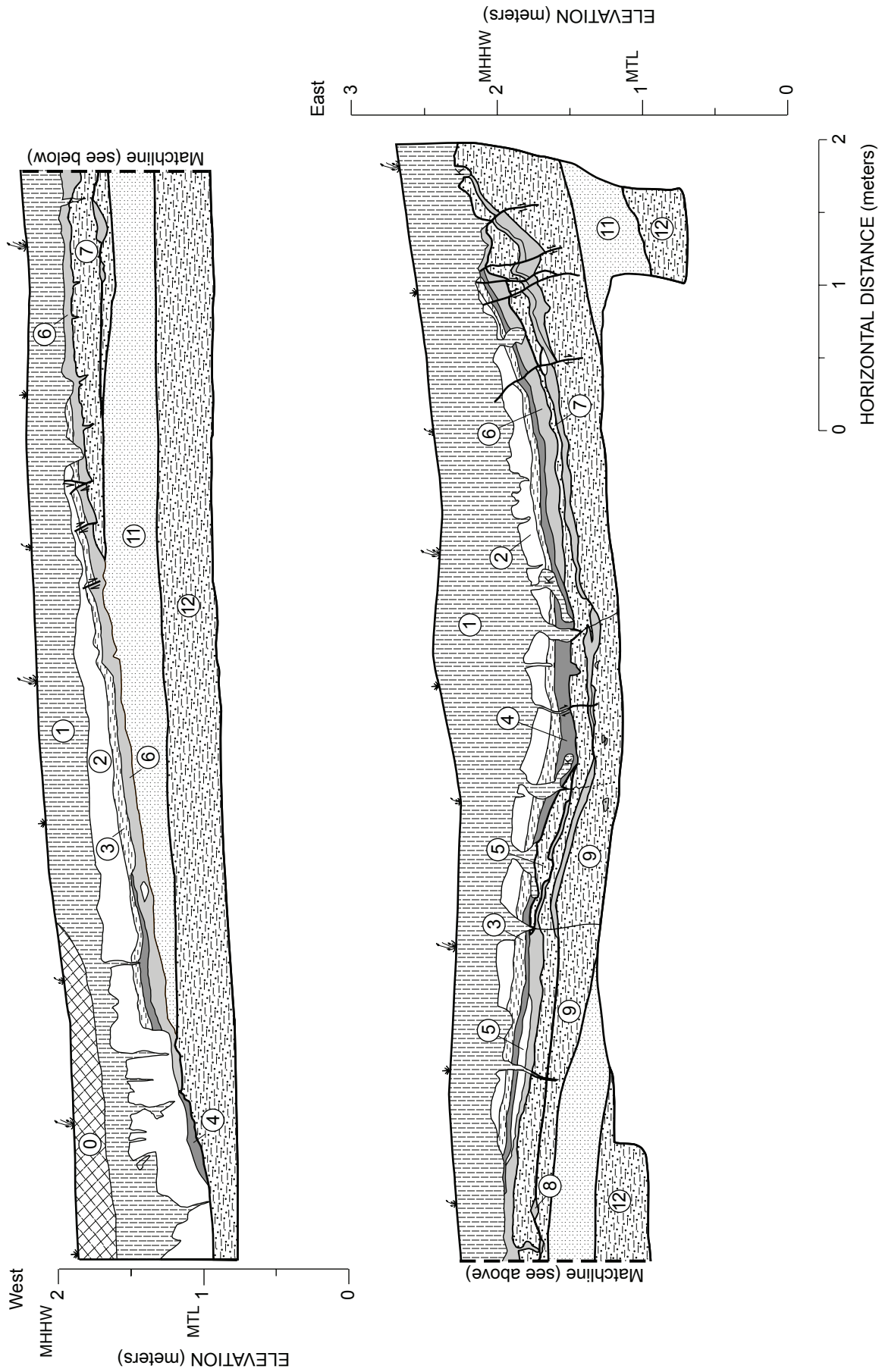


Figure 7. Detailed log of trench T-3 at the Swiss Hall site. See Figure 5 for explanation.

Finally, submergence of nearly the entire scarp is recorded by an angular unconformity at the base of unit 2 (Figures 5 and 6). The thick grey mud of unit 2 buries units 3 and 4 on the lower scarp and overlaps unit 6 higher up on the scarp and further west in the hanging wall (Figure 8). Near the crest of the scarp, the sharp contact between unit 6 and unit 2 and a corresponding shift in fossil diatoms, indicate a sudden drop from high marsh to tidal flat conditions. The submergence occurred sometime after 970 to 1,230 cal yr BP, the age of spruce needles from unit 3 (Witter et al., 2002). However, clear evidence for a similar episode of submergence near Hookton Slough at the same time is lacking because no tidal marsh soils are buried by unit 2 directly west of the scarp and because the second youngest buried soil along Hookton Slough is limited in its lateral extent and remains undated.

DISCUSSION

Late Holocene Earthquake Chronology, Western Trace Little Salmon Fault

From structural and stratigraphic relations observed in the trenches and sediment cores we interpret that deformation produced by three earthquakes built the scarp through progressive folding, normal faulting and *en echelon* fissuring in the hanging wall of a shallow, blind, thrust fault. Several of these events were coincident with or followed closely after coseismic subsidence in the footwall. Below, we propose an earthquake chronology derived from our interpretation of folded and disrupted intertidal deposits that lap onto the western flank of the scarp and radiocarbon age estimates from above and below stratigraphic evidence of an earthquake. Earthquake 'event horizons' were identified from angular unconformities in the section, progressive folding, upward fault terminations, and fissures produced by secondary surface rupture.

Evidence for the oldest earthquake, event 3, comes primarily from folding of unit 6 that can be distinguished from slightly shallower folding of younger deposits. We interpret that unit 6 has been progressively folded during two subsequent slip events because unit 6 dips more steeply than younger onlapping sediments higher in the scarp (Figures 5 and 6). Radiocarbon ages that bracket the event horizon, inferred as the contact between units 5 and 6, estimate the time of this event to between 1,310 and 1,710 cal yr BP. Evidence for coseismic subsidence of both the hanging wall and the footwall includes the submergence and burial of unit 6, which is best explained by regional subsidence caused by rupture of the Cascadia megathrust. However, the amount of submergence did not exceed the elevation of the scarp because the mud (unit 5) that abruptly buries unit 6 laps onto the base of the scarp but does not over top it. We speculate that coseismic slip on the western Little Salmon fault caused local uplift of the hanging wall that locally decreased the amount of subsidence along southeastern Humboldt Bay.

The penultimate earthquake, event 2, is recorded by folding of units 2, 3 and 4 and further warping of unit 6. Normal faults that offset an angular unconformity at the base and terminate in the lower part of unit 2 indicate coseismic extension in the hanging wall above a shallow, blind, thrust fault tip (Figures 6 and 7). Radiocarbon ages from the upper part of unit 2 provide a minimum limit to the time of faulting because normal faults terminate in the lower part of the unit. If the unconformity at the base of unit 2 records subsidence induced by a megathrust earthquake, then slip on the western Little Salmon fault occurred decades or possibly centuries later. Maximum age estimates come from unit 3. Together, the bracketing ages span a range of 540 to 1,230 cal yr BP for the penultimate slip event. We found no conclusive evidence for submergence in the footwall related to event 2.

Trench exposures show that the most recent event involved folding, *en echelon* surface cracking and normal faulting above a blind thrust fault. Vertical fissures filled with material from unit 1 taper downward into cracks that normally offset strata forming a graben above the paleo channel (trench T-1A; Figure 5). In trench T-2 (Figure 6), normal faults offset units 2 and 6 consistent with bending-moment faulting produced by fault-bend folding in the hanging wall. Reworked charcoal recovered from a fissure filled with unit 1 provided a radiocarbon age estimate of less than 460 cal yr BP (Witter et al., 2002) for the time of the most recent earthquake. Although no stratigraphic evidence for coseismic subsidence of unit 1 occurs directly west of the scarp, extensive submergence of soil A along Hookton Slough 2-km west of the Swiss Hall trench site may record downward vertical displacement of the footwall during the most recent event.

Trench T-1B

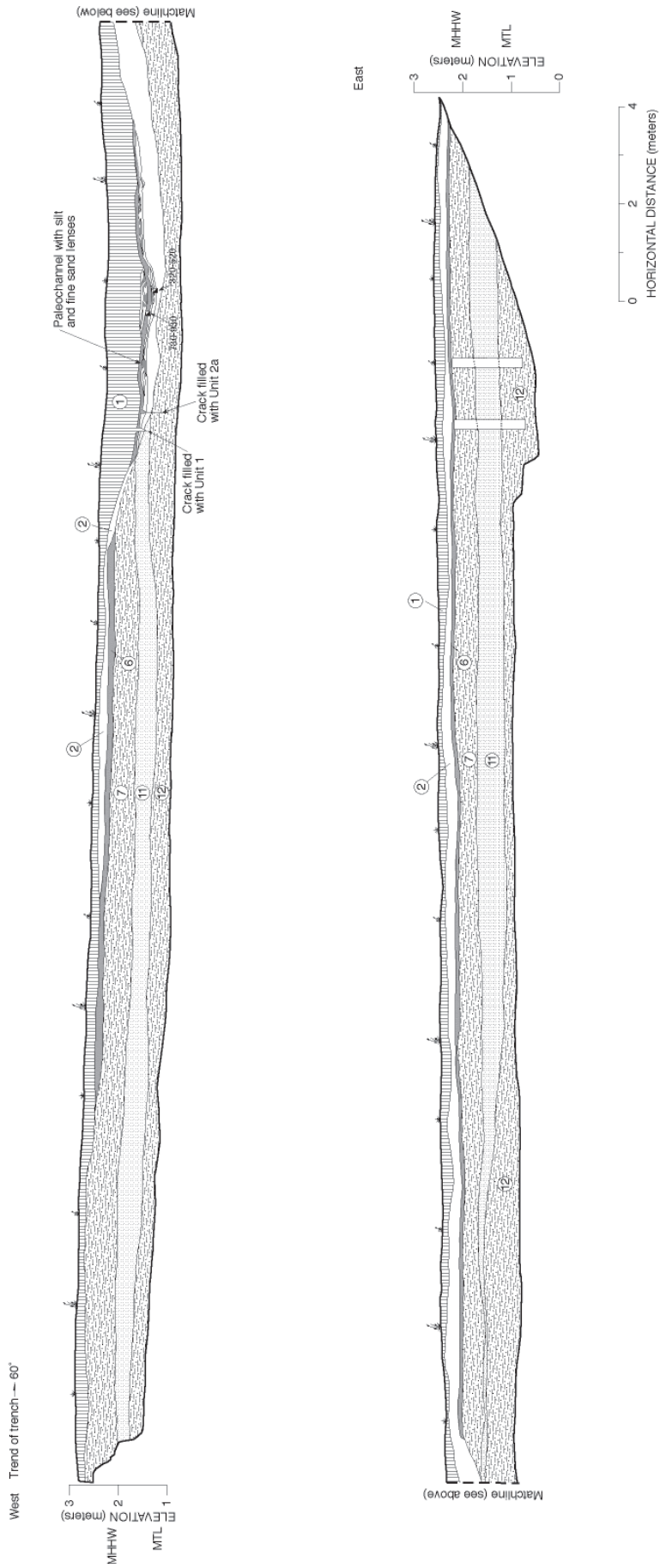


Figure 8. Detailed log of trench T-1B at the Swiss Hall site. See Figure 5 for explanation.

Slip Rate and Average Earthquake Recurrence Interval

Stratigraphic relationships and radiocarbon data (Figures 5 and 6) provide a slip rate estimate of 2.9 to 6.9 mm/yr over the past ca. 1.6 ka (Table 1). This relatively broad slip rate estimate is calculated using the age of unit 6 (1,530 to 1,710 cal yr BP), the inferred age of the most recent earthquake (A.D. 1700), the estimated cumulative vertical displacement across unit 6 (2.6 to 3.2 m), and the estimated near surface fault dip of 15° to 30° (Table 1). The range of slip rates determined by this method, 2.9 to 6.9 mm/yr, encompasses the range of slip rates, 5.3 to 6.3 mm/yr, estimated by Carver and Burke (1988). The amount of slip per event estimated assuming 3 events occurred over the last ca. 1.6 ka ranges between 1.7 and 4.1 m (Table 1). Previous estimates of coseismic slip for earthquakes on the western trace of the Little Salmon fault range between 3.6 and 4.5 m (Carver and Burke, 1988).

The average earthquake recurrence interval calculated from the results of this investigation ranges from 640 to 730 years. This estimate assumes that three slip events occurred on the Little Salmon fault between 1,530 and 1,710 years ago and that the most recent event coincided with the A.D. 1,700 Cascadia earthquake (Satake et al., 1996). The average time interval between earthquake-subsided soils at Mad River Slough (Clarke and Carver, 1992) is 275 to 360 years. Average earthquake recurrence intervals for the Cascadia subduction zone derived from studies in coastal Oregon and Washington vary from 500 to 590 years (Atwater and Hemphill-Haley, 1997; Kelsey et al., 2002; Witter et al., 2003).

Comparison to Cascadia Plate-Interface Earthquake Histories

Cascadia subduction zone earthquake histories derived from estuary studies in southwestern Washington, southwestern Oregon, and at Mad River Slough provide comparisons to evaluate whether upper-plate earthquakes on the western Little Salmon fault and subsidence in South Bay possibly were triggered by plate-boundary seismicity or occurred independently (Figure 9). We compared the record of subsidence at Hookton Slough (South Bay) (Patton, 2004) to four regional earthquake chronologies at Willapa Bay in southwestern Washington (Atwater and Hemphill-Haley, 1997; Atwater, unpublished data), the Coquille estuary and Sixes River in southwestern Oregon (Kelsey et al., 2002; Witter et al., 2003), and Mad River Slough in northern Humboldt Bay (Clarke and Carver, 1992). Further comparisons of the slip history for the western Little Salmon fault from the Little Salmon Creek trench site (Clarke and Carver, 1992) and the Swiss Hall site (this study) provide the basis to evaluate the synchronicity or lack of it between upper-plate and plate-interface seismicity.

Overlapping radiocarbon ages for paleoseismic events at sites from southwestern Washington to northern California suggest that earthquakes about 250 and 1,600 years BP ruptured the entire Cascadia subduction zone. Data from South Bay are consistent with abundant evidence for the M_w 9 1,700 AD Cascadia earthquake that subsided estuaries from Vancouver Island, British Columbia to northern California (Jacoby et al., 1997; Nelson et al., 1995; Yamaguchi et al., 1997) and generated a tsunami that reached Japan (Satake et al., 1996). The range of ages that constrain the timing of events 1 and 3 on the western trace of the Little Salmon fault allow, but do not require, the interpretation that large magnitude plate-interface events triggered upper-plate faulting (Figure 9). However, broad uncertainty in the age estimates leave open the possibility that the Little Salmon fault ruptured independently within decades of plate-interface earthquakes.

Still more uncertainty surrounds the speculation that the penultimate event on the Little Salmon fault was triggered by a great Cascadia earthquake. Age estimates for event 2 on the Little Salmon fault overlap the ages of three subsided soils at Mad River Slough and a Cascadia earthquake recorded in southwestern Washington (event W). However, the penultimate event horizon, defined by the upward termination of faults in the hanging wall, does not coincide with a laterally extensive buried soil in South Bay. The lack of or, at best, equivocal evidence for regional subsidence in southern Oregon and South Bay at the time of event 2 on the Little Salmon fault casts doubt on the possibility that a great Cascadia earthquake triggered crustal faulting. Alternatively, if the Little Salmon fault ruptured independently of the subduction zone around 1,000 years ago, then it may have closely coincided in time with an earthquake that subsided northern Humboldt Bay at Mad River Slough (Vick, 1988; Clarke and Carver, 1992).

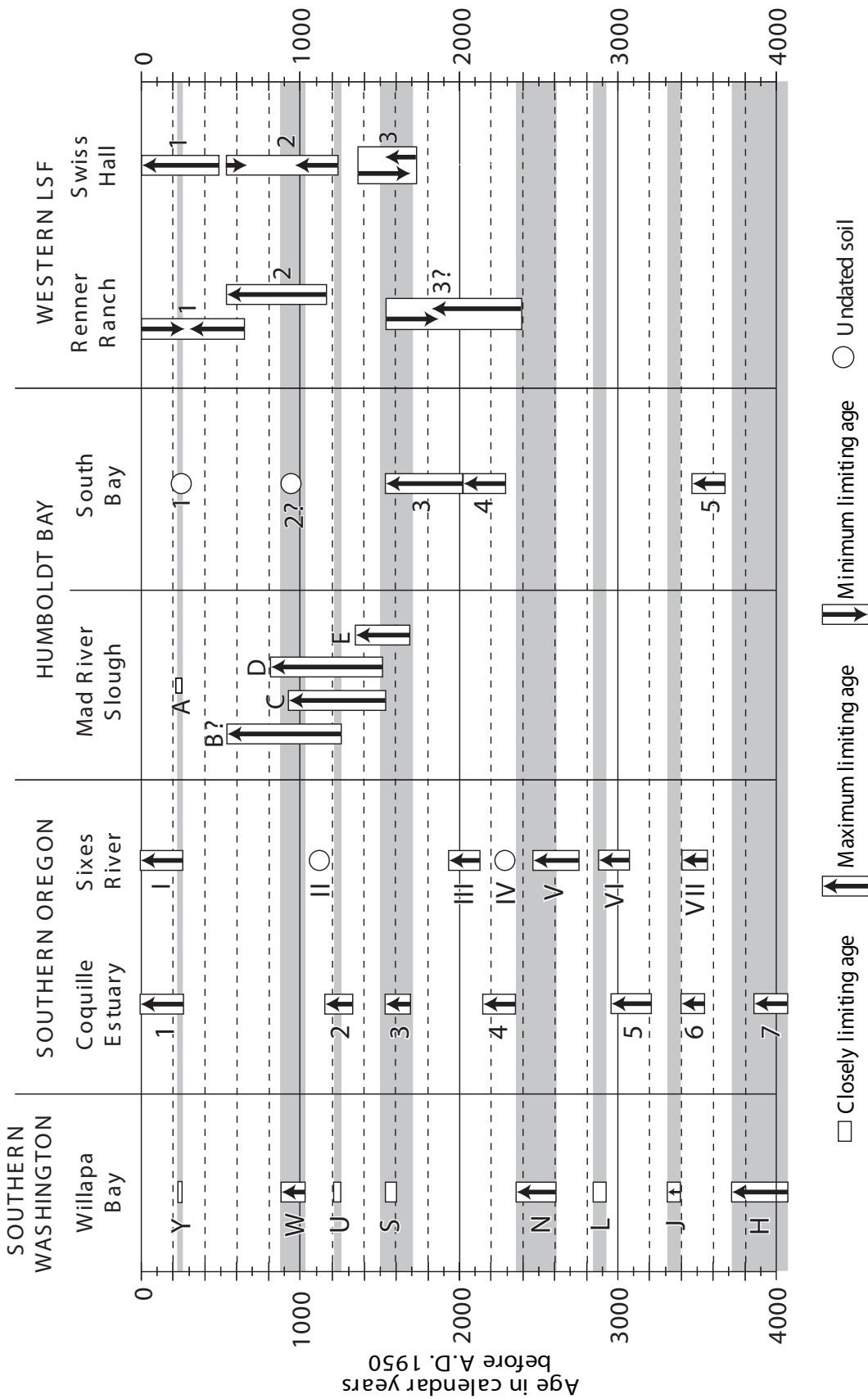


Figure 9. Comparison of calibrated radiocarbon ages for buried tidal marsh soils at estuaries in southwestern Washington, southern Oregon and at Humboldt Bay to paleoseismic data from trench studies of the western Little Salmon fault at two sites: the Little Salmon Creek site and the Swiss Hall site (Figure 2). Shaded regions represent the preferred ages for Cascadia subduction zone earthquakes at Willapa Bay, southern coastal Washington (Atwater and Hemphill-Haley, 1997). Other Cascadia earthquake chronologies include southern Oregon data from Kelsey et al. (2002), and Witter et al. (2003), and Mad River slough data from Clarke and Carver (1992) and Nelson et al. (1995). Western LSF earthquake chronologies include Renner Ranch data from Clarke and Carver (1992) and Swiss Hall data from Witter et al. (2000, 2001).

CONCLUSIONS

Earthquake-related deformation of estuarine and tidal marsh deposits identified in trenches and shallow borings across a 1-to-1.5-m-high moletrack scarp at the Swiss Hall site chronicle a late Holocene slip-history caused by earthquakes on the western Little Salmon fault. We found no evidence for primary surface fault rupture at the site. Instead, growth of the scarp is produced by folding and secondary normal faulting that has developed an asymmetric monocline in the western part of the fault scarp, and produced a fault-bounded graben in the hanging wall overlain by subvertical soil-filled cracks. The moletrack scarp investigated by this study occurs where the western trace of the Little Salmon fault traverses across the southeastern margin of South Bay, about 2.5-km northwest of the site studied by Carver and Burke (1988). Evidence for progressive warping and secondary reverse faulting documented by Carver and Burke (1988) reflect similar fold-related deformation above the buried tip of the western Little Salmon fault that we observed in trenches across the fault scarp at the Swiss Hall site.

Stratigraphic and structural relations, radiocarbon age data and diatom paleoecology provide evidence for 3 episodes of surface deformation caused by earthquakes on the western Little Salmon fault within the past 1,710 years. Broad radiocarbon age ranges constrain the times of earthquakes to the following intervals: 1,530 to 1,710 cal yr BP for event 3; 540 to 1,230 cal yr BP for event 2; and less than 460 cal yr BP for event 1. The average earthquake recurrence interval for the western trace of the Little Salmon fault is 640 to 730 years. Our results provide a slip rate estimate for the western Little Salmon fault of 2.9 to 6.9 mm/yr with slip per event ranging from 1.7 to 4.1 m; both estimates encompass or overlap similar data reported by Carver and Burke (1988).

Extensive buried tidal marsh soils provide evidence for five episodes of sudden earthquake-related subsidence in South Bay based on a detailed investigation of marsh stratigraphy near Hookton Slough (Patton, 2004). Sand layers that sharply overlie some of the soils record tsunamis that overtopped the South Spit and inundated South Bay up to 6-km inland (described by Patton, this guidebook). Two or three of the buried soils overlie the hanging wall of the western Little Salmon fault and are deformed in the scarp. At least one of the soils coincides with an interpreted 'event horizon' that records upper-plate faulting during event 3. We conclude that where evidence for slip on the Little Salmon fault and regional coseismic subsidence coincide, the simplest explanation is that slip on upper-plate faults was accompanied by rupture on the southern Cascadia plate-interface. However, uncertainties in radiocarbon age estimates do not provide conclusive evidence of coseismically triggered rupture of western Little Salmon fault by Cascadia megathrust events. In contrast, evidence in the scarp for fault slip during event 2 lacks correlation with a buried soil in the hanging wall and leaves open the possibility that the penultimate earthquake may have ruptured alone and was not triggered by a subduction zone event.

ACKNOWLEDGMENTS

This research project was supported by the Pacific Gas and Electric Company and the U.S. Geological Survey (USGS) under USGS award number 01HQGR0125. A comprehensive documentation of the results of this investigation is presented in Witter et al. (2002). We gratefully acknowledge our co-workers G. Carver, H. Kelsey, C. Garrison-Laney, R. Koehler, and E. Hemphill-Haley for their contributions in the field and laboratory and with help preparing the original report. We are indebted to W. Page for advocating and recognizing the potential of this project. J. Redwine, S. Bacon, A. Lutz and D. Cox helped in the field. The Department of Geology at Humboldt State University provided vibracoring equipment. We thank S. Caserza and D. Hansen for access to property. W. Lettis, B. Swan, L. Cluff, and C. Allen contributed constructive reviews in the field. A. Barron, C. Mosher, and R. Zeeb assisted with graphics.

REFERENCES CITED

- Atwater, B. F., and E. Hemphill-Haley, 1997, Recurrence intervals for great earthquakes of the past 3500 years at northeastern Willapa Bay, Washington, Washington, D. C., United States Geological Survey.
- Carver, G. A., and R. M. Burke, 1988, Trenching investigations of northwestern California faults, Humboldt Bay region, U.S. Geological Survey, National Earthquake Hazard Reduction Program Final Technical Report, 53 p.
- Carver, G. A., A. S. Jayko, D. W. Valentine, and W. H. Li, 1994, Coastal uplift associated with the 1992 Cape Mendocino earthquake, northern California: *Geology*, v. 22, p. 195-198.
- Carver, G. A., and J. P. McCalpin, 1996, Paleoseismology of compressional tectonic environments, in J. P. McCalpin, ed., *Paleoseismology*, New York, Academic Press, p. 183-270.
- Carver, D.H. and G.A. Carver, 1996, Earthquake and thunder—native oral histories of paleoseismicity along the southern Cascadia subduction zone [abs], Geological Society of America, Cordilleran Section, Abstracts with Program, Annual Meeting, v. 28, no. 5, p. 54.
- Carver, G.A., C. D., Peterson, C.E., Garrison, and R. Koehler, 1996, Paleotsunami evidence of subduction earthquakes for northern California [abs], Geological Society of America, Cordilleran Section, Abstracts with Program, v. 28, no. 5, p55.
- Clarke, S. H., Jr., and G. A. Carver, 1992, Late Holocene tectonics and paleoseismicity, southern Cascadia subduction zone: *Science*, v. 255, p. 188-192.
- Flück, P., R.D. Hyndman, and K. Wang, 1997, Three-dimensional dislocation model for great earthquakes of the Cascadia subduction zone, *Journal of Geophysical Research*, 102, B9, 20,539-20,550.
- Heaton, T.H., and H. Kanamori, 1984, Seismic potential associated with subduction in the northwest United States, *Bulletin of the Seismological Society of America*, v. 74, p. 933-941.
- Kelsey, H.M., R.L. Ticknor, J.G. Bockheim, and C.E. Mitchell, 1996, Quaternary upper plate deformation in coastal Oregon, *Geological Society of America Bulletin*, 108, 843-860.
- Kelsey, H.M., R.C. Witter, and E. Hemphill-Haley, 2002, Plate-boundary earthquakes and tsunamis of the past 5500 yr, Sixes River estuary, southern Oregon, *Geological Society of America Bulletin*, 114, 3, 298-314.
- McLaughlin, R.J., S.D. Ellen, M.C. Blake, Jr., Angela S. Jayko, W.P. Irwin, K.R. Aalto, G.A. Carver, and S.H. Clarke Jr., 2000, Geology of the Cape Mendocino, Eureka, Garberville, and Southwestern Part of the Hayfork 30 x 60 Minute Quadrangles and Adjacent Offshore Area, Northern California, U.S. Geological Survey, Miscellaneous Field Studies MF 2336.
- McNeil L.C., C. Goldfinger, R.S. Yeats, L.D. Kulm, 1998, The effects of upper plate deformation on records of prehistoric Cascadia subduction zone earthquakes, In: I.S. Stewart, and C. Vita-Finzi (eds), *Coastal Tectonics*, Geological Society, London, Special Publications, 146, 321-342.
- National Ocean Service, 1982, Tidal benchmark data published at: www.co-ops.nos.noaa.gov/benchmarks/9418686.html.
- Nelson, A. R., B. F. Atwater, P. T. Bobrowsky, L.-A. Bradley, J. J. Clague, G. A. Carver, M. E. Darienzo, W. C. Grant, H. W. Krueger, R. Sparks, T. W. Stafford, Jr and M. Stuiver, 1995, Radiocarbon evidence for extensive plate-boundary rupture about 300 years ago at the Cascadia subduction zone: *Nature*, v. 378, p. 371-374.
- Ogle, B. A., 1953, Geology of the Eel River valley area, Humboldt County, California: *Bulletin of the California Division of Mines*, v. 164, 128 p.
- Oppenheimer, D., G. Beroza, G. Carver, L. Dengler, J. Eaton, L. Gee, F. Gonzalez, A. Jayko, W. H. Li, M. Lisowski, M. Magee, G. Marshall, M. Murray, R. McPherson, B. Romanowicz, K. Satake, R. Simpson, P. Somerville, R. Stein, and D. Valentine, 1993, The Cape Mendocino, California, earthquakes of April 1992: Subduction at the triple junction: *Science*, v. 261, p. 433-438.
- Patton, J., 2004, Late Holocene coseismic subsidence and coincident tsunamis, southern Cascadia subduction zone, Hookton Slough, Humboldt Bay, California: M.S. thesis, Arcata, California, Humboldt State University, 71 p.
- Satake K., K. Shimazaki, Y. Tsuji, and K. Ueda., 1996, Time and size of a giant earthquake in Cascadia inferred from Japanese tsunami records of January 1700, *Nature*, 379, 246-251.
- Valentine, D. W., 1992, Late Holocene stratigraphy as evidence for late Holocene paleoseismicity of the southern Cascadia subduction zone, Humboldt Bay, California: M.S. thesis, Arcata, California, Humboldt State University, 84 p.
- Vick, G. S., 1988, Late Holocene paleoseismicity and relative sea level changes of the Mad River Slough, northern Humboldt Bay, California: M.S. thesis, Arcata, California, Humboldt State University, 87 p.
- Witter, R.C., Patton, J.R., Carver, G.A., H.M. Kelsey, C. Garrison-Laney, R.D. Koehler, and E. Hemphill-Haley, 2002, Upper-plate earthquakes on the western Little Salmon fault and contemporaneous subsidence of southern Humboldt Bay over the past 3,600 years, northwestern California, *U.S. Geological Survey, National Earthquake Hazard Reduction Program Final Technical Report*, [Grant award number 01HQGR0125], 44 p.
- Witter, R.C., H.M. Kelsey, and E. Hemphill-Haley, 2003, Great Cascadia earthquakes and tsunamis of the past 6,600 years, Coquille river estuary, southern coastal Oregon, *Geological Society of America Bulletin*, *Geological Society of America Bulletin*, 115, 10, 1289-1306.

Latest Pleistocene to Holocene Paleoseismology of the Southern Little Salmon Fault, Strong's Creek, Fortuna, California

Mark A. Hemphill-Haley, Robert C. Witter and Humboldt Friends of Geology (F.O.G.)

ABSTRACT

A trench was excavated along a southern splay of the Little Salmon fault near Fortuna, California. The Little Salmon fault is one of the southernmost reverse faults within the onland fold and thrust belt associated with the Cascadia subduction zone. The trench exposed evidence for at least 3 fold and fault events in terrace gravels and overbank deposits associated with nearby Strong's Creek. A prominent 1 m-wide fault zone dipping between 30 and 60° displaces all but the uppermost unit in the trench which is anthropogenic fill. The majority of deformation appears related to non-brittle folding of the fine-grained deposits. The most recent event consisted of about 2.5 m of vertical uplift and 2.9 m of horizontal shortening in a broad monoclinial fold of a prominent clayey silt deposit accompanied by about 20 cm of reverse offset. This event occurred between about 10,000 to 12,000 years ago. Based on retrodeformation of trench units and radiocarbon-based estimates of deposit ages, we conclude that a total of 5.1 m of fault parallel offset has occurred since about 13,000 to 14,000 years ago providing a slip rate of about 0.4 to 0.5 mm/yr. The three deformation events occurred within a span of less than 4,000 years followed by 10,000 years of quiescence. We conclude that this may represent temporal clustering of events on this particular splay of the fault which is not characteristic of the Little Salmon fault as a whole. Ample evidence for multiple Holocene ruptures on the Little Salmon fault at locations to the north lead us to believe that the splay trenched at Strong's Creek is likely subsidiary to a more active, yet unmapped structure nearby.

¹ Department of Geology, One Harpst St. Humboldt State University, Arcata, CA 95521 Phone (707) 826-3933; E-mail: markhh@humboldt.edu

² Oregon Department of Geology and Mineral Industries Coastal Field Office, 313 SW 2nd St., Suite D., Newport, OR 97365 Phone (541) 574-7969; Fax: (541) 265-5241 E-mail: rob_witter@dogami.state.or.us

ACKNOWLEDGEMENTS

This project would never have been possible without the amazing volunteer work of numerous people. We would like to thank them all personally but there is a limit to the size of the paper. Pacific Lumber Co. was extremely gracious to this study. Not only did they give us permission to excavate the trench but they also provided an excavator and operator at no charge. We'd like to thank John Oswald and his staff at PALCO for all of their logistical and geological help. The Humboldt Friends of Geology (F.O.G.) is an informal group of earth scientists that meets every two months to talk about geology and geology-related topics. A large number of members of the group provided countless hours to the task of cleaning, shoring, flagging, gridding, logging and photographing the trench, thank you. Of this group, several local area consulting firms provided staff to help in the project, they include SHN Engineers and Geologists, Pacific Watershed Associates, LACO Associates, Stillwater Sciences. We would specifically like to thank Dr. Tom Stephens of SHN Engineers for showing us the Little Salmon fault exposed in a nearby road cut, especially since he had not seen it for many years. Thomas Dunklin photographed the south wall of the trench and provided valuable insight into how to collect digital trench images. We were also assisted by faculty at Humboldt State University, especially Dr. Harvey Kelsey and Dr. Sue Cashman. Many students from the Department of Geology at HSU provided mental- and labor-intensive hours to the project. I would like to specifically thank Andy Tate and Emily Fudge who conducted specific projects under the guidance of Dr. Sue Cashman at the trench. We were also assisted by geologists from Humboldt County. This project was generously funded by the U.S. Geological Survey National Earthquake Hazards Reduction Program Grant #04HQPA0001.

INTRODUCTION

The Little Salmon fault (LSF) is one of the southernmost faults within the Little Salmon fault zone (LSfz), a major contractional structure located at the southern end of the Cascadia onland fold and thrust belt (Carver and Burke, 1992). The onland fold and thrust belt represents the upper plate deformation front associated with the Cascadia subduction zone (CSZ) (Figure 1).

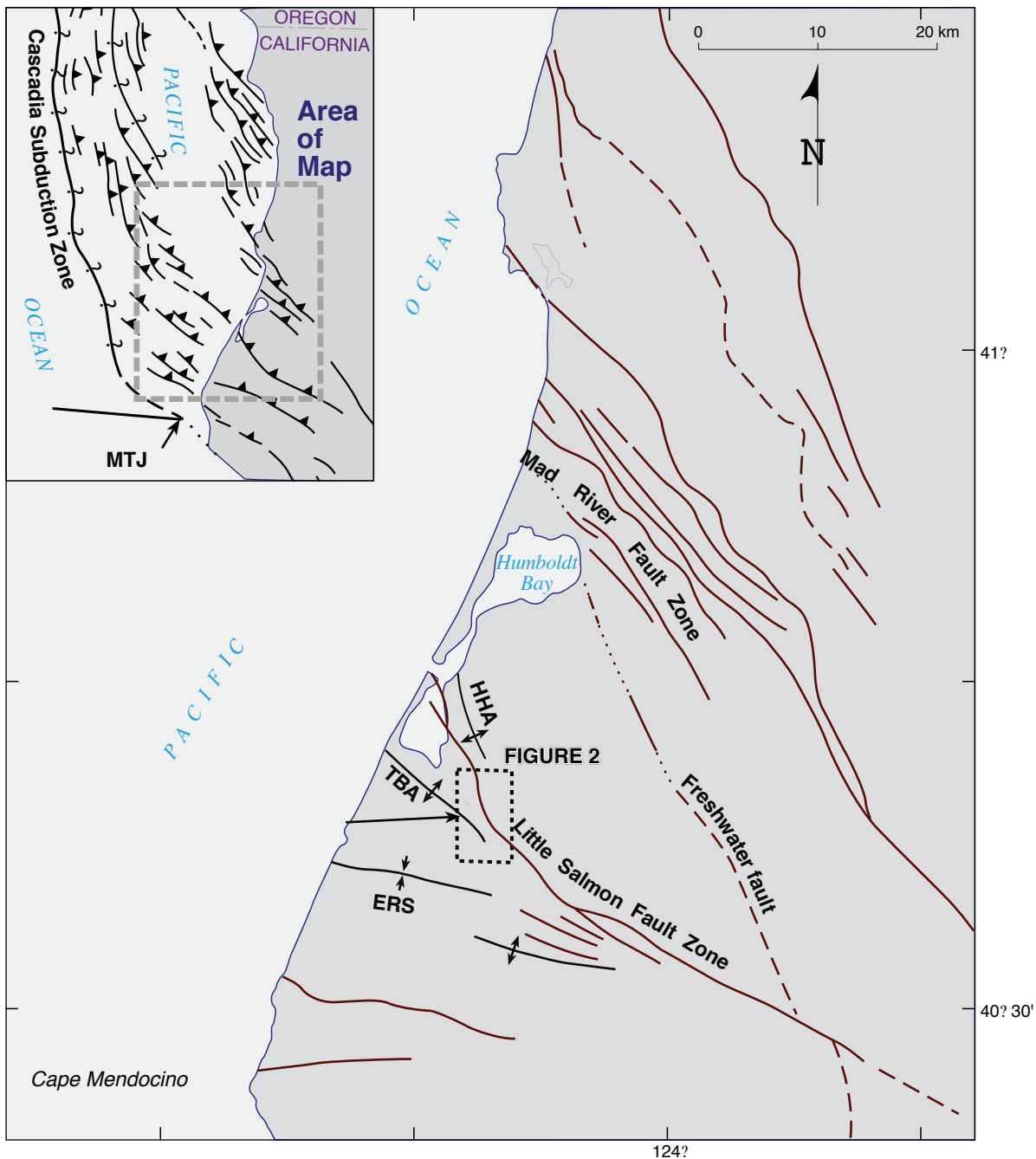


Figure 1 - Tectonic map of coastal California north of Cape Mendocino in context of the plate tectonic setting (inset). Crustal contraction in the lower Eel River valley occurs along the Little Salmon fault zone and along imbricate thrust faults of the Mad River fault zone north of Humboldt Bay. The Little Salmon fault study area is shown in Figure 2. HHA, Humboldt Hill anticline; TBA, Table Bluff anticline; ERS, Eel River syncline; MTJ, Mendocino Triple Junction (From Witter et al., 2002).

Objectives of this investigation included: 1) better constraint of the timing and size of upper-plate earthquakes along the Little Salmon fault and 2) establish a deformation chronology on an inland portion of the fault away from the influences of marsh-related geology that might be attributable to coseismic coastal subsidence.

One complexity regarding the history of rupture along the LSF is its association with the CSZ. Does the LSF act as an independent seismogenic structure or is it somehow structurally linked to the subduction zone megathrust (Clarke and Carver, 1992; Witter et al., 2002). One consequence of direct association between the two structures might be that the LSF ruptures in tandem with the megathrust. Conversely, if the LSF is not tied structurally to the megathrust it may then have a rupture history independent of the subduction zone.

Detailed Holocene surface rupture and coseismic subsidence chronologies have been developed at locations along the northern portion of the fault on land (for example Woodward-Clyde Consultants (1980), Carver and Burke (1988), Witter et al. (2002) and Patton (2004)) (Figure 2). Several of these investigations have compared deformation events known Cascadia megathrust coseismic events (for example Nelson et al. (1995), Atwater and Hemphill-Haley (1997) and Goldfinger et al. (2003)) to assess whether there is one-for-one correlation between the sources. However, within the influence of tidal marshes and potential tsunami-related deposits, it is difficult to separate the evidence for an LSF-induced rupture versus deformation attributable to the subduction zone.

One recent study by Witter et al. (2002) provides evidence of a likely event on the Little Salmon fault, at their Swiss Hall site, that occurred approximately 1,000 years ago and does not coincide with a known CSZ event.

APPROACH

This project consisted of a simple, fault normal excavation across a splay of the Little Salmon fault. We chose a location to the south of the main body of previous investigations (Figure 2) in order to collect surface rupture data for the fault away from the marsh environment and to characterize the lateral paleoseismic history of the fault.

The study area is located in Strong's Creek drainage, in the area of the former town site of Newberg directly northeast of Fortuna (Figure 2). We chose this location on the basis of previous mapping of the LSF near the range front alluvium contact (Tom Stephens, 2004, personal communication). Additionally, for much of its southern extent the fault is located in hilly terrain that is largely occupied by large landslides. The Strong's Creek site afforded us with a location absent of apparent landslide features.

The fault is exposed in a road cut along a private logging road along the north side of the drainage (Figure 3a). Based on the along strike projection of the fault, apparent fault related geomorphology of the drainage and mapping to the south of Strong's Creek by Stephens and by Kelsey (1980) we initially sited our trench across an inactive log deck (Figure 3a). We had prior information that, previously, a large lumber mill occupied the entire site (Figure 3b). Our intention was to trench through the deck fill and into the fault scarp that was buried below. However, a former timber company employee informed us that the logging deck contained large amounts of steel, including a railroad flatbed car, so we decided to abandon the primary trench site. Instead, we excavated a small, < 2 m high, broad, west-facing scarp immediately to the west of the logging deck (Figure 3a and 3c).

We excavated a single 24 m long, 4.5 m deep, 1.2 m wide, trench along a portion of the Little Salmon fault within the floodplain of Strong's Creek at an elevation of about 50 m (Figure 3c). The surface of the site is clearly disturbed by activities of the former mill site (Figure 3b) so we did not focus on geomorphic analysis of the site. This activity also impacted the upper portion of the trench stratigraphy that appears to be truncated and then backfilled.

Once we cleaned and gridded the trench walls we flagged stratigraphic contacts, structures and potential radiocarbon sample sites. We photographed, in sequence, each side of the trench in 1- by 1-m increments using a digital camera and wide-angle lens. We rectified each photo frame to remove distortion and combined the images to produce a photo record and logging base for the trench (Figure 4). We printed the mosaic for each side of the trenched and logged details using a Mylar overlay.

RESULTS

The trench exposes a deep section of fine-grained sediments that we interpret to be overbank deposits related to Strong's Creek. This thick section of fine sand and silt overlies a medium to coarse-grained sand and sandy gravel deposit exposed in the base of the eastern side of the trench (Figures, 4, 5 and 6, Unit 1). A low-angle zone of shearing and associated folding truncates the basal gravel layer and deforms overlying fine-grained deposits (Figure 4). The shear zone is approximately 1 m wide but is associated with a zone of folding that extends for more than 6 m (Tate et al., 2005). The average dip of the fault is about 45NE with the E side up relative to

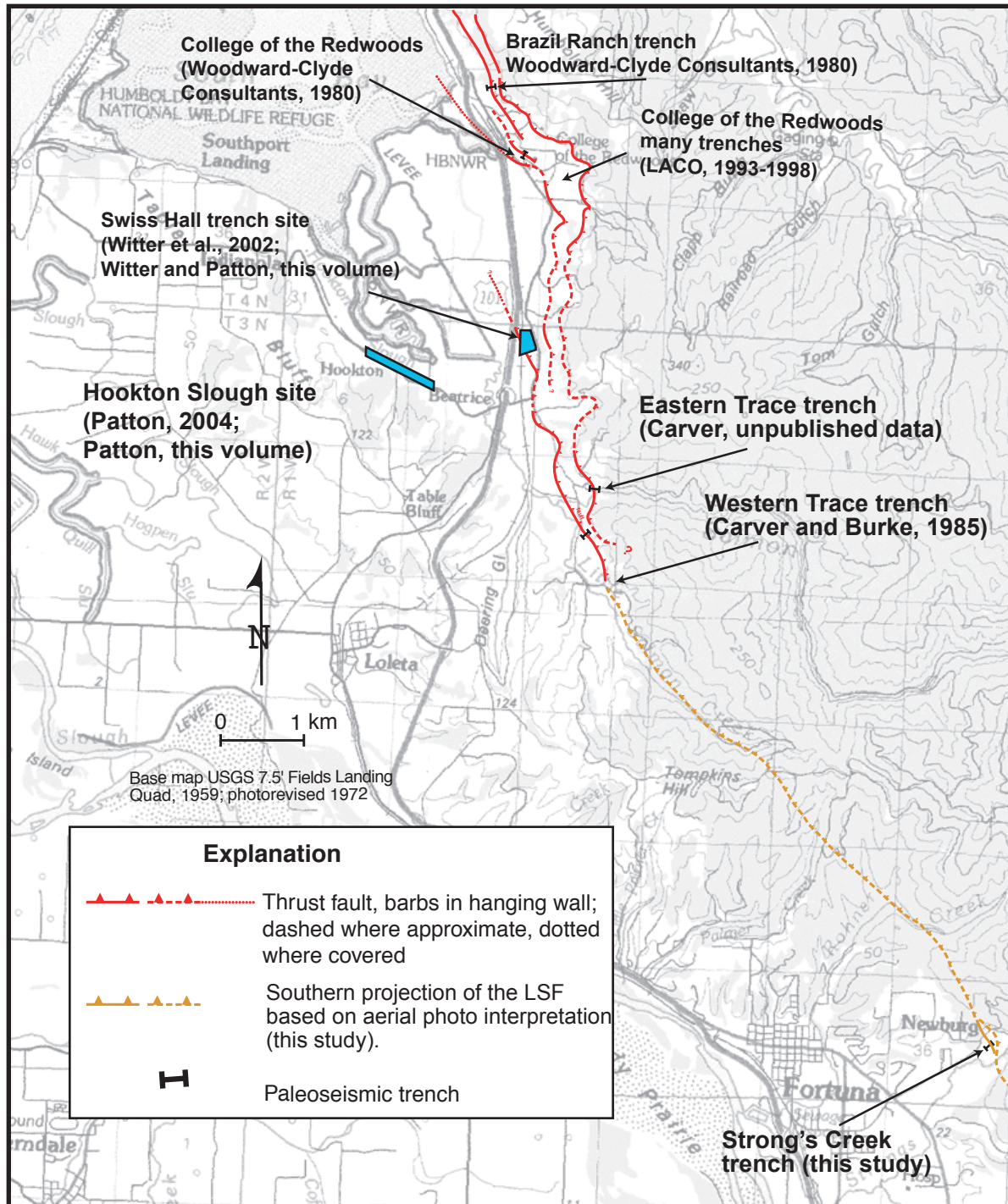


Figure 2 – Location map of a portion of the Little Salmon fault. Locations of earlier paleoseismic (Woodward-Clyde Consultants, 1980; Witter et al., 2002; Witter and Patton, this volume; Carver, unpublished and Carver and Burke, 1985), marsh stratigraphic (Patton, 2004; Patton, this volume), and fault location (Laco, this volume) studies are shown. Location of the fault south of the Carver and Burke (1985) study is uncertain and depicted here based on aerial photographic interpretation.

deposits on the W (Figure 4, 5 and 6). Based on detailed structural and stratigraphic analysis of the fault and folded sediments, Tate et al. (2005) conclude that motion along the fault is almost entirely reverse dip-slip with associated drag folds in both the hanging wall and footwall.

We interpret the stratigraphic units exposed by the trench to be a sequence of rapidly deposited flood overbank deposits. They are likely related to hydraulic backfilling associated with the confluence of Strong's Creek located

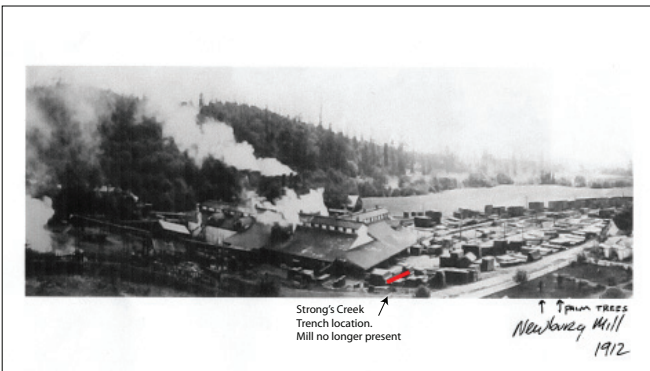
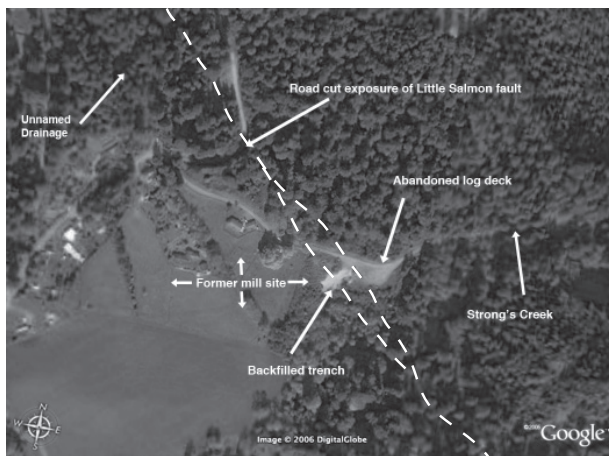


Figure 3 – Strong's Creek trench location photographs. a) aerial photograph taken from *Google Earth* map application. The backfilled trench is included in this photo. In addition, the locations of roadcut exposure of the Little Salmon fault originally mapped by Tom Stephens (SHN Engineering), Strong's Creek drainage, an unnamed drainage to the north of the site and the abandoned logging deck are shown. b) 1912 photograph of the Newberg mill. The location of the Strong's Creek trench is shown in the lower center of the photograph. The mill is no longer present, however, substantial evidence for mill-related surface disturbance still exists, c) photograph of the Strong's Creek trench taken while the trench is being visited by a Humboldt State University soils science class. Camera is pointed to the northeast. Note the broad, gentle warp toward the log deck used to park abandoned yarders).

immediately south of the trench site and a nearby, unnamed drainage that enters the valley to the north (Figure 3a). Within the trench, a repeated sequence of clayey silty units overly sandy and silty units (Figure 5 and 6, Units 4, 6, 8, and 10). We interpret these sequences to represent either weak soils formed on the flood deposits or upward fining sequences in the overbank depositional environment. A thick anthropogenic fill deposit truncates stratigraphy across the upper part of the trench (Figure 5 and 6, Unit 12). Units are laterally truncated but traceable across the shear zone.

Detrital charcoal is plentiful throughout the trench. Eleven samples were submitted for accelerator mass spectrometer (AMS) analysis (Table 1). These radiocarbon dates allow us to estimate the ages for the faulted and folded stratigraphic section. They also provide us with a means to estimate the age of deformation events.

The basal gravel layer (Unit 1) is approximately $23,770 \pm 200$ yr BP (uncalibrated) while the uppermost layer that is not anthropogenic (Unit 11) has an age of 10,250 to 10,190 cal BP (Table 1, Figures 5 and 6). Charcoal within the clayey deposit at the top of the sediments directly overlying the basal gravel provides an age of approximately 13,000 to 14,000 cal BP (Table 1). Thus, there is an unconformity above the gravel unit that represents about 10,000 years of missing time. The remainder of the trench section spans about 2,500 to 3,000 years of sedimentation. Possible explanations for the origin of the unconformity above the basal gravels are purely speculative but may include a) a period of lateral planation and abandonment by Strong's Creek, tectonic uplift of the sequence by a splay of the fault to the east of the trench, or creek incision in response to sea level change.

Although the zone of faulting was clearly represented in the trench, it was evident that much of the deformation was related to folding. In order to estimate the amount of folding per event, we performed a per-event retrodeformation of the trench sediments using a meshing routine (Figures 7 and 8). This required two assumptions. The first is that the finest-grained units were originally deposited nearly horizontally and not on a pre-existing slope. The second is that surface scarps or warps related to prior deformation events were either removed by erosion or burial. These two assumptions would

left intentionally blank for HH tabloid figure 5

Figure 5 – Photo mosaic and interpretation of the north wall of the Strong’s Creek trench. Highlighted areas represented clayey silt units that are used in the retrodeformation exercise.

left intentionally blank
for
HH tabloid figure 5

left intentionally blank for HH tabloid figure 6

Figure 6 - – Photo mosaic and interpretation of the south wall of the Strong’s Creek trench. Highlighted areas represented clayey silt units that are used in the retrodeformation exercise.

left intentionally blank
for
HH tabloid figure 6

be confirmed if a) there is relatively little change in lateral thickness of the relatively thin, fine-grained deposits (Figures 7 and 8, Units 4, 6, 8 and 10) and b) sedimentary units directly overlying these fine-grained units thicken laterally representing sedimentation across a scarp.

We retrodeformed the north and south wall trench logs from the top (youngest deposits and youngest deformation event) to the bottom. The mesh was deformed in a direction roughly parallel to the dip of the fault. In each retrodeformation step the clayey silt deposits (Figures 7 and 8, Units 4, 6, 8 and 10) were returned to a flat-lying position. That unit was then removed and underlying units were, in turn, retrodeformed. This allowed us to account for all deformation recorded in the trench in the form of faulting and folding. The oldest, lowest units were progressively deformed during the subsequent events. We recognize that estimates of deformation for these units should include increased error relative to the younger, less deformed deposits. This information allows us to estimate per event fault slip as well as the net offset due to folding (Figures 7 and 8, Table 2).

We identified three distinct deformation events from the trench stratigraphic and structural relations (Figures 7 and 8, Table 2). The amounts of each component of slip were consistent between the two trench walls but varied between the individual events. The net slip (averaged between the two walls) is $\sim 4 \pm \sim 1$ m, $0.75 \pm \sim 0.2$ m and $2 \pm \sim 0.5$ m for the youngest (Z) to oldest (X) events, respectively. We estimate the amount of net discrete brittle rupture of Unit 10 (Figure 7 and 8) for the most recent event to be about 0.2 m, about 5 % of the total deformation during that event. We can estimate the total net slip based on total deformation of the oldest measurable deposit, Unit 4, through the three events. We estimate an average net slip (from both trench walls) of 5.1 ± 0.4 m. In all but the intermediate event (Y) the horizontal component of slip exceeds the vertical component (Table 2).

We constrain the timing of the deformation events using radiocarbon-based estimates of ages of faulted and unfaulted units. The oldest event, “X” deforms only the deposits as young as Unit 4 (Figures 7 and 8). Sediments deposited subsequent to that unit thicken to the west across the fault reflecting burial of the surface fold. Calibrated ages from samples within Unit 4 range from 13,020 to 13,810 cal BP (SC-N04 and SC-N05, Table 1). A sample collected in the fine sand unit above Unit 4 provides an age of 13,150 to 13,780 cal BP (SC-S27, Table 1). Thus, this event is constrained to have occurred between about 13,000 and 14,000 years BP.

The next deformation event, “Y” involves deposits as young as Unit 8 (Figures 7 and 8). The maximum limiting age for the deposit is 13,150 to 13,780 cal BP (SC-S27, Table 1). Age estimates from samples taken from directly above the unit, range from 11,230 to 11,930 cal BP (SC-N07 and SC-S22, Table 1). Thus the event is constrained between about 11,000 to 13,000 years B.P.

The most recent event is constrained by samples within Unit 10 at 11,570 to 12,270 cal BP (SC-S37, Table 1) and within Unit 11, at 10,190 to 10,250 cal BP (SC-S39) directly above the contact. This constrains the most recent event at between about 10,000 to 12,000 years BP.

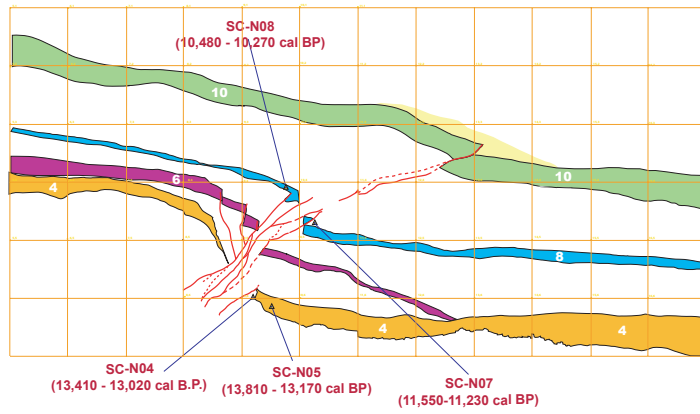
Obviously the trench is missing a Holocene section either due to mill-related activity or simply because of change in sedimentation conditions. We still can conclude that this strand of the Little Salmon fault has not experienced a Holocene deformation event unless folding within Unit 10 is due to more than one episode of activity on the fault. The very small amount of discrete rupture of the unit, however, implies that the deformation of this unit is not the product of multiple events.

We calculate a slip rate based on the average total deformation of Unit 4 (Figures 7 and 8, Table 2) of 5.1 m and an age range of 11,000 to 13,000 years for that event, we can estimate a slip rate of between 0.4 and 0.5 mm/yr.

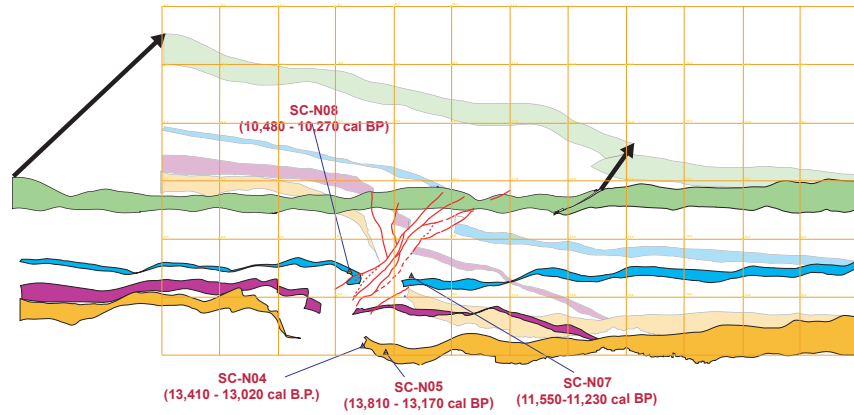
It appears that this splay of the fault has had a temporal clustering of events based on the presence of three events in a range of between 1,000 to 4,000 years followed by an absence of activity for the next 10,000 years.

Since other studies provide evidence for substantial Holocene activity on the fault we conclude that there is another splay, likely located beneath the log deck to the east.

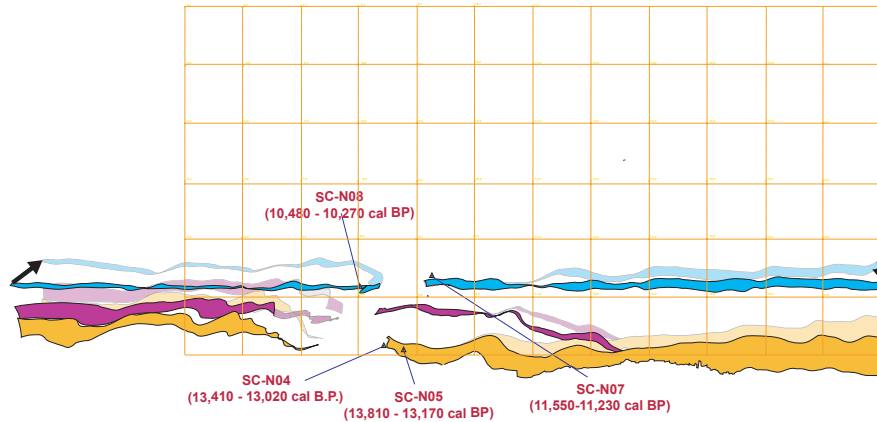
Present stratigraphic configuration of trench



Stratigraphy prior to most recent event "Z"



Stratigraphy prior to penultimate event "Y"



Stratigraphy prior to event "X"

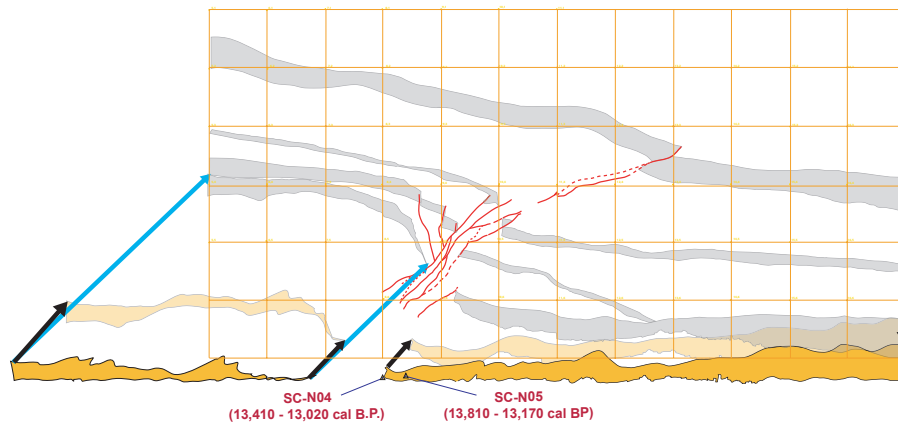


Figure 7 – Retrodeformation of the north wall of the trench. Individual steps in figure represent back step in time of the trench. Faint units represent location of retrodeformed sediments after each faulting event.

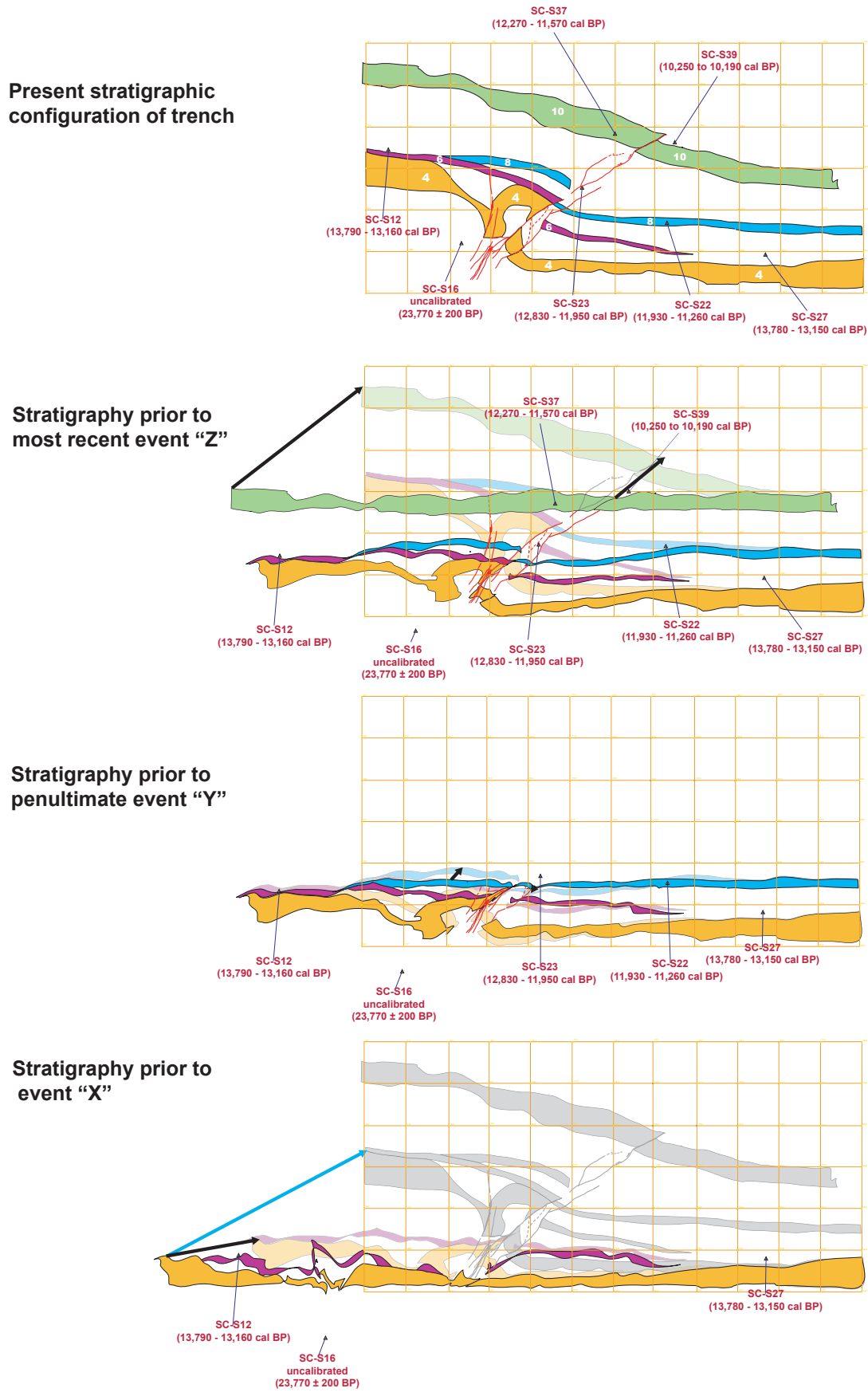


Figure 8 – Retrodeformation of the south wall of the trench. Individual steps in figure represent back step in time of the trench. Faint units represent location of retrodeformed sediments after each faulting event.

REFERENCES CITED

- Atwater, B.F., and Hemphill-Haley, E., 1997, Recurrence Intervals for Great Earthquakes of the Past 3,500 Years at Northeastern Willapa Bay, Washington: United States Geological Survey Professional Paper 1576, p. 108.
- Carver, G.A., and Burke, R.M., 1988, Trenching investigations of northwestern California faults, Humboldt Bay region, Final report, National Earthquake Hazards Reduction Program,, United States Geological Survey, p. 53.
- , 1992, Late Cenozoic Deformation on the Cascadia Subduction Zone in the Region of the Mendocino Triple Junction, *in* Burke, R.M., and Carver, G.A., eds., Pacific Cell, Friends of the Pleistocene Guidebook for the Field Trip to Northern Coastal California: Arcata, CA, p. 31-63.
- Clarke, S.H., Jr., and Carver, G.A., 1992, Late Holocene tectonics and paleoseismicity, southern Cascadia subduction zone: *Science*, v. 255, p. 188-192.
- Goldfinger, C., Nelson, C.H., Johnson, J.E., Erickson, D., Winkler, M., Kalk, P., Pastor, J., Camarero, A., Morri, C., Dunhill, G., Ramos, L., Raab, A., Piasias, N., Jr., Pourmanoutscheri, M., van Rooij, D., Amy, L., and Liu, C.-C.C., 2003, Holocene earthquake records from the Cascadia subduction zone and northern San Andreas Fault based on precise dating of offshore turbidites: *Annual Review of Earth and Planetary Sciences*, v. 31, p. 555-577.
- Kelsey, H.M., 1980, A sediment budget and an analysis of geomorphic process in the Van Duzen River basin, North coastal California, 1941-1975: *Geological Society of America Bulletin*, v. 91, p. I 190-I 195.
- Nelson, A.R., Atwater, B.F., Bobrowsky, P.T., Bradley, L.-A., Clague, J.J., Carver, G.A., Darienzo, M.E., Grant, W.C., Krueger, H.W., Sparks, R.J., Stafford, T.W., and Stuiver, M., 1995, Radiocarbon evidence for extensive plate-boundary rupture about 300 years ago at the Cascadia subduction zone: *Nature*, v. 378, p. 371-374.
- Patton, J.R., 2004, Late Holocene Coseismic Subsidence and Coincident Tsunamis, Southern Cascadia Subduction Zone, Hookton Slough, Wigi (Humboldt Bay), California: Arcata, Humboldt State University.
- Tate, A.W., Cashman, S.M., Hemphill-Haley, M.A., Kelsey, H.M., Witter, R.C., and Anonymous, 2005, A deformation analysis of the Little Salmon Fault at Strong's Creek, Humboldt County, California: Abstracts with Programs - Geological Society of America, v. 37, p. 48.
- Witter, R.C., Patton, J.R., Carver, G.A., Kelsey, H.M., Garrison-Laney, C., Koehler, R.D., and Hemphill-Haley, E., 2002, Upper Plate Earthquakes on the Western Little Salmon Fault and Contemporaneous Subsidence of Southern Humboldt Bay Over the Past 3,600 Years, Northwestern California: Final Technical Report U.S. Geological Survey National Earthquake Hazards Reduction Program Award No. 01HQGR0125, p. 44.
- Woodward-Clyde Consultants, 1980, Evaluation of the Potential for Resolving the Geologic and Seismic Issues for Humboldt Bay Power Plant Unit No. 3 - Appendixes, prepared for Pacific Gas and Electric Company.

The 1906 Earthquake in Humboldt and Del Norte Counties, California

Dengler, L.

ABSTRACT

The State Earthquake Investigation Commission (Lawson, 1908) documented the 1906 earthquake in Humboldt County. This study examines that report and additional information including newspapers, diaries and retrospectives and previously unpublished photographs to describe the earthquake and compare its impacts to recent large local earthquakes. Humboldt County of 1906 had thriving timber and agricultural industries, six newspapers in print and populations in the Eel River Valley similar to current levels. Local Historical Societies have compiled a large collection of primary materials. Losses in Humboldt County from the 1906 earthquake are estimated at \$200,000 in 1906 dollars. Damage and eyewitness accounts do not support the Lawson Report isoseismal map for Humboldt County. The Lawson map shows a zone of strongest ground motions around Humboldt Bay. Strongest ground motions (MMI IX) actually occurred in the Eel River Valley and Petrolia areas where all structures reported some damage and a number of injuries occurred. In the Eel River Valley and Ferndale, fewer than 2% of chimneys survived and nearly every structure was damaged. Liquefaction was observed in the Mattole Valley and throughout the Eel River Valley and occurred on a larger scale than any more recent events. Damage in Eureka was much less than in Ferndale and rapidly decayed to the north. Based on the severity of damage and scale of liquefaction, the 1906 earthquake was Humboldt County's strongest historic event with an intensity VII or larger area more than twice the size of the 1992 Cape Mendocino (M_w 7.1) earthquake. The 1906 earthquake triggered at least 22 smaller earthquakes on the North Coast in the 6 weeks following including the largest aftershock ($M \sim 6.7$) of the 1906 sequence.

INTRODUCTION

The earthquake of April 18, 1906 on the northern segment of the San Andreas fault was the greatest earthquake disaster in US history. The earthquake, estimated to have a magnitude of 7.8, ruptured nearly 300 miles of the fault from south of Santa Cruz to Shelter Cove in Humboldt County. At least 3000 people are believed to have died in the earthquake and ensuing fire that consumed much of San Francisco.

Humboldt County was the northernmost region to suffer significant damage in the 1906 earthquake (Figure 1). At the turn of the century, the County had a population of about 30,000 people (25% of the current population) and was the largest timber and dairy exporter in the state. The county seat and largest city was Eureka, located on Humboldt Bay with a population of close to 10,000 people. After Eureka, the largest communities were Arcata (2000), Fortuna (1500) and Ferndale (1600). The 1903 County Directory lists 50 towns of population between 20 and 1000 primarily located in the Eel River Valley and in the Humboldt Bay region. There were five daily newspapers and a weekly in print and a number of professional photographers who documented the 1906 effects

in the area. Del Norte County to the north was considerably smaller with a population just over 2400 people, concentrated in the Crescent City area and one daily newspaper.

This paper examines newspaper reports, letters, weather service entries and other primary data sources to estimate the impacts of the 1906 earthquake on California's north coast and compare this to the Report of the State Earthquake Investigation Commission (SEIC) (Lawson, 1908) and other published reports.

1906 FAULT TRACE IN HUMBOLDT COUNTY

The SEIC documents the 1906 fault rupture zone in Humboldt County noting several fissures on Point Delgada. that the State Earthquake Investigation Commission interpreted as primary fault rupture (Figure 2). F.E. Mathes conducted the fieldwork in the Shelter cove area and observed no horizontal

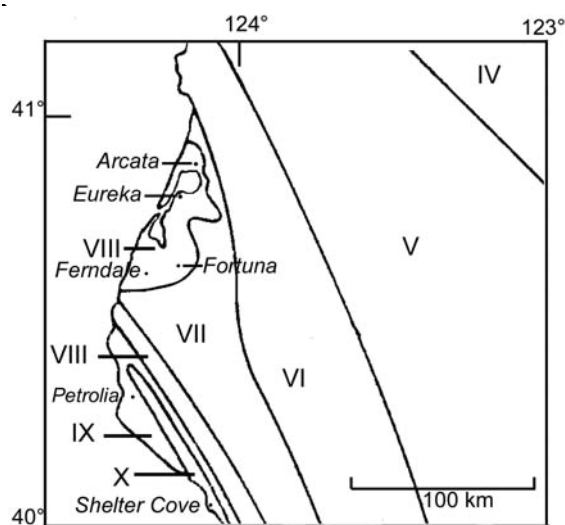


Figure 1. 1906 rupture and damage area. Outlined area is Humboldt County, modified from USGS.

displacement but more than a meter of vertical throw near Wood Gulch. The SEIC acknowledges that the Shelter Cove fissures may not be continuous with the well-defined rupture near Point Arena and that some of the observed displacement may have occurred previous to 1906. Brown (1995) re-examined Mathes' original field notes and concluded that the Shelter cove fissures did represent primary fault rupture. McLaughlin et al. (2000) question whether the Shelter Cove features are an expression of the San Andreas fault because the fissures were located in a major landslide complex and the displacements are more consistent with rotational slide displacement. Prentice et al. (1999) also examined Mathes' notes and trenched the site, confirming the existence of Holocene faulting

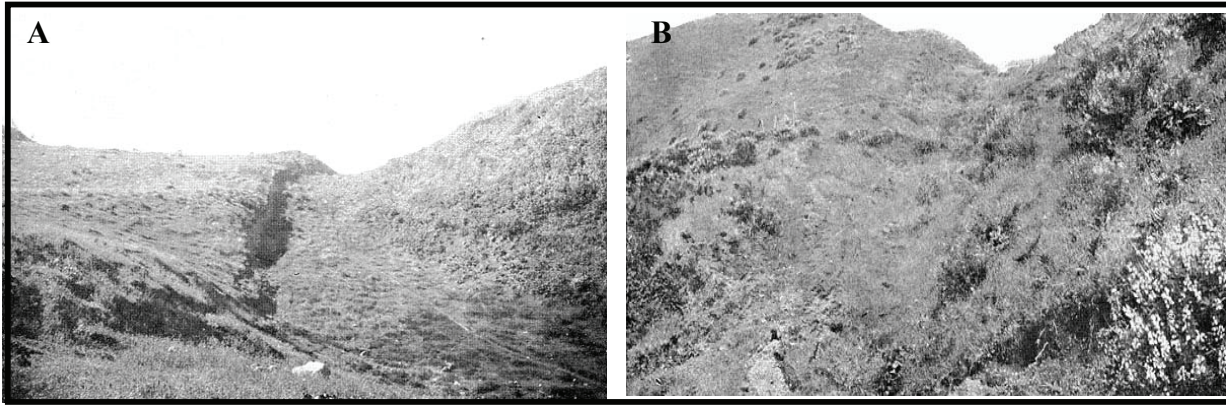


Figure 2. A. Mathes' map of 1906 surface rupture in the Shelter Cove area from the Lawson report (1908). B. SEIC photograph of the scarp at the head of Wood Gulch looking to the southwest, noted by the letter A on Mathes' map.

offsetting the Point Delgada landslide complex but observing little strike-slip displacement on the feature. The general consensus is that the northernmost segment of the San Andreas fault zone and its intersection with the Mendocino fault are poorly defined, and while significant ground disruption occurred at Shelter Cove, there is no agreement that it represented primary fault rupture.

1906 GROUND SHAKING

Figure 3 is a modification of the SEIC isoseismal map of ground shaking in Humboldt County based on the Woodward-Clyde (1980) examination of Humboldt ground shaking hazards. Isoseismals were based primarily on the field reconnaissance of UC Berkeley Mineralogist Arthur Eakle, a member of the State Earthquake Commission Committee on Isoseismals who visited Trinidad, Eureka, Arcata, Petrolia and Ferndale in May, 1906, about three weeks after the earthquake and eyewitness accounts he collected from eight local residents. Regional newspapers apparently were not examined by the SEIC. The consensus of local newspapers (McCormick, 1984) was that the total loss (1906 dollars) was about \$200,000 in the County. The summaries below are based on articles in the Ferndale Enterprise, Blue Lake Advocate, Humboldt Times, The Beacon and Arcata Union except where otherwise noted.

Arcata: (pop. 2000) Nearly 30 chimneys toppled, numerous windows broken on the Plaza. Brizard's Store (currently the Jacoby Store House exhibited spreading of brick walls but no collapse. Nearly all items in stores thrown from shelves. Many stacks of lumber collapsed and water sloshed from tanks. Lumber and shingles fell from the Arcata and Bayside docks into the Bay. More damage was observed in the south part of town than in the hills. Intensity VII.

Blue Lake: (pop. 800) Every store in town lost items off of shelves and 15 chimneys toppled. Plaster was damaged at the school. Damage was less than at Arcata or Eureka. Intensity VI – VII.

Crescent City: Felt by nearly everyone, several pendulum clocks stopped. Intensity IV.

Eel River Valley: (pop. 5000) The Ferndale Enterprise notes that fewer than 2 % of chimneys in the Eel River Valley remained intact and that county water tanks and windmills were thrown from foundations (Figure 4). The largest communities (Ferndale and Fortuna) are described in more detail below. The islands near the mouth of the Eel were particularly hard hit. The Ferndale Enterprise notes “Cock Robin Island came in for its share of the shake, chimneys being torn down and many holes and cracks in the ground made. The same destruction visited Cannibal Island, it being said that the land there that was quite high before the shake-up is now lowered from one to ten feet, while low places have been filled up. In many instances where the ground opened a kind of black sand or sediment oozed forth, showing that it must have been thrown from the very bowels of the earth. On the Hamner ranch on the Island, under lease to Rasmus Nielsen, we are told that this sand or sediment was very warm and that smoke arose from it for several hours after the convulsion.” Liquefaction features were prominent at many sites near the Eel River (Figure 5). At Port Kenyon the Ferndale Enterprise reported that several acres of land settled several feet. All along the Salt River land slid into the river and was reported cracked for distances of several hundred feet on either side. At Centerville Beach near the mouth of the Eel River, The Enterprise reports a half-mile wide landslide into the Pacific near Oil Creek, obstructing the view between the Cape Mendocino and Table Bluff lighthouses. All reports suggest ground motions throughout the Eel River Valley as far east as Grizzly were at least as strong as at Ferndale and should be assigned a IX. At Pepperwood, the SEIC reports most chimneys downed and “10 percent of the property was destroyed by breakage”. Large limbs and some tops of Redwood trees snapped. Topozada and Parke assign an VIII to Pepperwood.

Eureka: (pop. 10,000) By the time Eakle visited Eureka, most of the damage had been repaired. He notes the lack of damage to brick buildings and that no books had been thrown from library shelves. The SEIC relies in large part on the reports of Weather Observer Aaron H. Bell who noted daily observations in the Eureka Weather Service Daily log (U.S. Weather Bureau, 1906). The Weather Service Office was in downtown Eureka and Bell describes numerous downed chimneys and broken glass panes and 47 seconds of strong shaking that was more severe than any previous event in the area. The Ferndale Enterprise notes “Eureka escaped very lightly”. A letter by 18-year old Joseph Tracy (1906) provides the most detailed account of ground shaking in Eureka. He describes great volumes of water pouring out of water tank sloshing 100 gallons at a time, half the plate glass in town broken and numerous downed chimneys. All of the items in Daly’s store in downtown Eureka were knocked from shelves. The Humboldt County Courthouse, a tall ornate brick building, suffered no structural damage but caused the statue of Minerva to tip at an angle of nearly 45°. Damage was mainly minor, in addition to broken glass, Tracy reports, damaged plaster and cracks consistent with MMI VII values.

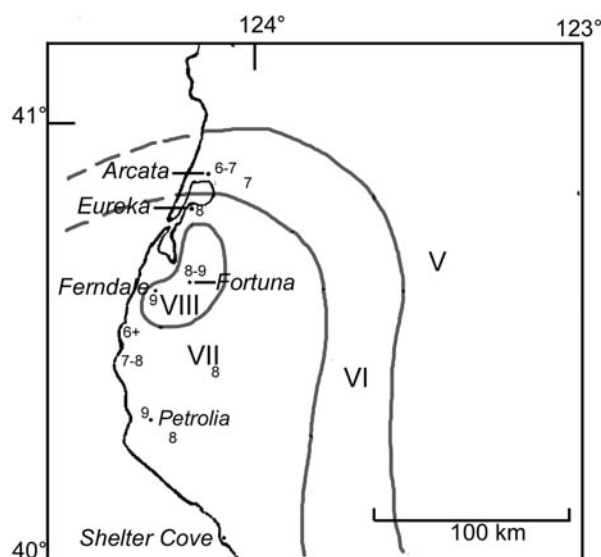


Figure 3. 1906 MMI Isoseismals in Humboldt County, From the SEIC, modified from Woodward Clyde, 1980.



Figure 4. Downed windmill in the Eel River Valley. Photo by E. Garrett, courtesy of the Peter Palmquist Collection

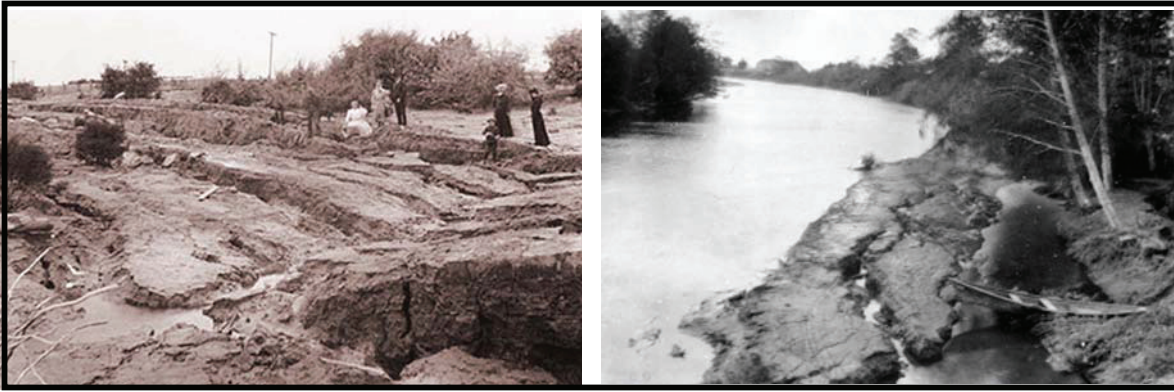


Figure 5. Liquefaction on the banks of the Salt River in the Eel River Valley, Edna Garrett photograph courtesy of the Peter Palmquist Collection.

Ferndale: (pop. 1600) Eakle notes Ferndale as the most heavily damaged community in Humboldt County. There were two brick buildings in the town at the time of the earthquake. The General Mercantile (339 Main St.) owned by the Russ, Early and Williams Co. had been completed only 4 months before the earthquake suffered complete loss of the brick parapet and all the glass windows (Figure 6a). The collapse of the front wall of the building killed two cows (Ferndale Enterprise). The building was repaired and continued as a commercial establishment until 1992 when it suffered similar damage in the Cape Mendocino earthquake (described below). The J. Gollober building (Figure 6b) suffered more severe damage and was demolished after the earthquake. Most of the structures in Ferndale were of wood frame construction and most were not secured to foundations. The largest wood structure was the Knights of Pythias Hall (Figure 7a). It was severely twisted and required shoring to prevent collapse. It was subsequently demolished. Most homes were knocked from foundations and porches and chimneys typically collapsed (Figure 7b). The Ferndale Enterprise reports describe almost every window in town broken, plaster damaged and all stock within buildings scattered. There were no serious injuries although a number of close escapes. The general pattern of damage and injuries was remarkably similar to what happened in the 1992 Cape Mendocino earthquake (see below). Stover and Coffman (1993) place Ferndale in the MMI VIII isoseismal and Topozada and Parke (1982) assign Ferndale a IX. Ferndale was assigned an VIII in the 1992 Cape Mendocino earthquake (Oppenheimer et al., 1992). 1906 damage was more extensive and is consistent with the Topozada and Parkes estimate of IX.

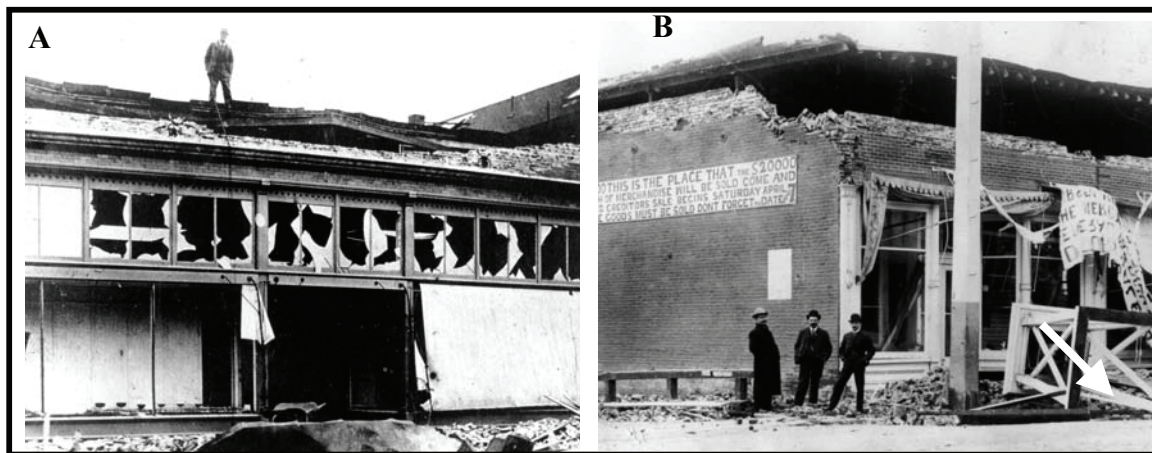


Figure 6. Damage to brick buildings in Ferndale. A) The General Mercantile. The building was repaired and subsequently damaged in 1992 (see figure 8). B) J. Gollober store. The cupola (arrow) housed the fire bell and was thrown to the ground. The building was demolished. Photographs by Ed and Edna Garrett, courtesy of the Peter Palmquist Collection.

Fields Landing: (pop. 100) Located at the southern end of Humboldt Bay, Fields Landing apparently marked the northern extent of significant liquefaction. The SEIC includes a report from H. Buhne, a prominent Eureka citizen who describes downed chimneys but relatively little other damage south of Eureka until Fields Landing. At Fields Landing, Buhne describes fissures in roads and 3 feet of subsidence near Pelican Island. The Pacific Lumber Company's wharf collapsed and damage was estimated at \$15,000 (Figure 8). A railroad water tank toppled over and fences were thrown down. Intensity VII – VIII.

Fortuna: (pop. 1500) The brick walls of the McIntyre store were badly damaged. Over half the chimneys in Fortuna were downed and several houses slid off foundations. Most stores suffered significant loss of merchandise. Clocks stopped and even the heaviest furniture displaced. The concrete breakwater at the East ferry landing on the Eel River was cracked and displaced. Intensity VIII.

Freshwater: (pop. 150) Every chimney in the Freshwater Valley was reported downed and substantial damage to dishes and other household items. Intensity VII.



Figure 7. Damage to wood frame buildings in Ferndale. A) The Knights of Pythias Hall, repaired after the earthquake, eventually replaced by a gas station. B) Unidentified home. Photographs by Edna Garrett, courtesy of the Peter Palmquist Collection.

Garberville: (pop. 300) Many buildings “knocked out of plumb”. Most chimneys and stovepipes knocked down. All items off shelves. Intensity VII - VIII.

Loleta: (pop. 400) Nearly every chimney collapsed. Water tanks collapsed and several people injured by falling objects. The trunks of several large spruce trees were snapped. A cow toppled over while being milked. Intensity VIII.

Pepperwood: (pop. 100) Most chimneys downed and “10 percent of the property was destroyed by breakage”. Numerous cracks and subsidence. Large limbs and some tops of redwood trees snapped. Intensity VIII.

Petrolia: (250) Petrolia is located near the mouth of the Mattole River. Eakle reported nearly every house off its foundation, noting that the houses were poorly constructed and had poor foundations. The Ferndale Enterprise reports conclude that the shaking in Petrolia was stronger than Ferndale as every structure was severely damaged and several people injured by falling bricks. “The bridge near Levant Cook’s place sunk at one end about 18 or 20 inches. Across the river from Petrolia a huge slide occurred, the mountain side partly going into the water and throwing a dam half way across the stream.” The damage is consistent with the Toppozada and Parke (1982) estimate of IX.

Samoa Peninsula: (pop. 200) In 1906 the Samoa Peninsula west of Eureka was home to the community of Samoa and a number of mills. Two warehouses were destroyed and subsidence observed. Log decks toppled and at least one mill was closed for an undetermined amount of time. Only one chimney toppled. Intensity VII.

Shelter Cove: (pop. 40) Shelter Cove in 1906 was a community of 40 residents and isolated ranches. The McKee Ranch was “entirely ruined by fissures” but that Notley’s Ranch, less than 1 mile from the inferred fault rupture suffered no damage. A man was milking a cow and the shaking threw the cow against him “knocking him over with the cow on top of him. The other animals were thrown to the ground also.” Wharves and warehouses suffered great damage displacing heavy creamery equipment. All chimneys were damaged but no one was injured. About 20 acres of land washed into the ocean. The wharf road was completely covered by a slide. Roads were also blocked by fallen trees. Intensity VIII.

Southern Humboldt: (pop. 500) In 1906 there were a number of small settlements scattered between the Eel River Valley and Shelter Cove including Blocksburg, Garberville, Briceland, Ettersburg, Harris, and Thorn. At Briceland the damage is described as severe but not as intense as at Petrolia. The Briceland store was displaced from its foundation and considerable stock fell from shelves. Local resident J. Bowden reported chimneys downed and the rupture of water and gas pipes. Between Briceland and Shelter Cove there were only two houses and both lost their chimneys. Intensity VIII.

Trinidad: (pop. 250) Felt by most people but no damage. Intensity IV - V.

COMPARING THE 1906 EARTHQUAKE TO LOCAL EVENTS

Humboldt County and the adjacent offshore area are one of the most seismically active areas in the contiguous 48 states (Dengler et al., 1992a). Five earthquakes in the past century have exceeded magnitude 7.0 and 14 earthquake since 1853 have produced peak MMI intensities of VIII or greater. Most of these earthquakes have been centered offshore or near Cape Mendocino, sparing the more populated Humboldt Bay region the strongest shaking levels. The best studied and the most damaging North Coast earthquake was the 1992 Cape Mendocino (M_w 7.1) earthquake centered onshore near Petrolia (Oppenheimer et al., 1993). The Humboldt Earthquake Education Center compiled a detailed isoseismal map of the event based on over 1000 surveys and damage reconnaissance (Dengler et al, 1992b). The 1992 earthquake resembled the 1906 shaking pattern in a number of ways. The strongest ground motion for both events was centered in the Petrolia area and the Eel River Valley where intensities were in the VIII to IX range. One building that was damaged in both earthquakes illustrates the similarities (Figure 9). In 1906, the General Mercantile in Ferndale was only 4 months old. The entire brick parapet collapsed in the earthquake and all the windows were broken (Figure 9a).



Figure 8. Pacific Lumber Company’s dock at Fields Landing, photographer unknown, courtesy Ferndale Museum.

In 1992 the building had become the Valley Grocery and suffered nearly identical damage (Figure 9b). However, not as much of the parapet wall failed in 1992 and only the large windows broke, suggesting that the 1992 ground motions, at least at this site, were less than 1906. The 1992 earthquake took place at the same time of year under very similar conditions – a high ground water table after a winter of heavy rainfall.

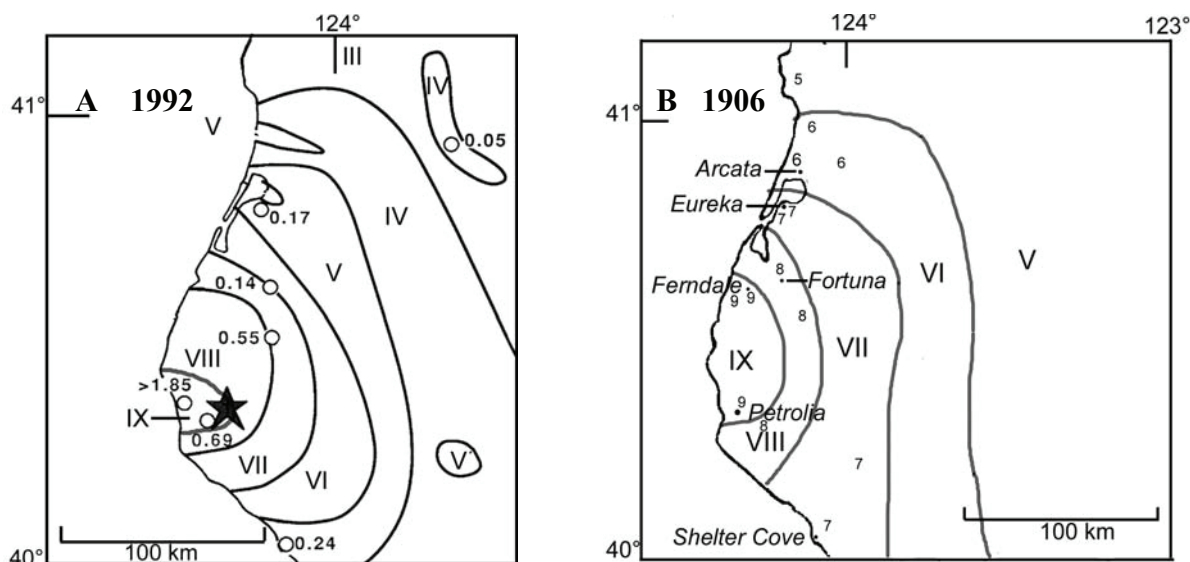


Figure 9. History repeats in Ferndale. A) The General Mercantile a few days after the 1906 earthquake, photograph by E. Garrett, courtesy of the Peter Palmquist Collection. B) The same structure (now the Valley Grocery) 86 years later, photograph taken April 25, 1992 by K. Bayless.

Liquefaction was observed at a number of sites in both the Mattole Valley near Petrolia and in the Eel River Valley. As in 1906, the most dramatic liquefaction features were linear lateral spreading cracks along the Salt River near Port Kenyon were three 20 to 30-foot long cracks with up to 6 inches of extension and 2 to 3 feet of vertical displacement were observed (Taylor, 1992). However the 1992 were nowhere as extensive as the liquefaction features produced in 1906 (Figure 10).

Figure 11 compares the isoseismal maps from the 1992 earthquake with a revised 1906 map based on the present study. While the 1906 isoseismals are far less certain than 1992, the general pattern is similar. For all zones the 1906 areas are larger. The 1906 intensity VII and larger area is about twice the size as in 1992.

AFTERSHOCKS

In the six weeks following the 1906 earthquake, at least 22 earthquakes were reported felt in Humboldt County (Table 1), including the largest event in the post April 18 sequence. There is no question that this spurt of activity was triggered by the 1906 main shock; no felt earthquakes had been reported in Humboldt County during the preceding year (Townley and Allen, 1939). These events were all likely centered in Humboldt County and the adjacent offshore area as none, with the exception of the largest event on April 23, were felt outside of Humboldt County. Meltzner and Wald (2003) in their examination of 1906 aftershocks and triggered events note two additional large events, an $M \sim 6.3$ earthquake near Shelter Cove on 11 August 1909 and a $M \sim 6.7$ near Cape Mendocino on 28 October 1909 which they also link to the 1906 earthquake. While the August 1909 event was possibly on the San Andreas, the two 6.7's were clearly not. The April 23, 1906 event was most likely centered within the Gorda basin, on a fault similar to the 1980 and 2005 $M 7.2$ earthquakes, and the August 1909 was most likely located on the Mendocino fault. While all of the magnitude 5 and larger aftershocks/triggered events occurred at or beyond the termination of the rupture zone (Meltzner and Wald, 2003), much more of the energy release was at or beyond the northern termination where all of the $M > 6$ events occurred.

Table 1. Aftershocks felt in Humboldt County between April 18 – May 30

18-Apr	5:22 AM	Slight and short duration, MMI III	1,2
18-Apr	12:25 PM	Slight and short duration	1,2
19-Apr	night	Slight shock in night	1
19-Apr	3:00 AM	slight	2
19-Apr	5:22 AM	slight	2
19-Apr	6:07 AM	slight	2
19-Apr	10:30 AM	slight	2
19-Apr	11:10 PM	Felt in Eureka	2
20-Apr	3:00 AM	Slight earthquake, duration 3 seconds	1,2
23-Apr	12:48 AM*	Stopped clocks Trinidad and Cape Mendocino	2
23-Apr	1:10 AM	Quite a severe shock, stopped clocks, MMI VII, M 6.7	1,2,3,4
23-Apr	1:17 AM	Felt at Cape Mendocino	2
23-Apr	6:07 AM	Slight shock, lasted 4 seconds	1,2
23-Apr	6:30 AM	Severe in Ferndale	2
27-Apr	10:30 AM	Sharp shock, also reported in Ferndale	1,2
30-Apr	1:10 PM	Slight shock, Felt in Eureka	1,2
30-Apr	10:58 PM	Felt at Cape Mendocino	2
9-May	7:25 PM	Slight shock, sufficient violence to shake buildings	1,2
9-May	9:30 PM	3 second duration in Ferndale	2
10-May	6:47 AM	Felt at Blocksburg, may be the same event as below	2
10-May	6:59 AM	Sudden jolt, 4 seconds duration, felt Eureka and Ferndale	1,2
18-May	8:30 PM	Felt at Cape Mendocino, may be the same event as below	2
18-May	8:54 PM	Slight at Ferndale	2
19-May	4:47 AM	Very slight at Ferndale	2
22-May	early AM	Very slight at Ferndale	

CONCLUSION

The 1906 earthquake directed considerable energy into Humboldt County north of the termination of rupture. The zone of MMI VII and stronger shaking extends from the southern edge of the county to Eureka and most of the Humboldt Bay region. The greatest damage was in the Eel River and Mattole River Valleys where intensities reached IX. The impacts and general pattern of damage was similar to the strongest local event, the 1992 Cape Mendocino earthquake but the 1906 intensity VII and larger zone is nearly twice as large. The 1906 earthquake triggered a number of large events on the North coast in the two years following the main shock including the three largest events in the 1906 aftershock sequence.

ACKNOWLEDGEMENTS

This study drew extensively on the collections at the Humboldt Room, Humboldt State University Library, Humboldt County Historical Society, Ferndale Museum and Historical Society and the Clarke Museum in Eureka. Thanks to the efforts of local historians Ellin Beltz, Ann Roberts, Pamela Service and the late Evelyn McCormick. Thanks to the late Peter Palmquist for preserving the photographs of Ed and Edna Garrett and making them available for this study.

REFERENCES

Brown, R.D., and Wolfe, E.W., 1972, Map showing recently active breaks along the San Andreas fault between Point Delgada and Bolinas Bay, California, U.S. Geological Survey Miscellaneous Investigations Series Map I-692, scale 1:24,000 2 sheets.

- Brown, R.D., 1995, 1906 surface faulting on the *San Andreas* Fault near Point Delgada, California, *Bulletin of the Seismological Society of America*, vol.85, no.1, pp.100-110.
- Dengler, L., Carver, G., and McPherson, R., 1992, Sources of north coast seismicity, *California Geology*, v. 45, p. 40-47.
- Dengler, L., K. Moley, A. Lehre, and D. Masten, D. (1992). Isoseismal Maps of the April 25-26, 1992 Cape Mendocino Earthquake Sequence, *EOS Trans. Am. Geophys. Union*, 73, n.43, 503.
- Ferndale Enterprise, 1906, Ferndale, California (on line at <http://ebeltz.net/fieldtrips/1906quake-fdale.html>)
- Lawson, A.C. 1908, The California earthquake of April 18, 1906: Report of the State Earthquake Investigation Commission: Carnegie Institute, Washington, Pub. 87, 2 vols., atlas.
- McLaughlin, R.J., Ellen, S.D., Blake, M.C., Jayko, A.S., Irwin, W.P., Aalto, K.R., Carver, G.A., Clarke, S.H., 2000, Geology of the Cape Mendocino, Eureka, Garberville, and Southwestern part of the Hayfork 30 x 60 minute quadrangles and adjacent offshore area, Northern California, U.S. Geological Survey Miscellaneous Field Studies MF 2336
- McCormick, Evelyn, 1984, *Living With The Giants*, 303 Orchard St., Rio Dell, CA 95562
- Meltzner, Aron J, Wald, David J, 2003, Aftershocks and triggered events of the Great 1906 California earthquake, *Bulletin of the Seismological Society of America*, vol.93, no.5, pp.2160-2186
- Oppenheimer D. H., G. Beroza, G. Carver, L. A. Dengler., J.P. Eaton, L. Gee, F. Gonzales, M. Magee, G. Marshall, M. Murray, R.C. McPherson, B. Ramanowicz, B., K. Satake, R. Simpson, P. Somerville, R. Stein, D. Valentine, 1993, The Cape Mendocino, California, Earthquake of April 1992: Subduction at the triple junction, *Science*, 261, 433-438
- Prentice, Carol S., Merritts, Dorothy J., Beutner, Edward C., Bodin, Paul, Schill, Allison, Muller, Jordan R., 1999, Northern San Andreas fault near Shelter Cove, California, *Geological Society of America Bulletin*, Vol. 111, 512-523
- Stover, C.W., Coffman, J.L., 1993, *Seismicity of the United States, 1568-1989 (Revised)*, U.S. Geological Survey Professional Paper 1527.
- Taylor, C., 1992, Ground Failures and liquefaction investigated in EERI Special Earthquake Report – July 1992.
- Topozada, T. R., Parke, D.L., 1982, Areas damaged by California Earthquakes, 1900 – 1949, Annual Technical Report to U.S. Geological Survey Open File Report 82-17 SAV, California Division of Mines and Geology.
- Townley, S.D., Allen, M.W., 1939, Descriptive Catalog of earthquakes of the Pacific Coast of the United States 1769 to 1928, *Bulletin of the Seismological Society of America*, Vol. 29, 297 pp.
- Tracy, J.P., 1906, Earthquake Letter by Joseph Prince Tracy (1879-1952), Eureka, written to his sister, original in the Humboldt County Historical Society, 703-8th St., Eureka, CA 95501.
- U.S. Weather Bureau, 1906, Daily Local Record, U.S. Department of Agriculture, Weather Bureau, Eureka California.
- Woodward-Clyde Consultants, 1980, Evaluation of the potential for resolving the geologic and seismic issues at the Humboldt Bay Power Plant Unit No. 3 / Prepared for Pacific Gas and Electric Company, Woodward-Clyde Consultants, Walnut Creek, California, Report for Pacific Gas and Electric Co.

This page is left intentionally blank for notes.

Late Holocene Coseismic Subsidence and Coincident Tsunamis, Southern Cascadia Subduction Zone, Hookton Slough, Wigi (Humboldt Bay), California

Jason R. Patton¹ and Robert C. Witter²

ABSTRACT

In the past 3,650 years (cal. yr. B.P.) evidence of coseismic subsidence was recorded five times in stratigraphy of bay margin deposits in southern Humboldt Bay, California. There are five buried marsh soils along a 1-kilometer long transect adjacent to Hookton Slough, a tidal channel tributary in Humboldt Bay. Using the lateral extent of burial, the abrupt upper contacts to the soils, and the diatom biostratigraphy, soils subsided coseismically and those soil burials were accompanied by abrupt rises in relative sea level. Tsunami-transported sand, observed in the stratigraphy from Hookton Slough, was deposited directly on two soils at the time of subsidence. Buried soils at Hookton Slough are best explained by coseismic subsidence during Cascadia subduction zone earthquakes. Radiocarbon age estimates constrain timing of subsidence and allow me to estimate a recurrence interval of Cascadia subduction zone earthquakes in the Humboldt Bay region. A recurrence interval for these large earthquakes ranges from 650 to 720 years for the last 2,400 years. Three of the buried soils correlate to similar buried soils found at other sites around Humboldt Bay, and timing of subduction zone earthquakes at Hookton Slough overlaps with timing of earthquakes on the Little Salmon fault.

The largest subsidence estimates based on the paleoelevation method are determined to be a minimum of 0.9 meters. This minimum estimate is increased by utilizing the relief of the upper contact for one buried soil. The relief of the upper contact was over two meters. Since the paleoecology of the soil was freshwater pre-submergence, and the entire soil was coseismically buried by tsunami sands and then by tidal silts to clay-silts, the subsidence estimate is increased from less than one, to greater than two meters.

1. Cascadia Geosciences Cooperative, P.O. Box 392, Arcata, CA 95518, E-mail: jrp2@humboldt.edu
2. Oregon Department of Geology and Mineral Industries Coastal Field Office, 313 SW 2nd St., Suite D, Newport, OR 97365
Phone: (541) 574-7969; Fax: (541) 265-5241 E-mail: rob.witter@dogami.state.or.us

INTRODUCTION

The principal objective of this study is to identify buried tidal marsh soils in sediments near Hookton Slough and assess whether each soil was buried due to abrupt tectonic subsidence and whether land level changes are concurrent with tsunamis. Timing of the abrupt change is constrained with radiocarbon age determinations. Finally, correlations are made between the Hookton Slough earthquake chronology and the regional earthquake history.

Hookton Slough core sites are in a low-lying brackish marsh that mostly exists below mean higher high water, MHHW (Figure 1). Levees constructed up to the late 1920s (Shapiro and others, 1980) now prevent tidal inundation to core sites. However, portions of the study area are perennially submerged because levees restrict drainage of ground and surface water. At times the study site becomes flooded with as much as two meters of standing water, and flooding contributes to the preservation of subsurface stratigraphy.

METHODS

Paleoseismic investigations provide data on earthquake history. Atwater (1987) first suggested evidence of coseismic deformation of late Holocene estuarine deposits along the coast of Washington. Atwater (1987); Clarke and Carver (1992); Clague and Bobrowsky (1994); Nelson and others (1996a, 1996b, 1998); Hemphill-Haley (1995); Atwater and Hemphill-Haley, (1997); Kelsey, and others (2002); and Witter and others (2003) interpret mid- to late-Holocene buried tidal marsh soils to be caused by vertical land-level changes related to Cascadia subduction zone (CSZ) earthquakes. Since buried soils are not often exposed in cut banks in southern Humboldt Bay, research on buried soils requires coring in tidal marshes.

Fifty-three, 3-centimeter diameter gouge cores were hand driven to sample subsurface stratigraphy along the one kilometer transect: West, Center, and East Sections (Figure 1). In addition to gouge cores, nine vibra cores (7.5-centimeter diameter aluminum tubes) were taken at sites where gouge cores had the most complete stratigraphic section. The cores were driven down to 6 meters depth or until resistance by coarse sediment (pebbles up to 3-centimeter diameter) prevented further penetration. The core transect is sub-parallel to the break in slope, along the historic high tide line. Three main sub-transects, West, Center, and East sections, are separated by historic channels (blue lines; Figure 1).

If buried soils are to be considered evidence for coseismic subsidence, there are five criteria that could be satisfied (Nelson, 1996b). They include (1) suddenness of submergence, (2) submergence greater than or equal to 0.5 meters, (3) lateral extent of submergence over hundreds of meters, (4) coincidence of submergence with tsunami sands, and (5) synchronous submergence of correlative buried soils. In addition, Hemphill-Haley (1995) suggests three additional criteria: a significant change in diatom assemblage across a stratigraphic contact inferring a sudden change in land elevation, submergence indicated by the persistence of environmental change, and the presence of sand flat diatom species in the sand capping the mud. In this study not all five criteria were satisfied in order to demonstrate coseismic subsidence.

Fossil diatoms sampled from specific strata in vibra cores are used to infer changes in paleoenvironment relative to mean tidal level. Paleoenvironmental interpretation is based on the observation that Humboldt Bay organisms live in tidal range-restricted habitats based on salinity (Li, 1992; Manhart, 1992; Carver and others, 1998). Hemphill-Haley (1995) developed techniques to estimate paleoenvironment based on diatom assemblages in Willapa Bay, Washington using the Brackish Intertidal Diatom Index (BIDI). The BIDI is a ratio of the counts of groups of diatoms based on their modern tidal range and provides a qualitative estimate of paleoenvironment. BIDI values range from zero, inferring a sub-tidal environment, to one, inferring a more freshwater, high-marsh environment.

Age control for deposits is constrained using accelerator mass spectrometry ^{14}C age estimates (Jacoby and others, 1995; Nelson and others, 1996b; Atwater and Hemphill-Haley, 1997). Only identifiable plant material was used for age control. Samples that likely persist through time (large chunks of wood, charcoal) were not chosen because they are more likely to be reworked, thus overestimating the age of the deposit.

RESULTS

The Hookton Slough cores show evidence of soils recurrently buried suddenly by mud to muddy peat. Sandy deposits abruptly overlie three buried soils. Abrupt and persistent paleoenvironmental change, as inferred from diatom analysis, accompanies the abrupt and persistent lithostratigraphic change. Accelerator mass spectrometry ^{14}C age estimates constrain the timing of these changes.

Lithostratigraphy

Five buried muddy-peat to peat horizons are found (buried soils 1-5). Soil 1 is the most recent buried soil and soil 5 is the oldest buried soil. The soils are abruptly buried by either muds (soils 5 and 2) or by sands (soils 1, 3, and 4). The soils contain up to 100% fibrous peat.

The mud found between the buried soils has an abrupt (< 2 cm) lower contact (Figure 2) and a gradual (5 to 15 cm) upper contact. The abrupt lower contact indicates a rapid stratigraphic change and the gradual upper contact indicates a slower stratigraphic change. The mud consists of silty clay to silt loam.

The sand overlying soils 3 and 4 commonly consists of multiple normally graded beds of sand to sandy loam. The sand's lower contact is abrupt, often with a wavy 1- to 4-centimeter relief. Commonly incorporated within the sand are 0.5- to 3-centimeter diameter rip-up clasts consisting of pieces of mud and pieces of fibrous peat (possibly from the underlying soil; Figure 2).

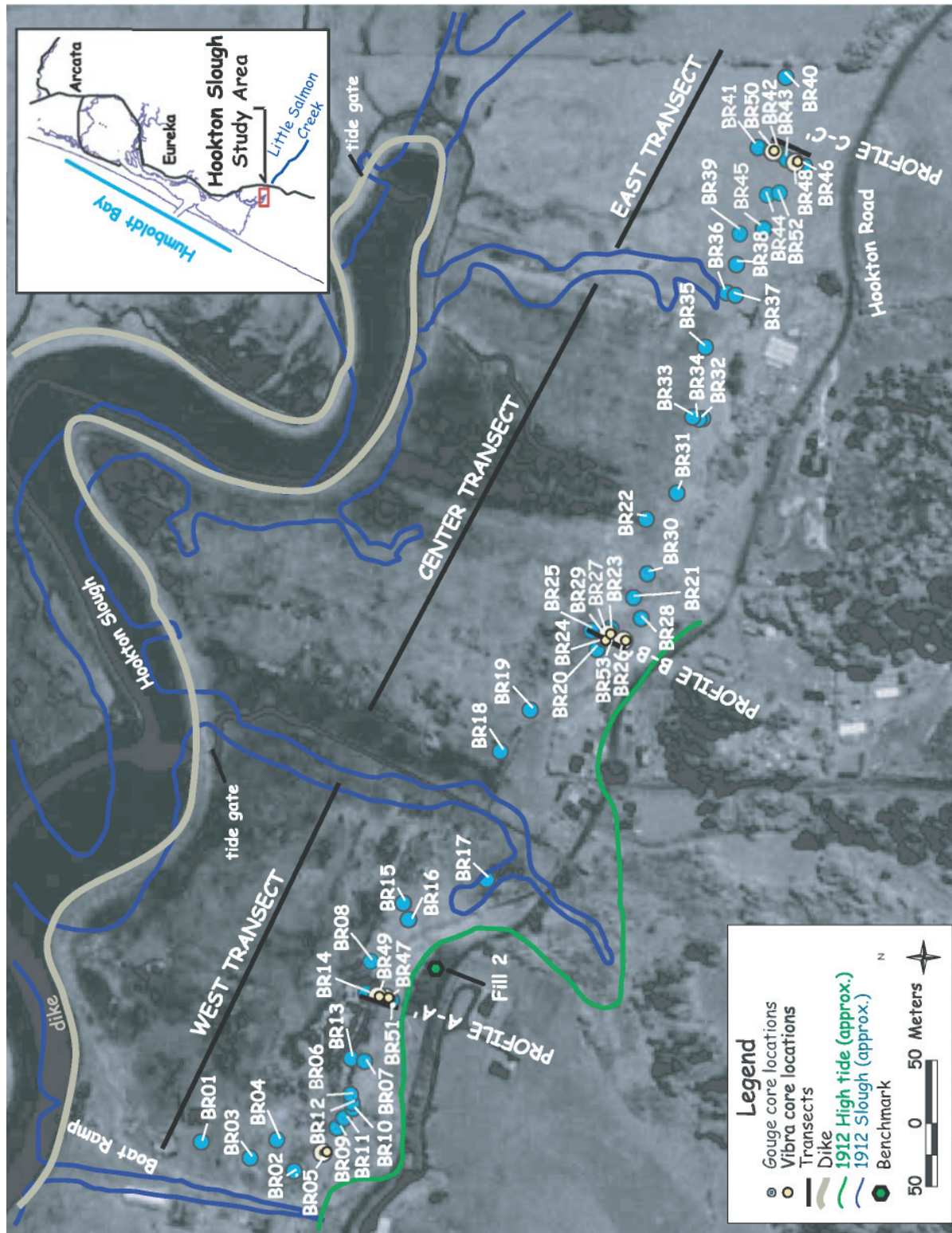


Figure 1. Hookton Slough core location map. Blue circles mark locations of gouge cores. Yellow circles mark locations of vibra cores. West, Center, and East transects are separated by historic tidal channels in green. 1912 high tide line in blue shows that all core locations were tidally inundated before the levees were constructed (Coast and Geodetic Survey, chart 18622, 1912). Tide gates permit partial tidal influence to study area. Imagery is a USGS panchromatic Digital Orthophoto Quarter Quadrangle, Fields Landing, 1989, with one meter pixels. Figure 4 photo point is shown along boat ramp. Hexagon indicates the location of the USGS benchmark (PID LV0658) "Fill 2."

Coarse gravelly sand to sandy loam defines the depth of core refusal, which ranges from 1.5 to 6.1 meters depth (Figure 2). These deposits are interpreted to be colluvium from the Pleistocene Hookton Formation, found in outcrop directly upslope to the south of the coring transect.

Biostratigraphy

Based on plants (Triglochin) and diatom assemblages, soils found at Hookton Slough were likely developed in high marsh to upland environments and the overlying muds were deposited in low marsh environments (Figure 3). Environmental change inferred from fossil diatoms in cores 5A and 49 (analysis by Eileen Hemphill-Haley) reflects a high marsh to upland paleoenvironment abruptly changing to a tidal flat paleoenvironment for burial of soil four and a low marsh paleoenvironment to tidal flat paleoenvironment for burial of soil three (Figure 3). The abrupt change in inferred environment correlates with an abrupt lithostratigraphic change. A freshwater paleoenvironment of the coarse gravelly sand to sandy loam below the oldest buried soils is based on diatoms and the presence of phytoliths.

Radiocarbon Age Determinations

Hookton Slough buried soils 1, 3, 4, and 5 contained materials suitable for radiocarbon age determinations. Age control is poor to non-existent for soils 1 and 2. Radiocarbon age determinations for soils 3, 4, and 5 are summarized in figure 4.

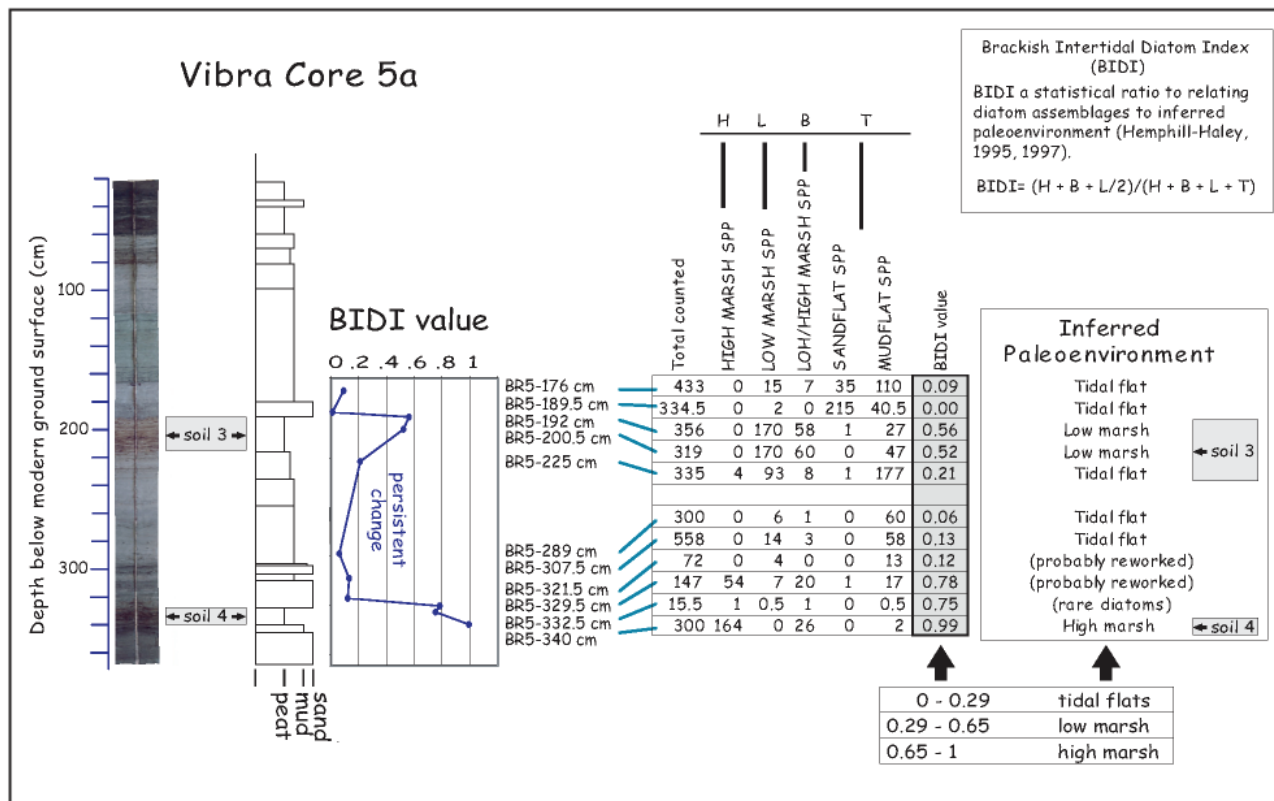


Figure 3. Diatom biostratigraphy in core 5a using the Brackish Intertidal Diatom Index (BIDI), developed by Hemphill-Haley (1995). In conjunction with disconformities above peats three and four, an abrupt change in inferred paleoenvironment occurs. Note that environmental change is persistent.

THIS PAGE LEFT INTENTIONALLY
BLANK
FOR
PATTON TABLOID FIGURE 2

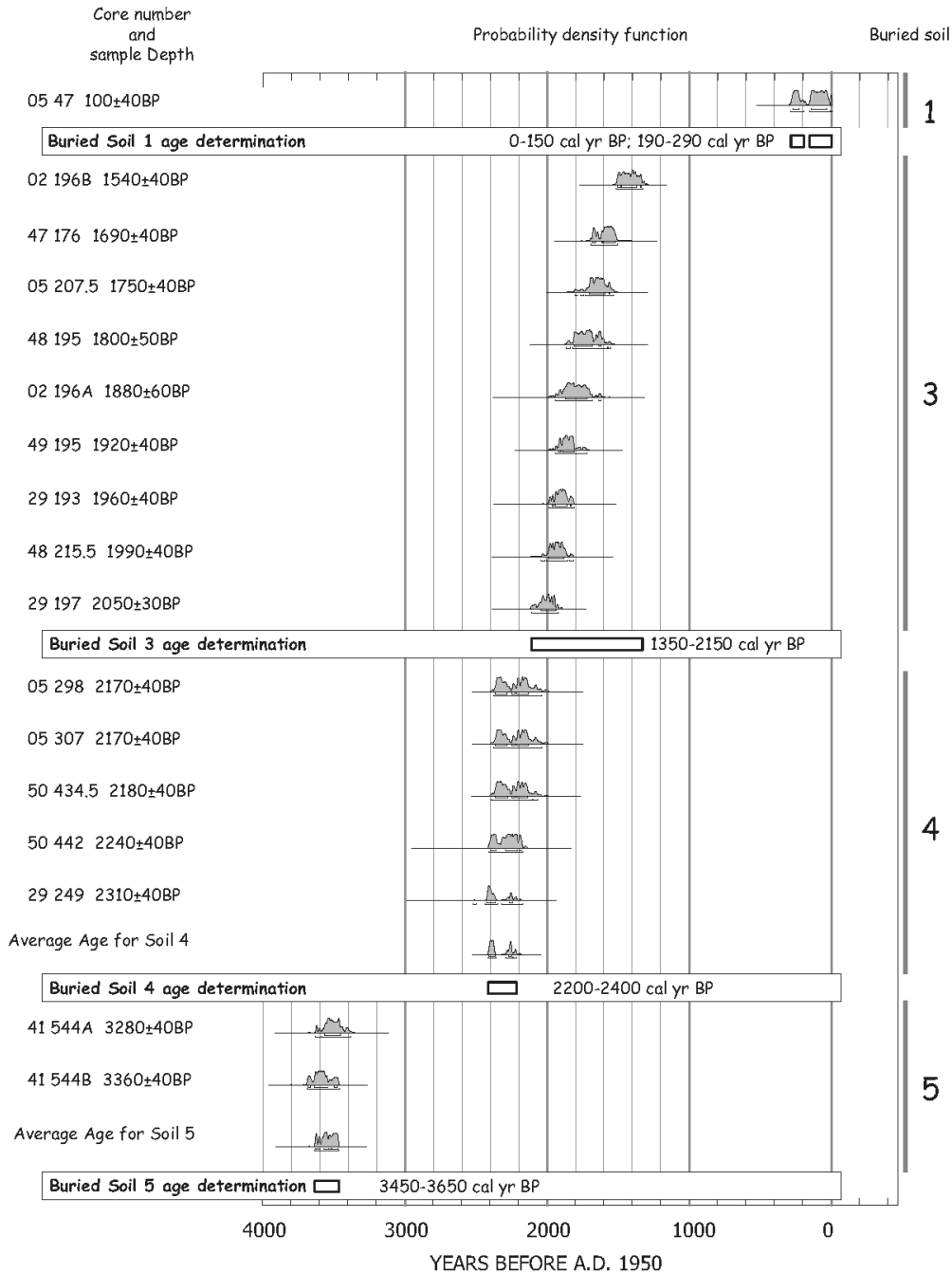
Figure 2. Hookton Slough vibra core stratigraphy for nine vibra cores. Triangles mark location of age control samples for vibra cores only. BIDI values indicate fossil diatom sample locations. Photo mosaic for each column is composed of six to fifteen overlapped photos. Peats are labeled with encircled numbers. Tsunami deposits are shown with encircled "t." Elevation is relative to MLLW for NOAA tidal benchmark (PID K1087).

THIS PAGE LEFT INTENTIONALLY
BLANK
FOR
TABLOID FIGURE 2

DISCUSSION

Subsidence Mechanism

Criteria used to infer coseismic subsidence of the five soils identified from cores in Hookton Slough include: 1) suddenness of change in depositional environment, 2) amount of subsidence, 3) lateral extent, 4) presence of sand capping peat, and 5) synchronicity of buried soils (Nelson, 1996b; Hemphill-Haley, 1995). These criteria are satisfied robustly for three of the five soils (Table 1).



These criteria are satisfied robustly for three of the five soils (Table 1).

Possible alternative explanations for all soil burials include cut-and-fill by tidal streams, sediment deposition by storms or floods, fluctuations in sea level, or intermittent closure of the mouth to Humboldt Bay. None of these alternative explanations is supported by field data.

In summary, abrupt and persistent lithostratigraphic and biostratigraphic changes coincide in sufficient frequency and over a sufficiently broad area (at least 48,000 m²) to verify the inference that several tidal marsh soils at Hookton Slough were buried by coseismic subsidence accompanying CSZ earthquakes. Coseismic subsidence occurred five times in the Hookton Slough region in the last 3,700 years.

Figure 4. Radiocarbon Probability Density Function plots of sequence analysis procedure using Bronk-Ramsey (1995, 2001). Lab reported age estimates are combined before calibration resulting in averaged calibration ages. Interpreted age ranges for each buried soil are delineated by rectangles. Due to potential problems with soil 3 sample material, soil 3 age is determined with the span of individual calibrated ages. Soils 4 and 5 ages are interpreted from calibrated average ages. Sample nomenclature and axis values are the same as for figure 9. Atmospheric data from Stuiver and others (1998a, 1998b); Calibration software: OxCal v3.5 (Bronk Ramsey 1995, 2001); and Calib (Stuiver and Reimer, 1986, 1993)

Table 1. Lateral extent and stratigraphic characteristics for the buried soils at Hookton Slough, Humboldt Bay.

Buried Soil	Number of cores that sampled buried soil *	Minimum lateral extent of buried soil *	Depth range of buried soil (MLLW, cm) †	Number of cores with overlying sandy deposit *	Maximum thickness (cm) of sandy deposit	Maximum number of beds in sandy deposit
1	44	940 m	111 to 41	1	10	1
2	17	900 m	75 to 22	0		
3	29	1,000 m	-28 to -153	4	24	5
4	20	920 m	-121 to -353	9	45	9
5	1	1 m	-380	0		

* see Figure 10

† Mean Lower Low Water (MLLW)

Subsidence Magnitude

Estimates of subsidence magnitude may be made using the paleoelevation estimate and augmented by the pre-burial ground surface relief estimate. Paleoenvironment based on fossil diatoms is used to estimate paleoelevation range (Kelsey and others, 2002; Witter and others, 2003; Figure 5). Paleoenvironment is based on elevation relations between modern vascular plants and modern diatom zonation in southern Oregon (Nelson and Kashima, 1993). Changes of paleoelevation are determined by subtracting paleoelevation ranges of the buried soil from the overlying mud (Figure 5-A). Minimum and maximum paleoelevation estimates of submergence for soil 4 are 0.9 and 3.1 meters, respectively. Minimum and maximum paleoelevation estimates of submergence for soil 3 are 0.0 and 1.6 meters, respectively. Because the upland and mudflat elevation ranges are limited to 1 meter by truncating the unbounded upper and lower ends respectively (Figure 5), this method does not measure maximum submergence greater than 0.9 meters. Therefore, the maximum submergence estimate can be larger and is thus a lower limiting maximum.

For estimates using the pre-burial ground surface relief measurements, minimum submergence is larger than the paleoelevation method. Assuming the relief of buried soil 4's upper contact represents pre-existing topography, all of soil 4 was in an upland setting, and mud overlying buried soil 4 was deposited in a tidal flat setting (Figures 3 and 5), pre-subsidence elevation of soil 4 is constrained by paleoelevation estimate for sediment sampled from core 5A (Figure 5-B, a). Post subsidence elevation control is based on the highest position for soil 4 being at the highest elevation in the mudflat ecological range. Minimum submergence estimates are made by subtracting the lowest possible elevation of the topographically highest position of soil 4 in core 5A (pre-subsidence elevation minimum = 3.2-meters MLLW) from the highest possible elevation of the same highest topographic position of soil 4 in core 5A (post-subsidence elevation maximum = 0.3-meters MLLW). Modern tidal range is almost as large as the relief of soil 4. Only soil 4 upper contacts are sufficiently large with respect to tidal range to reliably use the relief method for a submergence estimate.

The paleoelevation minimum subsidence estimate cannot measure submergence larger than 0.9 meters. Given the uncertainty in paleoelevation estimates for the range of elevations of soil 4, topographically above soil 4 in core 5A, the relief derived minimum submergence estimate for soil 4 is 2.9 meters.

Maximum submergence cannot be completely measured with either method, because upper bounds of upland environments and lower bounds of mudflat environments cannot be constrained. Maximum submergence estimate methods need to be improved to better estimate subsidence maxima. Because the paleoelevation method cannot measure minimum submergence greater than 0.9 meters, the soil relief method is necessary in future studies to make better estimates of submergence in cases where subsidence may be greater than 0.9 meters, in this case, 2.9 m.

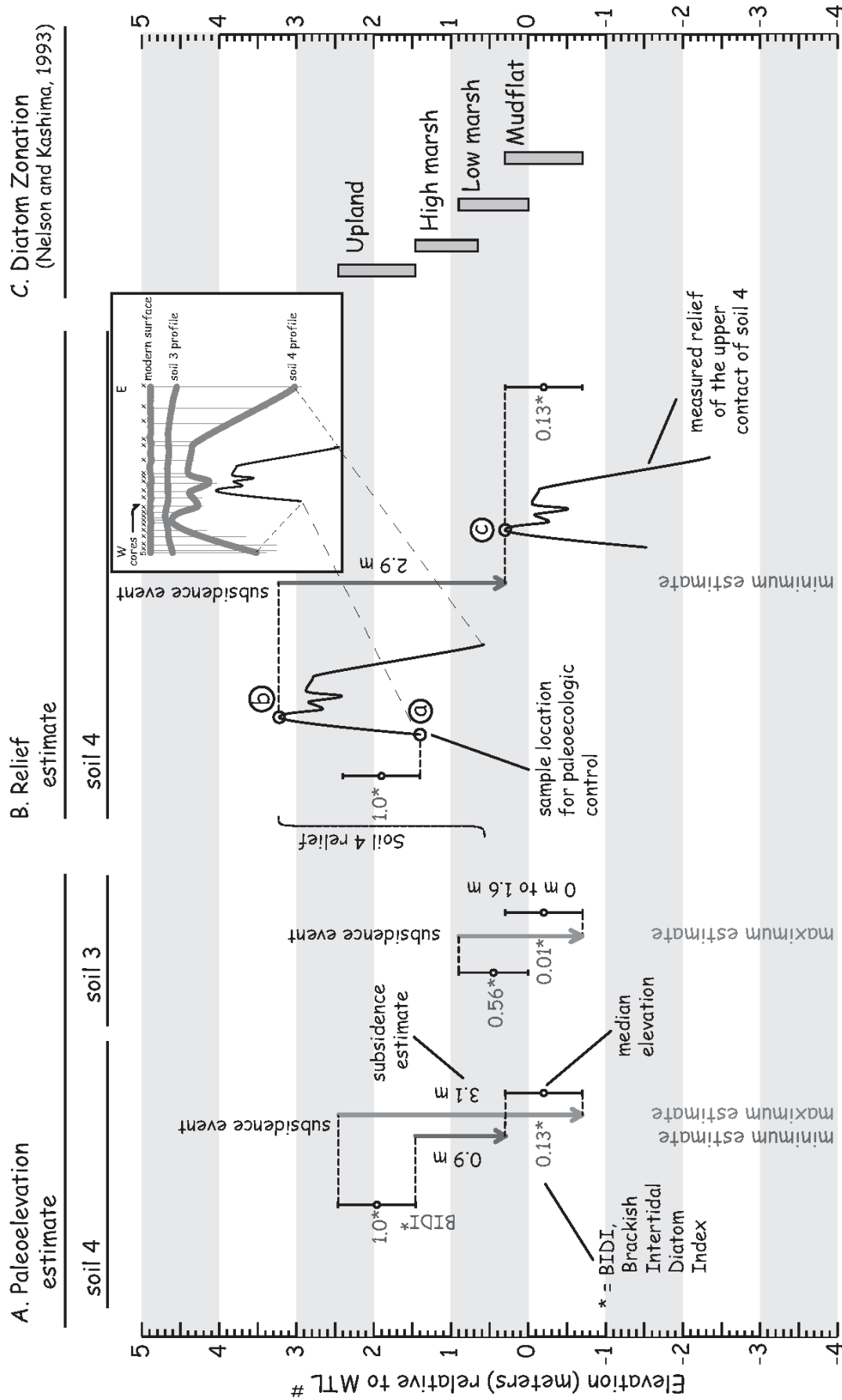


Figure 5. Subsidence magnitude estimates are made using paleoelevation and topographic relief methods. A. Changes of paleoelevation are determined by subtracting paleoelevation ranges of the buried soil from the overlying mud. B. Minimum submergence estimates are made by subtracting the lowest possible elevation of the topographically highest position of soil 4 in core 5A (post-subsidence elevation minimum = 3.2-meters MLLW; Fig. 12-B, b) from the highest possible elevation of the same highest topographic position of soil 4 in core 5A (post-subsidence elevation maximum = 0.3-meters MLLW; Fig. 12-B, c). Pre-subsidence elevation of soil 4 is constrained by paleoelevation estimate for sediment sampled from core 5A (Fig. 12-B, a). Post subsidence elevation control is based on the position of the highest position for soil 4 being at the highest elevation in the mudflat ecological range (Fig. 12-B, c). C. Diatom zonation is based on modern diatom ecology from coastal marshes in Oregon. The upper limit of the upland elevation range is truncated so that the range is 1 meter (Kelsey and others, 2002, Witter and others, 2003). Likewise, the mudflat elevation range is truncated on the lower end so that the range is 1 meter.

Coarse Sediment Deposition

There are several stratigraphic and paleontologic attributes of the Hookton Slough sandy sediment (“sand”) that permit an interpretation that it is of tsunamigenic origin. A sand-laden tsunami inundated Hookton Slough following at least two coseismic subsidence events. Rip-up clasts and sand intrusions into the underlying soil imply the tsunami had high flow velocities sufficient to erode the buried soil substrate. Multiple fining-upward sandy beds imply that the tsunami for each earthquake consisted of multiple waves. The coincidence of the tsunami deposits and the magnitude of soil burial, taken together, support the conclusion that CSZ earthquakes caused the subsidence at Hookton Slough.

In addition to tsunami deposits associated with buried soils 3 and 4 at Hookton Slough, Carver and others (1998) identified tsunami deposits in southwestern Humboldt Bay, six kilometers west of the Hookton Slough site.

Ages of Coseismic Subsidence Events

Hookton Slough stratigraphy records at least five coseismic events within the last 3,700 years. Radiocarbon age estimates are made on four of the inferred events (Figure 4).

In summary, five subduction zone earthquakes occurred in the last ca. 3,500 years in southern Humboldt Bay. The most recent was the A.D. 1700 earthquake and the other three age constrained buried soils (3, 4, and 5) record earthquakes in the age windows of 1,350 to 2,150 yrs BP, 2,200 to 2,400 yrs BP, and 3,450 to 3,650 yrs BP respectively.

Recurrence Interval for Subduction Zone Earthquakes

A recurrence interval estimate for subduction zone earthquakes causing coseismic subsidence near Hookton Slough is 650 to 720 years. This estimate assumes buried soils 1, 2, 3, and 4 each record a subduction zone earthquake. Three interseismic intervals that span these four soils have a cumulative age span of 1,950 to 2,150 years assuming soil 1 subsided in 250 years BP and soil 4 subsided 2,200 to 2,400 years BP. Three intervals in a 2,200 to 2,400 year period yield a 650 to 720 year recurrence interval.

Correlation of Hookton Slough Earthquake Record to other Humboldt Bay Paleoseismic Sites and Tectonic Role of Little Salmon Fault

Using radiocarbon ages and stratigraphic relations, earthquake records at Hookton Slough are correlated to other Humboldt Bay paleoseismic sites at Salmon Creek valley (Carver and Burke, 1988; Clarke and Carver, 1992), Swiss Hall (Witter and others, 2002), and Mad River Slough (Vick, 1988; Jacoby and others, 1995)(Figure 6).

Inferred earthquakes near Swiss Hall (located two to three kilometers east of Hookton Slough) are correlated with inferred coseismic subsidence events at Hookton Slough (Figure 6). At the Swiss Hall site there is evidence for three, and possibly four earthquakes in sediment cores and trenches that crossed the western trace of the LSF at the bay margin (events 1, 2, 3, and 4, Figure 6). Based on stratigraphic relations and fossil diatom evidence, Witter and others (2002) conclude that the study site coseismically subsided three times, over an estimated area of at least 5,500 m² (events 2, 3, and 4, Figure 6). Witter and others (2002) also conclude that the study site also folded the buried soils during at least one event on the LSF (event 1, Figure 6). Within radiocarbon error, three buried soils (Hookton Slough events 2, 3, and 4, Figure 6) at Hookton Slough appear to correlate with three buried soils at Swiss Hall (Swiss Hall events 2, 3, and 4, Figure 6). Within radiocarbon error Hookton Slough buried soil 1 correlates to the Swiss Hall folding event 1(Figure 6). At Hookton Slough three of the correlative buried soils (soils 1, 3, and 4) are capped by sand sheets that include multiple graded beds and mud or peat or peaty mud rip-up clasts.

Salmon Creek valley fault trench studies conclude at least three earthquakes occurred in the last 2,000 years (Figure 6). Within large radiocarbon age determination error, three earthquakes at Hookton Slough (Hookton Slough events 1, 2, and 3, Figure 6) correlate with three earthquakes at Salmon Creek Valley (Salmon Creek valley events 1, 2, and 3, Figure 6). Salmon Creek valley fault relations record LSF history. Hookton Slough strata record CSZ earthquake induced subsidence. If these three earthquakes are correlative, then LSF and CSZ earthquakes coincide.

If Hookton Slough is sensitive to both CSZ and LSF earthquakes, and LSF earthquakes are independent and chronologically distinct, then we would expect more earthquakes in the stratigraphic record at Hookton Slough (which we don't). Therefore, either 1) CSZ and LSF earthquakes are coincident and Hookton Slough is sensitive to both earthquakes' deformation, 2) CSZ and LSF earthquakes are not coincident and Hookton Slough is not sensitive to LSF earthquake deformation, but sensitive only to CSZ deformation, or 3) CSZ and LSF earthquakes are coincident and Hookton Slough is not sensitive to LSF earthquake deformation, but sensitive to CSZ deformation. Swiss Hall is probably sensitive to both CSZ earthquakes and LSF earthquakes. Witter and others (2002) conclude that subsidence at Swiss Hall may be due to either the CSZ or the LSF. However, for the earthquake that buried soils ca. 540 – 1,230 years BP, subsidence occurred in both the footwall and the hanging wall (Witter and others, 2002). Therefore, the CSZ is probably responsible for the subsidence during this earthquake.

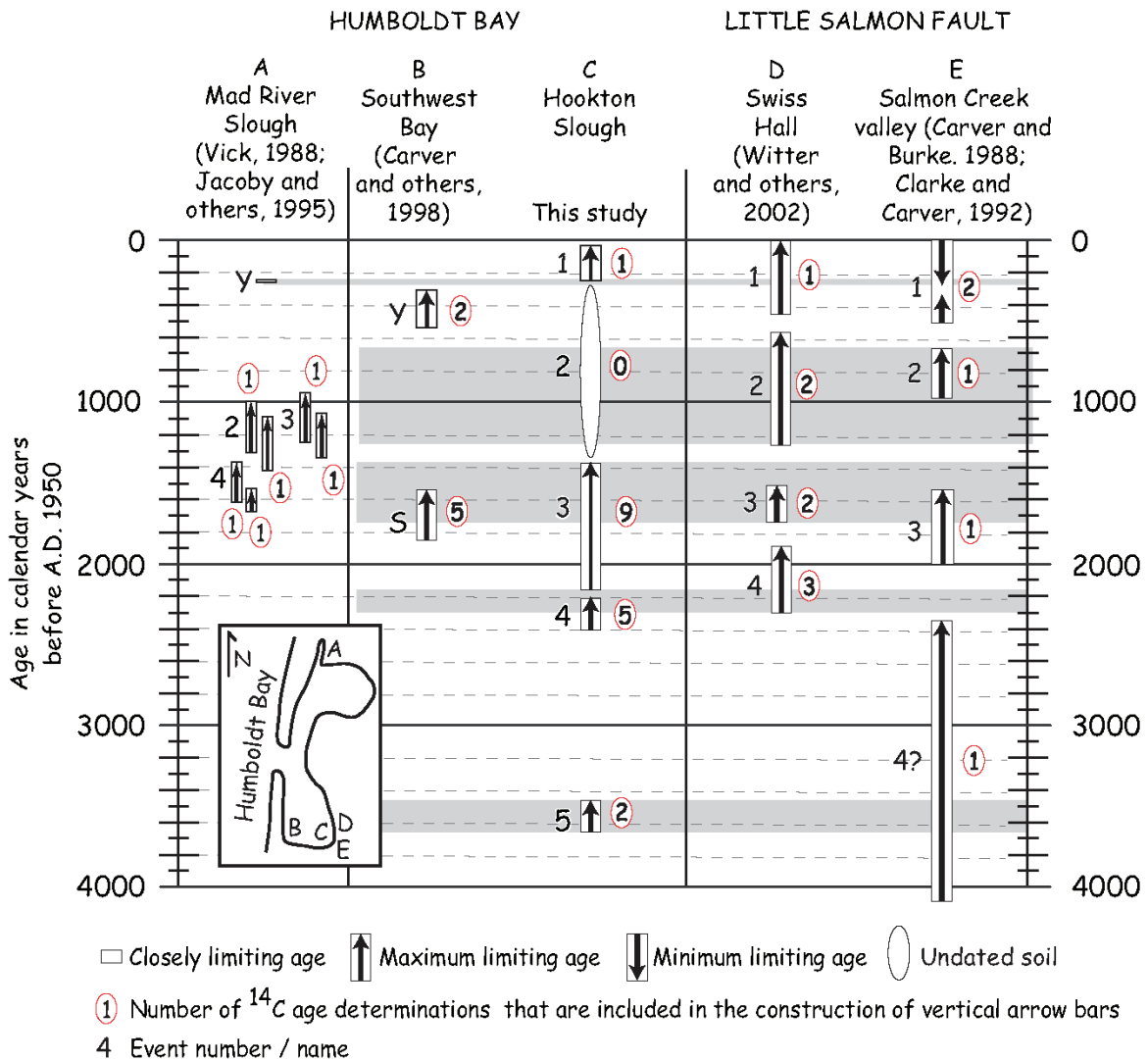


Figure 6. Correlation of earthquakes among Humboldt Bay study sites based on radiocarbon ages and stratigraphy.

Together the Hookton Slough and Swiss Hall studies demonstrate that, at least for some earthquakes, coseismic subsidence caused by earthquakes on the CSZ extends thousands of meters in the southern Humboldt Bay region and was coincident with generation of large tsunami and may be coincident with earthquakes on the LSF.

CONCLUSION

Southern Humboldt Bay has experienced at least four and possibly five CSZ earthquakes that caused subsidence and burial of tidal marsh soils in the past 3,700 years. Tsunami incursion in southern Humboldt Bay coincided with at least two earthquakes in the last 2,450 years. Preservation of tsunami deposits is highly localized.

Earthquakes at Hookton Slough occurred between 3,650 and 3,450, between 2,400 and 2,200, between 2,150 and 1,350, probably between 1,350 and 250, and finally around 250 years before A.D. 1950.

Four of these soils are correlated with earthquakes at the Swiss Hall site and they may correlate to the last three earthquakes at the Salmon Creek Valley trench site. A recurrence interval estimate for subduction zone earthquakes causing coseismic subsidence near Hookton Slough is 650 to 720 years.

Coincidence of tsunami deposits with abrupt subsidence provides evidence that CSZ earthquakes caused the subsidence observed at Hookton Slough and Swiss Hall. Within radiocarbon age determination error, upper-plate LSF earthquakes are coincident with CSZ earthquakes and thus the LSF may not be a source of coseismic subsidence independent of the subduction zone.

REFERENCES CITED

- Atwater, B. F., 1987. Evidence for Great Holocene Earthquakes Along the Outer Coast of Washington State, *Science*, vol. 236: 942-944.
- Atwater, B. F., Nelson, A. R., Clague, J. L., Carver, G. A., Yamaguchi, D. K., Bobrowsky, P. T., Bourgeois, J., Darienzo, M. E., Grant, W. C., Hemphill-Haley, E., Kelsey, H. M., Jacoby, G., Nishenko, S., Palmer, S., Peterson, C. D., and Reinhart, M.-A., 1995, Summary of Coastal Geologic Evidence for Past Great Earthquakes at the Cascadia Subduction Zone, *Earthquake Spectra*, vol. 11: 1-18.
- Atwater, B., and Hemphill-Haley, E., 1997. Recurrence Intervals for Great Earthquakes of the Past 3,500 Years at Northeastern Willapa Bay, Washington, States Geological Survey Professional Paper 1576. United States Government Printing Office, Washington, 108 p.
- Bronk Ramsey C., 1995, Radiocarbon Calibration and Analysis of Stratigraphy: The OxCal Program, *Radiocarbon*, vol. 37: 425-430.
- Bronk Ramsey C., 2001, Development of the Radiocarbon Program OxCal, *Radiocarbon*, vol. 43: 355-363.
- Carver, G.A., Burke, R. M., 1988, Final Report Trenching Investigations of Northwestern California Faults Humboldt Bay Region, United States Geological Survey Grant 14-08-0001-G1082, 53 p.
- Carver, G.A., Abramson, H.A., Garrison-Laney, C.E., and Leroy, T., 1998, Paleotsunami evidence of subduction earthquakes for northern California: Final Report for Pacific Gas and Electric Co., 164 p., plus appendices.
- Clague, J. J., Bobrowsky, P. T., 1994, Tsunami deposits beneath tidal marshes on Vancouver Island, British Columbia, in *Geological Society of America Bulletin*, vol. 106: 1293-1303.
- Clarke, S. H., and Carver, G. C., 1992. Late Holocene Tectonics and Paleoseismicity, Southern Cascadia Subduction Zone, *Science*, vol. 255: 188-192.
- Hemphill-Haley, E., 1995. Diatom evidence for earthquake-induced subsidence and tsunami 300 yr ago in southern coastal Washington, *Geological Society of America Bulletin*, vol. 107: 367-378.
- Jacoby, G., Carver, G., Wagner, W., 1995. Trees and herbs killed by an earthquake ~300 yr ago at Humboldt Bay, California, *Geology*, vol. 23: 77-80.
- Jacoby, G., Bunker, D. E., and Benson, B. E., 1997. Tree-ring evidence for an A. D. 1700 Cascadia earthquake in Washington and northern Oregon, *Geology*, vol. 25: 999-1002.
- Kelsey, H. M., Witter, R. C., and Hemphill-Haley, E., 2002. Plate-boundary earthquakes and tsunamis of the past 5,500 yr, Sixes River estuary, southern Oregon, *Geological Society of America Bulletin*, vol. 114: 298-314.
- Li, Wen-Hao, 1992, Evidence for the late Holocene coseismic subsidence in the lower Eel River Valley, Humboldt County, northern California: an application of foraminiferal zonation to indicate tectonic submergence: M.S. thesis, Arcata, California, Humboldt State University, Department of Geology, 87 p.

- Manhart, C. S., 1992, High-Resolution Foraminiferid Stratigraphy as Evidence for Rapid, Coseismic Subsidence: Preliminary results, in Carver, G. A., Burke, R. M. [eds.] *Friends of the Pleistocene Field Guidebook*, Humboldt State University, Department of Geology, Arcata, CA, 265 p.
- Nelson, A. R., Kashima, K., 1993. Diatom Zonation in southern Oregon Tidal Marshes Relative to Vascular Plants, Foraminifera, and Sea Level, *Journal of Coastal Research*, vol. 9: 673-697.
- Nelson, A. L., Jennings, A. E., and Kashima, K., 1996a. An earthquake history derived from stratigraphic and microfossil evidence of relative sea-level change at Coos Bay, southern coastal Oregon, *Geological Society of America Bulletin*, vol. 108: 141-154.
- Nelson, A. R., Shennan, I., and Long, A. J., 1996b. Identifying coseismic subsidence in tidal-wetland stratigraphic sequences at the Cascadia subduction zone of western North America, *Journal of Geophysical Research*, vol. 101: 6115-6135.
- Nelson, A. R., Ota, Y., Umitsu, M., Kashima, K., and Matsushima, Y., 1998. Seismic or hydrodynamic control of rapid late-Holocene sea-level rises in southern coastal Oregon, USA?, *The Holocene*, vol. 8: 287-299.
- National Oceanographic and Atmospheric Administration, NOAA, 2000. Gill, S. K. and Schultz, J. R., [eds.] *Tidal Datums and Their Applications*, NOAA Special Publication NOS CO-OPS 1, U. S. Department of Commerce, National Ocean Service, Center for Operational Oceanographic Products and Services, Silver Spring, Maryland, 115 p.
- Shapiro and Associates, (1980). Humboldt Bay Wetlands Review and Baylands Analysis, Report to Army Corps of Engineers, Vol. 1, 2, and 3.
- Stuiver, M., and Reimer, P. J., 1986, A computer program for radiocarbon age calibration, *Radiocarbon*, vol. 28:1022-1030.
- Stuiver, M., and Reimer, P. J., 1993, Extended 14C database and revised CALIB radiocarbon calibration program, *Radiocarbon*, vol. 35:215-230.
- Stuiver, M., Reimer, P.J., Bard, E., Beck, J.W., Burr, G.S., Hughen, K.A., Kromer, B., McCormac, F.G., v. d. Plicht, J., and Spurk, M., 1998a. INTCAL98 Radiocarbon age calibration 24,000 - 0 cal BP, *Radiocarbon*, vol. 40:1041-1083.
- Stuiver, M., Reimer, P.J., and Braziunas, T. F. 1998b. High-precision radiocarbon age calibration for terrestrial and marine samples, *Radiocarbon*, vol. 40:1127-1151.
- Vick, G., 1988, Late Holocene Paleoseismicity and relative vertical crustal movements, Mad River Slough, Humboldt Bay, California: M.S. thesis, Arcata, California, Humboldt State University, 88 p.
- Witter, R. C., Patton, J. R., Carver, G. C., Kelsey, H. M., Garrison-Laney, C., Koehler, R. D., and Hemphill-Haley, E., 2002. Final Technical Report: Upper Plate Earthquakes on the Western Little Salmon Fault and Contemporaneous Subsidence of Southern Humboldt Bay over the past 3,600 Years, Northwestern California. United States Geological Survey, National Earthquake Hazards Reduction Program, Award No. 01HQGR0215, 37 p.

Relative Tsunami Hazard Mapping for Humboldt and Del Norte Counties, California

Jason R. Patton¹ and Lori A. Dengler²

1. jrp2@humboldt.edu, Cascadia Geosciences Cooperative, P.O. Box 392, Arcata, CA 95521

2. lad1@humboldt.edu, Humboldt State University, Dept. of Geology, Arcata, CA 95521

ABSTRACT

Based on paleoseismic evidence from coastal marshes and on historic teletsunami inundation, coastal Humboldt and Del Norte Counties entertain a considerable tsunami hazard. Tsunami hazard maps are constructed using a raster-based geographical information systems (GIS) approach to depict the relative tsunami hazard of coastal Humboldt and Del Norte County in northern California (<http://www.humboldt.edu/~geodept/earthquakes/rctwg/toc.html>). The raster model is primarily based on topography, so the parameters may be easily adjusted as new hazard-elevation relations are developed through numerical modeling or other methods. In contrast to maps depicting hazard by a single inundation line, the raster model uses a gradational scale. Elevation, normally used for 2.5D surfaces, is substituted with safety units. Hazard is displayed as a safety index, a continuous gradational color scale ranging from red (high hazard) through orange (medium), yellow (low) to white (no hazard). Hazard-elevation relations were developed using existing numerical modeling, paleoseismic studies, historical tsunami flooding, and impacts of recent tsunamis elsewhere. Hazard units are further modified by distance to open water. An advantage to this approach is that tsunami hazard maps can be constructed even when numerical modeling does not exist and can be readily adjusted as new information/modeling results become available. The GIS framework facilitates ready adaptation by planners and emergency managers for use at different map scales. The maps are intended for educational purposes, to improve awareness of tsunami hazards, and to encourage emergency planning efforts of local and regional organizations by illustrating the range of possible tsunami events. The maps have been adopted by the Humboldt County Office of Emergency Services as part of their tsunami hazard mitigation plan.

INTRODUCTION

Humboldt Bay, the lower Eel River Valley, the Klamath River Valley, and Crescent City (Figures 1, 2, 3, and 4; Humboldt and Del Norte Counties) are located on the western edge of the North America Plate near the southern end of the Cascadia subduction zone (CSZ). Based on paleoseismic records along coastal North America (Atwater and others, 1995) and historic records in Japan (Satake and others, 1996), earthquakes generated by rupture on the CSZ have generated tsunamis. In addition to locally generated tsunami hazard, teletsunami from Chile (1960) and Alaska (1964) had devastating effect in Crescent City. Coastal northern California communities will better successfully survive coastal disaster when people are better educated about tsunami safety and preparedness. Maps are effective tools to help educate people about hazard safety.

Past inundation projections for the Humboldt Bay region (Toppazada and others, 1995, Bernard and others, 1994) depicted hazard as a single line that users found difficult to apply (Dengler and Preuss, 2003). More recently hazard mapping efforts were developed using a TIN to model hazard (Dengler and others, 2003). Both the Humboldt Bay and the lower Eel River Valley regions have previously been mapped with a similar method using a triangulated irregular network (TIN) model. This project was used to develop the relations between hazard, elevation, and distance to the open coast. One limitation of this method is that it is a cumbersome data model to edit and modify. This paper discusses the methods used to display tsunami hazard gradationally to promote a better understanding of the tsunami hazard and foster regional tsunami planning efforts.

METHODS

Relative tsunami hazard is displayed on maps as a color gradient that represents gradually decreasing hazard. The wide range of tsunami hazard is partitioned into three levels based on three different sources of tsunami. Hazard-elevation relations are used to display the hazard through these three levels.

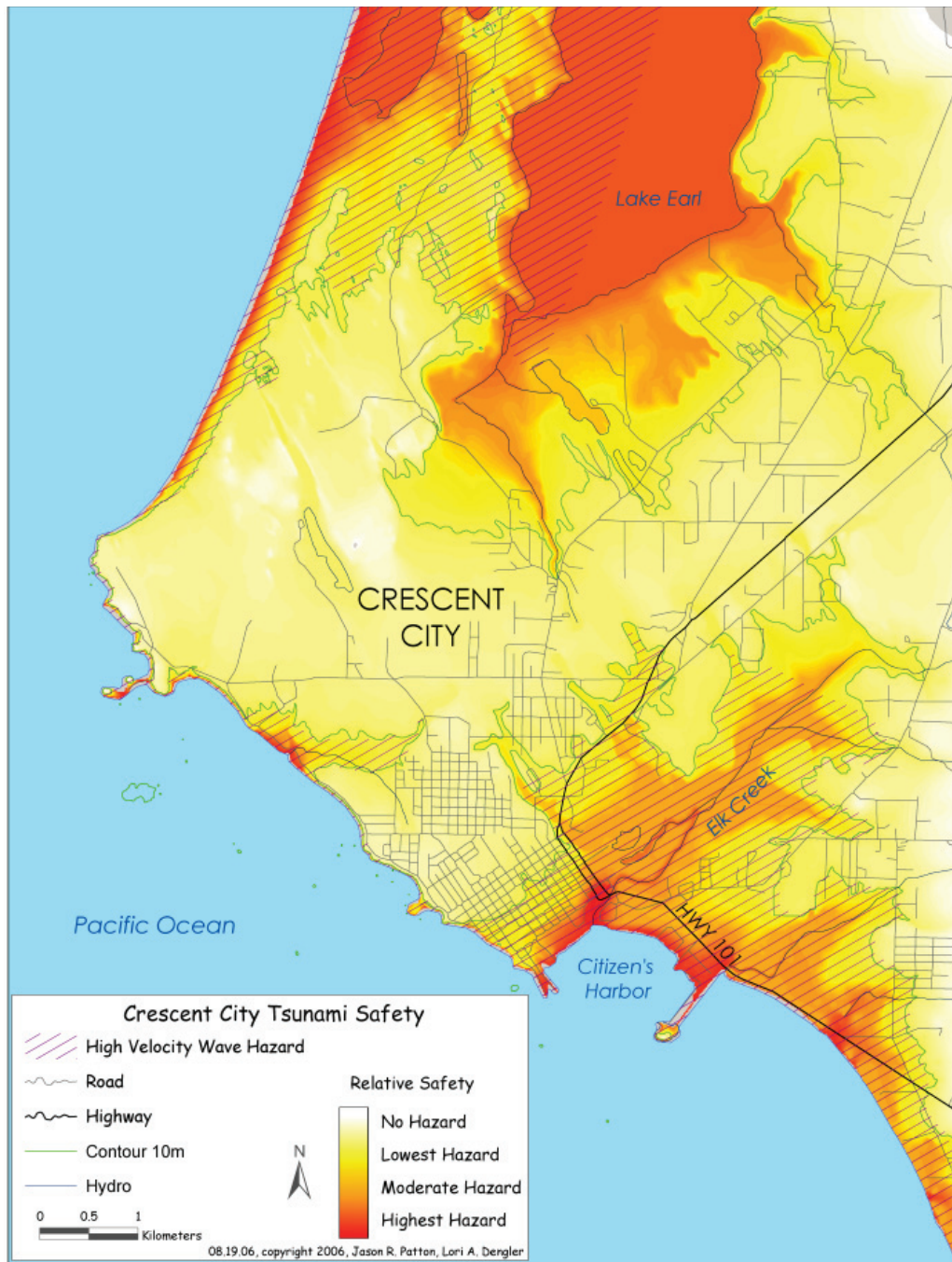


Figure 1. Crescent City relative tsunami hazard map. High velocity wave hazard is indicated by purple cross hatching. Ten m contour can be used to compare convergence of relative hazard in relation to distance to the coastline.

Tsunami hazard mapping for the north coast of California considers three levels of hazard including both teletsunami and local tsunami sources. The most hazardous level is the area that has likely been inundated historically by teletsunami. The moderately hazardous area includes areas likely to be inundated during a Cascadia subduction zone rupture generated tsunami. The lowest hazard area includes areas likely to be inundated during a worst-case scenario CSZ rupture with associated submarine landslide generated tsunami, during high tide, during a storm surge, and during high river discharge.

Each of these three levels of hazard has an associated run-up elevation range (Dengler and others, 2003, Patton and Dengler, 2004). On the open coast the high hazard run-up elevation is three meters, the moderate

hazard run-up elevation is ten meters, and the low hazard run-up elevation is thirty-five meters (Table 1). Hazard-elevation relations are developed by correlating increasing hazard with increasing elevation. A binomial regression equation (for the hazard-elevation relation) is used to convert elevation units to safety units.

There is a difference in the hazard between the open coast and further inland. Similar to Priest (1995) we further refine this estimate of range of tsunami hazard by including a component of the equation that considers distance to the coast. A grid is generated with cells that have values that diminish linearly to zero, twelve km from the coastline. Using map algebra a ten-meter resolution digital elevation model (DEM) is converted from elevation units to safety units with an equation that includes expressions standing for the hazard-elevations relations and the coastline-distance relations.

Another difference between the hazard along the open coast and that near more protected bodies of water, like Humboldt Bay, is the nature of the waves. The open coast is subjected to both elevated water levels and high velocity wave impact. In contrast, flooding within Humboldt Bay is more likely to resemble other flooding with locally high currents forced by changing water levels but no large wave impacts. In order to discriminate high-hazard on the open coast from high-hazard in tidally inundated areas that are protected from the coast, cross hatching representing high velocity wave hazard is displayed to a distance of 3km from the coastline. High velocity wave hazard is not displayed above 10 meters in elevation. Others have also limited how hazard is displayed based on topography (Priest, 1995).

Table 1. Elevation ranges for three hazard levels.

Hazard area boundaries are initially defined for each zone above based on elevation:

<u>Zone</u>	<u>Description</u>	<u>High</u>	<u>Moderate</u>	<u>Low</u>	<u>None</u>
Open Coast	Everywhere within 3km of coast	0 - 3 m elev	3 - 10 m elev	10 - 35 m elev	above 35 m elev

Finally a color gradient including red, orange, yellow, and white are applied to the associated safety unit values. By adjusting the percent of CMYK values for each step between the levels of hazard, a smooth color gradient is applied to the safety surface.

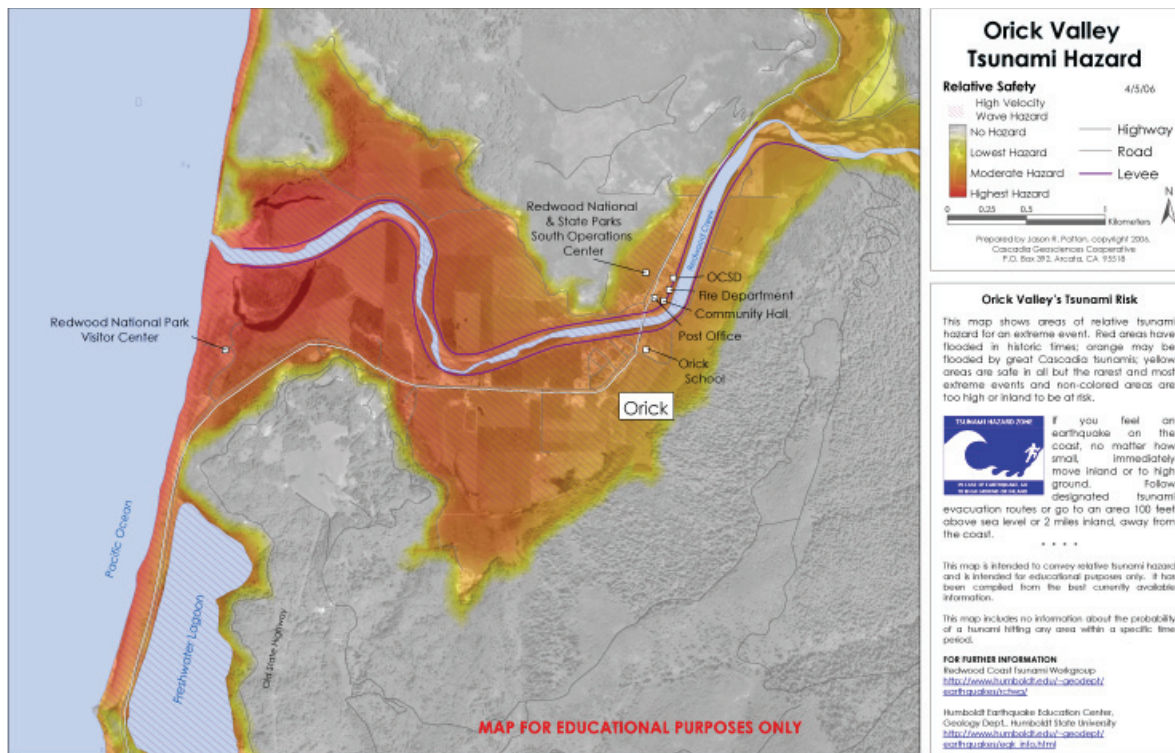


Figure 2. Orick Valley relative tsunami hazard map. This is very similar to the map used as placemats for a community fish fry as part of planning for the Orick community participation in the NOAA “Tsunami Ready Community” program. High velocity wave hazard is indicated by purple hatch marks. Orick is located in northern Humboldt County.

RESULTS

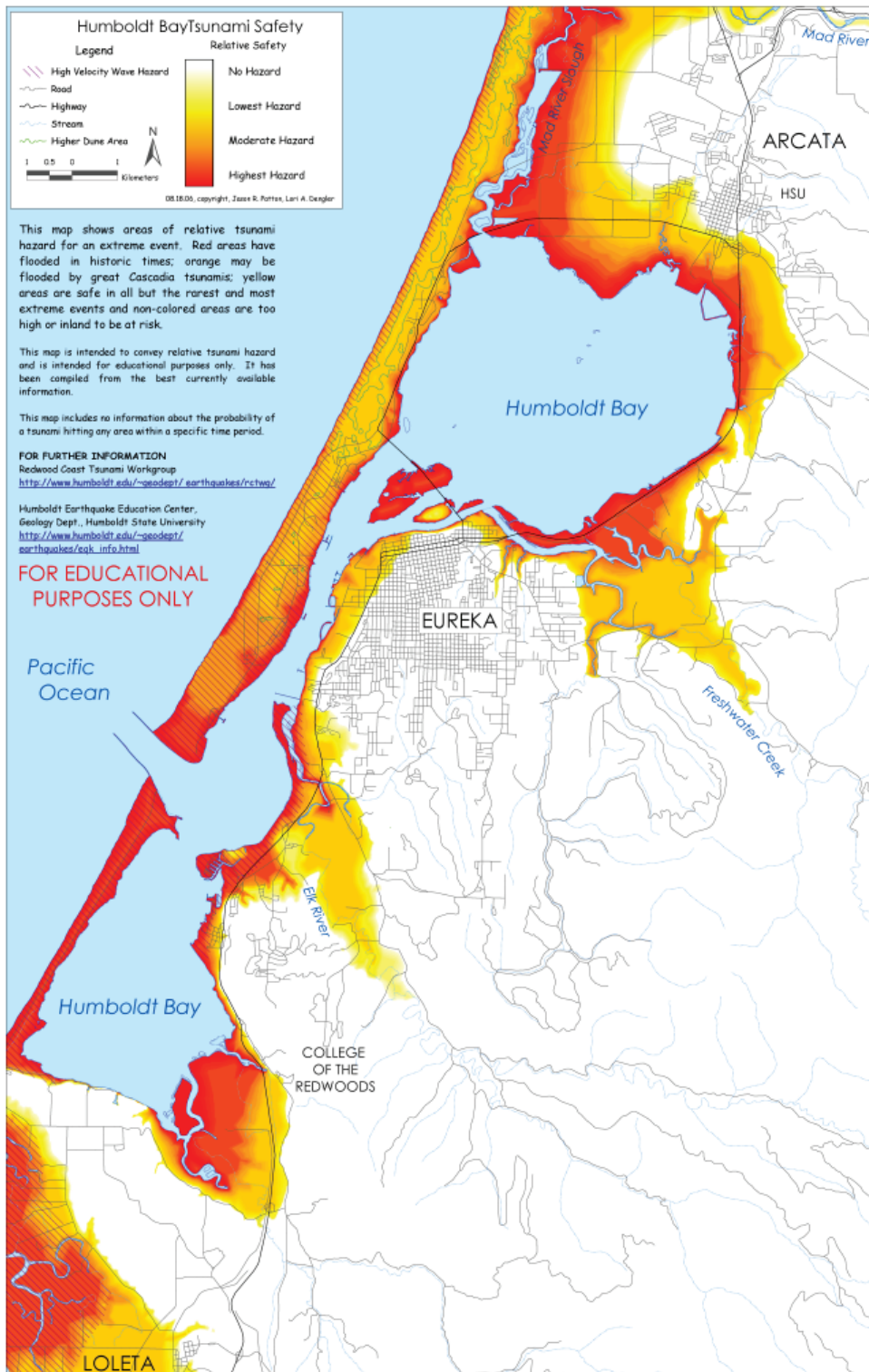


Figure 3. Humboldt Bay relative tsunami hazard map. High velocity wave hazard is indicated by purple hatches.

Since much of the community is low lying and close to the coast, tsunami awareness and education is extremely important.

The Humboldt Bay and lower Eel River Valley regions have been updated with the raster based method (Fig. 5). Humboldt County is currently adopting the Humboldt County Office of Emergency Services tsunami mitigation plan where a map series was produced with the results from this study.

Crescent City, Orick Valley, and the Humboldt Bay region have been mapped using this method. Products include placemats, county level hazard mitigation planning, and county fair educational posters.

Crescent City was the first region to be mapped with this method (Figure 3). Several places show how this mapping technique can adjust hazard based on the variables used. Low topography along Elk Creek is represented by higher hazard colors than the surrounding lower hazard, higher ground. The distance grid expression that reduces hazard with distance from the coast can be seen in Lake Earl that is safer on the east side since it is further from the coastline. A second way to see how the distance grid affects the safety index is by looking at the 10m contour line and how it converges and diverges from the safety index.

Orick Valley was the second map product generated with this method (Figure 4). The Orick Community Services District is using this map as part of their planning for the NOAA Tsunami Ready Community Plan.

DISCUSSION

Tsunami hazard can be determined using different methods including, but not limited to, numerical modeling, historic mapping, paleoseismic mapping, and mapping based on actual observations. Each of these methods has unique benefits and limitations. The benefits and limitations are based on what level of hazard is considered and how that hazard is displayed.

To date no direct relations have been developed between numerical models of inundation depth and hazard for this region. In the absence of numerical modeling, this method is a simple way to share essential material to communities in tsunami hazard zones. Once numerical modeling of inundation depth has begun, this study's model can be adjusted to incorporate the numerical modeling.

While many tsunami hazard maps represent single types of tsunami hazard, multiple levels of tsunami hazard are considered for north coastal California. Since numerical models of single types of hazard cannot display these multiple levels of various hazards, three lines would be required to display the hazard we display as a single color gradient. Three lines, with different relative hazard, would be confusing to the end user.

Single lines used in previous mapping efforts were also unable to display the uncertainty in the level of hazard. In maps from this study, since there are no lines separating distinct areas of varying hazard, it is difficult for one to be confused by the precise location where one moves from one type of hazard to another because the hazard changes gradually. However, uncertainty in the hazard-elevation relation is encompassed by the gradational nature of the color gradient in the maps from this study.

CONCLUSION

Relative tsunami hazard is clearly the best way to communicate geospatial relations of this hazard. Residents in low lying coastal areas have the opportunity to “see their house” on these maps, especially when panchromatic imagery (eg. DOQQs) is underlain below the safety index (Fig. 3). As effected regions are far reaching and emergency responders have limited affect in the immediate time following large earthquakes, people need to have these maps in their body of knowledge to ensure their survival. A picture is worth a thousand words and this type of modeling can be achieved at very little cost since DEMs are available globally. An added bonus is that numerical simulation data can be incorporated into the model to further substantiate its certainty.

REFERENCES CITED

- Atwater, B.F., Nelson, A.R., Clague, J.J., Carver, G.A., Yamaguchi, D.K., Bobrowsky, P.T., Bourgeois, J., Dari-enzo, M.E., Grant, W.C., Hemphill-Haley, E., Kelsey, H.M., Jacoby, G.C., Nishenko, S.P., Palmer, S.P., Peterson, C.D., and Reinhart, M.A., 1995, Summary of coastal geologic evidence for past great earthquakes at the Cascadia subduction zone: *Earthquake Spectra*, v. 11, no. 1, p. 1-18.
- Bernard, E., C. Mader, G. Curtis, and K. Satake (1994): Tsunami Inundation Model Study of Eureka and Crescent City, California. NOAA Technical Memorandum ERL PMEL-103, National Oceanic and Atmospheric Administration, Seattle, Washington, 80 pp.
- Dengler, L., Preuss, J., 2003, Mitigation Lessons from the July 17, 1998 Papua New Guinea Tsunami, *Pageoph*, Vol. 160, No. 10-11. 2001-2031.
- Dengler, L. A., B. R. Ludy, and J. R. Patton. 2003. Relative tsunami hazard maps, Humboldt County, California. *Eos Trans. AGU*, 84(46), Fall Meet. Suppl., Abstract OS22B-1162, 2003
- Patton, J. R., Dengler, L. A. (2004), GIS based Relative Tsunami Hazard Maps for Northern California, Humboldt and Del Norte Counties, *Eos Trans. AGU*, 85(47), Fall Meet. Suppl., Abstract OS23D-1353.
- Priest, G.R. (1995), Explanation of mapping methods and use of the tsunami hazard maps of the Oregon coast: Oregon Department of Geology and Mineral Industries, Open-File Report O-95-67, 95 p.
- Satake, K., Shimazaki, K., Tsuki, Y., and Ueda, K., 1996, Time and size of a giant earthquake in Cascadia inferred from Japanese tsunami records of January 1700, *Nature*, vol. 379: 246-249.
- Toppozada, T., G. Borchardt, W. Haydon, W., Petersen (1995): Planning Scenario in Humboldt and Del Norte Counties, California for a Great Earthquake on the Cascadia Subduction Zone, California Division of Conservation, Division of Mines and Geology Special Publication 115, 159 pp.

Long-Term Relative Sea Level Change and Implications to the Nuclear Waste Storage Facility at Buhne Hill, Humboldt County, California

Thompson, S.C., Page, W.D., and Witter, R.C.

ABSTRACT

A temporary, dry storage facility of nuclear waste (ISFSI) is being constructed at Buhne Hill on Humboldt Bay, the site of the Pacific Gas & Electricity Company (PG&E) Humboldt Bay Power Plant. In response to a request by the California Coastal Commission, PG&E evaluated the site conditions of their proposed facility for stability 'in perpetuity' by forecasting up to 100,000 years in the future potential changes from two geologic hazards: (1) the tectonic uplift of Buhne Hill, and (2) coastal erosion from projected sea level rise and Pacific storm variability that may result from global warming. This paper summarizes the analysis for coastal erosion hazard to Buhne Hill related to projected relative sea level rise over time periods of 100, 1,000, 10,000, and 100,000 years.

Relative sea level change results from both land level change and global sea level change. Land level change at Buhne Hill is dominated by long-term tectonic uplift at a rate of 1.2 ± 0.5 feet per thousand years (0.4 ± 0.1 mm/yr). Short-term land level change is dominated by elastic strain accumulation and release on the Cascadia subduction zone and Little Salmon fault zone, with permissible abrupt uplift or subsidence of up to a few meters during an earthquake on one or both of the sources. Global warming over the next century and beyond will cause a rise in sea level. Current emissions of greenhouse gasses, most notably carbon dioxide and methane, have produced higher atmospheric concentrations of those gasses than at any time in the past 420,000 years, and projected increases in temperature and sea level are expected to occur at rates that are an order of magnitude or higher than rates typical of the past few thousand years. The context for evaluating sea level change over the very long term is an assumption that the earth's climate remains in the cycle of glacial and interglacial intervals that have persisted for the past 2.5 million years. Changes in earth's orbit around the sun cause predictable variations in the solar insolation on earth, and these orbital variations closely correlate with glacial and interglacial cycles in the past. Current and projected solar insolation, combined with present day and near-future anthropogenic rise in greenhouse gasses, suggest that the earth may miss the next opportunity to enter the next glacial interval and hence global cooling may not start for another 50,000 years.

Over the next few hundred years sea level is expected to rise between less than one to as much as six feet, based on the 2001 report on climate change by the Intergovernmental Panel on Climate Change. In the thousand to ten thousand year time period sea level may rise and approach the ISFSI elevation of 44 feet (MLLW) with the extreme scenario of it being over topped. The maximum rate of sea level rise is not expected to exceed about 3.3 feet per century (10 mm/yr), the maximum rate of sea level rise recorded during an interglacial interval in the geologic record for the past 400,000 years. In the forecasts that consider climate change over for tens of thousands of years, glacial intervals are expected to resume with a corresponding drop in sea level. In all scenarios the long-term tectonic uplift of the site counters sea level rise.

Rise in sea level is a slow process (0.26 to 3.3 feet/100 years) and will be monitored. As the riprap protection at Buhne Hill is damaged, or possibly impacted, during increased storm activity and other changed conditions, additional riprap or other protection would be placed in front of Red Bluff and around Buhne Hill to insure the protection of the ISFSI. Over the next 100 years, barring a major earthquake on the Cascadia subduction zone, interseismic uplift will likely keep pace with sea level rise. However, a major earthquake on the Cascadia subduction zone would down drop King Salmon but may or may not cause abrupt coseismic subsidence of Buhne Hill. In this occurrence, PG&E would evaluate the integrity of the coastal protection works following the event and place additional riprap or other protection in front of Red Bluff to insure the protection of the ISFSI. In the unlikely scenario that the sea level rose above the elevation of the ISFSI in several thousand years, the site would be moved to a safe location.

INTRODUCTION

Pacific Gas & Electricity (PG&E) is constructing a temporary facility for dry storage of nuclear waste (ISFSI) at Buhne Hill, located adjacent to the PG&E Humboldt Bay Power Plant. For permitting, the California Coastal Commission requested additional technical information to demonstrate that the facility would be protected "in perpetuity" from the potential effects of global warming including rise in sea level and change in storm conditions. In response, PG&E prepared a report (Page, 2005) by

addressing the potential hazards from: (1) erosion caused by future sea level rise and changing wave heights and durations in response to projected global warming, and (2) an analysis of the potential tectonic uplift. This paper summarizes portions of PG&E's Coastal Commission report. Surface faulting potential is considered low and is described in detail elsewhere (PG&E, 2003).

SETTING

The Humboldt Bay ISFSI site lies directly east of the entrance to Humboldt Bay on the lee side of Red Bluff, the northwest facing side of Buhne Hill (also called Buhne Point) (Figures 1 and 2A). Buhne Hill is a small topographic high that is bordered by marshes to the northeast and south and by the bay to the northwest. The village of King Salmon is built on the sand spit that projects to the southwest of Buhne Point and on artificial fill of the adjacent marsh.

The proposed storage site will consist of a reinforced concrete vault that contains six separate cells into which robust canisters containing the waste are placed. These fault cells will be capped with a bolted cover whose top will be at grade with the ground surface at an elevation of 44 ft (13 m) above mean lower-low water (MLLW).

A seaward-sloping berm of riprap that is about 15 to 20 feet in front of Red Bluff has protected Buhne Hill from coastal erosion since it was installed in the 1950s and up graded in the 1980s (Figures 1 and 2B). Prior to this mitigation, wave erosion caused Red Bluff and Buhne Point to retreat an estimated 1300 feet (~400 m) since the 1850s (Page, 2004). Much of this erosion occurred as the result of the opening of the entrance to Humboldt Bay for a deep, stable shipping channel. PG&E addressed the potential erosion of Buhne Hill for the next 50 years, the design life of the ISFSI storage casks for its permit from the Nuclear Energy Commission (PG&E, 2003; Page, 2004).

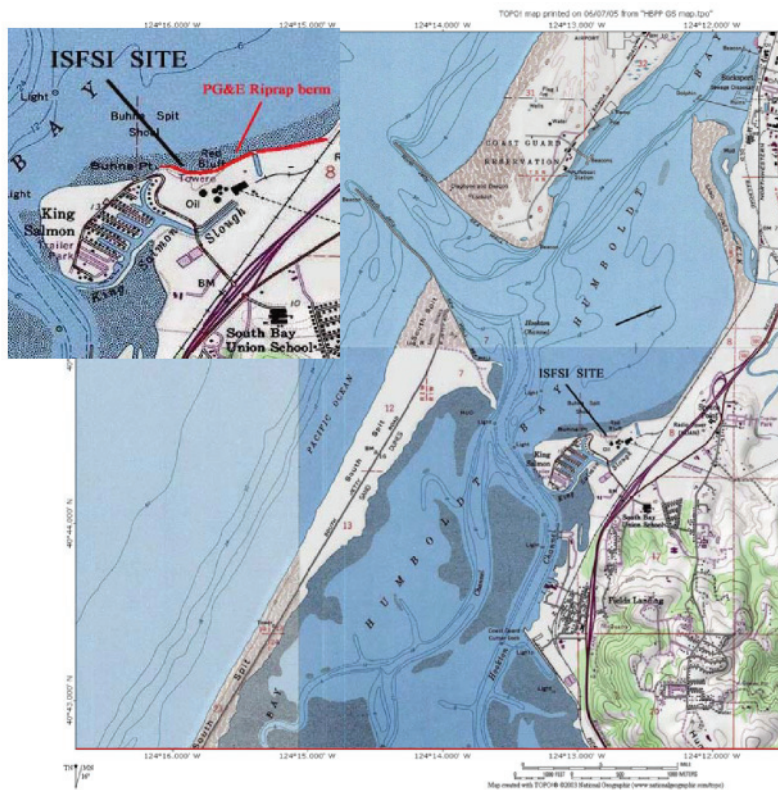
For the Coastal Commission, PG&E evaluated possible future changes to the site over time scales from decades to centuries to many thousands of years. PG&E's approach (Page, 2005) involved five components:

1. Assessing local land level change by determining the long-term pattern of tectonic uplift of Buhne Hill and short-term land level changes due to the earthquake cycle;
2. Forecasting global sea level change in a global environment predicted to be warmer than present for the next several centuries to millennia;
3. Characterizing changes in wave heights and patterns that may result from modifications in the strengths and directions of Pacific storms;
4. Reviewing tsunami hazards and maximum run-up heights in the context of relative sea level change; and
5. Analysis of the coastal protection for Buhne Hill as it is affected by the above changes.

The changes in wave heights and patterns anticipated from global warming and analysis of revetment stability are discussed in a consultant report prepared for PG&E (TerraCosta, 2005). The tsunami hazard for the ISFSI is discussed in detail in PG&E (2003). The risk to the ISFSI posed by tsunami is considered low, because in the unlikely chance that the vault is overtopped, the casks—which are designed to be submerged—would not be damaged by water. In addition, the vault is set below grade, so impact from large floating objects and debris is not a significant hazard.

TECTONIC SETTING AND LAND LEVEL CHANGE

A)



B)

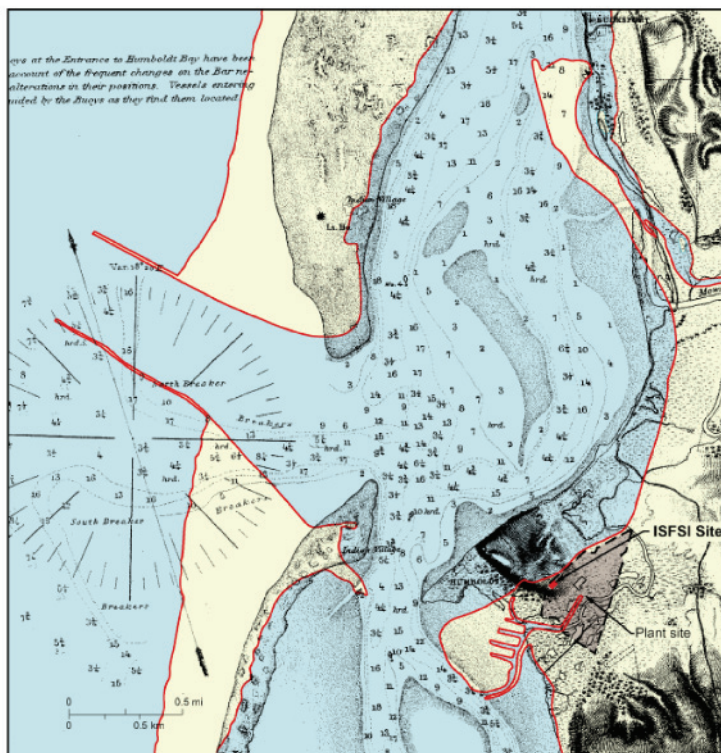


Figure 1. A) Location of ISFSI site at Buhne Hill in Humboldt Bay. B) Retreat of Red Bluff in Humboldt Bay since 1858. Figure shows preliminary survey of Humboldt Bay, U.S. Coast Survey 1858 (edition of 1879). Depths are in feet below mean lower low water to lowest dotted line; then in fathoms. Red line delineates present shoreline and jetties from USGS Fields Landing 7.5 minute Quadrangle. Brown area is plant site. From PG&E (2003).

Buhne Hill is located within the convergent plate boundary between the subducting Gorda Plate and the overriding North America Plate (Figure 3). The two primary tectonic elements that comprise the plate boundary and characterize the region are (1) the offshore Cascadia subduction zone and (2) the onshore fold-and-thrust belt that includes the Little Salmon fault zone (PG&E, 2003). Buhne Hill is located within the hanging wall of the Little Salmon fault zone. Short-term land level change at Buhne Hill is affected by the earthquake cycle related to these two tectonic elements, including abrupt “coseismic” uplift or subsidence during earthquakes and longer term “interseismic” uplift or subsidence between earthquakes. Long-term tectonic uplift at the site is recorded by ancient marine terraces that underlie the site and extend eastward. To evaluate future land level change, we construct a relatively simple model that includes both the long-term and short-term components.

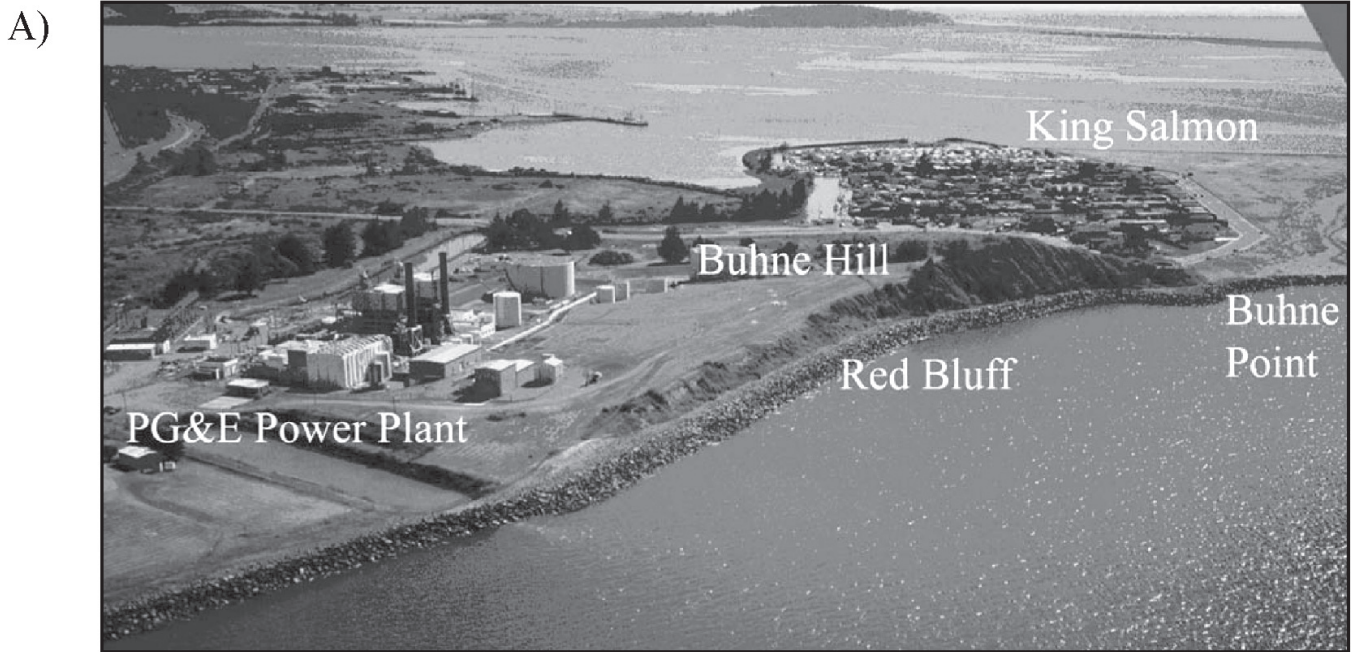
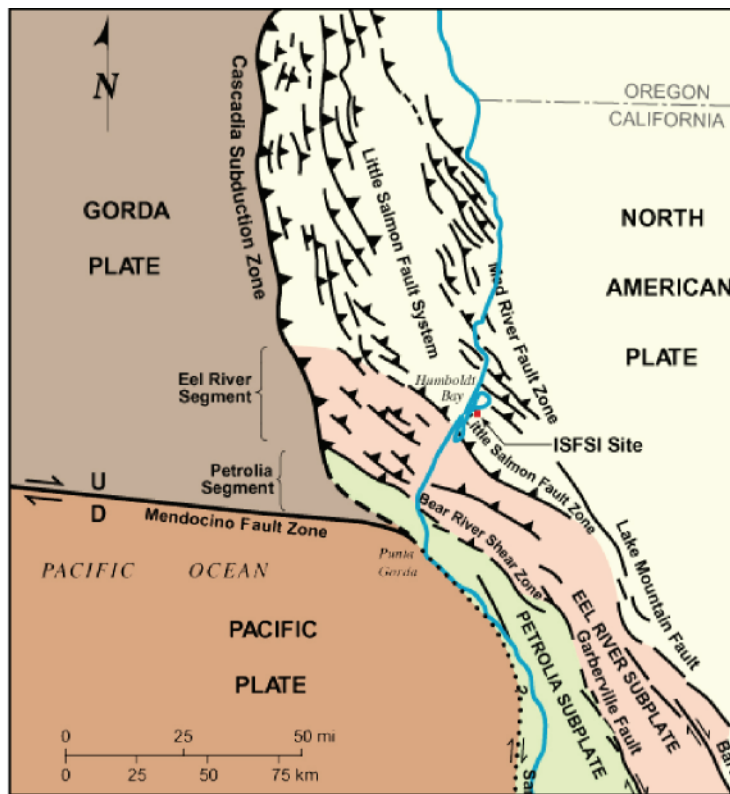


Figure 2. A) Aerial view of Buhne Hill, Red Bluff, and the PG&E plant site. B) View to northeast from Buhne Point of riprap berm in front of Red Bluff (photo by W.D. Page, 6/25/05).

Long-Term Uplift

A sequence of uplifted marine terraces is preserved on Humboldt Hill, a linear ridge that extends eastward from Buhne Hill (Figure 3B). The terraces provide a record of long-term tectonic uplift of the

A)



B)

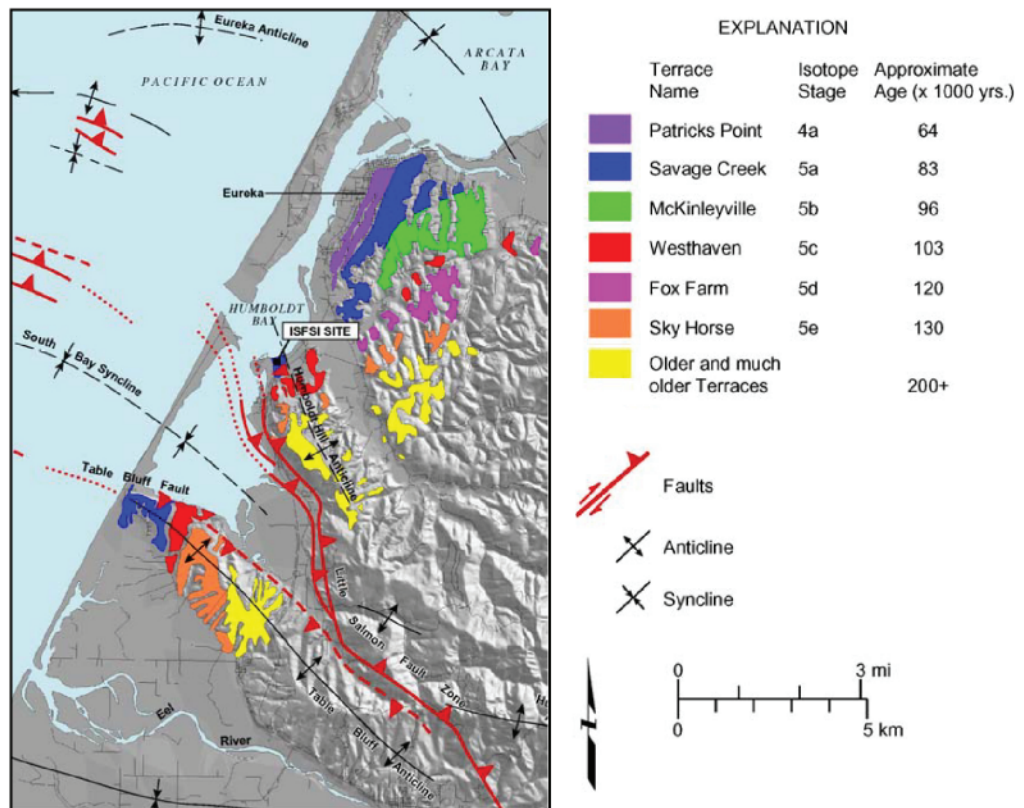


Figure 3. A) Map of the southern Cascadia subduction zone and major faults in northwestern California. B) Marine terraces around Humboldt Bay and the ISFSI site, including surface traces of the Little Salmon fault zone south of the ISFSI site. Both figures modified from PG&E (2003).

ridge over the past several hundred thousand years. The terraces were formed by wave erosion during past sea level high stands, and thus the highest point of each wave-cut terrace coincides approximately with a former position of mean sea level (paleo-sea level). We estimate the long-term rate of land level change at the proposed ISFSI site from the uplifted marine terrace that forms the gently sloping top of Buhne Hill, near the ISFSI site. The long-term rate of tectonic uplift at Buhne Hill is calculated from the age of the terrace, the modern elevation of the terrace at the ISFSI, and the paleo-sea level at the time the terrace was formed. The age, t , of the marine terrace is estimated to be $\sim 80,000$ or $\sim 105,000$ years old, coinciding with the sea level high stands of marine isotope stages 5a or 5c (PG&E, 2003). The modern height, h_m , of this terrace is about 50 ft (15 m) above mean sea level. Reconstructions of past sea level high stands from coral reefs in the Caribbean Sea suggest that paleo-sea levels, h_p , during stages 5a and 5c were about 62 ± 16 ft (19 ± 5 m) and 46 ± 13 ft (14 ± 4 m) below modern sea level (Potter and others, 2004). The long-term uplift rate, u , of Buhne Hill at the ISFSI site is determined by the equation: $u = (h_m - h_p) / t$. This equation yields uplift rates of 1.4 ± 0.3 feet per thousand years (0.4 ± 0.1 mm/yr) assuming the terrace was formed during stage 5a and 0.9 ± 0.2 feet per thousand years (0.3 ± 0.05 mm/yr) assuming the terrace was formed during stage 5c. For this study, we consider the full range of uncertainty in the long-term rate and forecast a future uplift rate of 1.2 ± 0.5 feet per thousand years (0.4 ± 0.1 mm/yr).

Short-Term Land Level Change

Land level at Buhne Hill is expected to fluctuate about the long-term rate due to the abrupt release of elastic strain energy during earthquakes and the gradual buildup of elastic energy between earthquakes (i.e., the “earthquake cycle”). There are two primary earthquake sources for the ISFSI site that affect short-term land level changes: the Cascadia subduction zone and the Little Salmon fault zone. For our model of short-term fluctuations in land level, we consider end-member models in which each source is considered to rupture independently in an earthquake. The scenario in which both sources rupture simultaneously (e.g., PG&E, 2003) will yield a result that lies somewhere in between the end-member models.

Cascadia Subduction Zone

The Cascadia subduction zone, which lies offshore between southern Vancouver Island, British Columbia and northern California, ruptures during large earthquakes on average every 300 to 700 years (PG&E, 2003). Evidence for these earthquakes includes buried marshes and tsunami deposits at several sites along the coast that record abrupt land subsidence of up to several meters during each earthquake and inundation by large waves generated by sea-floor displacements, respectively (e.g., Clarke and Carver, 1992; Atwater and Hemphill-Haley, 1997; Kelsey and others, 2002; Witter and others, 2003). Elastic dislocation models of the Cascadia subduction zone predict abrupt subsidence along the coast during earthquakes and gradual uplift along the coast between earthquakes as elastic strain energy accumulates (Hyndman and Wang, 1995). This model clearly applies to Washington, Oregon and the California coast north of the Klamath River and is constrained by estimates of present-day vertical uplift of the coast derived from tide-gage data and geodetic leveling (e.g., Mitchell and others, 1994).

Regional present-day uplift rates at the latitude of Humboldt Bay, similar to the uplift to the north, range from about 1.3 feet per century (4 mm/yr) based on leveling surveys tied to the Crescent City tide gage (Mitchell and others, 1994). Another uplift rate in this area is about 0.3 feet per century (1 mm/yr) based on three to seven years of GPS data (Williams, 2002). Thus, as one end-member model for land level change at Buhne Hill, we anticipate abrupt subsidence of a few meters at the site during a Cascadia

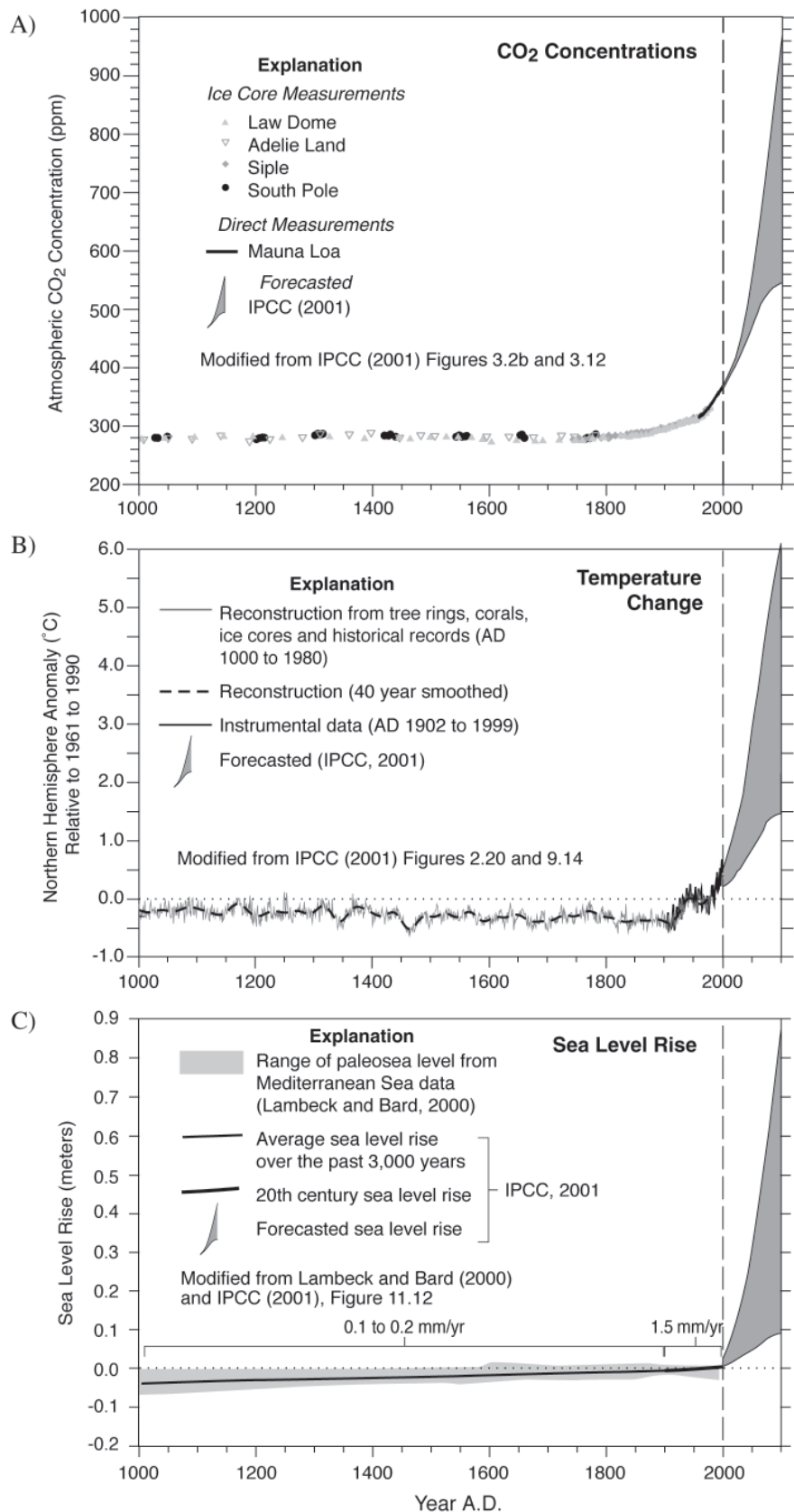


Figure 4. Glacial-interglacial cycles of the past 500,000 years. A) Marine oxygen isotope record of deep-sea sediments (from Imbrie et al., 1984). B) Solar insolation curve for 65 degrees North latitude in July. Insolation curve for the next 100,000 years also shown. A possible interglacial - glacial transition in about 50,000 years is indicated by the dashed and queried line. From Laskar et al. (2004).

subduction zone event, and uplift rates between earthquakes on the order of 1.3 feet per century (4 mm/yr). We note that there is no direct geologic evidence for coseismic subsidence in tidal marshes around the ISFSI site (PG&E, 2003), and that this end member model places a conservative limit on the earthquake cycle tied to the subduction zone.

Little Salmon Fault Zone

The other end-member model considers fault rupture during an earthquake on the Little Salmon fault zone. Paleoseismic data southeast of Buhne Hill constrain dip-slip displacement, d , across the moderately dipping fault zone to be up to 15 to 26 ft (4.5 to 8 m) per event (PG&E, 2003). Given a fault zone dip, δ , of 45 to 55°, the vertical displacement, v , per event is given by the equation: $v = d \sin(\delta)$. This equation yields vertical displacements of 10.5 to 21 ft (3.2 to 6.5 m) per event. Two alternatives are possible. Assuming equal portions of hanging wall uplift and footwall subsidence occur, we estimate that an earthquake on the Little Salmon fault zone could produce land level uplift of about 5 to 10 ft (1.6 to 3.2 m) in the hanging wall, and an equal amount of land level subsidence in the footwall. The second alternative, which is supported by the

lack of evidence of significant uplift or subsidence at Buhne Hill, is that Buhne Hill neither rises nor subsides appreciably during the faulting event with respect to sea level but all the fault displacement is taken in the subsidence of South Bay, including King Salmon.

Expected Land level Change

The result of uplift and subsidence from earthquakes on the Cascadia subduction zone and Little Salmon fault zone, whether they occur independently as end-member models described above, or occur dependently as described by PG&E (2003), when integrated over several earthquake cycles will produce coastal uplift at Buhne Hill equal to the long-term uplift rate recorded by the uplifted marine terrace sequence on Humboldt Hill. For this study, we choose an alternative for short-term land level change at Buhne Hill that is characterized by interseismic uplift followed by coseismic subsidence (Figure 8) [note: figure is out of sequence]. The rate of interseismic uplift, u_p , is constrained by the present-day rate of uplift of the Humboldt Bay area of 1.3 feet per century (4 mm/yr) published by Mitchell and others (1994). The magnitude of coseismic subsidence, s , is estimated by the equation: $s = (u_p - u_l) * R$, where u_l is the long-term uplift rate of the Buhne Point terrace (1.4 feet/thousand years (0.4 mm/yr)) and R is the recurrence interval between earthquakes. The long-term uplift rate, u_p , accounts for permanent uplift accommodated by slip on

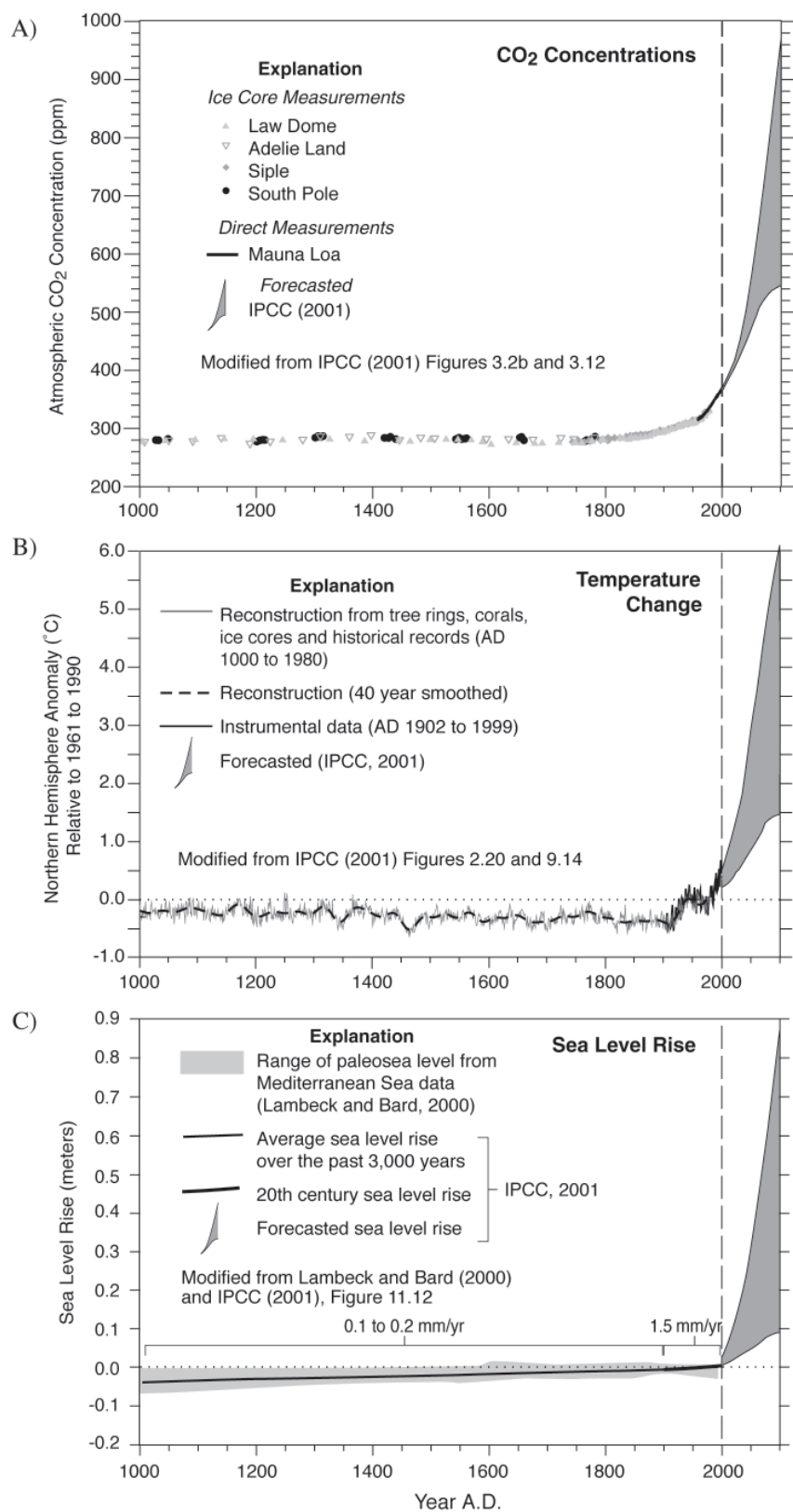


Figure 5. Climate change over the past 1000 years and forecasted for the next 100 years, based on data presented in IPCC (2001). Projected increases in CO₂ emissions are expected to cause increases in global temperature and sea level. A) Changes in atmospheric CO₂ concentrations. B) Changes in northern hemisphere temperature. C) Changes in global sea level.

the Little Salmon fault zone. An average recurrence interval of 500 years for Cascadia earthquakes results in a coseismic subsidence estimate of 5.9 ft (1.8 m). We emphasize that this value of coseismic subsidence is a direct function of the assumed interseismic uplift rate as published by Mitchell and others (1994).

Our estimates for coseismic subsidence are consistent with published subsidence estimates derived from elastic dislocation models and geologic evidence of buried marshes that dropped several meters during past Cascadia subduction zone earthquakes (e.g., Hyndman and Wang, 1995; Witter and others, 2003), and are conservative with respect to coastal erosion hazard. Lower uplift rates suggested by GPS data (Williams and others, 2002) and geologic data that does not detect evidence for abrupt subsidence near Buhne Hill (PG&E, 2003) suggest that amounts of coseismic subsidence may be much less than our selected estimate, or even negative (i.e., coseismic uplift of Buhne Hill) (G. Carver, personal communication, 2005).

We incorporate the considerable uncertainty in short-term land level change caused by future earthquakes on the offshore subduction zone and the Little Salmon fault zone by adding an error term above and below the long-term uplift curves (Figure 8). Because neither the timing nor the exact rupture scenario of future earthquakes is certain, we conservatively assume that at any future point in time, an earthquake may cause land level to subside up to 6.6 ft (2 m) below the minimum long term land level, or an earthquake may cause land level to uplift up to 10 ft (3.2 m) higher than the maximum long term land level.

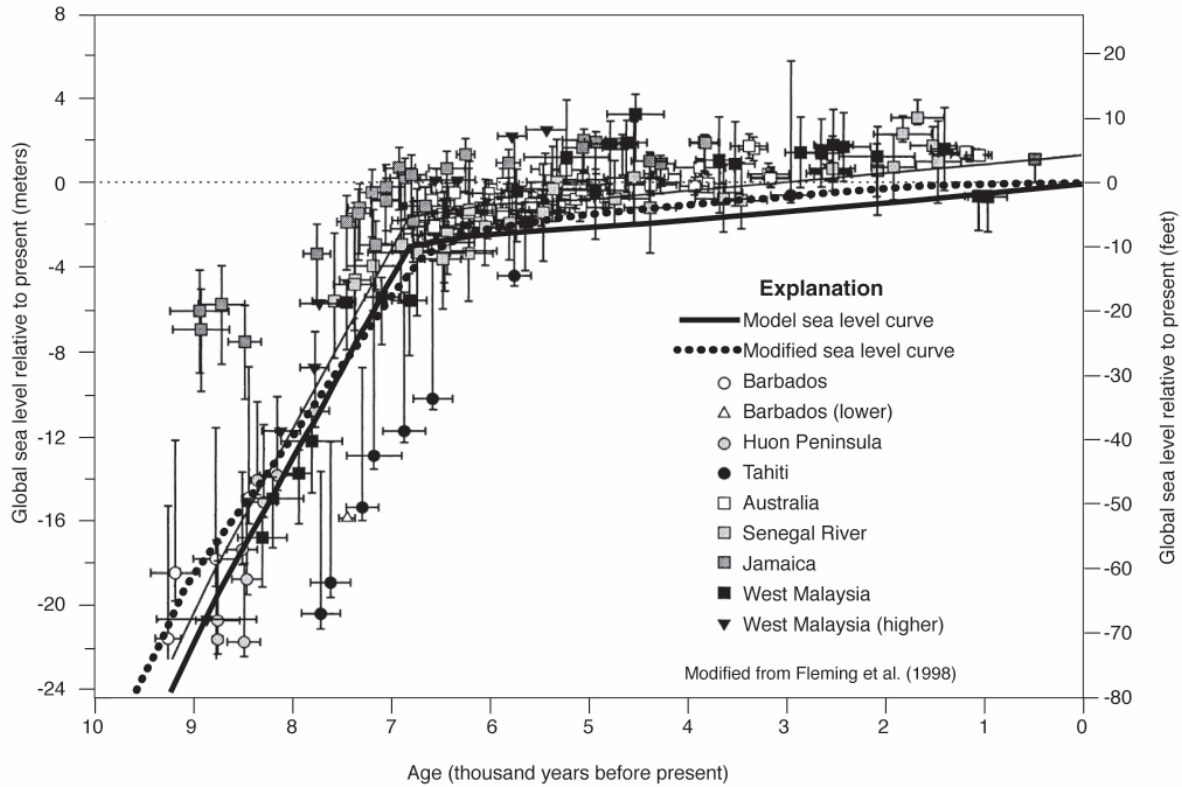
GLOBAL SEA LEVEL CHANGE

Global sea level is tied closely to global climate, and is the product of numerous variables and their complex interactions. Estimating future sea level change is speculative, and different approaches are required to capture the variability of possible sea level change over different time scales. We approach the goal of characterizing sea level change at the proposed ISFSI site by examining possible changes over the next 100, 1,000, 10,000 and 100,000 years. For the 100-year time scale, we rely on forecasted global sea level rise published in the United Nations Intergovernmental Panel for Climate Change report (IPCC, 2001). For time scales of several hundreds to a few thousands of years, we rely on extrapolations of the 100-year forecasts, and modify them based on evaluating the major individual contributors to sea level change such as thermal expansion of sea water, change in mass of the Greenland and Antarctic ice sheets, and change in mass of mountain glaciers (IPCC, 2001). For time periods longer than a few thousand years, forecasts of sea level change rely on: (1) the geologic record of past sea level change (Martinson and others, 1987; Thompson and Goldstein, 2005; Hearty and others, 1999) as a proxy for future sea level change; (2) numerical models and supporting geologic data that evaluate possible maximum sea level changes from each of the major individual contributors; and (3) relationships between past changes in Earth's orbit and glacial-interglacial intervals to predict future changes (Berger and Loutre, 2002). Estimates over these longer time periods incorporate the assumption that the earth remains within the climatic paradigm of the Quaternary Period, characterized by glacial and interglacial intervals that change in phase with variations in Earth's orbit around the sun (Imbrie and others, 1984) (Figure 4).

Historical and 21st Century Climate and Sea Level Change

Human-induced increases in greenhouse gases (mainly carbon dioxide (CO₂) and methane (CH₄)) are partially responsible for the historical rise in the Earth's average temperature, and are believed to

A)



B)

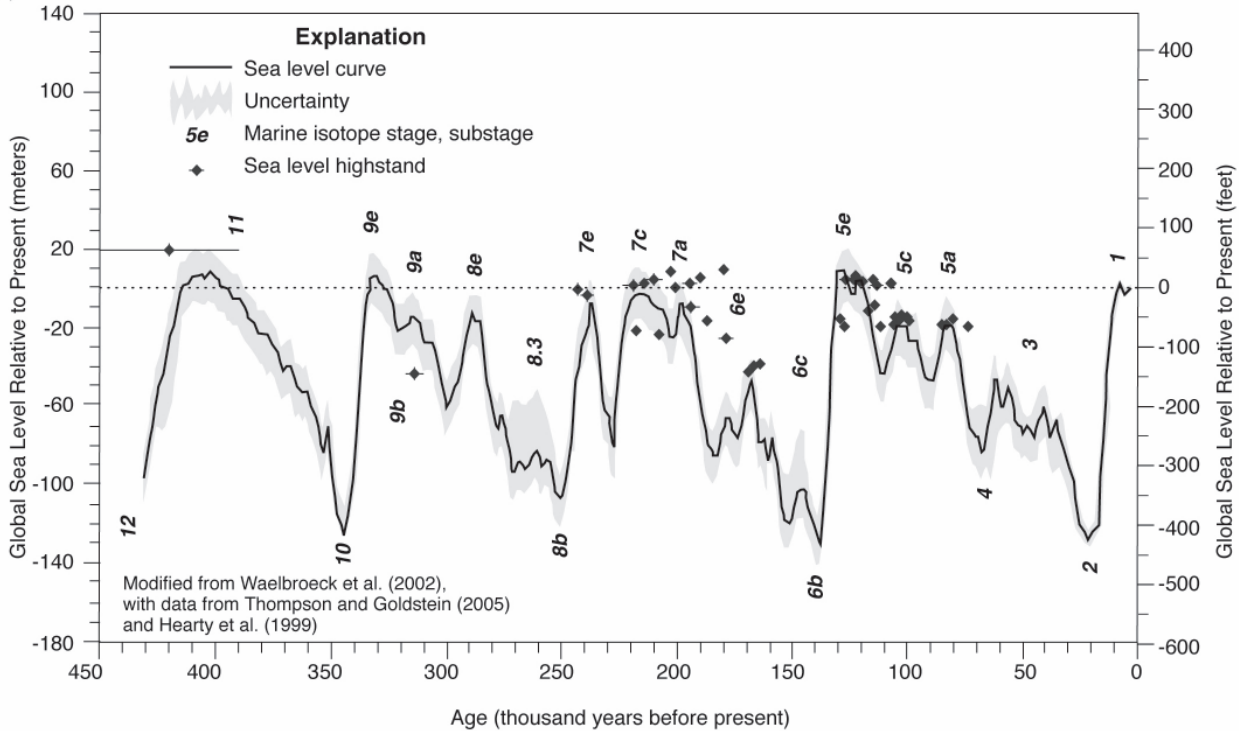


Figure 6. A) Reconstructed sea level curve for the Holocene based on data from coral reefs at several sites around the globe. Solid line is modeled sea level. Dotted line represents a modified sea level curve based on authors' subjective screening of the data. Modified from Fleming et al. (1998). B) Reconstructed sea level curve, 430,000 years ago to the present. The black sea level curve with shaded uncertainty is a composite of Atlantic and Pacific ocean core data, corrected for changes in ocean temperature. The numbers next to the curve are marine isotope stages and substages. Symbols with uncertainty bars are sea level highstand data from coral reefs and beach deposits. Curve from Waelbroeck et al. (2002). Coral highstand data from Thompson and Goldstein (2005) and references therein, and Hearty et al. (1999).

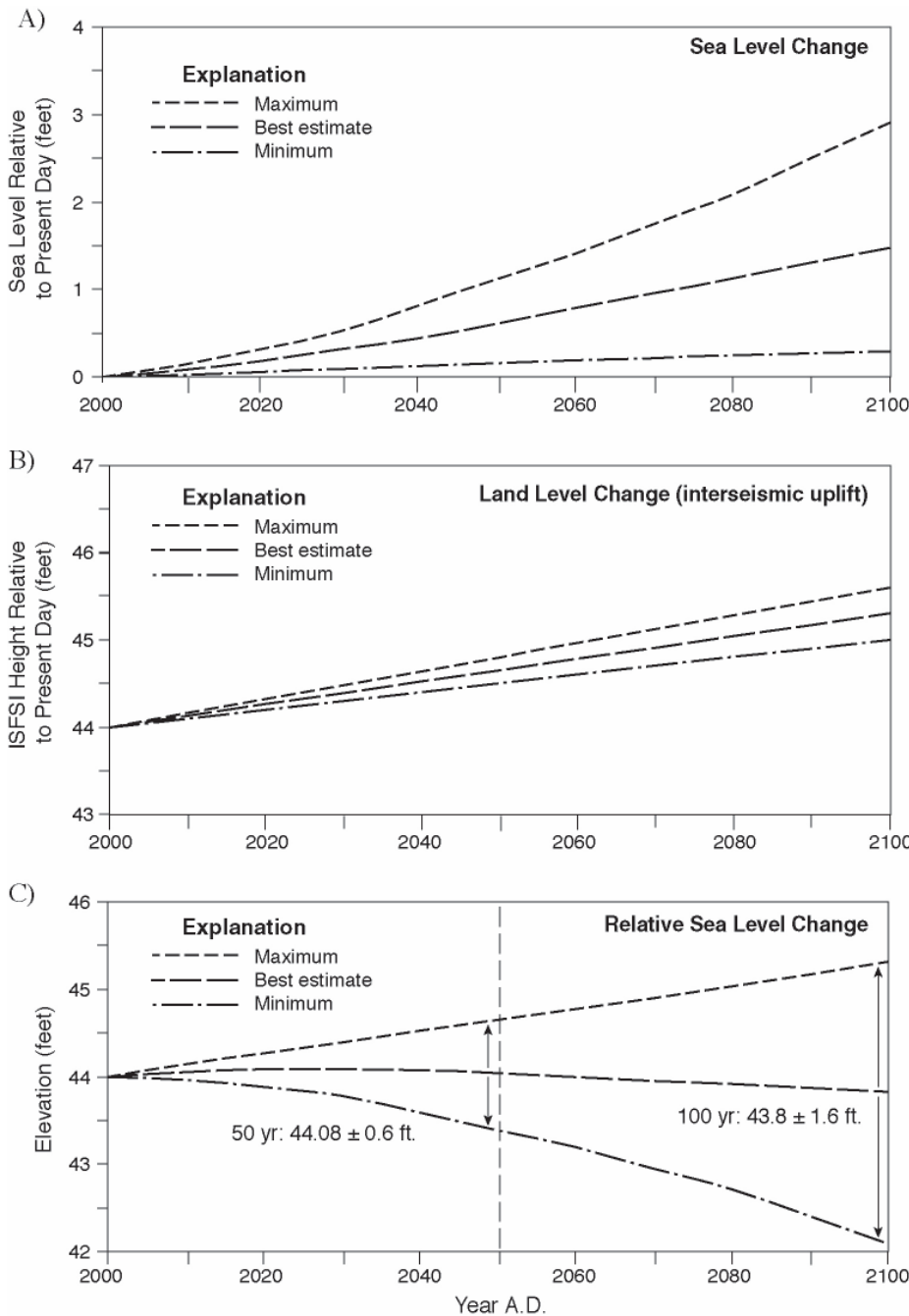
contribute to the projected 1.4 to 5.8°C rise in global temperature over the 21st century and beyond (IPCC, 2001) (Figure 5). Although temperature has probably varied by several degrees Celsius over the past 10,000 years (IPCC, 2001), present levels of CO₂ and methane are higher than at any point documented in the past ~420,000 years (Petit and others, 1999), and are projected to increase to about twice the 1990 levels by the end of the 21st century (IPCC, 2001). Although changes caused by global warming are most clearly recorded as temperature increases in high latitude regions, global warming is expected to influence local climates through changes in mean annual temperature, temperature extremes, annual precipitation (i.e., overall wetter or drier climate) and/or changes in the duration, pattern, and intensity of storms (IPCC, 2001).

A major consequence of historical and near-future global warming is global sea level rise, caused primarily by the melting of ice in mountain glaciers and by the expansion of ocean water caused by heating at the ocean surface (IPCC, 2001). During the past century average temperature increased 0.6°C (IPCC, 2001) and global sea level rose as much as 4 to 10 inches (10 to 25 cm) (Gornitz, 1995). Present-day rates are estimated at about zero (Mörner, 2004) to as much as 0.7 to 1.2 inches per decade (1.8 to 3 mm/yr) (Peltier and Tushingham, 1989; Douglas, 1991; 1997). By the year 2100, average temperatures are projected to increase 1.4 to 5.8°C, and sea level is expected to rise globally from about 4 to 35 inches (10 to 90 cm), which implies an average rate of global sea level rise up to four times the twentieth century rate (IPCC, 2001).

Holocene climate and sea level change

For the past 11,000 years or so, Earth has been in an interglacial interval that has been remarkable for its climatic stability relative to the geologic record of the past ~420,000 years (Petit and others, 1999; Ruddiman, 2003). The early Holocene warm interval occurred near the start of the Holocene in the high latitude regions (about 11,000 to 8,000 years ago) but did not start until about 8,000 years ago across much of North America and Europe (COHMAP, 1988). For much of the middle and late Holocene, global temperatures were cooler than present, though variable on time scales of decades to millennia. The twentieth century was the warmest in the past millennium (IPCC, 2001).

Holocene sea level change is characterized by decreasing rates of sea level rise as the ice sheets adjusted to warm, interglacial conditions and their melt water filled the oceans (Figure 6A). Sea level during the early Holocene rose rapidly as glaciers and ice sheets melted from their maximum glacial extent (Fairbanks and others, 1989). The average rate of sea level rise between 15,000 and 6,000 years was about 3.3 feet per century (10 mm/yr), although considerable variation in the rate occurred during the early part of the deglaciation processes (IPCC, 2001). During the last ~6,000 years, sea level rise slowed dramatically to rates of about 0.16 feet per century (0.5 mm/yr), and during the last 3,000 years sea level rise occurred at about an average rate of 0.03 to 0.07 feet per century (0.1 to 0.2 mm/yr) (IPCC, 2001). Although geologic evidence indicates a middle Holocene relative sea level that was as much as six feet (2 m) higher than present in low latitude regions (e.g., Blum and others, 2002), this relative sea level high stand is thought to be the result of hydro-isostatic effects and does not represent a global change in sea water volume (e.g., Fleming and others, 1998; Peltier, 1999). For comparison to an area close to the ISFSI and Eureka, relative sea level on the south-central Oregon coast rose gradually at a rate of 0.33 feet per century (~1 mm/yr) over the past 6700 years, and at a rate of 0.1 feet per century (~0.3 mm/yr) over the past 3,000 years, reaching a maximum level at the present day (Witter and others, 2003).



The relative stability of climate and sea level over the past few thousand years contrasts with the measured and projected rapid increases in temperature and sea level from the start of the 20th century into the 21st century. Figure 5 shows past and future changes in atmospheric CO₂ concentration, global temperature, and sea level for the time period A.D. 1000 to A.D. 2100. The departure from past Holocene stability can be seen around the start of the 20th century, when atmospheric CO₂ concentration and temperature increase. This increase coincides with an order of magnitude increase in sea level rise, from an estimated 0.1 to 0.2 mm/yr average over the past 3000 years to an estimated ~1.5 mm/yr average in the 20th century (IPCC, 2001). Twenty-first century estimates of CO₂, temperature, and sea level predict even greater rates of change.

Pleistocene Climate and Sea Level Change

Over the past 2.5 million years, Earth’s climate has fluctuated between glacial and interglacial intervals, with changes in global temperature, atmospheric greenhouse gas

Figure 7. Forecasted changes in relative sea level at Buhne Hill over the next 100 years. A) Sea level change from IPCC (2001). B) Land level change based on interseismic uplift rates from Mitchell et al. (1994). C) Relative sea level calculated as the difference between land level and sea level. The curves assume no major earthquake on the Cascadia subduction zone or Little Salmon fault zone over this time period.

concentrations, glacier and ice sheet extent, and sea level occurring on time scales that range from less than a thousand to hundreds of thousands of years (Imbrie and others, 1984; Petit and others, 1999) (Figure 4). Temperature changes between full glacial and interglacial conditions were about 20°C over Greenland and about 3°C in the tropics (IPCC, 2001). Rapid changes in temperature are recorded at rates up to 10°C in fifty years over much of the Northern Hemisphere, and up to about 7°C in a decade over Greenland (IPCC, 2001). The Vostok ice core from Antarctica shows almost in-phase changes of

temperature, CO₂, and methane through the glacial-interglacial ice age cycles over the past ~420,000 years (Petit and others, 1999).

Long-term records of sea level over the past several hundreds of thousands of years are based primarily on variations in the oxygen isotopic concentration in fossil organisms in marine sediment cores (e.g., Waelbroeck and others, 2002; Siddall and others, 2003) (Figure 6B). The time scales for these records are constrained by limited radiometric dating of young sediments, correlations with volcanic ashes or and magnetic reversals, and are “orbitally tuned” such that major fluctuations in the oxygen isotope records are matched with predictable changes in the earth’s orbit around the sun and the resulting changes in solar insolation (Figure 4) (Imbrie and others, 1984). Sea level records show oscillations of hundreds of feet of sea level change between glacial conditions, when sea level drops as water is stored in ice sheets, and interglacial intervals, when sea levels rise as ice sheets melt. At the most recent glacial maximum, about 20,000 years ago, sea level was about 400 ft (120 m) lower than present day (Fairbanks, 1989).

High-resolution records suggest that sea level changes up to 115 ft (35 m) occurred at rates of up to 6.6 feet per century (20 mm/yr) during abrupt changes in climate (Siddall and others, 2003). These high rates and rapid fluctuations are more typical during glacial intervals and glacial-interglacial transitions than during full interglacial intervals, but millennial-scale changes of tens of feet (and tens of meters) characterized previous interglacial intervals (Lea and others, 2002; Siddall and others, 2003).

Although sea level proxy data from oxygen isotopes in marine cores provides continuous records of sea level, more precise data for past sea levels at specific points in time come from uplifted coral reefs and marine terraces in environments where tectonic activity is assumed constant (e.g., Chappel, 2002; Potter and others, 2004). Uplifted coral reefs and marine terraces record past sea level high stands that place limits on what has been possible during past intervals of warm climate (Figure 6B). The highest sea level over the past ~500,000 years appears to have occurred about 400,000 years ago, during marine isotope stage 11, and reached a maximum height of about 43 to 66 ft (13 to 20 m) above present-day sea level (Hearty and others, 1999; Droxler and others, 2003). A more recent high stand of +13 to +26 ft (+4 to +8 m) occurred during the last interglacial interval, at marine isotope stage 5e, about 125,000 years ago (Thompson and Goldstein, 2005). Another similar high stand that consisted of multiple sea level standstills between about +6.6 to +20 ft (+2 to +6 m) occurred during the prior interglacial interval (marine isotope stage 7) about 190,000 to 220,000 years ago (Thompson and Goldstein, 2005). Peak rates of sea level rise were about 3.3 feet per century (10 mm/yr) during previous interglacial intervals (Thompson and Goldstein, 2005), although the uncertainties of these peak rates are unclear.

The largest contributors to major sea level changes over the Pleistocene have been the North American ice sheets (Laurentide, Cordilleran, and Greenland, of which only the Greenland ice sheet partially remains), the Fennoscandian ice sheet (which likely melted in the first half of the Holocene), and the Antarctic ice sheets, which consist of the East Antarctic ice sheet and the much smaller West Antarctic ice sheet (IPCC, 2001). The majority of the ~400 ft (120 m) of sea level rise since the last glacial maximum 20,000 years ago was due to the melting of the North American ice sheets. The water stored in the three remaining ice sheets is equal to about 250 ft (~80 m) of sea level rise.

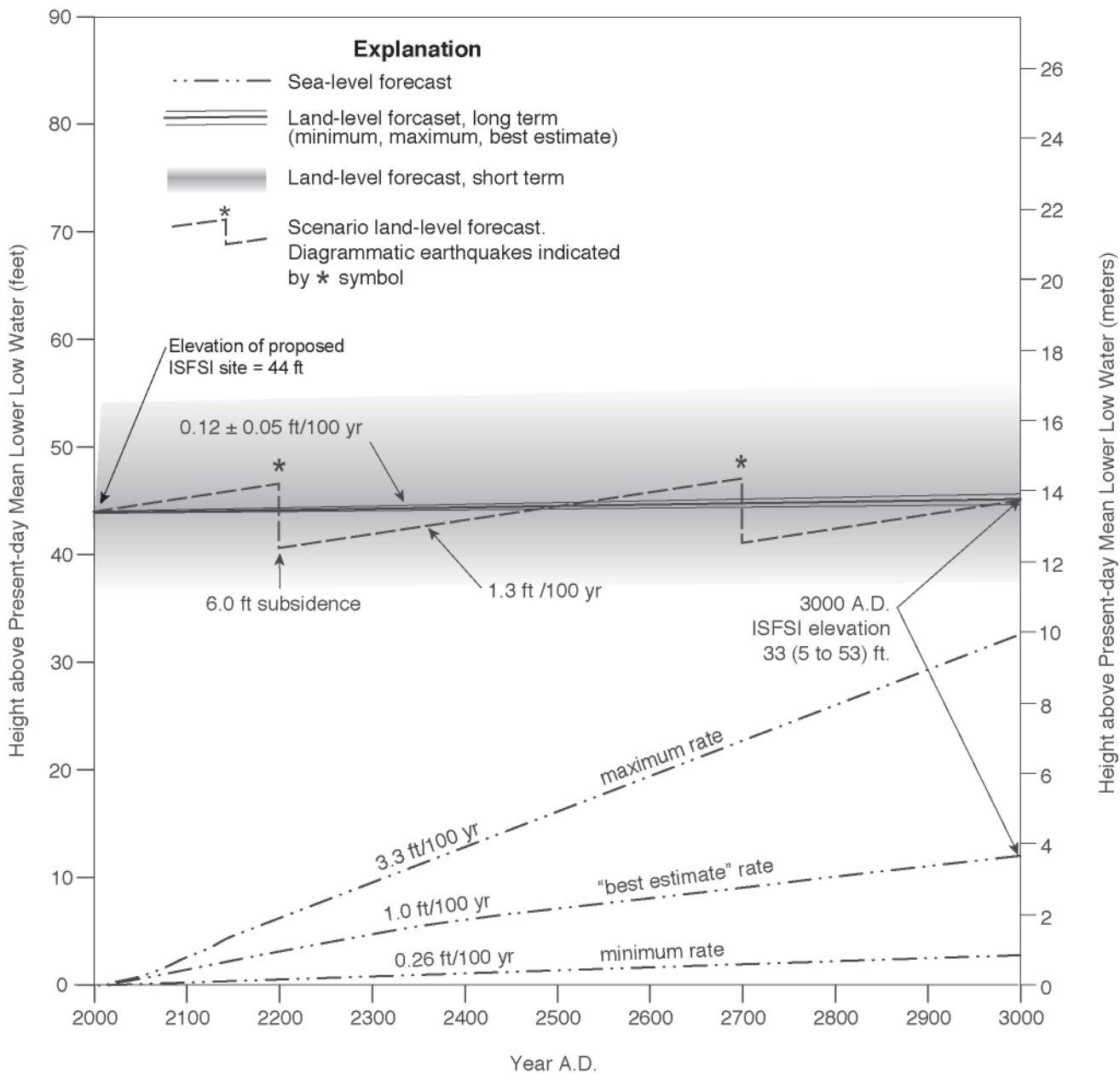


Figure 8. Forecasted land level and sea level changes at the proposed ISFSI site over the next 1000 years. Upper part of figure shows black lines reflecting long-term tectonic uplift at a rate of 0.7 to 1.7 feet per thousand years (0.25 to 0.5 mm/yr) with the center line representing the best estimate rate of 1.2 feet per thousand years (0.36 mm/yr). Short-term changes in land level due to abrupt coseismic uplift or subsidence, or due to gradual interseismic uplift or subsidence, are indicated by the area shaded gray. Dashed line shows a scenario land level forecast dominated by interseismic uplift and coseismic subsidence. Lower part of figure shows minimum, best estimate, and maximum sea level forecasts over the next 1000 years, based on an extrapolation of the IPCC (2001) reported rates.

ESTIMATES OF FUTURE GLOBAL SEA LEVEL CHANGE

Model predictions of future sea level change over the next century (and beyond) rely on quantifying the effects of global warming on four main contributors (IPCC, 2001):

- thermal expansion of ocean water from heating of surface ocean water,
- melting or growth of mountain glaciers,
- melting or growth of the Greenland ice sheet, and
- melting or growth of the West and East Antarctic ice sheets.

Because these systems are large, their responses to climatic perturbations occurring today and in the near future would be expressed over several centuries to millennia. Below, we summarize the major individual components that could contribute to future sea level change.

Thermal Expansion

The rate of sea level rise due to thermal expansion of ocean water is predicted to be 1.6 to 6.6 ft (0.5 to 2.0 m) to 3.3 to 13 ft (1 to 4 m) for atmospheric CO₂ levels that are two and four times pre-industrial levels, respectively (IPCC, 2001). This contribution to sea level rise is predicted to reach half its total value in about 500 years and will take several thousand years to reach the full value.

Mountain Glaciers

Melting of mountain glaciers due to global warming will contribute a significant, if not major component of sea level rise over the next century. Mountain glaciers cumulatively contain about 1.5 ft (0.5 m) of total sea level equivalent, and currently are in a state of general retreat and loss of mass (e.g., Arendt and others, 2002). With continued global warming, most of the world's mountain glaciers likely will continue to lose mass over the next several thousands of years.

Greenland Ice Sheet

Although the Greenland ice sheet is the most vulnerable of the Earth's ice sheets to climatic warming (IPCC, 2001), its contribution to future sea level change is highly uncertain. The Greenland ice sheet contains enough ice to raise sea level by 20 to 23 ft (6 to 7 m) (IPCC, 2001). At its relatively low latitude, the Greenland ice sheet is susceptible to melting given moderate increases in summer temperatures. Small increases in temperature, however, result in increased accumulation of snow during the winter, which may partially offset the increased summer melting. Glacier mass balance calculations suggest that a "mid-range" scenario of 5.5°C warming over Greenland will produce about 10 ft (3 m) of sea level rise over about 1000 years, and an 8°C warming will produce about 20 ft (6 m) of sea level rise, essentially eliminating the ice sheet over several thousands of years. Evidence from ice cores and sediment cores is consistent with partial melting of the Greenland ice sheet during the last interglacial period about 125,000 years ago, with a plausible contribution of 13 to 18 ft (4 to 5.5 m) to sea level (Cuffey and Marshall, 2000). This contributed to the oxygen isotope stage 5e sea level high stand of about 20 ± 6 ft (6 ± 2 m) above present-day sea level 125,000 years ago.

West Antarctic Ice Sheet

The West Antarctic ice sheet contains enough ice to raise sea level by about 13 to 20 ft (4 to 6 m) (Oppenheimer, 1998). The base of the ice sheet rests below sea level, and the outer margins of the ice sheet are floating ice shelves that extend seaward. These conditions make the West Antarctic ice sheet susceptible to changes in ice dynamics due to changes in sea level and ocean temperature. Analysis of sediment cores and geophysical data suggests that the ice sheet has repeatedly advanced and retreated over the ocean floor during the Quaternary period, including a major retreat about 400,000 years ago (Scherer and others, 1998). Evidence for such instability in the face of 20th century climate change has led several authors to conclude that the ice sheet is susceptible to rapid melting and retreat in short time periods (reviewed in Oppenheimer, 1998). Currently, however, there is considerable consensus that major loss of the ice sheet is unlikely during the 21st century, and significant contributions to sea

level change likely will require time scales of thousands of years (IPCC, 2001). Conservative estimates suggest that the West Antarctic ice sheet could melt at rates corresponding to 0.9 mm/yr of sea level rise, which projects to disappearance of the ice sheet in 4000 to 7000 years (Bindschadler, 1998). Total melting of both Greenland and the West Antarctic ice sheet would be required to reproduce the +43 to +66 foot (+13 to +20 m) sea level high stand that may have occurred about 400,000 years ago (Hearty and others, 1999; Droxler et al., 2003).

East Antarctic Ice Sheet

Although the East Antarctic ice sheet contains enough ice to raise sea level by about 200 ft (60 m), the ice sheet has persisted for as long as 20 million years (Oppenheimer, 1998), and is unlikely to lose any significant mass in the foreseeable future. The threshold for loss of mass of the ice sheet requires a temperature warming above 20°C, an amount well beyond forecasted levels (IPCC, 2001). A warming of the ocean and atmosphere near the East Antarctic ice sheet will likely cause an increase in mass due to increased snow fall, which would contribute to short and long-term draw-downs of sea level. This increase in East Antarctic ice sheet mass balance may partly offset sea level rise from other sources. However, it is also possible that sea level rise could cause melting around the margins of the ice sheet that may contribute to short-term sea level rise. Some net melting of the East Antarctic ice sheet probably was necessary to achieve the +66 foot (+20 m) sea level about 400,000 years ago as suggested by Hearty and others (1999).

RELATIVE SEA LEVEL CHANGE AT BUHNE HILL

Estimates of future sea level changes and relative sea level changes at Buhne Hill are divided into several time periods, including short time scales of 10 to 100 years, intermediate time scales of about 1,000 years, and long time scales of 10,000 to 100,000 years.

A major limitation for forecasting sea level change over short time scales at Buhne Hill is the variability in sea level change that exists both spatially and temporally around the globe. The variability of sea level due to changes in atmospheric and ocean circulation currently exceeds the amplitude of any background trends at any particular location (Douglas, 1991). Anticipating that variability at Buhne Hill is a challenging task. Quantifying global sea level change over the past century has traditionally relied on a subset of globally-distributed tide-gage data in tectonically stable areas with 60 years or more of record (e.g., Douglas, 2001). Although most tide-gage records, after corrections for land level change, show similar trends over the historical period, the rates of sea level change vary by location. Numerical models of 21st century sea level change consistently show that sea level rise is expected to be geographically non-uniform, but they do not agree about the geographical pattern (Gregory and others, 2001). Thus, the global average of both historic changes in the 20th century and forecasted sea level change over the 21st century should be considered only proxies for sea level change near Buhne Point. In other words, a global average forecast of sea level change does not predict precise sea level at a particular location and time, but should indicate a direction of change.

Short (10- to 100-year) Time Scales

Forecast Over the Next 100 Years

Sea level is predicted to rise globally 3.5 to 35 inches (0.09 to 0.88 m) between 1990 and 2100 (IPCC, 2001) (Figure 5). The majority of the predicted rise comes from thermal expansion and melting of

mountain glaciers, as most models predict that neither Greenland nor Antarctica will contribute to significant amounts of sea level change over the next 100 years (e.g., Huybrechts and others, 2004). The maximum sea level curve shows an increasing rate of sea level rise from 1.4 to 4.1 feet per century (4 to 12 mm/yr). The minimum sea level curve shows an increasing then decreasing rate of sea level rise from 0.2 to 0.3 to 0.2 feet per century (0.6 to 1.0 to 0.5 mm/yr). A best estimate of sea level rise that we consider for this study has a gradually increasing rate of sea level rise from 0.6 to 1.7 feet per century (1.8 to 5.2 mm/yr), and we adopt the full range in model predictions in the IPCC study in our uncertainty.

The range of rates of sea level rise encompasses rates that are comparable with and up to about six times greater than the rates measured over the 20th century. The highest predicted rate, 4.1 feet per century (12 mm/yr), is comparable in magnitude to the 3.3 feet per century (10 mm/yr) average rate of sea level rise during deglaciation between 15,000 and 6,000 years ago (Fairbanks, 1989) and the approximate rate of 3.3 feet per century (10 mm/yr) that occurred during interglacial intervals between about 70,000 and 250,000 years ago (Thompson and Goldstein, 2005).

100-year Relative Sea Level Change at Buhne Hill

Relative sea level change for the next 50 and 100 years is determined by subtracting forecasted sea level change from predicted land level change (Figure 7). For land level change, we assume a constant rate of interseismic uplift of 1.3 ± 0.3 feet per century (4 ± 1 mm/yr) based on level line surveys published in Mitchell and others (1994). We explicitly assume that no major Cascadia subduction zone or Little Salmon fault zone earthquake will occur during this time period. The resulting relative sea level curves show the ISFSI site at 44.0 ± 0.6 feet elevation by 2050 and at 43.8 ± 1.6 ft by the year A.D. 2100. The relative sea level curves show that, over the next century and barring any change in land level due to a major earthquake, the rate of interseismic uplift at Buhne Point will keep up with expected sea level rise. If a major Cascadia subduction zone event occurs within this time, however, land level may abruptly drop by up to about 6 ft (~2 m).

Intermediate (1000-year) Time Scales

Forecast Over the Next 1,000 Years

Our maximum sea level projection assumes a maximum sea level rise over the 21st century as forecasted by IPCC (2001), followed by an average rate of sea level rise of about 3.3 feet per century (~10 mm/yr) from the end of the 21st century to the end of the next millennium (Figure 8). The average rate is consistent with the maximum rates during interglacial intervals in the geologic record (Thompson and Goldstein, 2005). The sustained high rate reflects initial high rates of thermal expansion and meltwater from glacial ice, followed by high rates of melting of the Greenland and West Antarctic ice sheets that would probably lag behind the near-term abrupt rise in global temperatures (IPCC, 2001). The maximum sea level curve over the next 1000 years allows for partial melting of both Greenland and the West Antarctic ice sheets, negligible contribution from the East Antarctic ice sheet, significant sea level rise caused by thermal expansion of ocean water, and melting of the majority of ice presently stored in mountain glaciers.

Our minimum sea level scenario assumes a linear increase of sea level of about 0.26 feet per century (~0.8 mm/yr), comparable to the minimum average rate forecast over the next 100 years (IPCC, 2001). The minimum curve allows for sea level rise from more limited melting of both Greenland and West

Antarctica ice and a negligible change to an increase in mass balance of the East Antarctic ice sheet. The minimum curve also allows for limited thermal expansion of sea water and limited melting of mountain glacier ice.

Our best estimate for sea level change over the next 1,000 years follows our 100-year forecast based on the median rate of sea level rise of IPCC (2001) and then shows a gradually decreasing rate of sea level rise from 1.7 feet per century (5.2 mm/yr) to 1.0 feet per century (3.0 mm/yr). The best estimate curve allows for considerable thermal expansion and melting of mountain glacier ice in the short term followed by later melting of the Greenland and West Antarctic ice sheets that is moderated by sea level drawdown by an increase in snowfall and mass balance of the East Antarctic ice sheet.

1,000-year Relative Sea Level Change at Buhne Hill

Buhne Hill may range between 5 to 53 ft above sea level in 1,000 years, with a best estimate of 33 ft (Figure 8). Our relative sea level predictions provide that land level change during the next 1,000 years will fluctuate around the long-term uplift rate of about 0.12 ± 0.05 feet per century (0.4 ± 0.1 mm/yr), with short-term variations that may include up to 6.6 ft (2 m) of coseismic subsidence or up to 10 ft (3.3 m) of coseismic uplift.

Long-Term (10,000- to 100,000-year) Time Scales

Forecast Over the Next 10,000 to 100,000 Years

Over time scales beyond several thousands of years, forecasting sea level change is not accomplished by integrated numerical models but rather is constrained by considering past variations in sea level and maximum sea level high stands recorded in the geologic record over the past ~500,000 years (Thompson and Goldstein, 2005; Cutler and others, 2003; Siddall and others, 2003), and by placing limits on the maximum likely contributions from each ice sheet, plus the relatively minor contributions from thermal expansion and mountain glaciers. Thus, our forecasts of sea level change at Buhne Hill rely on considering the possible magnitudes and duration of the present interglacial, the start of the next glacial interval, and future glacial-interglacial cycles. Two major factors to consider over the next 10,000 years and longer are: (1) the probability that most fossil fuels will be depleted over the next several thousand years, and that the vast ocean system will have absorbed much of the excess human-induced atmospheric CO₂ and cause global cooling (Ruddiman, 2003), and (2) variations in Earth's orbit and resulting solar insolation will cause more- and less-favorable conditions for initiation of glacial intervals in the future (Berger and Loutre, 2002).

It is uncertain when the present interglacial interval will end and the next glacial interval (and start of major sea level lowering) will begin. Most interglacial (or interstadial) intervals over the past million years or so have lasted on the order of 5,000 to 10,000 years, with a maximum interglacial interval of about 30,000 years occurring about 400,000 years ago (Droxler and others, 2003). The ends of past interglacial and the onset of past glacial intervals have coincided with decreasing levels of solar radiation that are approaching minimum values on the 22,000 year orbit cycle (Berger and Loutre, 2002) (Figure 4), and a lowering of atmospheric CO₂ levels (Petit and others, 1999). Presently, the solar radiation on Earth is decreasing towards a low point in the 22,000-year cycle, which is predicted to occur in about 3000 years (Berger and Loutre, 2002). The present, therefore, is an appropriate opportunity for the next glacial interval to begin. Instead of indications of continued global cooling recorded in the 18th and

19th centuries and a lowering of atmospheric CO₂, however, global warming and CO₂ increases typify the 20th century and the present climate. Based on future orbital and solar radiation variations and present-day CO₂ levels, there is a compelling hypothesis that suggests Earth is bypassing the present “opportunity” to begin the next glacial interval (Berger and Loutre, 2002; Archer and Ganopolski, 2005). Although uncertain, the present window of opportunity to begin the next glacial interval may last for another 3000 years. Although it is possible that most fossil carbon reserves will be depleted within the next few hundred years, excess greenhouse gas emissions caused by the burning of that fossil carbon likely will persist in the atmosphere for up to several thousand years, as the ocean and land uptake of excess CO₂ is likely to be slow and gradual. If the present opportunity is bypassed, the next minimum in solar intensity likely to initiate another glacial interval (and a major draw down in sea level) may not occur for another 50,000 years, because the amplitudes of the next 22,000-year cycles will be dampened by the effects of longer-term cycles (Berger and Loutre, 2002) (Figure 4).

10,000-year Relative Sea Level Change at Buhne Hill

Forecasted relative sea level change at the Humboldt Bay ISFSI site over the next 10,000 years is shown in Figure 9. Buhne Hill rises at the long-term permanent uplift rate of 0.12 feet per century. The maximum sea level curve rises at a rate of about 3.3 feet per century for the first ~1200 years, then rises more slowly to attain a maximum height of about +66 ft (20 m) above present-day sea level. The maximum height is consistent with the maximum sea level high stand about 400,000 years ago, and represents complete melting of the Greenland and West Antarctic ice sheets, significant sea level rise from thermal expansion of sea water, and slight melting of the East Antarctic ice sheet. This scenario is consistent with long-term projections described in IPCC (2001). The projection shows inundation of Buhne Hill in about 2000 years. The forecasted height of Buhne Hill in 10,000 years is about 15 ft below sea level.

The minimum sea level curve increases at a rate of about 0.3 feet per century, representing lower amounts of thermal expansion, partial melting of the Greenland and West Antarctic ice sheets, and no change to an increase in the mass balance of the East Antarctic ice sheet. The rate of sea level rise is lower than the rate of land level rise, which has the effect of increasing the elevation of the ISFSI. The forecasted height of the ISFSI under the minimum sea level curve scenario is as great as 53 ft above sea level. The minimum sea level curve also shows an “Early glacial onset” alternative curve, which indicates the possible drop in sea level due to onset of the next glacial interval in the next several thousand years. This early onset alternative is indicated to produce a drop in sea level starting at A.D. 7000, several thousand years after a scenario of global cooling and initiation of the next glacial interval. A several thousand year difference in time between global cooling and sea level fall may be expected given the long response time of the massive ice sheets to adjust to changes in climate.

The best estimate sea level curve shows a decreasing rate of sea level rise from A.D. 3000 to about A.D. 8000, then a negligible change in sea level to A.D. 12,000 (Figure 9). The rate of sea level rise is less than the long-term rate of land level rise after about A.D. 6000, when the ISFSI is shown to be at minimum elevation of about 21.5 ft. After this time, land level change is expected to increase at a higher rate than sea level change, and the ISFSI will attain higher elevations. The best estimate sea level curve follows the path of a delayed onset of the next glacial interval, assuming that Earth will bypass the present opportunity of a solar insolation minimum to initiate the next glacial interval.

100,000-year Relative Sea Level Change at Buhne Hill

Over time intervals of 100,000 years and longer, relative sea level at Buhne Hill will be dominated by large-magnitude sea level changes related to major glacial-interglacial cycles (Figure 10). Buhne Hill rises at the long-term permanent uplift rate of 0.12 ± 0.05 feet per century (0.4 ± 0.1 mm/yr). The maximum sea level curve is based on a maximum level of +66 ft (+20 m), and then is shown to stay at higher than present-day levels for about 50,000 years. The minimum sea level curve attains a maximum height of about +20 ft (+6 m). The early onset alternative curve shows a rapid drop in sea level, indicating a return to glacial conditions in about 5000 years. The delayed onset alternative curve indicates a return to glacial conditions in about 50,000 years, consistent with the next low in solar insolation. The delayed onset curve is partially based on Berger and Loutre (2002). The best estimate curve is intermediate between the minimum and maximum curves, and follows the path of the delayed onset curve.

IMPLICATIONS TO COASTAL PROTECTION AT BUHNE POINT

The assessment of the coastal protection works at Buhne Hill is discussed in some detail by Page (2004) and TerraCosta (2005). The performance of the existing riprap berm in front of Red Bluff is reevaluated in light of potential long term changes of sea level as discussed below.

Current Coastal Protection Works

Red Bluff and Buhne Hill are protected currently by a riprap berm (Figures 1 and 2). Riprap was first placed along the bay shoreline in front of Red Bluff in the 1950s to help arrest wave erosion after PG&E acquired the property. The berm protects all of Buhne Hill, extending southwest for about 3,100 ft from the Northwestern Pacific Railroad's riprap berm on the north to the protective berm placed by the Corps of Engineers in front of the village of King Salmon to the south.

The original riprap, which consisted of silicified, micaceous schist and silicified diorite (maximum lengths 8 ½ ft; median length 6 ½ ft) was eroded during winter storms in the 1980s. In 1989 the riprap berm was completely refurbished by repairing the remnants of the earlier berm and placing additional 4- to 9-ton stones in two layers on the berm. The repairs significantly added to the seaward toe of the berm and decreased the seaward slope to 2.5:1 or 2:1 from the steeper older berm. The 1989 repair also called for setting 6- to 9-ton stones in a trench on the seaward toe of the berm. As measured in 2005 the seaward slope varies between 15 to 30 degrees (3:1 to 4:1) with an average of about 20 degrees. The foundation of the berm is a layer of naturally occurring fine sand (estimated to be 1 to 3 foot thick) that forms the sand flat in front of Red Bluff; the sand layer overlies the wave-cut bench on 'bedrock' that is moderately to well consolidated sand, silt and clay beds of the Pleistocene Hookton Formation. The berm is set 15 to 20 ft in front of the foot of Red Bluff. This set back allows for repairs to be made easily if the berm is damaged and permit easy public access along the coast.

The riprap berm as designed and constructed should withstand waves about 12 to 13 ft high, assuming an average slope of about 20 degrees, and an average stone as 7 tons. Since the augmentation of the riprap berm in 1989, a period of typical waves has been recorded off shore, including relatively high waves in 1999. The riprap has remained stable and performed well, with several areas of minor erosion and settlement.

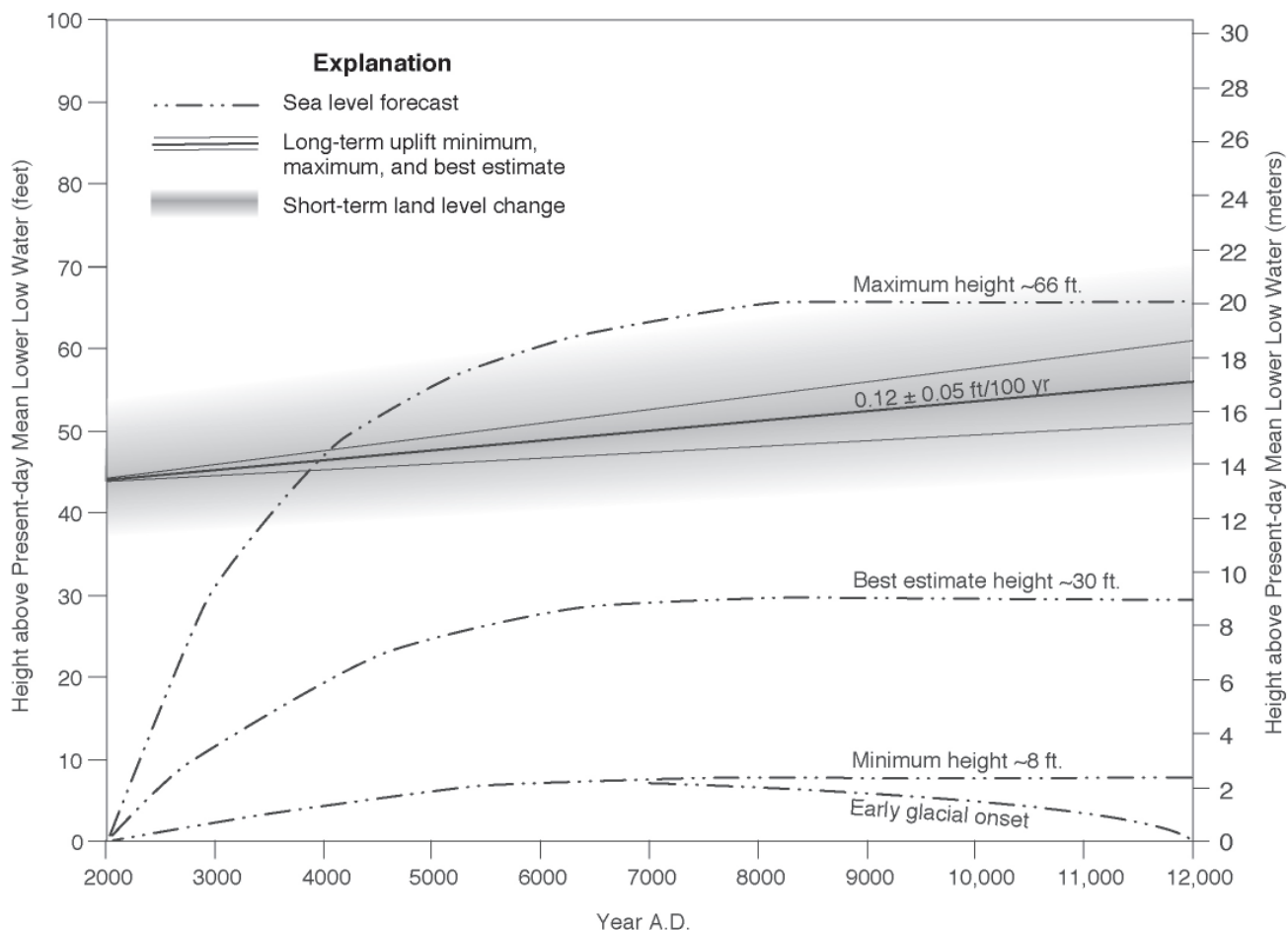


Figure 9. Forecasted changes in land and sea level at Buhne Hill over the next 10,000 years.

Changed Conditions from Rise in Sea Level

As new knowledge about global warming and rise in sea level are gained during the next 100 to 1,000 years, the potential effectiveness of the coastal protection at Buhne Hill will be reassessed. These reassessments will be performed periodically to consider how the projected changes in sea level and variations in storm waves may impact the coastal protection works. Under the minimum sea level rise scenario, tectonic uplift keeps pace with sea level rise. However, if sea level rises significantly with respect to the ISFSI as illustrated under the best and extreme estimated projections (Figures 7 and 8) the rise will be slow and hence needed modifications can and will be implemented to continue to protect the ISFSI. The wide area between the existing berm and the bluff allows for the berm to be raised with a minimum effort. Only under the maximum possible scenario in the 10,000-year projection (Figure 9) does the ISFSI become inundated by the rise in sea level. If conditions similar to those given in the maximum scenario are apparent a thousand years from now, the casks would be moved to another location.

Damage from Storms, Tsunamis and Earthquake Events

As stated in Page (2004), the riprap berm at Buhne Hill may be damaged in future storms or tsunami events. The implications of possible increased wave heights and increased frequency of storms resulting from global warming to the stability of the riprap berm at Buhne Hill has minimal consequence. The

berm may be damaged more frequently than under current conditions but such damage likely would be slight to moderate, and would be repaired by rebuilding the riprap berm with larger-sized boulders and possibly other improvements to account for the changed wave characteristics and other conditions. Any repairs would be undertaken only after significant damage occurred to the existing berm.

Damage from tsunamis is expected to be minor to extensive depending on the size of the runup surges. If the runup is high enough, the riprap berm may be significantly damaged by the wash and backwash of

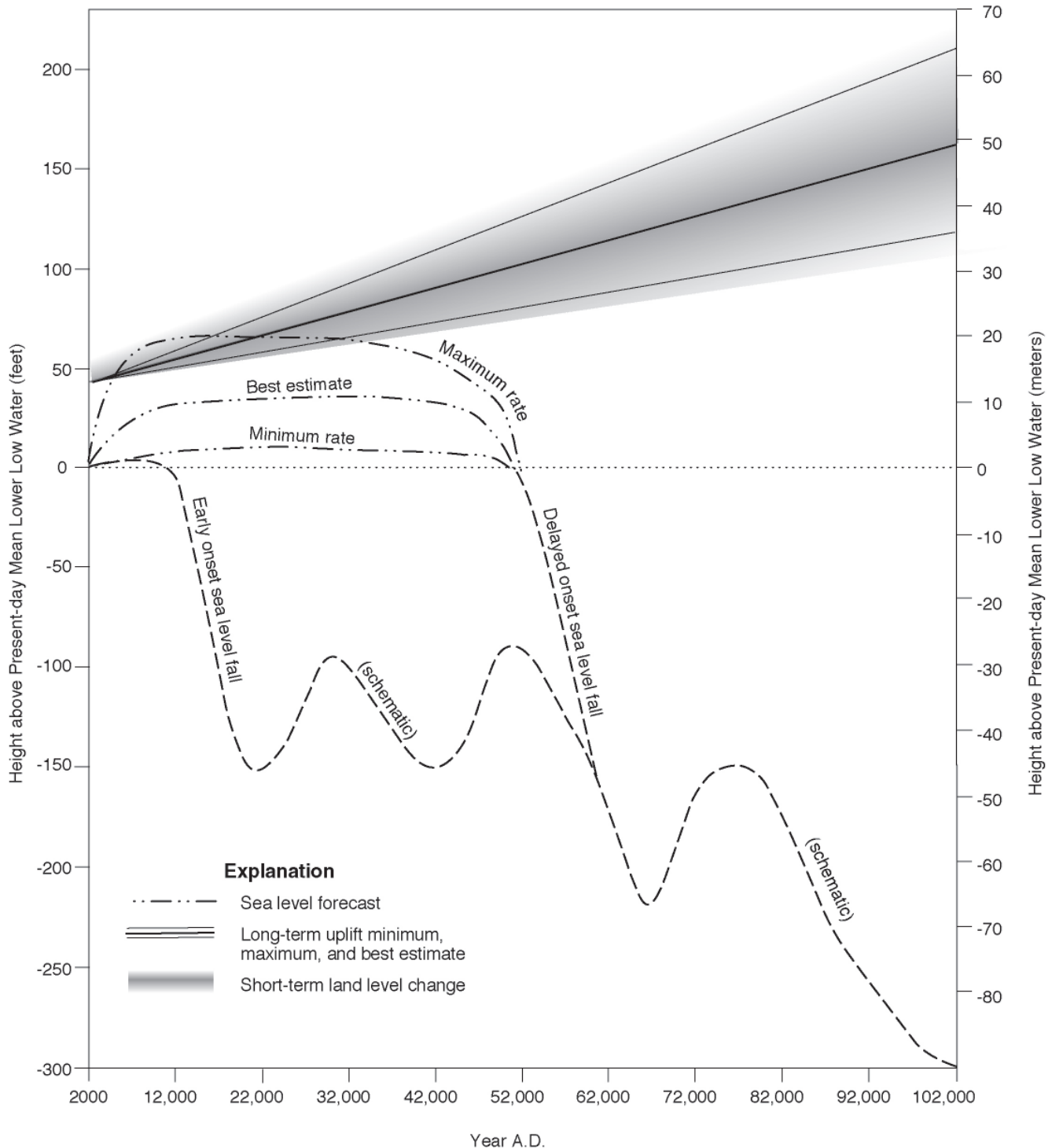


Figure 10. Forecasted changes in land and sea level at Buhne Hill over the next 100,000 years.

the tsunami surges and the vegetation will probably be stripped from the sides of Buhne Hill. However, erosion is expected to be minimal because tsunami are limited to only a few runups surges and the velocity is relatively slow. If a tsunami is larger than the maximum estimated for the ISFSI and floods the vault, no damage is expected because the casks are designed to be submerged and the vault is at ground level so no floating projectiles will impact the ISFSI. This conclusion is supplemented by the evidence from the 2004 Sumatra tsunami: while numerous houses were washed away by the 2004 Sumatra tsunami, most foundation pads remained intact. If and when a tsunami damages the protective berm or erodes Red Bluff, the riprap and other protection works will be repaired and augmented as needed. This is relatively easily done because of the wide strip between the berm and Red Bluff allow for easy equipment access and room to raise the berm.

An earthquake on Cascadia subduction zone and/or Little Salmon fault zone is expected to produce subsidence or uplift of up to several meters at Buhne Hill and the ISFSI site, and a simultaneous subsidence at the village of King Salmon, which lies on the footwall of the Bay Entrance and Buhne Point faults. This will inundate King Salmon and the south side of Buhne Hill and expose this area to erosion from storm waves that will more easily reach the area after the earthquake. The berm may need repairs and be heightened to accommodate the relative rise in sea level from the footwall subsidence. Additional protection of the south-facing aspect of Buhne Hill may be required, but this part of the hill is not subject to significant wave erosion. If significant erosion develops, it can be mitigated by adding a riprap berm at the base of the hill, similar to the existing berm.

ACKNOWLEDGEMENTS

Harvey Kelsey of Humboldt State University and Gary Carver of Carver and Associates, Kodiak, Alaska, provided input to the analysis of the short-term tectonic uplift, although our conclusions do not necessarily reflect the opinions of these experts. Ron Flick, San Diego State University, provided the information on sea level rise and wave parameters for the near-term up to 100 year scenarios. Walter Crampton, Principal Engineer, TerraCosta Consulting Group, assessed the effectiveness of the coastal protection works and formulated the revised mitigation to counter sea level rise and changing wave patterns. Stuart Nishenko, PG&E Geosciences Department, assessed the impact of tsunami on Buhne Hill. William Lettis & Associates provided professional development support to Thompson for preparation of this paper. Lloyd S. Cluff, PG&E, Director of the PG&E Geosciences Department and Larry Pulley, Project Manager, Humboldt Bay ISFSI, supported the wide scope needed to address the Coastal Commission request.

REFERENCES CITED

- Archer, David; Ganopolski, Andrey, 2005, A movable trigger: Fossil fuel CO₂ and the onset of the next glaciation: *Geochem. Geophys. Geosyst.*, Vol. 6, No. 5, Q05003 DOI 10.1029/2004GC000891
- Arendt, A.A., Echelmeyer, K.A., Harrison, W.D., Lingle, C.S., and Valentine, V.B., 2002, Rapid wastage of Alaska glaciers and their contribution to rising sea level: *Science*, v. 297, p. 382-386.
- Atwater, B.F. and Hemphill-Haley, E., 1997, Recurrence intervals for great earthquakes of the past 3500 years at northeastern Willapa Bay, Washington: U.S. Geological Survey Professional Paper 1576, 108 p.
- Berger, A. and Loutre, M.F., An exceptionally long interglacial ahead?: *Science*, v. 297, p. 1287-1288.
- Bindschadler, R., 1998, Future of the West Antarctic Ice Sheet: *Science*, v. 282, p. 428-429.
- Blum, M.D., Carter, A.E., Zayac, T, and Goble, R., 2002, Middle Holocene sea level and evolution of the Gulf of Mexico coast (USA), *Journal of Coastal Research*, Special Issue 36, pp. 65-80.
- COHMAP Members, 1988, Climate changes of the last 18,000 years: observations and model simulations: *Science*, v. 271, p.1043-1052.
- Chappell, J., 2002, Sea level changes forced ice breakouts in the last glacial cycle: New results from coral terraces: *Quaternary Science Review*, v. 21, p. 1229-1240.
- Clarke, S. H., Jr., and G. A. Carver, 1992, Late Holocene tectonics and paleoseismicity, southern Cascadia subduction zone: *Science*, v. 255, p. 188-192.
- Cuffey, K.M. and Marshall, S.J., 2000, Substantial contribution to sea-level rise during the last interglacial from the Greenland ice sheet: *Nature*, v. 404, p. 591-594.
- Cutler K.B., Edwards R.L., Taylor F.W., Cheng H., Adkins J., Gallup C.D., Cutler P.M., Burr G.S., Chappell J., and Bloom A.L. (2003). Rapid sea level fall and deep-ocean temperature change since the last interglacial. *Earth and Planetary Science Letters*, v. 206, p. 253-271.
- Douglas, B.C., 1991, Global sea level rise: *Journal of Geophysical Research*, v. 96, p. 6981-6992.
- Douglas, B.C., 1997. Global sea level rise: a redetermination, *Surveys Geophys.*, v. 18, p. 279-292.
- Douglas, B.C., 2001, An introduction to sea level, in, Douglas, B.C., Kearney, M.S., and Leatherman, S.P., eds., *Sea Level Rise: History and Consequences*, International Geophysics Series, v. 75, Academic Press, 232 p.
- Droxler, A.W., Alley, R.B., Howard, W.R., Poore, R.Z., and Burckle, L.H., 2003, Introduction: Unique and exceptionally long interglacial marine isotope stage 11: window into Earth warm future climate: In, A. Droxler, R. Poore, L. Burckle, and L. Osterman, Eds., *Earth's Climate and Orbital Eccentricity: The Marine Isotope Stage 11 Question*: American Geophysical Union Geophysical Monograph 137, pp. 69-85.
- Fairbanks, R.G., 1989. Glacio-eustatic sea level record 0-17,000 years before present: influence of glacial melting rates on Younger Dryas event and deep ocean circulation. *Nature*, 342, 637-642.
- Fleming, K., Johnston, P., Zwart, D., Yokoyama, Y., Lambeck, K., and Chappell, J., 1998, Refining the eustatic sea-level curve since the Last Glacial Maximum using far- and intermediate-field sites: *Earth and Planetary Science Letters*, v. 163, p. 327-342.
- Gornitz, V., 1995, Sea level rise: A review of recent past and near-future trends: *Earth Surface Processes and Landforms*, v. 20, p. 7-20.
- Gregory, J. M., J. A. Church, G. J. Boer, K. W. Dixon, G. M. Flato, D. R. Jackett, J. A. Lowe, S. P. O'Farrell, E. Roeckner, G. L. Russell, R. J. Stouffer, and M. Winton, 2001, Comparison of results from several AOGCMs for global and regional sea level change 1900-2100: *Climate Dynamics*, v. 18, p. 225-240.
- Hearty, P.J., Kindler, P., Cheng, H. and Edwards, R.L., 1999, A +20 m middle Pleistocene sea level high stand (Bermuda and the Bahamas) due to partial collapse of Antarctic ice: *Geology*, v. 27, p.375-378.
- Huybrechts, P., Gregory, J., Janssens, I., and Wild, M., 2004, Modeling Antarctic and Greenland volume changes during the 20th and 21st centuries forced by GCM time slice integrations: *Global and Planetary Change*, v. 42, p. 83-105.
- Hyndman, R.D. and Wang, K., 1995, The rupture zone of Cascadia great earthquakes from current deformation and the thermal regime: *Journal of Geophysical Research*, v. 100, p. 22,133-22,154.
- Imbrie, J., Hays, J.D., Martinson, D.G., McIntyre, A., Mix, A.C., Morley, J.J., Pisias, N.G., Prell, W.L., and Shackleton, N.J., 1984, The orbital theory of Pleistocene climate: Support from a revised chronology of the marine $\delta^{18}\text{O}$ record, in Berger, A.L., and others, eds., *Milankovich and Climate*: Hingham, Massachusetts, Riedel Publishing, p. 269-305.
- IPCC, 2001, Climate Change: The scientific basis, Third assessment report by the Intergovernmental Panel on Climate Change: Cambridge University Press, Oxford. See especially Chapter 11: Changes in sea level, p. 641-693. Available online at: http://www.grida.no/climate/ipcc_tar/
- Kelsey, H.M., Witter, R.C., and Hemphill-Haley, E., 2002, Plate-boundary earthquakes and tsunamis of the past 5500 years, Sixes River estuary, southern Oregon: *Geological Society of America Bulletin*, v. 114, p. 298-314.
- Laskar, J., Robutel, P., Joutel, F., Gastineau, M., Correia, A.C.M., Levrard, B., 2004, A long term numerical solution for the insolation quantities of the Earth: *Astronomy & Astrophysics*, v. 428, p. 261-285, DOI: 10.1051/0004-6361:20041335.

- Lea D. W., Martin P. A., Pak D. K., and Spero H. J. (2002) Reconstructing a 350 ky history of sea level using planktonic Mg/Ca and oxygen isotopic records from a Cocos Ridge core. *Quat. Sci. Rev.* 21(1-3), 283-293.
- Martinson, D.G., Pisias, N.G., Hays, J.D., Imbrie, J., Moore, T.C., Shackleton, N.J., 1987, Age dating and the orbital theory of the ice ages: development of high-resolution 0 to 300,000-year chronostratigraphy: *Quaternary Research* 27, 1–29.
- Mitchell, C.E., Vincent, P., Weldon, R.J., and Richards, M.A., 1994, Present-day vertical deformation of the Cascadia margin, Pacific Northwest, United States: *Journal of Geophysical Research*, 99, p. 12,257-12,277.
- Mörner, N.-A., 2004, Estimating future sea level changes from past records: *Global and Planetary Change*, v. 40, p. 49-54.
- Oppenheimer, M., 1998, Global warming and the stability of the West Antarctic Ice Sheet: *Science*, v. 393, p. 325-332.
- Page, W.D., 2005, Implications of Long-Term Global Warming and Tectonic Displacements at Buhne Hill, Humboldt County, California: PG&E Geosciences Department report to the California Coastal Commission, 39p. plus figures.
- Page, W.D., 2004, Assessment of Erosion at Buhne Hill, Humboldt Bay ISFSI, Humboldt County, California; PG&E Geosciences Department report, 32p.
- PG&E, 2003, Humboldt Bay ISFSI safety analysis report, December 2003, Section 2.6: report to the Nuclear Regulatory Commission, Washington, D.C.; produced from PG&E (2002), Seismic Hazard Assessment for the Humboldt Bay ISFSI Project: Humboldt Bay ISFSI Project Technical Report TR-HBIR-2002-01, revision 0 – 27 December 2002, Section 3, Regional Geology, 47 p.; Section 4, Site Geology, 49p.; Section 5, 47 p.; Section 8, Surface faulting potential, 26 p.; Section 9, Tsunami hazard, 64p.
- Peltier, W.R., 1999, Global sea level rise and glacial isostatic adjustment: *Global and Planetary Change*, v. 20, p. 93-123.
- Peltier, W.R. & Tushingham, A.M., 1989. Global sea level rise and the Greenhouse effect: Might they be connected?: *Science*, v. 244, p. 806-810.
- Petit, J.R., J. Jouzel, D. Raynaud, N.I. Barkov, J.-M. Barnola, I. Basile, M. Benders, J. Chappellaz, M. Davis, G. Delayque, M. Delmotte, V.M. Kotlyakov, M. Legrand, V.Y. Lipenkov, C. Lorius, L. Pépin, C. Ritz, E. Saltzman, and M. Stievenard, 1999, Climate and atmospheric history of the past 420,000 years from the Vostok ice core, Antarctica: *Nature*, v. 399, pp. 429-436.
- Potter, E.-K., Esat, T.M., Schellmann, G., Radtke, U., Lambeck, K., and McCulloch, M.T., 2004, Suborbital-period sea-level oscillations during marine isotope substages 5a and 5c: *Earth and Planetary Science Letters*, v. 225, p. 191-204.
- Ruddiman, W.F., 2003, The anthropogenic greenhouse era began thousands of years ago: *Climate Change*, v. 61, p. 261-293.
- Scherer, R.P., Aldahan, A., Tulaczyk, S., Possnert, G., Engelhardt, H., and Kamb, B., 1998, Pleistocene collapse of the West Antarctic ice sheet: *Science*, v. 281, p. 82-85.
- Siddall M., E.J. Rohling, A. Almogi-Labin, Ch. Hemleben, D. Meischner, I. Schmelzer, & D.A. Smeed, 2003, Sea level fluctuations during the last glacial cycle. *Nature*, 423, 583-588.
- TerraCosta Consulting Group, 2005, Revetment Stability at Buhne Hill, Humboldt Bay, California: unpublished consultant report to PG&E, Project No. 2350, dated October 5, 2005.
- Thompson, W.G. and Goldstein, S.L., 2005, Open-system coral ages reveal persistent suborbital sea level cycles: *Science*, v. 308, p. 401-404.
- Waelbroeck, C., Labeyrie, L., Michel, E., Duplessy, J.C., McManus, J.F., Lambeck, K., Balbon, E., and Labracherie, M., 2002, Sea-level and deep water temperature changes derived from benthic foraminifera isotopic records: *Quaternary Science Reviews*, v. 21, 295-305.
- Williams, T.B., 2002, The Geodetic Signature of Modern Deformation (1993-2002) within the Southern Cascadia Margin, Northwestern California: unpublished M.S. Thesis, Humboldt State University, Department of Geology, 102 p.
- Witter, R.C., Kelsey, H.M., and Hemphill-Haley, E., 2003, Great Cascadia earthquakes and tsunamis of the past 6700 years, Coquille River estuary, southern coastal Oregon: *Geological Society of America Bulletin*, v. 115, pp. 1289-1306.

Day 3 Introduction (Saturday)

Congratulations for making it to Day 3!

We'll begin by gathering at the fire circle in Pamplin Grove at 8:00 AM to briefly discuss trip stop logistics and carpooling. We'll then line up, *with as few a vehicles as possible*, and roll out of Pamplin Grove at 8:30 AM.

DAY 3 – Logistical Considerations: Total driving for the day will be about 90 mi, for the most part on paved public roads with the exception of a 3.6 mi length of private road behind a locked gate in the North Fork Elk River valley (**drive slowly and watch for equipment involved in timber operations**). Services are available at numerous locations along the route, but to stay on schedule and keep everyone together, please **plan on stopping for services in route back to Pamplin Grove at the end of the day**. The best place to stock up on supplies is Eureka, where there are numerous gas stations and grocery stores on south bound Hwy 101. We will make two stops today, both of which include short hikes (1- 2 mi) and opportunities to poke at exposures – so bring your hiking boots, miners pick or soil knife, and plenty of food and water.

Science of the day: Day 3 will build on the themes of Days 1 and 2 by focusing on the continental, estuarine, dune, and nearshore marine geomorphic and stratigraphic responses to deformation, baselevel change, and climate forcing in the northern Humboldt Bay area.

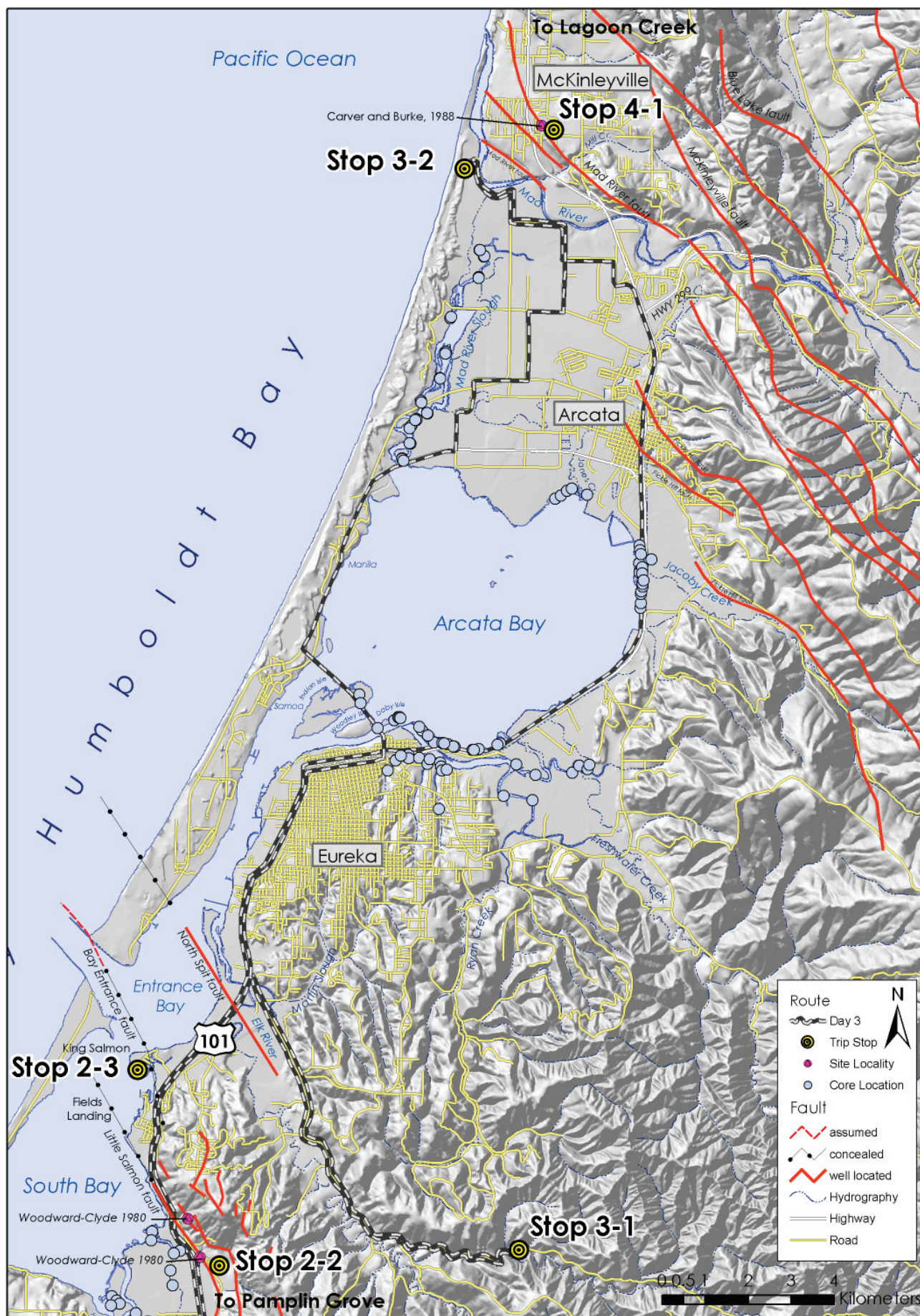
Stop 3-1 is located in the North Fork Elk River Valley, north of the Little Salmon fault and south of Eureka. We will examine relations between late Pleistocene uplift, denudation, and bedrock river incision rates as well as the influence of large landslides on landscape evolution.

Stop 3-2, located at Mad River Beach, examines three adjacent coastal geomorphic environments. We will start by walking south in the dunes for about a mile. There, we'll discuss continental shelf sedimentation and Holocene development of the northern California coast, coastal sand dune stratigraphy, and the results of a coring campaign in the Arcata Bay and Mad River Slough tidal flats. After the presentations and discussions, folks can further examine the coastal dune stratigraphy, walk to an excellent view of Arcata Bay marsh at the eastern edge of the dunes, walk to the beach, or start the hour-long drive back to Pamplin Grove.

See you tonight at the business meeting!

Day 3 Itinerary

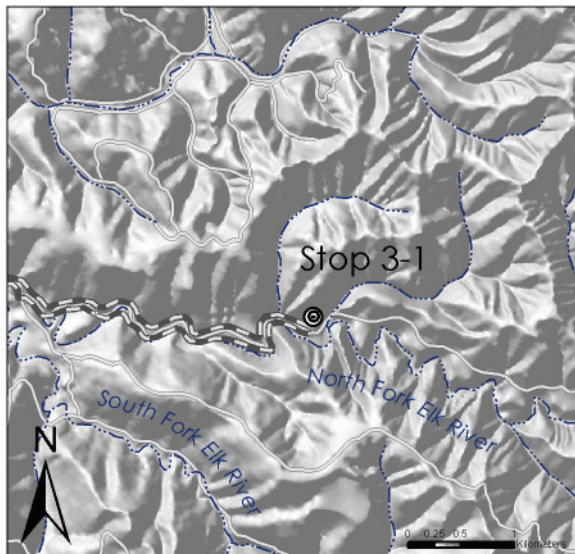
Day 3 (Saturday) North Humboldt Bay Area			
Field Trip Stop	Authors	Title	Reading Material
Stop 3-1: Lower North Fork Elk River: Fluvial terraces, large landslides, and driving forces.	Jay Stallman and Harvey Kelsey	Transient geomorphic response to late Pleistocene baselevel change and climate forcing in the southern Cascadia thrust-and-fold belt	paper 3-1-A
	Ben Mackey and Joshua Roering	Identifying deep-seated landslides through the use of high resolution airborne laser mapping – implications for landscape evolution	paper 3-1-B
	Gerald Marshall	Elk River geology, landsliding and related features	abstract
Stop 3-2: Mad River Beach: Holocene dune stratigraphy, coseismic tidal marsh stratigraphy, and offshore sediment dynamics.	Danny O'Shea	Marine stratigraphy of the Eel continental shelf: coastal response to sea level rise since the latest glacial maximum	paper 3-2-A
	Chad Prichard	Coseismic subsidence of Arcata Bay	paper 3-2-B
	Tom Leroy	Coastal Sand Dune Stratigraphy and Geomorphology of the North Spit of Humboldt Bay	paper 3-2-C



Day 3 Road Log

<u>Mileage</u>	<u>Distance</u>	<u>Description</u>
0.0	0.0	Pamplin Grove gate
0.3	0.3	TURN LEFT onto Hwy 36 - watch for traffic!
1.0	0.8	Martin & Shirley's Store
3.7	2.7	City of Carlotta - Continue west on Highway 36. Please drive slowly through town.
5.1	1.4	Carlotta Sign
5.4	0.3	Yager Creek Bridge
5.6	0.2	Little Salmon fault cuts hills on skyline (see trip map)
8.1	1.9	Gas Station. There is only about 50 miles of driving to get to the first stop. There are only 2 stops today, and each has a fair amount of walking to see the outcrops. We will drive thru Eureka between stops 1 & 2 today, so please only gas up here if you are in real need.
8.2	0.1	BEAR LEFT and continue East on Hwy 36. Do not go right towards Rhonerville.
9.0	0.9	View of the Van Duzen River valley to the south (9 o'clock).
10.9	2.8	Highway 36 ends. TURN RIGHT ONTO HWY 101
30.7	19.8	TURN RIGHT AND EXIT Highway 101 at Herrick Ave. At the stop sign, turn right onto Herrick Ave.
30.8	0.1	Intersection of Herrick Ave. and Elk River Road. TURN RIGHT on Elk River Road. View south is toward marine oxygen isotope stage 5 (MIS 5) marine terraces at the northwest end of Humboldt Hill. View northeast is toward MIS 5 marine terraces in Eureka (see Figure 3b in Thompson et al. paper 2-3C, this volume). The difference between 5a (80 ky) and 5c (105 ky) terrace elevations in Eureka and their respective paleo-sea levels (Muhs et al. 1992) divided by terrace ages inferred from reference chronosequences near Trinidad and McKinleyville (Carver and Burke 1992) yield a long-term uplift rate of $0.46 \pm 0.03 \text{ m ky}^{-1}$ for the Eureka block.
32.3	1.5	Intersection of Elk River Road and Ridgewood Drive. TURN RIGHT to stay on Elk River Road (do not proceed straight on Ridgewood Drive). Ridgewood Drive continues up a flight of six marine terraces and onto the surface used to calculate denudation of the Ryan Creek basin (Stallman and Kelsey, paper 3-1A, this volume). Long-term denudation was estimated from the volume removed by erosion into a paleo-topographic surface enveloping broad, accordant ridge crests capped by shallow marine and fluvial deposits of middle to late Pleistocene age (330–590 ka). Denudation rate ($0.10 \pm 0.03 \text{ m ky}^{-1}$) is 3 to 7 times slower than long-term uplift rate, indicating the landscape is not in a topographic steady state.
32.6	0.4	South of Elk River Road, late Pleistocene fluvial terraces are cut into deltaic and shallow marine deposits.
34.4	1.7	Three levels of fluvial terraces step up the north valley wall left of Elk River Road.

<u>Mileage</u>	<u>Distance</u>	<u>Description</u>
		At 3 o'clock, Railroad Gulch is visible south of the Elk River valley. Railroad Gulch is the type section for the 590 ± 10 ka Railroad ash, correlative to the Rockland ash (Sarna-Wojcicki et al. 1985, Lanphere et al. 2005). The Railroad Gulch basin contains excellent examples of large, deep-seated landslides formed in Pleistocene soft sediments (Kilbourne and Morrison 1985, Marshall this volume), and is one of the study basins for testing "Deep-seated Landslide and Earthflow Detection" (DSLED) algorithms using LiDAR data (Mackey and Roering, paper 3-1B, this volume). Ben Mackey will present some of the DSLED findings at this stop.
35.6	1.2	Intersection of Elk River Road and Wrigley Road. TURN LEFT on Wrigley Road (DO NOT cross bridge over North Fork Elk River).
36.1	0.6	Gate into Pacific Lumber Company property. Please leave the gate open and respect the property owner by driving slowly and remaining on the route described in the FOP guidebook. WATCH FOR LOG TRUCKS and other equipment involved in timber operations. BE PREPARED TO GET OFF THE ROAD AND LET LOGGING TRAFFIC GET BY IF NEED BE.
		The gate is located on the longitudinally continuous and paired T3 strath terrace (Stallman and Kelsey, paper 3-1A, this volume). Minimum age estimates for strath cutting provided by AMS dates from the channel facies on T3 (18.5–19.5 ky) and T5 (39.0–40.2 ky) terraces yield incision rates of 0.85 ± 0.05 m ky ⁻¹ and 0.89 ± 0.09 m ky ⁻¹ . Incision rates are similar to the average post-lowstand (~21 ka) sedimentation rate (0.95 ± 0.25 m ky ⁻¹) on the nearby margin, but are roughly twice the long-term uplift rate and 6–14 times faster than long-term denudation rate. Correlation of strath cutting to paleoclimate proxies in nearby marine sediment cores suggests a millennial-scale climate signal superimposed on baselevel lowering.
36.5	0.4	Gaging station. Flight of two Holocene terraces on left bank (south of road). T3 terrace occurs above Holocene terraces.
36.9	0.4	North Coast Bible Camp occupying the Holocene terrace on the right (south of road). Broad, paired T3 terraces occur above the Holocene valley bottom on both left and right banks (both sides of road).
37.1	0.2	Road crosses an unnamed creek and ascends T3 riser.
37.2	0.1	Top of riser, slope break to T3 surface.
37.7	0.5	Road crosses Dunlap Creek and ascends T3 riser.
37.9	0.2	Road intersection. TURN LEFT and ascend riser between T3 and T4 terraces. Look for parking directions in this vicinity.



Stop 3-1 Lower North Fork Elk River: Fluvial terraces, large landslides, and driving forces

We will have three short presentations (Ben, Gerald, and Jay) followed by a walk to several exposures of strath terrace cover sediments.

[0900-1230]

STOP 3-1 ABSTRACTS

Transient geomorphic response to late Pleistocene baselevel change and climate forcing in the southern Cascadia thrust-and-fold belt, north coastal California

Jay D. Stallman and Harvey Kelsey

Fluvial terraces, marine terraces, and accordant ridge-capping surfaces in the North Fork Elk River (59 km²) and Ryan Creek (33 km²) basins record transient geomorphic response to baselevel and climatic change in the southern Cascadia thrust-and-fold belt since the middle to late Pleistocene. Denudation rate ($0.10 \pm 0.03 \text{ m ky}^{-1}$), estimated from the rock volume eroded beneath a paleotopographic surface enveloping ridge-capping shallow marine and fluvial deposits of middle Pleistocene age (330–590 ka), is 3 to 7 times slower than long-term uplift rate ($0.46 \pm 0.03 \text{ m ky}^{-1}$) determined from the relative age and altitude of MIS 5a and 5c marine terraces near Eureka. Rapid bedrock incision ($0.85 \pm 0.05 \text{ m ky}^{-1}$) below an 18–20 ka fluvial strath terrace in the North Fork Elk River valley, however, exceeds long-term uplift rate and is similar to the average post-lowstand (~21 ka) sedimentation rate on the margin ($0.95 \pm 0.25 \text{ m ky}^{-1}$). Correlation of strath cutting to paleoclimate proxies in marine sediment cores suggests a millennial-scale climate signal superimposed on baselevel lowering, a conclusion consistent with models of climate-controlled strath terrace genesis in the northern Cascadia forearc and other temperate, unglaciated mountain ranges. Transient geomorphic response is well-represented in North Fork Elk River strath terraces compared to terrace records in nearby coastal basins due in part to the effects of contrasting lithology on bedrock erodibility. Resistant lithologies sourced from Yager terrane and competent blocks within Eastern belt Franciscan mélangé in the upper basin persist as bedload, and when supply rates are optimal, effectively erode the weaker siltstone and mudstone channel boundaries in the lower North Fork Elk River valley. Climate control on terrace genesis and disparity between uplift, denudation, and bedrock incision rates suggests a decoupling of valley bottom and hillslope geomorphic responses from baselevel lowering by climatically forced variability in sediment supply and stream power. Increased activity of currently dormant deep-seated landslides in Central belt Franciscan mélangé and soft sedimentary rocks may account for increased hillslope sediment production during wet climate intervals.

Identifying Deep-Seated Landslides Through the Use of High Resolution Airborne Laser Mapping – Implications for Landscape Evolution

Mackey, B.H., and Roering, J.J

The availability of extensive high-resolution Lidar datasets is revolutionizing the approaches we take in analyzing landscapes and how they evolve. Deep-seated landslides have proven particularly suited to identification and analysis with this high resolution digital topography. Large scale mass movements characteristically exhibit a rough surface generated during movement and host a suppressed drainage network when compared with terrain that has not undergone landsliding. Here we present techniques that can utilize surficial roughness and impeded drainage to distinguish landslides from unfailed terrain. The Elk River catchment, California, hosts a range of deep-seated landslide features which our algorithms are able to identify. In concert with radiometric dating, these approaches to analyzing Lidar data can be calibrated with landslide age and ultimately used to address the question of what controls the timing and location of deep-seated landslides.

Elk River Geology, Landsliding and Related Features and Relative Landslide Potential Maps

Gerald J. Marshall

In 2005 the California Geological Survey (CGS) released 1:24,000 scale maps of the Elk River Watershed titled: “Geologic and Geomorphic Features Related to Landsliding in Elk River Watershed” and “Relative Landslide Potential with Geomorphic Features, Elk River Watershed”. The maps present a compilation of data pertaining to the geology and relative stability of the landscape, including but not limited to the presence and type of past landsliding. This map set was compiled from multiple sources including published and unpublished maps and reports, aerial photograph mapping, and reconnaissance geologic mapping.

Clues to the presence of landsliding or unstable conditions used in the aerial photographic analysis and reconnaissance mapping included slope morphology. These morphological indicators are listed in detail in many widely used publications including notes issued by the California Division of Mines and Geology (DMG, now California Geological Survey or CGS). For brief example, convex slopes downslope of semi-lunar arcuate concave slopes are evidence of possible deep-seated landsliding. Scalloped, striated slopes are evidence for shallow debris sliding. Discontinuous, disrupted poorly incised drainages are indications of unstable terrain typical of large earthflows or translational landslides as are possible displaced watercourses at the toe regions. Distinctive vegetation differences such as an area of even-aged trees within a homogeneously aged forest or a patch of differing species can also be evidence of previous ground disturbance.

Of interest is the observed evidence for widespread deep-seated landsliding that is recorded on these maps. With recognition that the real world tends toward continua and actual landslides tend to display multiple process defined characteristics, these apparent landslides were classified according to the perceived dominate process type. Relative activity states were assigned using a published and widely used relative age classification scheme.

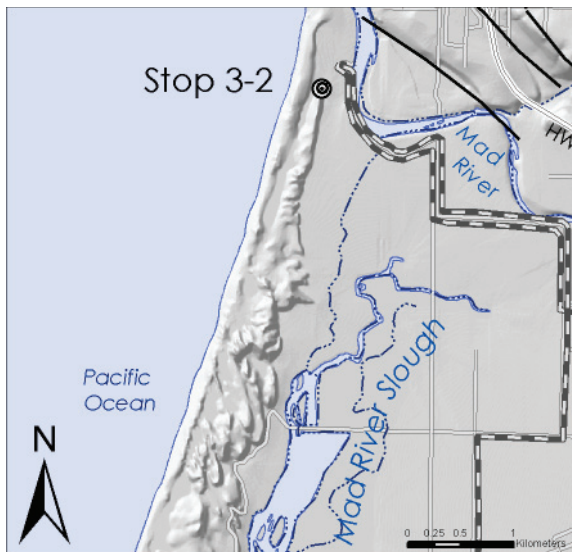
It is apparent from the maps that these deep-seated landslide features are pervasive across the Elk River Watershed and most are at various states of dormancy. It appears that some correlation between process types and localities could be derived that could be linked to underlying geology and structure. It is our interpretation that that areas underlain by Yager and Central Belt Franciscan materials display more deep-seated earthflow landsliding and as a result are often characterized by longer, gentler and smoother slopes. Areas underlain by Wildcat Group materials tend to be steeper with rotational/translational the dominant deep-seated landsliding process. It can be observed that the unambiguously historically active deep-seated landslides, while still relatively large do not approach the size of the larger indicated older dormant features.

From the CGS Elk River geologic and geomorphic features related to landsliding map it is intuitive that deep-seated landsliding has been a major shaper of the current landscape configuration and the dominant operating landsliding process has left a distinctive signature in various parts of the watershed. Relatively few and smaller historically active landslides in comparison to larger, older dormant features suggest the possibility of periods of more intense landsliding in the past. Detailed studies of many individual landslides appear necessary to tease out any pattern of age grouping that may be present.

California Geological Survey, 2120 Campton Road, Suite E, Eureka, CA 95503 (707) 441-5742 Gerald.Marshall@conservation.ca.gov

<u>Mileage</u>	<u>Distance</u>	<u>Description</u>
37.9		Return to cars and DRIVE CAREFULLY back down the road we came in.
39.8	1.9	Gate - leaving Pacific Lumber Company property.
40.4	0.6	Intersection of Elk River Road and Wrigley Road. TURN RIGHT
43.7	3.3	Intersection of Elk River Road and Ridgewood Drive. TURN LEFT
45.2	1.5	Intersection of Elk River Road and Herrick Ave. TURN LEFT
45.3	0.1	Northbound Highway 101 on-ramp. TURN RIGHT on to Hwy 101 towards Eureka
45.8	0.5	Pierson's stoplight ("home of the big hammer") CONTINUE STRAIGHT following 101 North thru Eureka. If you need to stop for gas or lunch staples, please do so <i>VERY QUICKLY</i> . Stop 3-2 involves a walk down the beach to look at tsunami deposits, and you'll want to hear this one, so, we need to get thru Eureka ASAP. !
46.1	0.3	Ft Humboldt stoplight. Continue straight thru the stoplight.
48.2	2.1	To the left is the Bayshore Mall. The parking lot is built on bay mud and is subject to liquefaction during strong ground shaking. To the right is the back edge of the MIS 4a (64 ky) marine terrace mapped by Carver and Burke (1992). West of the mall is where 85% of the gasoline delivered to Humboldt County is pumped from tankers.
50.1	1.9	Follow 101 N around a SHARP RIGHT TURN as Broadway turns to 5th Street.
50.5	0.4	Carver and Burke (1992) map this slope break as the riser to the MIS 5a (83 ky) marine terrace.
50.9	0.4	Move to the left lane and prepare to turn left onto R St (SR 255). We will turn left, then cross the Southbound 101 at a traffic light before continuing across the bridge to Samoa. Turning the group will almost certainly cause a traffic jam, so be careful.
51.1	0.2	TURN LEFT onto R St (SR 255), proceed across southbound Hwy 101, and over the Samoa Bridge. The Samoa Bridge underwent a seismic retrofit in 2005 to shore up the footings. Wooden, drop-down gates were also installed to stop traffic from driving on the bridges in the event of earthquake.
51.3	0.2	View left is of Woodley Island, location of the National Weather Service Eureka Forecast Office and the Eureka marina.
51.6	0.3	SR 255 crosses Indian Island, site of the 1860 massacre of the Wiyot ("Weott") tribe.
52.4	0.8	View to the west is stable, forested sand dunes on the North Spit of Humboldt Bay.
52.9	0.5	TURN RIGHT at the intersection of State Route 255 and Samoa Blvd.
53.6	0.7	The low lying marsh to the left is the location of the south Manila core transect. The transect starts where the forested dunes meet the marsh, and ends where the road fill meets the marsh on the western side of the road. The transect revealed a submerged dune with a buried and submerged wetland soil stratigraphically above it (Leroy and Patton, 2005 unpublished).

<u>Mileage</u>	<u>Distance</u>	<u>Description</u>
54.9	1.3	Crossing Mad River Slough. The Mad River Slough has been one of the most studied coastal areas in the Humboldt Bay area. It archives at least 4 submerged wetland soils and has a submerged forest at the north end which has been dated using dendrochronology. The dating and stratigraphic context suggests it was submerged after the 1700 AD Cascadia subduction zone earthquake (Jacoby et al. 1995). Other notable studies are by Vick (1988) and Prichard (2005).
56.2	0.8	TURN LEFT on Jackson Ranch Road and follow the winding road into the Arcata bottoms. The Humboldt Bay margin, including much of the bottoms, was dominated by expansive coastal salt marsh and brackish wetlands prior to European settlement. The sloughs and dry channels over the next half mile are remnants of these wetlands. Note the stable, parabolic dunes to the west adjacent to the Mad river slough.
57.0	2.0	TURN LEFT on Seidel Road
59.0	1.0	TURN RIGHT on Lanphere Road. Stop 3-2 will in the dunes at ~ 8 o'clock. We will hike in about a mile (one-way) from a public access beach to our north.
60.0	0.2	TURN LEFT on Mad River Road. Follow the main road as it turns left, right, then left again along the south bank of the Mad River.
60.2	3.1	Passing thru Tyee City, a site of habitation since native times. On the right is the Mad River. The levee to the right was topped during several recent floods ('95, 97, '06) and provides little protection from future high flows.
63.3	0.2	Looking downstream on the right bank, note where erosion by the Mad River has exposed the southern branch of the Mad River fault. This exposure is essentially a fractureless monocline warping the 83 ky terrace and associated silt cap.
63.5	0.4	TURN RIGHT into Mad River Boat Ramp and park in the boat ramp parking lot. From here we will gather and walk down the backside of the dunes for about a mile. As you walk along the deflated surfaces behind the foredune, observe the dune morphology, gravels, and large woody debris. In what depositional environment do large gravels get deposited with clean beach sands?



Stop 3-2: Mad River Beach. Holocene dune stratigraphy, North Bay and offshore sediment deposits

We will have three short presentations (Danny, Chad, and Leroy) followed by a walk to several beach and tsunami deposits.

[1400-1700]

STOP 3-1 ABSTRACTS

Marine Stratigraphy of the Eel Continental Shelf: Coastal response to sea level rise since the latest glacial maximum

Danny O'Shea

Sediment cores and high-resolution Chirp seismic reflection profiles on the Eel Shelf reveal four distinct facies: 1) inner shelf sands; 2) transitional sands-muds; 3) mid-shelf muds; 4) relict lowstand and transgressive muds and gravels. A lobate subaqueous delta near the Eel River, composed of well-sorted, fine-grained, inner shelf sands. The inner shelf sand facies north of the Humboldt Bay entrance amalgamate with mid-shelf muds, shell fragments and relict sediments. Sand-mud transition facies of interbedded sands and flood muds are emplaced by hyperpycnal flows and form subtle bathymetric terraces. The mid-shelf mud facies located, seaward of the 60 m isobath, contain terrigenous silts and clays with high porosities (> 60%) and onlap the transgressive surface.

The subaqueous delta west of the Eel River represents at least 20 m of Holocene sediment accumulation and moderate sedimentation rates (>2mm/yr). The inner shelf Holocene sediment thickness north of the Humboldt Bay entrance has as little as 2 m of accumulation and very low sedimentation rates (<0.2mm/yr). A northwest plunging anticlinal fold west of Arcata Bay aligns with the onshore Humboldt Hill Anticline. The anticline brings the transgressive surface boundary to within 2 m of the seabed and is located near a gas seep. Rapid sea level rise during 4 discrete melt water pulses since latest glacial maximum allowed incised channels to trap fluvial sediments depriving the shelf of a sediment supply and increased erosion of unconsolidated backedge seacliffs. Infilling allowed fluvial sediments to bypass estuaries and construct barrier bays and spits during relative stillstands.

Coseismic Subsidence of Arcata Bay

Chad Pritchard

Paleoseismic investigations to identify late Holocene upper crustal movement beneath Arcata Bay has confirmed four buried marsh soils that represent up to four great southern Cascadia subduction zone earthquakes. Estimated ages of earthquakes are: 250, 1350 to 1190, and 1590 to 1390 cal yr BP, with a possible earthquake at 1290 to 1100 cal yr BP. Coseismic subsidence in Arcata Bay was originally theorized to occur due to coseismic movement of the Freshwater Syncline (See Fig 1). Offshore seismic images published in Burger, et al. 2002 indicate that the Freshwater Syncline has ceased folding and that upper crustal faulting in the off-coast section of Humboldt Bay has occurred in the Holocene (See Fig 2).

To test for late Holocene movement of the onshore section of the Freshwater syncline buried low salt marsh soil horizons were correlated around Arcata Bay. Coseismically buried soils were identified using lithostratigraphy, estimated diatom

biostratigraphy, and radiocarbon age determinations. Sites used for the final study included: Mad River Slough (MRS), Arcata Salt Marsh (ARC), Jacoby Creek (JAC), Eureka Slough (ESB), and Daby Island (DAB). The only continuous buried soil horizon in Arcata Bay is the youngest, which probably subsided coseismically in A.D. 1700 during a regional megathrust event along the Cascadia subduction zone. The youngest buried soil was not warped by the Freshwater syncline (See Fig 3). Marsh accretion rates were calculated using diatom biostratigraphic data and surveyed elevations and were similar at multiple sites (See Fig 4). All data suggests that each site had similar depositional histories at the margin of Arcata Bay. Therefore, evidence suggests that the Freshwater syncline has not deformed during, or since, the most recent Cascadia subduction zone earthquake.

Coastal Sand Dune Stratigraphy and Geomorphology of the North Spit of Humboldt Bay

Thomas H. Leroy

The northern North Spit of Humboldt Bay is primarily composed of Holocene sand dunes in various states of stability. The dune field as a whole appears to be part of a transgression where active dunes are slowly advancing over older dunes and into the existing estuary environment.

The forested and stabilized portion of the dune field is composed of successive parabolic dune pulses, each one stacking up against a previous dune pulse from east to west. The active sand dunes are transverse type dunes and are currently advancing east, often as discrete "slugs" of sand. Previously stable sand dunes are often being eroded and incorporated into the active dune sequence.

Radiocarbon age control from a coastal forest, buried by the youngest dune sequence, defines three age ranges compatible with dune movement through the forest. The age ranges are 1725-1790, 1805-1885, and 1915-1960. Of these three age ranges the most likely candidate is 1725-1790.

There are coarse grained gravel deposits found discontinuously along the western margin of the stabilized dune field. Physical characteristics of the gravel suggest different means of deposition at different geographic areas along the spit. From the northern most forested dunes most of the gravel can best be explained by historic river mouth migration. South of the northern most forested dune, the gravel may better be explained by a paleo-shoreline related to vertical movements in the earths crust. An inland-most gravel exposure is deposited on sand dunes and may be tsunamigenic in origin.

The combined evidence from local paleoseismic and paleotsunami investigations, dune morphology and distribution, gravel deposition mechanisms, and age control, may suggest the North Spit was subjected to regional subsidence and tsunami inundation associated with the 1700 AD Cascadia Subduction Zone earthquake. The associated destabilization of the western margin of the spit could have initiated the current dune advancement.

<u>Mileage</u>	<u>Distance</u>	<u>Description</u>
63.5		Return to cars and head out of the parking lot.
66.6	3.1	Turn left on Mad River Road.
67.0	0.4	At the Stop Sign, TURN LEFT onto Janes Road.
67.2	0.2	Passing by Mad River Hospital on your right (emergency room entrance)
67.5	0.3	Follow road as it takes a HARD RIGHT
67.3	0.1	STAY RIGHT at the round-a-bout to get onto HWY 101 SOUTHBOUND. Return to Pamplin Grove by continuing south on Hwy 101 through Eureka, past College of the Redwoods, and turn left on Hwy 36 back to Pamplin Grove. There is gas available on the east side of the freeway, or on your way back thru Eureka.
77.5	10.0	Intersection with SR 255. CONTINUE STRAIGHT, southbound on 101 (4th St.)
68.3	1.0	Follow 101 southbound, as it TURNS LEFT
81.8	4.3	Pierson's stoplight ("the big hammer"). Continue south on 101.
88.6	20.3	TURN LEFT onto Hwy 36
92.7	10.9	TURN RIGHT into Pamplin Grove campsite See you all at tonight's business meeting!

Day 3 Papers

Transient geomorphic response to late Pleistocene baselevel change and climate forcing in the southern Cascadia thrust-and-fold belt, north coastal California

Jay D. Stallman¹ and Harvey Kelsey²

ABSTRACT

Fluvial terraces, marine terraces, and accordant ridge-capping surfaces in the North Fork Elk River (59 km²) and Ryan Creek (33 km²) basins record transient geomorphic response to baselevel and climatic change in the southern Cascadia thrust-and-fold belt since the middle to late Pleistocene. Denudation rate (0.10 ± 0.03 m ky⁻¹), estimated from the rock volume eroded beneath a paleotopographic surface enveloping ridge-capping shallow marine and fluvial deposits of middle Pleistocene age (330–590 ka), is 3 to 7 times slower than long-term uplift rate (0.46 ± 0.03 m ky⁻¹) determined from the relative age and altitude of MIS 5a and 5c marine terraces near Eureka. Rapid bedrock incision (0.85 ± 0.05 m ky⁻¹) below an 18–20 ka fluvial strath terrace in the North Fork Elk River valley, however, exceeds long-term uplift rate and is similar to the average post-lowstand (~21 ka) sedimentation rate on the margin (0.95 ± 0.25 m ky⁻¹). Correlation of strath cutting to paleoclimate proxies in marine sediment cores suggests a millennial-scale climate signal superimposed on baselevel lowering, a conclusion consistent with models of climate-controlled strath terrace genesis in the northern Cascadia forearc and other temperate, unglaciated mountain ranges. Transient geomorphic response is well-represented in North Fork Elk River strath terraces compared to terrace records in nearby coastal basins due in part to the effects of contrasting lithology on bedrock erodibility. Resistant lithologies sourced from Yager terrane and competent blocks within Eastern belt Franciscan mélangé in the upper basin persist as bedload, and when supply rates are optimal, effectively erode the weaker siltstone and mudstone channel boundaries in the lower North Fork Elk River valley. Climate control on terrace genesis and disparity between uplift, denudation, and bedrock incision rates suggests a decoupling of valley bottom and hillslope geomorphic responses from baselevel lowering by climatically forced variability in sediment supply and stream power. Increased activity of currently dormant deep-seated landslides in Central belt Franciscan mélangé and soft sedimentary rocks may account for increased hillslope sediment production during wet climate intervals.

¹Stillwater Sciences, Arcata, Ca 95518

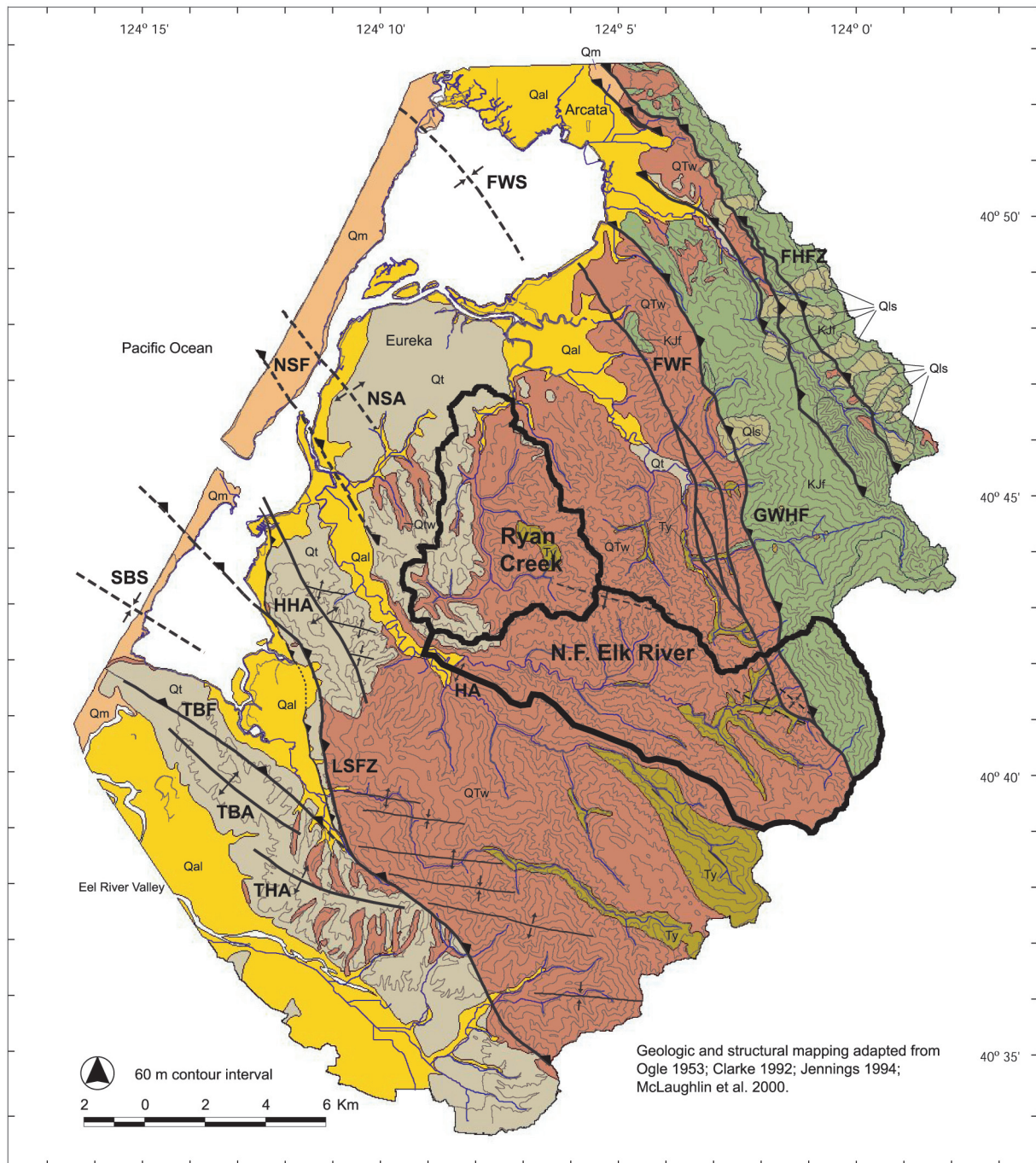
²Department of Geology, Humboldt State University, Arcata, CA 95521

INTRODUCTION

A half century of geophysical, stratigraphic, and paleoseismic research has revealed the geometry and kinematic development of the southern Cascadia thrust-and-fold belt over Holocene and > 100 ka time scales, but comparatively little about continental geomorphic response to baselevel change and climatic forcing over the 10–100 ka time scale. Fluvial terraces, marine terraces, and ridge-capping geomorphic surfaces in the North Fork Elk River (59 km²) and Ryan Creek (33 km²) basins, tributaries to Humboldt Bay, record transient geomorphic response to baselevel and climatic change during the middle to late Pleistocene. We use these geomorphic datums to test the hypothesis that uplift, denudation, and bedrock channel incision in the study area over the 10–100 ka time scale are decoupled by climate controls on the long-term mass balance between hillslope sediment production and sediment flux through mainstem river valleys.

SETTING

The North Fork Elk River and Ryan Creek basins drain the relatively undeformed Eureka block, bound on the southwest by the Little Salmon fault zone and on the northeast by the Freshwater fault (Figure 1). Quaternary to Holocene displacement on the Little Salmon thrust fault and related upper plate folding (Clarke and Carver 1992, Vadorro et al. this volume) influences regional uplift and northeast tilting of the Eureka block. The block is comprised of a thick transgressive-regressive overlap assemblage of Neogene sediments (undifferentiated Wildcat Group) unconformably overlying more resistant Paleogene trench slope deposits of argillite, sandstone turbidites,



- | | |
|--|---|
|  Qls landslide deposits |  QTw marine and nonmarine overlap deposits of the Wildcat Group and Falor Formation |
|  Qal Holocene alluvial deposits |  Ty Yager terrane |
|  Qm undeformed marine shoreline and aolian deposits |  KJf Central belt Franciscan complex |
|  Qt undifferentiated marine and nonmarine terrace deposits | |

Figure 1. Geologic and structural map of the Study Area. Tompkins Hill anticline (THA), Table Bluff anticline (TBA), Table Bluff fault (TBF), South Bay syncline (SBS), Little Salmon fault zone (LSFZ), Humboldt Hill anticline (HHA), Humboldt anticline (HA), North Spit fault (NSF), North Spit anticline (NSA), Freshwater fault (FWF), Greenwood Heights fault (GWHF), Fickle Hill fault zone (FHFZ), Freshwater syncline (FS).

and pebbly conglomerate (Yager terrane). A Jurassic to Cretaceous accretionary melange (Central belt Franciscan Complex) is juxtaposed against Paleogene and younger rocks in the easternmost study area by the Freshwater fault, a high angle reverse fault active into the Late Pliocene (Knudsen 1993). Undifferentiated shallow marine and fluvial deposits of middle to late Pleistocene age cap accordant interfluves across the study area.

The basins integrate steep drainage networks that originate from the unglaciated seaward slope of the outer Coast Range and flow across the low gradient coastal plain to Humboldt Bay. Climate is characterized by mild, wet winters and a prolonged summer dry season moderated by fog. Winter rainfall intensity and storm runoff are highly variable due to orographic lifting of moisture-laden frontal air masses as they intersect the outer Coast Range. Intense seasonal rainfall, steep topography, and erodible materials result in high sediment yields predominantly from debris slides on headwall and inner-gorge slopes, and from deep seated landsliding in Central belt Franciscan melange and soft sedimentary rocks. Rapid sediment accumulation on the continental shelf off Humboldt Bay exceeds the average rate of subaerial tectonic uplift and controls shelf surface morphology (Sommerfield and Nittrouer 1999, Orange 1999).

Paleoclimate proxies in lacustrine and marine sediment deposits indicate systematic changes in millennial-scale oceanographic conditions and climate in north coastal California (Figure 2). Cool, wet climate during full glacial intervals led to a Bering Sea assemblage of radiolarian fauna, dominantly herbaceous and montane coniferous vegetation (white fir, Douglas-fir, and pine), and high rates of terrigenous sediment deposition on the margin (Heusser et al. 2000, Hovan et al. 2000, Pisias et al. 2001, Barron et al. 2003). Warm, wet climate during deglaciation (e.g., Younger Dryas 13–11.5 ky) is marked by a transitional radiolarian assemblage and an abrupt increase in alder coincident with a decrease in pine (Heusser et al. 2000, Pisias et al. 2001, Barron et al. 2003). Increase in alder is followed by expansion of oak woodland and culminates during interglacial intervals (e.g., Holocene) in the contemporary coniferous lowland forest community dominated by redwood, western hemlock, Sitka spruce, and Douglas fir (Heusser et al. 2000, Barron et al. 2003). Interglacial intervals are also indicated by an Eastern Boundary Current assemblage of radiolarian fauna associated with coastal upwelling and lower rates of terrigenous sediment deposition (Hovan et al. 2000, Pisias et al. 2001).

UPLIFT

Erosional remnants of raised shore platforms formed by wave erosion during past sea level high stands are preserved at many locations along the approximately 100 km coastline in the southern Cascadia subduction zone (sCsz). The altitudinal distribution and age of these late Pleistocene marine terraces enable calculation of long-term uplift rates for fault-bound blocks. Due to the lack of datable materials in older marine terrace sediments, terrace ages have been estimated from the degree of soil development and by comparing the altitudinal distribution of terrace flights to eustatic sea level high stands. Chronosequences near Trinidad and McKinleyville provide reference age-assignments for other marine terrace flights in the sCsz (Carver and Burke 1992).

Carver and Burke (1992) identified at least 7 uplifted shore platforms in the Eureka area. Based on soil profile development at sites in Eureka and reference age assignments from Trinidad and McKinleyville, Carver and Burke (1992) correlated Eureka terraces located at approximately 47 m and 27 m (above modern sea level) to MIS 5c (105 ka) and MIS 5a (80 ka), respectively (see Figure 3 from Thompson et al. this volume). Paleo-sea levels during MIS 5a and 5c were about 7 m and 2 m below modern sea level, respectively (Muhs et al. 1992). The difference between modern terrace elevations and paleo-sea levels divided by the terrace age yields a long-term uplift rate of $0.46 \pm 0.03 \text{ m ky}^{-1}$ for the Eureka block.

DENUATION

Few estimates of long term denudation exist for tectonically active drainage basins in north coastal California, despite the relevance for testing landscape evolution models and understanding interactions between baselevel change and climate forcing. Long term erosion rates in coastal basins have been inferred from geologic datums (Warhaftig and Curry 1967, Janda et al. 1975), soil production rates (Heimsath et al. 1999, 2001), cosmogenic

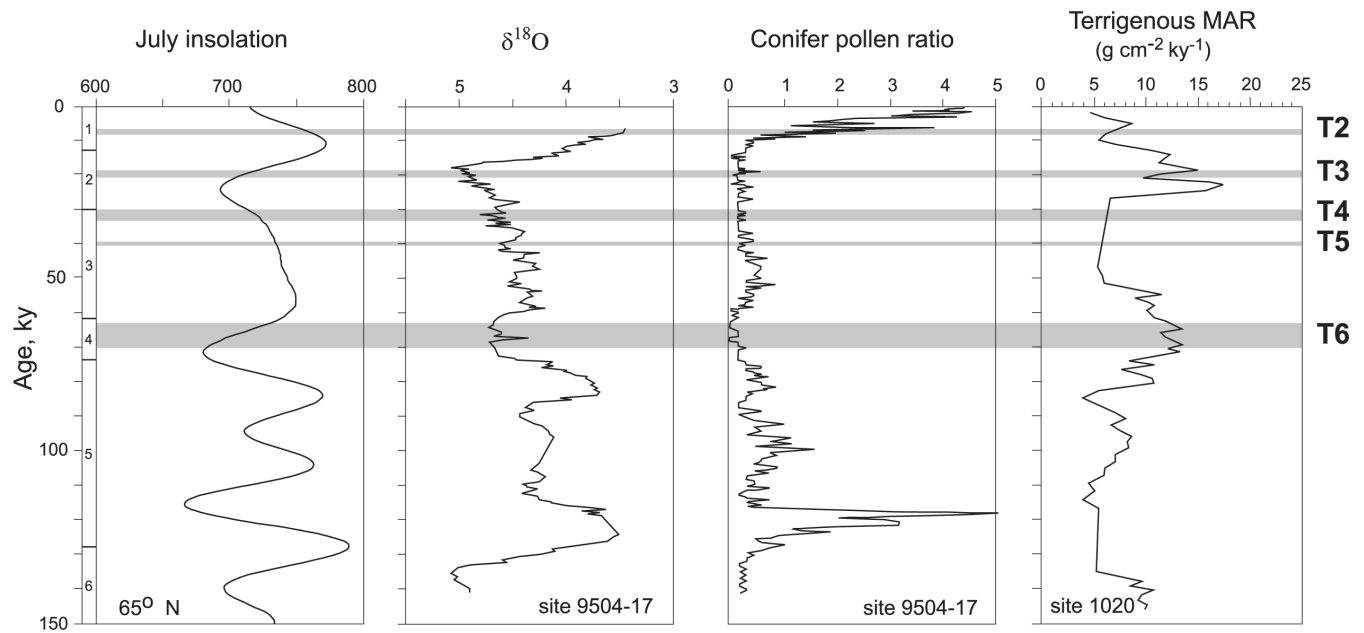


Figure 2. Paleoclimate proxies from Ocean Drilling Program Leg 167 sites 1020 and 9504-17 (located on the northern California margin) shown with the timing of strath terrace cutting in the North Fork Elk River valley. Insolation from Berger (1978), $\delta^{18}\text{O}$ and conifer pollen ratio (redwood + western hemlock/spruce) from Heusser et al. (2000), mass accumulation rate of terrigenous sediment (terrigenous MAR) from Hovan et al. (2000).

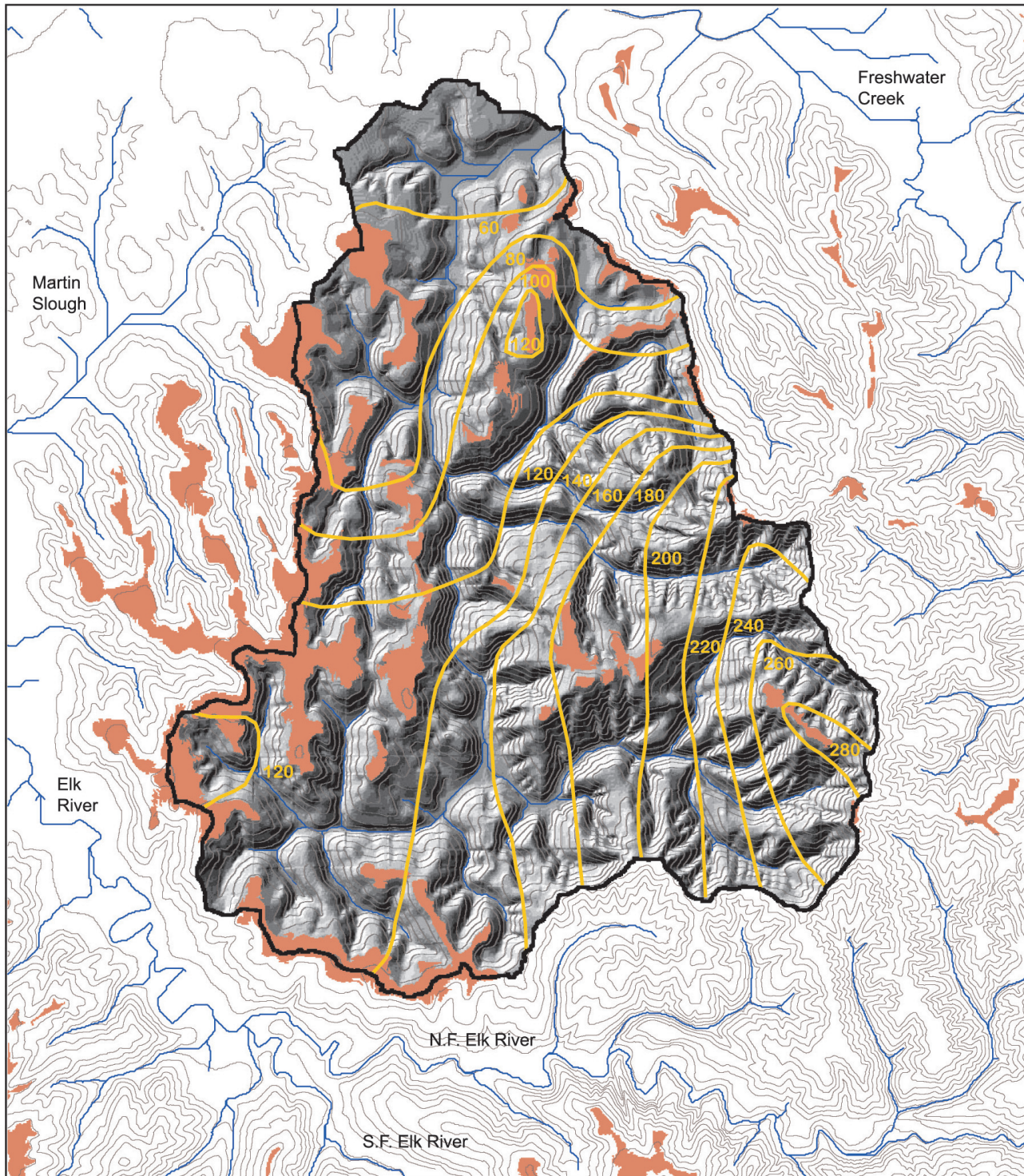
dating of alluvial sediment (Ferrier et al. 2005), and sedimentation rates on the inner continental shelf (Sommerfield and Nittrouer 1999, Hovan et al. 2000, Sommerfield et al. 2002). Historical erosion rates have been estimated using short gaging station and aerial photographic records (since about 1950).

An under-exploited approach to estimating long-term denudation involves assessing landform changes resulting from erosion into a regional geomorphic surface (Stanford et al. 2002, Amato et al. 2003). Long-term denudation of the Ryan Creek basin was estimated from the sedimentary rock volume removed by erosion into a paleo-topographic surface enveloping broad, accordant ridge crests capped by shallow marine and fluvial deltaic deposits of middle to late Pleistocene age. Ogle (1953) interpreted these deposits as remnants of an uplifted coastal plain deposited by the paleo- Eel, Van Duzen, and Elk rivers.

Methods

The paleo-topographic surface was constructed over an area east of Humboldt Bay from Jacoby Creek to the northern margin of the Eel River valley, where ridge-capping deposits are mapped as the Hookton formation (Kelley 1984, Kilbourne 1985a, 1985b, 1985c, Kilbourne and Morrison 1985). A 10 m digital terrain model was used to extract surface elevations from contiguous map units greater than 1 ha and enclosing planar surfaces sloping 0.05 or less. Limited air photo mapping and ground truthing were conducted in the south and eastern drainage divides of the Ryan Creek basin to verify the presence of shallow marine and fluvial cover sediments. A triangulated irregular network was created from extracted surface elevations and converted to a 10 m grid that was used to contour the envelope surface and calculate lowering relative to present-day topography. The envelope surface represents topography following sea level regression but prior to dissection of the shallow marine and fluvial cover sediments by Ryan Creek.

That portion of the paleo-topographic surface encompassing the Ryan Creek basin at the center of the map area where middle to late Pleistocene surfaces are best preserved was used to calculate eroded volume, thereby limiting edge effects of surface construction (Figure 3). Eroded volume was calculated as the sum of the elevation differences between the envelope surface and the present-day digital terrain model topography multiplied by the grid cell area. Denudation was calculated by dividing the eroded volume by the Ryan Creek drainage area



- Channel network
- Drainage basin boundary
- Hookton formation (map units > 0.01 km² and sloping < 0.05)
- 20 m envelope contours

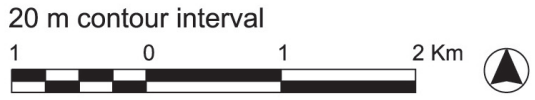


Figure 3. Envelope and digital terrain model surfaces used to calculate denudation in the Ryan Creek basin

and by the time period over which erosion has occurred. Initiation of erosion is bracketed by an inferred age of 330 ka (~MIS 9e) for the accordant interfluvial surfaces (minimum age) extrapolated from uplift of MIS 5a and 5c marine terraces near Eureka, and the 590 ±10 ka Rockland ash (Sarna-Wojcicki et al. 1985, Lanphere et al. 2005) located near the base of the Pleistocene section (maximum age). The method assumes landform changes are accomplished by stream incision and slope diffusion in response to glacio-eustatic baselevel fall and constant, uniform uplift, negligible differential erosion due to folding or faulting, and no long term sediment storage in the basin.

Results

Approximately 1.38 km³ of rock has been eroded from the Ryan Creek basin since the middle to late Pleistocene (330–590 ka). Denudation rate over this period (0.10 ± 0.03 m ky⁻¹) is consistent with other region estimates of millennial-scale denudation, ranging from 0.09 to 0.20 m ky⁻¹ (Warhaftig and Curry 1965, Janda et al. 1975, Lehre and Carver 1985, Ferrier et al. 2005), and is within about 20% of historical erosion rates in the Elk River determined from short-term sediment gauging records (PALCO unpublished data). Denudation rate is 3 to 7 times slower than uplift rate in the Eureka area over the last 80–105 ky (0.46 ± 0.03 m ky⁻¹), suggesting the landscape is not in a topographic steady state. The method may underestimate denudation if rock volume removed during low sea level is obscured by high-stand deposits, the envelope surface is diachronous or is cut by younger marine terrace surfaces to the northwest, erosion has lowered ridge crest elevations, or there is substantial long-term sediment storage in the basin.

BEDROCK CHANNEL INCISION

Latest Pleistocene and Holocene fluvial terraces occur in many north coast river valleys and have been used to describe fluvial response to eustatic and tectonic baselevel lowering (Merritts et al. 1994), regional uplift and deformation (Bickner 1993, Personius 1995, Koehler 1999), active faulting (Berry 1981, O’Dea 1992, Verhey 1992), and climate change (Personius et al. 1993, Adkins 1996). Terrace age correlations and the relative importance of common forcing mechanisms between valleys remain poorly understood.

The 12 km reach of the North Fork Elk River valley downstream of South Branch North Fork Elk River widens to more than 0.5 km and the active valley bottom is entrenched within late Pleistocene and Holocene strath terraces (Figure 4a). These river terraces, originally formed by fluvial processes at a former valley bottom and subsequently preserved in hillslopes above the modern river through rock uplift, provide a datum for examining the pattern and rates of long-term channel incision in response to baselevel change and climate forcing.

Methods

Terraces were mapped from 1:12,000 scale aerial photography and field traverses. Altimeter surveys (2σ error ±1.2 m) of terrace straths (76 points) and treads (186 points) were tied to GPS bench marks. Elevations were orthogonally projected to a vertical plane defined by the valley midpoint at the elevation of the highest mapped terrace level. Longitudinal distance of projected elevations was measured upstream from the confluence of the North Fork Elk River and the South Fork Elk River (km 0.0). The map relations and high density of survey points provided the initial basis for terrace correlations that were refined based on terrace stratigraphy and age estimates.

Surficial morphology of terrace treads and characteristics of the strath (e.g., rock type, color, and jointing), cover sediments (e.g., thickness, lithology, size, shape, roundness, sorting, and sedimentary structures), and soil were described at 33 of 76 exposures, including 15 backhoe pits excavated on lesser-disturbed terrace surfaces. Strath cover sediments are uniformly thin (generally 1.5–2.0 m) and typically comprised of a lower, clast-supported and imbricated cobble-gravel facies capped by fining-upward sands and silts. By assuming that the thin cobble-gravel channel facies deposited above a bedrock strath represents the scour depth and characteristic bedload thickness mobilized during a large flood and that abrasion of the bedrock channel bed by mobile bedload is responsible for strath cutting, the channel facies provides an upper limit on the altitudinal position of the channel bed and a minimum age for strath cutting (Merritts et al. 1994, Personius 1995, Pazzaglia and Brandon 2001, Wegmann

and Pazzaglia 2002). The overbank facies was deposited during infrequent large floods after the channel was abandoned and may be thousands of years younger than the underlying gravels (Merritts et al. 1994).

Minimum age estimates for strath cutting are provided by three radiocarbon dates from in situ, fluvially-deposited organic material (detrital charcoal, wood fragments, and leaf detritus) preserved in or near the channel facies of terrace deposits (Table 1). Minimum age estimates assume that deposition of the channel facies was coincident with strath cutting, straths were not subsequently reoccupied by the active channel, and organic material is not recycled from older deposits.

In the absence of widespread numerical dating of terrace deposits, clast weathering rind thickness was used in combination with elevation data and radiocarbon ages to longitudinally correlate terrace remnants. Thirty to fifty arkosic to feldspathic graywacke clasts from 50 to 150 mm in diameter were sampled from the depth of maximum soil profile development at 25 sites. Clasts were cut in half, and several rind measurements were made on the cut face to the nearest 0.1 mm. Rind thickness ranged from 0.45 mm to 2.80 mm, with thickness increasing in the upstream direction for any one longitudinally continuous terrace level. Rind measurements were calibrated to radiocarbon ages using a logarithmic least squares regression model.

Table 1. Radiocarbon of North Fork Elk River terrace deposits.

Lab number ¹	Longitudinal distance, km	Terrace surface	Laboratory age, ² yr	Calibrated age, ³ yr	Stratigraphic description
151432	4.37	T3	15,900 ±90	18,500–19,500	platy wood fragment channel facies 0.55 m above strath
153846	5.97	T4 (?)	16,300 ±50	19,000–19,800	leaf detritus overbank facies 2.5 m above strath
157389	2.78	T5	34,400 ±390	39,000–40,200	detrital charcoal channel facies 0.49 m above strath

1. All dates determined by accelerator mass spectrometry by Beta Analytic Inc.

2. Errors for laboratory ages represent 1 standard deviation. 3. 2σ calibrated age ranges. Samples 151432 and 153846 use calibration of Stuiver et al. (1998).

Sample 157389 uses calibration of Bard et al. (1998) (Reimer pers. comm. 2001).

Results

Six terrace levels (T1 through T6) were identified above the active North Fork Elk River channel based on geomorphic mapping and surveying, sedimentology and stratigraphy, radiocarbon ages, and relative weathering characteristics (Figure 4b). At least two late Holocene fill terraces form the valley bottom throughout the study reach (T1a and T1b). Upstream of km 6.5, the valley bottom is underlain by a bedrock strath cut in undifferentiated lower Wildcat Group. The strath can be traced upstream to about km 7.0, where it is obscured by recent flood and debris flow deposits. A higher Holocene strath terrace (T2) occurs 6 m above the lowest strath between km 5.5 and km 7.0. T2 projects beneath Holocene fill terraces downstream of km 5.5. Estimated age of T2 strath cutting at km 4.4 based on incision rate is 6.5–8.1 ky.

Four late Pleistocene terraces occur above the Holocene valley bottom between South Branch North Fork Elk River and the confluence with the South Fork Elk River, where straths are cut into siltstone and fine-grained sandstone of the undifferentiated lower Wildcat Group. A longitudinally continuous and paired strath terrace (T3) occurs 16–21 m (average 17 m) above the active channel between km 0.0 and km 7.8. The T3 strath is the most significant datum for interpreting incision, response to baselevel change, and deformation. Calibrated radiocarbon age of T3 strath cutting at km 4.4 is 18.5–19.5 ky. Remnants of three higher strath terraces (T4–T6) occur on the

THIS PAGE LEFT INTENTIONALLY
BLANK

FOR

STALLMAN TABLOID FIG 4

Figure 4. North Fork Elk River valley trip stop.

Figure 4a. Shaded relief map of the 12 km terraced reach of the North Fork Elk River valley from 1-m LiDAR DEM

Figure 4b. Map of late Pleistocene and Holocene fluvial terraces in the North Fork Elk River valley. (source: North Coast Regional Water Quality Control Board).

THIS PAGE LEFT INTENTIONALLY
BLANK

FOR

STALLMAN TABLOID FIG 4

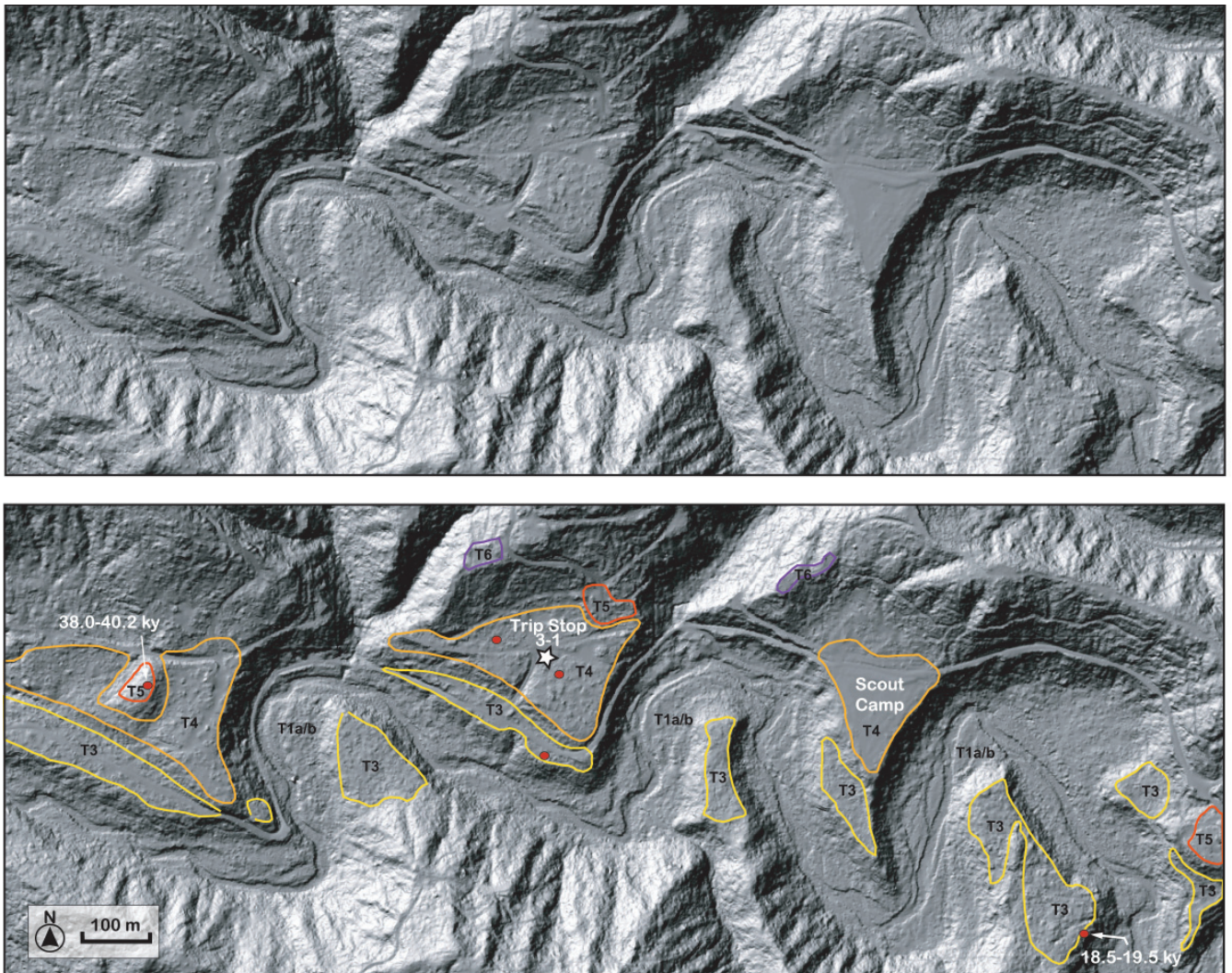


Figure 5. Inset map for trip stop 3-1. Red circles are backhoe pit exposures of strath terrace cover sediments. Minimum age estimates for strath cutting, provided by AMS dates from the channel facies on T3 (18.5–19.5 ky) and T5 (39.0–40.2 ky) terraces, give incision rates of $0.85 \pm 0.05 \text{ m ky}^{-1}$ and $0.89 \pm 0.09 \text{ m ky}^{-1}$.

north side of the valley from 29 m to 56 m above the active channel. The ages of strath cutting on T4 (25.2–33.3 ky), T5 (39.0–40.2 ky), and T6 (60.8 ka to 75.3 ky) were extrapolated from radiocarbon calibrated incision rates and weathering rinds.

Terrace longitudinal profiles in the North Fork Elk River valley are predominantly concave-up and downstream divergent (Figure 6). Upstream younging in the estimated age of strath cutting (Stallman 2003) suggests diachronous terrace genesis related to headward migration of baselevel lowering (Gardner 1983, Miller 1991, Seidl and Dietrich 1992). A convex-up segment of the T3 terrace profile between km 0.5 and km 3.5 and a local decrease in the sinuosity of the entrenched Holocene valley are coincident with the inland projection of a fault-propagation fold imaged in nearshore seismic reflection profiles located west of Humboldt Bay (McCulloch et al. 1977, Gulick and Meltzer 2002).

Bedrock incision rates derived from the height and calibrated radiocarbon age of the T3 and T4 terrace levels are $0.85 \pm 0.05 \text{ m ky}^{-1}$ and $0.89 \pm 0.09 \text{ m ky}^{-1}$, respectively. These incision rates are similar to the average post-lowstand ($\sim 21 \text{ ka}$) sedimentation rate ($0.95 \pm 0.25 \text{ m ky}^{-1}$) on the adjacent continental shelf (Spinelli and Field 2003), and are comparable to incision rates derived from strath terrace sequences preserved elsewhere along the Pacific margin of North America (Merritts et al. 1994, Personius 1995, Wegmann and Pazzaglia 2002, Pazzaglia and Brandon 2001).

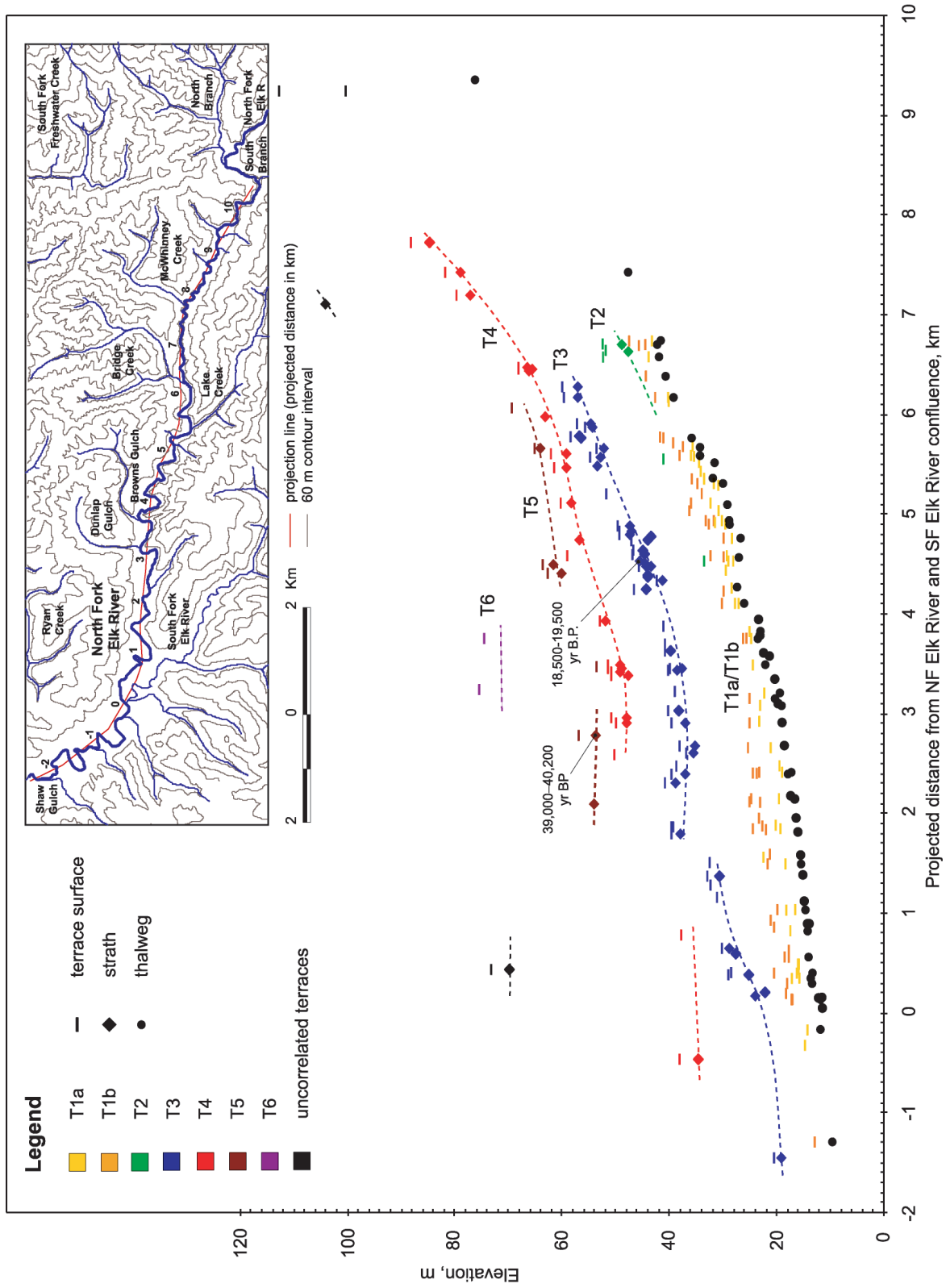


Figure 6. North Fork Elk River terrace profiles.

DISCUSSION

Correlation of strath cutting to paleoclimate proxies in nearby marine sediment cores (Figure 2)(Heusser et al. 2000, Piasias et al. 2001, Barron 2003) suggests a millennial-scale climate signal superimposed on baselevel lowering, a conclusion consistent with current models of climate-controlled strath terrace genesis in the northern Cascadia forearc and other temperate, unglaciated mountain ranges (Personius et al. 1993, Sugai 1993, Tucker and Slingerland 1997, Pazzaglia and Brandon 2001, Wegmann and Pazzaglia 2002, Hancock and Anderson 2002). Although climate controls on strath terrace genesis should be reflected in a common timing of strath cutting in north coastal California terrace chronologies, a common signal is not apparent likely due to differences in the type of terrace datums used (e.g., strath vs. fill) and large uncertainties in age inferred from uplift rates, incision rates, and relative weathering indices. Transient geomorphic response is well-represented in North Fork Elk River strath terraces compared to terrace records in other nearby coastal basins due in part to the effects of contrasting lithology on bedrock erodibility. Resistant lithologies sourced from Yager terrane and competent blocks within the Eastern belt Franciscan mélange in the upper basin persist as bedload, and when supply rates are optimal, effectively erode the weaker siltstone and mudstone channel boundaries in the lower North Fork Elk River valley.

Climate control on terrace genesis and disparity between uplift, denudation, and bedrock incision rates suggests a decoupling of hillslope and valley bottom geomorphic responses from baselevel lowering by climatically forced variability in sediment supply and stream power. According to this conceptual model, uplift rate exceeded bedrock incision rate during stadial or glacial intervals when cool, wet climate and rapid hillslope denudation forced aggradation in mainstem river valleys, increasing sediment storage and causing planation (strath cutting). Increased activity of currently dormant deep-seated landslides in the Central belt Franciscan mélange and soft sedimentary rocks (see Mackey and Roering, and Marshall, this volume) may account for higher hillslope sediment production during these intervals. Bedrock incision rate exceeded uplift during cool, dry late glacial and subsequent warmer and wetter deglacial intervals when slower hillslope denudation and/or increased stream power depleted channel sediment storage and forced incision in mainstem valleys. Establishment of maritime climate and a mesic redwood ecosystem during the middle to late Holocene led to approximate equilibrium.

REFERENCES CITED

- Adkins, B. R. 1996. Glaciofluvial origin of stream terraces at Big Flat, Smith River basin, northwestern California. Master's thesis. Humboldt State University, Arcata, California.
- Amato, A., P. P. C. Ancelli, and A. Cinque. 2003. The long-term denudation rate in the southern Apennines chain (Italy): a GIS-aided estimation of the rock volumes eroded since middle Pleistocene time. *Quaternary International* 101-102: 3-11.
- Barron, J. A., L. Heusser, T. Herbert, and M. Lyle. 2003. High-resolution climatic evolution of coastal northern California during the past 16,000 years. *Paleoceanography* 18(1), doi:10.1029/2002PA000768.
- Berry, M. E. 1981. Geomorphology and relative dating analysis of Quaternary fluvial terraces on the Mad River, near Blue Lake, California. Senior thesis. Humboldt State University, Arcata, California.
- Bickner, F. R. 1993. A soil chronosequence of the Mitchell Ranch fluvial terraces on the South Fork Eel River, age estimates and tectonic implications. Master's thesis. Humboldt State University, Arcata, California
- Carver, G. A., and R. M. Burke. 1992. Late Cenozoic deformation on the Cascadia subduction zone in the region of the Mendocino triple junction. Pages 31-63 in *Pacific Cell, Friends of the Pleistocene guidebook for the field trip to northern coastal California*, June 5-7, 1992..
- Carver, G. A., and R. M. Burke. 1988. Trenching investigations of northwestern California faults, Humboldt Bay region. Final report. National Earthquake Hazard Reduction Program, U. S. Geological Survey, Menlo Park, California.
- Clarke, S. H., Jr., and G. A. Carver. 1992. Late Holocene tectonics and paleoseismicity, southern Cascadia subduction zone. *Science* 255: 188-192.
- Gardner, T. W. 1983. Experimental study of knickpoint and longitudinal profile evolution in cohesive, homogeneous material. *Geological Society of America Bulletin* 94: 664-672.
- Gulick, S. P. S. and A. S. Meltzer. 2002. Effect of the northward-migrating Mendocino triple junction on the Eel River forearc basin, California: Structural evolution. *Geological Society of America Bulletin* 114: 1505-1519.
- Hancock, G. S., and R. S. Anderson. 2002. Numerical modeling of fluvial strath-terrace formation in response to oscillating climate. *Geological Society of America Bulletin* 114: 1131-1142.
- Heimsath, A. M., W. E. Dietrich, K. Hishiizumi, and R. C. Finkel. 1999. Cosmogenic nuclides, topography, and the spatial variation of soil depth. *Geomorphology* 27: 151-172.

- Heimsath, A. M., W. E. Dietrich, K. Hishiizumi, and R. C. Finkel. 2001. Stochastic processes of soil production and transport: erosion rates, topographic variation and cosmogenic nuclides in the Oregon Coast Range. *Earth Surface Processes and Landforms* 26: 531-552.
- Heusser, L. E., M. Lyle, and A. Mix. 2000. Vegetation and climate of the northwest coast of North America during the last 500 k.y.: high-resolution pollen evidence from the northern California margin. Pages 217-226 in M. Lyle, I. Koizumi, C. Richter and T. C. Moore, Jr., editors. *Proceedings of the ocean drilling program, scientific results, Volume 167*. Ocean Drilling Program, College Station, Texas.
- Hovan, S. A., S. W. Kish, and H. J. Renyck. 2000. Late Pleistocene record of terrigenous mineral deposition along the northern California margin (Sites 1018 and 1020). Pages 227-234 in M. Lyle, I. Koizumi, C. Richter and T. C. Moore, Jr., editors. *Proceedings of the ocean drilling program, scientific results, Volume 167*. Ocean Drilling Program, College Station, Texas.
- Ferrier, K. L., J. W. Kirchner, and R. Finkel. 2005. Erosion rates over millennial and decadal timescales at Caspar Creek and Redwood Creek, northern California Coast Ranges. *Earth Surface Processes and Landforms* 30: 1025-1038.
- Janda R. J., K. M. Nolan, D. R. Harden, and S. M. Coleman. 1975. Watershed conditions in the drainage basin of Redwood Creek, Humboldt County, California. USGS Open File Report 75-568.
- Kelley, F. R. 1984. Geology and geomorphic features related to landsliding, Arcata South 7.5' Quadrangle, Humboldt County, California, California Division of Mines and Geology Open-File Report 84-39.
- Kilbourne, R. T. 1985a. Geology and geomorphic features related to landsliding, Fortuna 7.5' Quadrangle, Humboldt County, California, California Division of Mines and Geology Open-File Report 85-01.
- Kilbourne, R. T. 1985b. Geology and geomorphic features related to landsliding, Hydesville 7.5' Quadrangle, Humboldt County, California, California Division of Mines and Geology Open-File Report 85-02.
- Kilbourne, R. T. 1985c. Geology and geomorphic features related to landsliding, McWhinney Creek 7.5' Quadrangle, Humboldt County, California, California Division of Mines and Geology Open-File Report 85-03.
- Kilbourne, R. T. and S. D. Morrison. 1985. Geology and geomorphic features related to landsliding, Fields Landing 7.5' Quadrangle, Humboldt County, California, California Division of Mines and Geology Open-File Report 85-04.
- Knudsen, K. 1993. Geology and stratigraphy of the Freshwater Creek watershed, Humboldt County, California. Master's thesis. Humboldt State University, Arcata, California.
- Koehler, R.D. III, 1999, Terrace formation, drainage adjustment, and tectonic geomorphology of the Van Duzen/North Fork Eel headwater region, northern California, M.S. thesis, Humboldt State University, Arcata, CA.
- Lanphere, M. A., D. E. Champion, M. A. Clynne, J. B. Lowenstern, A. M. Sarn-Wojcicki, and J. L. Wooden. 2005. Age of the Rockland tephra, western USA. *Quaternary Research* 62: 94-104.
- Lehre, A. K., and G. Carver. 1985. Thrust faulting and earthflows: speculations on the sediment budget of a tectonically active drainage basin. Pages 169-183 in M. E. Savina, editor. *Redwood country: American Geomorphological Field Group 1985 field trip guidebook*. Department of Geology, Carleton College, Northfield, Minnesota.
- McCulloch, D. S., A. T. Long, and P. A. Utter. 1977. Acoustic profiles offshore, Humboldt Bay, California. Open-file Report 77-667. U. S. Geological Survey.
- Merritts, D. J., K. R. Vincent, and E. E. Wohl. 1994. Long river profiles, tectonism, and eustasy: a guide to interpreting fluvial terraces. *Journal of Geophysical Research* 99: 14,031-14,050.
- Miller, J. R. 1991. The influence of bedrock geology on knickpoint development and channel-bed degradation along downcutting streams in south-central Indiana. *Journal of Geology* 99: 591-605.
- Muhs, D. R., T. K. Rockwell, and G. L. Kennedy. 1992. Late Quaternary uplift rates of marine terraces on the Pacific coast of North America, southern Oregon to Baja California Sur. *Quaternary International*, v. 15/16, pp. 121-133.
- O'Dea, K. M. 1992. Terrace formation and deformation on Yager Creek, Humboldt County, California. Pages 229-234 in *Pacific Cell, Friends of the Pleistocene guidebook for the field trip to northern coastal California, June 5-7, 1992*.
- Ogle, B. A. 1953. Geology of the Eel River valley area. Bulletin 164. Division of Mines.
- Orange, D. L. 1999. Tectonics, sedimentation, and erosion in northern California: submarine geomorphology and sediment preservation potential as a result of three competing processes. *Marine Geology* 154: 369-382.
- Pacific Gas and Electric Company. 2005. Implications of long-term global warming and tectonic displacements at Buhne Hill, Humboldt County, California. Report to the California Coastal Commission, San Francisco. July 18.
- Pazzaglia, F. J., and M. T. Brandon. 2001. A fluvial record of long-term steady-state uplift and erosion across the Cascadia forearc high, western Washington State. *American Journal of Science* 301: 385-431.
- Personius, S. F. 1995. Late Quaternary stream incision and uplift in the forearc of the Cascadia subduction zone, western Oregon. *Journal of Geophysical Research* 100: 20,193-20,210.
- Personius, S. F., H. M. Kelsey, and P. C. Grabau. 1993. Evidence for regional stream aggradation in the central Oregon Coast Range during the Pleistocene-Holocene transition. *Quaternary Research* 40: 297-308.
- Pisias, N. G., A. C. Mix, and L. Heusser. 2001. Millennial scale climate variability of the northeast Pacific Ocean and northwest North America based on radiolaria and pollen. *Quaternary Science Reviews* 20: 1561-1576.

- Sarna-Wojcicki, A. M., C. E. Meyer, H. R. Bowman, N. T. Hall, P. C. Russel, M. J. Woodward, and J. L. Slate. 1985. Correlation of the Rockland ash bed, a 400,000-year-old stratigraphic marker in northern California and western Nevada, and implications for middle Pleistocene paleogeography of central California. *Quaternary Research* 23: 236-257.
- Seidl, M. A., and W. E. Dietrich. 1992. The problem of channel erosion into bedrock. Pages 101-124 in K.-H. Schmidt and J. DePloey, editors. *Functional geomorphology: landform analysis and models*. Catena Supplement No. 23. Catena Verlag, Cremlingen-Destedt, Germany.
- Spinelli, G. A., and M. E. Field. 2003. Controls of tectonics and sediment source locations on along-strike variations in transgressive deposits on the northern California margin. *Marine Geology* 197: 35-47.
- Stallman, J. D. 2003. Strath terrace genesis in the North Fork Elk River valley. M.S. thesis, Humboldt State University, Arcata, CA.
- Stanford, S. D., G. M. Ashley, E. W. B. Russell, and G. J. Brenner. 2002. Rates and patterns of late Cenozoic denudation in the northwest Atlantic Coastal Plain and Piedmont. *Geological Society of America Bulletin* 114: 1422-1437.
- Sugai, T. 1993. River terrace development by concurrent fluvial processes and climatic changes. *Geomorphology* 6: 243-252.
- Sommerfield, C. K., and C. A. Nittrouer. 1999. Modern accumulation rates and a sediment budget for the Eel shelf: A flood-dominated depositional environment. *Marine Geology* 154: 227-241.
- Sommerfield, C. K., D. E. Drake, and R. A. Wheatcroft. 2002. Shelf record of changes in flood magnitude and frequency, north-coastal California. *Geology* 30(5): 395-398.
- Tucker, G. E., and R. Slingerland. 1997. Drainage basin responses to climate change. *Water Resources Research* 33: 2031-2047.
- Verhey, M. 1992. An investigation of active tectonics along the southern limb of the Eel River syncline. Pages 240-246 in *Pacific Cell, Friends of the Pleistocene guidebook for the field trip to northern coastal California, June 5-7, 1992*.
- Warhaftig, C., and R. Curry. 1965. Geologic implications of sediment discharge records from the northern Coast Ranges, California. P. 35-58 in *Man's effect on California watersheds*, prepared by the Subcommittee on Forest Practices and Watershed Management, Institute of Ecology, University of California at Davis.
- Wegmann, K. W., and F. J. Pazzaglia. 2002. Holocene strath terraces, climate change, and active tectonics: the Clearwater River basin, Olympic Peninsula, Washington State. *Geological Society of America Bulletin* 114: 731-744.
- Woodward-Clyde Consultants. 1980. Evaluation of the potential for resolving the geologic and seismic issues at the Humboldt Bay Power Plant Unit No. 3. Unpublished report. Prepared for Pacific Gas and Electric Company.
- Pisias, N. G., A. C. Mix, and L. Heusser. 2001. Millennial scale climate variability of the northeast Pacific Ocean and northwest North America based on radiolaria and pollen. *Quaternary Science Reviews* 20: 1561-1576.
- Potter, E., T. Esat, G. Schellmann, U. Radtke, K. Lambeck, and M. McCulloch. 2004. Suborbital-period sea-level oscillations during marine isotope substages 5a and 5c. *Earth and Planetary Science Letters*, v. 225: 191-204.
- Sarna-Wojcicki, A. M., C. E. Meyer, H. R. Bowman, N. T. Hall, P. C. Russel, M. J. Woodward, and J. L. Slate. 1985. Correlation of the Rockland ash bed, a 400,000-year-old stratigraphic marker in northern California and western Nevada, and implications for middle Pleistocene paleogeography of central California. *Quaternary Research* 23: 236-257.
- Seidl, M. A., and W. E. Dietrich. 1992. The problem of channel erosion into bedrock. Pages 101-124 in K.-H. Schmidt and J. DePloey, editors. *Functional geomorphology: landform analysis and models*. Catena Supplement No. 23. Catena Verlag, Cremlingen-Destedt, Germany.
- Stanford, S. D., G. M. Ashley, E. W. B. Russell, and G. J. Brenner. 2002. Rates and patterns of late Cenozoic denudation in the northwest Atlantic Coastal Plain and Piedmont. *Geological Society of America Bulletin* 114: 1422-1437.
- Sugai, T. 1993. River terrace development by concurrent fluvial processes and climatic changes. *Geomorphology* 6: 243-252.
- Sommerfield, C. K., and C. A. Nittrouer. 1999. Modern accumulation rates and a sediment budget for the Eel shelf: A flood-dominated depositional environment. *Marine Geology* 154: 227-241.
- Sommerfield, C. K., D. E. Drake, and R. A. Wheatcroft. 2002. Shelf record of changes in flood magnitude and frequency, north-coastal California. *Geology* 30(5): 395-398.
- Tucker, G. E., and R. Slingerland. 1997. Drainage basin responses to climate change. *Water Resources Research* 33: 2031-2047.
- Verhey, M. 1992. An investigation of active tectonics along the southern limb of the Eel River syncline. Pages 240-246 in *Pacific Cell, Friends of the Pleistocene guidebook for the field trip to northern coastal California, June 5-7, 1992*.
- Warhaftig, C., and R. Curry. 1965. Geologic implications of sediment discharge records from the northern Coast Ranges, California. P. 35-58 in *Man's effect on California watersheds*, prepared by the Subcommittee on Forest Practices and Watershed Management, Institute of Ecology, University of California at Davis.
- Wegmann, K. W., and F. J. Pazzaglia. 2002. Holocene strath terraces, climate change, and active tectonics: the Clearwater River basin, Olympic Peninsula, Washington State. *Geological Society of America Bulletin* 114: 731-744.
- Woodward-Clyde Consultants. 1980. Evaluation of the potential for resolving the geologic and seismic issues at the Humboldt Bay Power Plant Unit No. 3. Unpublished report. Prepared for Pacific Gas and Electric Company.

Identifying Deep-Seated Landslides Through the Use of High Resolution Airborne Laser Mapping – Implications for Landscape Evolution

Mackey, B.H., and Roering, J.J.^a

INTRODUCTION

Long-term average rock uplift rates in the northern California Coast Ranges are as high as 1-5mm/yr (Merritts and Bull 1989). Yet despite such high uplift rates, in many areas the relief remains modest (cf. Montgomery and Brandon 2002), an observation commonly attributed to pervasive slope instability. Here, we outline an approach with which to analyze deep-seated hillslope instability using extensive Airborne Laser Swath Mapping data (ALSM or ‘Lidar’). We apply these techniques to Lidar coverage from the South Fork Eel River and the Elk River in Northern California. The ‘bare earth’ datasets respectively cover approximately 230 km² and 150 km² at 1m² resolution.

Through a combination of geomorphic mapping and statistical terrain analysis, we identify ubiquitous deep-seated landslide and earthflow features, whose locations are strongly correlated with the Coastal and Central Belts of the underlying Franciscan mélangé lithology and other soft sedimentary rocks, large-scale structural features, and connectivity to channels. In this short contribution, we précis ongoing work which centers on the statistical analysis of high-resolution DEMs to address the causal mechanisms of deep-seated landsliding and their implications for landscape evolution.

Approach - Identifying Deep-Seated Landslides

Surface Roughness

In contrast to the well-ordered ridge-valley topography of unfailed hillslopes, deep-seated landslides characteristically present a rough or hummocky surface due to movement and internal deformation of the sliding mass. Such landslides are therefore ideally suited to recognition by various techniques that statistically measure small-scale variations in topographic roughness. To objectively identify and characterize landslide features using a process-based framework, we employ an adaptable algorithm termed “Deep-Seated Landslide and Earthflow Detection”, or DSLED.

‘DSLED-Rough’, detects surface roughness based on the eigenvalue ratio of cell-normal vector dispersion (McKean and Roering, 2004). A moving window walks through the DEM and at each point calculates a roughness within a given window size. By altering the window size over which roughness is calculated, the algorithm can detect different scales of roughness. Planar, stable hillslopes yield a high eigenvalue ratio, as most cells in the DEM point in a similar direction. In contrast, landslides generally generate a low eigenvalue ratio as in hummocky or disturbed terrain the cell-normal vectors are dispersed as shown in Figure 1. Figure 2 demonstrates DSLED-Rough applied to a portion of the Little South Fork Elk River catchment.

Impeded Drainage

In an alternative approach, we find a high correlation between slope instability and low values of drainage area per unit contour width (A/b). We term this algorithm ‘DSLED-Drain’. Active landslides have a marked impact on the hillslope hydrology by retarding the ability of the channels to incise and establish a drainage network. Slide movement thereby promotes large areas with significantly low A/b values compared to the surrounding unfailed or ‘well-drained’ ridge-valley topography. In Figure 3, low values of DSLED-Drain correlate well with the upper benches of deep-seated landslide deposits.

Improvements and Caveats

These techniques are able to identify and delineate the extent and surface features of much landslide prone terrain. Smoothing our resulting grids with a circular moving window of 50m radius has proven particularly valuable in identifying large deep-seated landslide features. Flat, stable surfaces such as terraces can generate both rough and poorly drained values, but can be filtered out using slope criteria. Care must also be taken in distinguishing the signature of landsliding from artificial roughness such as logging activity or residual unfiltered vegetation, primarily manzanita.

What is Driving Landsliding in the Coast Ranges?

Many of the landslide features we have identified are evidently thousands of years old, and a significant number

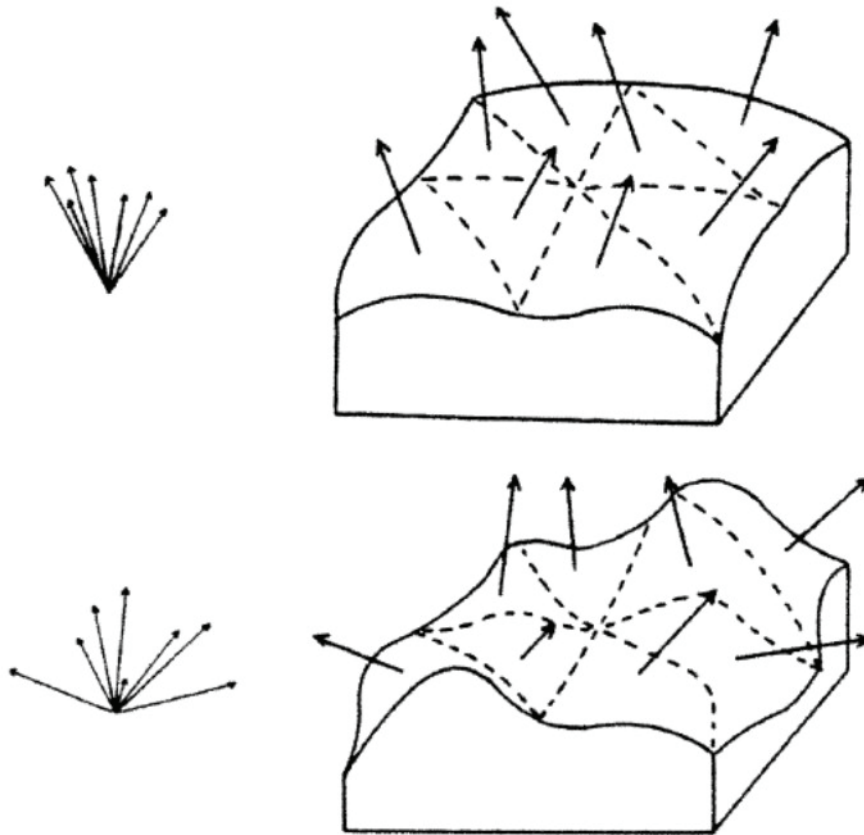


Figure 1. DSLED-Rough calculates the dispersion of cell-normal vectors within a specified window size. Ridge and valley topography exhibits semi-planar slopes (upper drawing) where the vectors will cluster close together generating a high eigenvalue ratio. In comparison, the surfaces of deep-seated landslides are frequently disturbed or ‘hummocky’, and this roughness manifests as a low eigenvalue ratio. Figure from McKean and Roering (2004).

show no evidence of late-Holocene movement. The corpus of our research is directed towards ascertaining a) when these slides were active, b) what caused the slide movement, and c) what is their contribution to mass-wasting over geomorphically significant spatial and temporal scales.

If a landslide stabilizes after movement, the initial surface roughness and hydrologic disturbance will likely be progressively smoothed by surface processes over time, and the degree of roughness can be used quantitatively as a guide to landslide activity. We anticipate that by constraining degrees of deep-seated landslide activity (with radiocarbon dating and using proxies such as surface roughness), combined with analyzing the spatial pattern of landsliding, we will soon be able to test hypotheses about what is driving deep-seated slope instability.

Preliminary Results:

Flows with a rougher surface, which we interpret to be more recently active than flows with smoother surfaces, are proximate to active stream channels suggesting undercutting of the toe is a primary control on the rate of slide movement. In analyzing longitudinal stream profiles, we frequently observe the signature of hillslope instability in the wake of knickpoints that appear to migrate upstream, suggesting that eustatic base-level fall and/or tectonic uplift are contributing to landsliding.

At the other end of the spectrum, climatically driven channel incision or elevated pore pressure associated with increased rainfall are other likely causes of deep-seated instability. Landsliding generated during a wet climatic

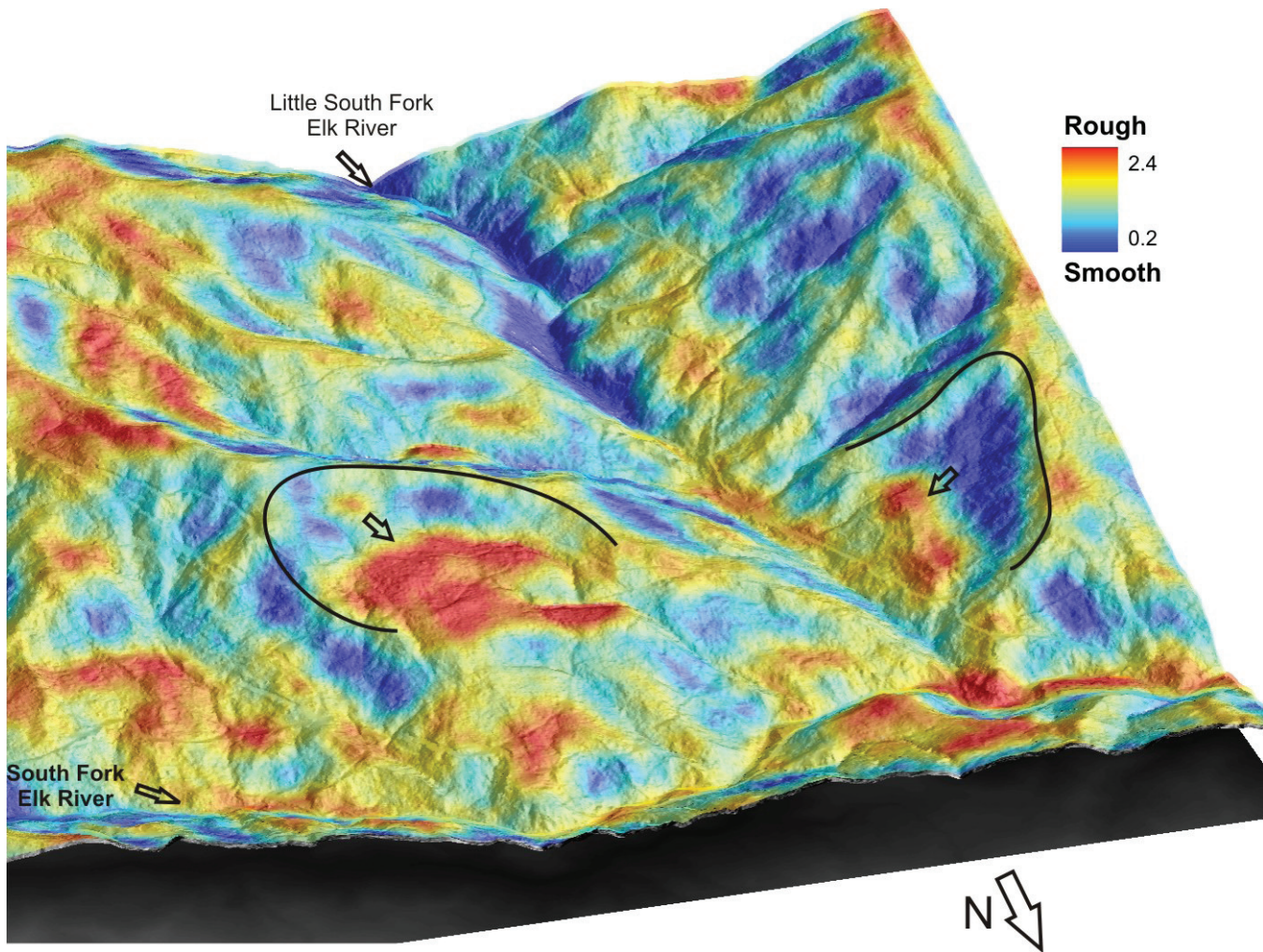


Figure 2. Oblique view up Little South Fork Elk River. The roughness algorithm DSLED-Rough calculated eigenvalue ratios within a 15m moving window, and was subsequently smoothed with a moving circle of radius 50m and draped over a digital elevation model. Two large deep-seated landslides are outlined, and the rough (red) slide bodies are clearly visible. We frequently observe smooth, steep headscarps which are distinct from the rougher landslide mass. Foreground approx 2km across.

period is likely to persist over a broad area – a spatial pattern distinct from that which we predict from the eustatically driven, headward-propagating, channel incision mechanism. Work is underway to ascertain the age of large landslide deposits. We hope then to correlate periods of slide activity or quiescence with Pleistocene-Holocene climatic conditions.

SUMMARY

This ongoing study illustrates the potential of Lidar in objectively analyzing large-scale hillslope instability with techniques that go beyond visually interpreting high-resolution shaded relief maps. Lidar will help underpin a process-based understanding of deep-seated landslide behavior and mechanistics.

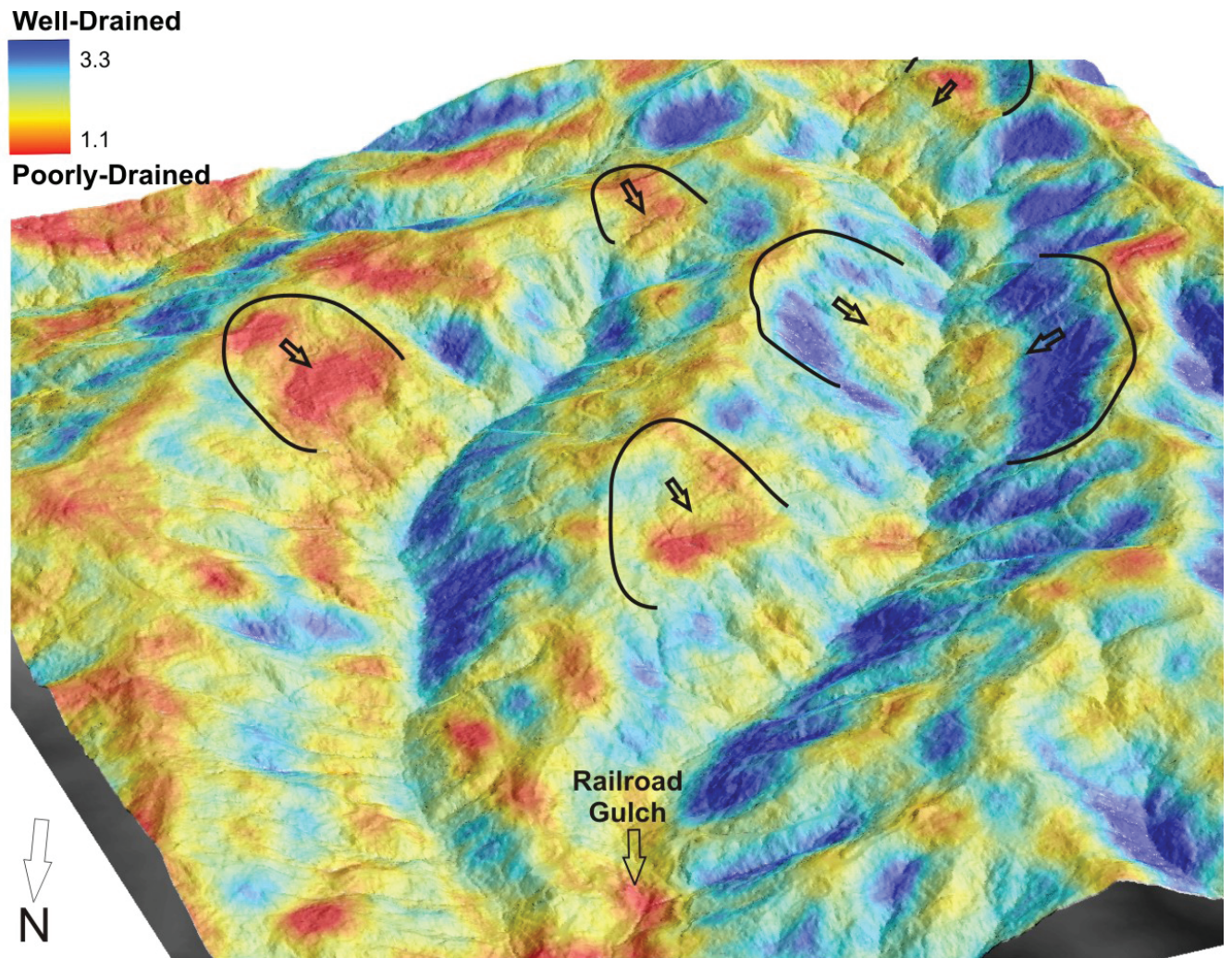


Figure 3. Oblique view up Railroad Gulch (tributary of Elk River). The flow accumulation algorithm DSLED-Drain has been smoothed with a moving circular window of 50m radius. Blue rendering indicates well drained (stable) topography, whereas red (unstable) suggests drainage has been disturbed, a process we attribute to deep seated landsliding. Outlines depict a selection of large landslides the algorithm successfully identifies. Again, the headscarps are frequently steep and well drained (blue). Length of Railroad Gulch catchment is approximately 2.5 km.

Marine Stratigraphy of the Eel Continental Shelf: Coastal response to sea level rise since the Latest Glacial Maximum

Danny O'Shea

ABSTRACT

Sediment cores and high-resolution Chirp seismic reflection profiles on the Eel Shelf reveal four distinct facies: 1) inner shelf sands; 2) transitional sands-muds; 3) mid-shelf muds; 4) relict lowstand and transgressive muds and gravels. A lobate subaqueous delta near the Eel River, composed of well-sorted, fine-grained, inner shelf sands. The inner shelf sand facies north of the Humboldt Bay entrance amalgamate with mid-shelf muds, shell fragments and relict sediments. Sand-mud transition facies of interbedded sands and flood muds are emplaced by hyperpycnal flows and form subtle bathymetric terraces. The mid-shelf mud facies located, seaward of the 60 m isobath, contain terrigenous silts and clays with high porosities (> 60%) and onlap the transgressive surface.

The subaqueous delta west of the Eel River represents at least 20 m of Holocene sediment accumulation and moderate sedimentation rates (>2mm/yr). The inner shelf Holocene sediment thickness north of the Humboldt Bay entrance has as little as 2 m of accumulation and very low sedimentation rates (<0.2mm/yr). A northwest plunging anticlinal fold west of Arcata Bay aligns with the onshore Humboldt Hill Anticline. The anticline brings the transgressive surface boundary to within 2 m of the seabed and is located near a gas seep. Rapid sea level rise during 4 discrete melt water pulses since latest glacial maximum allowed incised channels to trap fluvial sediments depriving the shelf of a sediment supply and increased erosion of unconsolidated backedge seacliffs. Infilling allowed fluvial sediments to bypass estuaries and construct barrier bays and spits during relative stillstands.

INTRODUCTION

Exploration of submarine geology throughout the oceans (Nicholson et al., 2006; Liu, et al., 2004), and on the northern California continental shelf (O'Shea, 2005), follows in part, from a substantial increase in the resolution of seismic reflection and coring technologies over the past decade. The record of continental shelf and slope stratigraphy reveal accommodation patterns that reflect a variety of controlling mechanisms, which interact over many temporal and spatial scales. Rates of incision, tectonic subsidence, sea-level rise, and sedimentation, inferred from identifiable sequence boundaries, provides a connection with recent advances in onshore mapping and plate boundary measurements to discoveries in marine stratigraphy.

Chirp seismic reflection profiles (Figure 1) and sediment cores (Figure 2) collected on the Eel continental shelf expose mid-shelf mud and inner-shelf sand deposits that onlap a transgressive, erosional surface, 5 km west of the North Spit of Humboldt Bay. A northwest plunging, asymmetric, fault-propagation anticlinal fold (i.e. the Axis of Doom) warps the marine stratigraphy on the inner shelf upward, emplacing a pre stage 2-lowstand surface to within 2 meters of the seafloor. The fold axis, which is ruptured closer inshore and not only releases gas into the water column, but also continues onshore near the U.S. Coast Guard Station on the North Spit peninsula, cuts diagonally across the Entrance Bay, continues underneath the Humboldt Bay Power Plant and nuclear waste storage facility, and eventually bifurcates beneath the local community College of the Redwoods and nearby adjacent South Humboldt Bay delta plain.

In addition to the Chirp seismic reflection profiles, box cores, vibra cores and slow cores ground truth the upper few meters of the seismic profiles and allow a quantitative analysis of continental shelf stratigraphy. Box cores provide high-resolution samples of the muddy deposits typical of the mid- and outer continental shelf and slope deposits. Vibra cores, which are effective in sandy sediments, but tend to disturb the sediments near the seafloor due to the intense vibration, are used in conjunction with slow cores that yield high-resolution, 30-cm diameter cores in both muddy and sandy locations. Synthesis of seismic stratigraphy and sediment cores along with other on and offshore research efforts provides the opportunity to enhance our understanding of tectonic, sedimentary, and eustatic processes that affect the margin.

Construction of the continental shelf north of Cape Mendocino is dominated by sediment input from the Eel River with only a minor contribution from the Mad River, 40 km to the north (Brown and Ritter, 1971). The Eel Continental Shelf extends northward from Cape Mendocino to the Trinidad Headlands and can be subdivided into 3 distinct regions based on water depth, sediment grain size characteristics and benthic faunal assemblages. The inner shelf extends from the 12-m to 55-m isobath and is dominated by fine sands that contain variable amounts of mollusk, arthropod and echinoderm shell fragments. The mid-shelf region extends seaward from the 55-m to the 90-m isobath, and on the Eel Shelf is the primary locus of episodic terrigenous flood mud deposits. The outer shelf extends to the shelf-slope break, located about the 130-meter isobath, and is dominated by bluish gray marine muds with increasing occurrence of ophiuroids, annelids as well as lesser amounts of mollusk, echinoderm and arthropod shell fragments.

The bathymetry of the Eel Shelf is for the most part is planar, but does contain several unique features that also serve as excellent geographical markers. The subaqueous delta, which forms the sediment lobe that extends along the shelf 8 km on either side of the Eel River mouth, builds the shelf seaward toward the head of the Eel Canyon. The Eel Canyon, which incises the Eel shelf to within 10 km of the coastline, provides a conduit for some of these sediments to abyssal depths. The Eel Canyon drops a precipitous 80-m to over 1000-m water depth within 22 km of the Eel River mouth. The entrance to Humboldt Bay, 10 km to the north-northeast of the Eel River mouth, is kept stationary by a pair of kilometer-long jetties that extend into the ocean to about the 10-meter isobath. The Humboldt Bar, another small lobe of sediment that forms seaward of the Humboldt Bay jetties, accumulates as ebb tidal currents from the bay and along shelf currents decrease and deposit their sediment load. The spoils from the annual dredging of the Humboldt Bay channels are dumped on the shelf 5 km WNW of the entrance, near the

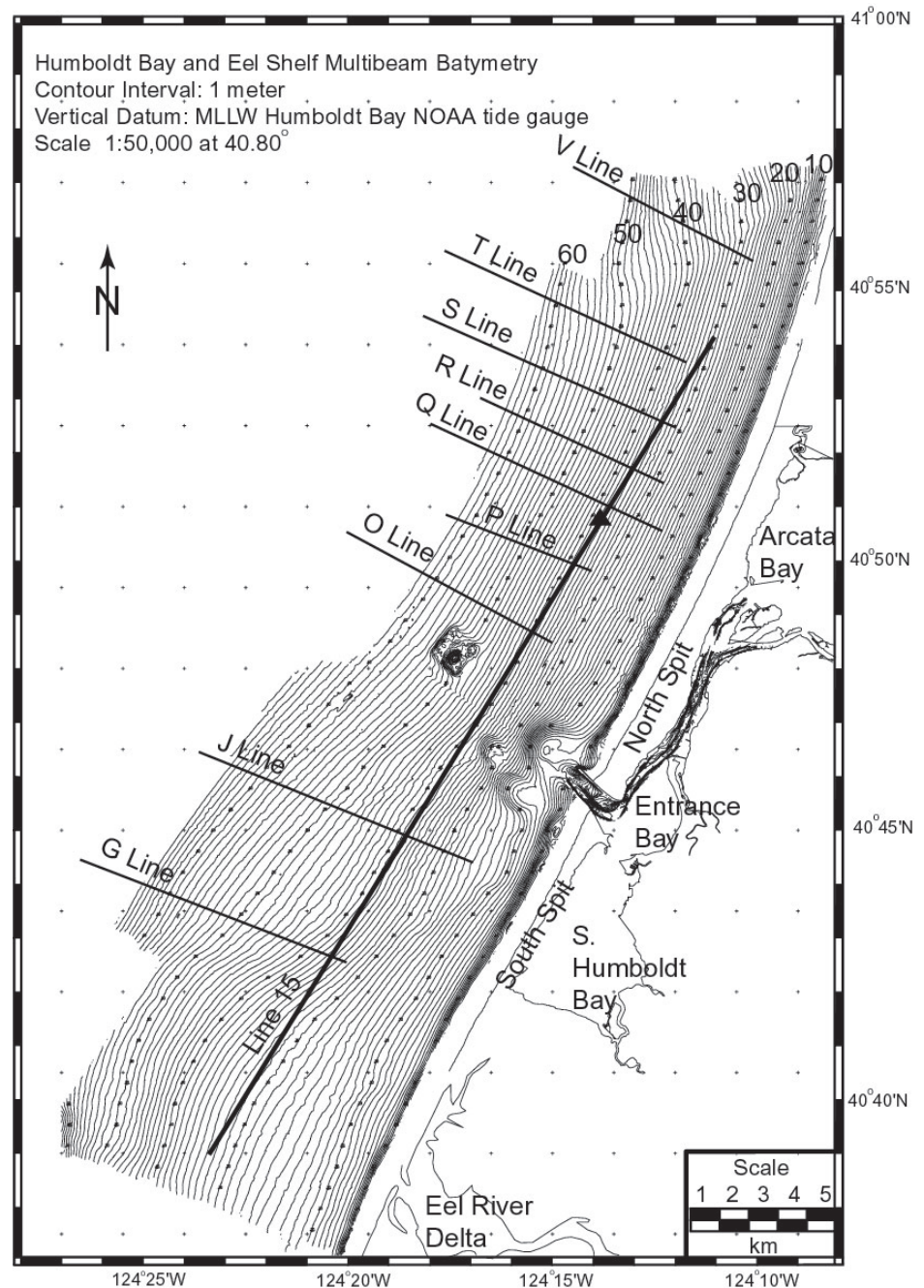


Figure 1: Survey lines of the high-resolution seismic reflection profiles collected on the Eel Shelf. The triangle between the Q and P Lines west of Arcata Bay on Line 15 is the location of the anticline seen in Figures 5.

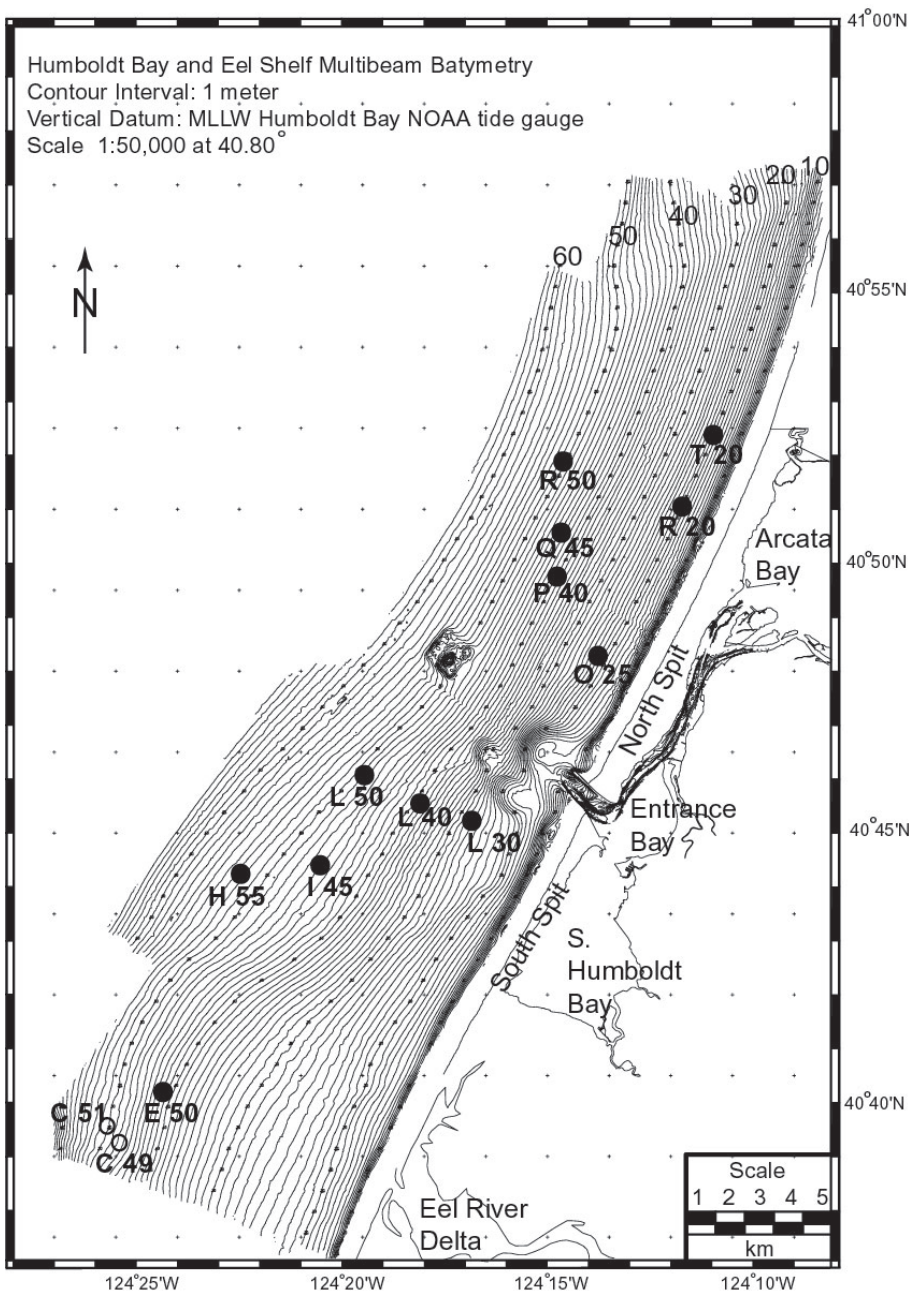


Figure 2: Core locations on the Eel shelf. Core locations are identified by the transect letters, A in the south to Z in the north, and a number indicating the nominal water depth in meters. Vibra cores are indicated by solid dots and Bothner slow cores are indicated by open dots.

below the seabed have a similar lithologic character as the core E 50 (Figure 3). Core data show that the massive well-sorted inner shelf sands of the Eel subaqueous delta lobe give way to a decrease in sorting and an increase of shell fragments northward toward the Humboldt Bay entrance.

The inner shelf sands west of Arcata Bay consist of poorly sorted, fine sands and gravels, with conspicuous cobbles of chert and quartz, and the remnants of benthic fauna including *Olivella olivella*, *Dendraster excentricus*, *Cancer* sp., and *Macoma* sp. fragments. The sands in this region are poorly sorted, grade downward through coarse sands and gravels and contain abundant shell fragments. Core Q 45 presents an unconformable, sharp contact between the poorly sorted inner shelf sands and underlying bluish-gray estuarine (?) muds.

50-meter isobath, and give rise to the 10-meter pile of dredge spoils mapped on the inner shelf. North of the Humboldt Bay jetties, there is a subtle increase in the gradient of the inner shelf, which is related to the sedimentary and tectonic accommodation patterns.

SEDIMENTARY FACIES

The synopsis of sediment cores and seismic reflection profiles have allowed the identification of four distinct facies on the Eel Continental Shelf: 1) inner shelf sands; 2) transitional sands-muds; 3) mid-shelf muds; 4) relict muds and gravels.

Inner Shelf Sands

The inner shelf sand facies extends from the storm-wave plunge point at about the 12-m isobath, seaward to the 55 m sand-mud transition and contain three distinct units of varying thickness. Surface sediments near the Eel subaqueous delta lobe directly west of the Eel River mouth contain fine to very fine, well sorted sands and sparse muddy, shelly or woody debris layers. Based on a lack of distinct reflectors in the Chirp seismic profiles it is suggested here that the 20 m of sediment

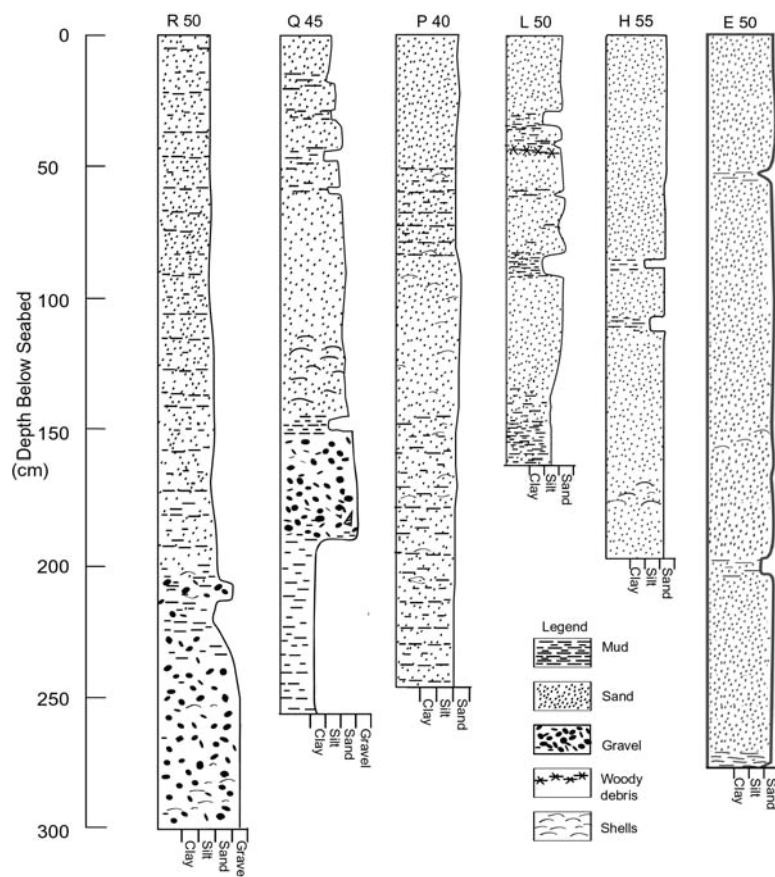


Figure 3: Core from the mid-continental shelf region west of the North Spit of Humboldt Bay (R50) to west of the Eel River mouth (E50). Core locations are identified by a transect letter, A in the south to Z in the north, and a number indicating the nominal water depth in meters.

100-m isobath and consists of terrigenous flood muds deposited on top of marine muds. The marine muds are recognized by their bluish to olive gray color and lower porosity, and are distinguished from the tan to brown terrigenous flood muds of higher porosity (>60%) and silt to clay size (< 64 μm) particles. As a result of the 1995 and 1997 Eel River floods, up to 10 cm terrigenous muds accumulated on the mid-shelf west of Humboldt Bay (Sommerfield et al., 1999). Bedform patterns preserved in the flood muds imply that hydrologic conditions at the seafloor are sufficient to generate 1- to 2-cm high ripples having wavelengths of 10 to 12 cm (Borgeld et al., 1999). Biogenic modification and chemical reduction of the terrigenous flood muds with the marine muds gradually causes the two to become indistinguishable from each other over relatively short periods of time (Wheatcroft et al., 1997).

Relict Sediments

Stratigraphy formed previous to the stage 2 lowstand and subsequently abraded during the transgressive period is characterized by infilling of drainage basins and erosion of weakly consolidated backshore regions (Driscoll, 1999). A sharp contact between the very coarse inner shelf sands and a fine-grained bluish gray mud deposit occurs 1.85 m below the seafloor in core Q 45 located on the axis of Doom. This stratigraphic relationship was observed in the Chirp seismic profiles and corroborated by this and other cores, which show direct evidence of an unconformable contact between the modern inner shelf sands and the underlying relict sediments.

Transitional sands-muds

A transition between the inner shelf sands and mid-shelf muds occurs along the 45-m to 60-m isobaths. On the bathymetric benches northwest of the Eel River mouth, tan to brown terrigenous flood muds that occasionally contain woody debris layers to 2-cm thick are interbedded with moderately sorted, very fine sands. Though limited in extent these layers are significant because they represent hyperpycnal fluid mud flow processes and are associated with high concentrations of fine grain sediments on the inner shelf (Traykovski, 2000).

Slumps and slides observed in side scan sonar data collected near the north entrant of the Eel Canyon indicate that small-scale slope instability processes are occurring on the continental shelf. Cores collected in and out of one such slope failure near the entrant of the Eel Canyon along the 50-m isobath, showed active mixing of inner shelf sands and interbedded mud layers.

Mid-shelf muds

The mid-shelf mud depocenter recognized by Wheatcroft et al. (1996) extends from the sand-mud transition zone to the

SEISMIC STRATIGRAPHY

The Chirp seismic data reveals an onlapping sequence boundary with high rates of sediment accumulation along the Eel River syncline and decreasing rates northward toward the inner shelf west of Arcata Bay (Figure 3). The most prominent feature imaged by the Chirp sonar is a tight, northwest plunging, asymmetric, fault-propagation anticlinal fold also located on the inner shelf 5 km west of Arcata Bay.

Sediments at the south end of Line 15 are acoustically transparent with occasional “blotchy” reflectors and exceed 20 meters in thickness. Between the Eel River mouth and the Humboldt Bay entrance, the thickness of inner shelf sandy sediments decreases and onlap the transgressive sequence boundary that formed since the latest glacial maximum (LGM). The inner shelf sands that cover the transgressive surface are at a minimum thickness over the axis of the anticline where the high rate of uplift precludes the accumulation of sediment. This location is coincident with an observed gas seep located at 40.8°N / 124.25°W.

The strata underlying the sequence boundary on the inner shelf north of the Bay entrance includes infilled channels, the tightly folded anticline and horizontal seismic reflectors. Reflectors seaward of the 50-m isobath (the mid-shelf mud facies) onlap the transgressive surface boundary from the south and the west. Gas wipeout is observed in several of the across-shelf seismic profiles seaward of the 70 m isobath (Figure 4).

The axis of the northwest plunging anticline 5 km west of the North Spit is located at 40° 50'N and 124° 16'W, and trends 150° (Figure 5). This fold is in the same region of the inner shelf west of Arcata Bay as an anticline

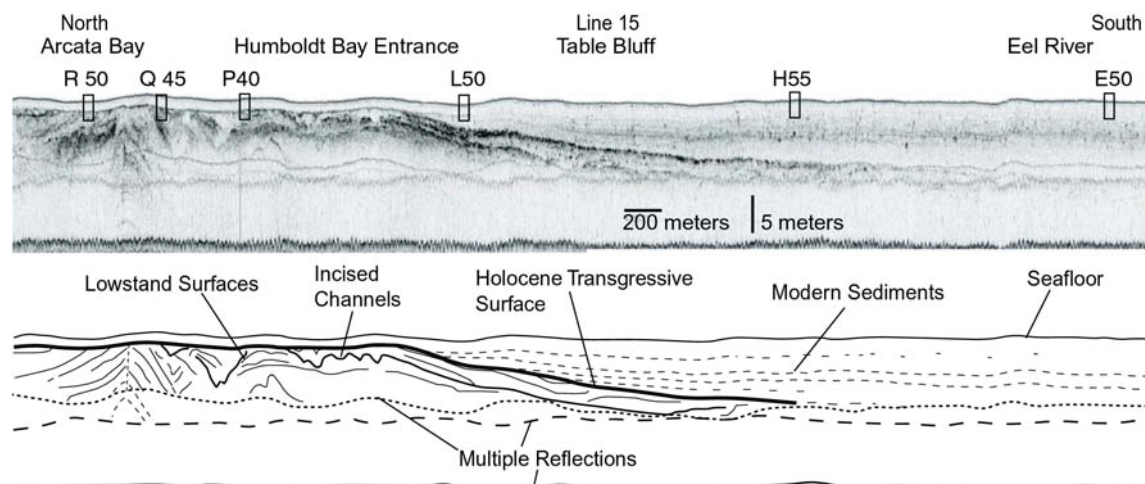


Figure 4: Line 15 is a high-resolution Chirp seismic reflection profile that extends along the 30-meter isobath from the Eel River mouth to west of Arcata Bay. Approximate locations of cores from Figure 3 are shown (Note that the water depths are different). The interpretation in the lower panel illustrates the modern Holocene strata onlapping the transgressive surface. Inner shelf sediment thickness north of the entrance to Humboldt Bay is at a minimum over the anticlinal fold. A detail of two separate Chirp profiles of the same anticline is shown in Figure 5.

mapped by Clarke (1992) and it aligns with the offshore extension of the Little Salmon Fault Zone. The trend of the fold axis, when projected to the southeast at 150° azimuth, crosses the North Spit near the public boat ramp in Humboldt Bay and closely aligns with the onshore Humboldt Hill Anticline (Figure 5).

COASTAL DEVELOPMENT DURING THE LATEST SEA LEVEL RISE

At the end of the LGM river mouths and intertidal waterways (e.g., sloughs, estuaries, lagoons) were located seaward of their present position (Shackleton et al., 1973; Swift, 1991). Sediments delivered by the paleo-Eel River to the lowstand shoreline near the modern day mid-shelf region (i.e. 100 m isobath) accumulated on a

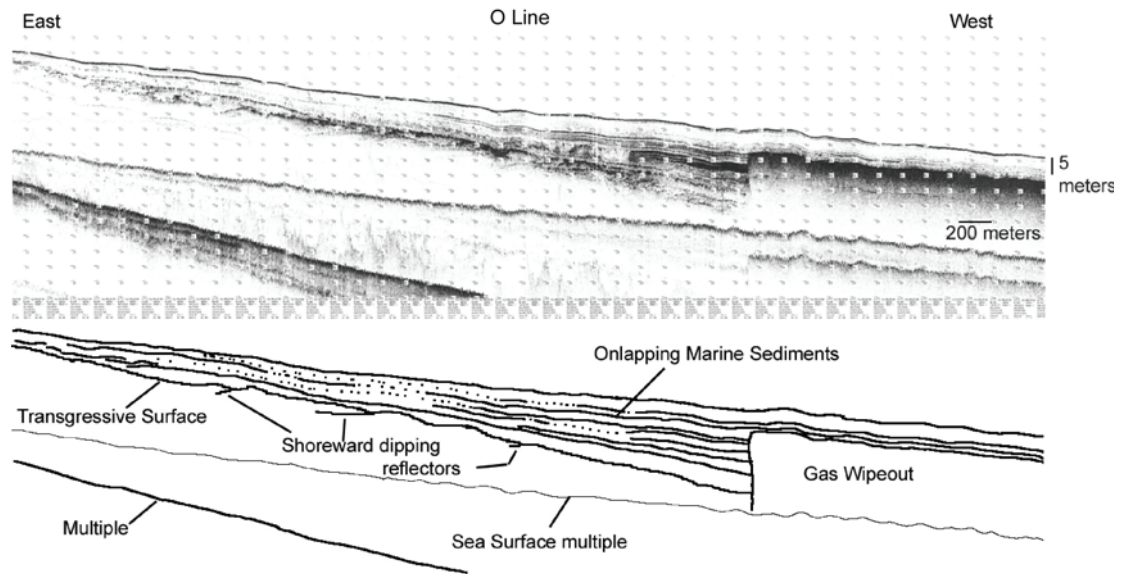


Figure 5: High-resolution seismic reflection profile generated by 0.6 to 15 kHz Chirp sonar. The “O Line” extends across the shelf from the 20-meter to the 100-meter isobath, north of the Humboldt Bay entrance. The lower panel illustrates the modern Holocene strata onlapping, from the west, onto the transgressive and lowstand surfaces. At the 70-meter isobath, a large area of gas wipes out the reflective surfaces.

narrow paleo-continental margin and formed the present day Humboldt Slide and continental slope plateaus (Alexander et al., 1999), or were advected westward into the Eel Canyon (Burger et al., 2002). As sea levels rose and low-lying coastal regions were flooded by seawater, an aggradational facies formed in the paleo-deltaic regions and trapped much of the fluvial sediment supply (Christie-Blick and Driscoll, 1995). Flooding of the incised paleo-Eel, Mad and Elk Rivers drainages during the sea level rise created accommodation space that filled with seawater and gradually infilled with sediment.

Liu et al. (2004) showed melt water pulses since the LGM have caused rapid rises of sea level that are punctuated by prolonged periods of slower sea level rise. Incised valleys trapped fluvial sediments derived from erosion of the upland regions as ocean waters flooded the continental shelf. The shelf adjusted to the new equilibrium profile based on the rate and size of sediment supply, water depth and hydrologic energy. The ability of marine waters to suspend and transport sediments generally decreases as water depths increase (Wright, 1995).

Uplifted coastal regions with more resistant lithologies formed seacliffs (e.g. Trinidad Headlands, Cape Mendocino), as the more poorly lithified seacliffs such as at Centerville, Table and McKinleyville Bluffs were more prone to mass wasting because of undercutting by waves. Seacliff erosion contributed to the development of the coastline by 1) providing a seacliff from which barrier spits can propagate, 2) adding sediments directly to the littoral zone, and 3) raising the level of the seabed on the inner shelf (Carter, 1988; Wright, 1995). Seacliff erosion and valley infilling have resulted in the modern coastal setting of delta plains separated by seacliffs and barred from coastal waters by barrier spits or dune fields.

Sand and gravel supplied to the coastal zones from the erosion of poorly lithified sea cliffs was transported along the paleo-littoral cell. Shallow marine sand bodies formed on sheltered regions of the inner shelf where currents had less ability to transport the bedload. As the incised and flooded regions aggraded, the suspended fluvial sediments eventually bypassed the paleo deltas, were transported to the mid- and outer shelf and gradually formed the onlapping mid-shelf mud facies observed in seismic profiles.

An upland region extended to the geographic location of the modern mid-shelf region west of the North Spit of Humboldt Bay. As sea level rose rapidly between 11.6 to 11.2 Ka, storm waves breached paleo-barrier spits

burying the back barrier lagoon deposits and preserving the lowstand surfaces now observed in the Chirp profiles west of the North Spit. Transgressive lag deposits of coarse sand, gravel and shells formed on top of the Late Pleistocene erosional surface. As the rate of sea level rise slowed approximately 6-7 Ka, a thin veneer of post transgressive inner shelf sands covers the erosional surface seen in the cores collected west of the North Spit of Humboldt Bay.

Aseismic and coseismic deformation also have an active role on the Eel Shelf via the creation of accommodation space. In areas of long-term subsidence, such as the Eel River syncline, creation of accommodation space allows for sediment accumulation over the long-term, and coseismic subsidence also creates the conditions for instantaneous sediment accumulation. The high rates of sediment accumulation in the Eel Syncline (>2 mm/yr) are the result of regional tectonic subsidence and compaction, whereas the sequence boundary observed near the seabed in core Q 45 and seismic profiles indicate interseismic uplift. Coseismic subsidence has preserved buried subtidal to supratidal estuarine surfaces observed in the Eel and Humboldt Bay regions (Li, 1992; Patton, 2004).

Eustatic sea level rise shifts the equilibrium profile of sea cliffs horizontally as the inner shelf seabed increases vertically in proportion to the amount of sea level rise (Bruun, 1962). Sediments are transported according to size and hydrologic conditions as seacliffs are undercut and erode (Wright, 1995; Van Wagoner, 1988). North of the Table Bluff Anticline a gradual reduction of accommodation space on the inner shelf, reaches a minimum west of the North Spit of Humboldt Bay where sediment thickness is less than 2 m above the tightly folded, anticline.

An interpretation of how the Eel continental shelf developed since the LGM is the result of the variable resistance of coastal seacliffs to erosion, infilling of lowstand incised regions, marine hydrodynamics, and a stepwise increase in sea level.

Eel River confined south by Table Bluff Anticline

The paleo-Eel River incised the modern day delta plain and flowed in a west-north westerly direction along the southern limb of the Table Bluff anticline. Multichannel seismic reflection profiles have identified paleo-channels incising the modern-day mid-shelf region west of Eel River syncline (Burger et. al., 2002). Chirp seismic records in this same region indicate that a thick sequence of modern sands have filled the basin resulting in a minimum sediment accumulation rate of 2 mm/yr.

Salmon Creek and Elk River separated by Humboldt Hill Anticline

The Elk River and Salmon Creek fluvial systems have long been isolated from the Eel River by the Table Bluff Anticline (Burger et al., 2002). Salmon Creek drains into South Humboldt Bay along the north limb of the Table Bluff anticline. The Elk River flows into the Entrance Bay and is presently separated from Salmon Creek by the Humboldt Hill Anticline. Chirp seismic profiles indicate the thalwegs of the paleo-Little Salmon Creek and the paleo-Elk River formed the channels and lagoons west of the present day Humboldt Bay entrance.

The Humboldt Hill and Eureka Anticlines were upland regions during the latest sea level lowstand and confined the Elk River to the valleys between the structural highs. Projection of the Humboldt Hill Anticline along its orientation of 330° aligns with the tightly folded anticline 5 km west of the North Spit.

Mad River confined to Arcata Bay by Eureka Anticline

The Mad River, Freshwater, Jacoby Creeks and other small drainage basins that flow into Arcata Bay were isolated from the Elk River by the Eureka Anticline. Horizontal seismic reflectors observed below the transgressive surface boundary on the inner shelf are interpreted as regressive back barrier deposits of the paleo-Mad River, Jacoby, Freshwater, and Janes Creeks. During periods between melt water pulses when rates

of sea level rise slowed, fluvial sediments infilled then bypassed the estuaries and formed barrier bays and spits. Periodic coseismic subsidence provided a mechanism for preservation of the horizontal reflectors and the transgressive sequence boundary, as the barriers were over-stepped. Preservation of the back barrier lagoonal deposits occurred as the next melt water pulse rapidly increased water depths. Interseismic uplift west of the North Spit has brought the lowstand and transgressive facies to within 2 m of the modern seabed. A lack of age control of the lowstand and transgressive facies precludes the correlation of specific reflectors with the eustatic and tectonic rates.

A modern day analog of the paleo-coastline during the period when sediment sources were limited by trapping occurs just north of the study area. Big, Dry, Stone and Freshwater Lagoons have morphologies similar to the coastline in the Humboldt Bay region during the period of rapid sea level rise associated with melt water pulses. Increased rates of seacliff erosion balance the deficit of sandy sediments supplied to the inner shelf when a limited source of fluvial sediment is available.

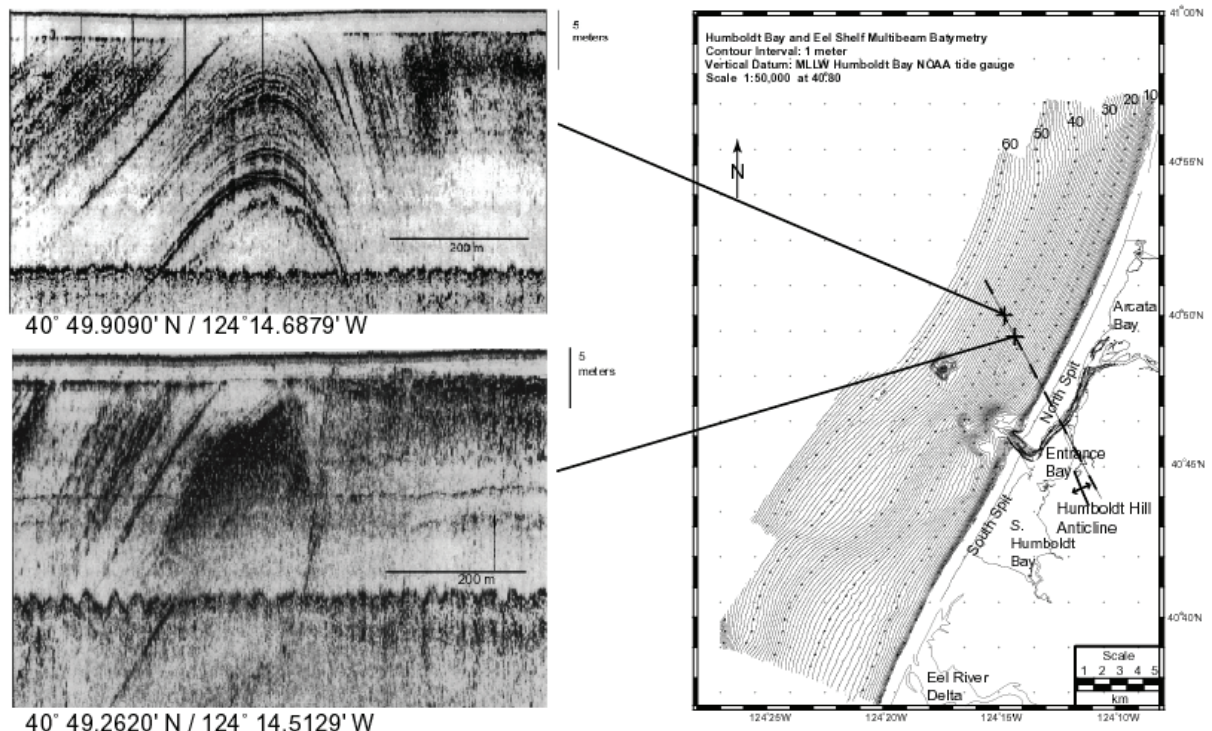


Figure 6: Two separate seismic reflection profiles of the same anticlinal, fault propagation fold located 5 km west of Indian Island in Humboldt Bay. The upper seismic profile located at $40^{\circ} 49.9090' N / 124^{\circ} 14.6879' W$ and is 1250 meters northwest of the lower seismic profile located at $40^{\circ} 49.2620' N / 124^{\circ} 14.5129' W$. The two profiles when projected southeast closely align with the mapped onshore Humboldt Hill Anticline

On the Eel Shelf during periods of rapid sea level rise, rates of seacliff erosion increased when Eel River sediments were trapped in the flooded paleo-estuaries. As sea levels stabilized 6 to 7 Ka the incised channels gradually infilled, sediments were again available to build the barrier spits, dunes, the Eel subaqueous delta and the mid-shelf mud depocenter.

The geomorphic expression of the erosional remnants of sea cliffs in south Eureka along U S route 101 and in Arcata from Valley West to Arcata High School, indicate that sea level has regressed and the coastline prograded as the sediments have infilled the Humboldt and Arcata Bays. The same process appears to have occurred on a larger scale in the Eel delta plain.

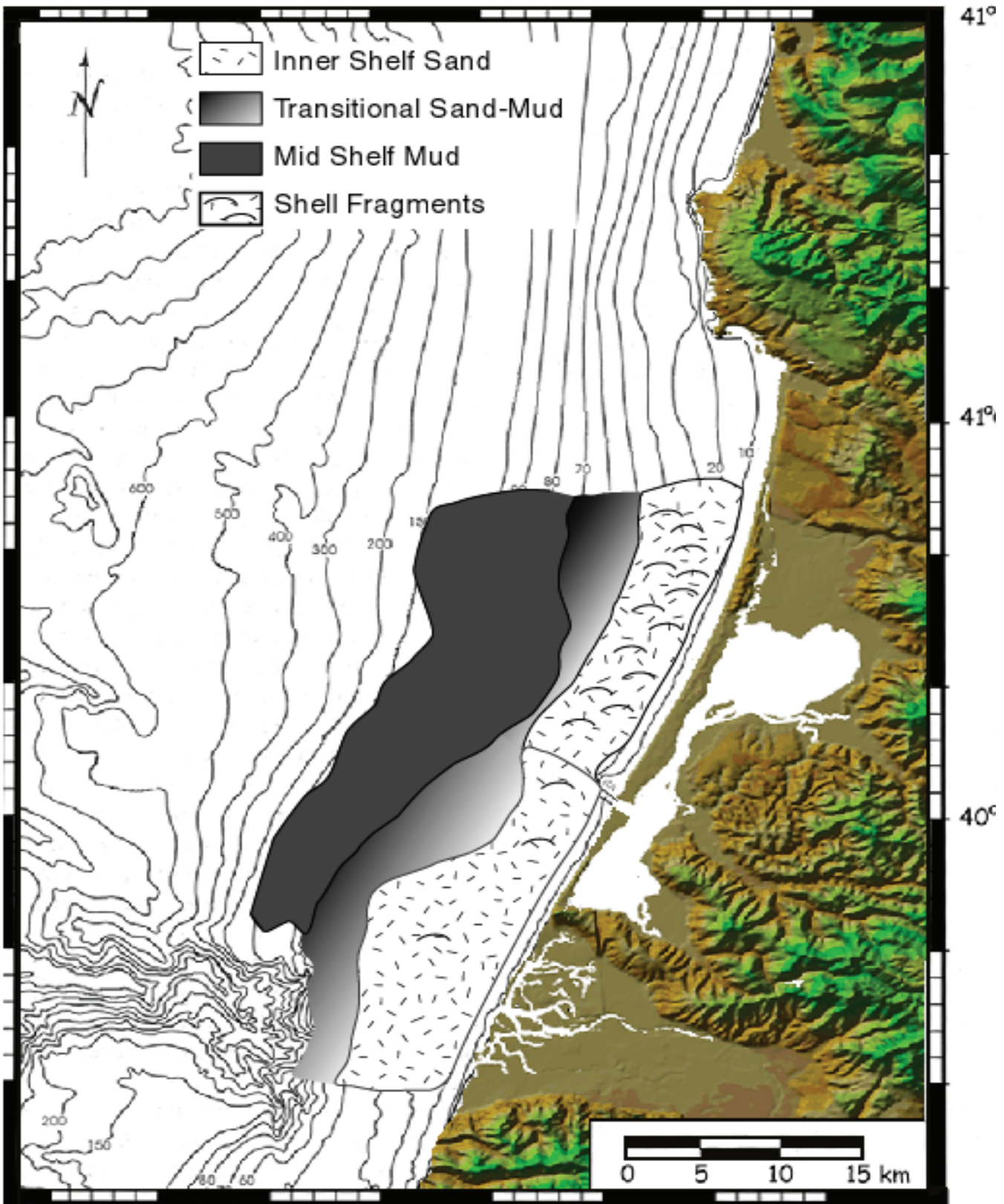


Figure 7: Facies on the Eel Shelf interpreted from vibra core and seismic reflection data. South of the Humboldt Bay entrance the inner shelf sands become interbedded muds and sands extend north and west of the Eel River mouth. North of the Humboldt Bay entrance, poorly sorted sands and shell fragments are in part reworked from the underlying relict sediments. The mid-shelf mud facies extends along the 55-meter isobath and extends seaward to approximately the 120-meter isobath.

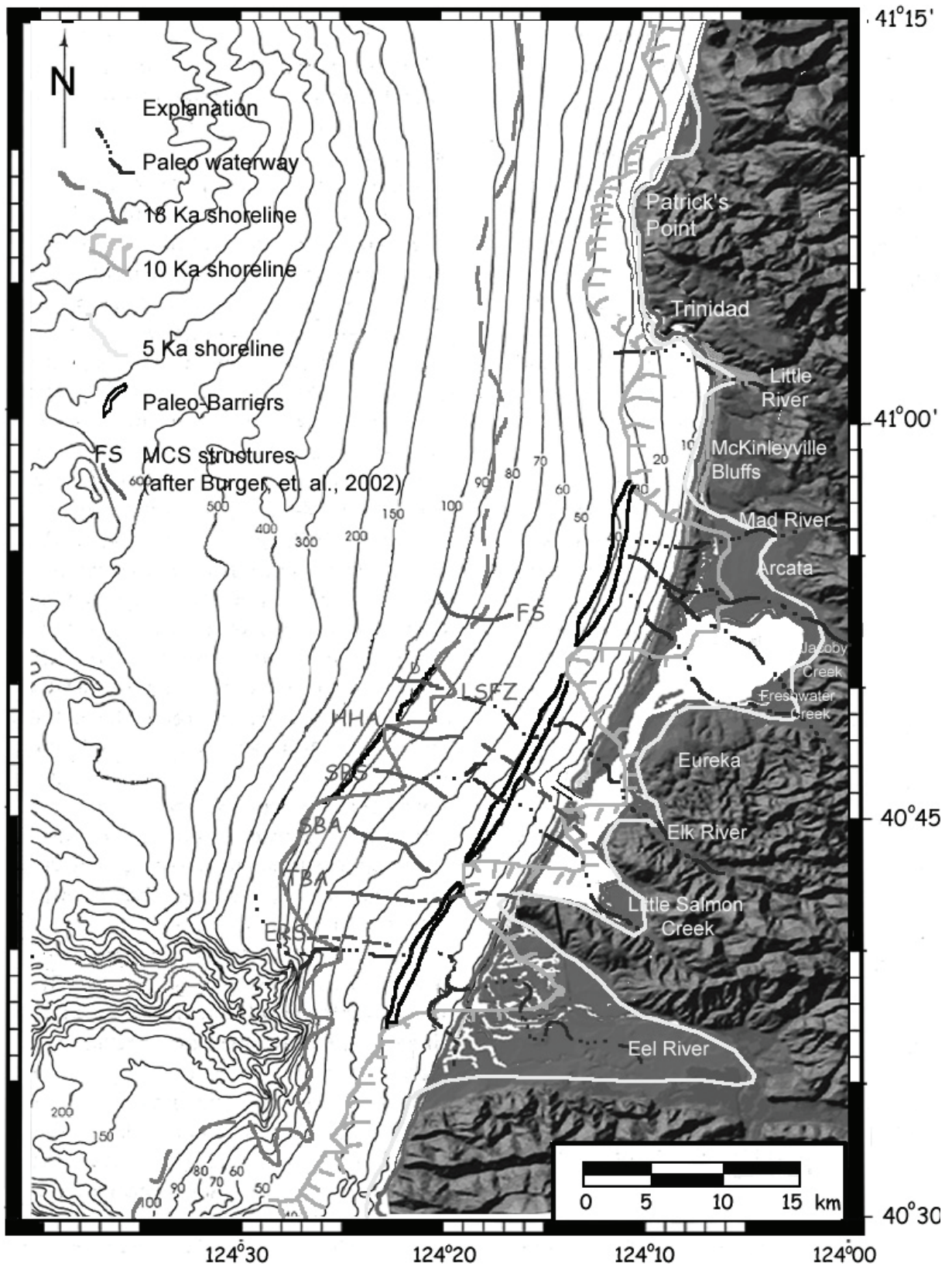


Figure 8: Paleo-coastline configuration interpreted from Chirp seismic reflection profiles, vibra core data, multi-channel seismic interpretations from Burger et al. (2002) and geomorphic features and sea level curve from Liu et al. (2004). ERS=Eel River Syncline, TBA=Table Bluff Anticline, SBA=South Bay Anticline, SBS=South Bay Syncline, HHA=Humboldt Hill Anticline, LSFZ=Little Salmon Fault Zone, FS=Freshwater Syncline.

REFERENCES CITED

- Alexander, C., Simoneau, A., 1999. Spatial Variability in Sedimentary Processes on the Eel Continental Slope, *Marine Geology*, vol.154: 243-254.
- Brown III, W. M., Ritter, J. R., 1971. Sediment transport and turbidity in the Eel River basin, California: United States Geological Survey Water-Supply Paper 1986, 70 p.
- Burger, R. L., Fulthrope, C.S., Austin, J.A., Gulick, S.P., 2002. Lower Pleistocene to Present structural deformation and sequence stratigraphy of the continental shelf, offshore Eel River basin, northern California. *Marine Geology*, vol. 185, p. 249-281.
- Clarke, S. H. Jr., 1992. Geology of the Eel River Basin and Adjacent Region: Implications for Late Cenozoic Tectonics of the Southern Cascadia Subduction Zone and Mendocino Triple Junction, *American Association of Petroleum Geologists Bulletin*, vol. 76, no. 2: 199-224.
- Christie-Blick, N., Driscoll, N. W., 1995. Sequence Stratigraphy, *Annual Review Earth Planetary Science*, vol. 23: 451-478.
- Driscoll, N. W., 1999. Marine Geology and Geophysics 12.710, in *Marine Field Trip Sat Nov. 13, 1999*, 35 p.
- Liu, J. P., Miliman, J. D., Gao, S., Cheng, P., 2004. Holocene development of the Yellow river's subaqueous delta, North Yellow Sea. *Marine Geology*, vol. 209: 45-67.
- Nicholson, C., Kennett, C., Sorlien, S., Hopkins, S., Behl, R., Normark, W., Sliter, R., Hill, T., Pak, D., Schimmelmann, A., Cannariato, K., 2006. Santa Barbara Basin Study Extends Global Warming Climate Record. *EOS, Transaction, American Geophysical Union*, Vol. 87, No. 21.
- O'Shea D., 2005. Continental Shelf Sedimentation and Holocene Development of the Northern California Coast, Eel River and Humboldt Bay Area. M. S. thesis, Humboldt State University, Arcata California, 135 pp.
- Sommerfield, C. K., Nittrouer, C. A., Alexander, C., 1999. ⁷Be as a tracer of flood sedimentation on the northern California continental margin. *Continental Shelf Research*, vol. 19, no. 3: 335-361.
- Traykovski, P., Geyer, W. R., Irish, J. D., Lynch, J. F., 2000. The role of wave-induced density-driven fluid mud flows for cross-shelf transport on the Eel River continental shelf, *Continental Shelf Research*, vol. 20, no. 16: 2113-2140.
- Shackleton, N. J., Opdyke, N. D., 1973. Oxygen isotope and paleomagnetic stratigraphy of equatorial Pacific core V28-238; oxygen isotope temperature and ice volumes on a 105 and 106 year scale, *Quaternary Research*, vol. 3: 39-55.
- Wheatcroft, R.A., Borgeld, J.C., Born, R.S., Drake, D.E., Leithold, E.L., Nittrouer, C.A., Sommerfield, K., 1996. Anatomy of an oceanic flood deposit, *Oceanography*, vol. 9: 158-162.
- Wheatcroft, R.A., Sommerfield, C.K., Drake, D.E., Borgeld, J.C., Nittrouer, C.A., 1997. Rapid and Widespread dispersal of Flood Sediment on the Northern California Margin, *Geology*, vol. 25, no. 2: 163-166.
- Wright, L. D., 1995. *Morphodynamics of Inner Continental Shelves*, CRC Press Inc., Boca Raton, Fla. 241 p.

Coseismic Subsidence of Arcata Bay

Chad Pritchard

Arcata Bay has a long history of paleoseismic stratigraphy, anthropogenic alterations, and as an important communing area for drunk guys with shotguns that don't like living ducks very much. A good number of geologic studies have been conducted in Arcata Bay, including: Vick (1988), Clarke and Carver (1992), Carver et al. (1992), Valentine (1992), Jacoby et al. (1995), and Pritchard (2004). Because the author of this abstract also did his thesis on the bay, the following is obviously "fact"; just joking, it comes from my thesis. Enjoy:

ABSTRACT

Paleoseismic investigations to identify late Holocene upper crustal movement beneath Arcata Bay has confirmed four buried marsh soils that represent up to four great southern Cascadia subduction zone earthquakes. Estimated ages of earthquakes are: 250, 1350 to 1190, and 1590 to 1390 cal yr BP, with a possible earthquake at 1290 to 1100 cal yr BP. Coseismic subsidence in Arcata Bay was originally theorized to occur due to coseismic movement of the Freshwater Syncline (See Fig 1). Offshore seismic images published in Burger, et al. 2002 indicate that the Freshwater Syncline has ceased folding and that upper crustal faulting in the off-coast section of Humboldt Bay has occurred in the Holocene (See Fig 2).

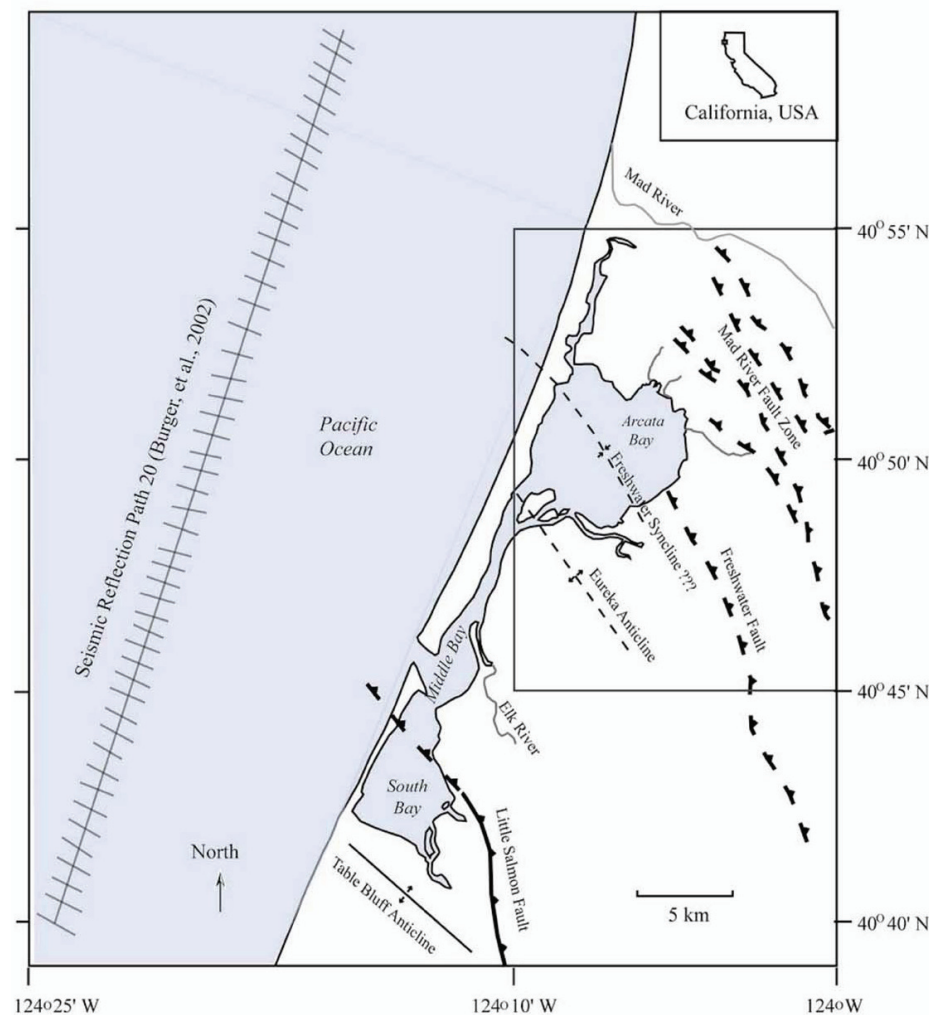


Figure 1: Map of Humboldt Bay, California with major onshore structural features. Seismic reflection survey path (Burger et al., 2002) is delineated by the offshore line in the western section of the map with smaller cross lines denoting intersection of crossing seismic profiles (Figure 2). Map modified from McLaughlin et al. (2000).

To test for late Holocene movement of the onshore section of the Freshwater syncline buried low salt marsh soil horizons were correlated around Arcata Bay. Coseismically buried soils were identified using lithostratigraphy, estimated diatom biostratigraphy, and radiocarbon age determinations. Sites used for the final study included: Mad River Slough (MRS), Arcata Salt Marsh (ARC), Jacoby Creek (JAC), Eureka Slough (ESB), and Daby Island (DAB). The only continuous buried soil horizon in Arcata Bay is the youngest, which probably subsided coseismically in A.D. 1700 during a regional megathrust event along the Cascadia subduction zone. The youngest buried soil was not warped by the Freshwater syncline (See Fig 3). Marsh accretion rates were calculated using diatom biostratigraphic data and surveyed elevations and were similar at multiple sites (See Fig 4). All data suggests that each site had similar depositional histories at the margin of Arcata Bay. Therefore, evidence suggests that the Freshwater syncline has not deformed during, or since, the most recent Cascadia subduction zone earthquake.

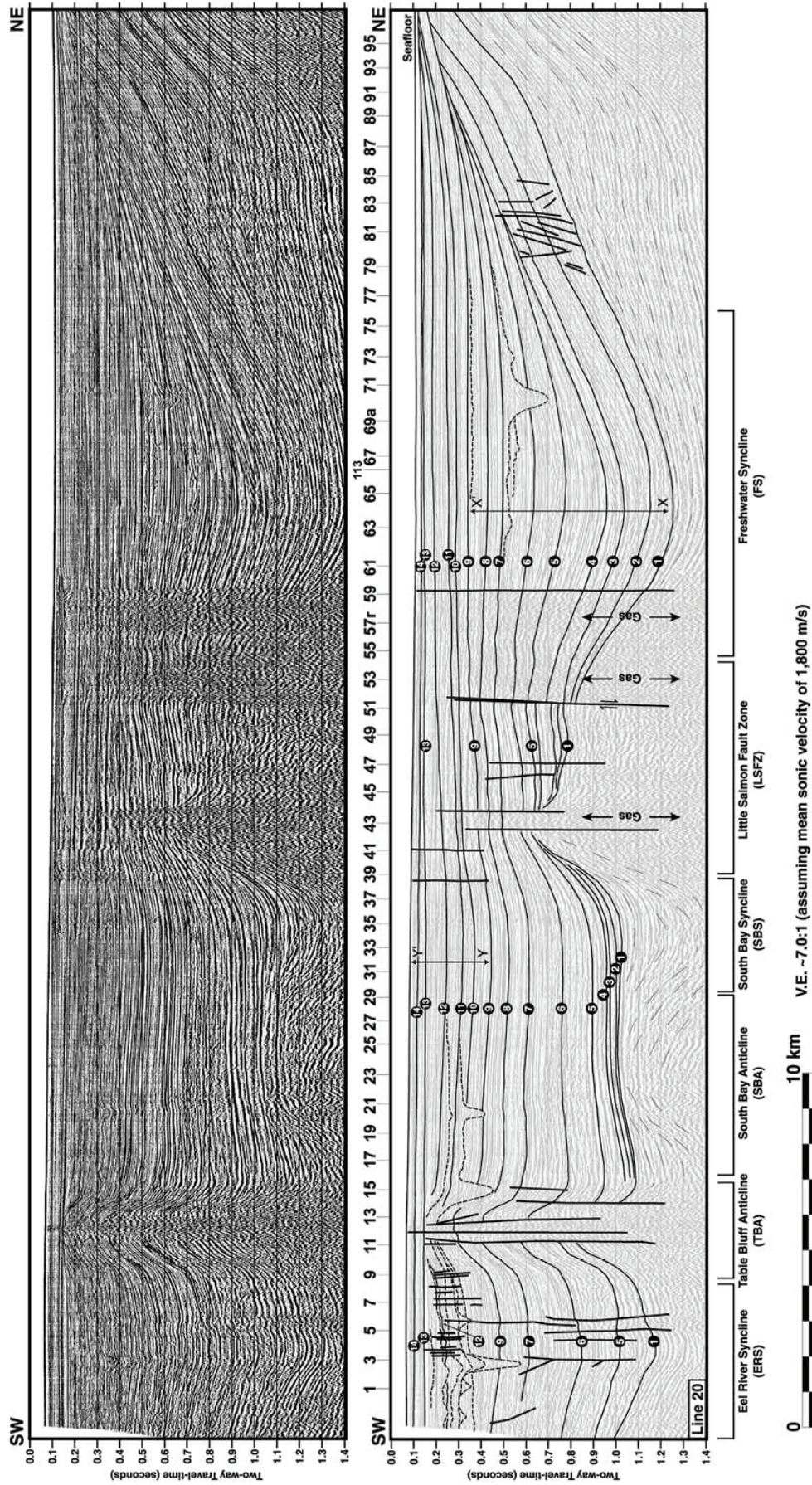


Figure 2: Seismic reflection survey of offshore Eel River Basin with uninterrupted survey (top) and interpreted survey (bottom), from Burger et al. (2002). The survey track lines for path 20, used in this paper, are located on figure 2. Based on the lack of folding in upper sediments, Burger et al. (2002) conclude that the offshore segment of Freshwater syncline ceased growth approximately 600,000 ka.

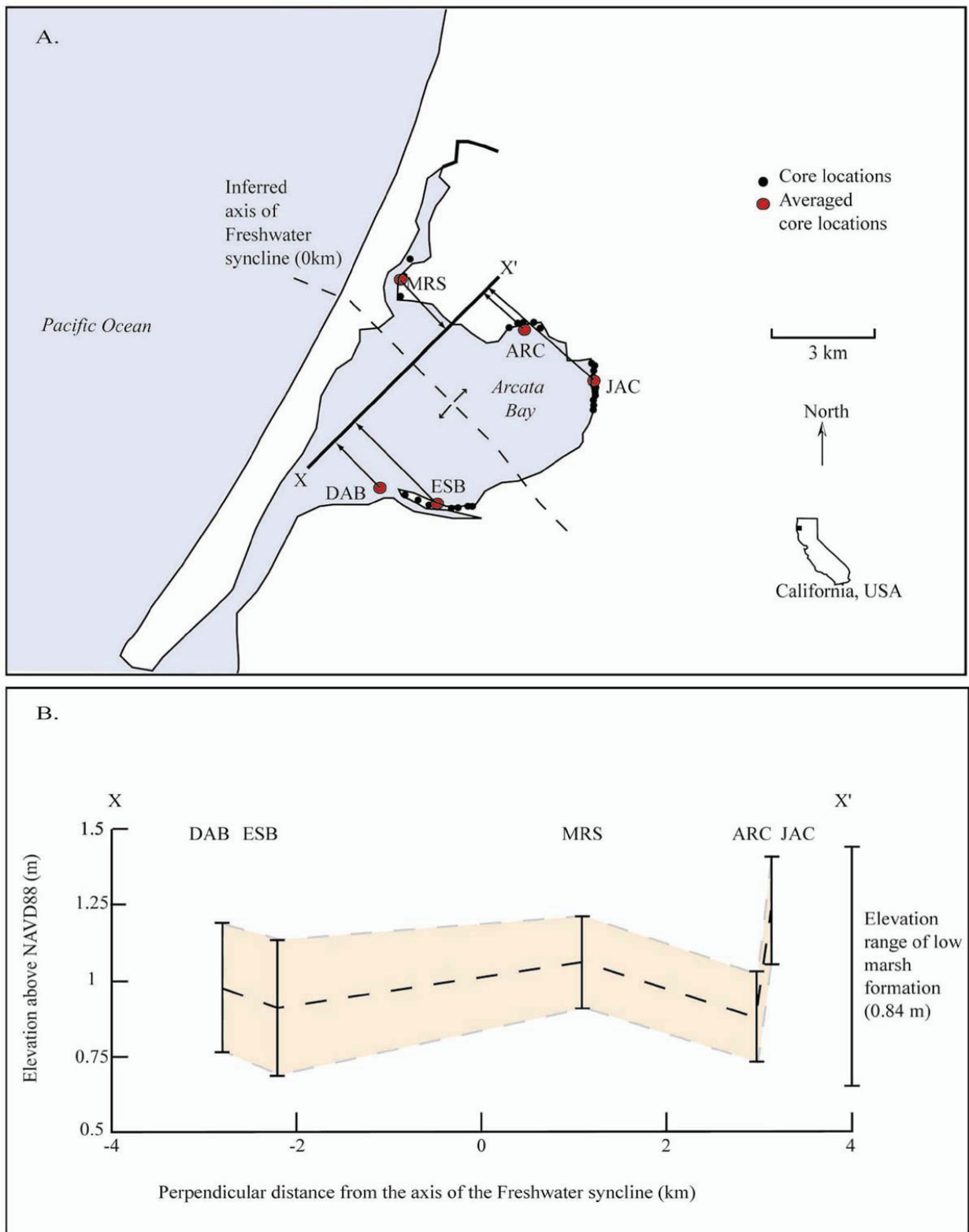


Figure 3: Cross section perpendicular to Freshwater syncline, Arcata Bay. A. Map showing orientation of cross section X-X' and method of projection of elevation onto X-X'. Core sites are: Mad River Slough (MRS), Arcata salt marsh (ARC), Jacoby Creek (JAC), Eureka Slough (ESB), and Daby Island (DAB). B. Cross section of the elevation of the top of the A.D. 1700 buried soil horizon. For each site, the elevation is average of all core elevations and error (shaded zone is the sum of standard error and closure error from surveys at each site). Cross section shows that there is little variation in the elevation of the buried soils. Elevational variation can be accounted for by the 84 cm elevation range of low marsh formation and paleo (i.e. pre -A.D. 1700) topography.

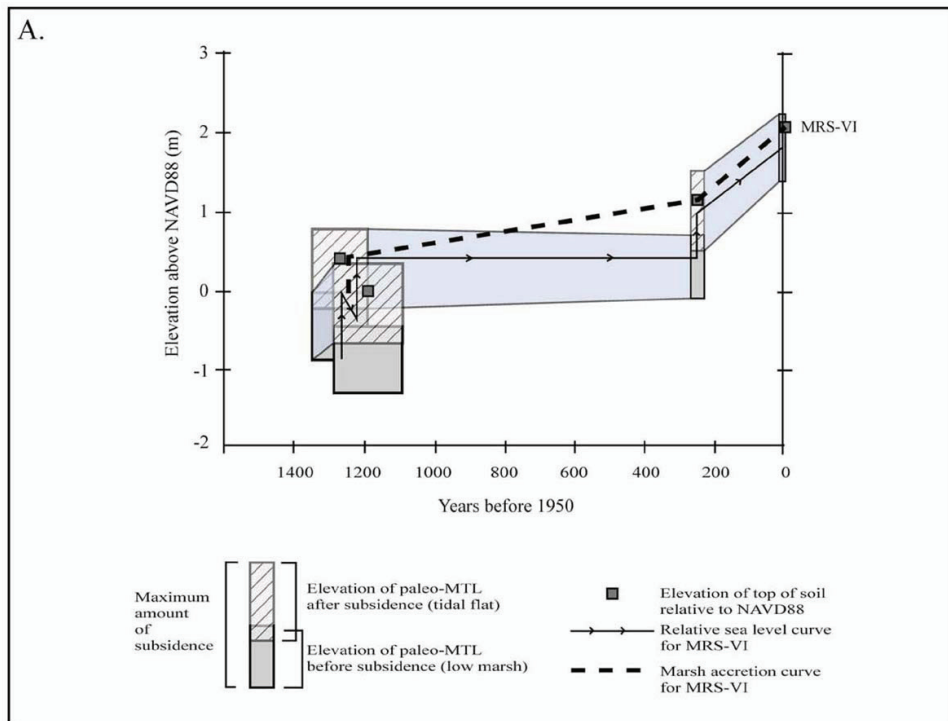
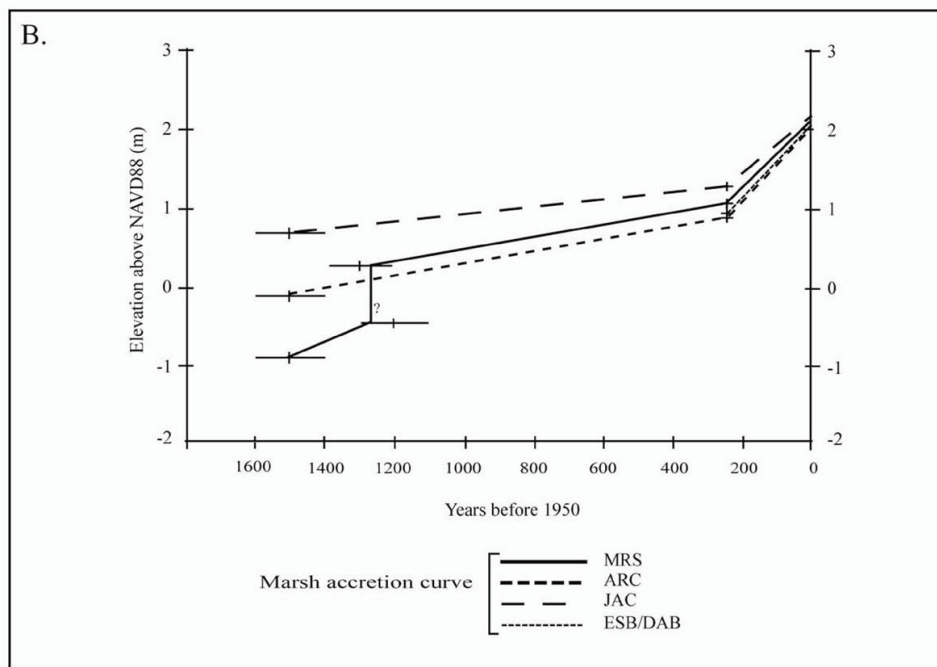


Figure 4 Estimated marsh accretion rates from core MRS-VI and all core sites. A. Relative sea level curve and marsh accretion curve for core MRS-VI. The solid line with arrows depicts increases in relative sea level with time, based on of low marsh (gray) and tidal flat (hashed) zones of formation relative to paleo-MTL. Length of boxes represents elevation ranges of low marsh or tidal flat formation (y-axis) and width of boxes delineates calibrated radiocarbon ages (x-axis). Marsh accretion curve for core MRS-VI shows an estimated rate of



sedimentation between buried soils. B. Marsh accretion curves for all sites from this study. Mad River Slough (MRS), Arcata salt marsh (ARC), Jacoby Creek (JAC), Eureka Slough and Daby Island (ESB/DAB). Elevation of the top of buried soils is averaged from each site, range of calibrated age is denoted by the horizontal line. The age of the fourth to youngest buried soil at Mad River Slough (Clarke and Carver, 1992; Valentine, 1992) was used to estimate a longer period of marsh accretion.

Coastal Sand Dune Stratigraphy and Geomorphology of the North Spit of Humboldt Bay

**Thomas H. Leroy
Pacific Watershed Associates
&
The Cascadia Geoscience Cooperative**

ABSTRACT

The northern North Spit of Humboldt Bay is primarily composed of Holocene sand dunes in various states of stability. The dune field as a whole appears to be part of a transgression where active dunes are slowly advancing over older dunes and into the existing estuary environment.

The forested and stabilized portion of the dune field is composed of successive parabolic dune pulses, each one stacking up against a previous dune pulse from east to west. The active sand dunes are transverse type dunes and are currently advancing east, often as discrete “slugs” of sand. Previously stable sand dunes are often being eroded and incorporated into the active dune sequence.

Radiocarbon age control from a coastal forest, buried by the youngest dune sequence, defines three age ranges compatible with dune movement through the forest. The age ranges are 1725-1790, 1805-1885, and 1915-1960. Of these three age ranges the most likely candidate is 1725-1790.

There are coarse grained gravel deposits found discontinuously along the western margin of the stabilized dune field. Physical characteristics of the gravel suggest different means of deposition at different geographic areas along the spit. From the northern most forested dunes most of the gravel can best be explained by historic river mouth migration. South of the northern most forested dune, the gravel may better be explained by a paleo-shoreline related to vertical movements in the earth's crust. An inland-most gravel exposure is deposited on sand dunes and may be tsunamigenic in origin.

The combined evidence from local paleoseismic and paleotsunami investigations, dune morphology and distribution, gravel deposition mechanisms, and age control, may suggest the North Spit was subjected to regional subsidence and tsunami inundation associated with the 1700 AD Cascadia Subduction Zone earthquake. The associated destabilization of the western margin of the spit could have initiated the current dune advancement.

INTRODUCTION

The coastal sand dunes of Humboldt Bay provide the foundation for one of the more unique geomorphic environments and environmental niches in Humboldt County. Dunes straddle the coast, in one form or another, from Clam Beach to Table Bluff, and protect Humboldt Bay and the coastline from wind and wave attack. The underlying geomorphic processes that contribute to form sand dunes, and hence coastal dune fields themselves, are very sensitive and dynamic and this is reflected in the diversity of the types, location, and size of the sand dunes that we see along the western margin of Humboldt Bay.

The dynamic variables that drive coastal dune processes include: wind, longshore sand transport, sediment supply, sea level fluctuations, and vegetative cover which vary over time and affect the small and large scale dune forms that we see along the coast. Slowly changing variables such as sea-level fluctuations effect the dune field on a time scale of hundreds to thousands of years. In contrast, vegetative cover can change quickly and have profound effects on natural dune processes in tens of years or less.

This paper is divided into 3 sections: 1) A description of basic dune features and the dune stratigraphy of the North Spit, 2) Age control on the dunes, and 3) Discussion, speculation, and conclusions

Basic Dune Features and Dune Stratigraphy of the North Spit

The North Spit of Humboldt Bay (Fig. 1) has extensive dune fields which exhibit many of the classic characteristics of typical coastal dunal landscapes; it also contains puzzling atypical stratigraphy which may reveal clues to the tectonic history of the Humboldt Bay region.

Like most of the other coastal dunes along the west coast of the United States, the introduction and subsequent invasion of non-native vegetation has had a profound affect on the natural dune morphology and processes on the North Spit (Fig. 2). On the North Spit in particular, the non-native vegetation has stabilized or slowed the advancement of dunes and artificially raised the elevation of the foredune complex. This vegetation colonization has changed the dynamics of the dune field by reducing or slowing the amount of sand moving off the beach and into the dune field. Although the non-native vegetation affects the dune field, the coastal dune processes that were operating thousands of years ago are still operating today, they've just been modified a bit.

Foredunes and Deflated Surfaces

By understanding the basic elements of coastal dune fields and their dynamic interaction with the beach, one can better hypothesize about the development of the older currently stabilized dunes on the North Spit, which may archive thousands of years of coastal development.

Two important and noticeable geomorphic features found on the western edge of the North Spit are the foredune and deflated surfaces (Fig. 3). These geomorphic features are typical of coastal dune fields and they interact with and profoundly influence the development of the large scale sand dune fields to the east.

The first or primary foredune ridge marks the boundary between the generally active upper strand, where beach processes dominate, and the dune system, which is controlled by aeolian processes. Behind the primary foredune ridge is a series of older foredune ridges that form a zone of accumulated sand blown off the beach which is slowly moving inland. This foredune complex, which varies in width, typically consists of complicated, hummocky

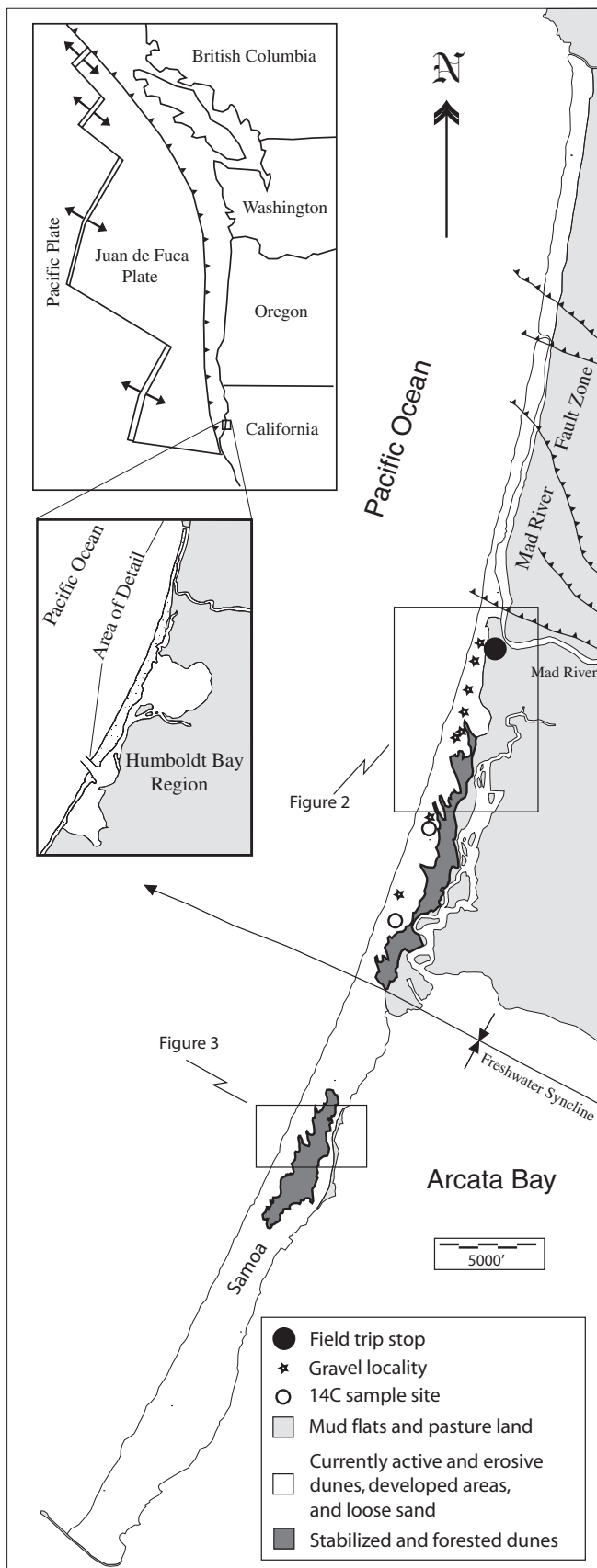


Figure 1. Generalized map of the North Spit of Humboldt Bay dune field. The figure also shows 14C sample locations and anomalous gravel localities.

topography and is the primary source of sand for dunes further inland.

On the North Spit, the foredune is a topographically distinct feature, bounded on the west by the beach and on the east (inland) by deflated surfaces created by the last major episode of inland dune movement.

In areas where foredune sand deposits have been blown inland and removed down to the water table or below the level of the effective winds, deflation plains form, and erosion slows dramatically or ceases (Fig. 3). These features can be seen in the multitude of seasonal wetlands that lie west of the large scale dunes. As with the dunes, these wetlands are constantly changing shape and extent in response to the slow inland migration of the growing foredune complex to the west, and as their inland margin migrates east at the trailing edge of the most recent dune movement.

Inland Coastal Sand Dunes of the North Spit

East of the foredune/ deflated surface complex lay the most prominent dunes on the North Spit. The eastern portion of the dune field is highly stabilized and overgrown with a thick coniferous forest; the western portion of the dune field is more dynamic with new dunes forming at the coast. The interface of the active and stable dunes is complex and dynamic (Fig. 2).

The dunes on the North Spit are most obviously subdivided into three categories; stable, active, and erosional. The stable dunes tend to occupy the eastern edge of the spit, the active dunes advance from the western portion of the spit, while the erosional dunes are commonly found along the margins of the stable dunes where active dunes or tidal flats interface with the stable portions of the dune field.

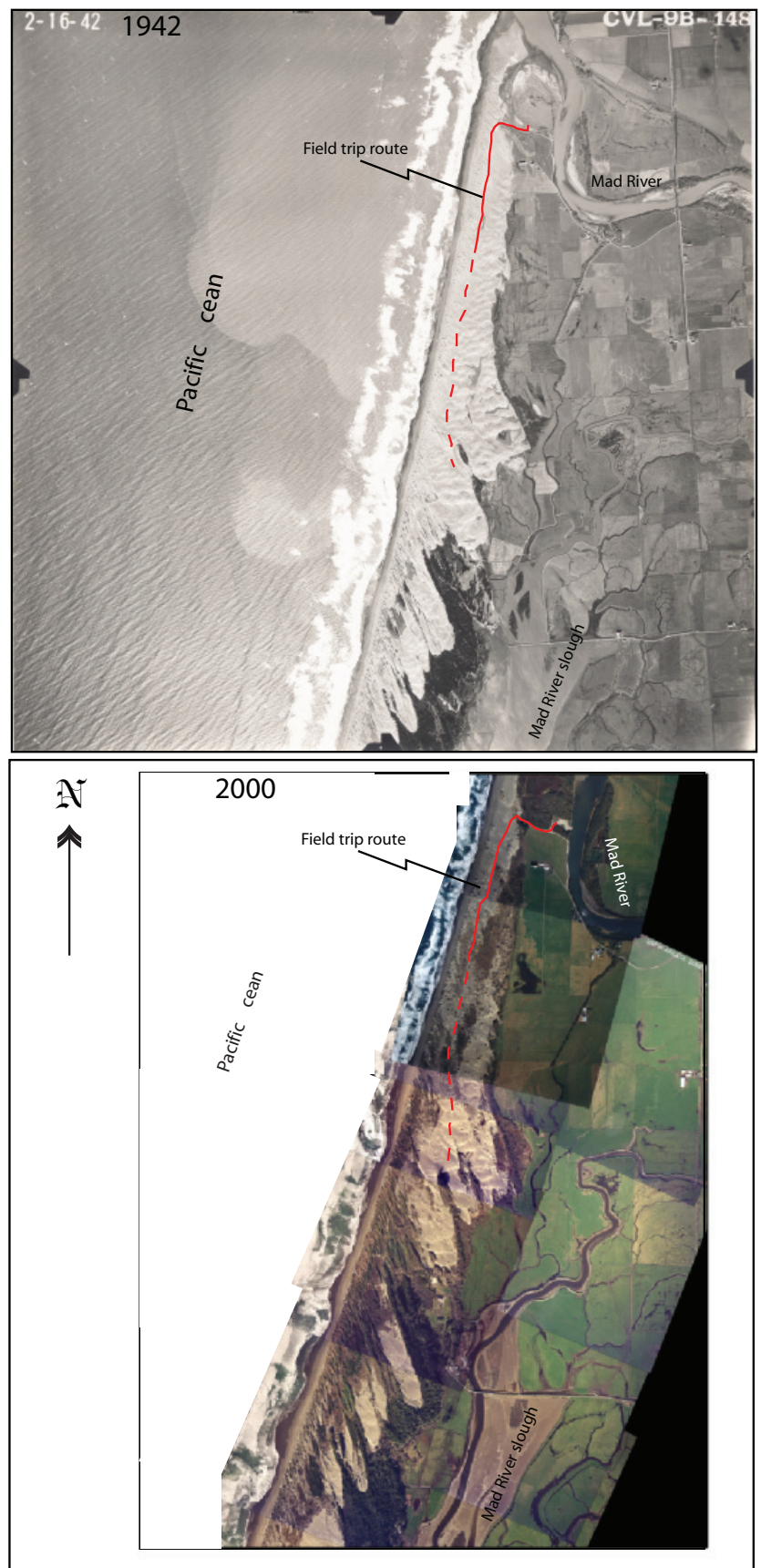


Figure 2. Aerial images from the same section of the North Spit, 1942 (above) and 2000 (below). Among other things, the images show the dune advancement and vegetation development on the northern North Spit.

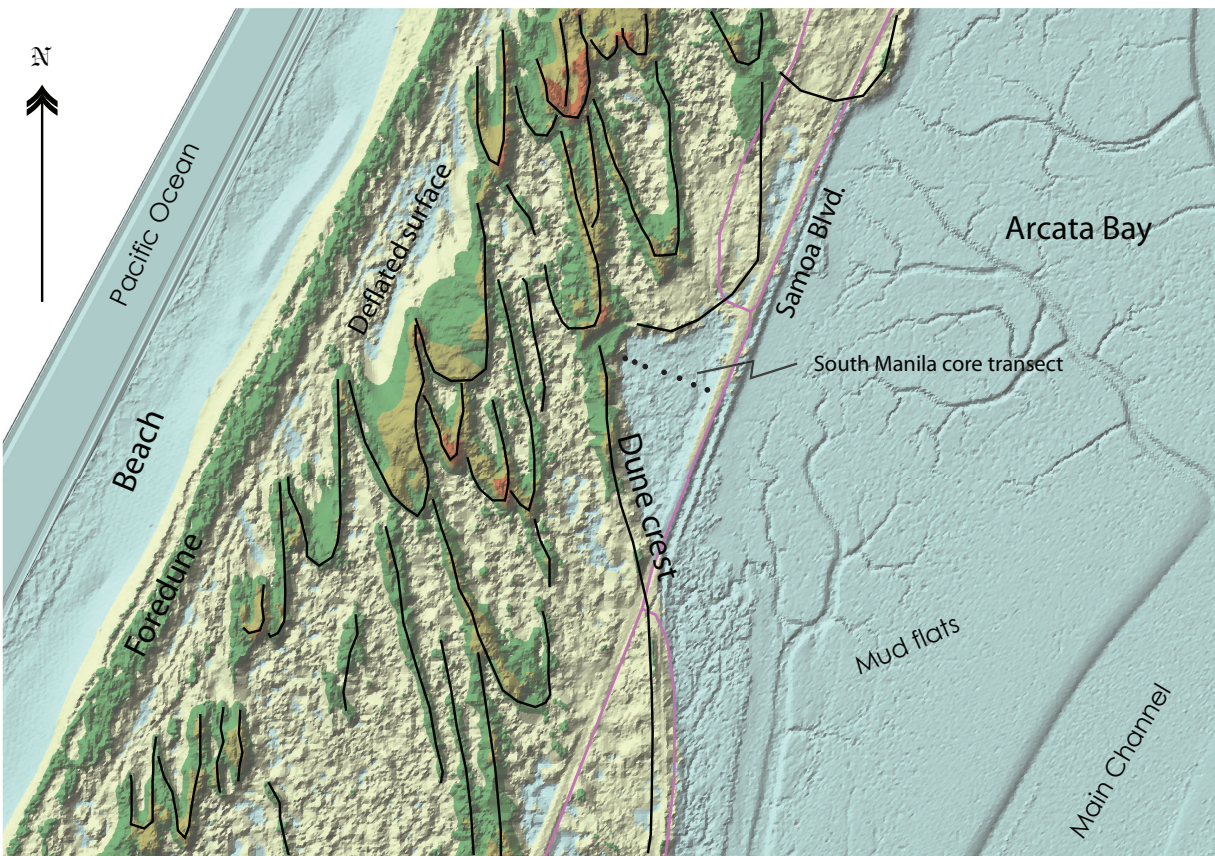
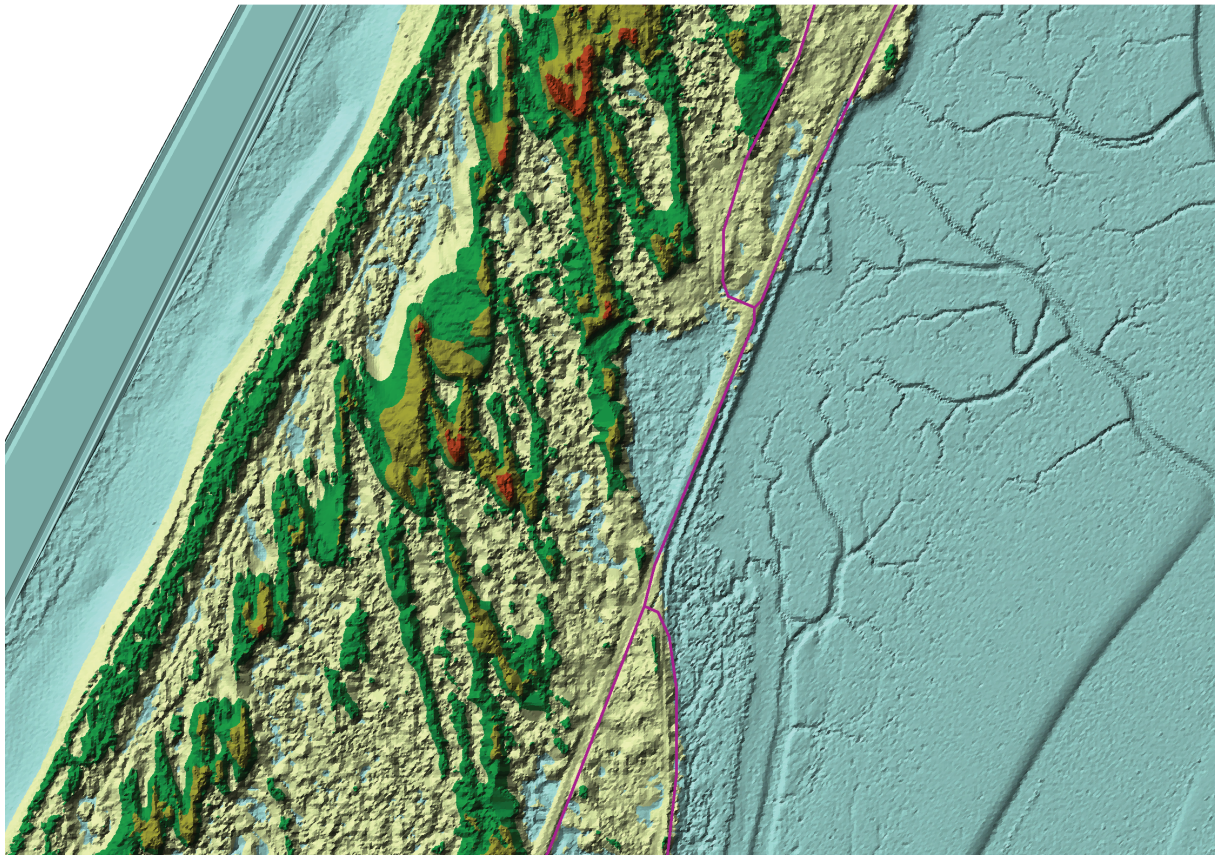


Figure 3. LiDAR imagery of a portion of the North Spit (Upper). With labels and geomorphic interpretation, (lower) of a portion of the North Spit dune field. This high quality image shows the classic coastal dune features, it also elucidates the complexity of the successive dune pulses.

The Stable dunes

The stable portion of the North Spit dune field resides along the eastern central portion of the spit where it interfingers with marsh and estuarine deposits to the east and younger dunes to the west (Fig. 1). The stable portion of the dune field likely represents thousands of years of dune accumulation. Figure 3 shows the stabilized portion of the dune field is composed of successive parabolic dune pulses, each one stacking up against a previous dune pulse from east to west. At this time there is no reliable numerical data to speculate on the time span between the successive pulses, although luminescence dating techniques may offer some resolution.

The forested and stabilized dunes currently extend from Samoa to just south of Tyee City (Fig. 1), but they likely had a greater extent. They are currently eroded on all sides and represent a fragment of a much more extensive dune field as is evidenced by the previously stable dune fragments that litter their less stable margins.

The eastern and western margins of the stable dune sequence are abnormally abrupt in some locations suggesting previous erosion from interaction with the estuary to the east and from the coast to the west. In many places on the western margin of the stable dunes, the tails of the youngest once stable parabolic dunes appear to be trimmed off in a shore parallel direction (Fig. 1). On the eastern margin there is evidence suggesting the oldest dunes have been co-seismically submerged and subsequently had wetland soils develop on them (Leroy & Patton unpublished data).

The Active Dunes

The active dune advancement occupies the western portion of the North Spit and is currently advancing eastward over the older dunes. It is primarily advancing into the topographically low sections of the older dunes, but in areas of higher sand supply, or easier advancement, it has formed large dune sheets that cover vast tracts of land (Fig. 1 & 2). In intermittent locations the active dunes have advanced over the entire existing dune field and are currently advancing into the tidal marshes of the Mad River Slough to the east (Fig. 2).

These active dunes are composed almost entirely of transverse sand dunes (Fig. 2). Transverse dunes consist of a mass of highly mobile sand that is moving over the body of the larger sand mass. The long, sinuous, transverse sand dunes are oriented with ridge crests roughly perpendicular to the NW summer winds. Primarily because of their high rates of movement, these dunes are rarely vegetated except on their margins.

The foredunes and deflated surface area to the east of the active dunes is the source area of the sand for those dunes, but because non-native vegetation has colonized the foredune, sand replenishment from the coast has been significantly reduced. This is causing the active dunes to behave like a “slug” of sediment in some areas, moving over the existing dune field with minimal replenishment of sand from the beach. Along the way it is incorporating sand from previously stable dunes, rather like cannibalizing its older brethren in the process of forward movement.

At the eastern margin of the currently advancing dunes a battle is waging between the forest and the sea. Here the active dunes are burying a coniferous forest on the stable dunes. The forest consists mostly of spruce trees but other coastal conifer species are present. On the western margin of the advancing dunes, where the dunes are cannibalizing their brethren because they're starving, and the dune sheet thins, the skeletal remains of previously consumed forests litter the landscape.

The erosional dunes

The most obvious areas of massive dune instability and erosion on the North Spit, are the areas directly north and south of the stabilized and forested dune areas (This would be the areas south of the Mad River beach parking lot where the field trip will stop and from the town of Samoa south) (Fig. 1). The erosional dunes are ones which had reached a degree of stability, and subsequently, for one reason or another, have become unstable and are in the process of erosion.

The margins of the currently stable dunes are the easiest place to observe these destabilized and eroding dunes, but careful observation will show that the stable dune field was considerably more extensive and that there are remnants of it thousands of feet from the currently forested and stable sections. These areas are composed of previously stable dunes that are now in various states of morphologic alteration. As the dunes destabilize they become more susceptible to active dune encroachment and are either buried, partially eroded and incorporated into the active dune advancement, or both.

The erosional dunes all lack their original morphology. Their degree of morphologic alteration spans the entire spectrum. These previously stable dunes, typically consist of the partially eroded lateral edges of parabolic dunes. All of the erosional dunes have one thing in common, although they may be actively incorporating into the active dunes, they are no longer moving as individual sand dunes.

Coarse grained deposits

There are coarse grained gravel deposits found discontinuously along the western margin of the stable dunes between Manila and Tyee City (Fig. 1). They are usually found as lag deposits on the deflated surfaces but they are occasionally found residing directly on top of dune deposits. Preliminary measurements suggest some of these gravels are up to 38' above sea level (Carver pers. Comm.), 100's of feet from the active coastline (the vertical estimations need to be verified with high precision surveying equipment tied to a NAVD benchmark). In some locations, stratigraphic evidence suggests this gravel was emplaced on the western margin of the stable parabolic dunes and that it predates the currently active transverse dunes.

The gravel has unique characteristics which may provide evidence of its origin. Much of the larger sized gravel is similar in physical characteristics to gravel currently found on the active beach. Much of the smaller sized gravel has characteristics similar to upper beach strand swash deposits observable near the current mouth of the Mad River. The gravel is abundant in all size ranges up to about 5 cm but rocks as big as 50 cm are not uncommon. It is smooth and almost exclusively blade and disk shaped although there are traces of rounded rocks. In many places the larger gravel is burned. Finally, although the overall density and distribution of the gravel is difficult to ascertain due to the extensive vegetation and active dunes, extensive field mapping suggests the density of the coarse grained deposits diminishes inland.

Age Control

The Stabilized Dunes

As mentioned above the stable dunes are comprised of what appears to be a complex sequence of successive sand pulses, piled against each other. Currently there are no reliable criteria to distinguish the successive dune pulses from one another in the field. Subdividing the stable dunes into distinct units is difficult over their entire range because of local variations in the dune stratigraphy, patchy topographic data, and virtually impenetrable vegetative cover.

Currently there are no reliable numerical dates that constrain the age of the stable dunes on the North Spit.

Although there are no numerical dates, there are lines of reasoning suggesting the dunes are Holocene in age.

- 1) Personal observations suggest most Pleistocene geomorphic features in coastal Oregon and locally here in Humboldt County, including marine terraces and sand dunes, have a wind blown silt cap deposited on them. This silt cap is absent on the dunes on the North Spit, possibly suggesting they formed after the silt accumulated.
- 2) Soil development on the dunes is minimal (essentially just a Cox), dunes of known Pleistocene age in Coastal Oregon, and locally, have more advanced soil development.

Dating the active dune advancement

Precision carbon 14 dating techniques and advanced data analysis were used to better constrain the age of the active dune sequence on the North Spit. Two Tree ring samples were taken from a tree that I believe was killed by advancement of the currently active dune migration. The stump was rooted in the tailing end of a partially eroded parabolic dune on the western margin of the stable dunes (Fig. 1). The tree had been buried and later exhumed by advancement of a transverse dune sheet mobilizing as a “slug” of sediment. Tree ring analysis showed rapid ring growth until 10, give or take a few unknown number of years before its death, in which time the tree rings showed highly diminished growth. I interpret this diminished growth to slow burial and eventual killing by dune advancement.

Two samples were taken from the tree for atomic mass spectrometry (AMS) analysis. Distinct tree ring samples from both the inner portion and outer portion of the tree were sampled with a counted 70 growth years between them. Sample # NSTR 70 was the best preserved ring near the center of the tree, and sample # NSTR 1 was one of the last rings to show rapid growth before the vitality of the tree declined. The results were calibrated using the program Oxcal (Bronk Ramsey, 1995, 2001) with a lab multiplier of 1.0 (Fig. 4).

Knowing the exact number of years between two carbon samples can, in this case, help better constrain the age of tree death. Figure 5 shows that at the 94.5% confidence interval there are four viable age ranges for carbon sample NSTR 70 and 2 for sample NSTR 1. When the sample age ranges from sample NSTR 70 are shifted 70 years forward in time (remember this is the known number of years between the ring samples) then the age ranges for the sample should represent the year the tree was first inundated by sand from the advancing active dune sequence (Fig. 5). The darkest areas, in the center timeline, on the lower portion of figure 5 show the age ranges in calendar years that are compatible with both carbon samples from NSTR 1 projected from below and NSTR 70 projected from above.

The results of this are that there are three distinct time ranges that could represent the calendar year the tree was initially inundated by advancing sand dunes. These are represented by the darkest boxes in figure 5. The age ranges are 1725-1790, 1805-1885, and 1915-1960. Of these three age ranges the most likely candidate is 1725-1790. The two younger age ranges are either close to or post European settlement of the area and have been discounted as likely candidates.

DISCUSSION

Overall understanding of the coastal sand dunes on the North Spit is continuously evolving. Current observations suggest eustatic sea-level rise and local and regional tectonic processes may both play a part in the long and short term development of the coastal dune environment in the Humboldt Bay region.

Over the long term, the dunes appear to be part of a transgression where the dunes are advancing over and into the existing estuary environment, possibly driven by Holocene sea level rise. Evidence from air photo interpretation suggests the dunes stack up, until larger advancements “punch through or over” the existing dune field and advance into the estuary. This leaves a corridor for future dune advancements to penetrate deeper into the pre-existing dune field where the process of dune stacking starts over again. The sum of this process repeating itself in intermittent sections of the dune field, over time, constitutes the transgression.

On the shorter term, the dunes on the North Spit appear to interfinger with estuarine sediments that archive evidence for co-seismic subsidence. The South Manila core transect (Leroy and Patton 2005 unpublished)(Fig. 3) shows a submerged wetland soil lapping up onto the remnant of a lateral edge of a parabolic dune. The soil indicates the dune had been rapidly submerged since its original stabilization. Further investigations of the western margin of the stable dunes may elucidate a unique interaction between the dunes and the estuary during co-seismic subsidence events in the Arcata Bay-Mad River slough area.

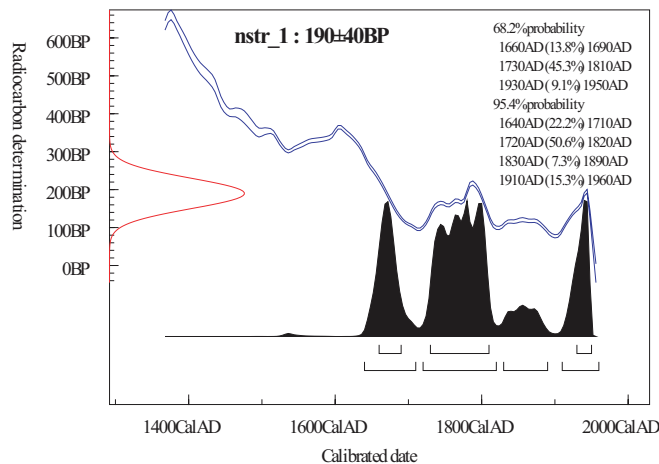
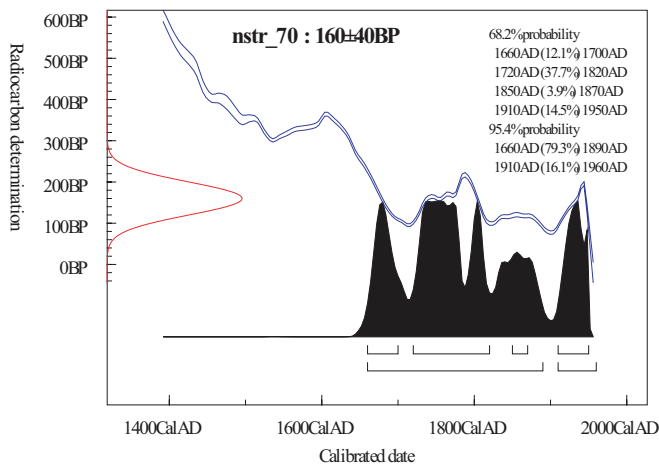


Figure 4. Probability density function of calibrated C-14 results for samples NSTR 1 and NSTR 70. Samples are from a tree rooted on the western edge of the stable parabolic dune sequence that was traversed by the actively advancing transverse dune sequence. Atmospheric data from Stuiver et al. (1998); OxCal v3.9 Bronk Ramsey (2003)

distribution of the observable gravel suggests a laterally continuous means of deposition, not an amassing of individual storm wave deposits.

Paleo-shoreline deposits

Abandoned shoreline deposits are a very appealing deposition mechanism for much of the observable gravel deposits. The sorting, compaction and particle size of the inland gravel, particularly in the deflated surfaces, is consistent with current upper beach strand deposits exposed where the Mad River has cut through the historic dune field and shoreline to the north.

Most of the gravel deposits observed for roughly 2500 feet south of the Mad River beach parking lot, may be explained as older shoreline deposits related to a previous configuration of the mouth of the Mad River.

North of the Mad River beach parking lot, the Mad River is running parallel to the beach, where it becomes the eastern margin of the active beach/dune field (Fig. 1 & 2). Historically, the Mad River has slowly migrated north then snapped back south repeatedly along this portion of the coastline. As the mouth of the river migrates north through a particular area, in its “wake”, it leaves a trail of distinctive stratigraphy which is soon covered by dune

Gravel Deposits

There are many alternative deposition mechanisms for the gravel deposits found in the north-central North Spit, and it is likely that more than one deposition mechanism is responsible for the observable deposits.

The most likely deposition mechanisms are:

- 1) Historic storm wash-over deposits,
- 2) paleo-shoreline deposits,
- 3) Tsunami deposits,
- 4) Anthropogenic deposits.

Historic Storm wave deposits

Storm waves do get impressively large in north coastal California and cannot be discounted as a potential mechanism for the gravel deposition. Historically storm waves have washed into or over both the North and South spits; usually in the topographically low areas, but occasionally, into the dune field itself. In most instances, the foredune on the North Spit provides the dune field significant protection from storm waves.

Although historic storm waves are a viable deposition mechanism, there are abundant lines of reasoning to suggest they may not be responsible for the observable gravel deposits. 1) There is often gravel at the historic wash-over sites, but the maximum particle size at these locations is typically smaller than is found in the inland gravel deposits. 2) Many of the inland gravel deposits are observed considerably further east into the dune field than any demonstrable historic storm deposit. 3) The beach-parallel

sands. This distinctive stratigraphy is often observable at the current northerly migrating mouth, where to the north, older beach and dune deposits are being eroded, and to the south, new stratigraphy is being created. This stratigraphy usually consists of a basal layer of inter-bedded sands and gravel, capped by dune deposits. The thickness of the dune deposits is partially related to the length of time since the river mouth passed.

Much of the observable inland gravel has similar characteristics as the current shoreline deposits at the mouth of the Mad River. Abandoned oxbows on the eastern margin of the dune field, south of the current course of the Mad River, suggest the river has run parallel to there also (Fig. 2). If this is the case then it is possible older beach stratigraphy is being exposed in the dune field, particularly in the deflated surfaces.

Although some of the gravel can be explained with the above scenario, it has trouble explaining other gravel deposits, particularly the gravel that seems to be at higher elevations and the gravel deposited with considerably older dunes and the Mad River Slough to the east (Fig. 1).

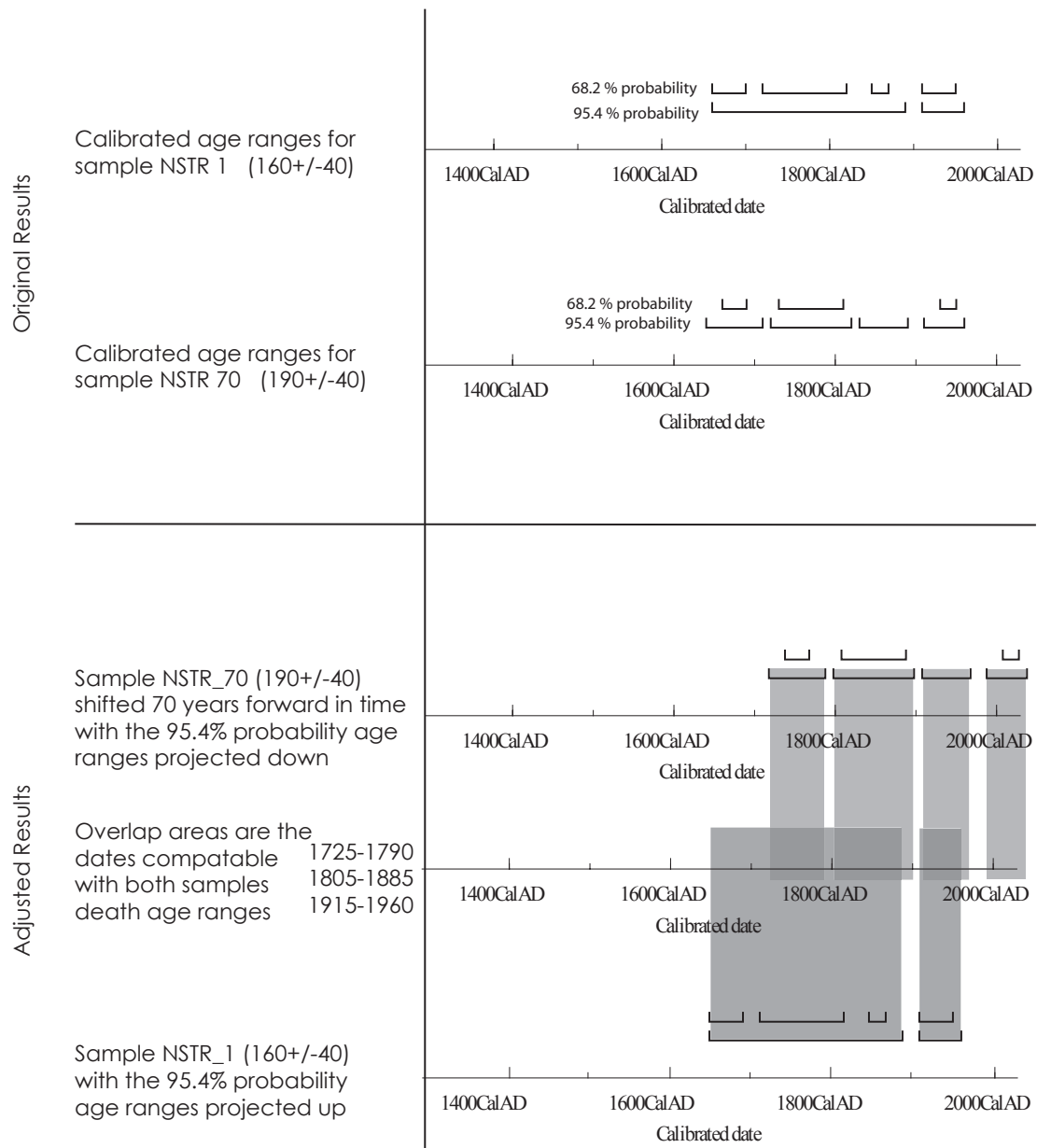


Figure 5. By using multiple 14C dates with known ages between them, one can better constrain the age of a trees death. The upper portion displays the original lab results from figure 4. The lower portion displays the results after sample NSTR_70 is shifted forward in time to reflect the onset of death age of the tree. The center lower time line shows the tree death age ranges compatible with both dated tree rings (the dark areas).

The smoothly curving, roughly shoreline parallel nature of the identifiable gravel deposits could suggest they are related to an abandoned shoreline that developed west of the oldest dunes but east of the current shoreline. The observable gravel deposits also line up well with the truncated western edge of the stable dune field (Fig. 1). The truncated nature of the western edge of the stable dune field could be interpreted as the wave-cut back edge of a beach. The sequence of gravel and truncated dunes could be interpreted as a beach and wave-cut back edge beach front. The older forested dunes to the east of these areas preclude the active beach wash-over mechanism for gravel deposition, but other scenarios could be consistent with these observations.

Two other possible scenarios for shoreline development, gravel deposition, and subsequent abandonment on the northern North Spit include:

- 1) Inter-seismic strain accumulation on the southern Cascadia subduction zone is causing regional uplift and shoreline recession in the Humboldt Bay region
- 2) The deposit archives a short lived coastal inundation related to co-seismic subsidence in the Humboldt Bay region.

Both of the above stated mechanisms have appeal, the first is simple in concept; inter-seismic strain accumulation from the Cascadia subduction zone is “flexing” the edge of North America and the North Spit is in a region of uplift. This is roughly consistent with predicted 3-D dislocation models of the southern Cascadia subduction zone proposed by (Fluck et. al 1997). Furthermore, because there is well demonstrated regional co-seismic subsidence in the Humboldt Bay region, inter-seismic uplift would be consistent with a typical seismic cycle of strain accumulation and release on a subduction zone.

An alternative mechanism; the deposit archives a short lived coastal inundation, related to co-seismic subsidence in the Humboldt Bay region, is slightly more elaborate but not out of the realm of possibilities.

Directly to the east of the observable gravel deposits is the Mad River Slough (MRS). The MRS archives 2000 years of net co-seismic submergence as evidenced by 4 buried wetland soil sequences (Vick 1988, Clark and Carver 1992, Pritchard 2004). The exact amount of co-seismic subsidence associated with these events is not well constrained.

If a portion of the coastline in the North Spit region subsided it would allow waves to attack deeper into the dune field. This might establish a short lived, dune incising, beach front in the subsided area. This rapidly forming shoreline would be an inflection in the normally smoothly curving, littoral influenced, coastline configuration between Trinidad and Table Bluff. Because the subsided area is out of equilibrium with the stable geometry of the regional shoreline, eventually it would reestablish its smoothly curving configuration by infilling with sand and abandoning the impinging beach front.

Although paleo-shoreline deposits as the source of the gravel deposits has allure, it can't explain gravel residing directly on sand dunes. Two mechanisms for placing gravel on sand dunes are proposed: Tsunami, and Anthropogenic

Tsunami deposit

Evidence for Tsunami inundating or over topping the North Spit dune field is mounting, but is not equivocal. Many localities in the Humboldt Bay region archive tsunami (Carver et al. 1998, Patton 2004). Most of these documented sites consist of clay and silt estuarine or marsh stratigraphy, punctuated by sand layers. The South Bay of Humboldt Bay, in both the south-east and south-west margins, archives multiple tsunami deposits within the last 3000 years (Patton 2004, Carver et al.1998). Particularly in the south-western margin of the bay, it is likely that tsunami inundation over-topped the south spit. Arcata Bay, although thoroughly cored, exhibits no identifiable tsunami deposits. It is likely the oldest dunes on the North spit acted as a sufficient barricade to tsunami overtopping.

In some locations, gravel residing directly on top of sand dune deposits is hard to explain by any mechanism other than tsunamis. This is particularly true for the location marked by the fifth star from the north on Figure 1. This locality is well east of both the linear trending gravel exposures and stratigraphically older dune deposits, and it appears to be lapped onto a sand dune. The only other likely mechanism of gravel deposition here would be anthropogenic, but this is unlikely because much of the observable gravel is too small to be of use to Native Americans.

Archeology deposits

The sheer abundance and size distribution of the gravel suggests Native Americans did not import it to the North Spit, although they most certainly took full advantage of the gravel that was there (especially the larger rocks). These were often used for cooking and were heated in fires as part of the process; this may explain many of the burned rocks, particularly when only the biggest rocks in a particular vicinity are observed to be burned.

Characteristics of the gravel at individual locations, suggest different depositional mechanisms are responsible for the gravel at different localities. North of the northern most forested dunes most of the gravel can best be explained by historic river mouth migration and upper beach strand washover deposits. South of the northern most forested dune, the gravel may better be explained by a paleo-shoreline related to vertical movements in the earth's crust. The inland-most gravel deposited on sand dunes may be tsunamigenic in origin.

It is possible that coseismic subsidence and subsequent tsunami from the 1700 Cascadia subduction zone event, damaged an existing coastline, and initiated the currently active dune advancement by destabilizing the western margin of the North Spit. Age control on the initiation of the currently advancing dunes is roughly coincident with the 1700 Cascadia Subduction zone event. The 1700 earthquake and tsunami event has been identified in many locations locally, and may have overtopped the south spit (Carver et al. 1998, Patton 2004). If the south spit was over-topped it would put the rough minimum elevation of the wave at over 20'. This is consistent with, if not lower than, current tsunami inundation models (Bernard et al. 1994)

There may be further evidence, in the dune geomorphology of the margins of the stable dunes, to support the conclusion the north spit has been inundated by tsunamis. Particularly the western and southern edges of the dune field are worthy of continued investigation.

CONCLUSIONS

The northern North Spit of Humboldt Bay is primarily composed of Holocene sand dunes in various states of stability. The stabilized portion of the dune field is composed of successive parabolic dune pulses, each one stacking up against a previous dune pulse from east to west. The active sand dunes are transverse type dunes and are currently advancing east, often as discrete "slugs" of sand. Previously stable sand dunes are currently being eroded and incorporated into the active dune sequence.

The invasion of non-native flora has stabilized the foredune, inhibiting sand replenishment to the active dunes, and allowing the deflated surfaces to increase in extent.

The dune field as a whole appears to be part of a transgression where active dunes are advancing over and into the existing estuary environment, possibly driven by Holocene sea level rise. Air photo interpretation suggests the dunes stack up, until larger advancements "punch through or over" the existing dune field and advance into the estuary. This leaves a corridor for future dune advancements to penetrate deeper into the pre-existing dune field where the process of dune stacking starts over again. The sum of this process repeating itself in intermittent sections of the dune field, over time, constitutes a transgression.

Radiocarbon age control from a coastal forest buried by the youngest dune sequence defines three age ranges compatible with dune movement through the forest. The age ranges are 1725-1790, 1805-1885, and 1915-1960. Of these three age ranges the most likely candidate is 1725-1790. The two younger age ranges are either close to or post European settlement of the area and have been discounted as likely candidates.

There are coarse grained gravel deposits found discontinuously along the western margin of the stable dunes. Multiple alternative deposition mechanisms for the gravel deposits are proposed for the north-central North Spit, and it is likely that all of the deposition mechanisms are responsible for the observable deposits. From the northern most forested dunes north, most of the gravel can best be explained by historic river mouth migration. South of the northern most forested dune, the gravel may better be explained by a paleo-shoreline related to vertical movements in the earth's crust. The inland-most gravel deposited on sand dunes may be tsunamigenic in origin.

The combined evidence from local paleoseismic and paleotsunami investigations, dune morphology and distribution, gravel deposition mechanisms, and age control, may suggest the North Spit was subjected to regional subsidence and tsunami inundation associated with the 1700 AD Cascadia Subduction Zone earthquake. The associated destabilization of the western margin of the spit could have initiated the current dune advancement.

Further research is needed to work out the development of the North Spit and to test some of the above conjecture. Future research projects include high precision GPS mapping of the gravel deposits to constrain the elevation of the deposits, continued investigation of the eastern margin of the dunes where they inter-stratify with the estuary environment, and hopefully a thermoluminescence campaign to establish better age control on the stable dunes. This research could not have been conducted if it were not for hours of discussion and field recognizance with Gary Carver, and generous funding from Pacific Gas & Electric Company.

REFERENCES CITED

- Bernard, E., Mader, C., Curtis, G., Satake, K., 1994. Tsunami inundation model study of Eureka and Crescent City, California. NOAA Technical memorandum ERL PMEL-103.
- Bronk Ramsey C., 1995, Radiocarbon calibration and analysis of stratigraphy: The OxCal Program, Radiocarbon, vol. 37: 425-430
- Bronk Ramsey C., 2001, Development of the radiocarbon program OxCal, Radiocarbon, vol. 43: 355-363
- Carver, G.A., Abramson, H.A., Garrison-Laney, C.E., and Leroy, T.H., 1998, Paleotsunami evidence of subduction earthquakes for northern California: Final report for Pacific Gas and Electric Co., 164p., plus appendices.
- Clark, S.H., and Carver, G.A., 1992, Late Holocene tectonics and Paleoseismicity, southern Cascadia subduction zone, Science, vol. 255: 188-192.
- Fluck, P., Hyndman, R.D., Wang, K., 1997. Three dimension dislocation model for great earthquakes of the Cascadia subduction zone, Journal of geophysical research, vol. 102: 20539-20550
- Patton, J.R., 2004, Late Holocene Coseismic subsidence and coincident tsunamis, southern Cascadia subduction zone, Hookton Slough, WIGI (Humboldt Bay), California.
- Pritchard, C.J., 2004 Late Holocene relative sea level changes, Arcata Bay, California: Evaluation of Freshwater syncline movement using coseismically buried soil horizons: M.S. thesis, Arcata California, Humboldt State University, 64p.
- Stuiver, M., and Reimer, P.J., 1986, A computer program for radiocarbon age calibration, Radiocarbon, vol. 28: 1022-1030
- Vick, G., 1988, Late Holocene Paleoseismicity and relative vertical crustal movements, Mad River Slough, Humboldt Bay, California: M.S. thesis, Arcata California, Humboldt State University, 88p.

Day 4 Introduction (Sunday)

So you made it to Day 4, the last official day of FOP 2006!

Shake the cobwebs out and **meet at 8:45 AM** to discuss access at Stop 4-1, and **leave Pamplin Grove at 9:00 A.M.**

PLEASE CLEAN UP YOUR CAMP SPACE!

THERE ARE TRASH AND RECYCLING BINS AVAILABLE NEAR THE MAIN FIRE PIT.

Day 4 - Logistical Considerations: Today's goal is to finish the 2006 FOP in Crescent City, located about 100 miles north of Pamplin Grove.

We will be parking in a residential area this morning at **Stop 4-1**, please do not block driveways or any other obvious access corridors. **Respect open space near Bugenig Rd. by not parking in anyone's front yard and staying on the pavement.** We will also be crossing School Rd. by foot, please walk on the south side of School Road toward the west to the open gate on the north side of School Rd. **Use extreme caution when crossing School Rd. on foot.**

Stop 4-2 at Lagoon Creek has a public parking area on the west of 101 North, **use extreme caution entering and exiting this parking lot to merge on to 101.**

Science of the day: Day 4 will focus on the earthquake history of the Mad River thrust fault; tsunami deposition in the Lagoon Creek estuary; depositional setting of the Pliocene Wimer formation; and paleo-tsunami deposition, historic tsunami damage, and present tsunami risks near Crescent City.

We will make 3 stops today:

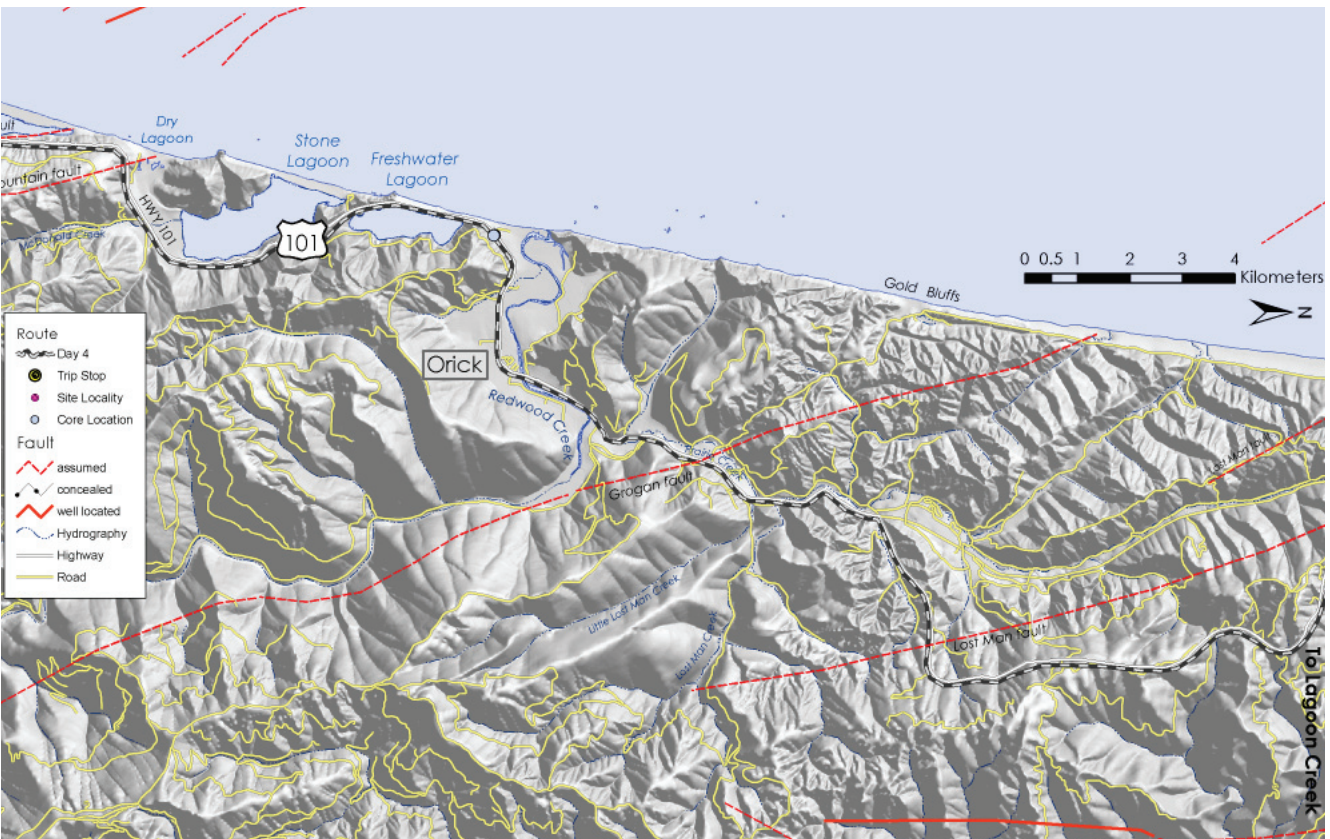
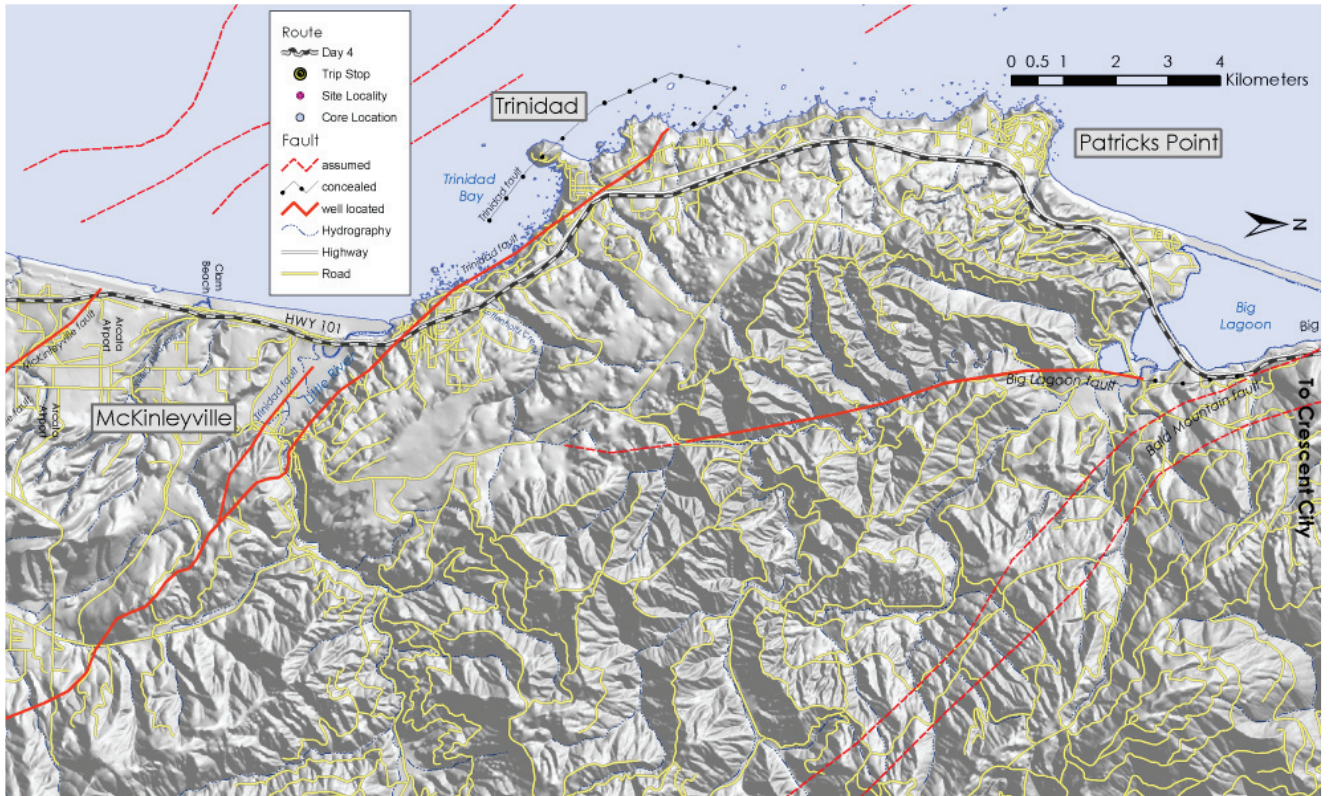
Stop 4-1, located on School Road in McKinleyville, will present the earthquake history of the Mad River thrust fault based on geomorphic and paleoseismic studies.

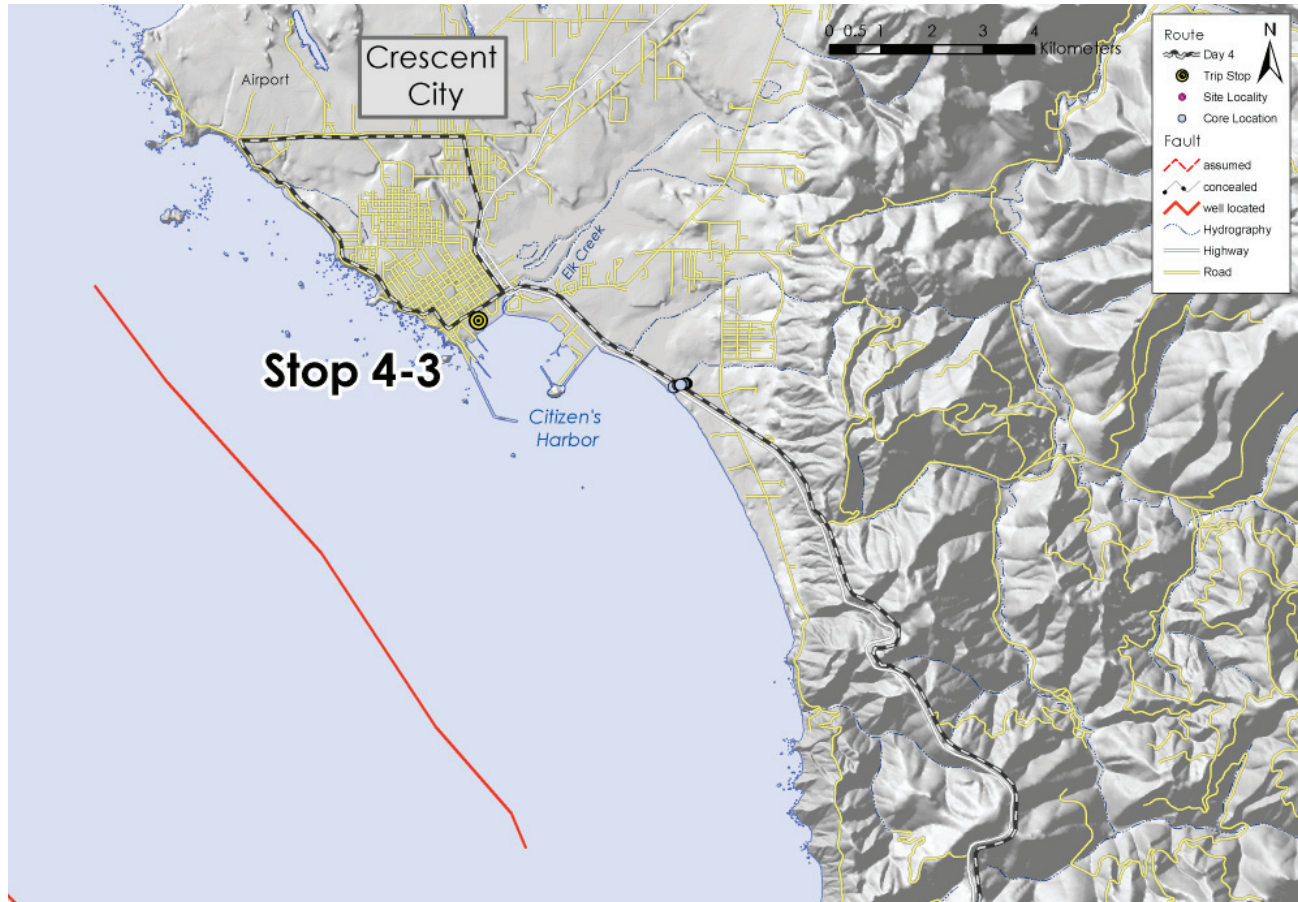
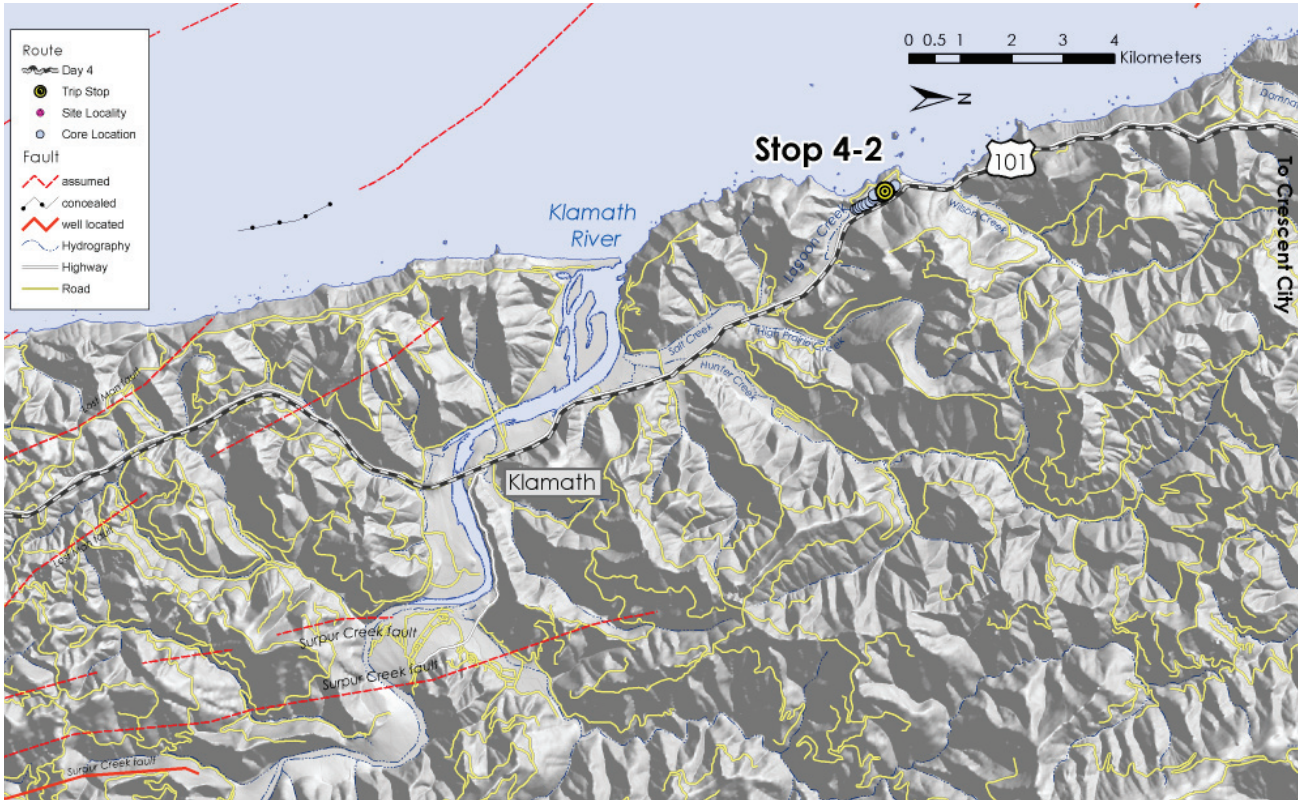
Stop 4-2, located at Lagoon Creek, will examine the 3000 yr. tsunami deposition history preserved there, and we'll discuss the remnant Neogene peneplain surface preserved in the coastal regions of the Klamath Mts.

Stop 4-3 will visit Tsunami Park in Crescent City. Here we will discuss past tsunami deposition, historic tsunami damage, and present tsunami risk in and around Crescent City.

Day 4 Itinerary

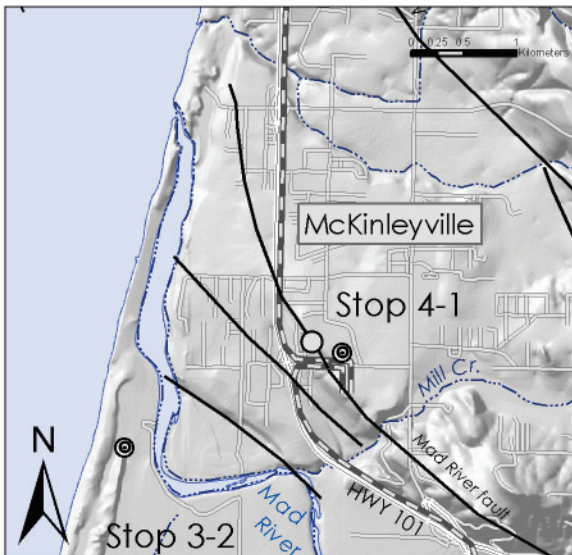
Day 4 (Sunday) North Humboldt Bay Area to Crescent City			
Field Trip Stop	Authors	Title	Reading Material
Stop 4-1: School Road McKinleyville: Mad River fault zone	Gary Simpson and Michelle Roberts	Morphology and structure of the Mad River fault from trench exposures at School Road, McKinleyville, CA	paper 4-1-A
Stop 4-2: Lagoon Creek: paleotsunami deposits	Carolyn Garrison-Laney, Hans Abramson, and Gary Carver	A 3,000 year record of tsunami deposition from the southern end of the Cascadia subduction zone	paper 4-2-A
	Caroline Lavenda	Depositional environments and characteristics of the late Miocene Wimer formation, Mill Creek drainage, Crescent City, Del Norte County, California	paper 4-2-B
Stop 4-3: Tsunami Park, Crescent City: 1964 tsunami	Lori Dengler and Orville Magoon	Reassessing Crescent City, California's tsunami risk	paper 4-3-A
	Bob McPherson and Hans Abrahamson	1964 tsunami deposits in the Crescent City area	
	Ken Aalto, Carolyn Garrison-Laney, and Dane Robinson	Evidence for paleotsunami at Crescent City, northern California	paper 4-3-B





Day 4 Road Log

<u>Mileage</u>	<u>Distance</u>	<u>Description</u>
0.0		Pamplin Grove Gate - reset daily trip mileage
0.3	0.3	Turn Left onto Hwy 36. Please drive defensively on these rural roads, the locals drive very fast!
0.8	0.8	Martin & Shirley's Store
3.5	2.7	City of Carlotta - Continue west on Highway 36. Please drive slowly through town.
6.1	0.3	Yager Creek Bridge
8.2	2.0	BEAR LEFT and continue East on Hwy 36. DO NOT go right toward Rhonerville Road
10.9	2.8	Highway 36 ends. TURN RIGHT ONTO HWY 101 NORTH
31.2	20.3	Pierson's stoplight. Continue NORTH on 101 thru Eureka.
35.5	4.3	Follow 101 as it TURNS RIGHT from Broadway onto 5 St
36.5	1.0	Intersection with SR 255. CONTINUE STRAIGHT, on 101 North (5th St.)
46.5	10.0	Guintolli Exit - Continue North on 101
47.6	1.1	Crossing over the Mad River bridge. Continue North on 101 and DO NOT EXIT the freeway at Central Avenue
48.9	1.3	Climbing several splays of the Mad River fault. Gary Simpson will discuss Mad River fault trenches at our first stop this morning
49.1	0.2	Exit 101 at School Rd.
49.3	0.2	TURN RIGHT (east) at the stop sign.
49.4	0.1	Straight ahead is another splay of the Mad River fault zone, and the topic of discussion this morning. We will park up the road, and walk back to the field below the yellow houses on the upper terrace. You may remember this church as one of the stops from the '92 FOP (Carver & Burke trenches)
49.6	0.2	TURN RIGHT on Bugenig St. Park along the right side of the street, being careful not to block private driveways. Park on the pavement (i.e. don't park south of the last cross street on Bugenig) - if we run out of room along Bugenig, park along side streets or turn around and park along the south side of School Road. To access the field, walk along the south side of School Road and cross the road near the eastern edge of the terrace riser, so you can watch for oncoming traffic from both directions.



**Stop 4-1: School Road, McKinleyville.
Mad River fault zone**

Gary will talk about findings from trenches along this stretch of the Mad River fault zone.

[1000-1200]

ABSTRACT STOP 4-1

Morphology and Structure of the Mad River Fault From Trench Exposures at School Road, McKinleyville, CA

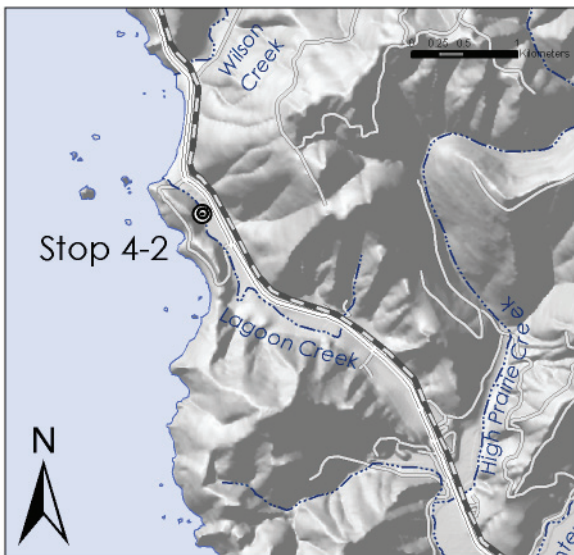
Gary D. Simpson and Michelle A. Roberts

To most Humboldt County geologists, the School Road scarp of the Mad River fault is something of a landmark. Perhaps it is the scarp’s appearance and location; the steep grassy slope offsets planar terraces along one of the main roads into the rapidly growing community of McKinleyville. There are two homes built directly on the crest of the scarp just north of School Road. Perhaps it’s the crazy trench log that came out of Carver and Burke’s initial research trench back in the mid 1980’s, with its over-turned terrace abrasion platform. We were here on the 1992 FOP trip because it’s the most vivid, accessible scarp in the area. Whatever the reason, development pressure on the otherwise prime building ground (flat marine terrace surface with ocean view) has resulted in a high density of fault rupture hazard investigations over the past 20 years. The close spacing of trenches allows a unique perspective of the fault structure and morphology of the Mad River fault at a relatively local scale. Further, because these studies occur at a fault terminus entering a broad step-over in the Mad River fault, they offer an interesting look at the mechanics of a significant, active thrust fault zone.

This paper presents a compilation of a series of trench exposures along an approximately 600 meter (2000 foot) long segment of the Mad River fault near School Road in McKinleyville, California (Figure 1). A minimum of 9 trenches have crossed the fault, and because the area is encompassed within an Alquist-Priolo Earthquake Fault Zone, extensive trenching has been completed on both foot wall and hanging wall blocks. Well-bedded marine terrace deposits throughout the area provide excellent stratigraphic control and generally allow definitive interpretation of fault location and character.

<u>Mileage</u>	<u>Distance</u>	<u>Description</u>
49.6		Return to cars and TURN LEFT on School Road
49.7	0.1	Leave Bugenig. Take left (west) towards 101 North.
49.9	0.2	Turn Right on to 101 Northbound
50.9	1.0	Murray Road Exit. If you need gas, you should get it here or in Trinidad.
51.9	1.0	Airport is on hanging wall of the McKinleyville fault. Scarp is visible just above hotel roof.
53.7	1.8	Clam beach and 105Ka marine terrace on right.
55.6	1.9	Little River

<u>Mileage</u>	<u>Distance</u>	<u>Description</u>
59.0	3.4	Crossing Trinidad thrust fault
66.5	7.5	Big Lagoon-Big Lagoon fault at base of Kane Ridge
71.8	5.3	Turn off to Dry Lagoon - BEWARE OF ELK
72.3	0.5	Stone Lagoon. Big, Stone, and Freshwater lagoons are located along a series of synclines associated with the fold and thrust belt.
75.3	3.0	Freshwater Lagoon
77.4	2.1	Entering Orick - Slow Down -
78.3	0.9	Redwood Creek
78.5	0.2	Largest building in Orick on left.
79.3	0.8	Bald Hills Rd on right
80.8	1.5	Fern Canyon/Gold Bluffs cutoff road
81.4	0.6	Lost Man Creek
82.9	1.5	Scenic Byway exit - STAY ON 101 NORTH
93.9	11.0	Del Norte County Line
96.7	2.8	Yurok Country
97.8	1.1	Klamath River bridge - the flat ridge tops to the east are remnants of the Klamath peneplain. Golden bears indicate that you're on the right track - we're almost there!
97.9	0.1	Fresh bridge repairs from 05/06 storm damage
99.1	1.2	Town of Klamath - Fuel, small store, café. This hamlet gets flooded periodically - '55, '64, '97, and 2006 all flooded the community.
100.1	1.0	At 9:00; Mouth of Klamath River off to the left (west)
102.7	2.6	Don's Gas and Woodland Villa Market
103.3	0.6	Trees of Mystery -- Paul Bunyan and Babe the Blue Ox
104.2	0.9	TURN LEFT into the Lagoon Creek Parking Lot.
104.2		Park in parking lot on west side of 101.



Welcome to the final scheduled stop of the 2006 FOP!

Stop 4-2: Lagoon Creek. Paleotsunami deposits, and late Miocene bedrock.

Hans will talk about late Holocene-to-recent tsunamis, Caroline will discuss bedrock mapping of the Wimer formation, and Ken and Dane will talk about older paleo-tsunamis near Crescent City.

[1400-1500]

ABSTRACTS STOP 4-2

A 3,000 Year Record of Tsunami Deposition from the Southern end of the Cascadia Subduction Zone

Garrison-Laney, Carolyn E., Abramson Ward, Hans F., and Carver, Gary A.

The stratigraphy of Lagoon Creek, a small freshwater pond on the coast of northern California, contains evidence of at least four and as many as six tsunamis from the Cascadia subduction zone over the last 3,500 years. We present evidence that plate boundary earthquakes generated tsunamis that inundated the southernmost portion of the CSZ at times synchronous with events documented along other parts of the subduction zone. These findings provide an important datapoint to the southernmost part of the CSZ, a heretofore undocumented area, that allows better characterization of CSZ rupture dynamics and recurrence intervals.

Six sand layers with characteristics typical of tsunami deposits interrupt the predominantly peaty and muddy stratigraphy of Lagoon Creek. Sand layer thinning and fining trends, sand layer structure, particle size, nature of contacts, presence of rip-up clasts, and biostratigraphy combine to make a compelling argument for tsunami deposition of sand layers. Two of the sand layers drape the toes of a landslide deposit derived from the adjacent hillside. In each case the sand layer contains angular rock fragments both above and as much as 200 m inland from the slide. We infer that the landslide and the tsunami resulted from the same earthquake.

We correlated sand layers using layer thickness and appearance, a volcanic ash layer, stratigraphic markers within the peat and mud, and radiocarbon ages of detrital twigs, spruce cones, and other woody debris within the tsunami deposits. Radiocarbon dates give the following two-sigma ranges of limiting maximum age for five of the inferred tsunamis: 1260-1290; 1360-1520; 1570-1690; 2470-2760; and 3210-3470 calibrated years before A.D. 1950 (cal yr B.P.). Four of these ranges fail to differ statistically from the timing of earthquakes and tsunamis from southern Washington and southern Oregon. The sixth and youngest of the tsunamis postdates peat dated 290-530 cal yr B.P. This tsunami probably resulted from the A.D. 1700 Cascadia earthquake.

Depositional Environments and Characteristics of the Late Miocene Wimer Formation, Mill Creek Drainage, Crescent City, Del Norte County, California

Caroline Levenda

The new state park acquisition in Mill Creek is located east of Highway 101 and is accessed through the gated Hamilton Road located just a couple miles south of Crescent City and north of the Mill Creek Campground. The park is currently under watershed and stream restoration and road decommissioning. This former timberland was extensively logged and is vegetated with large areas of second-growth redwoods. Two large streams, Mill Creek and Rock Creek are located in the new state park

acquisition. Mill Creek is tributary to the Smith River and has two main tributaries - the East Fork and West branch of Mill Creek. Rock Creek drains the east side of the new property and is a tributary to the South Fork Smith River. Wildlife, stream and forest ecology are being restored.

Franciscan complex basement rock, chiefly greywacke sandstone, and Quaternary fluvial terraces comprise the valley bottoms in the Mill Creek area (Aalto, 1984). Uplifted marine, estuarine, and fluvial sediments of the Late Miocene Wimer Formation have been discovered within the past 100 years to be associated with J.S. Diller's "Klamath Penepplain" and are situated on the ridgetops of the Coast Ranges including the Rattlesnake Mountains and the Little Bald Hills (Diller, 1902) (Figure 1). The Coast Range thrust fault trends northwestward and veers to the north as it approaches the Oregon border. Fractures, folds, and broken formations are associated with the thrust fault and the resistant Josephine ophiolite that constitutes the hanging wall of the fault accounts for the rugged terrain seen in the park.

The Wimer Formation has an estimated diatom age of Late Miocene (Stone, 1993). It consists of estuarine (brackish facies) sediments located approximately one to three kilometers inland of the Pacific Ocean coastline. The Wimer estuarine facies outcrops are uplifted, tilted, and highly fractured laminated sequences of mudstones and shales. Angular unconformities of uplifted Franciscan sandstones overlain by Wimer Formation sediments are visible along road cuts.

Further inland and at higher elevations, the fluvial facies of the Wimer Formation was discovered at elevations up to 800 meters (Stone, 1993). The fluvial facies is typical of braided stream deposits consisting of lenses and layers of sands and gravels. Large outcrops of the fluvial Wimer consist of massive pebble to boulder size conglomerates indicative of armored stream deposits (Figure 2). The deposits are highly weathered and most clast lithology is almost impossible to identify in the field. However, previous research has identified clasts originating from the Galice formation, Josephine Ophiolite, and others (Stone, 1993). Clasts have been identified as serpentinite, peridotite, volcanics, mafic igneous, latite, porcelanite, and grey, red and green cherts.

<u>Mileage</u>	<u>Distance</u>	<u>Description</u>
		For those of you who want more FOP stops . . .
104.2		Exit Lagoon Creek parking lot. Turn Left (north) onto 101 N.
104.4	0.2	Wilson Creek bridge
108.1	3.7	Old Growth Redwoods
112.3	4.2	Mill Creek Campground
114.4	2.1	Vista Point - Crescent City overlook on left. Note the crescent-shaped harbor of Crescent City. The configuration of the offshore channel had a drastic effect on the tsunami waves in 1964, amplifying the waves' effect as they came onshore.
115.4	1.0	Entering Crescent City coastal plain
116.2	0.8	Lagoons on either side of 101. Marsh stratigraphy records paleo-tsunamis. If FOPpers have the desire, we have the tools to pull a core from these marshes and examine the underlying stratigraphy (anyone feeling the urge to core like Sasquatch?)
116.7	0.5	Crescent Beach
117.3	0.6	Citizen's Dock on left -- Crescent City limits
117.6	0.3	Elk Valley Rd. -- Continue straight through light
118.0	0.4	Turn Left (west) on Front St. -- After 2 sharp 25mph turns
118.1	0.1	Continue straight through light -- cross 101 S and continue west
118.3	0.2	H St.
118.4	0.1	TURN LEFT into Tsunami Park



Optional Stop 4-3: Tsunami Park, Crescent City

Lori's paper 4-3-A reassesses Crescent City's tsunami risk, and Ken and Dane's paper 4-3-B is an interesting essay about tsunami-generated sinuous grooves.

[1530-1630]

ABSTRACTS STOP 4-3

Reassessing Crescent City, California's Tsunami Risk

L.A. Dengler and O.T. Magoon

Twenty-two tsunamis have been recorded in Crescent City, California since 1938, eight exceeded 0.5 m amplitude and two caused significant damage. In 1964 at least four large waves were observed and peak water height was 6.7 m above MLLW, inundating twenty-nine city blocks damaging or destroying 300 homes and businesses. Eyewitnesses described a relatively gentle inflow with water elevation increasing at the rate of about 0.3 meters/minute reaching a peak elevation of about 3 meters above the land surface followed by stronger outflow that scoured rills into the margins of the harbor. Where water exceeded 1 m, a common cause of damage was floating houses off foundations. Mapped structure displacements indicate the outgoing flow was strongest. Tide gage recordings of other Crescent City tsunamis exhibit characteristic long duration with peak amplitudes occurring many cycles into the trace suggesting a strong influence of harbor resonance on wave characteristics. Spectral analyses of two records of the 1960 Chilean tsunami show a dominant 32 minute period (Wiegel, 1965) and duration of more than 20 hours. At least 6 paleotsunami events have been documented in cores from the Crescent City area, all larger than the 1964 event and attributed to megathrust earthquakes on the Cascadia subduction zone (CSZ). In the 41 years since the tsunamis, Crescent City has established a siren-based tsunami warning system and developed tsunami evacuation maps, posted signs along evacuation routes and is the only city in California currently designated "Tsunami Ready" by the National Weather Service's TsunamiReady program. During the June 14, 2005 tsunami warning for a M 7.2 Gorda Basin earthquake, Crescent City was the only community in the warning area to effectively evacuate the majority of its coastal residents. Offsetting recent mitigation efforts is recent development within the 1964 inundation zone and recognition of the significantly greater tsunami hazards posed by the Cascadia subduction zone. The Crescent City experience in 1964 is one of the few examples of how tsunami waves interact with typical West Coast architecture and infrastructure and its mitigation efforts provide a model for other California coastal communities.

Evidence for Paleotsunami at Crescent City, Northern California

K. R. Aalto, C. E. Garrison-Laney, and D. T. Robinson

A paleosol developed on the Mesozoic Franciscan Complex is depositionally overlain by 48 m of late Miocene (diatom age ca. 6.0-6.4 Ma), mostly shallow-marine Saint George Formation. At the base of this sequence is a buried paleoforest of rooted tree stumps and fallen logs, found at three separate sites. Many of the largest logs preserved within basal Saint George Formation strata lie with their long dimensions oriented generally north-northwest to north-northeast. Above the rooted stumps is a sequence of wave-reworked colluvium containing woody debris interpreted as a tsunami deposit, succeeded by beach deposits, and bioturbated, mollusk-rich mudstone having occasional hummocky cross-stratified sandstone interbeds. Although fossils are consistent with deposition in either a bay environment or open marine conditions, the appearance of hummocky cross-stratified sandstone suggests that the deposition site was open to the ocean and permitted incursion of large storm and/or tsunami waves. Destruction of the forest appears to have been a single sudden event and may relate to rapid subsidence engendered by plate-boundary earthquakes or large-scale slumping.

Recent bedrock-sculpturing of semilithified St. George Formation sandy mudstone exposed on a wave-cut platform has produced a variety of erosional forms, including grooves, which may be straight or sinuous. Straight grooves form preferential incision of regional joints. Sinuous grooves are not fracture-controlled, are oriented parallel to wave run-up (orthogonal to the coast), and exist as closely-spaced subparallel, non-connecting, internally-drained grooves that are best developed on higher platform ramparts and benches. Sinuous grooves have a mean length of 258 cm, mean maximum width of 14 cm, mean width/length ratio of 0.08, mean groove edge-to-edge minimum spacing of 16 cm, and mean trough-to-trough spacing of 28 cm. They are not as deeply incised as straight grooves, do not serve as conduits for low-tide runoff during winter months, and typically terminate by shallowing and narrowing in both seaward and landward directions. Sinuous appearance results from trains of linked comma-shaped depressions, commonly with the blunt, highly curved end of each being most deeply incised and oriented seaward. Corrasion of bedrock highs and/or cavitation associated with turbulent vortices during tsunami run-up may have contributed to the genesis and/or enlargement of grooves. Auguring and coring in a back-barrier bog and diatom analysis reveals a landward-thinning, ~17 cm-thick, laterally continuous clean, tsunami-emplaced sand layer with a sharp basal contact up to 125 m inland of the modern high tide line. Based upon depth of burial, distance of sediment transport and overall thickness, the Pebble Beach tsunami sand is most likely coeval with a tsunami-emplaced sand yielding calibrated radiocarbon ages between 1,300 and 1,820 yr. BP. While seasonal cycles of beach aggradation and degradation combined with sediment transport and bedrock erosion accompanying low-tide runoff and high-tide wave motion undoubtedly accounts for form modification of sinuous grooves, it is unlikely to account for their origin.

Day 4 Papers

Morphology and Structure of the Mad River Fault From Trench Exposures at School Road, McKinleyville, CA

Gary D. Simpson and Michelle A. Roberts
SHN Consulting Engineers & Geologists, Inc., Eureka, CA

INTRODUCTION

To most Humboldt County geologists, the School Road scarp of the Mad River fault is something of a landmark. Perhaps it is the scarp's appearance and location; the steep grassy slope offsets planar terraces along one of the main roads into the rapidly growing community of McKinleyville. There are two homes built directly on the crest of the scarp just north of School Road. Perhaps it's the crazy trench log that came out of Carver and Burke's initial research trench back in the mid 1980's, with its over-turned terrace abrasion platform. We were here on the 1992 FOP trip because it's the most vivid, accessible scarp in the area. Whatever the reason, development pressure on the otherwise prime building ground (flat marine terrace surface with ocean view) has resulted in a high density of fault rupture hazard investigations over the past 20 years. The close spacing of trenches allows a unique perspective of the fault structure and morphology of the Mad River fault at a relatively local scale. Further, because these studies occur at a fault terminus entering a broad step-over in the Mad River fault, they offer an interesting look at the mechanics of a significant, active thrust fault zone.

This paper presents a compilation of a series of trench exposures along an approximately 600 meter (2000 foot) long segment of the Mad River fault near School Road in McKinleyville, California (Figure 1). A minimum of 9 trenches have crossed the fault, and because the area is encompassed within an Alquist-Priolo Earthquake Fault Zone, extensive trenching has been completed on both foot wall and hanging wall blocks. Well-bedded marine terrace deposits throughout the area provide excellent stratigraphic control and generally allow definitive interpretation of fault location and character.

GEOLOGIC SETTING

Basement rock in the region is composed of late Jurassic to late Cretaceous age *mélange* of the Franciscan Complex (McLaughlin et al., 2000; Clarke, 1992). The *mélange* is part of the central belt subunit of the Franciscan and typically consists of blocks of conglomerate, greywacke sandstone, radiolarian chert, blueschist facies metamorphic rock, greenschist, and ophiolitic plutonic rock in an intensely sheared argillite matrix. In the McKinleyville area, Franciscan basement rock is unconformably overlain by early to middle Pleistocene age marine and continental deposits of the Falor Formation (Carver, Stephens, and Young, 1985). A geologic map of the McKinleyville region is shown in Figure 2.

In coastal Humboldt County, Franciscan basement rock and Falor Formation deposits are overlain by a series of late Pleistocene age marine terraces. These terraces typically consist of an abrasion platform cut across bedrock, and terrace cover sediments typically consisting of near-shore marine deposits and alluvial, colluvial, and eolian deposits. No datable material has been recovered from the marine terraces, so age assignments have been based on elevation distributions and comparisons with global sea level chronologies, as well as comparisons of relative amounts of pedogenic soil development. Based on these analyses, the McKinleyville terrace sequence is correlated to the Sangamon interglacial period, between about 83,000 and 125,000 years ago. The offset terrace in the study area is correlated to the 83 ka Stage 5a sea level high stand by Carver and Burke (1992); the surface is referred to locally as the "McKinleyville terrace."

MAD RIVER FAULT ZONE

The area discussed herein is located within the Mad River fault zone (MRfz; see Figure 3), a northwest-trending fold and thrust belt that intersects the coastline between Big Lagoon on the north and Arcata on the south. This zone consists of several major northwest-trending thrust faults and numerous minor, secondary synthetic and antithetic faults. Major faults within the MRfz include (from north to south); the Trinidad, McKinleyville, Mad

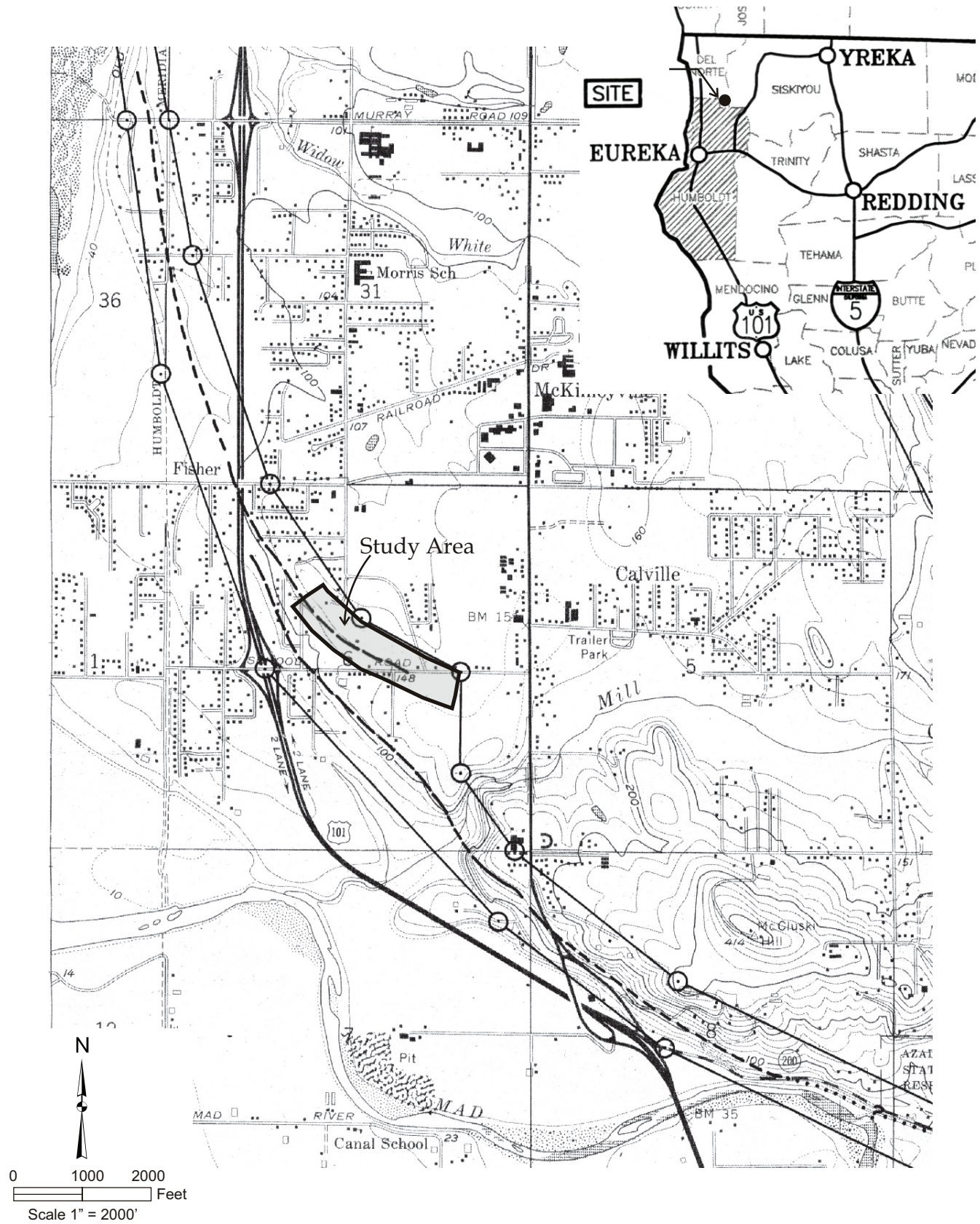
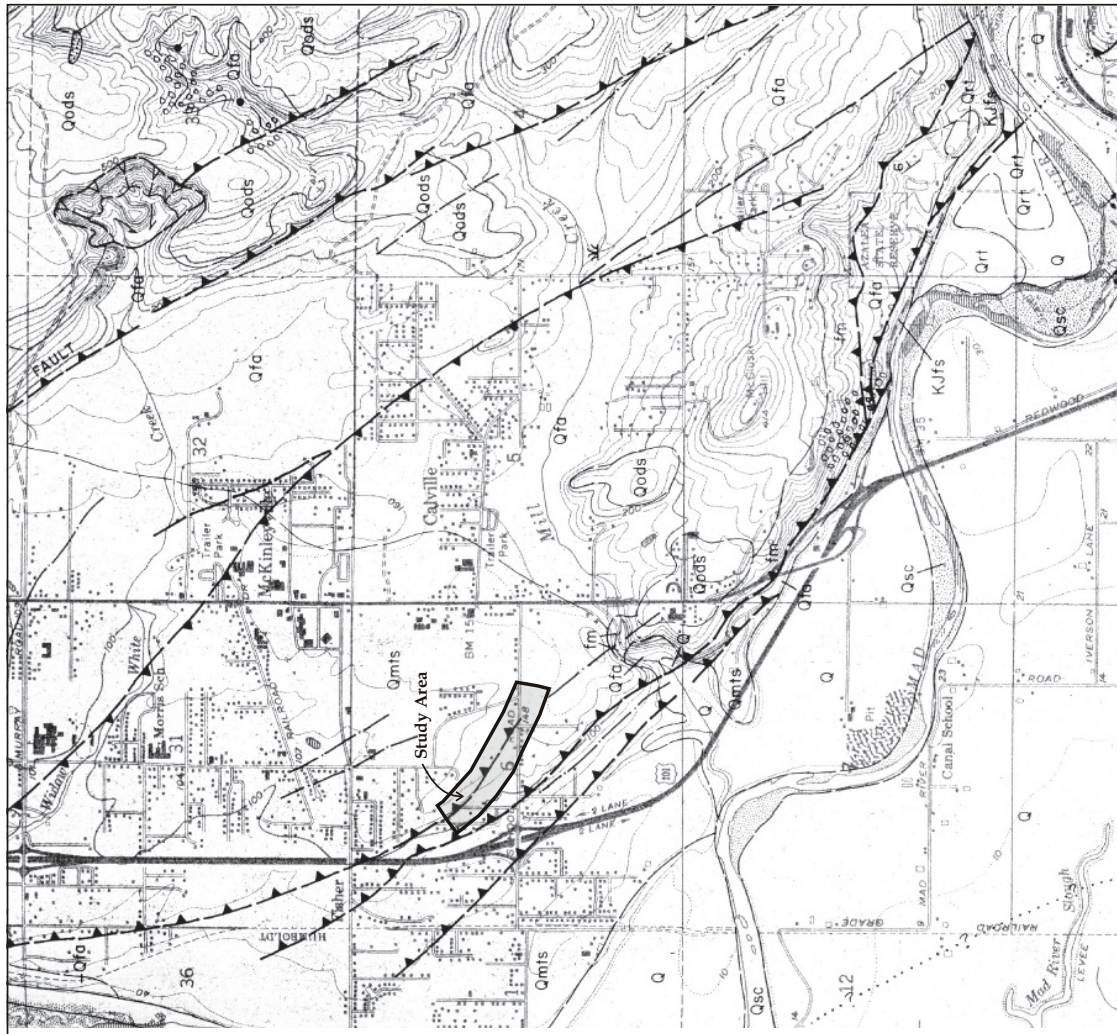


Figure 1. Location map. Base map: Alquist-Priolo Earthquake Fault Zone Map, Arcata North.



EXPLANATION

- Qsc **STREAM CHANNEL DEPOSITS (Holocene):** unconsolidated silt, sand, and pebble-to cobble-sized gravel in active river channel and flood-stage, gravel-bar areas.
 - Q **ALLUVIUM (Holocene):** unconsolidated, coarse-to fine-grained sand and silt on coastal plain, in valley bottoms, and along modern river flood plains; gravel in channel areas; may include some marine terrace deposits along Mad River flood plain.
 - Qrt **RIVER TERRACE DEPOSITS (Holocene-Pleistocene):** dominantly sand and gravel with minor amounts of silt and clay deposited during higher stands of major streams.
 - Qods **OLDER DUNE SANDS (Late Pleistocene):** unconsolidated deposits of fine-to coarse-grained sand; generally well vegetated.
 - Qm1s **MARINE TERRACE DEPOSITS (Quaternary):** poorly to moderately consolidated deposits of marine silts, sands, and gravels forming flat benches on wave-cut surfaces adjacent to the Mad River flood plain.
 - Qfa **FALOR FORMATION (Early to Middle Pleistocene):** fluvial and shallow-water marine sediments; includes pebbly conglomerate, sandstone, and silt; in some places, contains abundant animal and plant remains.
 - Kufs **CENTRAL BELT FRANCISCAN SEDIMENTARY ROCKS (Cretaceous-Jurassic):** well consolidated sandstone, siltstone, and shale with minor amounts of conglomerate; structurally, deformed and usually highly sheared; includes rocks mapped as Franciscan Broken Formation by Carver and others (1984).
 - fm **FRANCISCAN MELANGE (Cretaceous-Jurassic):** individual blocks of graywacke, sandstone, mudstone, conglomerate, greenstone, chert, and serpentinite in a sheared argillaceous matrix.
- LITHOLOGIC CONTACT:** dashed where approximately located.
- FAULT:** dashed where approximately located, dotted where projected or inferred, queried where uncertain.
- THRUST FAULT:** dashed where approximately located, dotted where projected or inferred, queried where uncertain; bars on upper plate.
- LINEAMENT:** linear feature of unknown origin observed on aerial photographs.

Figure 2. Geologic map of the McKinleyville region. Basemap and explanation from Arcata North USGS 7.5 minute Quadrangle "Geology and Geomorphic Features Related to Landsliding" OFR 84-38 SF

River, and Fickle Hill faults. The study area is located along the Mad River fault. Individual faults within the MRfz exhibit variable strikes, which is common along thrust faults, and shallow to moderate dips. At least 5 kilometers (3 miles) of middle and late Pleistocene displacement has occurred across the MRfz since deposition of the Falor Formation (Carver, 1987). In the McKinleyville area, the MRfz crosses and displaces the flight of marine terraces described above. The faults are typically well-expressed across the terraces as west- and southwest-facing scarps offsetting the otherwise planar terrace surfaces.

Limited paleoseismic data is available to constrain the timing of past earthquakes on faults within the MRfz, but available data suggest recurrence intervals on the order of thousands of years. The principal faults within the MRfz are considered active by the State and are included within Alquist-Priolo Earthquake Fault Zones.

MAD RIVER FAULT

Up to four traces of the Mad River fault have been mapped in the McKinleyville area (Carver, Stephens, and Young, 1985), although only the easternmost two traces are included by the State within Alquist-Priolo Earthquake Fault Zones (Figure 1). These faults form a southwest-stepping fault pair. The northern trace is mapped as extending from the coastal bluff near the western end of Murray Road, to the southeast beneath Highway 101, and across School Road. The fault forms a relatively steep, prominent 7-meter-high scarp just north of School Road (locally the "School Road scarp"), which becomes increasingly subdued as it extends southeastward across School Road. The scarp is not apparent within approximately 100 meters south of School Road. Trench studies (discussed below) have documented the termination of the northern fault trace 150 to 200 meters south of School Road. The northern trace trends about N15W on the west side of Highway 101 and progressively bends to the southeast towards its terminus. A relatively sharp bend in the scarp is present just north of School Road (south of Carver and Burke trench location; Figure 4), from about N45W to N70W. In the vicinity of School Road, the fault appears to strike about N70W, based on the trend of the geomorphic escarpment. In this area, scarp height and steepness decrease abruptly over a length of just a few tens of meters.

The southern Mad River fault trace overlaps the northern trace between about School Road and Highway 101, across an approximately 300- to 400-meter-wide step-over. The southern trace extends toward the southeast across the mouth of Mill Creek, to the northern valley wall of the Mad River drainage (Figure 1). This scarp becomes very high (20+ meters) directly south of School Road, although the scarp height may have been enhanced by past Mad River incision. The southern trace has not to date been trenched that we are aware of.

TRENCH INVESTIGATIONS IN THE SCHOOL ROAD AREA

As described above, numerous trench studies have been completed along the Mad River fault southeast of Highway 101 (Figure 4). We are aware of at least nine trenches that have crossed the fault, including Carver and Burke's initial trench; at least two other nearby studies including fault crossings have been described, but information on these is not readily available. Trenches have extended up to 300 meters onto the hanging wall block (southwest of the fault).

But it all started with Carver and Burke's trench back in the mid 1980's. That trench, included in the 1992 FOP guidebook and included herein as Figure 5, revealed the initially planar marine terrace abrasion platform deformed into a tight, overturned fault propagation fold that looked all the world like a cresting wave just about to break beneath the scarp. Multiple scarp-derived colluvial deposits were interpreted in that trench, which suggested repeated, episodic movement. Radiocarbon dates from two of the three shallowest buried colluvial horizons are on the order of 10 ka, suggesting 2 or 3 Holocene events on the fault. Six buried scarp-derived colluvial horizons were interpreted in all overlying presumably 83 ka marine terrace deposits, which suggests a relatively long interval between abrupt scarp-forming events.

Other nearby trenches, both northwest and southeast of the initial Carver and Burke trench, have not exposed similar relationships. About 200 meters to the northwest, a consultant trench (BGC, 1990) exposed the same

relationship of bedrock thrust over terrace sediments and scarp-derived colluvium, but did not observe the overhanging fold and did not distinguish individual colluvial horizons.

In the past year, we have completed four additional trenches crossing the fault directly southeast of the Carver and Burke study area (SHN, 2006). These trenches occur along the segment of the fault where scarp height and steepness rapidly decrease. The northwestern most of these trenches (Trench 5, log included as Figure 6) occurs on a steep segment of the scarp, and exposes bedrock thrust over scarp-derived colluvium. Bedrock in the trench is blocky and locally massive, although several distinct bedrock shears are present, as is a tight fault-bounded chevron fold (anticline) that suggests significant displacement along the adjacent shears. A distinct sheared fault gouge zone is apparent along the fault, which indicates rupture into the near-surface (as opposed to the blind

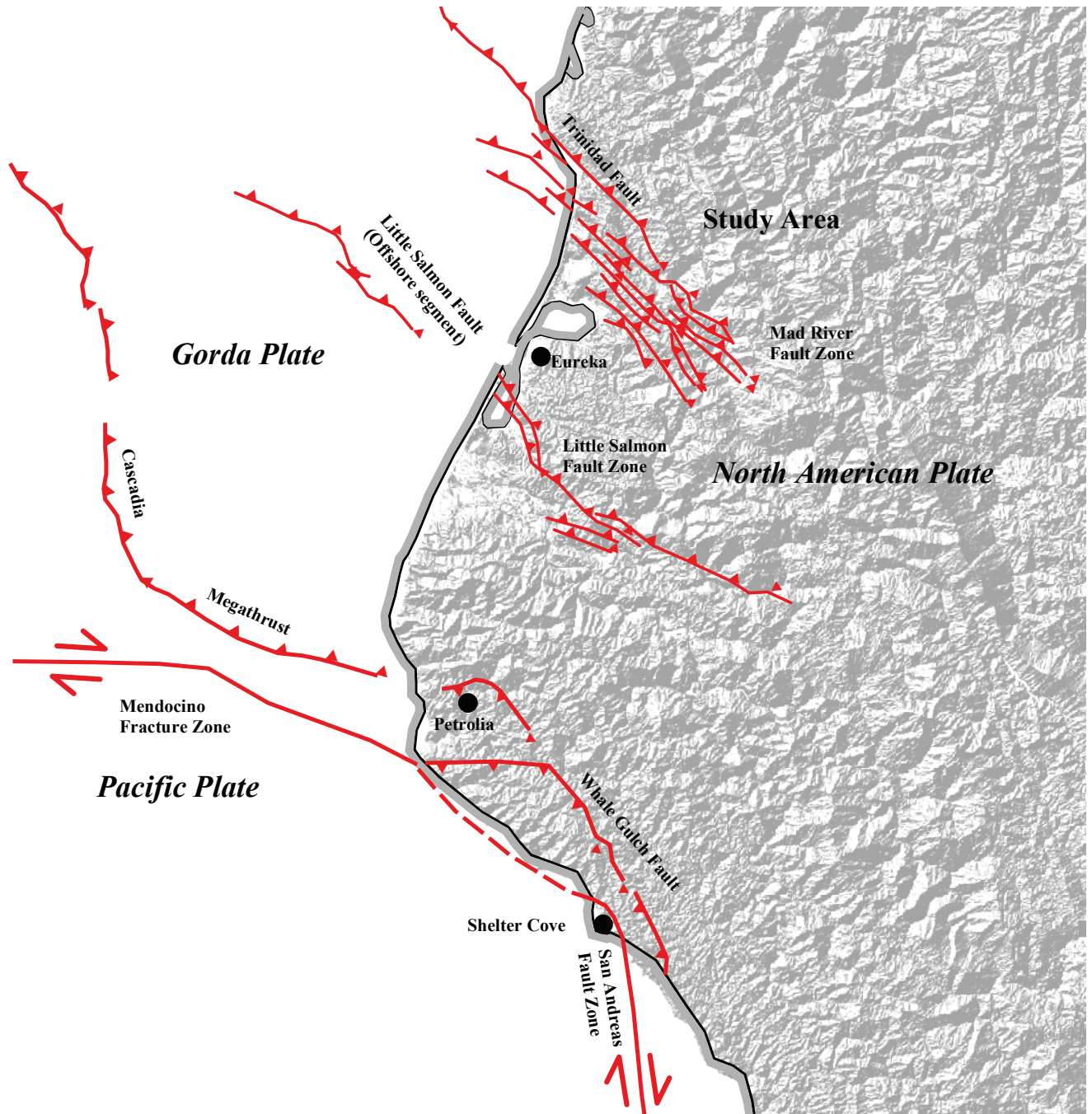


Figure 3. A schematic map showing the tectonic setting of northern California. Modified from: USGS California - Nevada Active Fault Map: <http://quake.wr.usgs.gov/info/faultmaps>; San Andreas Fault location taken from Prentice et al., 1999.

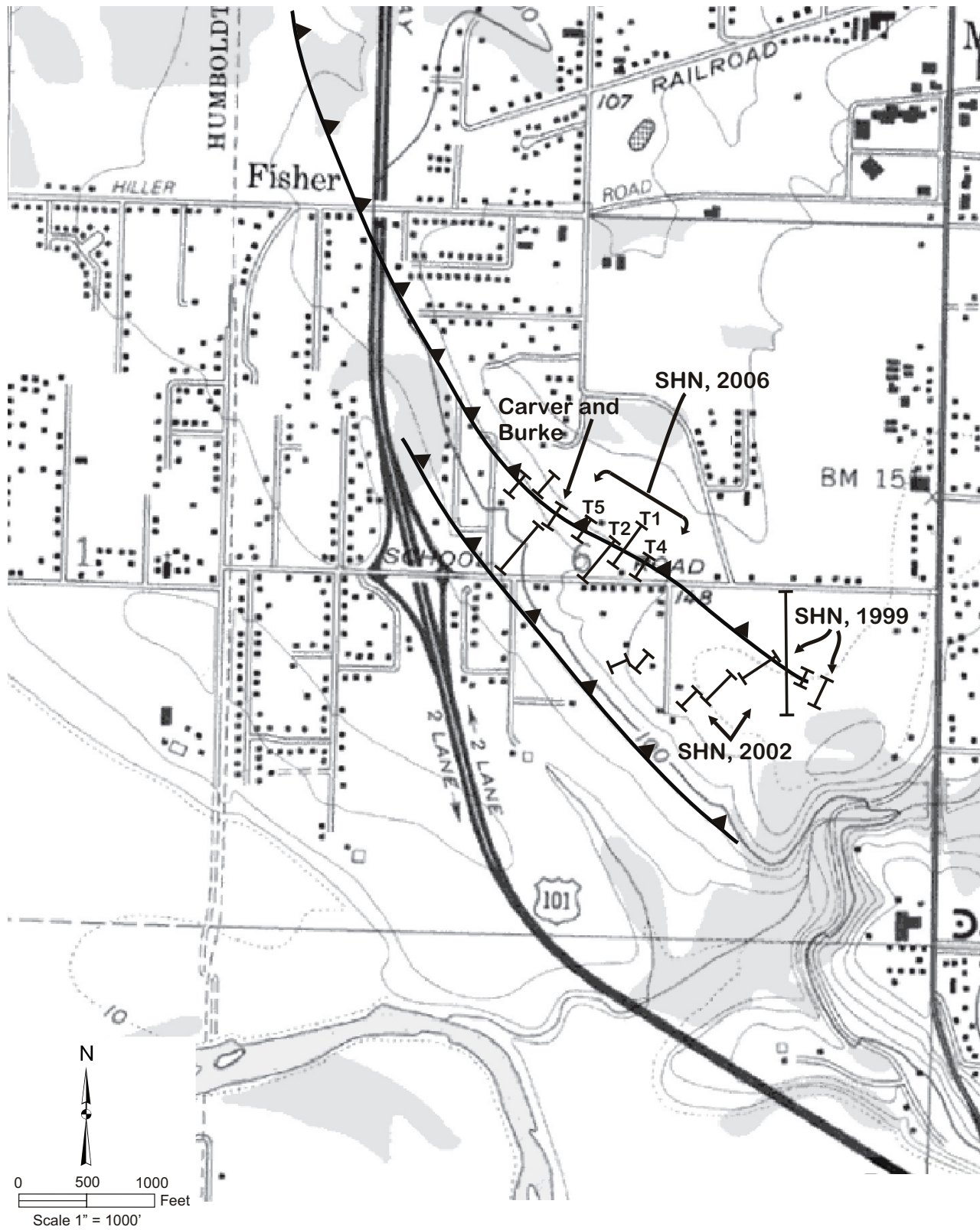


Figure 4. Locations of previous trench studies. T1, T2, T4, and T5 refer to SHN trenches 1,2,4, and 5, which are discussed in the text.

thrust/fault propagation fold exposed just a hundred or so meters to the northwest). We interpret two generations of scarp-derived colluvium that appear related to scarp-forming events, suggesting two paleo-earthquakes are recorded in the exposure. These apparently event-related colluvial deposits include distinct proximal facies (coarse, cobbly zones adjacent to the fault), presumably associated with collapse of the overhanging thrust tip following surface rupturing earthquakes, and a finer-grained distal facies that extends to the base of the scarp. The event-derived colluvial horizons are separated by colluvial horizons that lack this textural contrast, suggesting they represent slow, steady colluvial deposition during interseismic periods. Radiocarbon dating of a charcoal sample extracted from the upper event-derived colluvial horizon resulted in an age estimate of 2010 ± 40 cal yr BP. Presence of this sample in an area of darker soil color suggests it may be encompassed within a krotovina or root-fill; it may therefore be anomalously young and not representative of true horizon age.

About 65 meters to the southeast, our Trench 2 (Figures 7 and 8) crossed the scarp where it begins to become lower and less steep. That trench exposure was unique in that the bedrock in the hanging wall block was very blocky, with distinct planar joints. A broad, 2-meter-wide pervasively sheared gouge zone is present in the fault zone at this location, separating the blocky bedrock from marine terrace deposits. Due to the absence of a high scarp in this area, there is less scarp-derived colluvium, and it is not possible to interpret individual event-related deposits. Radiocarbon dating of a charcoal sample taken from the gouge zone resulted in an age estimate of $25,300 \pm 190$ cal yrs BP.

75 meters farther to the southeast, Trench 4 crossed the fault in an area where the scarp has become relatively short and low gradient. Again, bedrock is thrust over terrace/colluvial deposits, this time along a very sharp fault contact (Figures 9 and 10). Bedrock in the hanging wall block in this area is massive and deeply weathered, a stark contrast to the blocky rock farther northwest. A single scarp-derived colluvial horizon was observed at this site.

South of School Road, trenching investigations documented the termination of the northern Mad River fault strand (SHN, 1999). Three closely spaced trenches encountered progressively diminishing fault displacement, to the point where no offset was apparent in the southeasternmost trench, about 200 meters south of School Road. Displacement in the trenches diminished from about 1.4 meters, to .9 meters over a lateral distance of about 30 meters, to zero about 40 meters away. The termination of the fault in this area is coincident with the loss of a geomorphic escarpment. These trenches expose only terrace sediments; that is, the bedrock block present in the hanging wall block to the northwest is not present in this area.

Trenches crossing the upper (hanging wall) block locally expose evidence of distributed shear within the bedrock block in the area northwest of School Road. Bedrock near the fault exhibits zones of high-angle planar shears and joints that are presumably related to distributed shearing during surface rupturing earthquakes. Trenches across the lower (foot wall) block do not typically expose any faulting or shearing; terrace beds in the lower plate tend to be planar and undeformed.

SUMMARY, INTERPRETATION, AND SPECULATION

Trench studies along the Mad River fault near School Road result in the following observations and interpretations, in no particular order:

- Fault location can be refined based on these studies, especially south of School Road, where geomorphic expression of the fault is absent. The studies document the termination of the northern Mad River fault strand, just south of School Road.

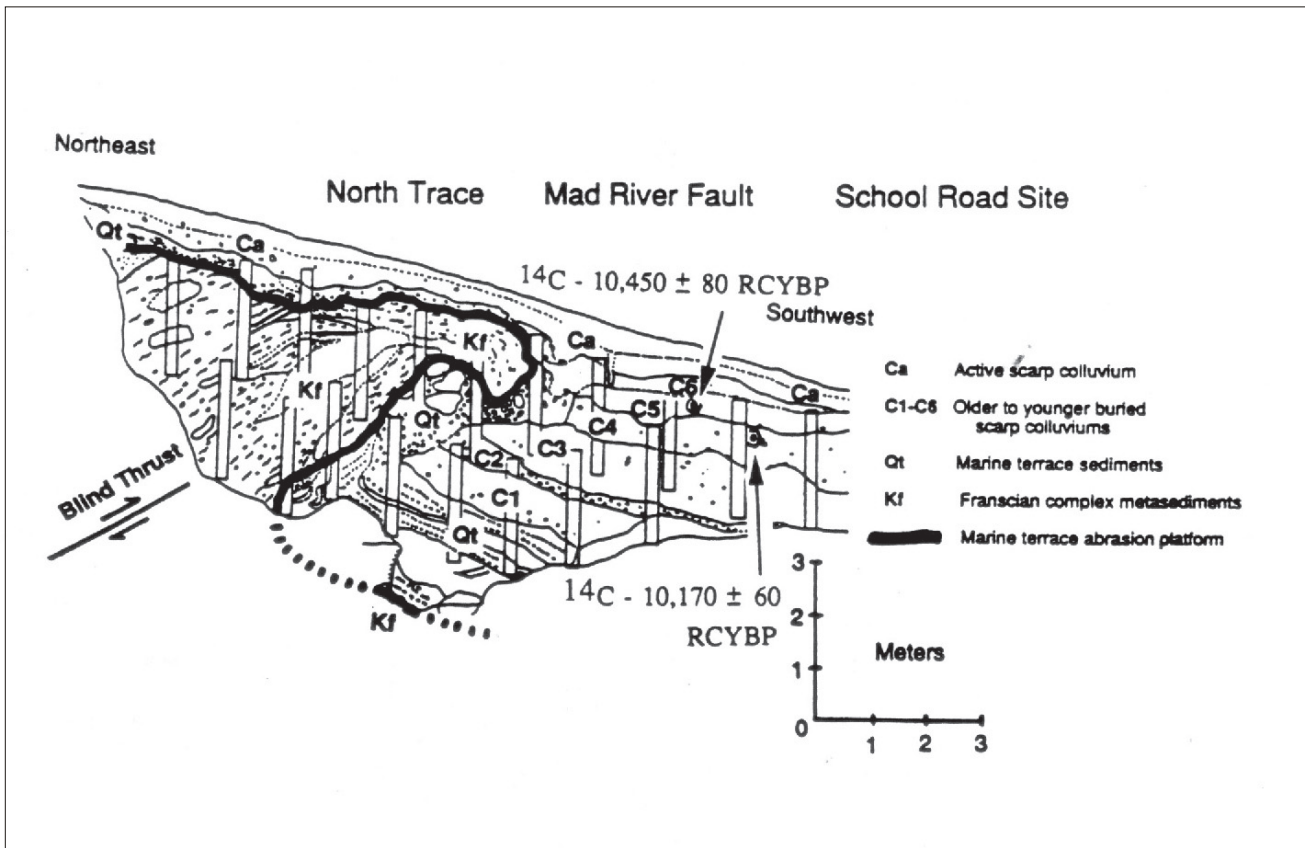


Figure 5. Trench log from Carver and Burke study, from 1992 FOP Guidebook.

- Scarp morphology in the area appears to be heavily influenced by the presence of a broad bedrock block that is being thrust over terrace sediments. The anomalously steep scarp in this area is directly coincident with the segment of the fault containing the rock block. Where the block is absent to the southeast, the scarp becomes more subdued and eventually terminates. It is conceivable that the bedrock block forms an asperity along the fault that may have played a role in the initiation of the broad fault step to the southwest.
- The internal character of the bedrock block appears to influence scarp morphology as well. The significant bend in the scarp directly north of School Road is coincident with the location of distinctly blocky, strongly jointed rock. Elsewhere in the vicinity the rock is massive and generally deeply weathered and pervasively sheared.
- As at other sites in the Mad River fault zone, the fault tends to daylight relatively low in the scarp face.
- The fault is expressed in the trenches as a relatively narrow zone, typically less than 2 to 3 meters wide. Locally, distributed shearing is observed in the upper (hanging wall) plate as high angle, fault-parallel

page left intentionally blank
for
simpson tabloid fig 6

Figure 6. Log of Trench 5 of the Mad River fault.

page left intentionally blank
for
simpson tabloid fig 6

page left intentionally blank
for
simpson tabloid fig 7

Figure 7. Log of Trench 2 of the Mad River fault.

page left intentionally blank
for
simpson tabloid fig 7

page left intentionally blank
for
simpson tabloid fig 9

Figure 9. Log of Trench 4 of the Mad River fault.

page left intentionally blank
for
simpson tabloid fig 9



Figure 8. Photograph of fault exposure in Trench 2. View is of southeast wall.



Figure 10. Photograph of fault exposure in Trench 4. View is of northwest wall.

REFERENCES CITED

- Busch Geotechnical Consultants, (1990). Results of an Alquist-Priolo Special Studies Zone Fault Investigation of the 15-acre Pialorsi Property, McKinleyville, CA. Unpublished Consultants Report. 32 pages with trench logs.
- Carver, G.A., Stephens, T.A., and Young, J.C., (1985). Quaternary Geologic Map of the Mad River Fault Zone, Arcata North 7.5' quadrangle. Unpublished preliminary map for the California Division of Mines and Geology State Map Project, scale 1:24,000.
- Carver, G.A. (1987). Late Cenozoic Tectonics Of The Eel River Basin Region, Coastal Northern California, In Schymiczek, H. And Suchsland, R. (Eds): Tectonics, Sedimentation And Evolution Of The Eel River And Associated Coastal Basins Of Northern California. pp. 61-72. Bakersfield: San Joaquin Geological Society.
- Carver, G.A., and Burke, R.M., (1992). Late Cenozoic Deformation on the Cascadia Subduction Zone in the Region of the Mendocino Triple Junction: in Burke, R.M. and Carver, G.A. (editors), 1992 Friends of the Pleistocene Guidebook, Pacific Cell, p. 31-63.
- Clarke, S.H., Jr. (1992). Geology of the Eel River Basin and Adjacent Region: Implications for Late Cenozoic Tectonics of the Southern Cascadia Subduction Zone and Mendocino Triple Junction: AAPG Bulletin, v. 76, no. 2, p. 199-224.
- Kelley, F.R. (1984). Geology and Geomorphic Features Related to Landsliding, Arcata North 7.5" Quadrangle, Humboldt County, California. CDMG Open File Report 84-38 SF.
- McLaughlin, R.J., and 7 others (2000). Geology of the Cape Mendocino, Eureka, Garberville, and Southwestern part of the Hayfork 30 x 60 Minute Quadrangles and Adjacent Offshore Area, Northern California: U.S. Geological Survey Miscellaneous Field Studies MF-2336.
- SHN (1999). Fault Rupture Hazard Evaluation; Proposed Subdivision, APN 508-061-16, McKinleyville, CA. Unpublished Consultants Report. 10 pages with trench logs.
- SHN (2002). Fault Rupture Hazard Evaluation; Proposed Subdivision of a Portion of APN 508-071-36, McKinleyville, CA. Unpublished Consultants Report. 10 pages with trench logs.
- SHN (2006). Fault Rupture Hazard Evaluation; Proposed Subdivision of APNs 508-351-39 and -40, McKinleyville, CA. Unpublished Consultants Report. 14 pages with trench logs.

A 3,000 Year Record of Tsunami Deposition from the Southern end of the Cascadia Subduction Zone

Garrison-Laney, Carolyn E.¹, AbramsonWard, Hans F.², and Carver, Gary A.³
Department of Geology, Humboldt State University, Founders Hall,
Arcata, California 95521, USA

ABSTRACT

The stratigraphy of Lagoon Creek, a small freshwater pond on the coast of northern California, contains evidence of at least four and as many as six tsunamis from the Cascadia subduction zone over the last 3,500 years. We present evidence that plate boundary earthquakes generated tsunamis that inundated the southernmost portion of the CSZ at times synchronous with events documented along other parts of the subduction zone. These findings provide an important datapoint to the southernmost part of the CSZ, a heretofore undocumented area, that allows better characterization of CSZ rupture dynamics and recurrence intervals.

Six sand layers with characteristics typical of tsunami deposits interrupt the predominantly peaty and muddy stratigraphy of Lagoon Creek. Sand layer thinning and fining trends, sand layer structure, particle size, nature of contacts, presence of rip-up clasts, and biostratigraphy combine to make a compelling argument for tsunami deposition of sand layers. Two of the sand layers drape the toes of a landslide deposit derived from the adjacent hillside. In each case the sand layer contains angular rock fragments both above and as much as 200 m inland from the slide. We infer that the landslide and the tsunami resulted from the same earthquake.

We correlated sand layers using layer thickness and appearance, a volcanic ash layer, stratigraphic markers within the peat and mud, and radiocarbon ages of detrital twigs, spruce cones, and other woody debris within the tsunami deposits. Radiocarbon dates give the following two-sigma ranges of limiting maximum age for five of the inferred tsunamis: 1260-1290; 1360-1520; 1570-1690; 2470-2760; and 3210-3470 calibrated years before A.D. 1950 (cal yr B.P.). Four of these ranges fail to differ statistically from the timing of earthquakes and tsunamis from southern Washington and southern Oregon. The sixth and youngest of the tsunamis postdates peat dated 290-530 cal yr B.P. This tsunami probably resulted from the A.D. 1700 Cascadia earthquake.

1. Current address: Dept. of Earth and Space Sciences, 63 Johnson Hall, Box 351310, University of Washington, Seattle, WA 98195-1310, cegl@u.washington.edu
2. Current address: Geomatrix Consultants, Inc., 2101 Webster Street, 12th floor, Oakland, California 94612, HAbrahamsonward@geomatrix.com
3. Current address: Carver Geologic, Inc., P.O. Box 52, Kodiak, AK 99615, cgeol@alaska.com

INTRODUCTION

This study presents evidence for repeated tsunami inundation from a heretofore-undocumented area adjacent to the southernmost segment of the Cascadia subduction zone (CSZ), on the coast of northern California. We use stratigraphy, lithology, grain size analysis, microfossil (diatom) biostratigraphy, and radiocarbon dates to evaluate sand layers in the sediment record of a small freshwater pond. We conclude that this record contains evidence for at least four, and possibly six, tsunami inundation events, as well as two episodes of shaking, in the last 3,500 years.

This study supplies an additional long record of tsunamis and earthquakes for the southernmost part of the CSZ. This additional site is critical to the understanding of CSZ rupture dynamics, as it is 135 kilometers south of the current southernmost long-record Cascadia site. In addition, it is the only long record site that is south of the Blanco fracture zone, and adjacent to subducting Gorda plate.

Long record sites from coastal estuaries and lakes that record earthquakes and tsunamis are important for characterizing rupture dynamics and recurrence intervals of subduction zones. Since the mid 1990s, several sites with long (>3,000 yr) records of earthquakes and tsunamis have been described along the CSZ. These records

are often represented by abruptly buried soils, and sometimes are accompanied by tsunami deposits (Atwater and Hemphill-Haley, 1997; Kelsey et al., 2002; Witter et al., 2003). Some of these studies describe records of tsunami deposits in coastal lakes (Hutchinson et al., 2000; Kelsey et al., 2005).

In this paper, we first present the results of our investigation of the tsunami and earthquake history of a site called Lagoon Creek. We then discuss the evidence that supports our conclusion that the sand layers are indeed tsunami deposits. Then we compare this new record with the records of earthquakes and tsunamis from Willapa Bay, Coos Bay, Coquille River, Bradley Lake, and the Sixes River estuary. These comparisons form a characterization of the rupture pattern and history of the CSZ.

SETTING

Lagoon Creek is a freshwater pond that is an ideal setting to trap and preserve tsunami deposits. A beach berm offers protection from winter storm waves, and the pond is above MHHW. The length of the pond is protected from the open coast by a relatively high ridgeline, providing only one access point at the mouth of the pond. This affords an opportunity to estimate how far inland each tsunami traveled. The pond's freshwater ecology allows any marine incursion to be detected by examining the microfossil content of the sediments.

Lagoon Creek pond is located in Redwood National Park, 4.5 km north of the mouth of the Klamath River and 20 km south of Crescent City, CA (Figure 1). The pond is about 1000 m long and about 100 m wide. The seaward

edge of the pond is 300 m from the surf zone on the beach and the beach berm (which has been modified by grading) currently rises 6 m above mean higher high water (MHHW). An outlet stream was dammed by Crescent Plywood Company, which stored logs in the pond in the 1940s to 1950s. The dam deepened the pond by about 1 m, and probably significantly increased the length of the pond upvalley.

The water depth in the pond varies from 4.3 m at the open seaward end (north side) to less than 1 m at the shallow inland marshy areas (south side). Two sinuous channels about 2 m deep extend across the marshy areas. The pond supports freshwater vegetation around its perimeter and in shallow areas including cattail (*Typha latifolia*), bulrush (*Scirpus microcarpus*), horsetail (*Equisetum arvense*), sedge (*Carex* spp.), and yellow pond lily (*Nuphar polysepalum*).

METHODS

The pond sediments were studied by collecting twenty-one 7.5 cm diameter vibracores and over fifty 2.5 cm diameter cores.

The vibracore locations are shown in Figure 2. Cores were split, described, and sampled in the lab. Samples were collected for grain size analysis, diatom analysis, and radiocarbon dating. Methods for grain size analysis of sand layers and peat are described in Abramson

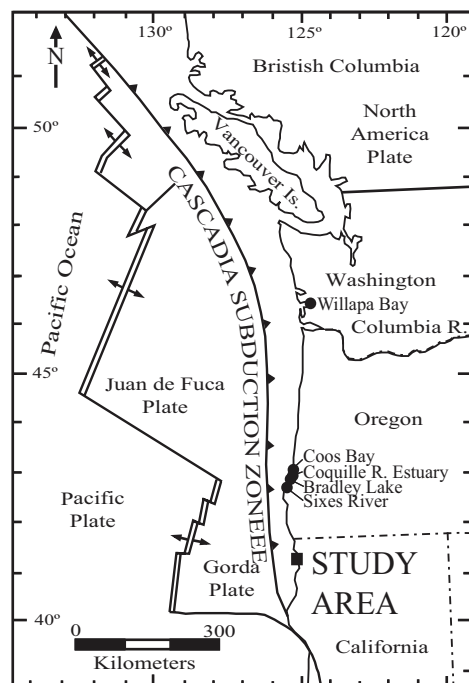


Figure 1. Location map showing locations of other CSZ study sites.

(1998). Methods for diatom analysis are described in Garrison-Laney (1998). In general, radiocarbon samples were selected from mixed layers of mud, peat and woody detritus at the top of sand layers. Delicate detrital material, such as small twigs with preserved bark, was selected when available. Most samples were dated using accelerator mass spectrometry (AMS) methods by Beta Analytic Labs, in Coral Gables, Florida. Calibrations were made using Calib version 4.3 software (Stuiver and Reimer, 1993), using a lab error multiplier of 1, and are reported at the 2σ (95%) confidence interval. Dates are reported as calibrated years before AD 1950 (cal yr BP).

RESULTS

In this section, we first describe the overall stratigraphy of Lagoon Creek, including a description of each sedimentary unit. Deposits described include peat, mud, sand layers, mixed deposits closely associated with the sand layers, a landslide deposit, sand veins, and an ash. Then we present our radiocarbon dates, the results of a grain size analysis of each of the sand layers, and the results of a diatom analysis.

Stratigraphy and Sedimentology

The general stratigraphy of Lagoon Creek is gray basal mud that grades upward into thick reddish-brown peat. This stratigraphy is punctuated by several layers of fine to medium-grained sand that contain occasional rip-up clasts, detrital forest material, and mixed peat and mud. Figure 2 shows the simplified stratigraphy and correlation between the 21 vibracores taken at Lagoon Creek. The sand layers are more numerous and thicker on the north (seaward) edge of the pond. In several cores, sand layers mark sharp changes from underlying peaty units to overlying muddy units. A localized wedge-shaped landslide deposit consisting of angular pebbles and cobbles in a muddy matrix occurs in the strata flanking the western valley wall roughly 600 m inland from the back edge of the beach. Several small (~1 cm diameter) sub-vertical veins of sand intrude sediments in all areas of the marsh. Each deposit is described in detail below.

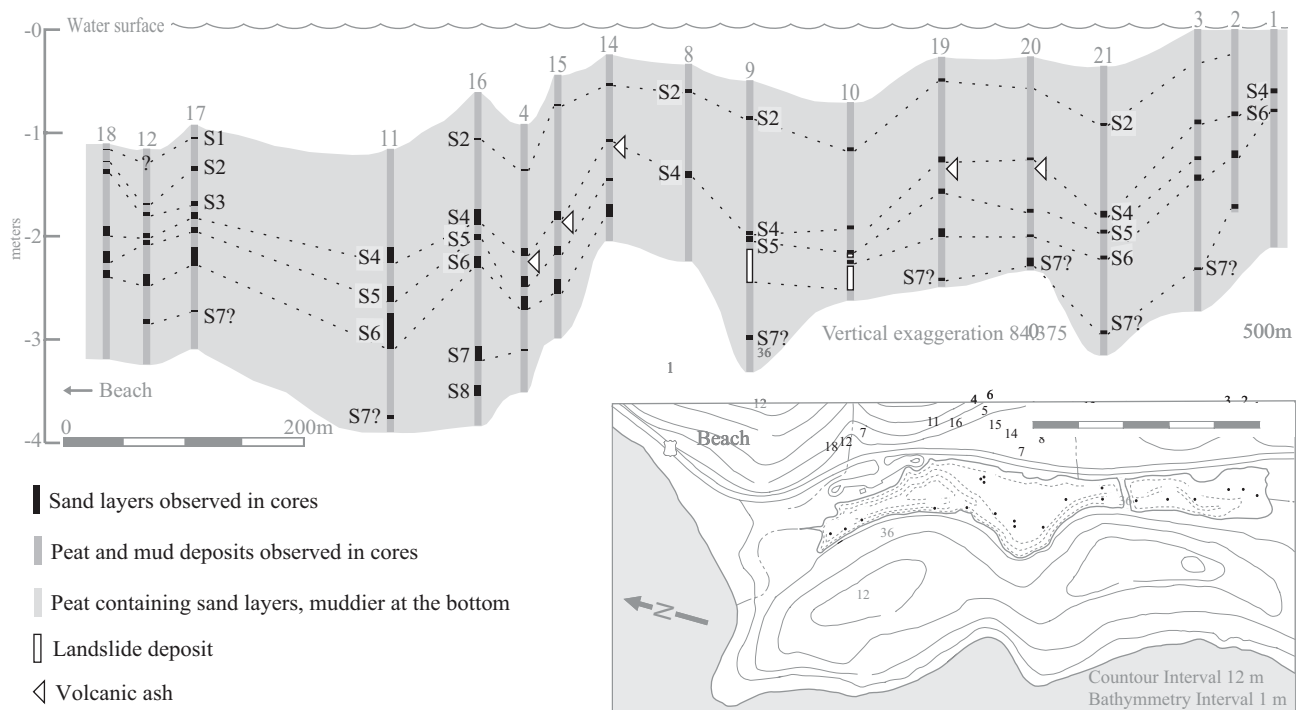


Figure 2. Lagoon Creek pond general tsunami deposit stratigraphy.

Peat Deposits

The peat deposits consist mainly of detrital plant material, in situ plant material, and lesser detrital woody plant material. Where individual fossils could be identified, they included seeds of the freshwater plants *Carex* spp. and *Nuphar polysepalum*, and stems of *Carex* spp. The peat deposits vary between light to dark shades of reddish-brown to yellowish-brown, and typically oxidize to black when exposed to air. Muddy peat and peaty mud deposits are typically slightly grayer than pure peat deposits. The organic content of peat deposits, as determined by percent weight loss on ignition, is generally over 40%, muddy peat deposits between 20-40%, and peaty mud deposits between 5-20%.

Mud Deposits

Mud deposits contain less than 5% organic material and contain little to no sand. The muds are typically light to dark gray and massive, but some deposits contain vascular plant roots, or are faintly laminated with 1 mm thick lighter and darker laminations. Most cores, especially from the landward section of the marsh, encountered massive gray mud with scattered thin (1-20 mm) sand layers at their bases.

Sand Layers

Eight sand layers were identified in the stratigraphy of Lagoon Creek, numbered from the youngest to the oldest as S1-S8. These layers are generally well-sorted, clean, fine- to medium- grained gray sand with variable thickness, structure, and stratigraphic signatures. The grain size and lithology are similar to sand samples taken

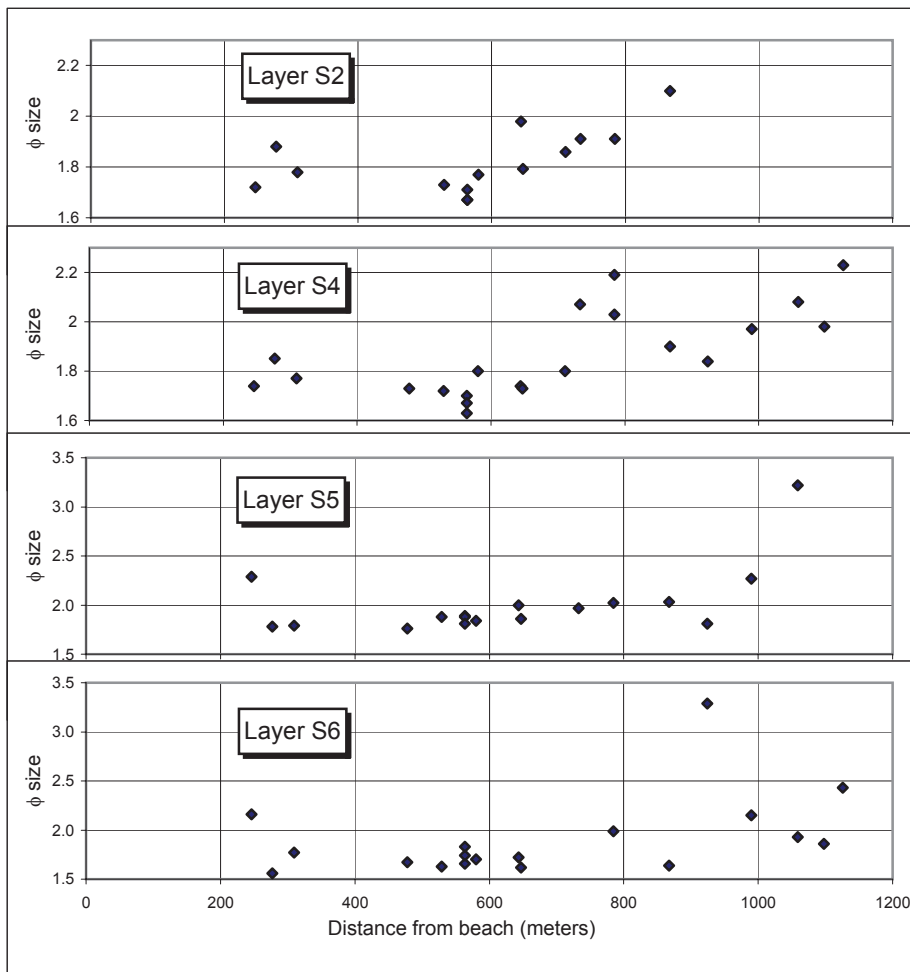


Figure 3. Median grain sizes plots for sand layers at Lagoon Creek. Grain size within each sand layer shows a slight fining trend away from the beach (inland). Note the wide variation in median grain sizes for cores inland of the landslide (about 600 meters from the beach) in Sand Layers S5 and S6, likely caused by entrainment of poorly sorted landslide debris into the landward-directed flows.

from the adjacent beach. Overall, sand layer thickness decreases inland (Figure 2), and the median grain size of samples from each sand layer fines inland (Figure 3). A summary of sand layer characteristics is presented in Table 1.

The sedimentary texture of the sand layers varies from massive to normally graded, locally containing multiple normally graded units within a single layer. In cores LC-11, 12, and 18, sand layer S6 is expressed as normally graded packages separated by thin (1 mm to 1 cm) muddy or peaty mud partings. Peat and/or mud rip-up clasts occur within most sand layers in the seaward part of the marsh, however they become smaller and less prevalent inland, eventually disappearing in the vicinity of cores LC-7 and LC-14. The rip-up clasts are typically concentrated near the base of the sand layer, and range from 0.5 cm to 5 cm wide. They are usually, but not always composed of the same material that immediately underlies the sand layer. Almost all the sand

layers have sharp basal contacts and most have gradational upper contacts. They are generally clean at the base, but grade upward into or are overlain by a 2-5 cm layer of mixed sand mud, peat and woody debris.

Sand Layer S2 can be traced farther inland than the extent of sand deposition. In core LC-20, the stratigraphic horizon of layer S2 consists of a layer of wood chunks, pieces of pond lily, and coarse black organic debris. The stratigraphic horizon changes farther inland so that at core LC-3 (Figure 2), it is represented by a horizontally-

Table 1. Sand layer characteristics.

Sand Layer	Age range ¹ (yr BP)	Number of cores layers found	Number of sharp basal contacts	Depth in core (cm)	Minimum observed inland extent of sand deposition (m)	Layer Thickness (cm)	Number of deposits showing normal grading	Number of pulsed deposits observed	Layer thins inland?	Grain size fines inland?	Rip-up clasts present?	Landslide clasts present?
S1	<S2	2	2	13	350	0.1-1.5	0	0	No	No	No	N/A
S2	<290-530	14	13	29-53	955*	0-4.5	1	0	Yes	Yes	Yes	No
S3	>S2	3	2	48-87	350	1-2.5	0	0	No	No	Yes	N/A
S4	1260-1290	21	21	68.5-174.5	1250	0.3-16.5	2	0	Yes	Yes	Yes	Yes
S5	1360-1520	17	16	123-184.5	1160	0.5-12.5	2	0	Yes	Yes	Yes	Yes
S6	1570-1690	18	18	139-204	1250	0.03-13	6	3†	Yes	Yes	Yes	Yes
S7	2470-2760	12?	11	203-292	1200(?)	15-22(?)	0	0	Yes?	unknown	Yes	Yes?
S8	3210-3470	1	1	337	580	9.5	0	0	unknown	unknown	Yes	unknown

1. Age ranges shown are the 2 σ calibrations of the pooled mean of samples interpreted to closely approximate the age of the sand layer. See Table 2, Summary of radiocarbon samples

*Tsunami deposit and disturbed stratigraphic horizon traceable inland beyond limit of sand deposition to 1190 m.

†Deposits observed with 3, 4, and 5 pulses

oriented matted layer of deciduous leaves. Seventeen meters farther inland at core LC-2, the same stratigraphic level is represented by only a sharp contact between reddish-brown peat (below) and brownish-gray muddy peat (above). Beyond the deposition of sand, the stratigraphic horizon of event S2 can be traced to about 1,190 m inland, an additional 235 m.

Mixed Deposits Above the Sand Layers

Most sand layers mark a distinct change in the stratigraphy from below the sand layer to above it. Below many of the sand layers there is a sharp contact with underlying peat, whereas above, there is a muddy layer mixed with sand and forest detritus including spruce cones, twigs, and peat and mud rip-up clasts. The muddy layer then grades upwards back into a peat deposit within ~ 20 cm. Figure 6 shows a generalized diagram of the pattern most often observed.

Landslide Deposits

A landslide deposit was encountered in several cores two meters below the sediment surface about 600 m inland from the beach. This unit flanks a steep hillside and tapers from about 1 meter thick on the west edge of the marsh to multiple thin (10-50 mm) layers near the middle of the marsh, implying the hillside is its source. No other such deposits were found anywhere else in the marsh.

This landslide deposit consists of poorly sorted, clast-supported, angular to sub-angular clasts that range from clay sized to > 5 cm. The lithology of the clasts consists of decomposed sandstone, metavolcanics, shale, and quartz (in decreasing order of abundance). Toward the middle of the marsh, the clast size decreases and the unit also contains a mix of peat and mud and forest detritus.

In core LC-10 (Figure 5), two distinct layers of landslide material are separated by peaty mud and in situ peat. Each of these layers is capped by a thin (5 mm) layer of clean well-sorted sand. These two sand layers are correlated to layers S5 and S6. A radiocarbon age of a twig with preserved bark taken from the distal end of the landslide deposit in core LC-9 yields a radiocarbon age between 1530 and 1260 yr BP. This age agrees with radiocarbon ages determined for sand layer S5 (Table 2).

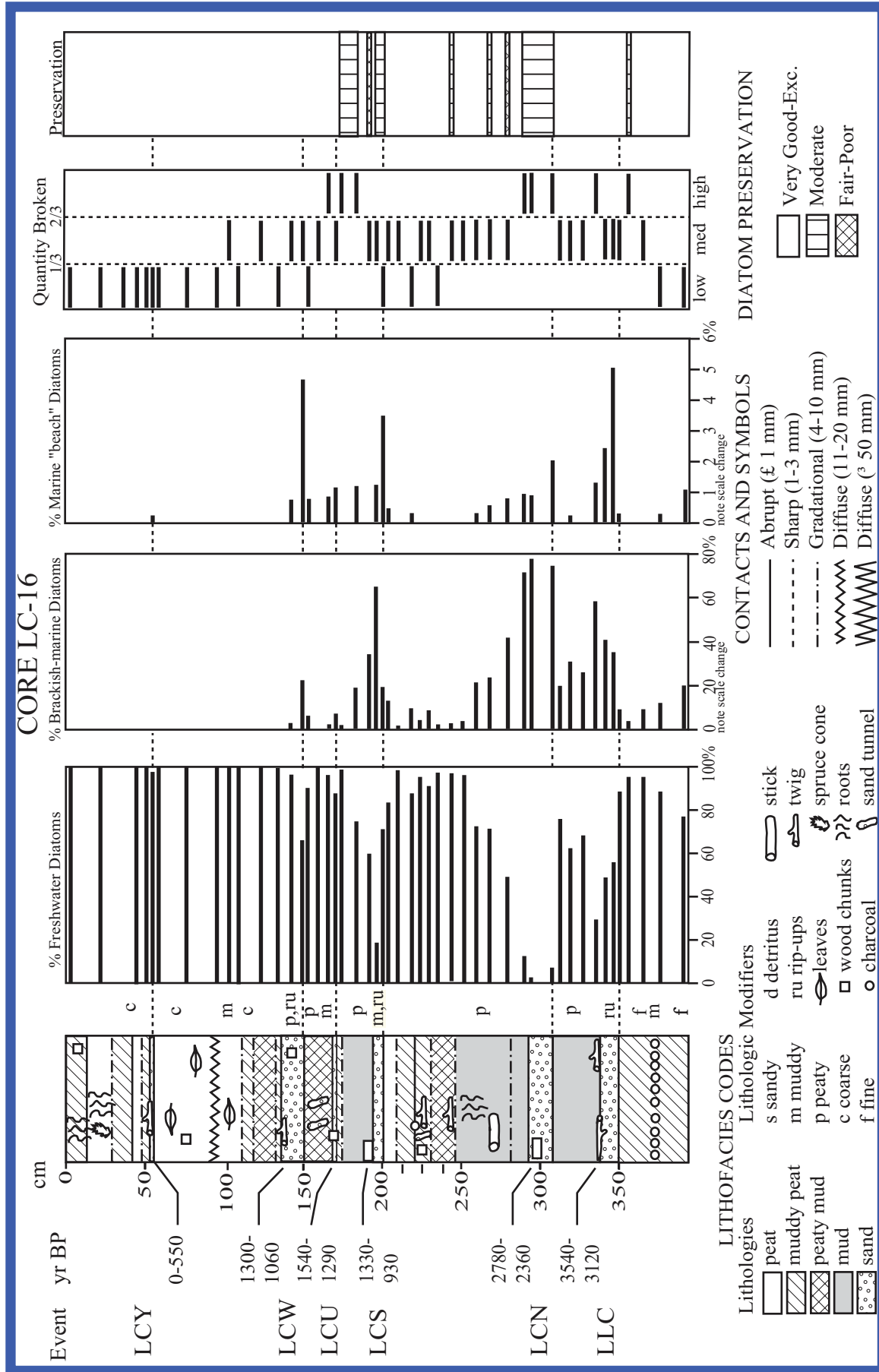


Figure 4. Stratigraphy of Core LC-16, showing the designated names of each sand layer; the ages of dated material; relative percentages of freshwater, brackish-marine, and marine "beach" diatom species; and quantity broken and valve preservation of diatoms for each sample.

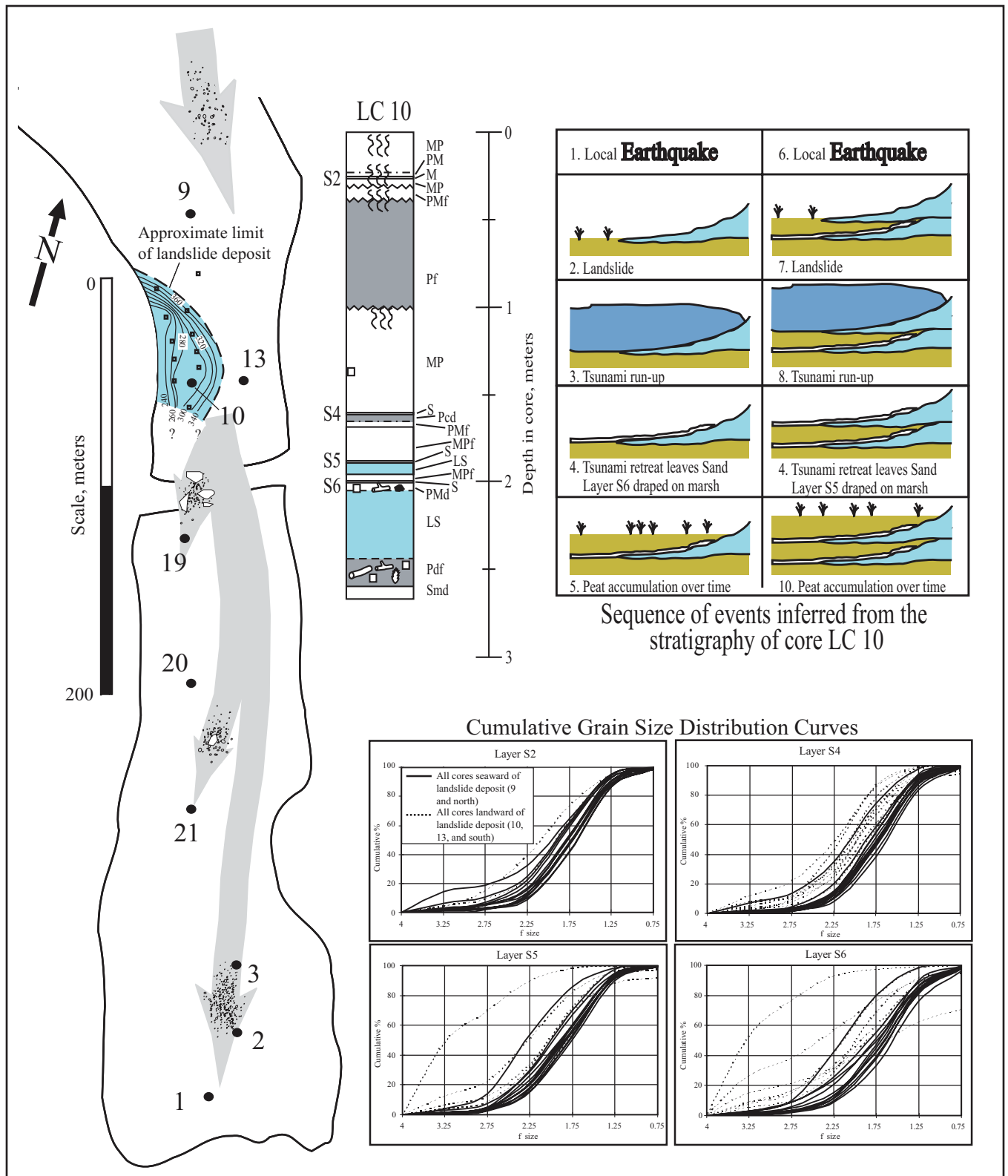


Figure 5. Summary of evidence for landsliding at Lagoon Creek. Contours shown around core LC 10 and the west side of the pond (upper left side of figure) indicate the depth in centimeters to the top of the landslide deposit below water surface. Depth contours were developed from transects of closely spaced gouge cores. Coincidence of landslide and tsunami deposits suggests both were triggered by the same earthquake and that the earthquake was local. The presence of landslide-derived material inland of the landslide deposit provides further evidence that inundation of the pond was landward-directed and maintained a high level of energy well inland of the beach.

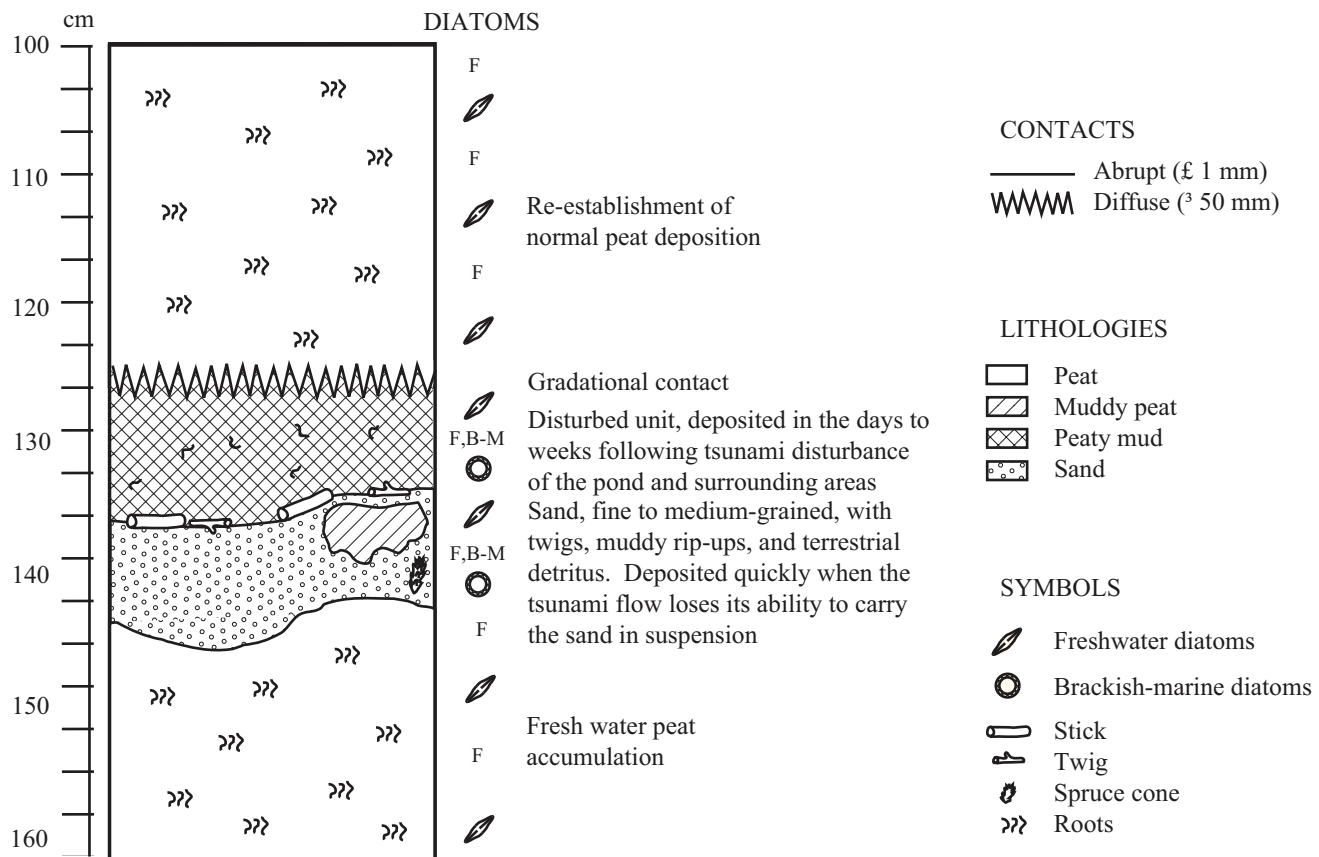


Figure 6. Depositional pattern of tsunami deposits. Generalized stratigraphy of a tsunami deposit from Lagoon Creek pond. The bottom of the pond is eroded by the turbulent flow of the tsunami, resulting in a deposit with incorporated rip-up clasts. Following the rapid sand deposition, the finer material settles on top of the sand layer. Marine diatoms are “trapped” in the sand and in the disturbed muddy unit above.

Sand Veins and Dikes

Several vertically oriented veins and dikes of clean, well-sorted sand intrude the peaty and muddy sediments. These veins vary in shape from tube to ribbon-shaped, and range up to 15 mm wide, and could be traced from about 2 to 20 centimeters in length. Many veins have a long plant root or stem running lengthwise down their center. A few tabular dikes were also encountered. The largest dike is 2 cm thick, wider than the core (> 8 cm) and extends down 6 cm from sand layer S5 in core LC-17. Sand within these features is similar in lithology, sorting, and grain size to the sand from the sand layers.

Most sand veins cluster above the thicker sand layers toward the seaward edge of the marsh, but they occur throughout the stratigraphy and are present in all cores except the most inland cores, LC-10, 20, 21, 3, 2, 1. Locally veins were observed to extend out of the tops of sand layers.

Ash Layer

A fine-grained white volcanic ash is present between 20-50 mm below sand layer S4 in cores LC- 4, 5, 7, 14, 15, 19, and 20. In most cases the ash forms a discontinuous layer less than 1 mm thick or a 2 mm diameter irregular pocket, but it was as much as 5 mm thick in core LC-15. Electron microprobe analysis of elemental composition has identified the probable source as the Little Glass Mountain, CA tephra (Sarna-Wojcicki, 1996, pers. comm.). Several radiocarbon dates from the source area of this tephra constrain the time of this eruption between 1,060 and 1,280 yr BP. (Heiken, 1978).

Radiocarbon

Table 2 summarizes all radiocarbon-dated samples reported in this study. These dates give the following two-sigma ranges of limiting maximum age for five of the inferred tsunamis: S4:1260-1290; S5:1360-1520; S6:1570-1690; S7:2470-2760; and S8:3210-3470 calibrated years before A.D. 1950 (cal yr B.P.). The sixth and youngest tsunami deposit postdates peat dated 290-530 cal yr B.P., and is most likely from the A.D. 1700 Cascadia earthquake.

Table 2. Summary of Lagoon Creek radiocarbon samples.

Sand Layer	Conventional 14C age BP	Calibrated Age* BP	13C/12C ratio	Core / Sample #	Beta Lab Number	Material	Method	Context
S2	370±70	0-550	-29.2	LC1-B6 (gouge core)	B-91553	bulk peat	RM	just below sand layer
S4	1270±40	1300-1060	-28.3	LC-16 - RC2	B-107490	twig with bark	AMS	detrital wood at top of sand layer
S4	1300±40	1310-1060	-28.8	LC-18 - RC2	B-113416	sticks	AMS	top of sand
S4	1330±40	1330-1080	-27.8	LC-3 - RC3	B-101544	spruce cone	AMS	in sand layer
S4	1400±40	1400-1180	-30.7	LC-21 - RC1	B-113419	stick	AMS	above sand layer
S5	1370±40	1360-1170	-24.7	LC-4 - RC2	B-101543	wood chunk	AMS	in mud 3 cm above sand
S5	1520±40	1540-1290	-32.4	LC-16 - RC3	B-107491	twig	AMS	in sand layer
S5	1530±40	1540-1300	-31.8	LC-21 - RC2	B-113420	twig	AMS	in sand layer
S5	1590±40	1610-1330	-27.7	LC-18 - RC3	B-113417	twigs with bark	AMS	top of sand
Landslide	1520±50	1550-1280	-27.8	LC-9 - RC4	B-107495	stick with bark	AMS	in landslide deposit
S6	1230±70†	1330-930	-24.9	LC-16 - RC4	B-107492	wood chunk	AMS	in mud just above sand layer
S6	1640±60	1730-1320	-29.2	LC-4 - RC1	B-101547	wood chunk	RM	in muddy peat below sand layer
S6	1720±40	1800-1500	-26.8	LC-18 - RC4	B-113418	twigs with bark	AMS	in top of sand layer
S6	1790±40	1870-1540	-26.4	LC-2 - RC3	B-113415	spruce cone	AMS	in sand layer
S6	3040±50§	3390-2970	-37.0	LC-3 - RC1	B-101539	small seed	AMS	in sand layer
S7	2550±50	2780-2360	-25.0	LC-16 - RC5	B-107493	bark	AMS	in sand layer
S8	3140±50	3540-3120	-28.6	LC-16 - RC6	B-107494	twig	AMS	in top of sand layer
basal mud	2910±40	3250-2860	-24.8	LC-3 - RC2	B-101545	spruce cones	AMS	not associated with sand layer

*Years before A.D. 1950, calibrated using 1.0 lab error multiplier and 2 σ (95%) age range (Stuiver and Reimer, 2000, Version 4.3)

† Erroneously young date? § Erroneously old date?

Diatom Analysis

Figure 4 presents the diatom analysis results of the most complete core, LC-16. In general, the diatoms from the sediments below the sand layers are predominately freshwater. The sand layers contain a mix of freshwater and brackish-marine species as well. Above the sand layers, there is a persistence of brackish-marine species for a time, followed by a gradual return to a freshwater environment.

Many modern diatoms collected in and near the Lagoon Creek pond are the same species as those found in the study cores. Freshwater species collected in the pond that were also found as fossils in the study cores included *Cymbella cuspidata*, *Staurosira construens* var. *venter*, *Fragilaria exigua*, *Sellaphora pupula*, *Tabellaria fenestrata*, and *T. flocculosa*. Many of the diatom species found in and above the sand layers were found living in the swash zone of the modern beach, including *Coscinodiscus marginatus*, *Stephanodiscus carconensis*, *Thalassionema nitzschoides*, and *Thalassiosira pacifica*.

Diatom preservation varied from very good-excellent to fair-poor in the study samples. Very good to excellent preservation describes samples where there are both delicate and heavily-silicified species present with sharp

valve features, implying very little or no dissolution or reworking. Moderate preservation in a sample indicates there is some deterioration to the valves, but there is still a range of delicate to heavily-silicified valves in the sample. Fair to poor preservation indicates that there are no delicate frustules in the sample, it consists of mostly heavily-silicified frustules, there is evidence for dissolution of the valves, or that there is abrasion of the valves or other evidence that the sediment was reworked.

The quantity of broken diatoms noticeably jumps to more than 2/3 of the valves broken in and just above most sand layers (high quantity broken, Figure 4). The highest concentration of broken diatoms is in muddy deposits directly above the sand layers, and in some cases at the base of the sand layers. There is a low (less than 1/3 broken) to medium (between 1/3 to 2/3 broken) amount of broken diatom valves elsewhere in the study core, especially in the top meter of section.

DISCUSSION

In this discussion we document the lines of evidence that support tsunami deposition for most of the sand layers at Lagoon Creek; and then describe the evidence for shaking that suggests that the earthquake that generated the tsunami was local. We then discuss the position of Lagoon Creek pond relative to sea level over time, and rule out storm surges as a possible depositional mechanism for these sand layers. Finally, we compare the timing of the record of Lagoon Creek tsunamis with the records of earthquakes and tsunamis from sites in Washington and Oregon.

Several characteristics of the laterally extensive sand layers at Lagoon Creek suggest they were deposited by tsunamis rather than any other mechanism: (1) the source of the sand was seaward of the pond; (2) the geometry and grain size distribution of the sand layers indicate that the sand was deposited by a landward-directed flow; (3) the distribution of landslide sediments also indicates a landward transport of sediment; (4) the flows that carried the sand were initially turbulent; and (5) the flows then lost energy and dropped the sand out of suspension. We discuss each of these points below.

Source of Sand

The diatom analysis confirms that the source area for the sand layers was the beach. Marine species found in and above the sand layers were also found living on the modern beach. Although the marine species are relatively rare with respect to the *in situ* freshwater population (>100:1 in some samples), this pattern is not uncommon for tsunami deposits in freshwater lakes or ponds. Diatom samples from tsunami deposits from Bradley Lake, OR (Hemphill-Haley and Lewis, 2003) showed similar small percentages of brackish-marine species compared to freshwater species. In addition, similar to the tsunami deposits at Bradley Lake, the highest concentration of marine species were found above, rather than within, sand layers.

The grain size distribution of the beach sand is similar to the distribution of grain sizes found within the sand layers. Also, the mineralogical composition of the sand in the sand layers is similar to the beach sand.

Sand Layer Geometry and Grain Size Distribution

Landward sand layer thinning and grain size trends are consistent with tsunami deposition (Figures 2 and 3). Sand layers S2, S4, S5, S6, S7, and S8 thin in a landward direction. Each of these sand layers also shows a landward fining trend.

Inland Transport of Landslide Clasts

Landward of the landslide deposits, sand layers S5 and S6 contain large angular sandstone and shale clasts in addition to the beach sand. Angular particles derived from the landslide deposit up to 10 mm in diameter were found in sand layer S6 in core LC-19, implying they were transported nearly 100 m by the surge, ending up over

1 km inland from the beach. This implies that the flow that deposited the sand was landward directed and that it entrained material from the landslide and moved it inland (Figure 5).

Turbulent Flows

Surges depositing sand layers at Lagoon Creek were violent and short, and maintained a high level of energy well inland. The sand layers have sharp, often erosive lower contacts. The flows that deposited sand layers S2, S4, S5, S6, S7, and S8, initially had basal shear stresses that were high enough to rip up peat and mud clasts over 500 m inland from the beach.

More evidence for the turbulence of the flow is the condition of the diatom valves within and above the sand layers. The highest concentration of broken diatoms are in the muddy deposits directly above and in some cases at the base of the sand layers. This implies that diatoms were both mechanically broken during turbulent flow and rapidly deposited as is consistent with deposition by a tsunami (Hemphill-Haley, 1996; Dawson et al., 1996).

Depositional Pattern of Deposits

The sediment depositional pattern and the concentration of brackish-marine diatoms in the sand layers provide additional evidence for tsunami deposition. Most of the sand layers and overlying muddy deposits from Lagoon Creek show a distinctive stratigraphy in which the sand layer is overlain by a mixed deposit of mud, sand, and forest debris (described above and illustrated in Figure 6). We interpret both the sand layer and the muddy layer above the sand as the tsunami deposit. This muddy layer contains the greatest percentage of brackish-marine diatoms in the tsunami deposit.

This distinctive pattern is the result of turbulent mixing of sand, other fine-grained sediments (including silt-sized diatoms), and forest debris during tsunami inundation. When the flow lost energy, and thus its ability to carry the sand in suspension, the sand was deposited rapidly in a normally graded bed, but the suspended silt, clay-sized material, and forest detritus was deposited afterward, perhaps over days to weeks. Good diatom valve preservation in and especially above the sand layers also suggests rapid deposition. This pattern of diatom preservation was also described by Dawson et al. (1996).

Evidence for Shaking -- Landslide deposit

The landslide deposit encountered in several cores provides evidence for earthquake ground shaking. In core LC-10, there are two distinct layers of landslide material, capped by sand layers that correlate to sand layers S5 and S6 (Figure 5). These two packages of landslide deposit capped by tsunami sand are separated by peaty mud. Layer S5 and S6 both contain landslide clasts inland of the landslide deposit.

The combined evidence of landsliding and tsunami deposition, including landward transport of landslide sediments suggests that the landslide was caused by shaking that was immediately followed by tsunami inundation. This suggests that the landslide and tsunami were generated by the same earthquake or perhaps a series of closely-spaced earthquakes.

Evidence for Shaking -- Liquefaction Features

The numerous sand veins present in many of the cores are most likely liquefaction features. Other explanations may include infilling of root holes or burrows. This may explain the genesis of cylindrical veins, but explains neither the tabular, dike-shaped veins, nor the long veins with roots or stems running through their centers. Proximity of most sand veins to the sand layers and abundance of veins in the seaward side of the marsh where sand layers are thicker suggests the source of sand for the veins is the sand layers. No alternative source of sand was found in the top 6 meters of stratigraphy.

Liquefaction at Lagoon Creek may have been induced by seismic shaking, or it may have resulted from artesian springs or flooding. No evidence was found favoring one mechanism over the other. The position of Lagoon Creek in the mouth of a narrow low-gradient valley with a small watershed makes it a poor candidate for artesian or flooding-induced liquefaction. This combined with the frequency of high magnitude earthquakes in the region (e.g., M 7.1 Cape Mendocino 1992; M 7.2 Trinidad 1980) suggests the liquefaction at Lagoon Creek results from earthquakes.

Tsunamis vs. Storm Surges

Three lines of evidence favor tsunamis over storm surges for the deposition of extensive sand layers at Lagoon Creek. The inland extent of sand, the presence of marine diatoms within these sands, and the sedimentary pattern of the sand layers support tsunami over storm deposition for all but two of the sand layers at Lagoon Creek.

Nelson et al. (1996a) suggest that sediment containing marine microfossils deposited well beyond the reach of the highest storm tides would be particularly diagnostic evidence of tsunami deposition. Five of the sand layers containing marine diatoms were deposited into a freshwater marsh well above the level of the highest storm tides to minimum distances ranging from 955 to 1,250 m inland. Steep hillsides bounding the east and west edges of Lagoon Creek (Figure 2) protect the pond from the full force of large storm waves. Nelson et al. (1996a) suggest that as storm surges raise water levels in protected inlets, current velocities drop below values required for widespread sand sheets. Sand layers S2, S4, S5, S6, S7, and S8 were deposited by erosive flows well inland of the reach of the highest storm tides.

Sand layers S2, S4, S5, and S6 locally exhibit normal grading. This suggests that they were deposited from suspension, as is consistent with deposition by a tsunami when the turbulent flow slows and the tsunami begins to recede. Layer S6 in core LC-11, has five stacked graded sections that may represent deposition from multiple pulses in a tsunami wave train. This structure was observed in deposits from the 1964 Alaskan tsunami (Benson et al., 1997). Historic storm surge deposits are usually either cross-bedded consistent with constant re-working by storm waves or thin and massive as seen in coastal Alabama in 1979 after Hurricane Frederic (Liu and Fearn, 1993).

While sand layers S2, S4, S5, S6, S7, and S8 are probably not storm deposits, sand layers S1 and S3 may be. These two layers are thinner, and are only preserved near the seaward edge of the pond (Figure 2). These layers could not be traced further than 300 meters inland, and have a massive texture. Several similar thin sand layers in the uppermost section of the Euchre Creek site in southern Oregon, have been interpreted as storm surge deposits and are possibly correlative to these (Witter and Kelsey, 1996).

Another possibility is that sand layers S1 and S3 are tsunami deposits from far-traveled, and presumably smaller tsunamis. A marsh near Crescent City, CA, 20 km to the north (Garrison and Abramson, 1997), contains evidence for the 1960 Chilean and 1964 Alaskan tsunamis. However, the sediment record of Lagoon Creek contains neither of these historical tsunami deposits.

Tsunami Timing: A Comparison of Lagoon Creek Tsunami Events to Other CSZ Earthquakes and Tsunamis

AMS ¹⁴C dates from the majority of the Lagoon Creek sand layers yield age ranges that overlap significantly with the ages of Cascadia earthquakes and tsunamis from the long record sites of Willapa Bay, South Slough, Coos Bay, Coquille River estuary, Bradley Lake, and Sixes River estuary. Figure 7 shows the timing of events at Lagoon Creek in comparison with the age ranges for events documented at these sites. As noted above, Sand Layer S2 is likely the Cascadia-wide event of January 1700. Ages of the older Sand Layers S4, S6, S7, and S8 overlap significantly with ages for events documented elsewhere, suggesting that tsunami inundation at Lagoon Creek was synchronous with events from the northern to southern end of the Cascadia subduction zone or subduction zone earthquakes on adjacent segments of the margin that are spaced apart by hours, days, week, or a few years.

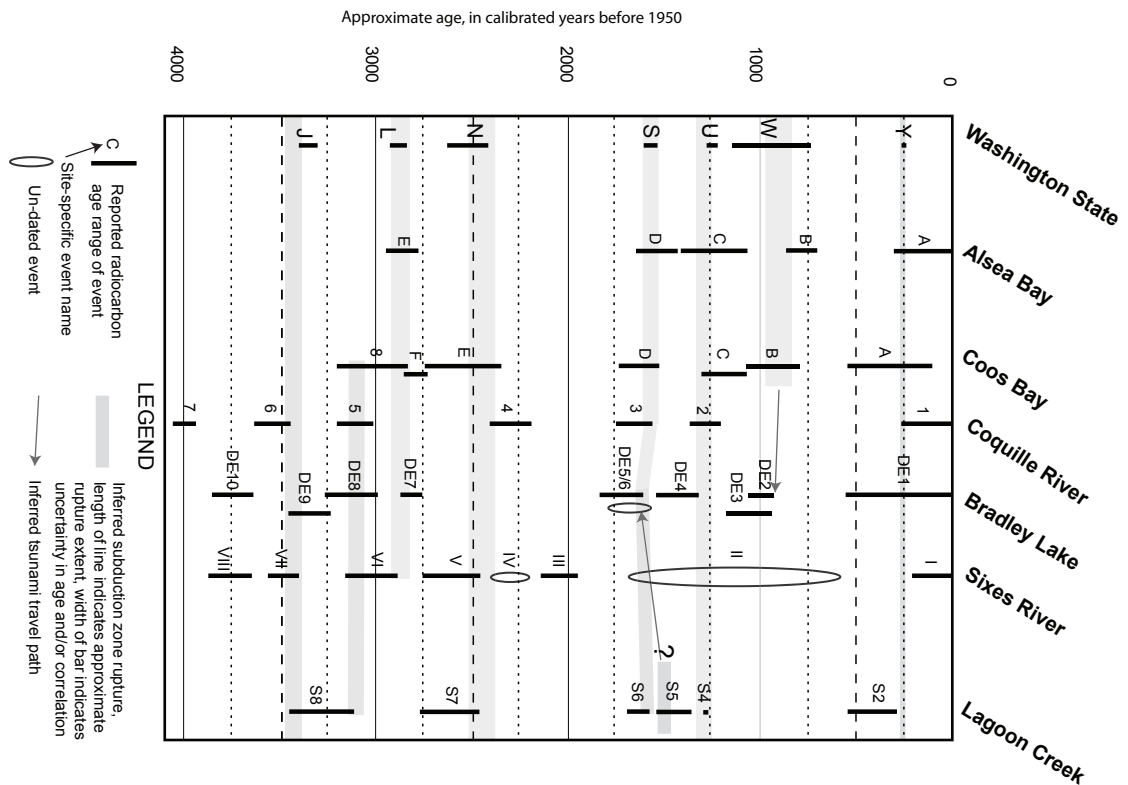


Figure 7. Comparison of calibrated radiocarbon age ranges for sand layers at Lagoon Creek to evidence for earthquakes and tsunamis from other long-record coastal sites on the CSZ. Ages of earthquakes come from tidal marshes at Sixes River (Kelsey et al, 2002), Coquille River (Witter et al, 2003), South Slough-Coos Bay (Nelson et al, 1996b; 2006), Alsea Bay (Nelson et al, 2006), and several sites in Southern Washington (Atwater and Hemphill-Haley, 1997, Atwater et al 2004), and from a coastal lake in southern Oregon (Bradley Lake; Kelsey et al, 2005).

Sand Layer S5 does not overlap with age ranges from any of the long record sites identified except Bradley Lake. The tsunami that deposited Sand Layer S5 may be the same event that created Disturbance Event 4 (DE4) at Bradley Lake. However, buried soils corresponding to this event were not identified at the Sixes River, Coquille River, or Coos Bay. DE4 more likely correlates with Sand Layer S4 at Lagoon Creek in addition to events documented at Coquille River, South Slough, Coos Bay, and in southern Washington and Northern Oregon, providing evidence for an earthquake that ruptured nearly the entire plate margin about 1,250 years BP, as implied by Nelson et al (2006). The tsunami that deposited Sand Layer S5 may have been generated by an earthquake that ruptured only the southern end of the Cascadia subduction zone (which explains the evidence for shaking and landsliding at Lagoon Creek), that did not rupture far enough north to cause ground deformation in the southern Oregon estuaries. It is possible that the tsunami from this earthquake did not maintain enough height as it propagated northward to inundate Bradley Lake. Alternatively, this tsunami may correlate with Disturbance Event 5 at Bradley Lake (the younger of the pair of Disturbance Events 5 and 6 that are interpreted to be separated by only a few decades).

CONCLUSIONS

The stratigraphy at Lagoon Creek contains evidence for inundation by six large tsunamis, tsunamis in the last 3,500 years. These tsunamis were likely generated by local earthquakes on the Cascadia subduction zone. This site, the only long-record site south of the Blanco fracture zone, and adjacent to subducting Gorda plate, provides an important data point that is necessary to further the understanding of Cascadia subduction zone dynamics.

Sand layer characteristics such as thinning and fining trends, sand layer structure, nature of contacts, presence of rip-up clasts, depositional pattern, and diatom evidence combine to create a compelling argument for tsunami deposition of sand layers S2, S4, S5, S6, S7, and S8.

Diatom evidence indicates that the environment has been primarily a freshwater setting for the last 3,500 years, with sharp increases in populations of brackish-marine diatoms coinciding with episodes of sand deposition. Diatom species found living in the surf zone of the adjacent beach were found in and above sand deposits as far as 1,400 m inland. The excellent preservation of delicate allochthonous marine species and a higher occurrence of broken valves in the sand deposits and in the muddy deposits above the sand indicates turbulent, rapid deposition, as would be consistent with a tsunami.

A landslide deposit encountered on the edge of the pond about 600 m from the coast. Based on the relationship of the landslide deposits and sand layers S5 and S6, we infer that these landslides were initiated by local shaking that was followed by tsunamis which entrained landslide material, and that the shaking and tsunami inundation were generated by the same earthquake on two separate occasions. Liquefaction features occurring throughout the stratigraphy at Lagoon Creek may provide additional evidence for local seismic shaking at this site.

The timing of most sand deposition events at Lagoon Creek agrees with time range estimates for CSZ earthquakes from long record sites from Washington to southern Oregon, suggesting that five of the Lagoon Creek tsunamis were generated by earthquakes on the CSZ; either the same earthquakes as those affecting sites to the north, or earthquakes within the same seismic cycle. However, one sand layer at Lagoon Creek (S5) probably resulted from an earthquake that ruptured only the southernmost end of the Cascadia subduction zone or a local upper plate fault. No evidence for ground deformation during this event was found at the southern Oregon sites, however a tsunami deposit was identified at Bradley Lake with a similar age as Sand Layer S5.

REFERENCES CITED

- Abramson, H.F., 1998, Evidence for tsunamis and earthquakes during the last 3500 years from Lagoon Creek, a coastal freshwater marsh, northern California [M.S. Thesis]. Humboldt State University, 76 p.
- Atwater, B.F., and Hemphill-Haley, E., 1997, Recurrence intervals for great earthquakes of the past 3500 years at northeastern Willapa Bay, Washington: U.S. Geological Survey Professional Paper 1576, 108 p.
- Atwater, B.F., Tuttle, M., Schweig, E.S., Rubin, C.M., Yamaguchi, D.K., Hemphill-Haley, E., 2004, Earthquake recurrence inferred from paleoseismology. In Gillespie, A.R., Porter, S.C., Atwater, B.F., eds. *The Quaternary period in the United States, Developments in Quaternary Science*, Elsevier, New York, p. 331-350.
- Benson, B.E., Grimm, K.A., Clague, J.J., 1997, Tsunami deposits beneath tidal marshes on northwestern Vancouver Island, British Columbia: *Quaternary Research*, v. 48, p. 197-204.
- Dawson, S., Smith, D. E., Ruffman, A., and Shi, S., 1996, The diatom biostratigraphy of tsunami sediments: Examples from Recent and Middle Holocene events: *Phys. Chem. Earth*, v. 21, no. 1-2, p. 87-92.
- Garrison-Laney, C.E., 1998, Diatom evidence for tsunami inundation from Lagoon Creek, a coastal freshwater pond, Del Norte County, California [M.S. Thesis]. Humboldt State University, 97p.
- Garrison, C.E., and Abramson, H.F., 1997, Evidence for repeated tsunami inundation from two freshwater coastal marshes, Del Norte County, California: *Geological Society of America Abstracts with Programs*, v. 29, no. 5, p. 15.
- Heiken, G., 1978, Plinian-type eruptions in the Medicine Lake highland, California, and the nature of the underlying magma, *Journal of Volcanology and Geothermal Research*, v. 4, p. 375-402.
- Hemphill-Haley, E., 1996, Diatoms as an aid in identifying late-Holocene tsunami deposits: *The Holocene*, v. 6, no. 4, p. 439-448.
- Hemphill-Haley, E., and Lewis, R.C., 2003, Diatom data from Bradley Lake, Oregon: downcore analyses: U.S. Geological Survey Open-File Report 03-190.
- Hutchinson, I., Guilbault, J.-P., Clague, J. J., and Bobrowski, P. T., 2000, Tsunamis and tectonic deformation at the northern Cascadia margin: a 3000-year record from Deserted Lake, Vancouver Island, British Columbia, Canada: *The Holocene*, v. 10, p. 429-439.
- Kelsey, H.M., Witter, R.C., and Hemphill-Haley, E., 2002, Plate-boundary earthquakes and tsunamis of the past 5500 yr, Sixes River estuary, southern Oregon: *Geological Society of America Bulletin*, v. 114, no. 3, p. 298-314.

- Kelsey, H.M., Nelson, A. R., Hemphill-Haley, E., and Witter, R.C., 2005, Tsunami history of an Oregon coastal lake reveals a 4600 yr record of great earthquakes on the Cascadia subduction zone: *Geological Society of America Bulletin*, v. 117, n. 7/8, p. 1009-1032.
- Liu, K., and Fearn, M.L., 1993, Lake sediment record of late Holocene hurricane activities in coastal Alabama, *Geology*, v. 73, p. 793-796.
- Nelson, A.R., Shennan, I., and Long, A.J., 1996a, Identifying coseismic subsidence in tidal-wetland stratigraphic sequences at the Cascadia subduction zone of western North America: *Journal of Geophysical Research*, v. 101, no. B3, p. 6115-6135.
- Nelson, A.R., Jennings, A.E., and Kashima, K., 1996b, An earthquake history derived from stratigraphic and microfossil evidence of relative sea-level change at Coos Bay, southern coastal Oregon: *Geological Society of America Bulletin*, v. 108, no. 2, p. 141-154.
- Nelson, A.R., Kelsey, H.M., Witter, R.C., 2006, Great earthquakes of variable magnitude at the Cascadia subduction zone: *Quaternary Research*, v. 65, p. 354-365.
- Stuiver, M. and Reimer, P.J., 1993, Extended ^{14}C data base and revised CALIB 3.0 ^{14}C are calibration program: *Radiocarbon*, v. 35, p. 215-230.
- Stuiver, M., Reimer, P.J., Bard, E., Beck, J.W., Burr, G.S., Hughen, K.A., Kromer, B., McCormac, G., Plicht, JvD., Spurk, M., 1998, INTCAL98 radiocarbon age calibration, 24,000-0 cal B.P.: *Radiocarbon*, v. 40, p. 1041-1084.
- Witter, R.C., and Kelsey, H.M., 1996, Repeated abrupt changes in the depositional environment of a freshwater marsh: a record of Late Holocene paleoseismicity at Euchre Creek, south coastal Oregon: *Geological Society of America Abstracts with Programs*, v. 28, no. 5, p. 125.
- Witter, R.C., Kelsey, H.M., and Hemphill-Haley, E., 2003, Great Cascadia earthquakes and tsunamis of the past 6,700 years, Coquille River estuary, southern coastal Oregon: *GSA Bulletin*, v. 115, n. 10, p. 1289-1306.

Depositional Environments And Characteristics Of The Late Miocene Wimer Formation, Mill Creek Drainage, Crescent City, Del Norte County, California

Caroline Levenda

ABSTRACT

The new state park acquisition in Mill Creek is located east of Highway 101 and is accessed through the gated Hamilton Road located just a couple miles south of Crescent City and north of the Mill Creek Campground. The park is currently under watershed and stream restoration and road decommissioning. This former timberland was extensively logged and is vegetated with large areas of second-growth redwoods. Two large streams, Mill Creek and Rock Creek are located in the new state park acquisition. Mill Creek is tributary to the Smith River and has two main tributaries - the East Fork and West branch of Mill Creek. Rock Creek drains the east side of the new property and is a tributary to the South Fork Smith River. Wildlife, stream and forest ecology are being restored.

Franciscan complex basement rock, chiefly greywacke sandstone, and Quaternary fluvial terraces comprise the valley bottoms in the Mill Creek area (Aalto, 1984). Uplifted marine, estuarine, and fluvial sediments of the Late Miocene Wimer Formation have been discovered within the past 100 years to be associated with J.S. Diller's "Klamath Peneplain" and are situated on the ridgetops of the Coast Ranges including the Rattlesnake Mountains and the Little Bald Hills (Diller, 1902) (Figure 1). The Coast Range thrust fault trends northwestward and veers to the north as it approaches the Oregon border. Fractures, folds, and broken formations are associated with the thrust fault and the resistant Josephine ophiolite that constitutes the hanging wall of the fault accounts for the rugged terrain seen in the park.



Figure 1. A view of Diller's "Klamath Peneplain" (photo taken facing west)

The Wimer Formation has an estimated diatom age of Late Miocene (Stone, 1993). It consists of estuarine (brackish facies) sediments located approximately one to three kilometers inland of the Pacific Ocean coastline. The Wimer estuarine facies outcrops are uplifted, tilted, and highly fractured laminated sequences of mudstones and shales. Angular unconformities of uplifted Franciscan sandstones overlain by Wimer Formation sediments are visible along road cuts.

Further inland and at higher elevations, the fluvial facies of the Wimer Formation was discovered at elevations up to 800 meters (Stone, 1993). The fluvial facies is typical of braided stream deposits consisting of lenses and layers of sands and gravels. Large outcrops of the fluvial Wimer consist of massive pebble to boulder size conglomerates indicative of armored stream deposits (Figure 2). The deposits are highly weathered and most clast lithology is almost impossible to identify in the field. However, previous research has identified clasts originating from the Galice formation, Josephine Ophiolite, and others (Stone, 1993). Clasts have been identified as serpentinite, peridotite, volcanics, mafic igneous, latite, porcelanite, and grey, red and green cherts.



Figure 2. Fluvial facies of the Wimer Formation including pebble to cobble size clasts (A Jacobs staff is located to the right for scale).

REFERENCES CITED

- Aalto, K.R., and Murphy, J.M., 1984, Franciscan Complex geology of the Crescent City area, northern California, in Blake, M.C., Jr., ed., *Franciscan geology of northern California: Pacific Section, Society of Economic Paleontologists and Mineralogists Book 43*.
- Diller, J. S., 1902, *Topographic development of the Klamath Mountains*: U.S. Geological Survey Bulletin 196.
- Stone, L., 1993, *Pliocene-Pleistocene Sedimentary & Tectonic History of the Crescent City Smith River Region, Del Norte County, California*

REASSESSING CRESCENT CITY, CALIFORNIA'S TSUNAMI RISK

L.A. Dengler¹ and O.T. Magoon²

ABSTRACT

Twenty-two tsunamis have been recorded in Crescent City, California since 1938, eight exceeded 0.5 m amplitude and two caused significant damage. In 1964 at least four large waves were observed and peak water height was 6.7 m above MLLW, inundating twenty-nine city blocks damaging or destroying 300 homes and businesses. Eyewitnesses described a relatively gentle inflow with water elevation increasing at the rate of about 0.3 meters/minute reaching a peak elevation of about 3 meters above the land surface followed by stronger outflow that scoured rills into the margins of the harbor. Where water exceeded 1 m, a common cause of damage was floating houses off foundations. Mapped structure displacements indicate the outgoing flow was strongest. Tide gage recordings of other Crescent City tsunamis exhibit characteristic long duration with peak amplitudes occurring many cycles into the trace suggesting a strong influence of harbor resonance on wave characteristics. Spectral analyses of two records of the 1960 Chilean tsunami show a dominant 32 minute period (Wiegel, 1965) and duration of more than 20 hours. At least 6 paleotsunami events have been documented in cores from the Crescent City area, all larger than the 1964 event and attributed to megathrust earthquakes on the Cascadia subduction zone (CSZ). In the 41 years since the tsunamis, Crescent City has established a siren-based tsunami warning system and developed tsunami evacuation maps, posted signs along evacuation routes and is the only city in California currently designated "Tsunami Ready" by the National Weather Service's TsunamiReady program. During the June 14, 2005 tsunami warning for a M 7.2 Gorda Basin earthquake, Crescent City was the only community in the warning area to effectively evacuate the majority of its coastal residents. Offsetting recent mitigation efforts is recent development within the 1964 inundation zone and recognition of the significantly greater tsunami hazards posed by the Cascadia subduction zone. The Crescent City experience in 1964 is one of the few examples of how tsunami waves interact with typical West Coast architecture and infrastructure and its mitigation efforts provide a model for other California coastal communities.

Professor, Department of Geology, Humboldt State University, Arcata, California 95521
 President, Coastal Zone Foundation, 600 Chestnut St. Unit 409, San Francisco, CA 94133-3279

2

INTRODUCTION

Crescent City has experienced more tsunamis and greater damage than any other community in the continental United States outside of Alaska in historic times (Dengler and Magoon, 2005). Since a tide gage was installed on Citizens Dock in the 1930's, twenty-two tsunamis have been recorded and eight were 0.5 meters or larger. The March 27, 1964 9.2(M_w) Alaskan earthquake was particularly damaging in Crescent City, killing 11 and causing an estimated 15 million in 1964 dollars in losses (Lander et al, 1993). After the tsunami, an Army Corps of Engineers team surveyed the inundation zone in Crescent City and documented structural damage (Magoon, 1966). This study re-examines data collected by the Army Corps study and other archival material on the impacts of the tsunami in Crescent City, summarizes current tsunami risk assessment and recent mitigation efforts.

1964 tsunami in Crescent City

In 1964, Crescent City residents were familiar with tsunamis. Six tsunamis had been observed in the eighteen years prior to 1964 and two caused damage. The 1960 tsunami from the great Chilean earthquake flooded the Citizens Dock area and the beachfront up to Front Street, peaking at about 13 feet relative to Mean Lower Low Water (MLLW) (Wally Griffith, Personal Communication).

The 1964 sequence of events is reconstructed from the eyewitness accounts in Griffith (1984) and interviews with Crescent City eyewitnesses and emergency personnel. At 11:08 PM PST March 27, about 3 1/2 hours after the Alaska earthquake, the California Disaster Office issued a bulletin to coastal police and local disaster office officials that a "tidal wave" was probable but not confirmed. At 11:50 PM a similar bulletin issued by the State Civil Defense Office estimated the arrival time of the first wave as 12:00 AM March 28. Del Norte County Sheriff's Department received the bulletin and deputies were sent to low waterfront areas. The Sheriff did not

Table 1. Tsunamis recorded in Crescent City

Date	Tsunami Source Area	Amplitude (m)	Comments
November 10, 1938	Alaska Peninsula	0.2	
April 6, 1943	N. Central Chile	trace	
April 1, 1946	Unimak Island, Alaska	0.9	
December 20, 1946	Nankaido, Japan	0.2	
March 4, 1952	SE Hokkaido, Japan	0.2	
November 4, 1952	Kamchatka	1.0	4 boats overturned, concrete buoys moved
March 9, 1957	Central Aleutians, Alaska	0.7	
May 22, 1960	S. Central Chile	1.7	2 ships destroyed, \$30,000 damage
October 13, 1963	Kuril Islands, Russia	0.5	
March 28, 1964	Gulf of Alaska	4.8	described in this paper
February 4, 1965	W. Aleutian Islands, Alaska	0.1	
October 17, 1966	Peru	0.1	
May 16, 1968	Honshu, Japan	0.6	
July 26, 1971	New Ireland, PNG	trace	
October 3, 1974	Peru	trace	
May 7, 1986	Aleutian Islands, Alaska	0.1	
April 25, 1992	Cape Mendocino, California	0.6	Seiche in harbor
October 4, 1994	Kuril Islands, Russia	1.1	
June 22, 2001	S. Peru	0.4	
December 26, 2004	Indonesia	0.21	
September 25, 2003	Hokkaido, Japan	0.35	
June 15, 2005	Gorda basin, N. Calif	0.13	

From Lander et al, 1993 and West Coast Alaska Tsunami Warning Center

order an evacuation but suggested people leave the area and the deputies had not completed the door-to-door notification when the first wave arrived at 11:52 PM. Anecdotal reports suggest that most people had left the waterfront area before the first wave arrived.

The onset of the tsunami was a small negative wave that was not observed (Figure 1). The first positive wave caused modest flooding and deposited debris on the beach and Front Street in the downtown Crescent City area and near Citizens Dock, reaching 4.3 m (14.5 ft) MLLW or about 2.7 m above the ambient tide level (a high tide of about 2 m at the time of the first wave arrival). It is important to note that the area inundated by the first wave was very similar to the 1960 tsunami only 4 years before. After the first wave, the harbor emptied completely before the arrival of a second, smaller wave at 12:20 AM on March 28. This wave crested at about 1.5 meters (5 ft) above the ambient tide and did not reach Front Street. Some people reentered the waterfront area to check on homes or businesses, assuming the worst of the event had past. Others, hearing about the tsunami, came to sightsee.

There is some discrepancy about the arrival time and size of the later waves as the tide gage in the Crescent city harbor ceased recording as the third wave arrived a little after 1 AM. Eyewitnesses generally agreed that the third and fourth waves were both larger than the first wave, the third arriving at about 1:20 AM and the fourth and largest at 1:45 AM. From measurements of high water marks on land, it reached a height of about 6.7 m above MLLW or nearly 16 feet above the ambient tide (Magoon, 1966). By the time of the fourth wave, the sheriff had closed off the entire waterfront district to keep out sightseers and potential looters, but a general alarm was not issued until after the largest wave struck. Almost all of the damage and all the deaths were caused by this surge.

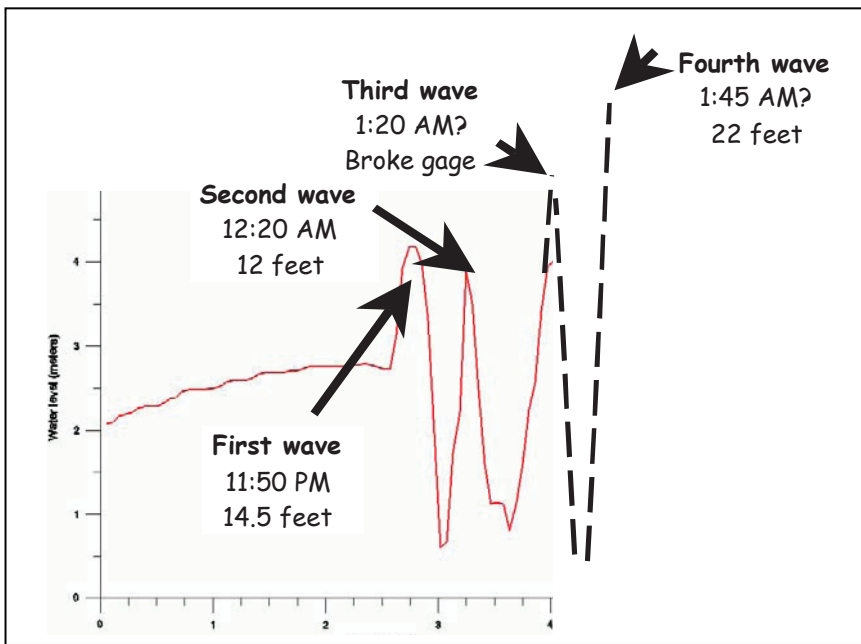


Figure 1: Marigram recovered from the Citizen's Dock tide gage after the 1964 tsunami (solid line). The instrument house was knocked over as the third positive wave arrived. Dashed line is a reconstruction based on eyewitness accounts.

Damage

The tsunami caused 11 deaths in Crescent City, destroyed 54 homes and damaged an additional 37 homes, displacing 150 people. One hundred seventy-nine businesses in a 29-block area were affected, 42 of which were totally destroyed. The cost (in 1964 dollars) is estimated at about \$15 million. Magoon (1966) conducted a post tsunami survey a week after the event, mapping the inundation zone, noting high water marks, and compiling an inventory of structural damage. High resolution air photos taken before and after the tsunami were used to observe the impacts (Figure 2).

By combining air photo analysis and field reconnaissance, Magoon (1966) constructed a contour map of water inundation depth and displaced structures (Figure 3).

The inundation at Crescent city reached a maximum depth on land of about 3 meters on Front Street between I and K and a maximum penetration inland of about 800 meters (.5 miles) in the Elk Creek Valley south of the Del Norte County Fair Grounds. Eyewitnesses generally described the incoming water as a gentle flow with water elevation increasing at the rate of about 0.3 meters/minute. The peak water elevation in the developed parts of the City reached about 2.5 meters above the land surface. At least 26 structures were floated off foundations and displaced. All of the displaced structures were wood-frame and unsecured to foundations and are only seen where the water depth is greater than 1 meter. National Flood Insurance Program data suggests that unsecured wooden homes float when flooding exceeds .3 meters (Chris Jones, Personal Communication 2004). In Crescent City, most homes sat on top of a .3 - .7 meter foundation (Figure 4), making the 1 meter water depth for floating



Figure 2: Air photos of the Crescent City Harbor area. A) October 1862, B) April 3, 1964. Note extensive evidence of scour. Arrow shows location of tide gage.

consistent with the NFIP data. Structures were most often displaced towards the harbor (Figure 3) suggesting that the outflow was stronger than the incoming waves.

At least 15 structures were damaged by the impact of debris. The most well-known example of the effect of impact is the 25 ton tetrapod near 2nd and N Street that was displaced 2.5 meters off of a concrete pad (Figure 5A). This displacement was erroneously used to estimate water flow velocity assuming that the displacement was caused by water pressure alone (Tudor, 1964). Eye witnesses observed the log in Figure 5 hit the tetrapod.

Some structures appear to have the walls blown outwards (Figure 5 B). The tsunami caused flooding of the buildings and when the waters receded, waters drained more slowly from within structures producing an outward pressure on the walls.

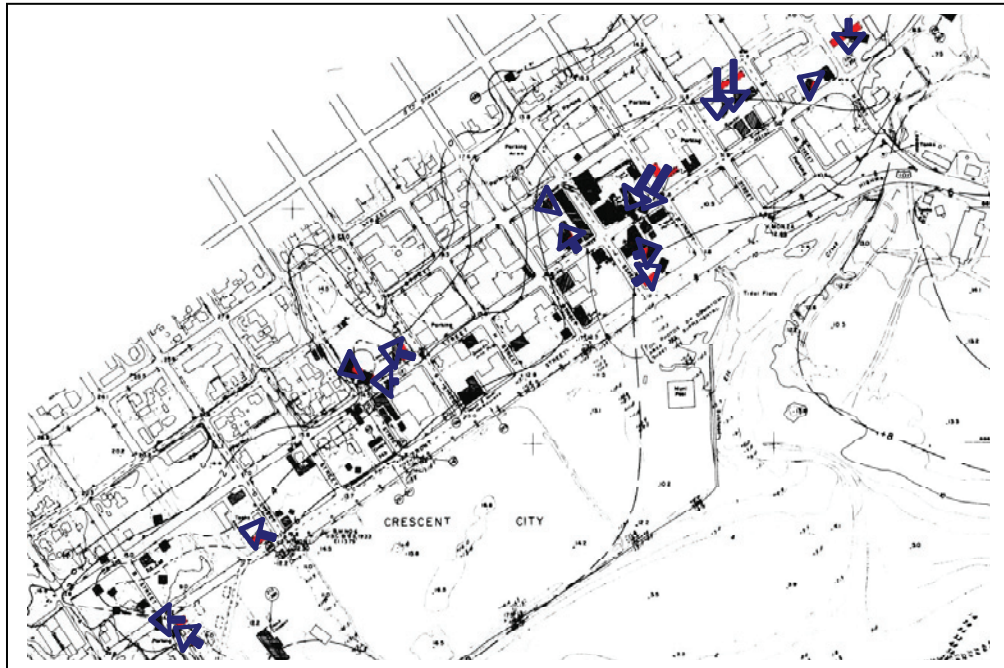


Figure 3: Contours of water inundation depth from Magoon (1966). Dark building displaced and/or destroyed. Arrows show displacement direction.

Redevelopment

The Army Corps of Engineers defined a redevelopment zone that encompassed most, but not all, of the inundation zone. Curiously the 4-story Surf Hotel on Front Street, then owned by movie mogul Lloyd Bridges, was excluded. For structures within the Redevelopment Zone, property owners were given the choice of bringing the building up to current codes or selling them at market value to the Redevelopment Agency for demolition. Almost everyone chose the latter and only a handful of pre-1964 structures still stand today. One of the structures in the zone was the Odd Fellows Hall, a 20-story wooden structure that had floated off its stone foundation with no significant damage. The sturdy old-growth redwood structure proved difficult to destroy.



Figure 4: Foundation of the Crider home, Front and J Street. Unsecured home floated and displaced 5 meters.

Rebuilding of residential structures was excluded from the redevelopment zone. Much of 2nd Street was replaced with “Tsunami Landing”, a covered walkway meant to encourage small shops and businesses. Unfortunately few materialized. A major addition to the area was in 1973 when the newly created Redwood National Park built its headquarters on K Street. Construction featured a tsunami resistant design with most of the work space built on piers on the second floor. Unfortunately the structure, built in 1973, does not meet the revised ground shaking estimates of the current UBC and its future is uncertain. The Surf Hotel remained derelict until 1998 when redeveloped funds were obtained from the Federal Agency on Aging and the building was converted into Senior Apartments. It is ironic that the only residents of the 1964 tsunami inundation zone are senior citizens.



Figure 5: A) 25 ton tetrapod displaced by log impact. B) Home damage by water pressure bursting out sides.

The bulk of new development in the past two decades has been along the 101 corridor south of Crescent City. This area, relatively undeveloped in 1964 but within the 1964 inundation zone is now home to 4 large hotels, an RV park, an aquatic park and numerous other commercial structures. Unlike the old downtown area flooded in 1964, the new development area poses a more difficult evacuation problem. The downtown area provides easy foot access to higher ground. The inland area northeast of South 101 is blocked by a series of fresh water marshes. Evacuees need to travel up to 2 miles north or south parallel to the coast before they can turn inland.

Reassessing Crescent City’s Tsunami Hazards

In 1992 a magnitude 7.1 earthquake occurred near Cape Mendocino in Humboldt County, about 90 miles (150 km) south of Crescent City. The earthquake caused about \$60 million in property damages related to ground shaking and also generated a small tsunami that was recorded in Crescent City and a several other locations in California and Oregon (Gonzales et al, 1995). The tsunami, while not damaging, reinvigorated interest in tsunami hazards and in assessing the potential vulnerability of not only distant source tsunamis like the 1964 event but also local sources like the Cascadia subduction zone (CSZ).

The CSZ extends from Cape Mendocino, California to Vancouver Island, Canada and has not produced a great earthquake ($M \geq 8.0$) in historic times. With the exception of the 1992 Cape Mendocino sequence at the southern end of the CSZ, the zone has been almost entirely devoid of earthquakes of any size. In the 1980’s a series of papers (summarized by Atwater et al, 1995) examined the seismic potential of Cascadia and there is now nearly unanimous agreement in the scientific community the CSZ produced at least seven great earthquakes in the past 2000 years. The most recent, in 1700, produced a tsunami that left deposits along the West Coast of North America from Humboldt Bay, California to Vancouver Island, Canada and caused damage in Japan and is estimated to have a magnitude of 9.0 (Satake et al, 2003).

The same freshwater marshes near Highway 101 in Crescent city that hinder evacuation are also excellent tsunami traps (Figure 7). The marsh was flooded by both the 1960 and 1964 tsunamis, leaving clearly delineated sand lenses behind. Above and below the tsunami sands are organic rich peat deposits; there is no evidence that winter storm waves have ever left deposits at this site. At about 70 cm below the surface and 40 cm below the 1960



Figure 7: A) Crescent Beach motel after the 1964 tsunami. B) Core taken from the pond in the upper right, just west of Highway 101.

deposit a prominent 20 cm thick sand lens is seen. There are no intervening peat layers and the deposit most likely represents a single event, the most recent CSZ event in 1700.

Tsunami inundation modeling of Crescent City (Bernard et al,

1994) show the likely inundation from a Cascadia earthquake to extend approximately twice as far inland as the 1964 zone leaving the entire downtown area south of 9th Street vulnerable.

Mitigation

Not surprisingly, interest in tsunami mitigation was high in 1964 immediately after the tsunami. The Del Norte County Civil Defense Office developed tsunami plans and installed two evacuation sirens. The Pacific Tsunami Warning System was reorganized and the Alaska Tsunami Warning Center was established in Palmer, Alaska and eventually became the West Coast/Alaska Tsunami Warning Center with responsibility for issuing warnings to Alaska and the West coast of the United States and Canada. However only two tsunami warnings have been issued for the Crescent City Area since 1964 (May 1986 and October 1994) and both produced no damaging waves. Interest in tsunamis waned, the sirens ceased to function and a generation grew up with no memory of the 1964 event. Population of Del Norte County significantly increased in 1990 with the establishment of Pelican Bay Prison and its large support staff, most from out of the area with little or no tsunami awareness.

The 1992 Cape Mendocino earthquake and tsunami caused concern for locally generated tsunamis from the Cascadia subduction zone and led to the formation of the National Tsunami Hazard Mitigation program (NTHMP) in 1996 (Bernard, 1998). The program strengthens the tsunami warning infrastructure, supports inundation mapping and promotes mitigation activities. Although Crescent City has not received direct funding through the program, the NTHMP has stimulated local tsunami mitigation efforts and improved tsunami planning. Tsunami Bulletins for earthquakes within the Pacific are now routinely issued and received within 20 minutes of the earthquake and North American earthquake information disseminated within 5 minutes of the event. Crescent City refurbished its sirens and now conducts monthly tests of the system. Using the 1994 inundation model results (Bernard et al, 1994) and paleotsunami data, the City compiled and evacuation map and installed tsunami evacuation signs (Figure 8). In September 2003, Crescent City became the first community in California to be designated *Tsunami Ready* under the National Weather Service TsunamiReady program.

On June 14, 2005 at 7:51 PM PDT a M 7.2 earthquake occurred in the Gorda Basin 157 km WSW of Crescent City. The earthquake was felt lightly (MMI IV) by most people in the Crescent City area. The West Coast Alaska Tsunami Warning Center sent out a Tsunami Warning Bulletin for the entire West Coast of the Continental United States 5 minutes after the event. The Sheriff's Office in Del Norte County received the warning message and an estimated arrival time of the first wave, if generated, at 8:29 PM. In spite of complete communications gridlock

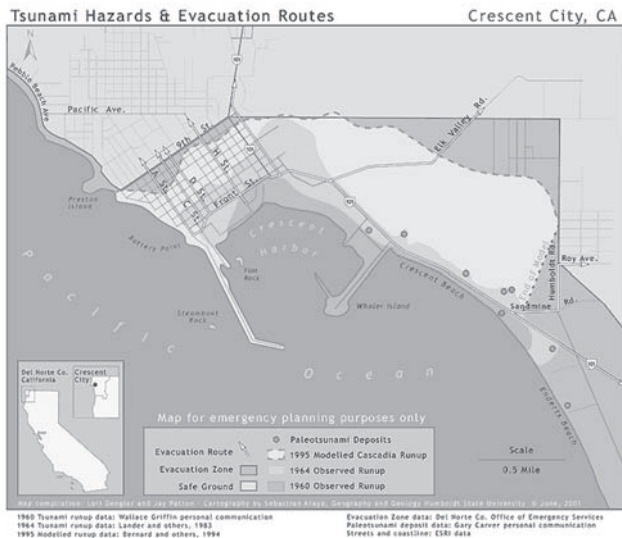


Figure 8: Crescent City tsunami hazards and evacuation zone

and the absence of a number of key emergency personnel including the County OES Director and the City and regional Fire Chiefs, a decision was made to sound the alarm and the siren rang continuously from 8:05 until 8:50 PM when the tsunami warning cancellation notice was received. Approximately 4000 people evacuated the coastal area (Renteria, 2005; Del Norte Triuplicate, 2005; Winogradov, personal communication). No other California County effectively evacuated coastal areas.

DISCUSSION

Crescent City is unusual on the US West Coast for the large amplitude and unusual long duration of tsunami signals compared to nearby coastal sites. Investigators considering this anomaly

have suggested a number of possible reasons or causes of this anomaly. Wilson and Torum (1968) suggest that the 30 to 35 minute period oscillations noted in the 1964 tsunami “would accord with the third harmonic of the incident tsunami wave” which they reported as a 1.77-hour period. They further state “That this frequency could have gained such large response suggests that some topographical feature of the region must provide resonant conditions and suggest the shape and bathymetry offshore between Pt. St. George and Patrick’s Point could be the cause. Keulegan et. al. (1969) in analyzing the high speed water level recordings taken during the May 1960 tsunami at Citizen’s Dock and Dutton’s Dock at Crescent City, note that “predominate periods of 80.0, 33.0, 22.0, and 18.0 minutes are clearly defined in all cases and can be accepted with confidence. These predominate periods are in good agreement with periods computed by consideration of the oscillations of the Crescent City area from the offshore area to the beach”. Roberts and Kauper (1964) suggest that the “submarine morphology and direction of propagation of the (1964) tsunami, appear to be the apparent cause of the focusing of the wave energy at Crescent City”. They note two seamounts approximately 400 miles and 150 miles northwest of the Crescent City harbor, Edge (personal communication, 2005) suggests that trapped edge waves may also be partly responsible for the relatively high waves at Crescent City. Wiegel (personal communication, 2005) suggested that consideration should be given to the combined effects of more than one cause in producing the high tsunami values at Crescent City.

Crescent City provides one of the best examples for the interaction of a developed area and tsunami waves. The main cause of damage in 1964 was the floating of wood frame structures and the impact of large debris. With the improved detection of potentially tsunamigenic events, rapid dissemination of warning bulletins, tsunami sirens and posted evacuation routes, Crescent City is in considerably better shape today to deal with a repeat of a 1964 tsunami. Crescent City’s evacuation after the June 2005 tsunami warning illustrates the success of their tsunami planning efforts. Of much more concern now is a locally-generated tsunami from the Cascadia subduction zone where the time for response is minutes and people will need to self-evacuate with little or no official assistance and the impacts will be exacerbated by strong ground shaking.

REFERENCES CITED

- Atwater, B. F., Nelson, A.R., Clague, J.J., Carver, G.A., Yamaguchi, D.K., Bobrowsky, P.T., Bourgeois, J. Darienzo, M.E., Grant, W.C., Hemphill-Haley, E., Kelsey, H.M., Jacoby, G.C., Nishenko, S.P., Pammer, S.P., Peterson, C.D., Reinhart, M.A., 1995, Summary of coastal geologic evidence for past great earthquakes at the Cascadia subduction zone, *Earthquake Spectra*, 11.1, p.1-10.
- Bernard, E.N., 1998: Program aims to reduce impact of tsunamis on Pacific states. *Eos, Transactions, American Geophysical Union*, 79(22), 258, 262-263.

- Bernard, E., Mader, C., Curtis, G., and Satake, K., (1994) *Tsunami Inundation Model Study of Eureka and Crescent City*, California, NOAA Technical Memorandum ERL PMEL-103, National Oceanic and Atmospheric Administration, Seattle, Washington, 80 pp.
- Gonzales, F., Bernard, E., Satake, K., 1995, The Cape Mendocino tsunami, 25 April 1992, in Tsuchiya, Y., Shuto, N. eds *Advances in Natural and Technological Hazards Research*, vol 4, p 151-158.
- Del Norte Triplicate, June 14 2005, Crescent City CA http://www.triplicate.com/news/story.cfm?story_no=1804
- Dengler, L., Magoon, O., 2005, The 1964 Tsunami in Crescent City, California: A 40-year retrospective, *Proceedings Solutions to Coastal Disasters, 2005*, ASCE.
- Griffin, W., 1984, *Crescent City's Dark Disaster*, Crescent City Printing Co., Crescent City, CA, 188 pp.
- Keulegan, G. H., Harrison, J., and Matthews, M.J., 1969, Theoretics in The Design or the Proposed Crescent City Harbor Tsunami Model
- Lander, J.F., 1996, *Tsunamis Affecting Alaska, 1737 – 1996*, NGDC Key to Geophysical Research Documentation No. 31, United States Department of Commerce, NOAA, 195 pp.
- Lander, J.F., Lockridge, P., 1989, *United States Tsunamis*, Publication 41-2, National Geophysical Data Center, U.S. Department of Commerce, Boulder Co., 265pp.
- Lander, J.F., Lockridge, P., Kozuch, M. (1993), *Tsunamis Affecting the West Coast of the United States 1806-1992*, NGDC Key to Geophysical Records Documentation No. 29, U.S. Dept. of Commerce
- Magoon, O.T., 1962, The tsunami of May 1960 as it affected Northern California, ASCE Hydraulics Division Conference, Davis, California 18 pp.
- Magoon, Orville T., 1966, Structural Damage by Tsunamis, Proceedings, American Society Civil Engineers, Specialty Conference on Coastal Engineering, Santa Barbara, California, Oct. 1965, 35-68.
- Renteria, H.R., 2005, *Preliminary Internal Review: June 14, 2005 Tsunami Warning M7.2 Gorda Plate Earthquake offshore of Humboldt County*, Governor's Office of Emergency Services State of California, 49 pp.
<http://www.oes.ca.gov/Operational/OESHome.nsf/PDF/Tsunami%20Review/>
- Roberts, James A., and Kauper, Edwin K., 1964, The Effects of Wind and Precipitation on the Modification of the South Beach, Crescent City, including An Appendix on the Focusing of Tsunami Energy at Crescent City. Atmospheric Research Group.
- Satake, K., Wang, K., Atwater, B., 2003, Fault slip and seismic moment of the 1700 Cascadia earthquake inferred from Japanese tsunami descriptions, *Journal Geophysical Research*, vol. 108, B11, 2535-2552.
- Tudor, W.J., 1964, *Tsunami Damage at Kodiak, Alaska and Crescent City, California, from Alaskan Earthquake of 27 March 1964*, Technical Note No. N-622, U.S. Naval Civil Engineering Laboratory, Port Hueneme, Calif., Nov. 1964, 128 pp.
- Wiegel, R.L., 1965, *Protection of Crescent City, California from tsunami waves*, Report for the Redevelopment Agency of the City of Crescent City, 5 March 1965 Berkeley, California 114 pp.
- Wilson, B.W., Torum, A., 1967, *Final Report: Engineering Damage from the Tsunami of the Alaskan Earthquake of March 27, 1964*, Coastal Engineering Research Center, Corps of Engineers, U.S. Army, Contract No. DA-49-055-CIVENG-66-6, Science Engineering Associates, San Marino, CA
- Wilson, B.W., Torum, A., 1968, *The Tsunami of the Alaskan Earthquake, 1964: Engineering Evaluation Tech. Memo No. 25*, Coastal Engineering Research Center, U.S. Army Corps of Engineers, Washington, D.C., 401 pp.

Evidence for Paleotsunami at Crescent City, Northern California

K. R. Aalto, Dept. of Geology, Humboldt State University, Arcata, CA 95521
C. E. Garrison-Laney, Quaternary Research Center, Univ. of Washington, Seattle, WA 98195
D. T. Robinson, Mission Geoscience Inc., 2082 Michelson Dr., Irvine, CA 92612

SUMMARY: PEBBLE BEACH FIELD TRIP STOP

A paleosol developed on the Mesozoic Franciscan Complex is depositionally overlain by 48 m of late Miocene (diatom age ca. 6.0-6.4 Ma), mostly shallow-marine Saint George Formation (Fig. 1 - 3). At the base of this sequence is a buried paleoforest of rooted tree stumps (Fig. 3a) and fallen logs, found at three separate sites. Many of the largest logs preserved within basal Saint George Formation strata lie with their long dimensions oriented generally north-northwest to north-northeast (Fig. 3a). Above the rooted stumps is a sequence of wave-reworked colluvium containing woody debris interpreted as a tsunami deposit, succeeded by beach deposits, and bioturbated, mollusk-rich mudstone having occasional hummocky cross-stratified sandstone interbeds (Fig. 1 - 3). Although fossils are consistent with deposition in either a bay environment or open marine conditions, the appearance upsection of hummocky cross-stratified sandstone suggests that the deposition site was open to the ocean and permitted incursion of large storm and/or tsunami waves. Destruction of the forest appears to have been a single sudden event and may relate to rapid subsidence engendered by plate-boundary earthquakes or large-scale slumping.

Recent bedrock-sculpturing of semilithified Saint George Formation sandy mudstone exposed on a wave-cut platform has produced a variety of erosional forms, including grooves, which may be straight or sinuous (Fig. 3cdf). Straight grooves form preferential incision of regional joints. Sinuous grooves are not fracture-controlled, are oriented parallel to wave run-up and exist as closely-spaced subparallel, non-connecting, internally-drained grooves that are best developed on higher platform ramparts and benches. Sinuous grooves have a mean length of 258 cm, mean maximum width of 14 cm, mean width/length ratio of 0.08, mean groove edge-to-edge minimum spacing of 16 cm, and mean trough-to-trough spacing of 28 cm. They are not as deeply incised as straight grooves, do not serve as conduits for low-tide runoff during winter months, and typically terminate by shallowing and narrowing in both seaward and landward directions. Sinuous appearance results from trains of linked comma-shaped depressions, commonly with the blunt, highly curved end of each being most deeply incised and oriented seaward (Fig. 3d). Corrasion of bedrock highs and/or cavitation associated with turbulent vortices during tsunami run-up may have contributed to the genesis and/or enlargement of grooves. Bryant and Young (1996) interpret sinuous grooves in Australia as erosional features developed by cavitation during tsunami run-up. These are carved into unweathered diorite and are somewhat similar in appearance to those at Pebble Beach. Shaw (1988) describes curved flutes arranged so as to intertwine in succession with their concave faces oriented towards a central axis and their blunt ends oriented downflow. These are quite similar in scale and appearance to many sinuous grooves exhibiting seaward scour preference at Pebble Beach. He ascribes their origin to impingement of curved, entwined helical vortices on bedrock accompanied by cavitation.

Crescent City was the site of a destructive tsunami following the 1964 Alaskan earthquake. Vibracoring in backbeach freshwater marshes in the Crescent City area reveals the presence of multiple (up to 13) tsunami-derived sands interstratified with peat horizons (Garrison et al., 1997; Garrison-Laney, 1998). Auguring and coring in a back-barrier bog at Pebble Beach and diatom analysis reveals a landward-thinning, ~17 cm-thick, laterally continuous clean, tsunami-emplaced sand layer with a sharp basal contact up to 125 m inland of the modern high tide line (Fig. 3e). Based upon depth of burial, distance of sediment transport and overall thickness, the Pebble Beach tsunami sand is most likely coeval with a tsunami-emplaced sand yielding

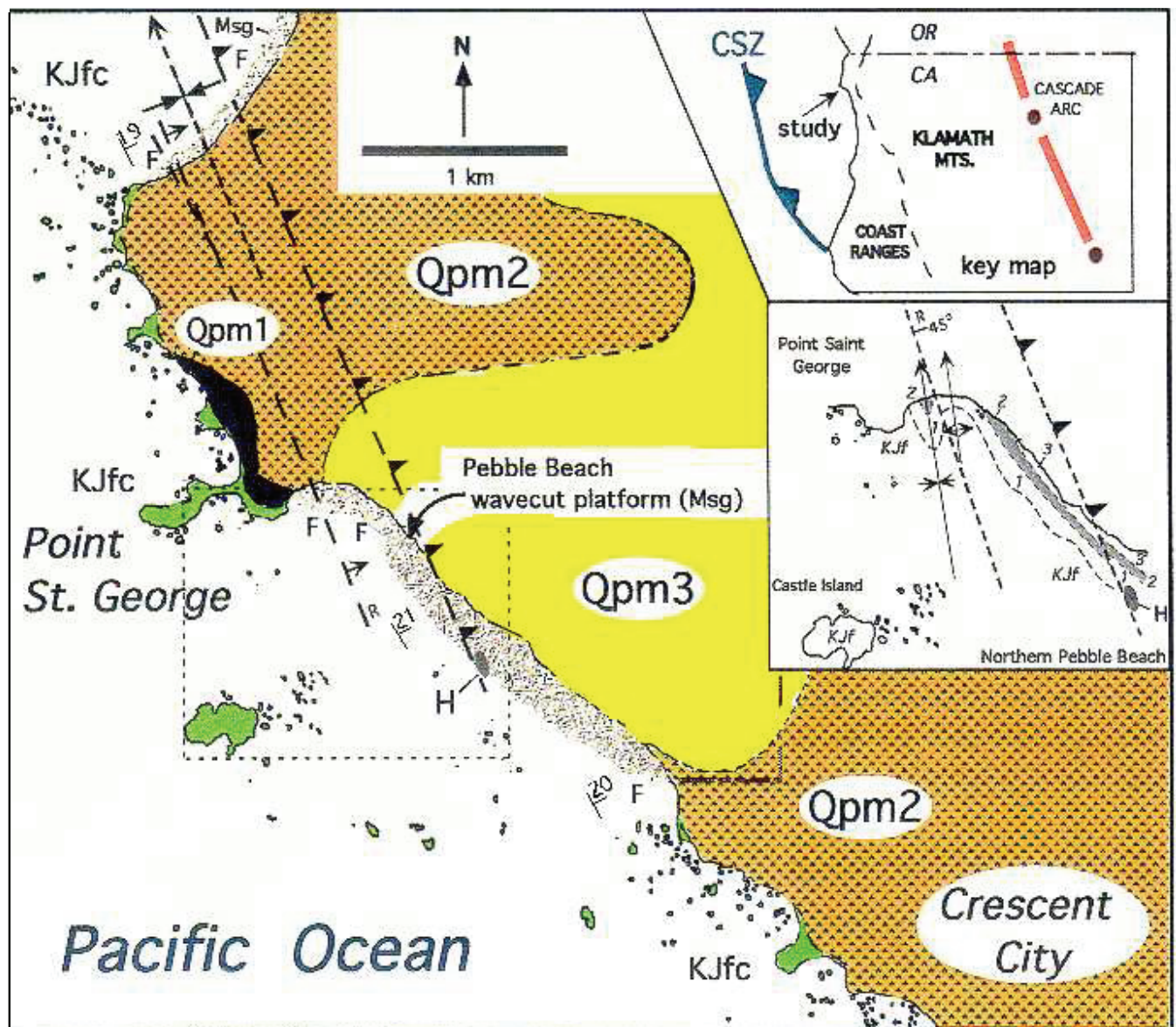
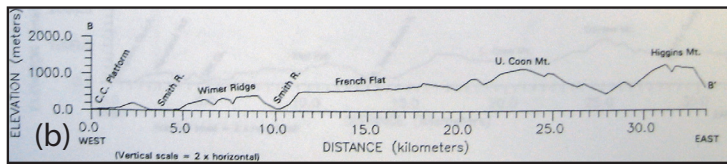
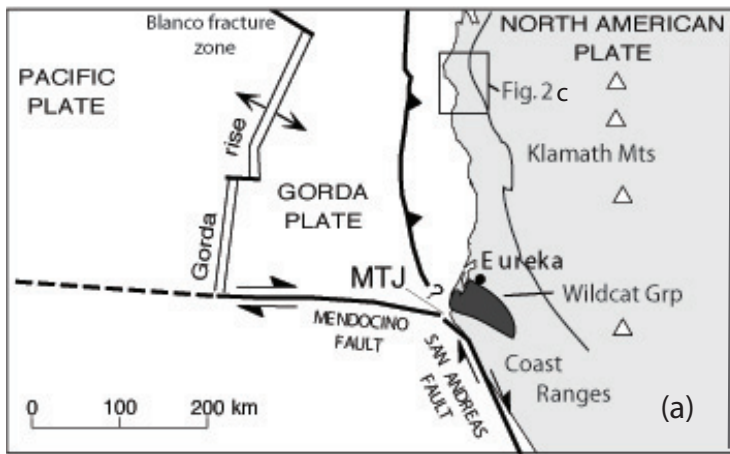


Figure 1. Geologic map of the Crescent City headland. Holocene peat at 'H' yielded a conventional radiocarbon date of 3000 \pm 60 BP from two pine cones from this peat (the 2 sigma calibrated range is Cal BP 3355 to 2980, Beta Analytic, Inc., Miami, FL). Inset map shows structural detail at the north end of Pebble Beach with Saint George units 1–3 delineated (mapping by Aalto). Geology is modified from Aalto (1989), Polenz and Kelsey (1999) and Robinson (2001).

calibrated radiocarbon ages between 1,300 and 1,820 yr. BP (Aalto, et al., 1999). The Crescent City headlands have repeatedly been the site of tsunami inundation during the Late Cenozoic, according to stratigraphic and paleontologic evidence found in the Late Miocene Saint George Formation and Holocene bog deposits. In addition, unusual bedrock erosional forms carved during supercritical flow are best ascribed to tsunami currents. Consideration of such high energy events (event stratigraphy) must be appreciated in our reconstruction of earth history.



(d)

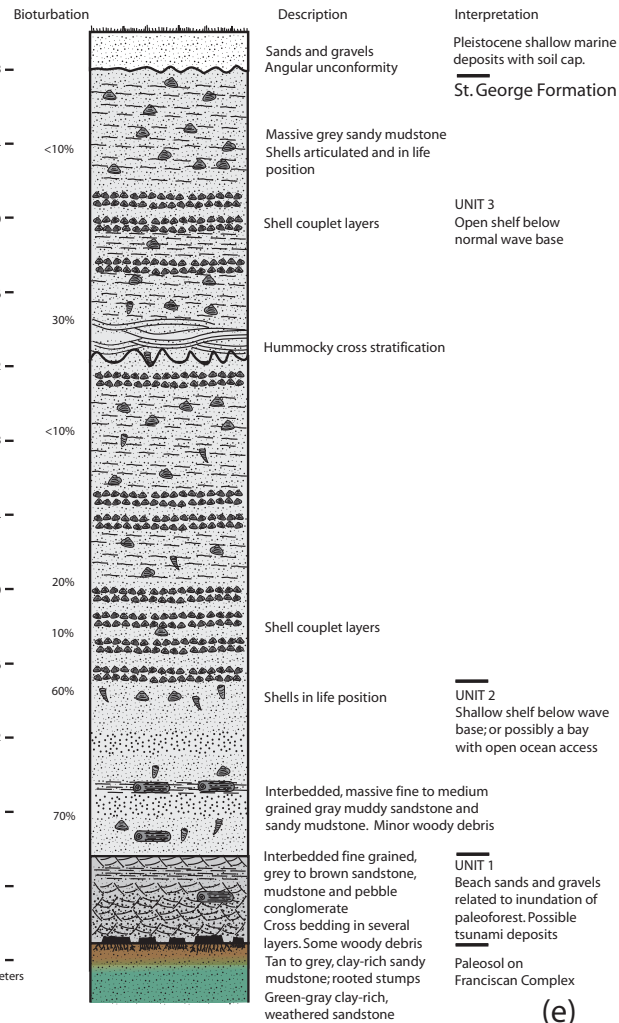
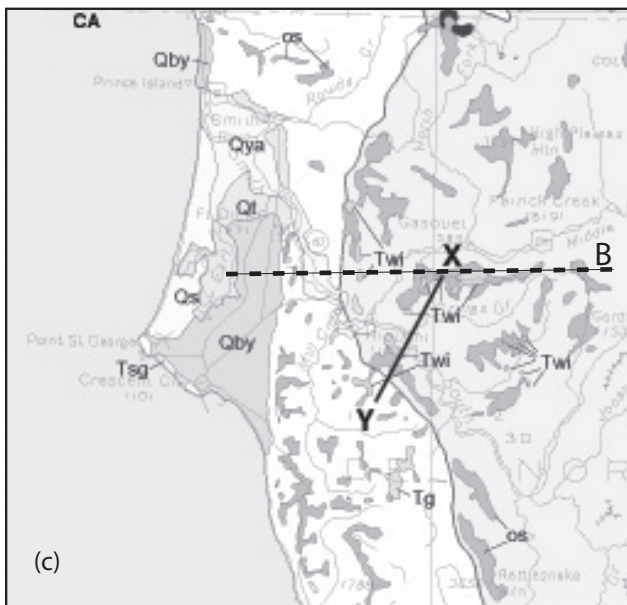


Fig. 2 a) Regional tectonic map, b) east-west topographic profile along line 'B' showing the westward-dipping Klamath erosion surface [Diller's 'Klamath Peneplain'] (from Stone, 1993), c) Cenozoic geology: of note are variously labeled Quaternary terraces [Q-deposits] and the Tertiary Saint George [Tsg] and Wimer [Twi] Fms. Line B is the profile above; X-Y delineates the marine-nonmarine Wimer facies contact (from Stone, 1993 and Irwin, 1997, d) view west from site near south end of line X-Y, e) generalized stratigraphic column measured at north Pebble Beach (Fig. 1). The bioturbation index is that of Miller and Smail (1997) (from Robinson, 2001).

(e)

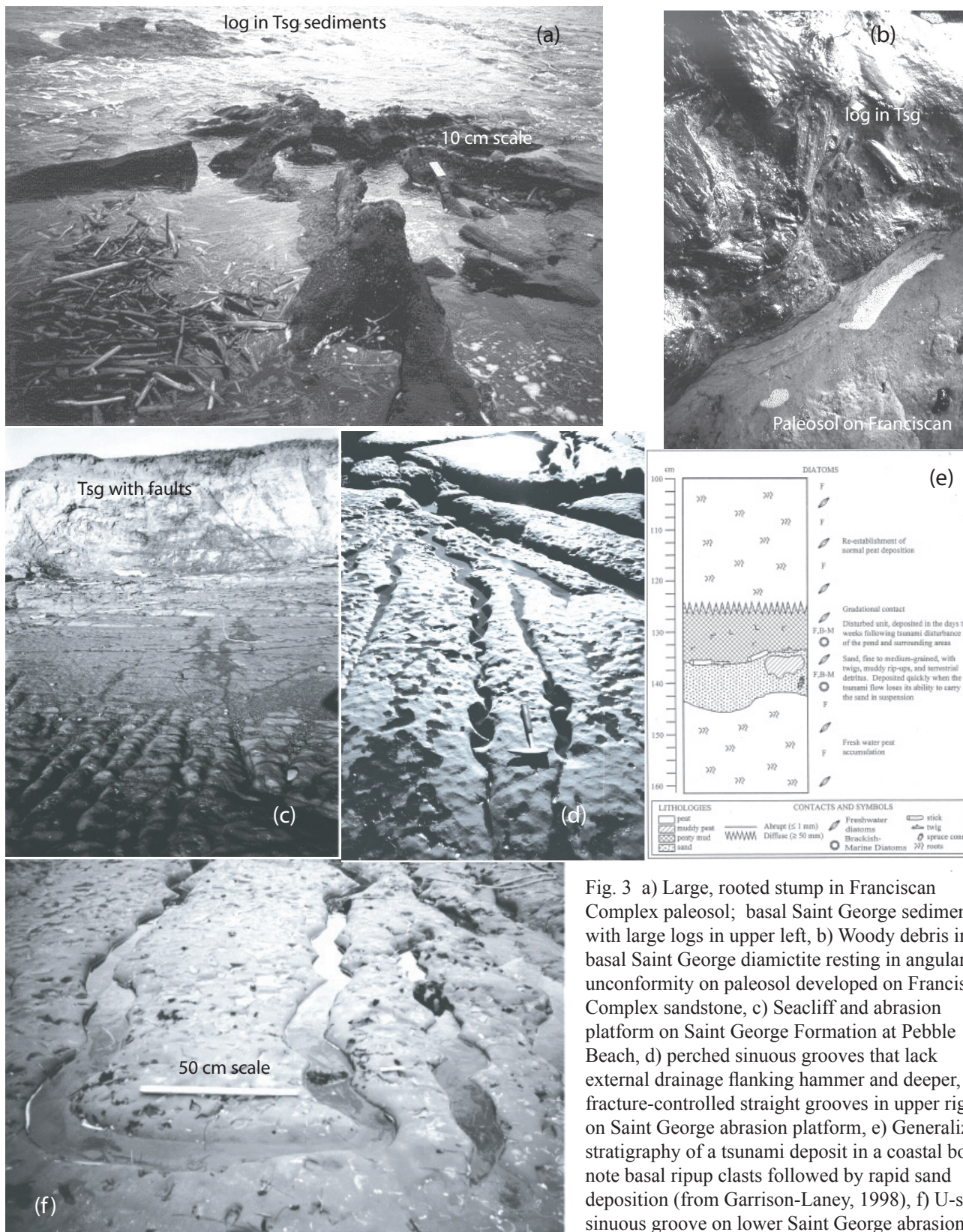


Fig. 3 a) Large, rooted stump in Franciscan Complex paleosol; basal Saint George sediments with large logs in upper left, b) Woody debris in basal Saint George diamictite resting in angular unconformity on paleosol developed on Franciscan Complex sandstone, c) Seacliff and abrasion platform on Saint George Formation at Pebble Beach, d) perched sinuous grooves that lack external drainage flanking hammer and deeper, fracture-controlled straight grooves in upper right on Saint George abrasion platform, e) Generalized stratigraphy of a tsunami deposit in a coastal bog-note basal ripup clasts followed by rapid sand deposition (from Garrison-Laney, 1998), f) U-shaped sinuous groove on lower Saint George abrasion platform (down-platform towards bottom).

REFERENCES CITED

- Aalto, K. R., 1989, Franciscan Complex olistostrome at Crescent City, northern California: *Sedimentology*: v. 36, p. 471 – 495.
- Aalto, K. R., Aalto, R., Garrison-Laney, C.E., and Abramson, H.F., 1999, Tsunami (?) sculpturing of the Pebble Beach Wave-cut Platform, Crescent City area, California: *Journal of Geology*, v. 107, p. 607-622.
- Bryant, E. A., and Young, R. W. 1996. Bedrock-sculpturing by tsunamis, South Coast, New South Wales, Australia: *Journal of Geology*, v. 104, p. 565-582.
- Garrison, C. E.; Abramson, H. F.; and Carver, G. A. 1997. Evidence for repeated tsunami inundation from two freshwater coastal marshes, Del Norte County, California: *Geological Society of America Abstracts with Programs*, v. 29, p. A15.
- Garrison-Laney, C. E., 1998, Diatom evidence for tsunami inundation from Lagoon Creek, a coastal freshwater pond, Del Norte County, California: unpublished M. S. thesis, Humboldt State University, 97 p.
- Irwin, W. P., 1997, Preliminary map of selected post-Nevadan geologic features of the Klamath Mountains and adjacent areas, California and Oregon: U. S. Geological Survey Open File Report 97-465, 29 p.
- Miller, M.F., and Smail, S.E., 1997, A semiquantitative method for evaluating bioturbation on bedding planes: *Palios*, v. 12, p. 391-396.
- Polenz, M., and Kelsey, H. M., 1999, Development of a Late Quaternary marine terraced landscape during on-going tectonic contraction, Crescent City coastal plain, California: *Quaternary Research*, v. 52, p. 217 – 228.
- Robinson, D. R., Aalto, K. R., Barron, J. A., Jayko, A. S., and Erwin, D. M., 2001, Marine inundation of a Late Miocene forest: stratigraphy and tectonic evolution of the St. George Formation, Crescent City, California: *California Geology*, v. 54, p. 10 – 22.
- Robinson, D., R., 2002, Marine inundation of a Late Miocene forest: Stratigraphy and tectonic evolution of the Saint George Formation, Crescent City, California: [unpublished M.S. Thesis] Humboldt State University, Arcata, CA, 86 p.
- Shaw, J., 1988, Subglacial erosional marks, Wilton Creek, Ontario: *Canadian Journal of Earth Sciences*, v. 25, p. 1256-1267.
- Stone, L., 1993, Pliocene-Pleistocene sedimentary and tectonic history of the Crescent City-Smith River region, Del Norte County, California: [unpublished M.S. Thesis] Humboldt State University, Arcata, CA, 234 p.

GEOLOGIC AND SEISMIC SETTING

Mark Hemphill-Haley, Todd Williams, and Jay Stallman

REFERENCES CITED

- Atwater, B., F., Nelson, A.R., Clague, J.J., Carver, G.A., Yamaguchi, D.K., Bobrowsky, P.Y., Bourgeois, J., Darienzo, M.E., Grant, W.C., Hemphill-Haley, E., Kelsey, H.M., Jacoby, G.C., Nishenko, S.P., Palmer, S.P., Peterson, C.D., and Reinhart, M.A., 1995, Summary of coastal geologic evidence for past great earthquakes at the Cascadia Subduction Zone: *Earthquake Spectra*, v. 11, p. 1-18.
- Atwater, B.F., and Hemphill-Haley, E., 1997, Recurrence Intervals for Great Earthquakes of the Past 3,500 Years at Northeastern Willapa Bay, Washington: United States Geological Survey Professional Paper 1576, p. 108.
- Atwater, T., 1970, Implications of plate tectonics for the Cenozoic tectonic evolution of western North America: *Geological Society of America Bulletin*, v. 81, p. 3513-3536.
- Bakun, W.H., 2000, Seismicity of California's north coast: *Bulletin of the Seismological Society of America*, v. 90, p. 797-812.
- Beaudoin, B.C., Godfrey, N.J., Klemperer, S.L., Lendl, C., Trehu, A.M., Henstock, T.J., Levander, A.R., Holl, J.E., Meltzer, A.S., Luetgert, J.H., and Mooney, W.D., 1996, Transition from slab to slabless; results from the 1993 Mendocino triple junction seismic experiment: *Geology*, v. 24, p. 195-199.
- Burke, R.M., Carver, G.A., Lundstrom, S.C., and Anonymous, 1986, Soil development as a relative dating and correlation tool on marine terraces of Northern California: Abstracts with Programs - Geological Society of America, v. 18, p. 91.
- Carver, G.A., Burke, R.M., and Dickinson, W.R., 1987, Late Pleistocene and Holocene paleoseismicity of Little Salmon and Mad River thrust systems, N.W. California; implications to the seismic potential of the Cascadia subduction zone: Abstracts with Programs - Geological Society of America, v. 19, p. 614.
- Carver, G.A., and McCalpin, J.P., 1996, Paleoseismology of compressional tectonic environments: *International Geophysics Series*, v. 62, p. 183-270.
- Clarke, S.H., Jr., and Carver, G.A., 1992, Late Holocene tectonics and paleoseismicity, southern Cascadia subduction zone: *Science*, v. 255, p. 188-192.
- Clarke, S.H.J., 1992, Geology of the Eel River Basin and adjacent region: Implications for Late Cenozoic tectonics of the southern Cascadia subduction zone and Mendocino triple junction: *AAPG Bulletin*, v. 76, p. 199-224.
- Dengler, L., Carver, G., and McPherson, R., 1992, Sources of North Coast seismicity: *California Geology*, v. 45, p. 40-53.
- Denlinger, R.P., 1992, A model for large-scale plastic yield of the Gorda deformation zone: *Journal of Geophysical research*, v. 97, p. 15,415 - 15,423.
- Furlong, K.P., and Govers, R., 1999, Ephemeral crustal thickening at a triple junction; the Mendocino crustal conveyor: *Geology*, v. 27, p. 127-130.
- Furlong, K.P., Lock, J., Guzowski, C., Whitlock, J., and Benz, H., 2003, The Mendocino crustal conveyor; making and breaking the California crust: *International Geology Review*, v. 45, p. 767-779.
- Goldfinger, C., Nelson, C.H., Johnson, J.E., Erickson, D., Winkler, M., Kalk, P., Pastor, J., Camarero, A., Morri, C., Dunhill, G., Ramos, L., Raab, A., Piasias, N., Jr., Pourmanoutscheri, M., van Rooij, D., Amy, L., and Liu, C.-C.C., 2003, Holocene earthquake records from the Cascadia subduction zone and northern San Andreas Fault based on precise dating of offshore turbidites: *Annual Review of Earth and Planetary Sciences*, v. 31, p. 555-577.
- Hyndman, R.D., and Wang, K., 1995, The rupture zone of Cascadia great earthquakes from current deformation and the thermal regime: *Journal of Geophysical Research*, v. 100, p. 22,133-22,154.
- Jachens, R.C., and Griscom, A., 1983, Three-dimensional geometry of the Gorda plate beneath northern California: *Journal of Geophysical Research*, v. 88, p. 9375-9392.
- Jacoby, G.C., Bunker, D.E., and Benson, B.E., 1997, Tree-ring evidence for an A.D. 1700 Cascadia earthquake in Washington and northern Oregon: *Geology*, v. 25, p. 999-1002.
- Kelsey, H.M., and Carver, G.A., 1988, Late Neogene and Quaternary tectonics associated with northward growth of the San Andreas Transform Fault, northern California: *Journal of Geophysical Research*, v. 93, p. 4797-4819.
- Kelsey, H.M., 2001, Active faulting associated with the southern Cascadia subduction zone in northern California, in Ferriz, H. and Anderson, R. (eds), *Engineering Geology Practice in Northern California*, Division of Mines and Geology Bulletin 210, Association of Engineering Geologists Special Publication 12, p. 259-274.
- Kelsey, H.M., Witter, R.C., and Hemphill-Haley, E., 2002, Plate-boundary earthquakes and tsunamis of the past 5500 yr, Sixes River estuary, southern Oregon: *Geological Society of America Bulletin*, v. 114, p. 298-314.
- McPherson, R., 1989, *Seismicity and Focal Mechanisms Near Cap Mendocino, Northern California: 1974-1984*: Arcata, CA, Humboldt State University.

- McPherson, R.C., and Dengler, L.A., 1992, The Honeydew earthquake, August 17, 1991: *California Geology*, v. 45, p. 31-39.
- Murray, M.H., Marshall, G.A., Lisowski, M., and Stein, R.S., 1996, The 1992 M = 7 Cape Mendocino, California, earthquake; coseismic deformation at the south end of the Cascadia Megathrust: *Journal of Geophysical Research B Solid Earth and Planets*, v. 101, p. 17,707-17,725.
- Oppenheimer, D.H., Beroza, G.C., Carver, G.A., Dengler, L., Eaton, J.P., Gee, L., Gonzalez, F.I., Jayko, A.S., Li, W.H., Lisowski, M., Magee, M., Marshall, G.A., Murray, M., McPherson, R., Romanowicz, B., Satake, K., Simpson, R.W., Somerville, P.G., Stein, R.S., and Valentine, D., 1993, The Cape Mendocino, California, earthquakes of April 1992; subduction at the triple junction: *Science*, v. 261, p. 433-438.
- Pryor, I., and McPherson, R., 2006, Seismicity and stress near the Mendocino Triple Junction, in Hemphill-Haley, M.A., McPherson, R., Patton, J.R., Stallman, J., Leroy, T., Sutherland, D., and Williams, T., eds., 2006 *Pacific Cell Friends of the Pleistocene Field Trip Guidebook, The Triangle of Doom: Signatures of Quaternary Crustal Deformation in the Mendocino Deformation Zone (MDZ)* Arcata, CA.
- Satake, K., Shimazaki, K., Tsuji, Y., and Ueda, K., 1996, Time and size of a giant earthquake in Cascadia inferred from Japanese tsunami records of January 1700: *Nature*, v. 379, p. 246-249.
- Savage, J.C., 1983, A dislocation model of strain accumulation and release at a subduction zone: *Journal of Geophysical Research*, v. 88, p. 4984-4996.
- Smith, S.W., Knapp, J.S., and McPherson, R.C., 1993, Seismicity of the Gorda Plate, structure of the continental margin, and an eastward jump of the Mendocino triple junction: *Journal of Geophysical Research, B, Solid Earth and Planets*, v. 98, p. 8153-8171.
- Thatcher, W., 1984, The earthquake deformation cycle, recurrence, and the time-predictable model: *Journal of Geophysical Research*, v. 89, p. 5674-5680.
- Verdonck, D., and Zandt, G., 1994, Three-dimensional crustal structure of the Mendocino triple junction region from local earthquake travel times: *Journal of Geophysical Research, B, Solid Earth and Planets*, v. 99, p. 23,843-23,858.
- Wakabayashi, J., 2006, Some thoughts on the instability and evolution of the Mendocino triple junction, in Hemphill-Haley, M.A., McPherson, R., Patton, J.R., Stallman, J., Leroy, T., Sutherland, D., and Williams, T., eds., 2006 *Pacific Cell Friends of the Pleistocene Field Trip Guidebook, The Triangle of Doom: Signatures of Quaternary Crustal Deformation in the Mendocino Deformation Zone (MDZ)* Arcata, CA.
- Wang, K., Wells, R., Mazzotti, S., Hyndman, R.D., Sagiya, T., 2003. A revised dislocation model of interseismic deformation of the Cascadia subduction zone. *Journal of Geophysical Research* 108(B1) 2026, doi:10.1029/2001JB001227.
- Wells, R. E., C. S. Weaver, R. J. Blakely, 1998. Forearc migration in Cascadia and its neotectonic significance. *Geology* 26, 759-762.
- Witter, R.C., Carver, G.C., Patton, J.R., Kelsey, H.M., Koehler, R.D., Garrison-Laney, C.E., Page, W.D., and Anonymous, 2001, Evidence for progressive folding of the late Holocene tidal marsh deposits along the western Little Salmon Fault, Humboldt Bay, Northern California: *Seismological Research Letters*, v. 72, p. 270.
- Witter, R.C., and Patton, J.R., 2006, Upper-Plate Earthquakes on the Western Little Salmon Fault and Contemporaneous Subsidence of Southern Humboldt Bay Over the Past 3,600 Years, in Hemphill-Haley, M.A., McPherson, R., Patton, J.R., Stallman, J., Leroy, T., and Sutherland, D., eds., 2006 *Pacific Cell Friends of the Pleistocene Field Trip Guidebook, The Triangle of Doom: Signatures of Quaternary Crustal Deformation in the Mendocino Deformation Zone (MDZ)* Arcata, CA.
- Witter, R.C., Patton, J.R., Carver, G.A., Kelsey, H.M., and Anonymous, 2000, Does the Little Salmon Fault rupture independently from the southern Cascadia subduction zone?; evidence for fault propagation folding of late Holocene tidal marsh soils, Humboldt Bay, California: *Eos, Transactions, American Geophysical Union*, v. 81, p. 1124.
- Witter, R.C., Patton, J.R., Carver, G.A., Kelsey, H.M., Garrison-Laney, C., Koehler, R.D., and Hemphill-Haley, E., 2002, Upper Plate Earthquakes on the Western Little Salmon Fault and Contemporaneous Subsidence of Southern Humboldt Bay Over the Past 3,600 Years, Northwestern California: Final Technical Report U.S. Geological Survey National Earthquake Hazards Reduction Program Award No. 01HQGR0125, p. 44.
- Williams, T., and McPherson, R., 2006, Gorda Plate Deformation Contributes to Shortening Between the Klamath Block and the On-land Portion of the Accretionary Prism to the S. Cascadia Subduction Zone, in Hemphill-Haley, M.A., McPherson, R., Patton, J.R., Stallman, J., Leroy, T., Sutherland, D., and Williams, T., eds., 2006 *Pacific Cell Friends of the Pleistocene Field Trip Guidebook, The Triangle of Doom: Signatures of Quaternary Crustal Deformation in the Mendocino Deformation Zone (MDZ)* Arcata, CA.
- Yamaguchi, D.K., Atwater, B.F., Bunker, D.E., Benson, B.E., and Reid, M.S., 1997, Tree-ring dating the 1700 Cascadia earthquake: *Nature*, v. 389, p. 922-923.

OVERVIEW OF NEOGENE WILDCAT GROUP

Excerpt from: NEOGENE STRATIGRAPHIC EVOLUTION OF NORTHWESTERN CALIFORNIA

K. R. AALTO

REFERENCES CITED

- Aalto, K. R., 1989b, Sandstone petrology and tectonostratigraphic terranes of the northwest California and southwest Oregon Coast Ranges: *Journal of Sedimentary Petrology*, v. 59, p. 561 – 571.
- Aalto, K. R., 1992, Late Cenozoic sediment provenance and tectonic evolution of the northernmost Coast Ranges, California: *in* G. A. Carver and K. R. Aalto (eds.), *Field guide to the late Cenozoic subduction tectonics and sedimentation of northern coastal California*: Pacific Section, American Association of Petroleum Geologists, Field Guide GB-71, p. 11 – 20.
- Aalto, K. R., Moley, K., and Stone, L., 1995, Neogene paleogeography and tectonics of northwestern California, *in* E. Fritsche (ed.), *Cenozoic Paleogeography of the Western United States-II*: Pacific Section, SEPM Book 75, p. 162 – 180.
- Aalto, K. R., Moley, K., and Miller, W., III, 1996, Evolution of a trench-slope basin within the Cascadia subduction margin: the Neogene Humboldt Basin, California: *Discussion: Sedimentology*, v. 43, p. 761 – 769.
- Aalto, K. R., Sharp, W. D., and Renne, P. R., 1998, $^{40}\text{Ar}/^{39}\text{Ar}$ dating of detrital micas from Oligocene-Pleistocene sandstones of the Olympic Peninsula, Klamath Mountains and northern California Coast Ranges: Provenance and paleodrainage patterns: *Canadian Journal of Earth Sciences*, v. 35, p. 735 – 745.
- Carver, G.A., and Aalto, K.R., eds., *Field guide to the late Cenozoic subduction tectonics and sedimentation of northern coastal California* : Pacific Section, American Association of Petroleum Geologists, Field Guide GB-71, 74 p.
- Clarke, S. H., Jr. 1992, Geology of the Eel River basin and adjacent region: implications for late Cenozoic tectonics of the southern Cascadia subduction zone and Mendocino triple junction: *American Association of Petroleum Geologists Bulletin*, v. 76, p. 199-224.
- Haller, C.R., 1980, The Miocene stratigraphy of California revisited: *American Association of Petroleum Geology Studies in Geology* no. 11, 349p.
- Ingle, J.C., Jr., 1987, The depositional, tectonic, and paleo-oceanographic history of the Eel River (Humboldt), Point Arena, and Bodega (Point Reyes) basins of northern California; a summary of stratigraphic evidence, *in* Schymiczek, H., and Suchsland, R., eds., *Tectonics, Sedimentation and Evolution of the Eel River and Other Coastal Basins of Northern California*: Pacific Section, American Association of Petroleum Geologists Miscellaneous Publications 37, p. 49-54.
- Knudson, K., 1993, Geology and stratigraphy of the Freshwater Creek watershed, Humboldt County, California: [unpublished M.S. Thesis] Humboldt State University, Arcata, CA, 84 p.
- McCrory, P.A. 1989. Late Neogene geohistory analysis of the Humboldt basin and its relationship to convergence of the Juan de Fuca Plate. *Journal of Geophysical Research* v. 94, p.3126-3138.
- Moley, K. 1992. A petrographic study of the Wildcat Group, Eel River basin, Humboldt County, California. *In* Field guide to the late Cenozoic subduction tectonics and sedimentation of northern coastal California. *Edited by* G. A. Carver and K. R. Aalto. Pacific Section, American Association of Petroleum Geologists Field Guide, GB-71, p. 31-38.
- Nilsen, T.H., and Clarke, S.H., Jr., 1987, Geological evolution of the late Cenozoic basins of northern California: *in* Tectonics, Sedimentation and Evolution of the Eel River and Other Coastal Basins of Northern California, edited by H. Schymiczek and R. Suchsland, Pacific Section, American Association of Petroleum Geologists Miscellaneous Publication 37, p. 15-30.
- Ogle, B.A., 1953, Geology of the Eel River area, Humboldt County, California: *California Division of Mines Bulletin* 164, 128 p.

A Soil Chronosequence of the Mitchell Ranch Fluvial Terraces of the South Fork Eel River Age Estimates and Tectonic Implications

Frank R. Bickner, LACO ASSOCIATES

INTRODUCTION

Fluvial terraces are abundant in northwestern California, yet few have been studied in detail and, as a consequence, age control and correlations are generally lacking. This study employs relative dating and soil geomorphological techniques to develop a soil chronosequence on a well preserved flight of terraces near Garberville, at the Mitchell Ranch. This soil chronosequence may help to provide a base of data to aid with correlation of similar geomorphic surfaces elsewhere in northwestern California.

At the Mitchell Ranch, a well preserved nested terrace sequence of fourteen surfaces steps upwards from the South Fork Eel River. This sequence of terraces is well suited to the study and development of a soil chronosequence because: 1) the terrace surfaces are spatially distinct; 2) alluvial parent materials for all of the soils are compositionally similar; 3) the depositional stratigraphy for all of the terrace deposits is similar; 4) soils occur as surface soils and most have not had appreciable profile rejuvenation; 5) radiometric ^{14}C (Stone and Vasey, 1968) age determination of a surface soil in the South Fork Eel River basin provides "low-end", 9.5 Ka (thousands of years before present), soil-age calibration; 6) magnetostratigraphic measurements of terrace soils (LaVen and Fine, 1987) provide supporting evidence for a tentative age of between 104 Ka and 17 Ka; and 7) the relative soil development and topographic data suggest that the terraces and soils can be grouped into age-classes.

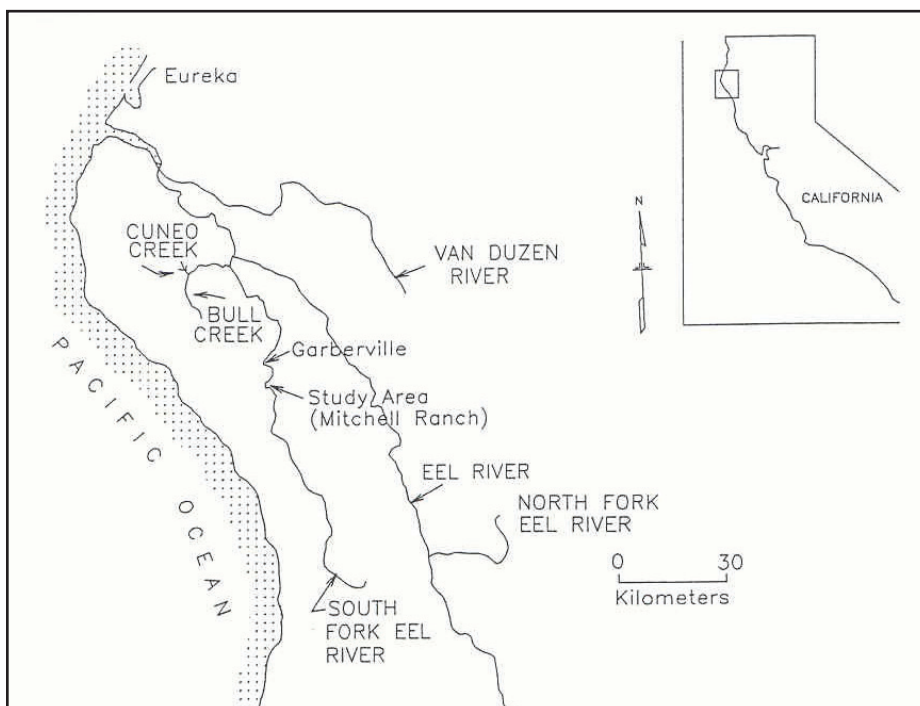


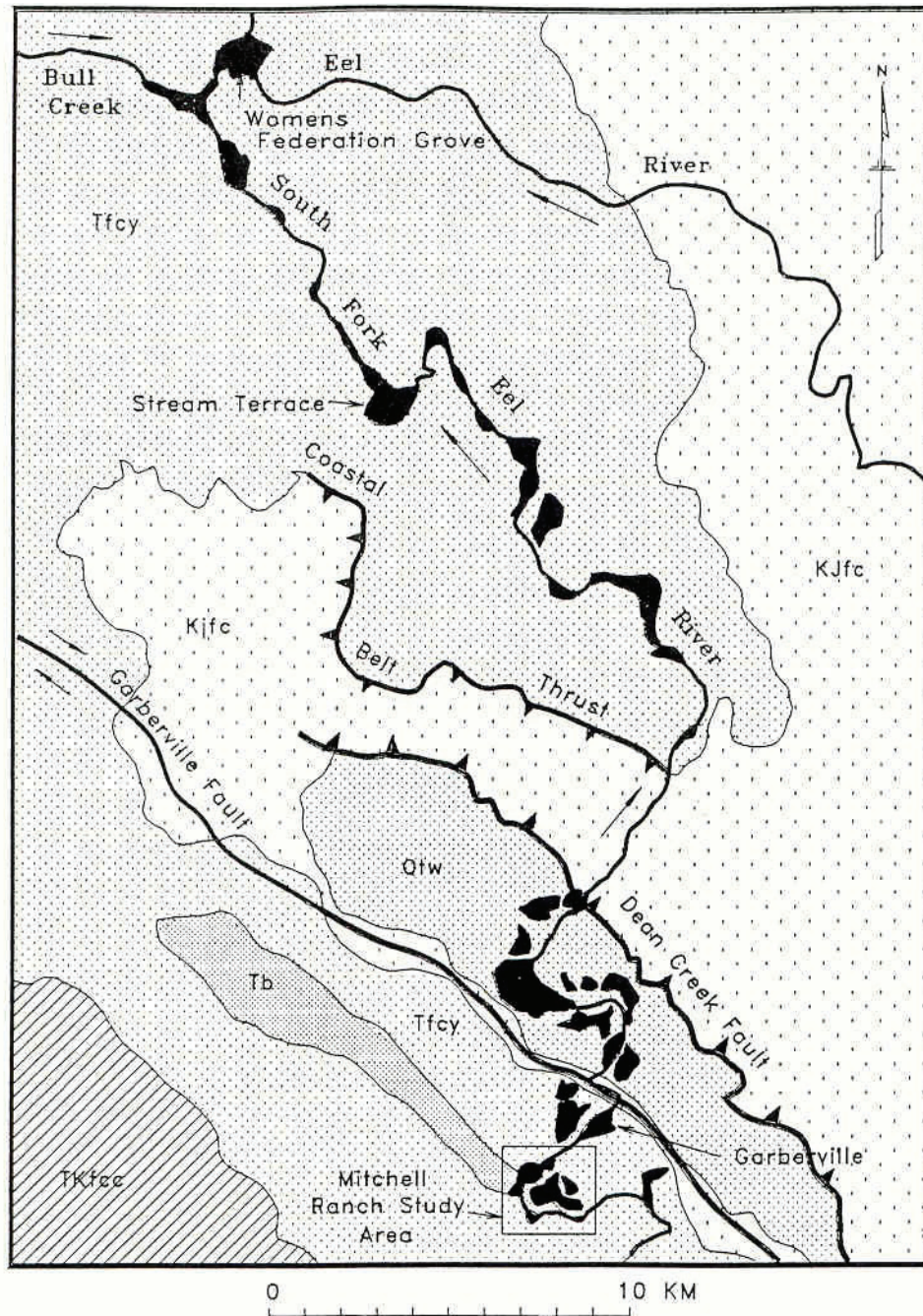
Figure 1. Location map of Mitchell Ranch near Garberville, northwestern California.

ABSTRACT

Alluvial history in the South Fork Eel River basin (1,750 sq. km) of northern California is recorded by strath and fill terraces. Fourteen nested terrace surfaces 3m, 4m, 6m, 8m, 10m, 50m, 62m, 65m, 97m, 108m, 259m, 279m, 305m, and 315m above the South Fork Eel River in the Garberville area at the Mitchell Ranch were studied in detail. The 3m, 4m, and 6m surfaces represent fill terraces composed of active channel gravel and flood deposits. Strath terraces at 8m, 10m, 50m, 62m, 65m, and 108m are composed of gravel and are capped by overbank deposits. The 259m, 279m, 305m, and 315m surfaces are eroded terrace remnants with only resistant chert and metamorphic lag gravel remaining.

Using quantitative data based on weathering and soil development phenomena, a soil chronosequence was developed for the Mitchell Ranch terraces. The Soil Profile Development Index (SPDI) methodologies of (Harden, 1982; Harden and Taylor, 1983) were used to quantify the soil development. Estimated ages based on soil development correlations using the UPDI's suggest that the terraces can be grouped into six age-classes, as follows: age-class 1, recent alluvium; age-class 2, 3.5 Ka - 8.3 Ka; age-class 3, 29 Ka - 48 Ka; age-class 4, 75 Ka - 80 Ka; age-class 5, 100 Ka - 120 Ka; age-class 6, greater than 300 Ka.

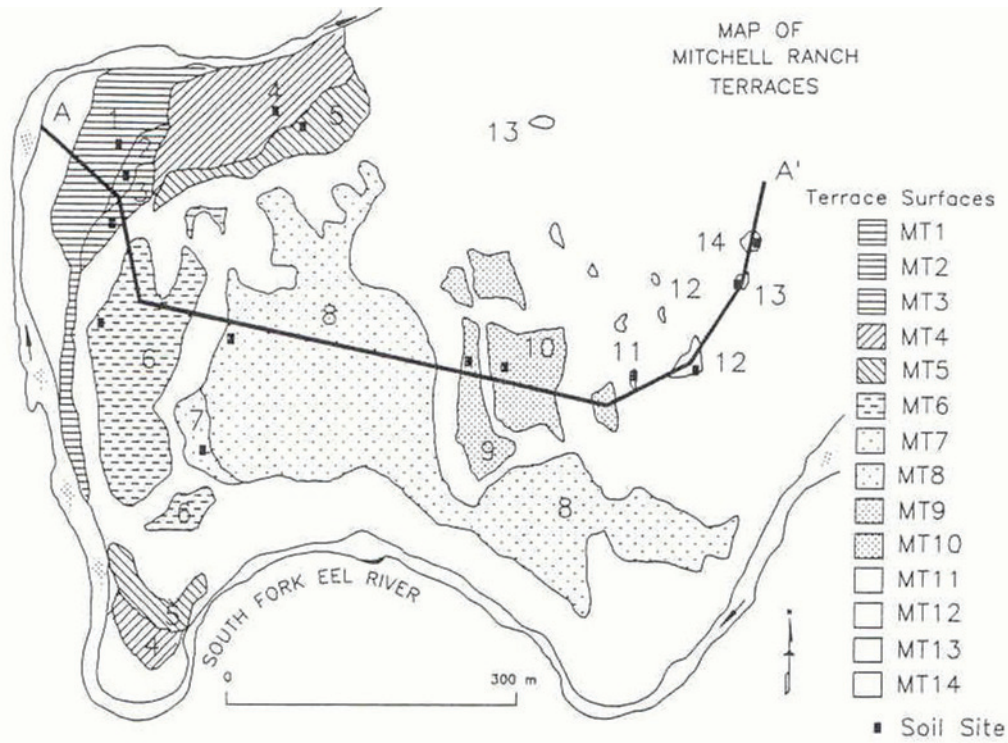
Based on soil development, the average uplift rate at the Mitchell Ranch, up to the age of MT10 is 1.3 m/ky. The long term, average uplift rate of 1.3 m/ky for the Mitchell Ranch terraces compares well to uplift rates inferred from: 1) regional denudation rate of 1.2 m/ky (Judson and Ritter, 1964); 2) work (Menack, 1986) on the edge of the Kimtu Unit of the Wildcat Group, which sets the age of this unit at 1,000 Ka with total incision into this unit of 1219 m, resulting in an uplift of 1.22 m/ky; and 3) published uplift rates ranging from 0.3 m/ky to 4 m/ky for elevated marine surfaces on the coast to the west (15km) of the study area (Lajoie et. al., 1982; Merritts and Bull, 1989).



KJfc = Central Belt Franciscan Melange
 TKfcc = Coastal Belt Franciscan
 Tfcy = Yager Formation
 Tb = Kimtu Unit of the Wildcat Group
 Qtw = Garberville Unit of the Wildcat Group

Figure 2. Terrace locations and regional geology along the lowermost 30 km of the South Fork Eel River

A



B

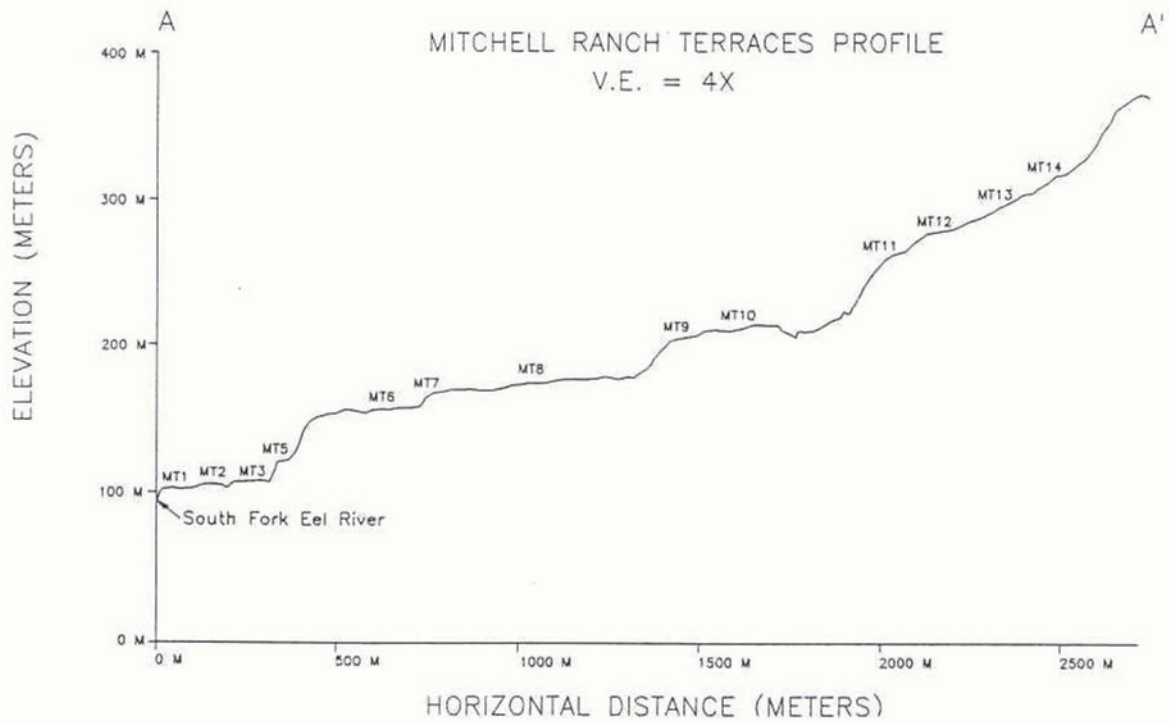


Figure 3. A. A map of the Mitchell Ranch showing the location of terrace surfaces, the profile, and soil pits. B. Topographic profile of the Mitchell Ranch Terraces.

INFLUENCE OF THE MENDOCINO TRIPLE JUNCTION ON THE TECTONICS OF COASTAL CALIFORNIA

Kevin P. Furlong

Geodynamics Research Group, Department of Geosciences, Pennsylvania State University, University Park, Pennsylvania 16801; email: kevin@geodyn.psu.edu

Susan Y. Schwartz

Earth Sciences Department and IGPP, University of California, Santa Cruz, California 95064; email: sschwartz@es.ucsc.edu

ABSTRACT

The migration of the Mendocino triple junction through central and northern California over the past 25–30 million years has led to a profound change in plate interactions along coastal California. The tectonic consequences of the abrupt change from subduction plate interactions north of the triple junction to the development of the San Andreas transform system south of the triple junction can be seen in the geologic record and geophysical observations. The primary driver of this tectonism is a coupling among the subducting Juan de Fuca (Gorda), North American, and Pacific plates that migrates with the triple junction. This coupling leads to ephemeral thickening of the overlying North American crust, associated uplift and subsequent subsidence, and a distinctive sequence of fault development and volcanism.

This page intentionally left almost blank.

Insert Furlong and Schwartz paper here.
This abstract is available as a separate
download.

Structural Geology South of Punta Gorda, Mendocino Triple Junction Region

**Senior thesis by Sunshine Mansfield
Humboldt State University**

ABSTRACT

An unnamed fault emerges from offshore just south of Punta Gorda in the Mendocino triple junction region. The fault is near vertical, NW-trending and most likely related to strike-slip faulting associated with the San Andreas transform, and separates Late Eocene Coastal terrane from middle Miocene King Peak Subterrane. The Coastal terrane forms steep cliffs and is massive and well indurated, and King Peak subterrane is more shaley, less well indurated and the site of extensive landslides. Where the bounding fault steps inland forming a restraining bend there is head ward erosion of King Peak subterrane from sea level to the ridge crest. The high uplift rate and nearness of the fault plane to ocean storm waves are what make this a dramatic landscape. Large tension cracks a few hundred meters long and deep in the break-inslope form small ridges above the cliffs along the shore and are located in the corner of the fault tear. Sea Lion Gulch exposes the contact and distinctive tan conglomeritic *mélange*, possibly reworked fault breccia from the downslope movement of King Peak subterrane along the fault plane. A fault in the King Peak subterrane juxtaposes *mélange* types found north along a drag fold with the folded turbidites found south. The fault trends WNW and dips steeply to the NE. Investigation of the contact found no large scale regional shear structures for the previously mapped Cooskie Shear zone in the study area shedding some doubt on R. J. McLaughlin's interpretation that the King Range terrane migrated along the transform margin. The *mélange* unit near the contact is described as type I and type II *mélange* [cf. Cowan] and originated in the accretionary prism accompanying prism growth which resulted in gravitational slides and lateral spreading of unconfined sediments. Progressive disruption by brittle-ductile deformation from dewatering sediments is identified by layer parallel extension of sand beds. Features of progressive stages of stratal disruption include: necking, boudinage and shear fractures; fragment foliation of lenticular shape; and fragments resulting from complete disruption. Type II *mélange* has similar features but includes a different lithology comprised of extensive black mudstone interbedded with thin layers of green tuff, white, grey or black chert and fine-grained sandstone. The fold hinges are parallel to the fault and gently plunge ESE. Many of the folds are overturned and inverted. A fold transect done perpendicular to the axis is a kinked fold hinge from a larger overturned fold. The folds may be overturned and rotated along the fault and hinges kinked or the fault is compressive and related to the formation of the fault.

Some Thoughts on the Instability and Evolution of the Mendocino Triple Junction

John Wakabayashi

Department of Earth and Environmental Sciences, California State University, Fresno, 2576 E. San Ramon Ave. MS ST-24, Fresno, CA 93740-8039, USA

The Mendocino triple junction (MTJ) marks the transition from the Pacific-North American transform plate boundary to the south and the Gorda/Juan de Fuca-North America convergent plate boundary (Cascadia subduction zone) to the north. Owing to the relative velocities of the three plates involved the triple junction migrates northwestward relative to stable North America at about the dextral slip rate of the San Andreas fault system (SAFS). Were it not moving northwestward at this rate, we would have either major shortening or extension across the Mendocino fracture zone (MFZ), and the MFZ is a purely right-lateral fault. We often hear the term “slab window” and envision a slab falling away leaving asthenosphere to well up in the wake of the triple junction. When one really thinks through the reference frames here, nothing really falls away south of the MTJ. It is more like the southern edge of the subducting Gorda slab is yanked out “sideways” to the northwest from beneath the Coast Ranges (the “rug is being pulled out sideways” at the approximate slip rate of the SAFS). Now that is the simple view of the triple junction, but there are complications, when we look at things more closely. Two of these complications concern the unstable geometry of the triple junction and the fact that the San Andreas fault system consists of multiple faults rather than simply the San Andreas fault itself.

The instability of the triple junction results from the non-colinearity of the San Andreas fault system and the Cascadia subduction zone. How this instability relates to the evolution of the triple junction depends in part on how one depicts the triple junction (Fig. 1). The usual way of depicting the triple junction is given in the alternative “A” in Figure 1 in which the San Andreas fault system is represented as a single fault, with a strike of N40°W (average strike of the northern part of the fault system), and the three plate boundaries join in a point. The evolution of this geometry predicts the opening of a gap in the triple junction region (Fig. 1, alternative A), but this prediction conflicts with field observations that show that the MTJ area is one of focused shortening and uplift. There is certainly a localized region of high paleogeothermal gradients and high late Cenozoic exhumation that might correspond to this opening and not the generalized slab window thermal anomaly, which is much broader and inboard (Underwood, 1989; Dumitru, 1991; Bürgmann et al., 1994; Underwood et al., 1999), although this belt does not appear to have the predicted northward-younging trend (Underwood et al., 1999). Another alternative (Alternative B in Figure 1) is to use the current local triple junction configuration as a reference state and examine how such a geometry might evolve. The current geometry departs from the idealized geometry above because the San Andreas fault takes a large right bend to a N5°W strike south of the MTJ. In addition, the northernmost San Andreas fault is inboard (east) of the daylighting (on the ocean floor) Cascadia subduction zone (Alternative B, Fig. 1). The N5°W strike is actually more northerly than the strike of the Cascadia subduction zone, so that migration of the triple junction along such a strike would result in the overrunning of North America; this predicts shortening. In addition, the bend of the San Andreas fault to a N5°W strike is a right (releasing) bend, predicting transtension in the area that trails south of the region of active shortening. The overall sequence of tectonic events predicted by the Alternative B scenario would be late Cenozoic shortening followed by transtension and possibly negative tectonic inversion.

One hypothesis suggests an additional (or alternative) mechanism for localized shortening in the MTJ region in the form of transfer of slip from the eastern faults of the northern San Andreas fault system (called “eastern faults” for short) (Wakabayashi, 1999; Wakabayashi et al., 2004; Wakabayashi, in press). This model treats this slip transfer as a regional scale restraining step-over or bend that migrates with respect to affected rocks (Fig. 2) as explained below.

Schematic Diagrams of the Hypothetical Evolution of the Mendocino Triple Junction (no scale implied)

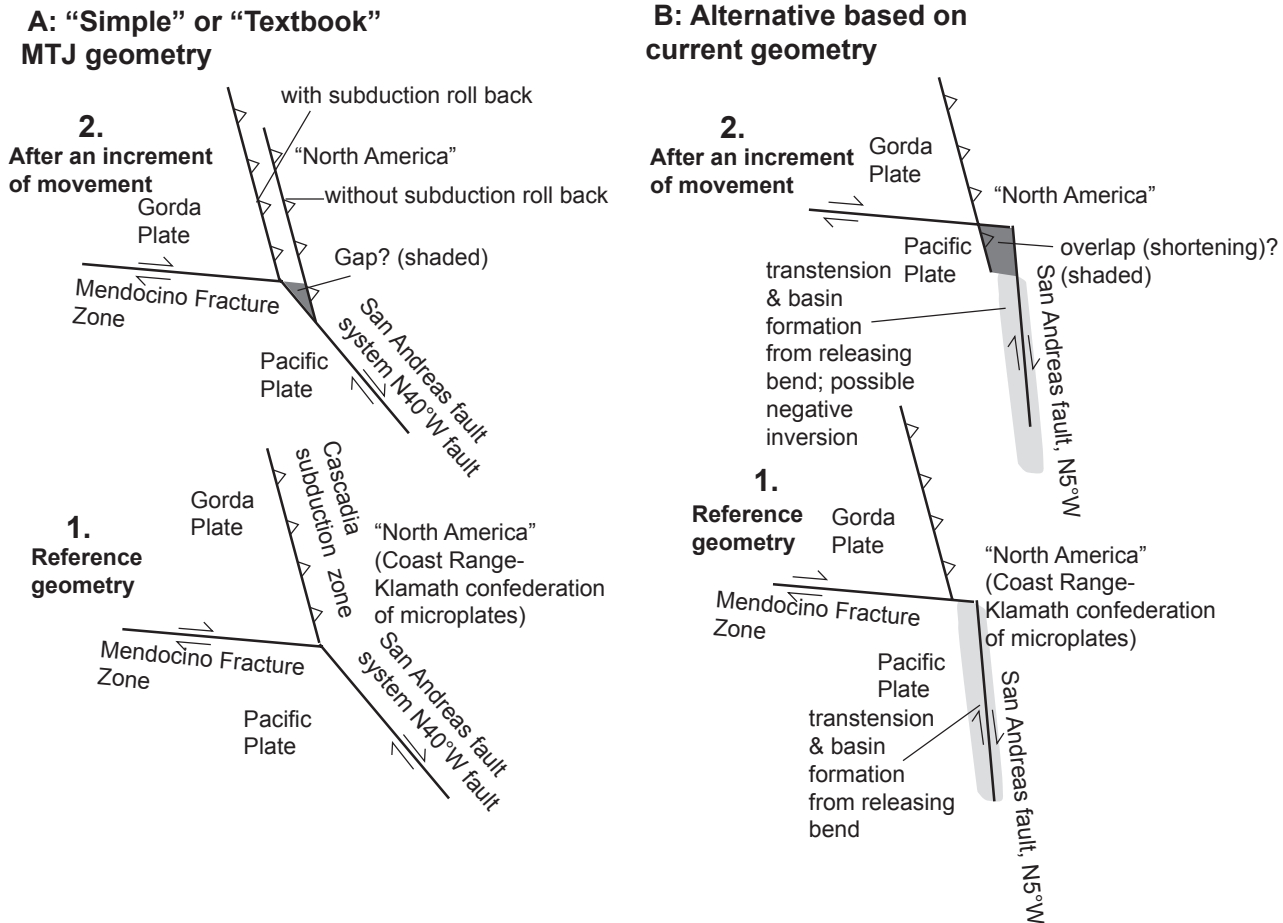


Figure 1. These diagrams present alternative scenarios for the evolution of the Mendocino Triple Junction and its evolution.

San Andreas-age dextral faults are not present north of the MTJ (Kelsey and Carver, 1988). In the northern SAFS, 230-250 km of dextral slip, the aggregate amount of displacement of the eastern faults, must transfer westward to the MTJ, otherwise there would be enormous slip incompatibilities along the eastern faults with zero displacement at their northern tips and a large displacements to the south (Wakabayashi, 1999). Transfer of slip from the eastern faults to the Mendocino triple junction is a restraining (left) slip transfer or step-over. For any range of transverse structure dips and strikes, this step-over geometry predicts an unrealistic amount of late Cenozoic rock uplift for which there is no evidence (tens of km, Wakabayashi et al. 2004). The actual geometry of transverse structures in the triple junction region may be complex. Some strike-slip faults south of the triple-junction transition into thrust faults north of the triple junction (Kelsey and Carver, 1988). The uplift rates are higher in the triple junction region than to the north along the subducting margin or to the south along the transform boundary (Merritts and Bull, 1989), and this uplift does not appear to be limited to that directly associated with reverse movement along the structures noted above. Tens of km south of the triple junction, discrete high-angle faults, that strike more westerly than the dextral strands of the San Andreas fault system, cut Franciscan nappe structures and later out-of-sequence thrust faults that imbricate the Franciscan nappes. Late Cenozoic deposits are not present along or across these structures, so it is difficult to verify whether these are paleo transverse structures as suggested by Wakabayashi (1999) and Wakabayashi et al. (2004).

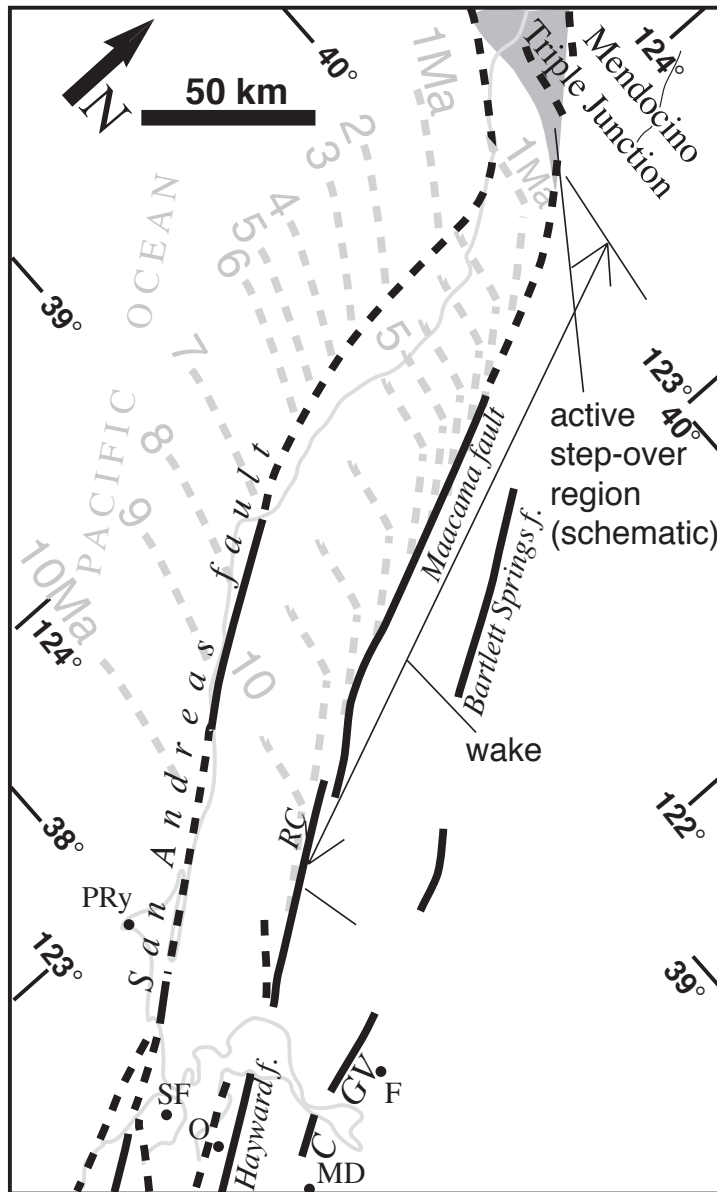


Figure 2. Migration of the restraining transfer zone to the Mendocino Triple Junction. Approximate past positions of the triple junction (west of the the San Andreas fault), and transverse structures (east of the San Andreas fault; this is the 'wake' or region formerly affected by oblique deformation associated with the step-over at an earlier position) shown in grayed dashed lines with corresponding age designations. Longitude/latitude and other reference points are valid only for present, given that they would differ upon restoration to the different time frames. Abbreviations: C: Concord fault, F: Fairfield, GV: Green Valley fault, O: Oakland, RC: Rodgers Creek fault, SF: San Francisco.

did not exist (or had low collective slip rates) prior to about 11 Ma (Wakabayashi, 1999). It may be coincidental that the thermal anomalies of Underwood et al. (1999) are rather uniform in age and are approximately 11-13 Ma old. Perhaps during that time the local geometry of the triple junction more closely resembled that depicted in Alternative 1 of Fig. 1 and without the shortening connected to slip transfer from eastern faults. Perhaps there was a relatively brief period of time in which a mechanism such as that shown in Fig. 1 alternative A operated,

The eastern faults, such as the Hayward-Rodgers Creek-Maacama trend, and the Green Valley-Bartlett Springs faults, die out northward as well-defined faults (Fig. 2). This may be because the eastern faults are young and propagating northward, while slip transfers to the triple junction that is migrating at about 25 mm/yr northwestward relative to the westernmost of the eastern faults (Wakabayashi, 1999; Wakabayashi et al. 2004). In other words, the eastern faults are trying to dump slip to a moving target. In order to transfer slip to the migrating triple junction, new transverse faults must continue to form (Fig. 2). Thus, the step-over region progressively migrates so that large-scale displacement or structural relief has not developed on any given transverse structure, similar to other so-called migrating step-overs interpreted along the SAFS (Wakabayashi et al., 2004; Wakabayashi, in press). It is difficult to estimate the length of the 'wake' (ie the strike length of the region formerly affected by this step-over), because the boundaries of the active step-over area are not well defined, and because the nature of late Cenozoic deformation in the region southeast of the triple junction has not been determined, owing to the lack of late Cenozoic deposits. The 'wake' of the step-over region may be 200-250 km long based the presence of possible old transverse structures cutting basement as far as south as the inboard 10 Ma contour on fig. 2, the lack of such structures in the San Francisco Bay area, and the temporal spatial distribution of slip on the eastern fault strands (Wakabayashi, 1999). This wake corresponds only to the activity history of the eastern faults, not the older Mendocino triple junction itself.

It is likely that transfer of slip from the eastern faults contributes to the shortening in the MTJ area, possibly enhancing shortening generated by the triple junction geometry itself. The eastern faults, however, probably

generating heating and hydrothermal activity close to the triple junction. The subsequent dispersion of the thermal anomalies along the San Andreas fault might be a product of shifting of the active zone of faulting through the history of the fault, a mechanism that may be characteristic of most of the major faults of the SAFS (e.g., Sims, 1993; Wakabayashi, 1999). It should be noted that the broader inboard belt of high geothermal gradients, associated with the better known northward-younging slab window volcanics, does not have anywhere near as high exhumation associated with it (suggesting far less shortening and uplift). In any case, it goes without saying that the MTJ is an area of extraordinary complexity. It has served as a brain teaser for many geologists in the past and promises to challenge geologists for many years to come.

REFERENCES CITED

- Bürgmann, R., Arrowsmith, R., Dumitru, T., and McLaughlin, R., 1994, Rise and fall of the southern Santa Cruz Mountains, California, from fission tracks, geomorphology and geodesy: *Journal of Geophysical Research*, v. 99, p. 20181-20202.
- Dumitru, T.A., 1991, Major Quaternary uplift along the northernmost San Andreas fault, King Range, northwestern California: *Geology*, v. 19, p. 526-529.
- Kelsey, H.M., and Carver, G.A., 1988, Late Neogene and Quaternary tectonics associated with northward growth of the San Andreas transform fault, northern California: *Journal of Geophysical Research*, v. 93, p. 4797-4819.
- Merritts, D., and Bull, W.B., 1989, Interpreting Quaternary uplift rates at the Mendocino triple junction, northern California, from uplifted marine terraces: *Geology* v.17, p. 1020-1024.
- Sims, J.D., 1993, Chronology of displacement on the San Andreas fault in central California: evidence of reversed positions of exotic rock bodies near Parkfield, California: in Powell, R.E., Weldon, R.J., II., and Matti, J.C., eds. *The San Andreas Fault System: Displacement, Palinspastic Reconstruction and Geologic Evolution*, Geological Society of America Memoir 178, p. 231-256.
- Underwood, M.B., 1989, Temporal changes in geothermal gradients, Franciscan subduction complex, northern California: *Journal of Geophysical Research*, v. 94, p. 3111-3125.
- Underwood, M.B., Shelton, K.L., McLaughlin, R.J., Laughland, M.M., and Solomon, R.M., 1999, Middle Miocene paleotemperature anomalies within the Franciscan Complex of northern California: Thermotectonic responses near the Mendocino triple junction: *Geological Society of America Bulletin*, v. 111, p. 1448-1467.
- Wakabayashi, J. 1999., Distribution of displacement on, and evolution of, a young transform fault system: the northern San Andreas fault system, California: *Tectonics* v. 18, p. 1245-1274.
- Wakabayashi, J., Hengesh, J.V. & Sawyer, T.L. 2004, Four-dimensional transform fault processes: progressive evolution of step-overs and bends: *Tectonophysics*, v. 392, p. 279-301.
- Wakabayashi, J., in press, Step-overs that migrate with respect to affected deposits: Field characteristics and speculation on some details of their evolution: in Cunningham, W.D., and Mann, P., eds. *Tectonics of strike-slip releasing and restraining bends in continental and oceanic settings*. Geological Society of London Special Publication.